DTU Mechanical Engineering
Department of Mechanical Engineering

Design and Performance Analysis of Plate Heat Exchangers for Heat Pumps using Pure and Mixed Refrigerants

Roberta Mancini

PhD Thesis

Design and Performance Analysis of Plate Heat Exchangers for Heat Pumps using Pure and Mixed Refrigerants

Ph.D. Thesis
submitted the 31st May 2019
and defended the 25th October 2019
at the
TECHNICAL UNIVERSITY OF DENMARK

for the degree of Doctor of Philosophy

by
Roberta Mancini

under suggestion of:
Professor Brian Elmegaard (DTU), main supervisor
Associate Professor Wiebke Brix Markussen (DTU), co-supervisor
Associate Professor Fredrik Haglind (DTU), co-supervisor

and under the recommendation of:
Associate Professor Knud Erik Meyer (DTU), examiner
Associate Professor Kim Sørensen (Aalborg University), examiner
Professor José Corberán (Polytechnic University of Valencia, Spain), examiner

Design and Performance Analysis of Plate Heat Exchangers for Heat Pumps using Pure and Mixed Refrigerants

Copyright ©2019 by Roberta Mancini. All rights reserved.

Ph.D. Thesis
DCAMM Special Report no. S268
Printed by STEP
Font: Utopia typeset with LaTeX 2ε

DTU Mechanical Engineering
Section of Thermal Energy
Technical University of Denmark

Nils Koppels Allé, Bld. 403
DK-2800 Kongens Lyngby
Denmark
Phone: (+45) 4525 4319
Fax: (+45) 4525 1961
www.mek.dtu.dk
ISBN:978-87-7475-578-4

Al mio papá,
che mi ha insegnato ad avere sogni senza limiti,
e ad inseguirli con passione, determinazione e onestá.

We cannot all succeed when half of us are held back.

— Malala Yousafzai

Preface

The present thesis was prepared at the Section of Thermal Energy, Department of Mechanical Engineering, Technical University of Denmark (DTU). It is submitted as partial fulfillment of the requirements for the degree of Doctor of Philosophy and is written as a monograph.

The work was carried out from December 2015 to May 2019, under the main supervision of Professor Brian Elmegaard (DTU) and co-supervision of Associate Professor Wiebke Brix Markussen (DTU) and Associate Professor Fredrik Haglind (DTU).

An external research stay was carried out at the Center for Environmental Energy Engineering (CEEE) at University of Maryland (College Park, US) under the supervision of Research Scientist Dr. Vikrant C. Aute, from January 2018 to July 2018. A short visit was undertaken in April 2019 to the Institut Français du Froid Industriel et de Génie Climatique at Conservatoire National des Arts et Métiers (Paris, France), under the supervision of Professor Pascal Tobaly.

The PhD project was funded within the frame of the THERMCYC project, "Advanced thermodynamic cycles utilizing low-temperature heat sources" with project ID 1305-00036B, (http://www.thermcyc.mek.dtu.dk/) by Innovation Fund Denmark, The Danish Council for Strategic Research in Sustainable Energy and Environment.

Additionally, EUDP (Energy Technology Development and Demonstration) within the project "Development of ultra-high temperature hybrid heat pump for process application" (grant number 64011-035), funded a three months research work from October 2018 to December 2018. The results of this research are not included in the present thesis.

Last, financial support was received from the Otto Mønsted A/S Fond, Tranes Fond, Reinholdt W. Jorck og hustrus Fond, and P.A. Fiskers Fond, within the frame of the external research stay in the US, and the participation to ECOS 2017 and IIR Gustav-Lorentzen 2018 international conferences.

Copenhagen, May 2019 Roberta Mancini

Acknowledgments

This PhD thesis represents the end of a wonderful journey during which I grew professionally and personally. It was very challenging to express with meaningful words my gratitude to all the people that shared this adventure with me.

First, my deepest gratitude goes to my supervisor Brian Elmegaard, for choosing me for this position three years ago. Thank you for giving me the freedom to pursue my research interests, for supporting my decisions, and contributing to my work with interesting discussions, useful feedback, and challenging questions. I wish to extend my gratitude to my co-supervisors Wiebke Brix Markussen, for her valuable contributions to this work, and to Fredrik Haglind, for many fruitful discussions.

My external research stay at University of Maryland would have not been possible without Vikrant Aute, who hosted me in his laboratory. Thank you for inspiring discussions on modelling and heat exchangers, and for a fruitful collaboration. I would also like to acknowledge Pascal Tobaly, who hosted me in his lab at CNAM in Paris.

A very big thank you goes to Søren Gundtoft from Sondex AS: for believing so much in my work, for giving an industrial application to my models, and for a very contagious enthusiasm. I am incredibly happy that we had the chance to meet and share knowledge, ideas, and work, in the last part of this project.

A huge thank you goes to all the colleagues contributing to this work: to Benjamin, for all the work we did together, the exchange of ideas, and for sharing this journey with me from the very beginning to the end; to Jonas, for contributing with many ideas on models, correlations and many different topics; to Martin, for all the challenging questions you asked me, and all the work on correlations and mixtures; to Ji, for all the experimental data you shared with me. A special thank you also goes to my colleagues Andrea, Gennaro, and Michael, for proofreading big chapters of this thesis. And of course, thank you Michael for helping me with the Dansk Resumé.

My long working days would have not been the same without all my colleagues at the Section of Thermal Energy, and I wish to thank all of them for creating an enjoyable environment. Special thanks go to my officemates Benjamin, Fabian, Henrik, Wiebke, Pernille, and Valentin, for the support, fun and chocolate shared together. Thank you

to all the members of the Cool Coffee Club, for long (sometimes short) afternoons of coffee, cakes, chocolate, and interesting conversations on our work. I extend my profound gratitude to my colleagues during my time in Maryland, especially Lukas, Jimmy, Ransisi, Rohit, and Zhenning, for welcoming me in their office and sharing with me fun moments during my time there. In particular, thank you Lukas for making my stay in the US a special memory that I will always keep with me.

The years in Copenhagen have been an amazing time of my life, and I found a home in the coldness of Denmark thanks to all the incredible friends that I met along the way. Thank you (in random order): Tivi, for all the adventures around the world (not to mention our dinners and spontaneous pyjama parties); Matthias, for our gin tonic nights and for helping me to break my limits with sports; Enrico, for our talks about the meaning of life, and a bit of everything else; Angelo, for constantly making fun of me and being a loyal friend; Andrea Mazzucco, for the jokes, the honest advices, and for teasing (and loving) Dani as much as I did; Danilo, for inspiring me with his attitude to life and parties, and for never saying no to the wildest proposals; Lorenzo, for being my very first mentor at DTU; Michael, for our deep talks during *danskepausen*, and for becoming a precious friend in my life; Nico, Rai, Ros and Manu for being a warm family during my time in Rolf Krakes, especially to Manu, for being my very first friend and still a very important one in Copenhagen; Luca, for all the Italian music sharing, and a contagious positive attitude to life; Rossana, for the super joyful *spirito terrone* finally imported in DTU; my girlfriends Chiara, Elena and Maria, for creating our special tradition of girls nights out, and for our teenager/adult conversations in front of a cocktail. Finally, to my small beloved family of Copenhagen: Thank you Andre, for sharing this journey with me, at work and at home, and filling my life with an incredible amount of joy, risottos, and friendship. Thank you Fede, for all the times you understood that I needed a hug coming back home. Thank you Chica, for being the sister I never had, because you always understand and support me, and we spent truly *unforgettable* moments together.

A special thank you goes to all the distant friends, spread around the world. In particular: Hussain, thank you for being an honest friend and for all the discussions about the most disparate topics, from love to PhD life, from politics to gossip. Monica, grazie per essere un'amica speciale nella mia vita, e per le nostre infinite chiacchiere su lavoro, vita da expat, e una buona dose di pettogolezzi. Alle mie amiche di sempre, Alessandra, Claudia, Fabiola e Giulia, grazie perché nonostante la distanza e il tempo, riesco a ritrovare la mia spensieratezza di adolescente quando sono con voi.

Il ringraziamento piú speciale va alla mia famiglia, che mi ha sempre supportato nelle mie scelte e nei miei lunghi periodi lontana da casa. Edo, il corraggio con cui affronti la vita, la tua sensibilitá, e il tuo spirito critico sono una fonte di ispirazione giornaliera. Mamma, grazie per essermi cosí vicina nonostante la distanza. La tua forza e la tua energia sono una continua motivazione ad andare avanti, e sai bene che senza di te tutto questo non sarebbe stato possibile.

Abstract

Optimal heat exchanger (HEX) design and accurate estimation of its performance is of paramount importance to improve the energy efficiency and the economic feasibility of heat pump systems. A plate heat exchanger (PHE) is a multi-channel HEX configuration, which attracted intense industrial attention due to enhanced heat transfer in a relatively compact design compared to traditional configurations. Moreover, due to the possibility of setting the flow in a counter-current arrangement, PHEs constitute an ideal solution to match the temperature glide of zeotropic mixtures during phase change with the secondary fluid temperature profile, thus reducing the irreversibility due to heat transfer.

This PhD thesis presents detailed numerical models of PHE evaporators and condensers using pure and mixed refrigerants. The numerical models were implemented based on both one-dimensional and two-dimensional discretization of the HEX, with the aim of simulating channel-to-channel flow maldistribution. The PHE models were further integrated with design and off-design models of single-stage vapour compression heat pumps, in order to evaluate the impact of HEX design and performance on the thermodynamic and economic performance indicators of the cycle. Additionally, the presented models were validated against available experimental data for both pure fluids and zeotropic mixtures.

The developed modelling framework was subsequently applied to case studies in order to address research gaps in the field of PHE technology. First, a comparison of different correlations to compute the evaporation heat transfer coefficient of zeotropic mixtures was carried out, with the aim of deriving recommendations on the most suitable ones. Each correlation was applied to the PHE model to compute the local heat transfer coefficient, and the calculated heat flow rate was subsequently compared to experimental data for zeotropic mixtures of carbon dioxide (CO_2)/propane at different mass compositions.

Second, guidelines for PHE evaporators and condensers design were derived. It was shown that condenser pressure drop solely affects the economic feasibility of the heat pump, while an optimal trade-off between heat transfer area and pressure drop of the PHE evaporator must be ensured to optimize the system thermodynamic and economic performance. Moreover, a methodology to derive simplified guidelines for the design of optimal PHE evaporators was formulated and applied to a case study of heat pump integration in a spray drying facility for waste heat recovery purposes.

Last, a study on the impact of flow maldistribution on the performance of PHE evaporators was carried out. Specifically, the impact of liquid/vapour non-uniformities at the evaporator inlet and the effect of end plates were estimated on a PHE evaporator using two pure fluids and two zeotropic mixtures as refrigerants. The impact of maldistribution on the heat pump thermodynamic performance was subsequently evaluated by an integrated PHE - heat pump model. The evaporator degradation was thus translated into a reduction of the thermodynamic performance of the heat pump, negatively impacting the system operating costs.

Resumé

Optimalt design af varmevekslere samt en præcis estimering af deres ydeevne er altafgørende for at kunne forbedre energieffektiviteten samt økonomien for varmepumpesystemer. En pladevarmeveksler (PHE) er en varmevekslerkonfiguration, som har tiltrukket sig stor industriel interesse pga. en forbedret varmetransmission i et relativt kompakt design sammenlignet med traditionelle konfigurationer. Desuden udgør PHEs en ideel løsning til at matche zeotropiske blandingers temperaturglidning under fasesovergang med den sekundære fluids temperaturprofil pga. muligheden for at anvende en modstrømskonfiguration i varmeveksleren. Derved reduceres den irreversibilitet som er grundet varmtransmissionen.

I denne ph.d. afhandling præsenteres detaljerede numeriske modeller af PHE fordampere og kondensatorer med både rene og blandede kølemidler. De numeriske modeller er baseret på både en-dimensionel og to-dimensionel diskretisering af varmeveksleren med det mål at kunne simulere en ulige strømningsfordeling mellem kanalerne i varmeveksleren. Komponentmodellerne er endvidere blevet integreret med design og off-design modeller af et-trins-kompressionsvarmepumper for at kunne evaluere effekten af varmevekslerdesign og -performance på indikatorer for den termodynamiske og økonomiske performance af varmepumpesystemet. De præsenterede modeller er valideret med eksperimentelle data for både rene kølemidler samt zeotropiske blandinger.

De udviklede modeller er blevet anvendt i forskellige case studies for at adressere forskningsmæssige huller på pladevarmevekslerområdet. Først blev en sammenligning udført af forskellige korrelationer til at beregne varmetransmissionskoefficienten under fordampningen af zeotropiske blandinger med det formål at udarbejde anbefalinger af de mest velegnede korrelationer. Det blev gjort ved at anvende korrelationerne i PHE modellen til at beregne den lokale varmetransmissionskoefficient, hvorefter varmestrømningshastigheden blev beregnet og sammenlignet med eksperimentelle data for karbondioxid/propan blandinger med forskellige blandingsforhold.

Derefter er retningslinjer blevet udledt for PHE fordamper- og kondensatordesigns. Det blev vist, at tryktab i kondensatoren kun påvirker økonomien for varmepumpen, mens et optimalt trade-off mellem varmetransmissionsareal og tryktab i PHE fordampere må sikres for at optimere systemets termodynamiske og økonomiske performance. Endvidere blev en metode til at udlede simplificerede retningslinjer for optimalt design af PHE fordampere formuleret og anvendt i et case study, hvor en varmepumpe integreres i et

sprøjtetørringsanlæg for waste heat recovery.

Til sidst er et studie af indflydelsen af en ulige strømningsfordeling i PHE fordampere på fordamperens performance blevet udført. Særligt blev indflydelsen af væske/dampuensartetheden ved indløbet til fordamperen samt effekten af endeplader på en PHE fordamperens performance estimeret ved anvendelse af to rene fluider og to zeotropiske blandinger som kølemidler. Indflydelsen af en ulige strømningsfordeling på varmepumpens termodynamiske performance blev efterfølgende evalueret med en integreret PHE-varmepumpe model. Fordamperens degradering blev derved omsat til en reduktion af varmepumpens termodynamiske performance, og påvirker dermed negativt på systemets driftsomkostninger.

Dissemination activities

Part of the work presented in this PhD thesis resulted in peer-reviewed publications and presentations at international conferences. Moreover, part of the modelling work was published open-access. Papers, presentations and numerical models are listed hereafter by category.

Peer Reviewed Journal Publications

[P1] **Roberta Mancini**, Benjamin Zühlsdorf, Jonas Kjær Jensen, Wiebke Brix Markussen, and Brian Elmegaard. Deriving guidelines for the design of plate evaporators in heat pumps using zeotropic mixtures. Energy, Vol. 156, p.492-508, 2018.
DOI: doi.org/10.1016/j.energy.2018.05.026

[P2] **Roberta Mancini**, Benjamin Zühlsdorf, Vikrant Aute, Wiebke Brix Markussen, and Brian Elmegaard. Performance of heat pumps using pure and mixed refrigerants with maldistribution effects in plate heat exchanger evaporators. International Journal of Refrigeration, Vol.104, p.390-403, 2019.
DOI: doi.org/10.1016/j.ijrefrig.2019.05.023

[P3] **Roberta Mancini**, Ines Ben El Mekki, Martin Ryhl Kærn, Wiebke Brix Markussen, Pascal Tobaly, and Brian Elmegaard. Assessment of evaporation heat transfer correlations for zeotropic mixtures of CO_2/propane in plate heat exchangers [To be Submitted].

Peer Reviewed Conference Publications

[C1] **Roberta Mancini**, Benjamin Zühlsdorf, and Brian Elmegaard. Derivation of guidelines for the design of plate evaporators in heat pumps using zeotropic mixtures. ECOS 2017: 30^{th} International Conference on Efficiency, Cost, Optimisation, Simulation and Environmental Impact of Energy Systems, July 2^{nd}-6^{th} 2017, San Diego, California, US.

[C2] **Roberta Mancini**, Jonas Kjær Jensen, Wiebke Brix Markussen, and Brian Elmegaard. Comparison of heat transfer and pressure drop correlations for evaporation of zeotropic mixtures in plate heat exchangers. 13^{th} IIR Gustav Lorentzen Conference on Natural Refrigerants, June 18^{th}-20^{th} 2018, Valencia, Spain.

[C3] **Roberta Mancini**, Vikrant Aute, Wiebke Brix Markussen, and Brian Elmegaard. Impact of liquid/vapour maldistribution on the performance of a plate heat exchanger evaporator for pure and mixed refrigerants. 17th International Refrigeration and Air Conditioning Conference at Purdue, July 9th-12th 2018, Lafayette, US.

[C4] **Roberta Mancini**, Benjamin Zühlsdorf, Wiebke Brix Markussen, and Brian Elmegaard. Design recommendations for plate heat exchangers in heat pumps using pure and mixed refrigerants. 25th IIR International Congress of Refrigeration, August 24th-30th 2019, Montréal, Canada.

Numerical models

[M1] **Roberta Mancini**, Benjamin Zühlsdorf, and Brian Elmegaard, Numerical models for assessing the performance of heat pumps with maldistribution effects in plate heat exchanger evaporators, 2019.
https://data.dtu.dk/articles/Numerical_models_for_assessing_the_performance_of_heat_pumps_with_maldistribution_effects_in_plate_heat_exchanger_evaporators/7565279. DOI:10.11583/DTU.7565279.v1.

Publications not included in the present thesis

[N1] Benjamin Zühlsdorf, Fabian Bühler, **Roberta Mancini**, Stefano Cignitti, and Brian Elmegaard. High temperature heat pump integration using zeotropic working fluids for spray drying facilities. 12th IEA Heat Pump conference, May 15th-18th 2017, Rotterdam, Netherlands

[N2] **Roberta Mancini**, Jonas Kjær Jensen, Lars Reinholdt, Wiebke Brix Markussen, and Brian Elmegaard. Design optimization of plate heat exchanger absorbers and desorbers for hybrid absorption compression heat pumps. ECOS 2019: 32nd International Conference on Efficiency, Cost, Optimisation, Simulation and Environmental Impact of Energy Systems, June 23rd-28th 2019, Wroclaw, Poland.

[N3] Ji Zhang, Enrico Baldasso, **Roberta Mancini**, Brian Elmegaard, and Fredrik Haglind. A general heat transfer correlation for a plate condenser and its impact on the design of organic Rankine cycle systems. 5th International Seminar on ORC Power Systems, September 9th-11th 2019, Athens, Greece

Other Publications

[O1] Benjamin Zühlsdorf, **Roberta Mancini**, Jesper Graa Andreasen, Andrea Meroni, Brian Elmegaard, and Fredrik Haglind. THERMCYC – Advanced Thermodynamic Cycles Utilizing Low Temperature Heat Sources. Abstract and Poster at SustainATV Conference, 2016. Kgs. Lyngby, Denmark.

Contents

Preface vii

Acknowledgements ix

Abstract (English/Dansk) xi

Dissemination activities xv

Contents xix

Nomenclature xxv

1 Introduction 1
- 1.1 Background . . . 1
- 1.2 Literature review . . . 2
  - 1.2.1 Plate heat exchangers: technology and applications . . . 3
  - 1.2.2 The use of zeotropic mixtures as working fluids in heat pumps . . . 5
  - 1.2.3 Heat exchanger design guidelines . . . 7
  - 1.2.4 Maldistribution in plate heat exchangers . . . 8
- 1.3 Thesis statement . . . 11
- 1.4 Methods . . . 12
- 1.5 Thesis structure . . . 12

2 Simulation tools 15
- 2.1 Background . . . 15
- 2.2 Plate heat exchanger model . . . 16
  - 2.2.1 PHE Geometry . . . 17
  - 2.2.2 Governing equations . . . 18
  - 2.2.3 Discretization approach . . . 19
  - 2.2.4 Numerical model . . . 20
  - 2.2.5 Iterative solution strategy . . . 23
  - 2.2.6 Computation of heat transfer coefficient and pressure drops . . . 25
  - 2.2.7 Fluid thermo-physical properties . . . 28
  - 2.2.8 Design solver . . . 29

2.3 Alternative PHE model for design . . . 30
2.4 Flow distribution solver . . . 32
2.5 Verification and validation . . . 34
2.5.1 Flow distribution solver verification . . . 35
2.5.2 Comparison with experimental data: evaporation data from DTU . . . 37
2.5.3 Comparison with experimental data: Sondex evaporators using ammonia . . . 39
2.5.4 Comparison with experimental data: pure CO_2 data from CNAM . . . 41
2.5.5 Comparison with experimental data: condensation data from DTU . . . 41
2.6 Coupled PHE - heat pump simulation framework . . . 43
2.6.1 Heat pump model . . . 44
2.6.2 Off-design without maldistribution effects . . . 46
2.6.3 Off-design with maldistribution effects . . . 48

3 Heat transfer correlations for evaporation of zeotropic mixtures 51
3.1 Introduction . . . 51
3.2 Literature survey . . . 52
3.2.1 Evaporation heat transfer in plate heat exchangers . . . 52
3.2.2 Zeotropic mixtures . . . 54
3.3 Comparison of prediction methods against experimental data . . . 61
3.3.1 Experimental apparatus and data reduction . . . 62
3.3.2 PHE model . . . 64
3.3.3 Results . . . 64
3.3.4 Main finding and recommendations . . . 69
3.3.5 Discussion . . . 70
3.4 Significance of the choice of the correlation to correct the nucleate boiling contribution . . . 71
3.4.1 Results . . . 71
3.4.2 Discussion . . . 73
3.5 Case study: impact of correlations on a performance problem . . . 74
3.5.1 Methods . . . 74
3.5.2 Results . . . 76
3.5.3 Discussion . . . 80
3.6 Summary . . . 81

4 Derivation of design guidelines 83
4.1 Introduction . . . 83
4.2 Design recommendations for evaporator and condenser design . . . 84
4.2.1 Methods . . . 84
4.2.2 Results . . . 86
4.2.3 Discussion . . . 92
4.3 A methodology to derive simplified guidelines to design plate heat exchanger evaporators in heat pumps using zeotropic mixtures . . . 93
4.3.1 Methods . . . 93

4.3.2 Results . . . 101
4.3.3 Discussion . . . 111
4.4 Summary . . . 115

5 Flow maldistribution **117**
5.1 Introduction . . . 117
5.2 Impact on evaporator performance . . . 118
5.2.1 Methods . . . 118
5.2.2 Results . . . 120
5.2.3 Significance of the prediction method to compute pressure drop . . 124
5.2.4 Significance of plate size and count . . . 125
5.3 Impact on cycle performance . . . 126
5.3.1 Methods . . . 127
5.3.2 Results . . . 129
5.4 Discussion . . . 139
5.5 Summary . . . 141

6 Conclusions **143**
6.1 Summary of findings . . . 143
6.1.1 Recommendations on heat transfer correlations for evaporation of zeotropic mixtures in PHEs . . . 144
6.1.2 Simplified design guidelines of evaporator and condenser design in heat pumps . . . 144
6.1.3 Impact of flow maldistribution on evaporator and cycle performance 145
6.2 Recommendations for future work . . . 146

Bibliography **148**

List of Figures **166**

List of Tables **169**

Papers **170**

Nomenclature

Abbreviations

1D	one dimensional
2D	two-dimensional
CO_2	carbon dioxide
CV	control volume
DH	district heating
DME	dimethyl ether
EU	European union
GHG	green house gas
GWP	global warming potential
HC	hydrocarbon
HEX	heat exchanger
HVAC	heating, ventilation, air conditioning
LHS	latin hypercube sampling
MC	Monte Carlo
ODP	ozone depletion potential
ORC	organic Rankine cycle
PHE	plate heat exchanger
SEWTLE	semi-explicit wall temperature linked equations

Roman letters

A_0	free flow area [m^2]

A_{ht}	heat transfer area [m^2]
b	corrugation height [m]
Bd	Bond number [-]
Bo	Boiling number [-]
CF	annual cash flow [€ y^{-1}]
COP	coefficient of performance [-]
CRF	capital recovery factor [y^{-1}]
C	yearly cost [€ y^{-1}]
c	specific cost/income [€ MWh^{-1}]
C_{me}	correction factor - convective boiling [-]
C_{un}	correction factor - nucleate boiling [-]
C_i	Chisholm parameter in Eq.(2.23) [-]
c_p	specific heat at constant pressure [J $\text{kg}^{-1}\text{K}^{-1}$]
D_h	hydrualic diameter [m]
D_p	port diameter [m]
e	error [-]
E,E_0	enhancement factors [-]
f	Fanning friction factor [-]
F_{cb}	two-phase convective boiling enhancement factor [-]
FC	fuel cost[€]
Fr	Froude number [-]
G	mass flux [kg s^{-1} m^{-2})]
g	gravitational acceleration [m/s^2]
h	heat transfer coefficient or specific enthalpy [W m^{-2} K^{-1})]
i	specific enthalpy [J kg^{-1}]
k_{wall}	wall conductivity [W m^{-1} K $^{-1}$]
L_{ht}	heat transfer length [m]

L_p	plate port-to-port length [m]
$\dot{m}$	mass flow rate [kg s^{-1}]
N	number of experimental points [-]
n	number of control volumes [-]
N_{ch}	number of channels [-]
n_{hp}	lifetime [y]
NPV	net present value [€]
OH	operating hours [h y^{-1}]
OMC	operation and maintenance cost[€]
P	heat transfer perimeter[m]
p	pressure [Pa] or [bar]
PEC	purchased equipment cost[€]
$\dot{Q}$	heat flow rate [W]
$\dot{Q}''$	heat flux [W m^{-2}]
$\dot{Q}^*$	non-dimensional heat flux [-]
res	residual [-]
Re	Reynolds number [-]
S_{LV}	slip ratio [-]
TCI	total capital investment [€]
T	temperature [°C]
t	plate thickness[m]
T^*	non-dimensional temperature [-]
tol	tolerance [-]
U	overall heat transfer coefficient [W $m^{-2}K^{-1}$]
$\dot{V}$	volumetric flow rate [m^3 h^{-1}]
$\dot{W}$	power [W]
W	plate width [m]

We	Weber number [-]
x	vapour quality or mass fraction [-]
X_{tt}	Martinelli parameter [-]
y	molar fraction [-]
Z	rate of sensible heat over latent heat [-]
z	spatial coordinate flow direction [m]

Greek letters

α	void fraction [-]
β	chevron angle [°]
Δ	difference [-]
δ	deviation [%]
η	efficiency [-]
Λ	corrugation pitch [m]
μ	viscosity [Pa s]
Φ	enlargement factor [-]
Φ_L	two-phase liquid frictional multiplier [-]
ρ	density [kg m^{-3}]
σ	surface tension [N $^{-1}$]
τ	time [hr]
θ	inclination angle [°]
ξ	multiplication constant in Eq.(2.24) [-]

Superscripts

$''$	per unit area
$*$	normalized
i	index discretization along flow direction
j	index discretization number of channel
k	index solver iteration

m	index wall number

Subscripts

1	more volatile component (CO_2)
acc	acceleration
bubble	bubble
cb	convective boiling
comp	compressor
cond	condenser
design	design
dew	dew
eff	effective
el	electricity
eva	evaporator
exp	experimental
fr	friction
gr	gravity
h	heat
hg	heat generation
hp	heat pump
hs	heat source
ht	heat transfer
id	ideal
in	inlet
is	isentropic
L	left
lo	liquid-only
min	minimum

nb	nucleate boiling
ng	natural gas
out	outlet
pinch	pinch
pool	pool boiling
R	right
ref	refrigerant
sf	secondary fluid
sh	super-heating
sink	sink
TP	two-phase
tot	total
V	vapour
vo	vapour-only
w	wall
wf	working fluid

1 Introduction

This chapter illustrates the state of the art on plate heat exchanger technology, and delineates the open research questions that motivated the work carried out during the PhD project. A literature review on plate heat exchangers is presented, followed by research objectives, methods and structure of the thesis.

1.1 Background

The Paris Agreement [1] signed by the United Nations in 2016 defined ambitious targets to mitigate the effects of global warming related to the greenhouse gas (GHG) emissions. A reduction of GHG emissions by 80 % to 95 % compared to the level in 1990 is targeted by 2050 by the European Union (EU), and national strategies were adopted by each country to achieve these goals. The International Energy Agency identified heating and cooling in buildings and industry to account for 40 % of the final energy consumption, with 65 % of the demand currently relying on fossil fuels [2]. Reducing the related GHG emissions is thus of paramount importance to achieve the goals set by the EU. Heat pumps, combined with district heating and cooling networks, and use of renewable energy sources, are envisaged as a promising technology for the targeted decarbonisation goals [3].

Denmark has a large potential for waste heat recovery, with the possibility to recover a total of 212 PJ per year, with 23 % coming from the industrial sector [4]. Moreover, 5% of the current Danish heating demand could be potentially covered by using industrial excess heat with economically feasible technologies [5]. In fact, excess heat can be used as the low-temperature level heat source of heat pumps, which can subsequently provide heat at the higher-temperature levels required by many industrial and domestic applications.

Due to the promising numbers in terms of waste heat recovery potential and availability of low-temperature heat sources in Denmark, the THERMCYC project - *Advanced thermodynamic cycles utilizing low-temperature heat sources* [6]- was initiated and coordi-

nated by the Technical University of Denmark. The project aimed at achieving further developments in the current state of the art of organic Rankine cycle (ORC) power systems and heat pumps. The improvements were estimated to yield a 15 % reduction in the Danish energy consumption for the industrial sectors, and a subsequent cut of 8.8 million tons of annual GHG emissions.

In the THERMCYC project framework, advances in cycles, components and working fluids were investigated. The present PhD thesis presents the research efforts aimed at further advancing the *heat transfer equipment* design. Heat exchangers (HEXs) are, in fact, core components in both heat pumps and ORCs, and their optimized design is thus a key-aspect to improve the energy efficiency and economic feasibility of these systems.

The focus of the work was the design and performance analysis of HEXs for heat pumps operating with waste heat recovery applications and district heating networks. In conventional vapour compression systems, heat exchangers are employed as both evaporator and condenser units, as well as internal HEXs. Among different HEX designs, plate heat exchangers (PHEs) attracted intense industrial attention, because of the possibility to enhance the heat transfer coefficient in a relatively compact design compared to other configurations. Compactness is of particular concern for future development in refrigerating and heat pumping equipment, since a smaller internal volume entails a reduction of the refrigerant charge. This consitutes an imperative feature to operate the equipment safely with flammable natural refrigerants (or mixtures of natural refrigerants), which will be replacing most conventional fluids due to their phase-out, according to the Kigali amendment to the Montreal protocol [7].

In light of the previous considerations, this PhD thesis aims at addressing current research gaps in the field of PHEs and their integration in heat pumps using pure fluids and zeotropic mixtures of natural refrigerants. The learnings gained during the project are thus envisioned to contribute with new relevant knowledge in the field of PHEs, together with fostering the development of the next generation heat pump systems.

1.2 Literature review

This section reviews the state of the art of PHE technology, followed by advantages and disadvantages of using zeotropic mixtures as working fluids for heat pump systems. Moreover, different considerations related to the estimation of PHE performance, also considering maldistribution effects, and the adoption of different design approaches, are presented. The objective of the literature review is to identify the research challenges addressed by the PhD thesis.

1.2.1 Plate heat exchangers: technology and applications

Plate heat exchangers are comprised of thin parallel rectangular plates, typically manufactured in stainless steel, stacked together to form parallel channels for fluid flow, as shown in Fig.1.1. The characteristic plate corrugation pattern provides a larger heat transfer area while modifying the flow pattern with the aim of enhancing the heat transfer performance. The plates are stacked together so that the mass flow rate of hot and cold fluids alternate in the passages. The figure shows a counter-current flow arrangement, with the cold and hot media flowing upward and downward, respectively.

The application of PHE started in 1923 for milk pasteurization in the dairy industry, as gasketed PHEs. In this configuration, the plates are sealed around the edges by gaskets and held by a frame. The gaskets are also employed to direct the flow to the inter-plate passages. Gasketed PHEs found a wide range of applications as liquid-to-liquid HEX, in different industrial sectors. Main advantages are given by the ease of mechanical cleaning, since individual components as plates, frame and gaskets can be easily de-assembled, and flexibility of design, since the heat transfer area can be modified by adding or removing plates. Typical operation of gasketed PHEs is however limited to 20 bar and 150 °C. Temperatures up to 250 °C can theoretically be achieved depending on the gasket material [9]. In order to extend the operation range of PHE, welded PHEs are available, and in particular brazed PHEs are very popular for evaporators and condensers of refrigeration and heat pumping units. Instead of using gaskets, the plates are brazed using copper or

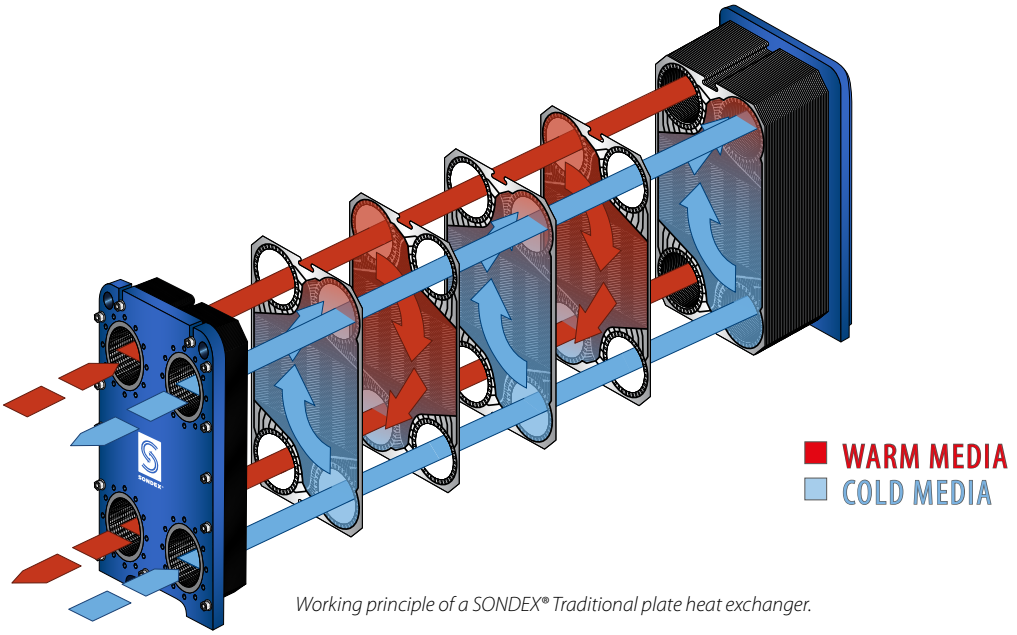

Figure 1.1: Working principle of a Sondex AS [8] gasketed PHE

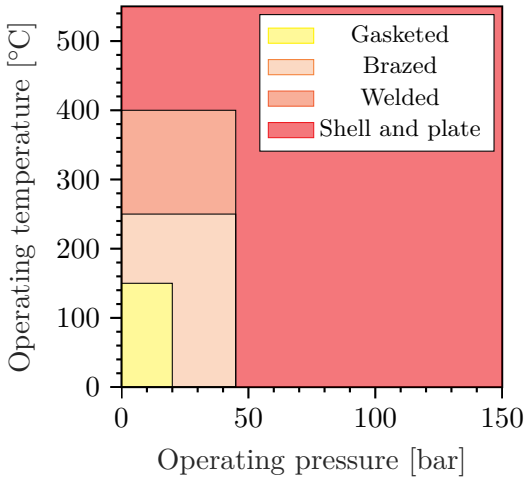

Figure 1.2: Operability limit of different PHE designs (adapted from [11, 12])

brazing material, resulting in a very compact, self-contained configuration. Fully welded PHEs are constituted by a completely welded pack of plates bolted to end plates and a frame. However, both brazed and welded PHEs do not have the flexibility and ease of cleaning of the gasketed PHE design, yet the welding process provides them with a structural integrity superior to gasketed PHEs [10].

The operability limits of the different types of PHEs are reported in Fig. 1.2. For higher operating pressure and temperature compared to welded PHEs (e.g. 50 bar and 400 °C), shell-and-plate configurations were introduced in the early 1990s, with the aim of merging shell-and-tube and PHE designs. Karellas et al. [11] proposed the application of shell and plate configuration in ORCs, since they can reach operating pressure up to 150 bar, while keeping the compactness of PHE design. In order to exploit the entire shell area, circular plates are typically manufactured.

Regardless of the type chosen, the most typical corrugation pattern that the plates are manufactured with, is termed *chevron* or *herringbone* corrugation. The corrugation geometry is a key-feature influencing thermal and hydraulic performances of PHEs. When the plates are stacked together, the corrugation of two successive plates is rotated of 180°so that the plates are in contact in multiple points. The corrugation serves to increase the plate heat transfer area, to enhance the heat transfer coefficient and to improve the mechanical integrity of the component [10].

In the following sections, three topics related to PHEs and their application in heat pump systems are introduced. First, the use of zeotropic mixtures in thermodynamic cycles is explained, and current issues in accurately determining the performance of these fluids in PHEs are highlighted. A reliable estimation of the performance of PHEs integrated

in thermodynamic cycles is, in fact, necessary to correctly design the components. Therefore, the review continues by presenting different approaches to design HEXs in thermodynamic cycles, and to obtaine optimized designs from both thermodynamic and economic perspectives. Last, the issue of flow maldistribution in PHEs, hindering the performance at both component and thermodynamic cycle level, is presented.

1.2.2 The use of zeotropic mixtures as working fluids in heat pumps

Zeotropic mixtures are blends of two or more components, with different mass fractions of the liquid and vapour phases at thermodynamic phase equilibrium. Therefore, the temperature at bubble and dew points differ at any saturation pressure and the mixture undergoes a temperature glide during phase change. The use of zeotropic mixtures as working fluids for heat pumps offers the possibility of optimizing the cycle thermodynamic efficiency by reducing the exergy destruction in the HEXs. Due to non-isothermal evaporation and condensation, the irreversibility in the HEXs can be reduced by matching the working fluid temperature glide with the heat source and heat sink temperature profiles.

Fig. 1.3 (a) shows a simple configuration of single-stage vapour compression heat pump, with four components, namely evaporator, compressor, condenser and throttling valve. In Fig. 1.3 (b) an example of temperature - heat (T-Q) diagram is shown for a mixture of propylene/butane at (0.5/0.5) mass composition, for both evaporator and condenser. The heat transfer irreversibility is related to the area included between the black temperature

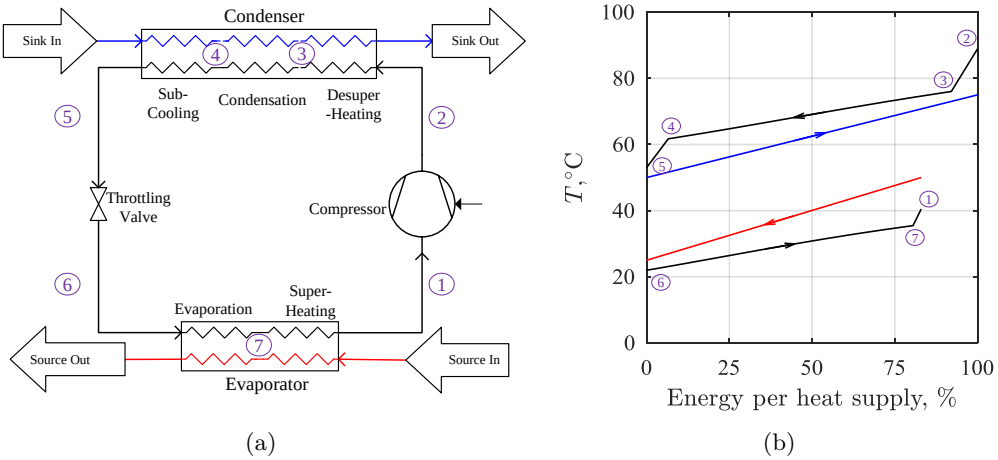

Figure 1.3: (a) Flow sheet of a single-stage vapour compression heat pump, and (b) Temperature - heat diagram for a case study with propylene/butane (0.5/0.5) as working fluid (adapted from [13])

profiles (refrigerant) and the heat source/sink temperature profiles (red/blue lines). Due to the mixture characteristic temperature glide, this irreversibility can be reduced compared to the constant temperature profile of pure fluids.

Zeotropic mixtures of natural refrigerants like hydrcocarbons (HCs) and carbon dioxide (CO_2) is one possibility of replacing the most conventional refrigerants, given their null Ozone Depletion Potential (ODP) and negligible Global Warming Potential (GWP) together with thermophysical properties favorable to heat transfer [14]. Moreover, utilizing mixtures of HCs and CO_2 mitigates typical problems encountered with system operating with pure CO_2 or HCs: high operating pressure and flammability [15]. In this regard, several experimental and numerical studies focused on the utilization of zeotropic mixtures of pure HCs or HCs and CO_2, demonstrating an increase in the cycle thermodynamic performance as well as reduced operating pressures [13, 15–23]. As an example, Bouteiller et al. [22] and Tobaly et al. [23] experimentally investigated the performance of a heat pump using CO_2/propane at different mass compositions in a transcritical vapour compression refrigerating cycle, obtaining a Coefficient of Performance (COP) increase between 10 % and 15 % without loosing cooling capacity. Garg et al. [24] further proposed to use mixtures of CO_2 with propane and isopentane in organic Rankine cycles for medium temperature applications. Zühlsdorf et al. [13, 20, 21] demonstrated the possibility of enhancing the heat pump COP by simulating the use of zeotropic mixtures as working fluids in conventional single-stage vapour compression systems. The effect of temperature glide matching in the evaporator was found to have a dominating effect compared to the condenser [20]. The performance improvement was quantified for different case studies. For a small-scale booster heat pump integrated in a district heating network, a 30 % improvement in the COP was found compared to the best performing pure refrigerant [21]. For a larger scale heat pump to recover waste heat from data centres a 30 % increase of system COP and best economic performance were obtained using a mixture of propylene/butane at (0.6/0.4) mass composition [13].

As a drawback entailed by zeotropic mixtures utilization, larger heat transfer areas are usually required for the HEXs, due to (i) a lower temperature difference between the refrigerant and the secondary fluids and (ii) a degradation of the heat transfer coefficient during both evaporation and condensation, which was observed in several experimental studies [25]. PHEs constitute thus a suitable evaporator and condenser configuration for these working fluids, due to the high compactness of their design and the possibility to set the flow in a counter-current configuration, which is imperative to attain the desired temperature glide matching between mixture and secondary fluid.

In light of the previous considerations, tools to correctly design and analyse the performance of PHEs are necessary to optimize the thermodynamic cycles where they are integrated. In particular, the use of suitable heat transfer and pressure drop correlations is of paramount importance to accurately simulate the HEX behaviour. Literature reports limited studies on condensation and evaporation in PHEs, and no study is currently available to predict the heat transfer and fluid flow characteristics of mixtures of natural

refrigerants in PHEs [26]. The only study concerning zeotropic mixtures in PHEs was conducted for ammonia/water [27], which is subject to very large glides and presents very different characteristics compared to other natural refrigerants. On the other hand, several studies focused on evaluating heat transfer and fluid flow characteristics of zeotropic mixtures in vertical and horizontal tubes. However, results for tubular geometry cannot be directly extended to smaller corrugated channels by simply substituting the tube diameter with the PHE hydraulic diameter, as demonstrated by Vakili-Farahani et al. [28].

1.2.3 Heat exchanger design guidelines

When designing HEXs for a given application, different criteria can be adopted to select the geometrical configuration. The pressure drop of one or both fluids may be limited to a maximum allowable value [9, 29], and the heat transfer area can be minimized for a full utilization of the available pressure loss, as applied by Gut and Pinto [30]. For single-phase HEXs, the pressure drop limitations could also be translated into maximum gas and liquid phase velocities at the inlet, and typical design values can be found in literature for a number of heat exchanger configurations [29]. These values are often based on empirical experience from manufacturers and the extension to other types of cases(e.g. zeotropic mixtures and/or phase change) is not straightforward.

Following other design approaches, the HEX can be optimized by carrying out a cost minimization problem without a maximum pressure drop limitation, thus evaluating the trade-off between heat transfer area and pressure drop. Several previous studies approached the problem by considering solely the cost related to the HEX, namely the investment cost and the pumping and compression costs related to the two working fluids, for a general HEX configuration [31, 32], for shell and tube HEXs [33] and for PHEs [34, 35]. However, the economic analyses lacked assessment of the interaction between the thermodynamic cycle and the HEXs, whose performance strongly affects the cycle operation and costs.

Furthermore, despite numerous studies [36–40] can be found on simultaneous optimization of PHE evaporators and/or condensers and thermodynamic cycle, pressure drop on the working fluid side is most often neglected. The pressure drops are in fact only considered as pumping cost on the heat source/sink side, and none of the studies assessed the impact of the working fluid pressure drop on the thermodynamic state at the component outlet. The results of the optimization are therefore solely valid if the HEX operates ideally at the design point with no pressure drop. Some works were for instance related to the assessment of the impact of some specific cycle parameters on the PHE design [36, 37], while other studies performed a combined cycle-PHE optimization procedure with the aim of maximizing the cycle efficiency [38], and by including also an economic analysis [39, 40].

Brignoli et al. [41], Cavallini et al. [42], Brown et al. [43, 44] on the other hand highlighted the importance of taking the refrigerant pressure drop into account for optimal HEX design, especially when comparing different working fluids. Cavallini et al. [42] introduced a Performance Evaluation Criteria for in-tube condensation, dividing it into two contributions: a Penalty Factor related to heat transfer irreversibility due to the finite temperature difference between the two fluids, and a Total Temperature Penalization Term related to the saturation temperature decrease following the refrigerant pressure drop. The method was applied to obtain an optimal tube length for a case study of an air-cooled condenser in an air conditioning system. The same method was extended by Brown et al. [43, 44] to flow boiling, and applied to compare different refrigerants for a given application. The main findings of their research were summarized by Brignoli et al. [41], with focus on fin-and-tube evaporator geometry, typical in Heating, Ventilation and Air-Conditioning (HVAC) systems in the US. The authors not only stressed the importance of taking pressure drop into account to optimize HEXs in refrigerating equipment, but additionally stressed how different refrigerants are differently sensitive to pressure drops, depending on their characteristic properties. Therefore, when comparing different refrigerants for the same application, the HEX geometry must be optimized as a trade-off between pressure drop and heat transfer area for each different fluid, since the same geometry may lead to suboptimal solutions in some cases. This is an opposite approach compared to fixing a maximum allowable pressure drop or inlet velocities, since the ranking of the working fluids in terms of both thermodynamic and economic performance may change depending on the heuristic criterion chosen.

The approach by Brignoli et al. [41] suggests to optimize the HEX design for each considered working fluid. However, a simultaneous component-system optimization may entail a demanding computational cost, especially during the preliminary system design phase. When screening several mixtures that are combinations of pure refrigerants evaluated at many different mass compositions, as suggested by Zühlsdorf et al. [13], this approach require too many evaluation of system performance, and the HEX design would be unnecessarily optimized for working fluids which will eventually not result as suitable candidates. A simplified approach and appropriate design guidelines would thus enable a faster screening of a wide range of fluids, while a full HEX optimization can be carried out at a later stage of the design process.

1.2.4 Maldistribution in plate heat exchangers

The occurrence of flow maldistribution can degrade the performance of multiple channels HEXs. Mueller and Chiou [45] published the first work defining maldistribution within the context of HEX design, namely as a non-uniform mass flow distribution of the working fluids entailing a degradation of heat transfer. They additionally conducted an extensive review on the main causes of maldistribution, identifying three main origins: entry problems due to improper nozzle design, self-induced maldistribution by fluid flow characteristics, e.g. viscous or two-phase flow, and fouling and corrosion effects. In PHEs,

maldistribution leads to three three main effects: (i) uneven channel-to-channel mass flow rate distribution, (ii) uneven in-channel (e.g. along the plate width) mass flow rate distribution , and (iii) effect of end plates, i.e. the different heat transfer area of the outer-most PHE channels causes a modification of the mass flow distribution.

Single-phase channel-to-channel maldistribution in PHEs has been described analytically [46–49], numerically [50] and experimentally [51–55]. Most of the works focused on the effects of channel-to-channel maldistribution. Bassiouny and Martin [46, 47] studied the uneven distribution of liquid-to-liquid PHEs for both U-type and Z-type flow arrangements by an analytical model. They propose to compensate the effect by tuning the area ratio between inlet and outlet fluid ports. A higher performance degradation was found to occur for smaller manifold port diameters, higher mass flow rates and a higher number of channels. Rao and Das [51] first studied experimentally the maldistribution effect on fluid pressure drop for a PHE for single-phase applications, and subsequently used their data in an analytical model [52], confirming a higher deterioration of heat transfer and pressure drop for smaller port size, and conversely higher number of channels and larger mass flow rate. Srihari et al. [48] and Srihari and Das [49] developed analytical models based on the work of Bassiouny and Martin, in order to study the transient response of PHEs in single pass and multi-pass configurations, showing how flow maldistribution affected the performance of the component in both steady state and transient operations. Further works by Bobbili et al. [53] and Tereda et al. [54] demonstrated the occurrence of flow maldistribution in U-type configuration PHEs experimentally, again showing a more severe maldistribution for higher mass flow rates, smaller port diameters and higher number of channels. Their experimental results displayed a good agreement with the analytical treatment first developed by Bassiouny and Martin. Li and Hrnjak [50] assessed the impact of in-channel flow maldistribution of upward nitrogen flow experimentally, using the results to validate a Computational Fluid Dynamics (CFD) model of the PHE header. Jin and Hrnjak [56] focused instead on effect of end-plates. They evaluated the overestimation of the PHE heat transfer coefficient when the end plates effect is not considered, and found that the effect is less than 2 % for PHE configurations with more than 20 plates.

Literature reports only a limited number of studies focusing on two-phase flow maldistribution in PHEs, while analogous works can be found for two-phase flow maldistristribution in fin-and-tube [57] or mini-channels evaporators [58–60]. Brix et al. [58, 59] showed that both air-side maldistribution and liquid vapour non-uniformities have an impact on the performance degradation of mini-channel evaporators using R134a and CO_2, with the latter being most sensitive to air-side maldistribution. Nielsen et al. [60] demonstrated how maldistribution effects imply a larger degradation of mini-channel HEX performance when the plate spacing between the channels is not uniform due to manufacturing tolerances. Fin-and-tube evaporators were instead investigated by Kærn et al. [57]: the authors compared face split and interlaced tube circuitries, and found that the interlaced circuitry outperforms face-split configurations only when flow maldistribution is accounted for.

In-channel two-phase maldistribution in PHEs was investigated by Jin and Hrnjak [61]. In their work, the flow of R245fa in a single plate channel with transparent walls was visualized, resulting in large non-uniformities of the mass flow rate and occurrence of dry-out zones. Nonethless, channel-to-channel maldistribution in evaporators is of particular relevance especially for vapour-compression cycles. In fact, being the refrigerant inlet in two-phase after the expansion valve, a non-uniform distribution of the mass flow rate entails a non-uniform distribution of the vapour quality. In this respect, Vist and Pettersen [62] investigated two-phase flow distribution in compact HEX manifold experimentally, dividing the mass flow into ten channels, in both upward and downward flow configurations. Some of their experimental results are reported in Fig. 1.4 for upward (a) and downward (b) flow. As shown by the figures, the vapor phase distributed more easily in the first channels for upward flow, while higher quality was detected in the last channels for downward flow arrangement. Moreover, a monotonic trend was observed in both cases. Fig. 1.4 (a) additionally shows the effect of mass flow rate, which resulted to be insignificant. On the other hand, Fig. 1.4 (b) shows the effect of inlet vapour quality, which resulted to improve the distribution at higher values. The same finding was confirmed in a recent study by Mahvi and Garimella [63], where a monotonic trend of the vapour quality was found as a result of a validated model of a micro-channel HEX header with two-phase flow. Moreover, for lower values of inlet vapour quality, the degree of maldistribution was found to be higher, as in [62]. Jensen et al. [64] assessed the impact of this type of liquid/vapour non-uniform distribution at the inlet of PHE evaporators by a numerical model, imposing different rates of linear quality variation at the PHE channels inlet. The study was conducted for a PHE comprised of 20 channels using R134a as working fluid, resulting in a 25 % reduction of the overall heat transfer coefficient when a 0.4 difference in inlet vapour quality was imposed to the model.

As an additional aspect to consider, the use of multi-component working fluids entails a further degree of complexity to the problem. Due to the different compositions of

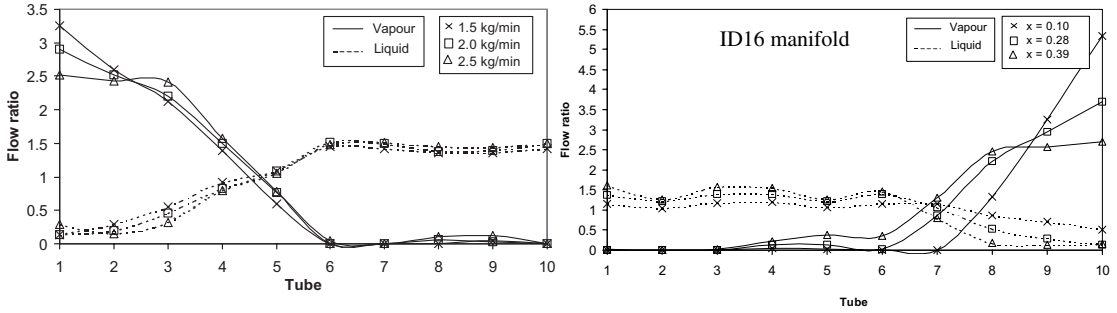

(a) (b)

Figure 1.4: Mass flow rate distribution for upward (a) and downward (b) flow [62]

liquid and vapour phases, a non-uniform distribution of the vapour quality between the PHE channels implies that mass flow rates of mixtures at different compositions are flowing in the inter-plate passages. The differences among refrigerants and the main design aspects influencing the sensitivity to maldistribution effects are still open research questions. Moreover, a performance degradation of the evaporator due to maldistribution effects additionally causes a degradation of the thermodynamic cycle thermodynamic performance, and this is an additional aspect to take into consideration. Previous works addressed the analysis of flow maldistribution effects in air conditioning systems [65] and heat pumps [66, 67] for fin-and-tube evaporators. Kærn et al. [65], for instance, quantified a COP reduction of 13 % and 43 % due to liquid/vapour maldistribution and air-side non uniform flow, respectively. A similar study, quantifying PHE maldistribution effects on the heat pump COP, would thus be relevant to quantify the potential degradation of the cycle performance due to the effect of end-plate and liquid/vapour maldistribution.

1.3 Thesis statement

Plate heat exchangers constitute a promising solution as evaporator and condenser units of heat pump systems using pure fluids and zeotropic mixtures of natural refrigerants as working fluids. However, the current state of the art lacks a comprehensive understanding of some aspects, which are summarized as the following research questions.

i **Methods to evaluate the performance of zeotropic mixtures in PHE evaporators**

1) What are the methods available to predict the heat transfer and fluid flow characteristics of zeotropic mixtures in PHE evaporators and what is the impact of using different methods on the estimation of the PHE evaporator performance?

ii **Derivation of simplified design guidelines**

1) What is the relative importance of evaporator and condenser design on the thermodynamic performance of heat pumps when using pure fluids and zeotropic mixtures as working fluids?
2) How is it possible to define an optimal trade-off between heat transfer area and pressure drop, accounting for the pressure drop impact on the cycle, without carrying out a full optimization of the component?
3) How is it possible to translate the optimal trade-off into a simplified guideline to ensure optimal design of PHEs for different working fluids in the preliminary design phase of heat pumps?

iii **Effect of flow maldistribution on evaporator and cycle performance**

1) What is the degradation of PHE evaporator performance if maldistribution effects are taken into account and what aspects affect the results to the largest extent?
2) How does the sensitivity to maldistribution differ for pure fluids and mixed refrigerants, and which fluid properties are most relevant?
3) What is the impact of maldistribution effects on the thermodynamic performance of heat pumps, and how does maldistribution affect the economic feasibility of the system?

The objectives of the PhD project are therefore defined as:

- to implement an open-access modelling framework to design and evaluate the performance of PHE evaporators and condensers to be integrated in heat pump cycles using pure and mixed refrigerants.
- to validate the modelling framework against experimental data of pure fluids and zeotropic mixtures at different working conditions.
- to develop a coupled PHE-heat pump modelling framework for design and off-design analysis of component and cycle.
- to use the modelling framework to answer the target research questions and expand the knowledge in the current state of the art of PHE technology.

1.4 Methods

In order to answer the research questions, simulation tools are developed to predict the performance of PHEs, as well as to size the component in relevant case studies. The models are subsequently validated against experimental data. The component models are then integrated to a heat pump cycle simulation framework. All the models are developed with the aim of being physically consistent and making use of general formulations that can be easily adaptable to different case studies and working fluids.

The reader is referred to Chapter 2 for a detailed and comprehensive description of the modelling work carried out within the PhD project.

1.5 Thesis structure

The PhD thesis is structured as follows:

- **Chapter 2** presents the simulations tools developed for design and rating of PHEs,

as well as the integration with cycle calculations. The validation and verification of the model is also presented.

- **Chapter 3** presents the research work aimed at comparing different prediction methods to evaluate the local heat transfer coefficient of zeotorpic mixtures in PHE evaporators, and at deriving recommendations on the most suitable methods based on a comparison with experimental data.
- **Chapter 4** illustrates a derivation of design guidelines for evaporator and condenser design in heat pumps using pure fluids and zeotropic mixtures.
- **Chapter 5** quantifies the impact of flow maldistribution on the performance of PHE evaporators and on the thermodynamic cycles in which they are integrated, focusing on thermodynamic performance and illustrating the potential impact on the economic feasibility of heat pumps for a case study.
- To conclude, **Chapter 6** highlights the main outcomes of this PhD thesis and summarizes recommendations for future work.

2 Simulation tools

This chapter presents a detailed description of the simulation tools that were developed during the PhD project. The tools include PHE models spatially discretized in both one-dimension (1D) and two-dimensions (2D). The models were integrated with design and performance solvers, and could simulate evaporating, condensing, and liquid flow of pure fluids and mixtures. Moreover, the PHE models were integrated into cycle models for both design and off-design calculations. The open-access database FigShare provides access to part of the modelling routines , while the chapter is partially based on the model documentation published in [M1].

2.1 Background

Physical models at different level of details are needed to solve *design*, *rating* and *performance* problems for HEXs. Shah [9] defines the design or sizing problem as the selection of a HEX configuration, flow arrangement, material and calculation of the geometry, to meet a specified thermal load, and constraining the maximum pressure drop. Rating problems are instead defined as estimating the heat transfer and pressure drop performance of HEX with a prescribed geometry. In the rating problem, the operating conditions of the HEX are specified. A performance problem, instead, is based on the solution of a rating problem, but the operating conditions are unknown. An example is given by solving evaporators coupled with heat pumps in off-design conditions: the geometry is specified as an input but the operating conditions are estimated as outputs based on specified control values as degree of superheat and suction volume flow rate.

The solution of design, rating and performance problems is typically based on simplified models of the HEX, which can be based on different approaches. A zero-dimensional model of the HEX, where a lumped mean heat transfer coefficient and average fluid properties are used, is a simple method to solve the HEX. The logarithmic mean temperature difference (LMTD) method and the ϵ-NTU method can also be applied to design and

estimate the performance of the component [9]. However, evaporators and condensers require a more accurate modelling due to the large variation of the heat transfer coefficient and fluid properties during phase-change.

The literature reports several models that were proposed to solve design and rating problems of HEXs for both single-phase and two-phase flow. Some of the most relevant work related to PHEs are reported hereafter. Corberán et al. [68, 69] proposed an explicit model to solve the rating problem of HEXs in any configuration, by a volume discretization along the flow direction. The model was termed SEWTLE as Semi-Explicit Wall Temperature Linked Equations, since the wall temperature was used as the iteration variable for the solution of the overall energy conservation equation. Moreover, the iterations were based on an explicit formulation of the wall temperature as a function of the temperature of primary and secondary fluids. Qiao et al. [70] proposed a validated simulation framework for the rating problem based on discretizing the PHE in slices of equal heat transfer area along the flow direction and in the different channels. The solver was able to handle multi-pass flow arrangement and two-phase flow. The model was further improved by Eldeeb et al. [71], proposing an alternate approach for a faster convergence. The approach consisted in updating the solution for the fluid flowing upward and downward alternatively. At a given iteration the local conservation equations were solved only for one of the fluid, while the properties of the other fluid were kept equal to the previous iteration values. Gullapalli [72, 73] developed a rating model for brazed PHEs, and his work was the basis for the commercial software by SWEP SSP G8 [74], which can size HEXs for different application. The approach was based on a 1D discretization along the fluid flow direction. Constant enthalpy steps were considered, and enthalpy and pressure chosen as independent variables to define the thermodynamic state of the working fluids at each volume. Last, Amalfi and Thome [75] proposed a rating model based on a one-dimensional discretization of the PHE at constant heat transfer area steps, with particular focus on modelling two-phase flow. Contrary to most common solvers, the model iterated on the heat flow rate in each CV. All of the aforementioned solvers needed to be complemented with calculation procedures for fluid properties, as well as prediction methods to estimate the local heat transfer coefficient and pressure drop.

2.2 Plate heat exchanger model

In this section, the formulation of the PHE model that was implemented as part of this thesis work, is presented. Depending on the type of analysis carried out, the different problems of design, rating and performance were addressed and different solvers were coupled with the model. However, the mathematical formulation of the PHE model was analogous in all the cases, i.e. aiming at solving mass, momentum and energy conservation equations in the PHE. In the following subsection, a detailed description of the PHE geometry, the governing equations describing the fluid flow and heat transfer mechanism,

as well as the adopted discretization method and the numerical implementation, is presented. MATLAB 2017b [76] was used as programming framework.

2.2.1 PHE Geometry

The geometry of a chevron-PHE is determined by plate size and count, and corrugation specific parameters. An illustrative example is depicted in Fig. 2.1, while Table 2.1 reports the list of the parameters. The plate size is defined by width W and length. The port-to-port length L_p characterizes the fluid flow lenght, affecting the pressure drop. The heat transfer length L_{ht} is the effective plate length determining the heat transfer area. The number of plates defines the number of channels for fluid flow N_{ch}, and thus the total heat transfer area. The plate thickness t determines the trade-off between mechanical integrity of the component and wall thermal conductive resistance. The plates are most commonly manufactured in stainless steel, with a thermal conductivity k_w equal to 16.2 W/(mK). Last, the port diameter D_p determines the inlet and outlet pressure drop.

The corrugation geometry is characterized by corrugation pitch Λ, plate spacing (or corrugation height) b, and chevron angle β. Literature reports different definitions of β as the angle with the vertical or horizontal axis. In this work, the chevron angle β is estimated with respect to the horizontal axis (see Fig.2.1), while the complement $\theta = 90° - \beta$ indicates the inclination angle, e.g. the angle with the vertical axis. A high β (equal to a low θ) corresponds to designs resulting in high heat transfer coefficients and high pressure drop, while a low β entails low pressure drop and lower heat transfer coefficient. The corrugation geometry is thus a key-set of parameters determining both heat transfer and pressure drop in the inter-plate passages.

The calculation of the channel hydraulic diameter, free-flow area, and effective heat transfer area was carried out by using the correlations proposed by Martin [77]. The hydraulic diameter D_h was estimated by Eq.(2.1).

$$D_h = \frac{2b}{\Phi} \tag{2.1}$$

Here, Φ indicates the enlargement factor, i.e. the ratio between effective and flat plate area. Φ is determined as a function of corrugation pitch and plate spacing, estimated by Eq.(2.2).

$$\Phi = \frac{1}{6}\left(1 + \sqrt{1 + \left(\frac{\pi b}{\Lambda}\right)^2} + \sqrt{1 + \frac{1}{2}\left(\frac{\pi b}{\Lambda}\right)^2}\right) \tag{2.2}$$

The free-flow area of each fluid was computed as:

$$A_0 = b \cdot N_{\text{ch}} \cdot W \tag{2.3}$$

where N_{ch} indicates the number of channels in which the considered fluid is flowing. The total heat transfer area is finally determined by Eq.(2.4). The number of channels in PHE is typicall an odd number, with the secondary fluid flowing in the outer channels. Due to the assumption of adiabatic end-plates, the number of channels in Eq.(2.4) must be referred to the value of the working fluid with the lowest number of channels.

$$A_{\text{ht}} = 2 \cdot \Phi \cdot (W \cdot L_{\text{ht}}) \cdot N_{\text{ch}} \tag{2.4}$$

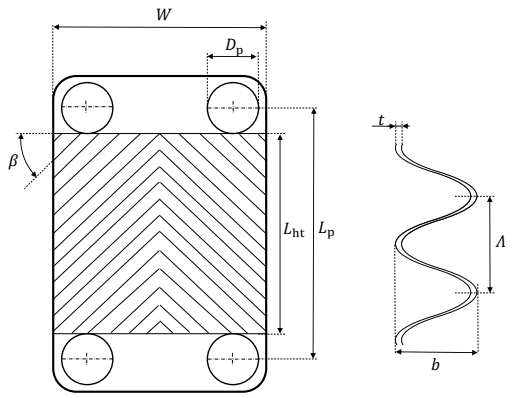

Figure 2.1: Chevron PHE geometry

Parameter	Description
W	Plate width
L_p	Port-to-port length
L_{ht}	Heat transfer length
N_{ch}	Number of channels
b	Corrugation height
Λ	Corrugation pitch
β	Chevron angle
θ	Inclination angle
t	Plate thickness
k_{w}	Thermal conductivity

Table 2.1: Geometrical parameters

2.2.2 Governing equations

The governing equations are given by mass, momentum and energy conservation equations. The following assumptions were considered:

(i) steady state conditions;

(ii) adiabatic end plates, i.e. no heat loss to the environment;

(iii) no longitudinal conduction through the plates;

(iv) liquid and vapour phases flowing at different velocities according to an estimated slip ratio;

(v) no pressure drop in the PHE manifolds;

(vi) Newtonian working fluids.

Given the PHE geometry, with constant free-flow area A_0 for each fluid path, the steady-state mass conservation equation results in:

$$G = const. \tag{2.5}$$

where G is the mass flux of the fluid flowing in the channel. The momentum equation was given by Eq.(2.6), where the three terms represent the frictional (fr), gravity (gr) and acceleration (acc) contributions to the total pressure drop, and f indicates the Fanning friction factor.

$$\frac{dp}{dz} = -2f\frac{G^2}{\rho D_h} - \frac{d(\rho g z)}{dz} - G^2\frac{1}{dz}\left(\frac{1}{\rho}\right) = \left(\frac{dp}{dz}\right)_{\text{fr}} + \left(\frac{dp}{dz}\right)_{\text{gr}} + \left(\frac{dp}{dz}\right)_{\text{acc}} \tag{2.6}$$

The energy conservation equation in steady state for both primary and secondary fluids was expressed by Eq.(2.7) for single-phase flow and by Eq.(2.8) for two-phase flow. In Eq.(2.8), the kinetic contribution to energy balance was neglected.

$$\dot{m}c_p\frac{dT}{dz} = \sum_{m=1}^{n_w} P^m U^m (T_{\text{w}}^m - T) \tag{2.7}$$

$$\dot{m}\frac{di}{dz} = \sum_{m=1}^{n_w} P^m U^m (T_{\text{w}}^m - T) \tag{2.8}$$

Here, i indicates the enthalpy, P^m represents the heat transfer perimeter, z is the direction of the fluid flow, and n_w is the total number of walls that are in contact with the fluid. The overall heat transfer coefficient U^m is determined by the convective heat transfer coefficient of the fluid and by the conductive resistance of half thickness of wall, and calculated by:

$$U^m = \left(\frac{1}{h^m} + \frac{t/2}{k_w}\right)^{-1} \tag{2.9}$$

2.2.3 Discretization approach

Two different approaches were implemented, applying a one-dimensional (1D) and a two-dimensional (2D) discretization, respectively. The 2D discretization was applied to the evaporator performance model, since it can account for the flow distribution in the different channels. The 1D discretization was applied to both evaporator and condenser design and performance models. The difference between the results of the 1D performance model of the evaporator and the 2D model with uniform vapour quality distribution at the inlet allows estimating the effect of end plates, since the flow is assumed to distribute perfectly even among the different channels in the 1D case. The different discretization approaches are shown for the example of the evaporator in Fig.2.2, where hs indicates the heat source (or secondary fluid) and ref the refrigerant cells.

The 2D discretization, represented in Fig.2.2 (b), divides the PHE into n slices along the flow direction. The grid is further discretized by dividing each slice by the total number

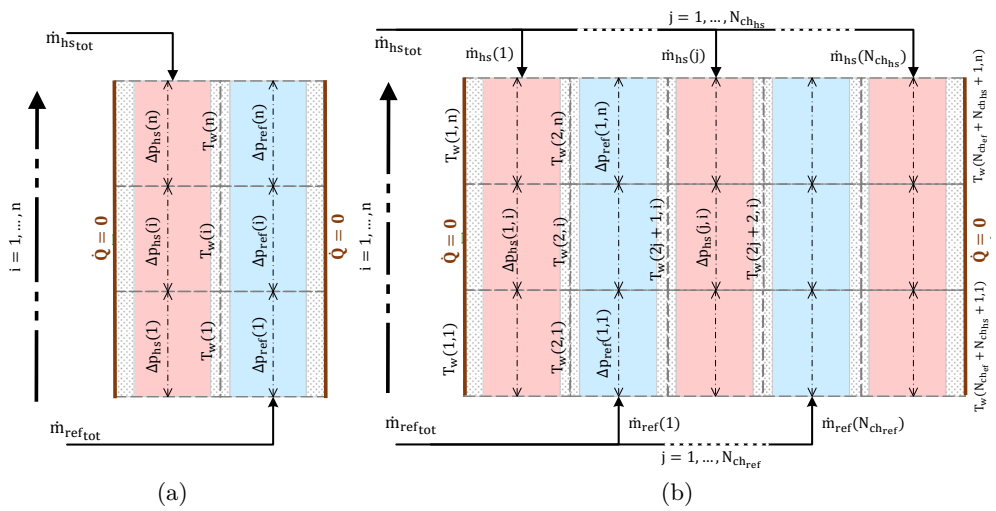

Figure 2.2: PHE model discretization approaches:(a) 1D ; (b) 2D

of channels. One CV is therefore constituted by a refrigerant or a secondary fluid cell and half thickness of the plate. Two adjacent refrigerant and secondary fluid CVs share thus a face at the midpoint of the wall. This kind of discretization allows considering different mass flow rates (shown by $\dot{m}_{\mathrm{ref/hs}}(j)$) at each channel j of the PHE. Fig.2.2 (a) represents the 1D discretization, solely applied along the flow direction. In each slice two different CV are considered to describe the refrigerant and the secondary fluid flows. One face of two adjacent CVs is shared also in this case, by placing each CV boundary at the midpoint of the plate wall.

Note that, in both cases, a centered approach was chosen for wall discretization. Two adjacent fluid cells shared a boundary at the midpoint of the plate thickness, and the wall temperature was estimated at the center point between inlet and outlet of both fluid paths [69].

2.2.4 Numerical model

The momentum (Eq.(2.6)) and energy (Eq.(2.7) and Eq.(2.8)) conservation equations were integrated in each cell by a finite volume method, since local conservation ensures global conservation over the entire fluid domain. As shown in Fig.2.2 the total mass flow rate of one fluid was considered to flow simultaneously in one equivalent channel with area equivalent to the sum of all channels in the 1D case, while each channel is considered separately in the 2D case.

Fig. 2.3 shows the details of the discretization schemes in both 1D and 2D. The black

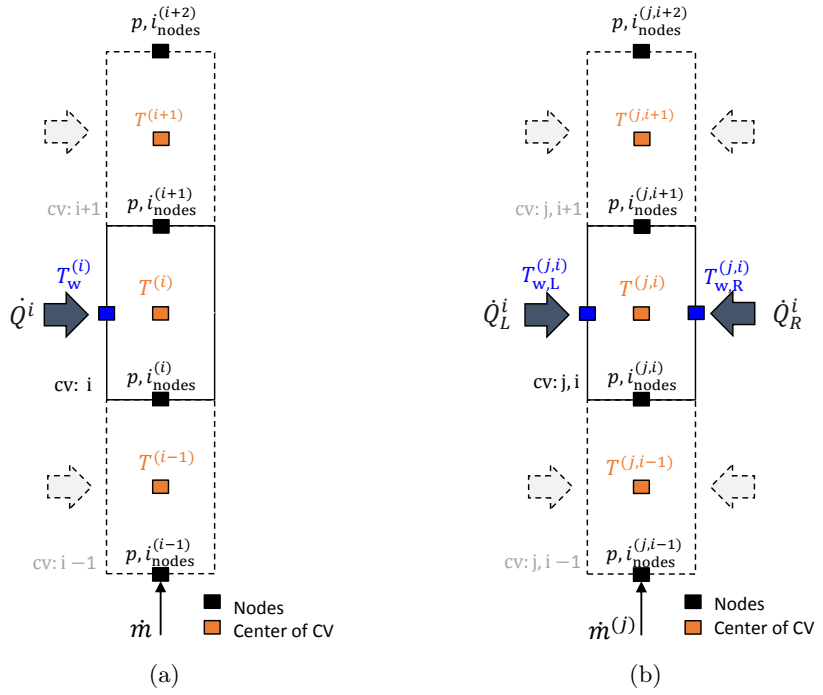

Figure 2.3: Detailed discretization schemes: (a) 1D, (b) 2D

squares (for pressure p and enthalpy i) indicate the values evaluated at the nodes, i.e. at the inlet/outlet of each cell. The orange square indicates the value at the center point, which was evaluated by a central differencing scheme assuming a linear variation between inlet and outlet. The wall temperature (blue square) in each CV was evaluated at the midpoint between inlet and outlet of one fluid cell.

For a specific CV (j,i) the integration of the momentum equation led to the formulation in Eq.(2.10). In this notation, the row index j identifies the channel, while the column index identifies the CV along the flow direction. The 1D formulation is analogous (with no index j).

$$p_{\text{nodes}}^{(j,i+1)} = p_{\text{nodes}}^{(j,i)} - \Delta p_{\text{fr}}^{(j,i)} - \Delta p_{\text{gr}}^{(j,i)} - \Delta p_{\text{acc}}^{(j,i)} \tag{2.10}$$

Note that the pressure drop $\Delta p^{(j,i)}$ is evaluated by using the fluid properties at the center of the CV, and then applied to estimate the value of the pressure at the outlet of the CV $p_{\text{nodes}}^{(j,i+1)}$. A more detailed explanation of the computation of frictional, gravity and acceleration contributions to pressure drop is presented in section 2.2.6.

The energy conservation equation for single-phase flow was solved by assuming a linear variation of the fluid temperature in the CV. In the 2D discretization scheme, each

channel has a right (R) and left (L) wall exchanging thermal energy with the fluid cell, thus the integral formulation of Eq.(2.7) for the CV (j,i) leads to:

$$\int_{j,i}^{j,i+1} dT = \int_{z^{j,i}}^{z^{j,i+1}} \left[\frac{P^{(j,i)}U^{(j,i)}}{\dot{m}^{(j)}c_p}(T_{w,R}^{(j,i)} - T) + \frac{P^{(j,i)}U^{(j,i)}}{\dot{m}^{(j)}c_p}(T_{w,L}^{(j,i)} - T) \right] dz \tag{2.11}$$

From the integration of Eq.(2.11), it holds:

$$T_{\text{nodes}}^{(j,i+1)} = \frac{\chi(T_{w,L}^{(j,i)} + T_{w,R}^{(j,i)}) + (1-\chi)T_{\text{nodes}}^{(j,i)}}{1+\chi} \tag{2.12}$$

with χ equal to:

$$\chi = \frac{\Delta A_{\text{ht}}^{(j,i)} U^{(j,i)}}{\dot{m}^{(j)} c_p} \tag{2.13}$$

The advantage of using the formulation of Eq.(2.12), is that the temperature at the outlet of the cell can be computed by solely using the inlet value and the wall temperature of the cell. In two-phase flows, the energy conservation must be expressed in terms of enthalpy i, and the integration of Eq.(2.8) leads to the formulation:

$$i_{\text{nodes}}^{(j,i+1)} = i_{\text{nodes}}^{(j,i)} + \frac{\Delta A_{\text{ht}}^{(j,i)} U^{(j,i)}}{\dot{m}^{(j)}}(T_{\text{w,R}}^{(j,i)} - T^{(j,i)}) + \frac{\Delta A_{\text{ht}}^{(j,i)} U^{(j,i)}}{\dot{m}^{(j)}}(T_{\text{w,L}}^{(j,i)} - T^{(j,i)}) \tag{2.14}$$

Here, since the temperature of the fluid at the center of the fluid cell $T^{(j,i)}$ is not known, the calculation was carried out as suggested by Corberán [68], e.g. to assume the temperature equal to the value at the inlet node plus a variation equal to the previous iteration variation. Moreover, in order to compute the different contributions to pressure drop in Eq.(2.10) and the heat transfer coefficients U in Eq.(2.12) and (2.14), fluid thermo-physical properties are evaluated at the center of the cell. Assuming a linear variation of the fluid thermo-physical properties, the same approach used for the temperature was adopted, and translated into:

$$\Psi_k^{(j,i)} = \Psi_{\text{nodes,k}}^{(j,i)} + \frac{\Psi_{\text{nodes,k}-1}^{(j,i+1)} - \Psi_{\text{nodes,k}-1}^{(j,i)}}{2} \tag{2.15}$$

where Ψ represents a general property or temperature, k indicates the iteration number and (j,i) the CV taken into account.

In the 1D case, the energy conservation equations were slightly modified for both single-phase and two-phase flow, since each fluid CV is in contact with one wall only ($n_w = 1$ in Eq.(2.7) and (2.8)). For single-phase flow, the formulation was [69]:

$$T_{\text{nodes}}^{(i+1)} = \frac{\chi T_w^{(i)} + (1-\chi/2)T_{\text{nodes}}^{(i)}}{1+\chi/2} \tag{2.16}$$

with χ expressed by Eq.(2.13). For two-phase flow, instead, it was obtained:

$$i_{\text{nodes}}^{(i+1)} = i_{\text{nodes}}^{(i)} + \frac{\Delta A_{\text{ht}}^{(i)} U^{(i)}}{\dot{m}} (T_{\text{w}}^{(i)} - T^{(i)}) \tag{2.17}$$

2.2.5 Iterative solution strategy

The solution of the energy and momentum equations for the CVs of the domain requires the values of the mass flow rates and inlet thermodynamics of both fluids, which are imposed as boundary conditions at the inlet of the first nodes. In the 2D discretization scheme, the inlet mass flow rate in each channel is required for solving energy and momentum equations in all the cells of the considered channel. However the solution of the energy and momentum conservation equations requires the values of the wall temperature. Therefore, the overall solution strategy was implemented as an iterative procedure, and the solver was based on the SEWTLE (Semi-Explicit Wall Temperature Linked Equations) approach, presented in [68, 69]. Moreover, the alternate iteration approach suggested in [71] was implemented to accelerate the model convergence.

The flow-chart of the successive substitution solver, iterating on wall temperature and refrigerant and secondary fluid pressure drops, is shown in Fig.2.4. The inputs to the solver were given by the working fluid and the fully defined PHE geometry, together with the inlet thermodynamic state and mass flow rate of both fluids. The inlet state was used as boundary condition for the solution. An initial guess of the distribution of wall temperature and pressure drop was also provided to the solver. The guessed distribution for the wall temperature was given by a linear temperature variation between inlet refrigerant and secondary fluid temperatures, in order to avoid temperature crossing. Pressure drops were preliminarily calculated considering the fluid properties at the inlet conditions and distributed uniformly in each CV.

At each iteration k the temperature and the fluid thermo-physical properties were evaluated at the center of each cell. In the first iteration, the properties were estimated by considering the inlet conditions of the fluid entering the CV, which were known from the outlet of the previous cell. From the second iteration the values were estimated as suggested by Corberán et al. [69], and previously illustrated by Eq.(2.15). The refrigerant and secondary fluid heat transfer coefficients were evaluated by using the properties at the center of the CV, by means of appropriate experimental correlations. The thermodynamic state of both fluids at the outlet of the CV were subsequently estimated by integrating the momentum and energy balance equations locally. After solving energy and momentum conservation equations in all the refrigerant and secondary fluid cells, an energy balance over two adjacent refrigerant and secondary fluid cells was applied to compute an updated value of the wall temperature.

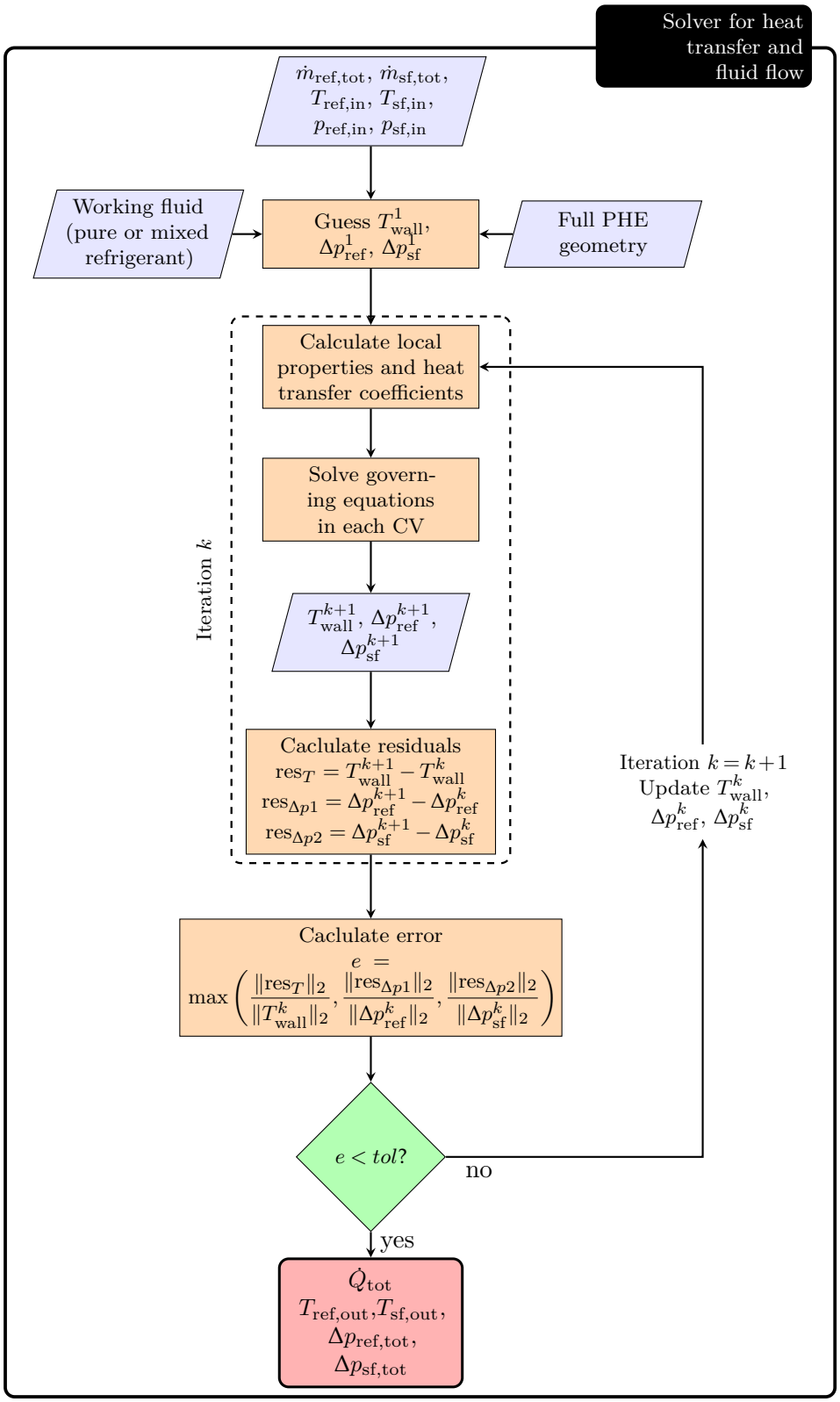

Figure 2.4: Work flow of the solver for heat transfer and fluid flow

The balance led to the formulation of Eq.(2.18), where the heat transfer area was simplified being equal for both fluids.

$$T_{\text{wall}} = \frac{U_{\text{ref}} T_{\text{ref}} + U_{\text{sf}} T_{\text{sf}}}{U_{\text{ref}} + U_{\text{sf}}} \tag{2.18}$$

Here the subscript ref indicates the refrigerant and sf the secondary fluid, namely the heat source and heat sink sink for the evaporator and condenser, respectively. Using the wall temperature as iteration variable has the advantage of avoiding the convergence to unfeasible solutions, for example temperature crossing between fluids, compared to using the heat flux [71]. This method is also completely explicit with respect to the wall temperature, which is updated by Eq.(2.18) [68] as a function of the fluids temperature profiles and heat transfer coefficients.

The residuals between two subsequent iterations were estimated and the error was calculated as the L^2-norm of the higher relative residuals between wall temperature, refrigerant and secondary fluid pressure drops. If the error was lower than the selected tolerance, the solution was given in terms of total heat flow rate, outlet thermodynamic states of the two fluids, as well as wall and fluid temperature and pressure distribution. If the error was higher than the tolerance, the solver updated the iteration variables and made an additional iteration. The solver in 2D needs as input the mass flow rate distribution of both fluids in the different channels. Therefore, the pressure drop across each channel was estimated as output of the model and it was not trivial that all the channels resulted in the same outlet pressure. The governing equations for the flow distribution were solved separately in the flow distribution solver, which will be presented in section 2.4.

2.2.6 Computation of heat transfer coefficient and pressure drops

Experimental correlations and theoretical models were implemented in order to calculate the heat transfer coefficients, the frictional pressure drops and the void fraction of the refrigerant and secondary fluid. Depending on the working fluid and specific case study, different models were chosen, and they are introduced and justified case by case in the case studies analysed in this thesis.

Since the PHE models were discretized in 1D or 2D, heat transfer coefficient local values were estimated as a function of refrigerant thermo-physical properties, vapour quality (or simply phase) and local heat flux. An extensive review of all the theoretical methods and correction factors implemented and used for pure fluids and zeotropic mixtures is presented in Chapter 3.

The pressure drops of both refrigerant and secondary fluid were estimated locally, similarly to the heat transfer correlations. As shown by the momentum conservation equation (2.6), the pressure drop was evaluated by summing the different contributions of static

(gravity), acceleration and frictional pressure drops.

The single-phase frictional pressure drops can be estimated by different correlations for the Fanning friction factor. The two-phase frictional pressure drops can be estimated by means of three different approaches, as described in [28] :

- i estimating a two-phase Fanning friction factor;
- i applying the Lockhart-Martinelli [78] method;
- i establishing a relation between pressure drops and kinetic energy per unit volume.

The two-phase Fanning friction factor can be estimated for both evaporation and condensation by different correlations, and pressure drop are subsequently calculated by:

$$\frac{dp_{\mathrm{fr,tp}}}{dz} = 2f_{\mathrm{tp}}\frac{G^2}{\rho_m D_h} \tag{2.19}$$

where G represents the mass flux, z indicates the direction of the flow, D_h is the hydraulic diameter and ρ_m is the momentum density, estimated - according to the assumption of separated flow model - by [79]:

$$\rho_m = \left(\frac{x^2}{\rho_V \alpha} + \frac{(1-x)^2}{\rho_L(1-\alpha)} \right)^{-1} \tag{2.20}$$

where x is the vapour quality, α is the void fraction (estimated by an appropriate correlation) and the subscripts L and V indicate the liquid and vapour phases, respectively.

The Lockhart-Martinelli [78] method is extensively used in the literature to estimate the two-phase frictional pressure drops by relating them to the single-phase *liquid alone* and *vapour alone* pressure drops as follows:

$$X^2 = \frac{dp_L/dz}{dp_V/dz} \tag{2.21}$$

$$\Phi_L^2 = \frac{dp_{\mathrm{fr,tp}}/dz}{dp_L/dz} \tag{2.22}$$

Her, X is the so-called Lockhart-Martinelli parameter and Φ_L^2 is the two-phase frictional multiplier. The terminology *alone* refers to the flow as the vapour or liquid occupied the entire cross-section of the channel, resulting in a mass flux multiplication by x and $(1-x)$ to estimate the vapour and liquid pressure drops, respectively. One widely used approach to estimate the two-phase liquid multiplier Φ_L is to use the fitting proposed

by Chisholm [80] and reported in Eq.(2.23), where C_i is a constant for which different values were proposed by different authors.

$$\Phi_L^2 = 1 + \frac{C_i}{X} + \frac{1}{X^2} \tag{2.23}$$

In order to use the Lockhart-Martinelli method, a single-phase correlation is necessary for the computation of the single-phase pressure drop.

The last method for the two-phase pressure drop calculation consists in the definition of a proportionality between the frictional pressure drops and the kinetic energy per unit volume, as suggested for evaporation and condensation in PHEs by Longo and Gasparella [81] and Longo [82]. By employing this method, the pressure drop is estimated as:

$$\frac{dp_{\mathrm{fr,tp}}}{dz} = \frac{d}{dz}\left(\xi \frac{G^2}{2\rho_m}\right) \tag{2.24}$$

where ξ is constant obtained by fitting experimental data for specific PHE geometries.

Due to the assumption of separated flow model between liquid and vapour phases, a void fraction correlation was implemented to estimate the cross-section void faction α, namely the ratio between the cross section area occupied by the vapour phase and the total cross section area. The void fraction is defined as [83]:

$$\alpha = \left(1 + S_{\mathrm{VL}} \frac{1-x}{x} \frac{\rho_V}{\rho_L}\right)^{-1} \tag{2.25}$$

The homogeneous model assumed that the slip ratio S_{VL} is equal to 1, e.g. the vapour and liquid phases flow at the same velocity. However, this is not a reasonable assumption for PHEs and Smith [84] proposed expressions to estimate S_{VL}, as function of the local vapour quality and vapour and liquid phase densities, as:

$$\alpha = \left(1 + \frac{\rho_V}{\rho_L} K \left(\frac{1}{x} - 1\right) + \frac{\rho_V}{\rho_L}(1-K)\left(\frac{1}{x} - 1\right) \cdot \left[\frac{\frac{\rho_L}{\rho_V} + K\left(\frac{1}{x} - 1\right)}{1 + K\left(\frac{1}{x} - 1\right)}\right]^{1/2}\right)^{-1} \tag{2.26}$$

with x being the vapour quality and K a constant equal to 0.4. The correlation by Smith [84] was extensively validated for two-phase annular flow [85], which is a reasonable assumption for two-phase flow in PHEs [28].

The void fraction is needed for the computation of the two-phase pressure drops. More specifically, it is needed to compute the momentum density ρ_m with Eq. (2.20), as well as the cross section weighted average density ρ, estimated by [79]:

$$\rho_{\mathrm{cs}} = (1-\alpha)\rho_L + \alpha\rho_V \tag{2.27}$$

The momentum density ρ_m is used to compute the acceleration contribution to the pressure drop in two-phase flow, as [79]:

$$\frac{dp_{\text{acc,tp}}}{dz} = G^2 \frac{d}{dz}\left(\frac{1}{\rho_m}\right) \tag{2.28}$$

On the other hand, the cross section average density serves for the computation of the gravity contribution to the pressure drop by [79]:

$$\frac{dp_{\text{gr,tp}}}{dz} = \frac{d(\rho_{\text{cs}} g z)}{dz} \tag{2.29}$$

where g is the gravitational acceleration constant.

In PHEs, the port contribution to pressure drop at the inlet and outlet can also be estimated and added to the overall momentum conservation. If considered, the port pressure drop must solely be added to the first and last CV, corresponding to the inlet and outlet ports. The Shah and Focke [86] correlation, expressed by Eq. (2.30), is commonly used to compute port pressure drops.

$$\Delta p_{\text{port}} = 0.75 \left[\left(\frac{G_p^2}{2\rho}\right)_{\text{in}} + \left(\frac{G_p^2}{2\rho}\right)_{\text{out}} \right] \tag{2.30}$$

where G_p indicates the mass flux at the port diameter D_p.

The PHE models were implemented to simulate evaporators and condensers, thus requiring the computation of the refrigerant heat transfer coefficient during transition to single to two-phase flow and viceversa. A smooth transition was ensured by calculating the refrigerant heat transfer coefficient and frictional pressure drop by interpolating the two-phase and single-phase contributions at the interface, as suggested by Corberán et al. [68]. The smoothing was applied to the CVs with a local vapour quality included in the intervals [0, 0.1] and [0.9, 1.0].

2.2.7 Fluid thermo-physical properties

The thermo-physical properties of pure fluids and zeotropic mixtures were estimated by REFPROP 10 [87], and CoolProp 6.2.1 [88]. Being the PHE model discretized in 1D or 2D, the model was able to estimate the local values of the properties. This aspect was particularly relevant to model zeotropic mixtures: due to the varying compositions of the liquid and vapour phases during the evaporation and condensation processes, the saturation properties are not constant. The large variation in liquid and vapour physical properties during flow boiling was estimated to contribute to 80 % of the total heat transfer degradation entailed by mixture utilization [89, 90]. Therefore, it is of paramount importance to include this effect in the modelling tool.

2.2.8 Design solver

The afore-described PHE models, i.e with the solver for heat transfer and fluid flow, were coupled with a design solver with the aim of estimating the required heat transfer area at the evaporator and the condenser to meet a certain design thermal load. Therefore, the inputs required were given by the total heat flow rate and inlet thermodynamic states of both working fluid and secondary fluid. The design solver was implemented by fixing the plate size and corrugation geometry, and using the solver for heat transfer and fluid flow, explained in section 2.2.5, to iterate on the required number of channels. This approach was chosen as an equivalent approach to commercial design solvers (e.g. [74]), where the plate size is fixed to the manufactured dimensions and the number of channels is calculated as output of the design. In these solvers, different solutions related different plate width and length are proposed. Maximum pressure drop, e.g.50 kPa, can be used as a criterion to suggest possible designs.

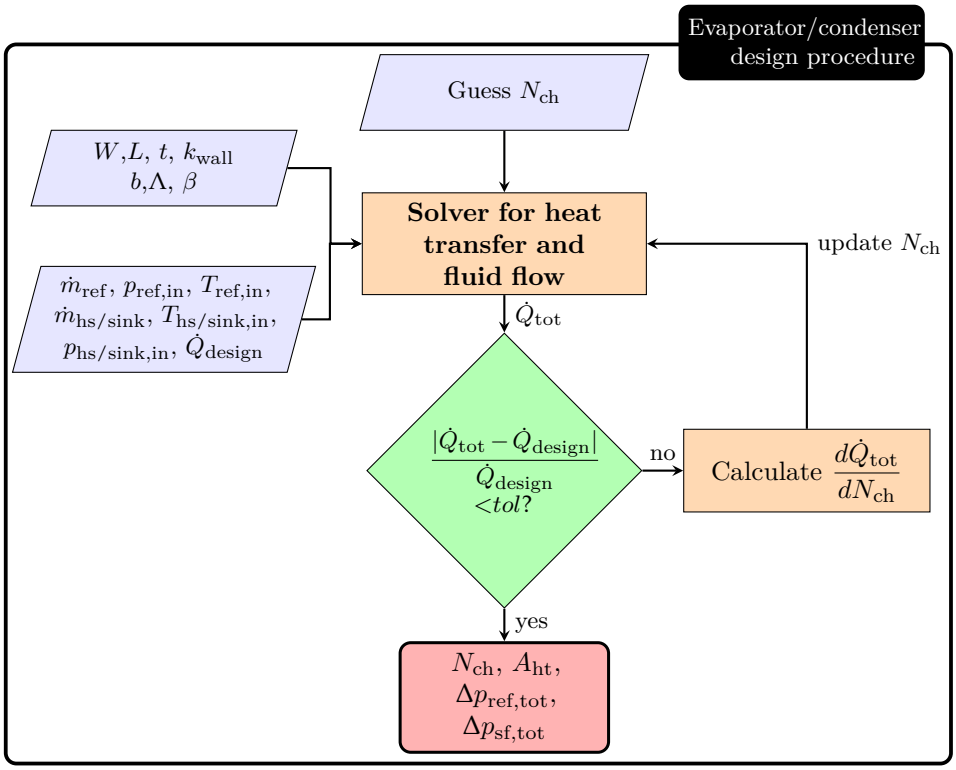

Figure 2.5: Work flow of the design solver

The flow-chart of the implemented design solver is shown in Fig.2.5. A guess values for the number of channels is provided as first step. Second, the solver for heat transfer and fluid flow estimates the outlet thermodynamic states of working fluid and secondary side, as well as the total heat flow rate. The convergence at the solution is checked by

estimating the relative residual of the total heat flow rate compared to the design value. If the residual is lower than the set tolerance, the solver converged to the set solution. If the residual is higher, the derivative of the heat flow rate with respect to the number of channels is estimated and the value of N_{ch} at the next iteration $k+1$ is updated following the Newtwon-Raphson method. Since the number of channels must be an integer odd value, the solution was set as the highest integer value of the exact output of the solver.

2.3 Alternative PHE model for design

The model described in section 2.2 presented a modelling approach aimed at solving the PHE rating problem. The model was integrated with a solver to address the design problem, as presented in subsection 2.2.8. Here, an alternative approach to model the PHE is presented, with the aim of solving the design problem: in fact, the previously presented approach entails the drawback related to the high computational time required. The solver for heat transfer and fluid flow has to solve at each iteration before converging to the required number of channels is reached. Moreover, a fast and successful convergence to the solution was found to be highly dependent on the initial guess. As an advantage, the solver was well suited for a realistic PHE design, when the plate size is fixed to typical manufactured dimensions. However, if the objective of the work is to obtain novel geometrical configurations of PHEs, for example by running optimizations on an extensive search space of different geometries, a faster and more robust approach is chosen.

The alternative PHE design model was based on a 1D discretization of the HEX along the flow direction and - differently from the solver for heat transfer and fluid flow - at constant enthalpy steps. This approach implies that a constant heat flow rate was obtained for each CV. Since the total design heat flow rate is known a-priori and used as input, this approach allows knowing the enthalpy values at each node of the discretized HEX from the first iteration. The input PHE geometrical parameters were given by the specifications on corrugation geometry, plate width W and number, and thickness of the plates. The model thus iterated on the total heat transfer length L_{ht} to meet the desired thermal load.

The solver is based on a successive substitution approach. First a guess value for the total heat transfer area (related to the total plate length by Eq.(2.4)) was provided, together with a guess value for the allocation of the discretized heat transfer area in each CV. Guessed pressure drops of both working fluids were also provided in the initial step, either by setting their value to zero or by calculating them using the inlet properties and the guessed plate length. The following steps were subsequently taken:

1. Based on the guessed pressure drops, the pressure was computed at each node of the CV, and the temperature was computed based on known values of enthalpy and pressure;

2. fluid thermo-physical properties were computed at each node, since the thermodynamic state was known;

3. the thermodynamic state and properties at the center of each CV were estimated based on a linear interpolation of the values at the nodes;

4. the local overall heat transfer coefficient was calculated for each CV as:

$$U^{(i)} = \left(\frac{1}{h_{\text{ref}}^{(i)}} + \frac{t}{k_w} + \frac{1}{h_{\text{sf}}^{(i)}} \right)^{-1} \tag{2.31}$$

   where h_{ref} and h_{sf} are the local heat transfer coefficients of the refrigerant and of the secondary fluid, respectively, estimated by appropriate correlations depending on the region;

5. the local UA- values were computed based on the LMTD between the two fluids at each CV as a function of the temperatures at the nodes, as expressed by Eq.(2.32):

$$\frac{\dot{Q}_{tot}}{n} = (U \Delta A_{\text{ht}})^{(i)} \cdot \frac{(T_{\text{sf}}^{(i)} - T_{\text{ref}}^{(i)}) - (T_{\text{sf}}^{(i+1)} - T_{\text{ref}}^{(i+1)})}{\ln \left(\dfrac{T_{\text{sf}}^{(i)} - T_{\text{ref}}^{(i)}}{T_{\text{sf}}^{(i+1)} - T_{\text{ref}}^{(i+1)}} \right)} \tag{2.32}$$

6. the value of heat transfer area ΔA_{ht} for each CV was updated by using Eq.(2.32) and (2.31), and the plate length associated to each CV was also estimated by Eq.(2.4).

7. the local pressure drop was updated by considering the updated plate length with each control volume. The approach to calculate it was presented in section 2.2.6;

8. the convergence was checked on the relative residual of the length and refrigerant and secondary fluid pressure drops, as:

$$e = \max \left(\left| \frac{\Delta A_{\text{ht}}^{k+1} - \Delta A_{\text{ht}}^{k}}{\Delta A_{\text{ht}}^{k}} \right|, \left| \frac{\Delta p_{\text{ref}}^{k+1} - \Delta p_{\text{ref}}^{k}}{\Delta p_{\text{ref}}^{k}} \right|, \left| \frac{\Delta p_{\text{sf}}^{k+1} - \Delta p_{\text{sf}}^{k}}{\Delta p_{\text{sf}}^{k}} \right| \right) \tag{2.33}$$

   where e represents the error and k the iteration number.

9. if the error was lower than the set tolerance, the solver was considered to have converged to the solution, while the discretized values of heat transfer area in each CV were updated for a new iteration if the error was larger than the tolerance.

The output of the design model was thus given by the PHE heat transfer area, corresponding to a related plate heat transfer length L_{ht}. Moreover, the PHE design corresponded to specific pressure drops on both the refrigerant and the secondary fluid side. By changing

the fixed geometrical parameters, such as plate width W and number of channels N_{ch}, it was possible to obtain different designs, which were able to satisfy the same design heat flow rate, yet entailing a different pressure drop and total heat transfer area.

2.4 Flow distribution solver

A flow distribution solver was coupled with the PHE model discretized in 2D, in order to compute the mass flow rate distribution in the different channels. The model was based on the principle of *identical pressure drop* [55] for each channel. The manifold pressure drop was considered to be negligible, thus the channel pressure drop was assumed to be the sole contributor of pressure drop along each flow path. The assumption is justified by the fact that inlet manifold of PHE is rather complex and would require many detailed geometrical inputs to be solved for. The contributions determining the overall channel pressure drop were therefore given by friction, acceleration and gravity.

The flow distribution solver was implemented for liquid-to-liquid PHEs and for evaporators. In the former case, the effect of end plates was investigated. The effect of end plates is determined by the outermost plates of the PHE, which ideally do not transfer heat to the external environment [56], and thus entail a modification of the mass flow distribution among the different channels. In the case of evaporators, two different effects were considered by the model, e.g. effect of end plates and liquid/vapour maldistribution. In fact, the refrigerant inlet is in the two-phase region for evaporators, placed after the throttling valve in vapour compression cycles. For upward refrigerant flow, the vapour phase distributes more easily in the first channels from the inlet port, and this effect was observed experimentally [62]. Therefore, a variation of the inlet vapour quality between the different channels was imposed as a boundary condition to the model before solving the flow distribution equations in order to estimate the effect of different rates of non-uniformity.

The solver for flow distribution solved the global mass conservation and the identical pressure drop equations, by using the MATLAB built-in algorithm *fsolve* [91]. A guessed distribution of the mass flow rate of both working fluid was provided to the solver, where a uniform distribution was imposed to the channels.

For liquid-to-liquid PHEs, the number of unknowns was equal to the total number of channels $N_{\text{ch,tot}}$, i.e. the mass flow rate of each fluid in the channels $\dot{m}_1^{(j)}$ and $\dot{m}_2^{(j)}$. The number of governing equations was also $N_{\text{ch,tot}}$, expressed by Eq.(2.34)-(2.37).

$$\sum_{j=1}^{N_{\text{ch},1}} \dot{m}_1^{(j)} = \dot{m}_{1,\text{tot}} \tag{2.34}$$

$$\sum_{j=1}^{N_{\mathrm{ch},2}} \dot{m}_2^{(j)} = \dot{m}_{2,\mathrm{tot}} \tag{2.35}$$

$$\sum_{i=1}^{n} \Delta p_1^{(j,i)} = \sum_{i=1}^{n} \Delta p_1^{(j+1,i)}, \qquad j = 1, ..., N_{\mathrm{ch},1} - 1 \tag{2.36}$$

$$\sum_{i=1}^{n} \Delta p_2^{(j,i)} = \sum_{i=1}^{n} \Delta p_2^{(j+1,i)}, \qquad j = 1, ..., N_{\mathrm{ch},2} - 1 \tag{2.37}$$

$N_{\mathrm{ch},1-2}$ represents the number of channels of the first and second fluid (whose sum is equal to the total number of channels), and j and i are the indexes indicating the channel and the CV along the flow direction, respectively. It is noted that n is the number of CV in which the PHE is discretized along the flow direction, while the subscripts 1 and 2 indicate the primary and secondary fluid, respectively.

For evaporators, an additional equation was added to the system of equations, to solve for the additional unknown of inlet vapour quality in the first channel $x_{\mathrm{ref}}^{(1,1)}$. A linear vapour quality variation of fixed slope was assumed between first and last channel, thus by knowing the value of the quality at the first channel, the remaining channels were computed accordingly. The liquid/vapour maldistribution was defined by fixing a parameter Δx, representing the difference in vapour quality between the two outermost refrigerant channels. The inlet quality at the j-th channel, assuming a linear profile, was therefore calculated by:

$$x_{\mathrm{in}}^{(j)} = x_{\mathrm{in}}^{(1)} + \frac{j-1}{N_{\mathrm{ch,ref}} - 1} \Delta x \tag{2.38}$$

where $x_{\mathrm{in}}^{(1)}$ is the vapour quality of the first channel. The parameter Δx represents the slope of the vapour quality variation. An example of the imposed variation of vapour quality for a case of 11 refrigerant channels and Δx varying between 0 and 0.25 is shown in Fig. 2.6.

When the parameter Δx was set equal to 0, an uniform vapour quality variation was imposed, thus no liquid/vapour maldistribution effect was considered in the PHE. Therefore, this case allowed estimating the effect of end plates. The effect of end plates resulted into a modification of the flow distribution of both refrigerant and secondary fluid, as the outer-most channels transfer a different amount of heat compared to the interior channels. This was taken into account by evaluating the evaporator model in 2D without imposing any variation of the vapour quality, e.g. $\Delta x = 0$.

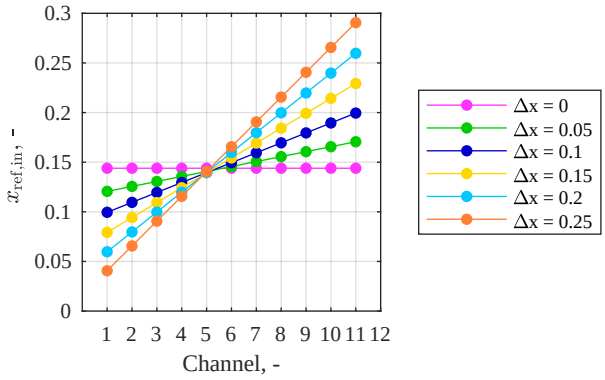

Figure 2.6: Vapour quality variation in different PHE channels for different values of Δx

The additional equation of mass conservation, applied to the vapour phase only, was thus added as:

$$\sum_{j=1}^{N_{\mathrm{ch,ref}}} \dot{m}_{\mathrm{ref}}^{(j)} \cdot x_{\mathrm{ref,in}}^{(j)} = \dot{m}_{\mathrm{ref,tot}} \cdot x_{\mathrm{ref,in}} \tag{2.39}$$

Here, the inlet vapour quality based on the total mass flow rate of the refrigerant $x_{\mathrm{ref,in}}$ was fixed to a value depending on the boundary conditions of the specific case study. By applying both Eq.(2.39) and (2.34) to the refrigerant, the mass conservation of the liquid-phase is also ensured.

2.5 Verification and validation

This section presents the verification of the flow distribution solver compared to a model from literature, and the validation of the PHE solver for heat transfer and fluid flow against experimental data. As suggested by Vakili-Farahani et al. [28], the deviation between the model results and the experimental data (or the reference model from literature) is reported for all cases in terms of the mean relative error δ and mean absolute error $|\delta|$, estimated by Eq.(2.40) and (2.41), respectively, in percentage points.

$$\delta = \frac{1}{N} \cdot \sum_{i=1}^{N} \left(\frac{\theta_{\mathrm{model}} - \theta_{\mathrm{exp}}}{\theta_{\mathrm{exp}}} \right) \cdot 100 \tag{2.40}$$

$$|\delta| = \frac{1}{N} \cdot \sum_{i=1}^{N} \left| \frac{\theta_{\text{model}} - \theta_{\text{exp}}}{\theta_{\text{exp}}} \right| \cdot 100 \tag{2.41}$$

θ represents the compared quantity, i.e. total heat flow rate and refrigerant total pressure drops, and N represents the number of the considered experimental data points. For the comparison with experimental data, the models were used in rating mode (see section 2.2). The model received as inputs the full PHE geometry and inlet thermodynamics of both fluids, as gave the total heat flow rate, pressure drops and outlet thermodynamics as outputs. Experimental heat flow rate and refrigerant pressure drop (when available from measurements) were then used to evaluate the model accuracy. For the flow distribution solver verification, the reference was given by the quantity evaluated by the reference model.

2.5.1 Flow distribution solver verification

The flow distribution solver was verified against the results of the model presented in [55]. Li and Hrnjak [55] developed an experimentally validated model to solve single-phase flow distribution in PHEs. The model was built using a similar approach compared to the present model, i.e. by imposing equations to ensure global conservation of mass and *identical pressure drop* for each flow path. Li and Hrnjak [55] accounted for frictional, gravity and manifold pressure drop, while they neglected the acceleration contribution. The manifold pressure drop is on the contrary neglected in the present model.

The outlet temperature in each channel for both primary and secondary fluid, as well as the heat flow rate exchanged by the channels, were compared with the results of the model by Li and Hrnjak for three PHEs, with a fixed plate geometry and different number of channels. Hot and cold water streams were used as primary and secondary fluid, respectively. By increasing the number of channels, the manifold pressure drop increases, thus enhancing the difference of the inlet pressure between the outermost channels. Therefore, it is expected to have larger discrepancies between the model results for higher number of channels.

Fig. 2.7 reports the result of the verification. The deviations between the models were quantified in terms of mean relative error and mean absolute error, thus computed by Eq.(2.40) and (2.41). The two models showed an overall satisfactory agreement with the highest deviation for both outlet temperature and heat flow rate achieved in the case of $N_{\text{ch}} = 99$. The highest deviation for temperature was found to be as low as 0.2 %.

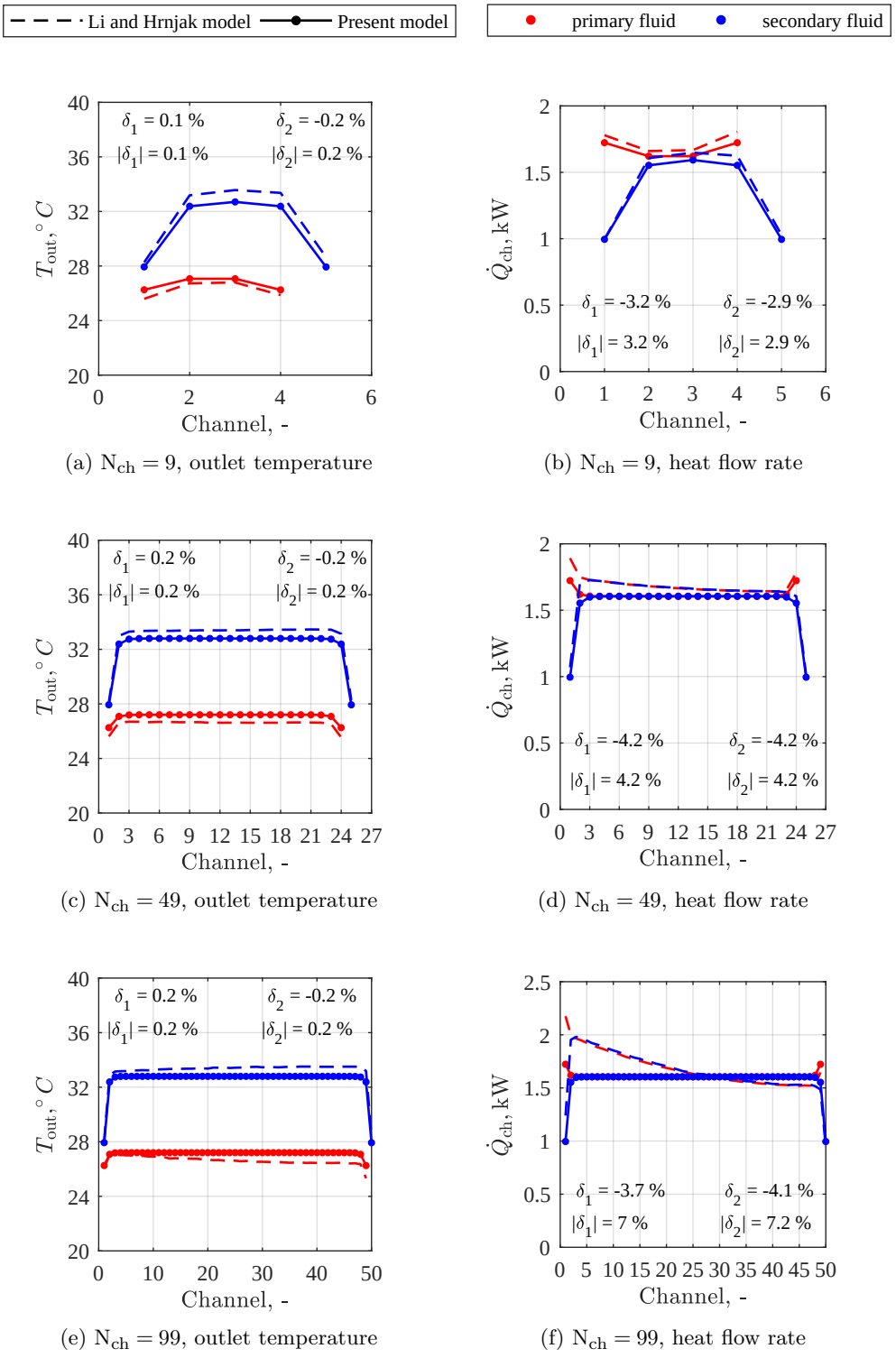

(a) $N_{ch} = 9$, outlet temperature

(b) $N_{ch} = 9$, heat flow rate

(c) $N_{ch} = 49$, outlet temperature

(d) $N_{ch} = 49$, heat flow rate

(e) $N_{ch} = 99$, outlet temperature

(f) $N_{ch} = 99$, heat flow rate

Figure 2.7: Comparison between the results of the present model and the results of the model by Li and Hrnjak [55]

In all cases, the present model overestimated the outlet temperature of the primary fluid (red line, hot fluid), while the outlet temperature of the cold water stream (blue line) was underestimated. This was due to a general underestimation of the heat flow rate exchanged between the channels. The highest deviation on heat flow rate was found in the case of $N_{ch} = 99$, with mean absolute errors of 7.0 % and 7.2 % on the heat flow rates in the hot and cold fluid channels, respectively. The mean relative errors were found to be -3.7 % and -4.1 %, thus the heat flow rate was overestimated or underestimated depending on the channel.

It is noted that the deviation for temperature was calculated for the temperature in K, even though Fig. 2.7 (a), (c) and (e) report the temperature in °C. Moreover, the results showed that it is acceptable to neglect manifold pressure drops when the number of channels is not too large, and that errors below 10 % are obtained even in the case of 99 total channels.

2.5.2 Comparison with experimental data: evaporation data from DTU

A total of 316 flow boiling data from the experimental study by Zhang et al. [92], for R134a (106 points), R1234yf (91 points) and R1234ze(E) (119 points) were used. The study was carried out in the laboratory of DTU Mechanical Engineering. The data included information on both total heat flow rate and refrigerant pressure drop. In the PHE model, the heat transfer coefficient was estimated locally by applying the correlation by Amalfi et al. [93], while the frictional pressure drop was estimated by calculating the Fanning friction factor according to Yan and Lin [94]. The comparison was carried out using the models discretized in both 1D and 2D. The 2D model was applied together with the flow distribution solver by imposing an uniform vapour quality distribution at the inlet of the PHE channels, thereby solely accounting for the effect of end plates.

Fig. 2.8 reports the comparison of the total heat flow rate and total refrigerant pressure drop for both the 1D and 2D model, considering all the experimental data points. Table 2.2 reports the deviations for each working fluid separately. The 1D model slightly overestimated the experimental values, with a relative deviation of +4.3 %, while in the 2D case the deviation was -2.3 %. The difference is likely due to the effect of end plates, which slightly degrades the heat transfer performance of the evaporator and is considered solely in the 2D model. Jin and Hrnjak [56] found that this effect is not negligible for configurations with less than 20 channels, and the experimental study was carried out on a PHE configuration with 7 channels in total [92].

R1234ze(E) resulted in the highest deviation for the 1D model,i.e. 6.1 % overestimation of the total heat flow rate. The discrepancy reduced however down to -1.3 % for the 2D model, resulting in the best match with the experimental data compared to the two other working fluids. This might be due to a higher sensitivity of R1234ze(E) to the effect of end plates compared to the other working fluids, hence leading to a higher deviation

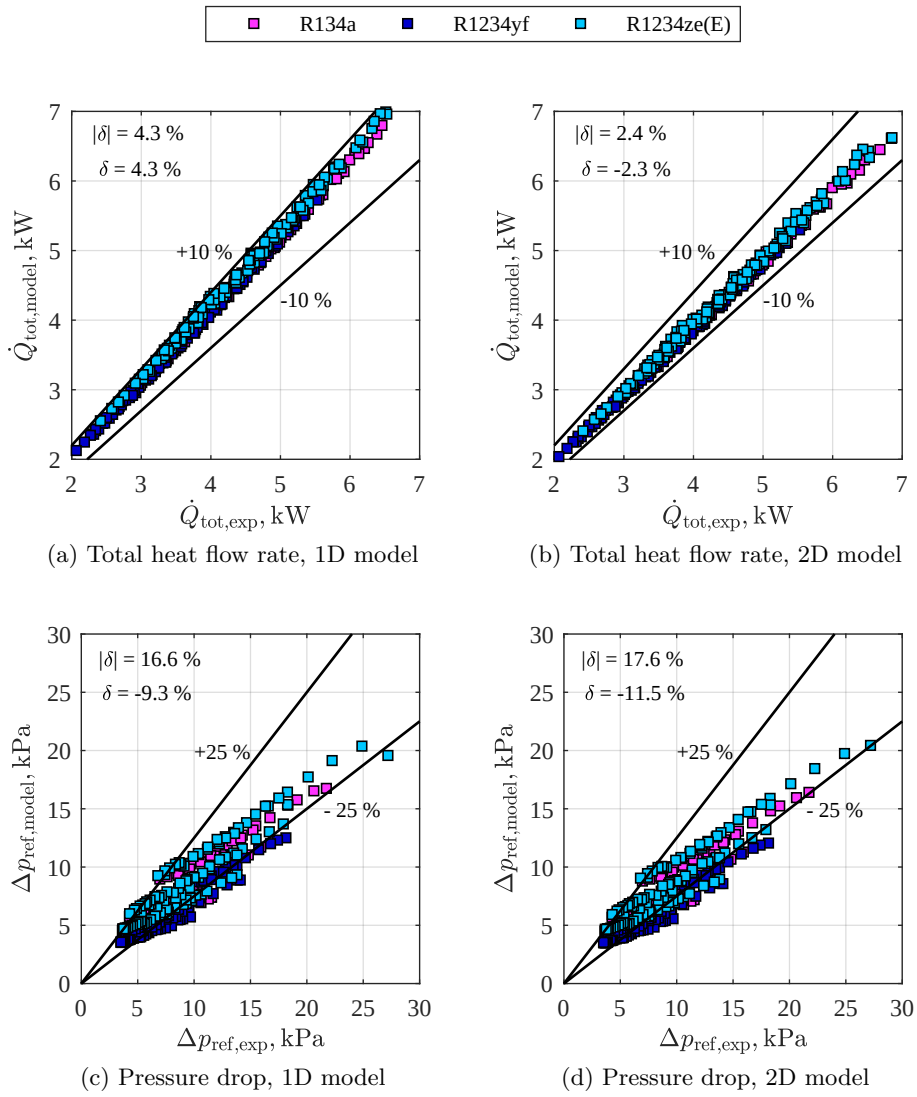

(a) Total heat flow rate, 1D model

(b) Total heat flow rate, 2D model

(c) Pressure drop, 1D model

(d) Pressure drop, 2D model

Figure 2.8: Comparison of simulated data points vs. experimental data for the (a), (b) total heat flow rate, and (c), (d) total refrigerant pressure drop

from experimental data when the effect was neglected with the 1D model.

Higher errors were reported for refrigerant pressure drop for all the fluids, with a general underestimation of the value calculated by the model, with the errors equal to -9.3 % and -11.5 % for the 1D and 2D models, respectively. R1234yf resulted in the highest deviation, while R134a and R1234ze(E) presented similar matches. It is noted that Zhang et al. [92] reports the maximum uncertainty on the measured pressure drop and heat flow rate equal to 6.6 % and 2.8 %, respectively. Therefore, the model results and the

Table 2.2: Deviations between experimental data and results of the evaporator model using 1D and 2D discretization (DTU data)

	1D model				2D model			
	Heat flow rate		Pressure drop		Heat flow rate		Pressure drop	
Working fluid	δ	$\lvert\delta\rvert$	δ	$\lvert\delta\rvert$	δ	$\lvert\delta\rvert$	δ	$\lvert\delta\rvert$
	%	%	%	%	%	%	%	%
R134a	3.6	3.6	-6.5	14.7	-2.9	2.9	-8.6	15.6
R1234yf	2.9	2.9	-21.1	21.2	-2.9	2.9	-22.9	23.0
R1234ze(E)	6.1	6.1	-2.8	14.6	-1.3	1.5	-5.3	15.3
Overall	4.3	4.3	-9.3	16.6	-2.3	2.4	-11.5	17.6

experimental data showed an overall good match, with maximum deviations in the same order of magnitude of the experimental uncertainty.

2.5.3 Comparison with experimental data: Sondex evaporators using ammonia

The PHE evaporator model discretized in 1D was further validated against experimental data from commercially manufactured PHEs from Sondex AS [8]. For confidentiality reasons, the cooling capacity and the geometry of the evaporator cannot be reported in the present thesis. The evaporator capacity was around 1000 kW. The PHEs were tested with ammonia as evaporating working fluid, and with a 40 % (mass) brine as heat source. The correlation by Palm and Claesson [95] was used to estimate the heat transfer coefficient of ammonia in two-phase, while the Martin [77] correlation was used for the single-phase heat transfer coefficient and pressure drop. The frictional pressure drop of ammonia was calculated as proposed by Amalfi et al. [93].

The comparison between the model and the experimental data is reported in terms of normalized value, e.g. each value of the experimental and calculated heat flow rate or pressure drop was divided by the maximum experimental value for the specific PHE model. The results of the comparison are shown in Fig.2.9. Each color represents a different PHE tested model, and total heat flow rate, ammonia and brine pressure drops are plotted in sub-figure (a), (b) and (c), respectively. Table 2.3 reports the mean absolute and relative errors for the different PHE models in terms of total heat flow rate and pressure drops of both fluids. The total heat flow rate presents a good match against the experimental data with a slight overestimation of the total heat flow rate for all PHE models. The deviation stayed however below 10 % for all PHE models, with the exception of HEX 1, which reported a mean absolute error equal to 12.7 %. The match between experimental and estimated pressure drop was not found to be as good as the thermal performance. The ammonia pressure drop was overestimated by the model, with a maximum deviation of 32.1 % for HEX 3. On the other hand, the pressure drop of the brine was largely underestimated and HEX 1 reported the maximum absolute error of

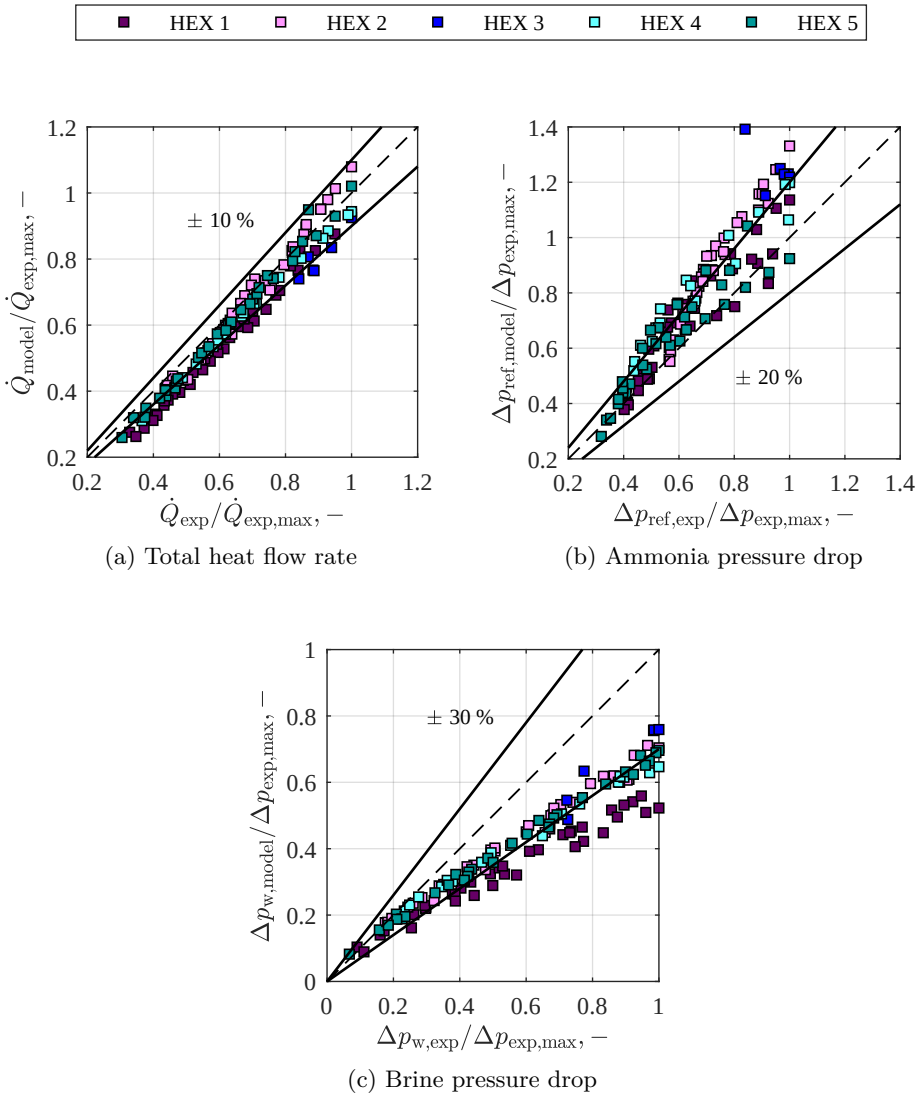

(a) Total heat flow rate

(b) Ammonia pressure drop

(c) Brine pressure drop

Figure 2.9: Comparison of simulated data points vs. experimental data for the estimation of (a) total heat flow rate, (b) total pressure drop of ammonia, and (c) total pressure drop of the brine

34.8 %. The discrepancies between model and experimental data can be due to different reasons. First, manifold pressure drop, contributing to the overall experimental pressure drop, was neglected by the model. Moreover, the suitability of Martin [77] correlation to estimate the heat transfer coefficient of the brine is not trivial. An underestimation of the heat transfer performance from the brine side might lead to an underestimation of the pressure drop. This might explain why a good match between model and experimental data was found by using Palm and Claesson [95], instead of more recent correlations (like

Table 2.3: Deviations between experimental data and results of the evaporator model (Sondex data)

PHE model	Heat flow rate		Ammonia pressure drop		Brine pressure drop	
	δ %	$\|\delta\|$ %	δ %	$\|\delta\|$ %	δ %	$\|\delta\|$ %
1	-12.7	12.7	9.6	11.4	-34.0	34.8
2	-1.5	4.8	22.4	22.6	-21.6	21.6
3	-10.8	10.8	32.1	32.1	-24.3	24.3
4	-7.2	7.2	24.1	24.1	-24.1	24.1
5	-4.7	5.5	10.9	12.7	-21.9	23.3

Amalfi et al. [93]), which were found to underestimate the total heat flow rate. Therefore, by using Palm and Claesson [95] and Martin [77], a slight overestimation of the ammonia heat transfer coefficient and underestimation of the brine heat transfer coefficient might be obtained. This can be explained by looking at the overestimation/underestimation of ammonia/brine pressure drop, despite the overall good match with the experimental heat flow rate - which is likely to compensate the two effects.

2.5.4 Comparison with experimental data: pure CO_2 data from CNAM

Experimental data on the heat flow rate for a PHE evaporator using pure CO_2 were used from an experimental study carried out at the Conservatoire National des Arts et Métiers (CNAM) in Paris [96]. 83 data points were therefore used to validate the evaporator model discretized in 1D. The experimental test-rig was subsequently used to test mixtures of CO_2/propane at different mass compositions, and a detailed description of the test rig and the results of the study are presented in details in Chapter 3.

The comparison was carried out by using Amalfi et al. [93] to compute the refrigerant two-phase heat transfer coefficient and pressure drop, and Martin [77] for single-phase. The heat source was given by a mixture of ethylene glycol/water at (0.32/0.68) mass composition. The validation results are presented in Fig.2.10 for the total heat flow rate. PHE model and data presented a good agreement with a mean relative error of -2.7 %, i.e. a very small underestimation of the model compared to the experiments.

2.5.5 Comparison with experimental data: condensation data from DTU

Experimental data from the campaign by Zhang et al. [97] for R134a, R1234ze(E), R245fa and R1233zd(E) were used. The data were collected in the same test-rig of the evaporation data of section 2.5.2. The correlations by Zhang et al. [97] were applied to compute the heat transfer coefficient and two-phase friction factor. For the condenser, only the 1D

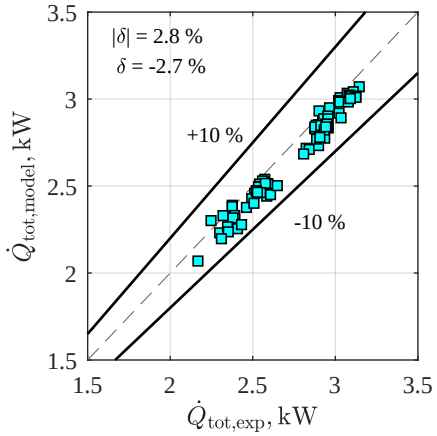

Figure 2.10: Comparison of simulated data points vs. experimental data for the estimation of total heat flow rate

discretization approach was implemented and thus compared against experimental data.

Fig. 2.11 reports the results in terms of total heat flow rate and total pressure drop of the refrigerants. The model underestimated overall the total heat flow rate with mean relative and mean absolute errors equal to -8.4 % and 9.9 %, respectively. The model underestimated the results for all working fluids with the exception of R245fa, which presented the best match with a slight mean overestimation of 4.1 %. On the other hand, the total pressure drop was overall overestimated by the model, with mean relative and mean absolute errors equal to 15.6 % and 20.6 %, respectively. The model overestimated the results for all working fluids, with R245fa showing the lowest mean relative error equal to 6.4 %, yet resulting in a higher absolute value of 16.6 %.

Zhang et al. [97] reported the maximum uncertainty on the experimental total heat flow rate and frictional pressure drop, as 4.1 % and 15.2 %, respectively. Therefore, similarly to the results of the evaporator model, the model results and the experimental data showed an overall good match, with maximum deviations in the same order of magnitude

Table 2.4: Deviations between experimental data and results of the model

Working fluid	Heat flow rate		Pressure drop	
	δ %	$\lvert\delta\rvert$ %	δ %	$\lvert\delta\rvert$ %
R134a	-6.8	6.8	20.3	25.3
R1234ze(E)	-16.2	16.2	11.6	16.3
R245fa	4.1	4.7	6.4	16.6
R1233zd(E)	-9.6	9.6	23.7	23.7
Overall	-8.4	9.9	15.6	20.6

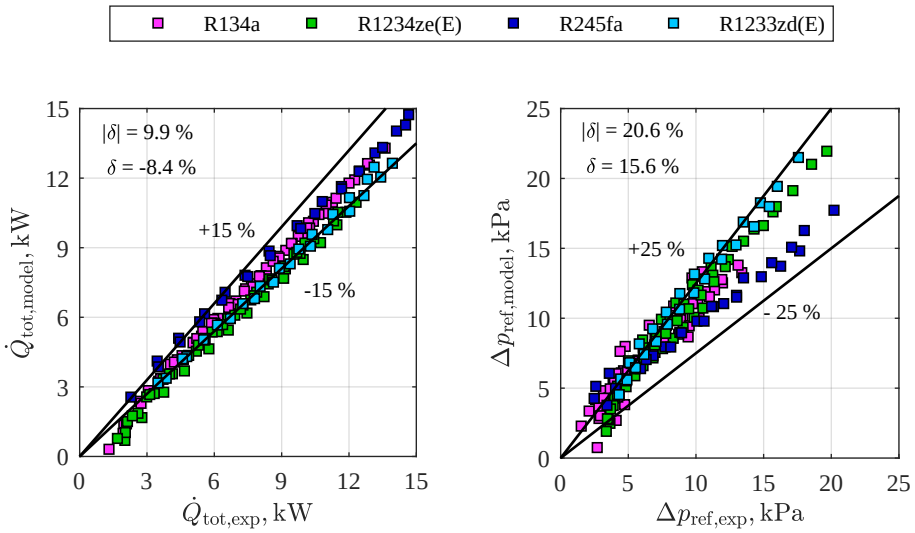

(a) Total heat flow rate

(b) Refrigerant total pressure drop

Figure 2.11: Comparison of simulated data points vs. experimental data for the (a) total heat flow rate and (b) total refrigerant pressure drop

of the experimental uncertainty.

2.6 Coupled PHE - heat pump simulation framework

The PHE models of both evaporator and condenser were integrated with a model of a single-stage vapour compression heat pump for both design and off-design calculations. The work flow of the simulation framework is presented in Fig. 4.5. The flow-chart shows how the different models are integrated in the overall procedure. Each orange rectangle represents a numerical model, while each parallelepiped represents input/output of the models. The rounded bold rectangles represent instead the main outputs.

The framework is structured as follow:

- *Heat pump design model*: after defining the boundary conditions of the cycle and the working fluid, the design of the heat pump is carried out. A brief explanation is also given in section 2.6.1.
- *Evaporator and condenser design models*: the design models used in the coupled framework were implemented following the approach presented in section 2.2.8.
- *Heat pump off-design model*: the off-design calculations were carried out by an overall simulation framework (yellow box in Fig.4.5), including a solver of heat

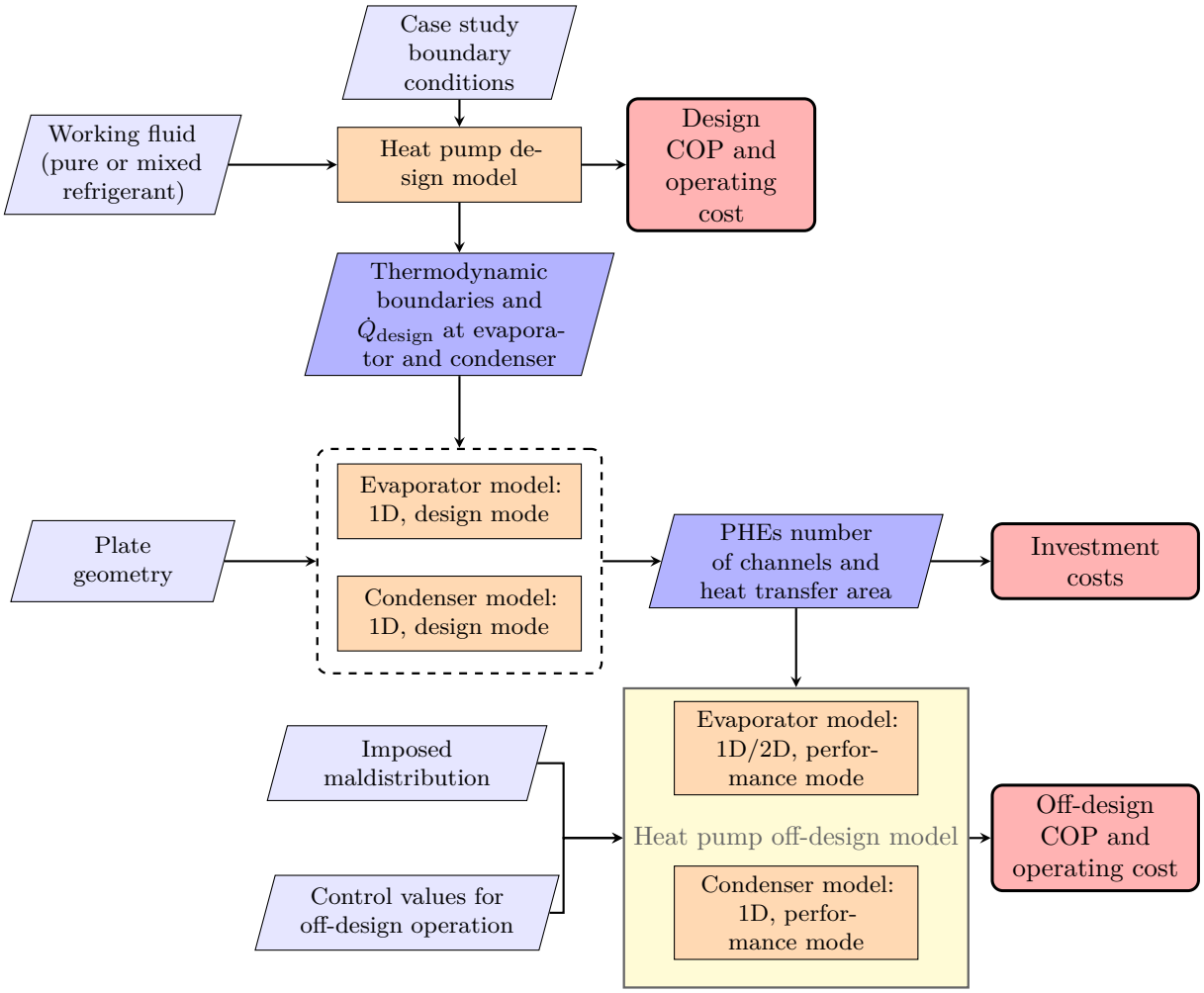

Figure 2.12: Work flow of the overall procedure. Rectangles represent a numerical model; parallelepipeds represent input/output; rounded bold rectangles represent main output

transfer and fluid flow for both evaporator and condenser, together with calculations of compressor and throttling valve operation in off-design. The off-design model was based on either a 2D or 1D discretization of the evaporator, thus estimating the performance of component and thermodynamic cycle with and without maldistribution effects.

2.6.1 Heat pump model

The reader is referred to Zühlsdorf et al. [13] for a comprehensive description of the modelling strategy adopted for cycle calculations. The thermodynamic cycle was modelled

in steady state and it consists of a single-stage configuration of a vapour compression heat pump. Fig.2.13 shows the sketch of the unit, with the different components integrated in the cycle, namely compressor, condenser, throttling valve and evaporator.

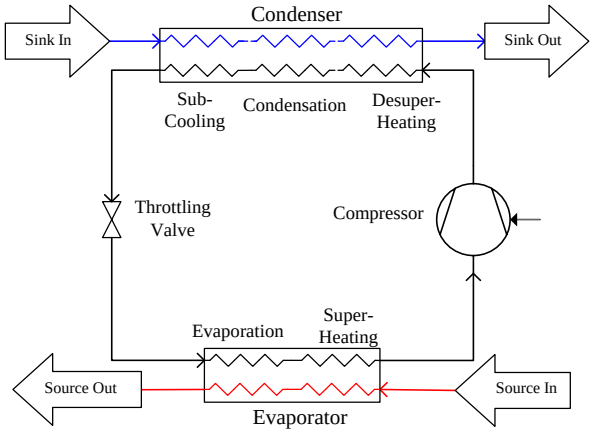

Figure 2.13: Schematic of the heat pump cycle (adapted from [13])

Depending on the application, the thermal load was fixed at either the evaporator or the condenser. The evaporation and condensation pressures of the working fluid were defined by the minimum required pinch point temperature difference between the working fluid and the fluid at the secondary side. The amount of subcooling was defined by the pinch point temperature difference and the sink inlet temperature in order to obtain the maximum efficiency. A minimum superheat of 5 K was typically included in the evaporator, in order to ensure a dry compression for all the fluids. At the design point, the compressor was modelled by assuming a constant isentropic efficiency, while the motor efficiency accounted for the power generation losses [98]. The throttling valve was assumed to expand the working fluid with an isenthalpic process.

The thermodynamic performance was evaluated by estimating the Coefficient of Performance (COP), defined by Eq.(2.42):

$$\mathrm{COP} = \frac{\dot{Q}_{\mathrm{sink}}}{\dot{W}_{\mathrm{comp}}} \tag{2.42}$$

where $\dot{Q}_{\mathrm{sink}}$ is the heat provided to the heat sink and $\dot{W}_{\mathrm{comp}}$ is the work required by the compressor.

2.6.2 Off-design without maldistribution effects

If maldistribution effects were neglected (both vapour quality maldistribution and effect of end plates), the off-design model was based on a 1D discretization of the evaporator. Fig.2.14 shows how the different component models are integrated in an overall solver for the cycle to solve for the operating conditions. First of all, the solver was initialized, e.g. the tolerance was set and the inputs were defined. The inputs were given by the full specified geometry of both evaporator and condenser (preliminary designed with design solver) and by the control values for off-design operation. Four control variables were specified:

(i) the degree of superheat at the evaporator outlet, fixed to the design value ΔT_{sh}

(ii) the degree of subcooling at the condenser outlet, namely a fixed temperature difference was imposed between the outlet refrigerant temperature at the condenser and the inlet heat sink temperature, equal to the minimum pinch point temperature difference $\Delta T_{\mathrm{sc}} = \Delta T_{\mathrm{pinch,min}}$

(iii) the suction volume flow rate at the compressor inlet, fixed to the design value $\dot{V}_{\mathrm{eva,out}}$

(iv) the heat sink outlet temperature, fixed to the design value $T_{\mathrm{sink,out-design}}$

These four control variables were related to four unknowns, defining the off-design operation of the cycle, namely:

(i) the total mass flow rate of the refrigerant $\dot{m}_{\mathrm{ref,tot}}$

(ii) the condensation pressure p_{cond}

(iii) the evaporation pressure p_{evap}

(iv) the total mass flow rate of the heat sink $\dot{m}_{\mathrm{sink,tot}}$

The last constraint was defined in light of an application in which a heat pump must provide heat to a district heating network at a fixed temperature level, therefore requiring a fixed heat sink outlet temperature also in off-design operation. The governing equations solved for the cycle operating parameters are also reported in Fig. 2.14.

In order to estimate the value of the four control variables for different heat pump operating conditions, the *fsolve* algorithm was set to solve all the components simultaneously, as shown in the yellow box of Fig. 2.14. The condenser and evaporator were solved by using the solver for heat transfer and fluid flow presented in section 2.2. The throttling valve was still thermodynamically described by an isenthalpic expansion process, while the

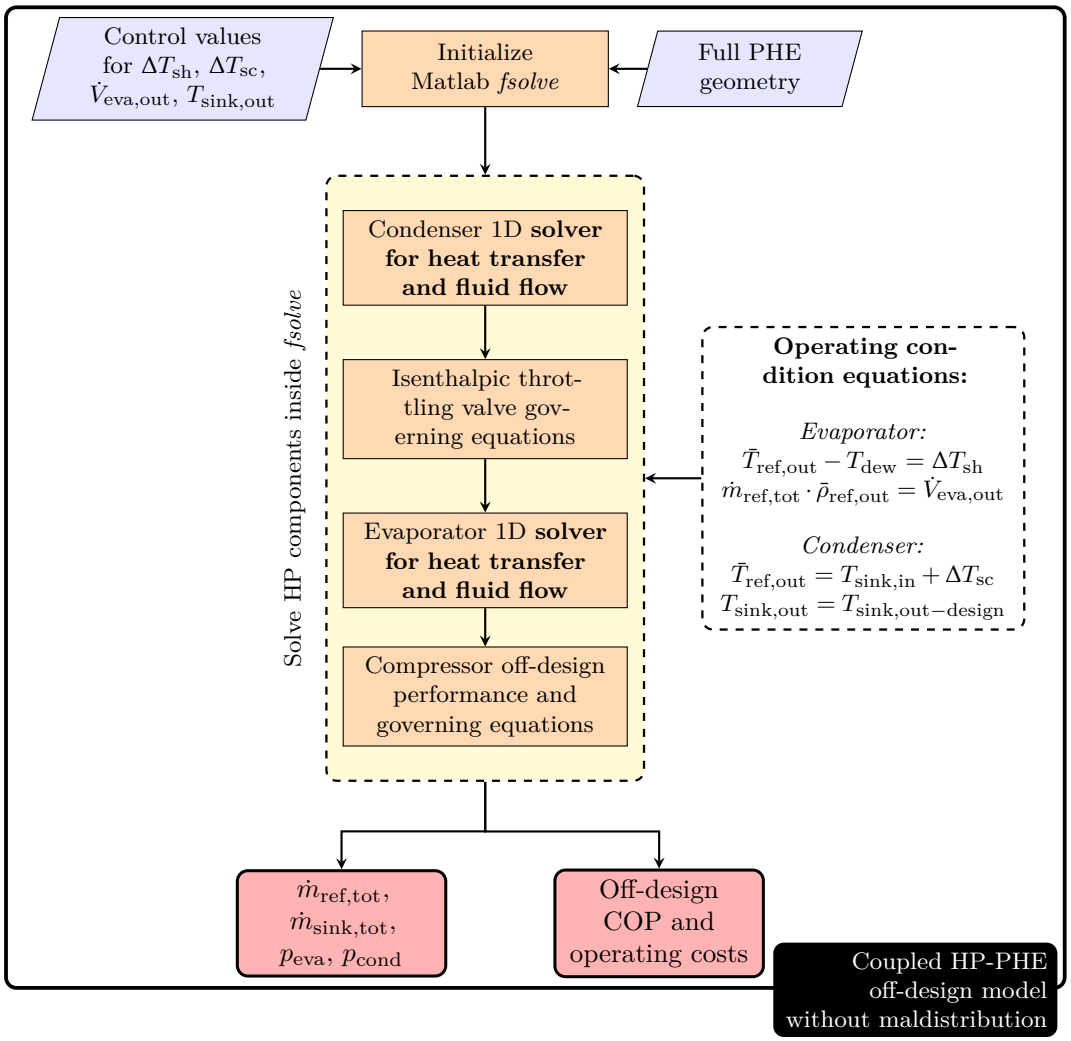

Figure 2.14: Work flow of the coupled off-design heat pump model and PHE performance models without maldistribution effects (1D evaporator model)

off-design performance of the compressor was formulated according to Granryd et al. [99], defined by Eq.(2.43), which related the isentropic efficiency to a pressure ratio deviating from the design value.

$$\frac{\eta_{is}}{\eta_{is,design}} = \frac{\left(\frac{p_1}{p_2}\right)^{\frac{k-1}{k}} - 1}{\pi_i^{\frac{k-1}{k}} - \frac{k-1}{k}\pi_i^{\frac{-1}{k}}\left(\pi_i - \frac{p_1}{p_2}\right)} \tag{2.43}$$

Here π_i represents a corrected built-in volume ratio, and k is the exponent of the polytropic process describing the compression process. π_i was found by imposing the value equal to

one for the design pressure ratio. This correlation is valid for volumetric compressors with built-in volume ratios.

The output of the coupled HP-PHE simulation framework was given by the operating conditions of the cycle, as mentioned previously. However, additional outputs were also given by the thermodynamic and economic performance indicators of the heat pump. The thermodynamic performance of the heat pump was indicated by the COP (Eq. (2.42)). The economic performance was instead evaluated by the (levelized) specific cost of heat, calculated in €/MWh by Eq.(2.44). The levelized cost of heat was defined as a function of the different cash flows (CF), i.e. the cost of electricity $\mathrm{CF_{el}}$, the income from supplying cold by cooling the heat source $\mathrm{CF_{hs}}$. Moreover, it was dependent on the Total Capital Investment (TCI), the Capital Recovery Factor (CRF), and the yearly production of heat, evaluated by multiplying the condenser load ($\dot{Q}_{\mathrm{sink}}$) by the yearly operating hours (OH). Further details can be found in Zühlsdorf et al. [13].

$$c_{\mathrm{h}} = \frac{\mathrm{CF_{el}} - \mathrm{CF_{hs}} + \mathrm{TCI} \cdot \mathrm{CRF}}{\dot{Q}_{\mathrm{sink}} \cdot \mathrm{OH}} \tag{2.44}$$

2.6.3 Off-design with maldistribution effects

The coupled HP-PHE simulation framework was also implemented to estimate the performance of heat pumps when maldistribution occurs in the evaporator. Therefore, the degree of liquid/vapour maldistribution was set as input, and used to solve the 2D evaporator model with the flow distributions solver, together with the heat pump off-design conditions. The input maldistribution was imposed as already presented in section 2.4, by fixing a value for the parameter Δx (Eq.(2.38)), defining the slope of the linear variation of the vapour phase distribution between the channels.

Fig. 2.15 shows the integration of the component models for the solution of both the heat pump operating conditions and the mass flow distribution inside the evaporator. In this case, the 2D evaporator solver for heat transfer and fluid flow was employed. The procedure was similar to the one showed in Fig. 2.14 for the estimation of the off-design heat pump performance without considering maldistribution effects. The main differences were given by the additional input of the maldistribution rate, as well as by the additional unknowns and equations. In fact, a total of $N_{\mathrm{ch,ref}} + N_{\mathrm{ch,hs}} + 1$ unknowns were added to the four operating variables defined by the control values. These were given by the mass flow rate distribution of the refrigerant in the $N_{\mathrm{ch,ref}}$ channels, the mass flow rate distribution of the heat source in the $N_{\mathrm{ch,hs}}$ channels and the inlet vapour quality in the first channel x_{in}^{1} (the vapour quality at the other channels is then estimated by Eq. (2.38)). The additional required governing equations were the same explained in section 2.4, e.g. imposing equal pressure drop in each channel together with global mass conservation equations for refrigerant, heat source and refrigerant vapour phase.

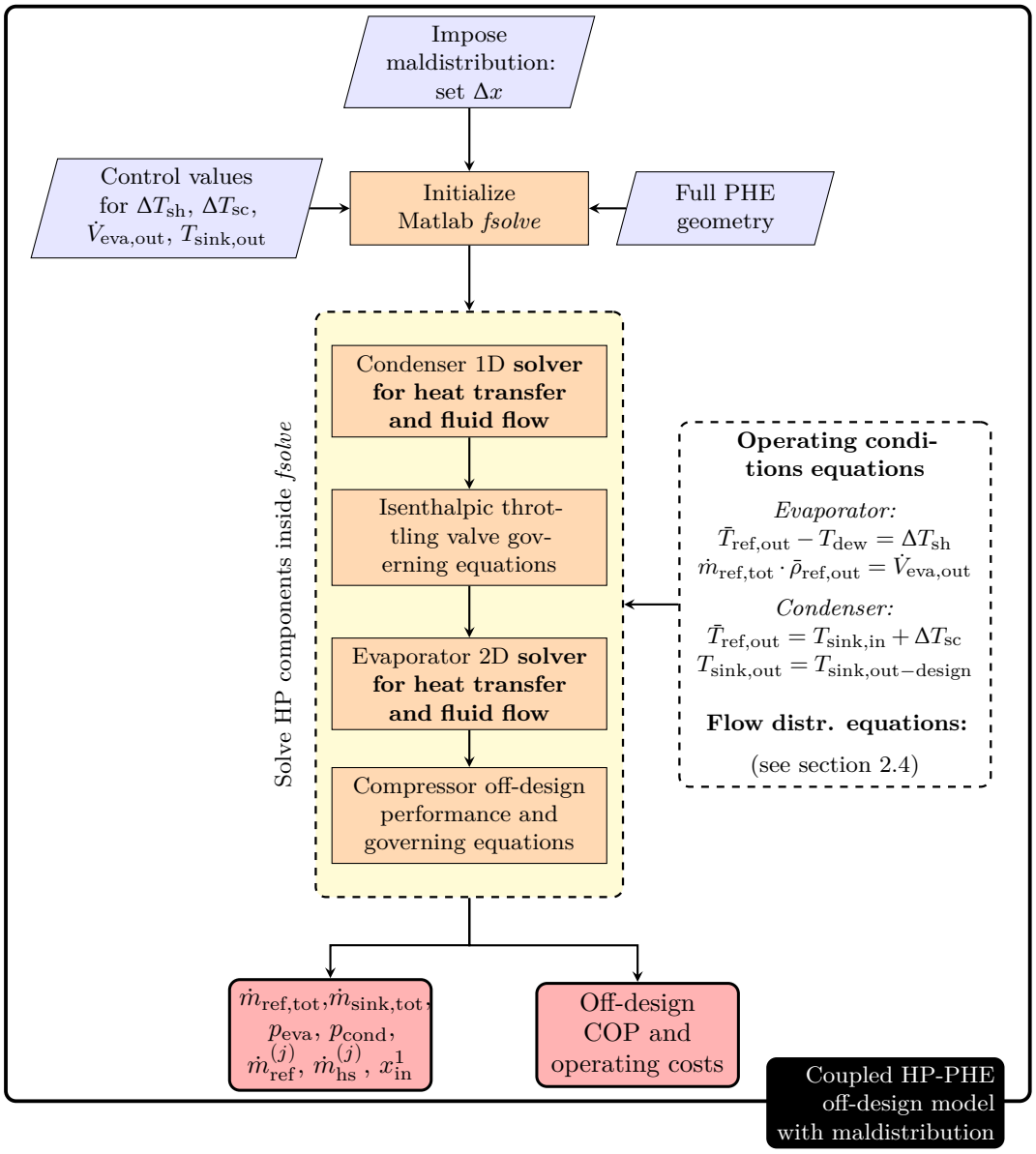

Figure 2.15: Work flow of the coupled off-design heat pump model and PHE performance models with maldistribution effects (2D evaporator model)

3 Heat transfer correlations for evaporation of zeotropic mixtures

This chapter presents the research work carried out with the aim of comparing different prediction methods to estimate the heat transfer coefficients of zeotropic mixtures in plate heat exchanger evaporators. The results were used to develop guidelines on the most suitable methods to predict the performance of PHE evaporators using zeotropic mixtures of natural refrigerants as working fluids. The chapter is based on [P3] and [C2].

3.1 Introduction

A comparison of prediction methods to estimate the heat transfer characteristics of zeotropic mixtures of natural refrigerants in PHE evaporators is presented in this chapter. A comprehensive literature review is carried out with the aim of defining available models from literature. The focus was given to evaporation studies in PHEs and to pool and flow boiling studies of zeotropic mixtures in horizontal and vertical plain tubes. After defining relevant prediction methods to investigate, a comparison against experimental data of CO_2/propane at different mass compositions is carried out. The comparison serves as a basis to define recommendations on the selection of appropriate prediction methods for zeotropic mixtures of natural refrigerants.

The chapter is structured as follows: section 3.2 presents a detailed literature survey. Section 3.3 describes the results of comparing different methods to the experimental data. Last, sections 3.4 and 3.5 present two sensitivity analysis for the choice of different correlations in the Silver [100] and Bell and Ghaly [101] method. The former study was focused on the impact of using different correction methods for the nucleate boiling contribution, while the latter investigated the impact of different correlations to compute convective boiling, nucleate boiling and vapour only contributions for a relevant case study.

3.2 Literature survey

This section presents a detailed literature survey on: (i) flow boiling correlations in PHEs and (ii) zeotropic mixtures and existing prediction methods for in-tube evaporation. The literature survey aims at presenting the prediction methods available in literature, which will be further analysed and compared to experimental data.

3.2.1 Evaporation heat transfer in plate heat exchangers

Heat transfer correlations for evaporation in PHEs are available in literature for different refrigerants and test conditions. Evaporation in PHEs is influenced by geometry, flow regime, working fluid thermo-physical properties, heat and mass fluxes, vapour quality range, and others, thus making the phenomenon particularly complex. Despite the large amount of experimental work carried out so far on plate evaporators, the majority of prediction methods was limited to the application for specific geometries, fluids and flow conditions [26].

Flow boiling is governed by three heat transfer mechanisms, namely nucleate boiling, two-phase convective boiling and single-phase and mist transfer to the vapour in the so-called drywall region, which potentially occurs at high vapour qualities depending on the magnitude of the heat flux. The latter mechanism is often neglected in prediction methods, and most of the available correlations are formulated by [28]:

$$h = [((h_{\mathrm{nb}} S_{\mathrm{nb}})^n + (h_{\mathrm{lo}} F_{\mathrm{cb}})^n)]^{1/n} \tag{3.1}$$

where the subscripts nb and lo represents the nucleate boiling and convective boiling contributions, respectively. S_{nb} indicates the nucleate boiling suppression factor accounting for suppression of nucleate boiling in flow boiling, due to force convective fluid flow, especially occurring at high mass fluxes. F_{cb} represents the enhancement factor of convective boiling, accounting for the higher two-phase heat transfer compared to liquid-only (subscript lo). When the exponent n is equal to 1, Eq.(3.1) is termed superposition model or Chen-type correlation [102]. Correlations in the form of Eq.(3.1) are widely available for in-tube flow boiling, yet Vakili-Farahani et al. [28] highlighted that in-tube flow boiling correlations do not well predict PHE heat transfer by substituting the tube diameter with the PHE hydraulic diameter, and PHE specific correlations must be instead utilized.

Eldeeb et al. [103] and Amalfi et al. [26] carried out comprehensive literature surveys on existing experimental correlations for flow boiling in PHEs. The most relevant work related to heat transfer correlations for evaporation in PHEs is reported hereafter.

Danilova et al. [104] developed a flow boiling correlation based on Reynolds number and Bond number, accounting for the ratio between gravitational and surface tension forces and defining the transition between macro and micro scale effects. They observed a high dependence of the heat transfer coefficient on the vapour quality and mass flux

that is typical of convective dominated boiling regimes. The effect of heat flux was accordingly lower. Yan and Lin [94] proposed a correlation based on data for R134a, and the two-phase Nusselt number was estimated as a function of both Reynolds and Boiling numbers. They however observed that the heat transfer is dominated by convection at high vapour quality, where the mass flux is the dominant parameter. On the other hand, high heat flux shows some effects at low vapour quality. Han et al. [105] investigated flow boiling of R410A and R22, testing three different chevron angles for the PHE. Their experimental correlation relates the heat transfer coefficient to the equivalent Reynolds number and Boiling number, by using the equivalent mass flux definition proposed by Akers et al. [106]. Palm and Claesson [95] concluded that heat transfer in PHEs is well correlated by pool boiling correlations, proposing to use the Cooper [107] correlation with a multiplication factor of 1.5. Another well known correlation to describe pool boiling was proposed by Gorenflo and Kenning [108], with a formulation taking into account properties of fluids, heating element and saturation pressure. Huang et al. [109] developed a correlation based on data for PHEs with three different chevron angles. A high dependence on heat flux was noted, while a weak dependence on vapour quality, mass flux and chevron angle was found, thus concluding that heat transfer is nucleate boiling dominated. Amalfi et al. [93] noted however that their correlation was based on a group that was not dimensionless. The afore-mentioned studies [94, 104, 105, 109] are regression correlations, i.e. the derivation was based on regression models using the experimental data sets and different non-dimensional groups. On the other hand, Palm and Claesson [95] and Gorenflo and Kenning [108] are pool boiling correlations, i.e. only the nucleate boiling contribution is taken into account, since it is assumed to dominate the heat transfer mechanism. A Chen-type correlation based on data for R410a was instead developed by Hsieh and Lin [110], where Dittus and Boelter [111] and Cooper [107] were proposed to estimate the liquid-only convective and pool boiling heat transfer coefficients, respectively. Longo et al. [112] developed instead a correlation to estimate the average boiling heat transfer coefficient, computed as the maximum between the convective boiling and nucleate boiling contributions. Two regression models were recently derived by Amalfi et al. [93] and Ayub et al. [113], considering larger dataset collected from literature, containing several refrigerants, geometries and operating conditions.

None of the correlations presented in this section, which were specifically developed for PHEs, included data for zeotropic mixtures, with the exception of ammonia/water, which however presents very large temperature glides and very different properties compared to natural refrigerants. The only additional mixtures considered in the experimental campaigns were the near-azeotropic mixture R410a and the azeotropic mixture R507. The following section further elaborates on the reasons why the prediction methods for pure fluids are not directly applicable to refrigerant mixtures.

Table 3.1 reports the formulation of four correlations, which are indicated as the most relevant and recent studies in the context of the flow boiling in PHEs.

Table 3.1: Some relevant PHE flow boiling correlations

Authors and reference	Correlation	
Hsieh and Lin [110]	$h = h_{\mathrm{nb}} S_{\mathrm{nb}} + h_{\mathrm{lo}} F_{\mathrm{cb}}$	(3.2)
	$h_{\mathrm{lo}} = 0.023 Re_{\mathrm{lo}}^{0.8} Pr_l^{0.4} (k_l / D_h)$	(3.3)
	$h_{\mathrm{nb}} = 55 p_{\mathrm{red}}^{0.12} (-\log_{10} p_{\mathrm{red}})^{-0.55} M^{-0.5} \dot{Q}''^{0.67}$	(3.4)
	$F_{\mathrm{cb}} = 1 + 24000 \cdot \mathrm{Bo}^{1.16} + 1.37 \left(\frac{1}{X_{\mathrm{tt}}}\right)^{0.86}$	(3.5)
	$S_{\mathrm{nb}} = \left(1 + 1.15 \cdot 10^{-6} F_{\mathrm{cb}}^2 \mathrm{Re}_{\mathrm{lo}}^{1.17}\right)^{-1}$	(3.6)
Longo et al. [112]	$h = \max(h_{\mathrm{nb}}, h_{\mathrm{cb}})$	(3.7)
	$h_{\mathrm{cb}} = 0.122 \Phi \mathrm{Re}_{\mathrm{eq}}^{0.8} \mathrm{Pr}_l^{1/3}$	(3.8)
	$\mathrm{Re}_{\mathrm{eq}} = \frac{G_{\mathrm{eq}} D_h}{\mu_l}, \quad G_{\mathrm{eq}} = G\left[(1-x) + x\left(\frac{\rho_l}{\rho_v}\right)^{1/2}\right]$ $h_{\mathrm{nb}} = h_0 \cdot 0.58 \cdot \Phi \cdot \left(\frac{\mathrm{Ra}}{\mathrm{Ra}_0}\right)^{2/15} \cdot F_p(p_{\mathrm{red}}) \cdot \left(\frac{\dot{Q}''}{\dot{Q}_0''}\right)^{0.467}$ $F_p = 1.2 \cdot p_{\mathrm{red}}^{0.27} + \left(2.5 + \frac{1}{1-p_{\mathrm{red}}}\right) p_{\mathrm{red}}$ $p_{\mathrm{red},0} = 0.1, \quad \dot{Q}_0'' = 20 \ \mathrm{kW/m^2}, \quad \mathrm{Ra}_0 = 0.4 \ \mu\mathrm{m}$	(3.9)
Amalfi et al. [93]	$h = 982 \cdot \left(\frac{\theta}{70^\circ}\right)^{1.101} \mathrm{We}_m^{0.326} \mathrm{Bo}^{0.320} \left(\frac{\rho_l}{\rho_v}\right)^{-0.224} \cdot \left(\frac{k_l}{D_h}\right), \quad \mathrm{Bd} < 0.4$	(3.10)
	$h = 18.495 \cdot \left(\frac{\theta}{70^\circ}\right)^{0.248} \mathrm{Re}_v^{0.135} \mathrm{Re}_{\mathrm{lo}}^{0.351} \mathrm{Bd}_m^{0.235} \mathrm{Bo}^{0.198} \left(\frac{\rho_l}{\rho_v}\right)^{-0.223} \cdot \left(\frac{k_l}{D_h}\right), \quad \mathrm{Bd} \geqslant 0.4$	(3.11)
Ayub et al. [113]	$h = \left(\frac{k_l}{D_h}\right)\left(1.8 + 0.7\frac{\theta}{65^\circ}\right) \mathrm{Re}_{\mathrm{eq}}^{(0.49 - 0.36\sigma^*)} \mathrm{Bo}_{\mathrm{eq}}^{-0.2}$	(3.12)
	$\mathrm{Bo}_{\mathrm{eq}} = \frac{\dot{Q}''}{G_{\mathrm{eq}} h_{\mathrm{lat}}}, \quad \mathrm{Re}_{\mathrm{eq}} = \frac{G_{\mathrm{eq}} D_h}{\mu_l}, \quad G_{\mathrm{eq}} = G\left[(1-x) + x\left(\frac{\rho_l}{\rho_v}\right)^{1/2}\right]$	
	$\sigma^* = \sigma_{\mathrm{ref}} / \sigma_{\mathrm{NH_3}}$	

3.2.2 Zeotropic mixtures

Zeotropic mixtures are blends of two or more components with different composition of liquid and vapour phases at thermodynamic equilibrium, thus undergoing a temperature glide during phase change. Zeotropic mixtures experience a degradation of heat transfer compared to concentration weighted pure counterparts, with respect to both nucleate and two-phase convective boiling. Nucleate boiling is mainly affected by the bubble growing mechanism and effective wall superheat. The evaporation of the more volatile component (i.e. the one with the lowest boiling point) creates a region around the bubble (at the liquid/vapour interface) that is richer in the less volatile component, thus increasing the

saturation temperature and decreasing the effective wall superheat driving the nucleation process. The region around the bubble, depleted of the most volatile component, entails the formation of an additional mass diffusion resistance, further deteriorating the heat transfer [114]. Degradation of heat transfer for two-phase convective boiling mostly occurs due to additional sensible heat, which must be provided to both liquid and vapour phases to increase the saturation temperature along the flow direction [115]. Additionally, Jung et al. [89, 90] claimed that up to 80 % of the overall heat transfer degradation compared to the ideal coefficient computed using the mixing rule, is determined by the large variation of refrigerant physical properties during evaporation, due to the varying liquid and vapour phases compositions. The degradation was measured experimentally for R22/R114 and R12/R152a mixtures at different mass fractions. Last, worse transport properties compared to pure fluids is an additional contribution to the heat transfer degradation [114]. Both nucleate and two-phase convective boiling contribute to the degradation of heat transfer coefficient during flow boiling of zeotropic mixtures, and appropriate corrections must be applied to extend the pure fluid correlations to mixtures. Previous studies proposed heat transfer correlations for both flow boiling and pool boiling of zeotropic mixtures in horizontal tubes.

In-tube flow boiling of zeotropic mixtures

In this paragraph, a literature review on the most relevant studies on predicting the heat transfer coefficients of zeotropic mixtures during in-tube flow boiling is presented.

Thome [115] proposed to modify two well-know correlations for pure fluids, namely Gungor and Winterton [116, 117], to account for mixture effects. The former correlation [116] is a superposition model where the Cooper [107] and Dittus and Boelter [111] correlations are suggested to estimate the nucleate and convective boiling contributions, respectively. Thome [115] introduced a mixture correction factor for the nucleate boiling term, in order to model the additional mass diffusion resistance.

In Gungor and Winterton (1986) [116], the correlation for mixture is applied by Eq.(3.13) [115]:

$$h = h_{\mathrm{nb}} S_{\mathrm{nb}} F_c + h_l E_0 \tag{3.13}$$

Thome [115] reccomended the use of Stephan and Abdelsalam [118] to compute h_{nb}, differently from the original formulation based on the use of Cooper [107]. E_0 and S_{nb} are estimated by the original correlation using Eq.(3.14) and (3.15), respectively [116].

$$E_0 = 1 + 24000 \cdot \mathrm{Bo}^{1.16} + 1.37 \left(\frac{1}{X_{\mathrm{tt}}} \right)^{0.86} \tag{3.14}$$

$$S_{\mathrm{nb}} = \frac{1}{1 + 1.15 \cdot 10^{-6} E_0^2 Re_l^{1.17}} \tag{3.15}$$

Here, X_{tt} is the Martinelli parameter, computed by [116]:

$$X_{\mathrm{tt}} = \left(\frac{1-x}{x}\right)^{0.9} \left(\frac{\rho_v}{\rho_l}\right)^{0.5} \left(\frac{\mu_l}{\mu_v}\right)^{0.1} \tag{3.16}$$

In Eq.(3.13) F_c indicates the mixture correction factor and it is estimated by the correlation introduced by Thome and Shakir [119]. Note that different correlations can be chosen in literature for the computation of F_c, and this will be further introduced in the following subsection.

In 1987 Gungor and Winterton [117] proposed an enhancement-type simplified correlation requiring less calculation steps compared to the original form and based on the replacement of the nucleate boiling term with a simpler expression that is a function of the convective term, as:

$$h = E h_l \tag{3.17}$$

where E takes both convective and nucleate boiling contributions into account. Thome [115] suggested the modification of the enhancement factor E as in Eq.(3.18), using the mixtuere correction factor F_c to reduce the Boiling number Bo.

$$E = 1 + 3000 \cdot (\mathrm{Bo} F_c)^{0.86} + 1.12 \left(\frac{x}{1-x}\right)^{0.75} \left(\frac{\rho_l}{\rho_v}\right)^{0.41} \tag{3.18}$$

The two correlations by Gungor and Winterton [116, 117] were originally developed for pure fluids and later modified to model mixture effects. Other prediciton methods were directly developed for specific working fluid mixtures. In this regard, Jung et al. [89] and Wettermann and Steiner [120] are two well-known specific correlations for in-tube flow boiling. Jung et al. [89] was developed based on data for R22/R114 and R12/R152a, and the heat transfer coefficient is computed as:

$$h = C_{\mathrm{me}} F h_l + \frac{S_{\mathrm{nb}}}{C_{\mathrm{un}}} h_{\mathrm{pool}} \tag{3.19}$$

Two mixture correction factors are defined as C_{me} and C_{un}, for convective and nucleate boiling, respectively. C_{me} is based on the molar fraction in the liquid and vapour phases of the most volatile component of the mixture, accounting for the mass transfer resistance between the two phases in the convective boiling region. h_{pool} and C_{un} are computed as suggested by Ünal [121]. Stephan and Abdelsalam [118] is recommended for the ideal nucleate boiling coefficient.

Wettermann and Steiner [120] developed a specific correlation based on data for R116/R134a, with the aim of characterizing the heat transfer degradation of "wide-boiling" mixtures, i.e. with temperature glides higher than 5 K [122]. Grauso et al. [122] compared several methods to predict heat transfer performance of wide boiling mixtures against experimental data for in-tube horizontal boiling of CO_2/propane blends. They found that the correlation developed by Wettermann and Steiner [120] performed better compared with other methods to predict their database, R116/R134a and CO_2/propane data from Cho et al. [123], with 60.8 % data points included within ± 30 % error. Wettermann and Steiner [120] used the onset of nucleate boiling, i.e. when the heat flux is lower than the onset the nucleate boiling contribution is neglected. Furthermore, the asymptotic model (Eq.(3.1) with $n = 3$) was used, where the suppression S_{nb} is commonly set equal to 1. The ideal nucleate boiling heat transfer coefficient was corrected to account for mixture degradation by a factor F_c, as proposed by [119]. The correlation proposed by Steiner and Kind [124] was recommended to compute the pure fluid components nucleate boiling contribution. The two-phase convective contribution was instead estimated by applying Dittus and Boelter [111] for the liquid-only heat transfer coefficient, and the enhancement factor F_{cb} was calculated by:

$$F_{\mathrm{cb}} = \left((1-x)^{0.01} \left[(1-x) + 1.2x^{0.4} \left(\frac{\rho_l}{\rho_v} \right)^{0.37} \right]^{-2.2} + \ldots \right.$$
$$\left. \ldots + x^{0.01} \left[\frac{h_{\mathrm{vo}}}{h_{\mathrm{lo}}} \left(1 + 8(1-x)^{0.7} \cdot \left(\frac{\rho_l}{\rho_v} \right)^{0.67} \right) \right]^{-2} \right)^{-0.5} \tag{3.20}$$

where x represents the vapour quality, l and v denote liquid and vapour phases, and lo and vo indicate liquid-only and vapour-only parameters, assuming the mass flowing entirely as liquid and vapour, respectively.

Two theoretical models can also be found in literature. One was developed by Silver [100] and Bell and Ghaly [101], with the original derivation carried out for annular condensation. A later work by Sardesai et al. [125] extended the utilization of this method to mixture evaporation, and the following formulation of the mixture heat transfer coefficient was obtained:

$$h = \frac{1 + \dfrac{F_c h_{\mathrm{nb}}}{h_{\mathrm{cb}}}}{\dfrac{1}{h_{\mathrm{cb}}} + \dfrac{Z}{h_{\mathrm{vo}}}} \tag{3.21}$$

In Eq.(3.21), the nucleate boiling heat transfer contribution must be corrected by an appropriate correction factor F_c, taking into account mixture degradation, e.g. the correlation by Thome and Shakir [119]. h_{cb} must be estimated by a convective boiling correlation and h_{vo} is the vapour phase heat transfer coefficient, estimated by considering the vapour flowing alone in the entire channel. Z is expressed by Eq.(3.22), as a function

of vapour quality, slope of evaporation curve and vapour specific heat capacity [100].

$$Z = q\frac{dT}{dh}c_{\mathrm{p,v}} \tag{3.22}$$

Z indicates the rate of sensible heat transfer over the total heat load, thus accounting for the heat loss due to the increase of saturation temperature during the evaporation process.

In the work by Shah [126], a different extension of the Silver [100] and Bell and Ghaly [101] method is proposed to evaporation. The heat transfer coefficient is computed by:

$$h = F_c h_{\mathrm{nb}} + \left(\frac{1}{h_{\mathrm{cb}}} + \frac{Z}{h_{\mathrm{vo}}}\right)^{-1} \tag{3.23}$$

where all the terms are analogous to Eq.(3.21), yet arranged in a different manner. Despite Shah [126] was developed as a theoretical method, thus any correlations can be chosen to compute h_{cb}, h_{nb} and h_{vo}, in their original paper some correlations to compute h_{cb} were compared to experimental data, while Dittus and Boelter [111] and Cooper [107] were suggested to evaluate the single-phase and ideal nucleate boiling heat transfer coefficients.

As a last work relevant to mention, Zhang et al. [127] proposed a correlation based on multiple regression of dimensionless numbers defined by the Buckingham π theorem, with the formulation:

$$h = 20.1439 \cdot \mathrm{Re}_l^{0.1505}\mathrm{Re}_{\mathrm{vo}}^{0.4551}\mathrm{Bo}^{0.5580}\mathrm{Fr}_v^{0.2538}T^{*-1.1466}Q^{*1.1084}\frac{k_l}{D_h}, T^* \leq 0.06 \tag{3.24}$$

$$h = 0.1672 \cdot \mathrm{We}_l^{-0.1457}\mathrm{Re}_l^{0.4771}\mathrm{Re}_{\mathrm{vo}}^{0.1829}\mathrm{Fr}_v^{0.1007}T^{*-0.2490}Q^{*-0.4878}\frac{k_l}{D_h}, T^* > 0.06 \tag{3.25}$$

where Q^* is defined as the ratio between sensible heat and latent heat and T^* represents a non-dimensional temperature glide, normalized by the saturation temperature. Their correlation is based on 2091 experimental data points from 22 independent research groups. Their proposed correlation, expressed by Eq.(3.24) and (3.25), achieved an agreement of 24.6 % against the entire experimental database. Note that the data only included evaporation in horizontal tubes. They identified two additional methods leading to good agreements with the data, e.g. the correlation by Gungor and Winterton [117] (Eq.(3.17)) with the correction to account for mixture degradation proposed by Thome [115] (49.0 %) and the method proposed by Shah [126] with the convective boiling correlation for pure fluids by Gungor and Winterton [117] (47.3 %).

Correction factor for nucleate boiling

As highlighted in the previous subsection, prediction methods for zeotropic mixtures require the computation of a correction factor F_c to take mixture degradation of nucleate boiling into account. Thome and Shakir [119] was mentioned as one widely used correlation, suggested by Thome [115], Wettermann and Steiner [120] and Shah [126]. Kærn et al. [128] carried out an extensive review of methods, focusing on correlations used for ammonia/water mixtures. Table 3.2 reports some relevant works. In Stephan and Körner [129], Jungnickel et al. [130] and Schlunder [131] the difference in molar composition of the most volatile component is used in order to take the mass diffusion resistance into account (note that the most volatile component is indicated as 1). In the correlation by Stephan and Körner [129], the parameter A_0 was fitted from experimental data for different mixtures, and values between 0.42 and 3.56 were obtained. Fujita and Tsutsui [132] recommends to use the average value of 1.53 for mixtures that are not included in the experimental database. In the correlation by Jungnickel et al. [130] instead, the parameter K_0 was found fitting the data for five freon mixtures and correlating it to the difference in normal boiling points of the two components. ΔT_{bp} indicates the mixture temperature glide, i.e. the difference between bubble and dew temperature at the given saturation pressure. It is used in Thome and Shakir [119], Fujita and Tsutsui [132, 133] and Inoue et al. [134]. Compared to the widely used correlation by Thome and Shakir [119], Fujita and Tsutsui [132, 133] claimed to correlate the experimental data points better at higher heat fluxes, for which a higher degradation of heat transfer was estimated.

In order to apply the correction factors reported in Table 3.2, the ideal nucleate boiling heat transfer coefficient must be evaluated, and two different approaches can be adopted. The former consists of estimating the ideal coefficient by using a pure fluid correlation, e.g. Cooper [107], using mixture properties. This approach was used in the Silver [100] and Bell and Ghaly [101] method, in both correlations by Gungor and Winterton [116, 117], and by Shah [126]. The latter consists of estimating the ideal nucleate boiling heat transfer coefficient as a function of the heat transfer coefficients of the two components. The formulation is based on the ideal nucleate boiling heat transfer coefficient as:

$$\frac{1}{h_{\mathrm{nb,id}}} = \frac{y_{l,1}}{h_{\mathrm{nb},1}} + \frac{y_{l,2}}{h_{\mathrm{nb},2}} \tag{3.26}$$

where h_{nb} is estimated by a pure fluid correlation and y is the molar fraction of the components in the liquid phase. This latter method was implemented in the correlations by Jung et al. [89] and Wettermann and Steiner [120]. The same approach is also adopted by Fujita and Tsutsui [132, 133] and Inoue et al. [134], where an ideal temperature difference ΔT_{id}, i.e. ideal wall superheat, is derived. The formulation is given by Eq.(3.28), which is obtained by substituting the definition of ΔT_1 and ΔT_2 of Eq.(3.27) inside Eq.(3.26).

$$\begin{aligned} \Delta T_1 &= \dot{Q}'' / h_{\mathrm{nb},1} \\ \Delta T_2 &= \dot{Q}'' / h_{\mathrm{nb},2} \end{aligned} \tag{3.27}$$

The value of ΔT_{id} is thus given by:

$$\Delta T_{\mathrm{id}} = y_{l,1}\Delta T_1 + y_{l,2}\Delta T_2 \tag{3.28}$$

Note that this latter method fails if boiling occurs between the critical pressures of each components, thereby making the first approach more generally applicable [128].

Table 3.2: Nucleate boiling correction factors for mixtures $F_c = h_{\mathrm{nb}}/h_{\mathrm{nb,id}}$

Authors and reference	Correlation
Stephan and Körner [129]	$\frac{h_{\mathrm{nb}}}{h_{\mathrm{nb,id}}} = \left[1 + A_0 \left\lvert y_{v,1} - y_{l,1} \right\rvert (0.88 + 0.12p)\right]^{-1}$ (3.29)
Jungnickel et al. [130]	$\frac{h_{\mathrm{nb}}}{h_{\mathrm{nb,id}}} = \left[1 + K_0 \left\lvert y_{v,1} - y_{l,1} \right\rvert \left(\frac{\rho_v}{\rho_l}\right) \dot{Q}''^{0.48+0.1y_{v,1}}\right]^{-1}$ (3.30)
Schlunder [131]	$\frac{h_{\mathrm{nb}}}{h_{\mathrm{nb,id}}} = \left(1 + \frac{h_{\mathrm{nb,id}}}{\dot{Q}''} \left\lvert T_{s,1} - T_{s,2} \right\rvert \left\lvert y_{v,1} - y_{l,1} \right\rvert \left[1 - \exp\left(\frac{-B_0 \dot{Q}''}{\rho_l h_{\mathrm{lat}} \beta_l}\right)\right]\right)^{-1}$, (3.31)
	$B_0 = 1, \beta_l = 0.0002\mathrm{m/s}$
Thome and Shakir [119]	$\frac{h_{\mathrm{nb}}}{h_{\mathrm{nb,id}}} = \left(1 + \frac{h_{\mathrm{nb,id}}}{\dot{Q}''} \Delta T_{\mathrm{bp}} \left[1 - \exp\left(\frac{-B_0 \dot{Q}''}{\rho_l h_{\mathrm{lat}} \beta_l}\right)\right]\right)^{-1}, B_0 = 1, \beta_l = 0.0003\,\mathrm{m/s}$ (3.32)
Fujita and Tsutsui [132]	$\frac{h_{\mathrm{nb}}}{h_{\mathrm{nb,id}}} = \left(1 + \frac{\Delta T_{\mathrm{bp}}}{\Delta T_{\mathrm{id}}} \left[1 - 0.8 \exp\left(\frac{\dot{Q}''}{10^5}\right)\right]\right)^{-1}$ (3.33)
Fujita and Tsutsui [133]	$\frac{h_{\mathrm{nb}}}{h_{\mathrm{nb,id}}} = \left(1 + \frac{\Delta T_{\mathrm{bp}}}{\Delta T_{\mathrm{id}}} \left[1 - \exp\left(\frac{-60 \dot{Q}''}{\rho_v h_{lat}} \left(\frac{\rho_v^2}{\sigma g (\rho_l - \rho_v)}\right)^{1/4}\right)\right]\right)^{-1}$ (3.34)
Inoue et al. [134]	$\frac{h_{\mathrm{nb}}}{h_{\mathrm{nb,id}}} = \left(1 + \frac{\Delta T_{\mathrm{bp}}}{\Delta T_{\mathrm{id}}} \left[1 - 0.75 \exp\left(\frac{-0.75 \dot{Q}''}{10^5}\right)\right]\right)^{-1}$ (3.35)

3.3 Comparison of prediction methods against experimental data

The literature survey in section 3.2 presented a review of the existing methods to predict the performance of refrigerants evaporating in PHEs, as well as correction methods and correlations for zeotropic mixtures evaporating in tubular geometries. This section presents the comparison of some of the presented methods against experimental data of zeotropic mixutures of CO_2/propane at different mass composition and operating conditions in PHEs. The correlations chosen for further investigation are reported in Table 3.3. They are divided in four categories. PHE specific correlations refer to flow boiling studies in PHEs, without accounting for mixture effects on the degradation of heat transfer. Theoretical models refer to the Silver [100] and Bell and Ghaly [101] methods, with different correlations chosen to compute nucleate, convective and single-phase contributions. Despite Amalfi et al. [93] was developed as an enhancement model taking into account both effects of convective and nucleate boiling contributions, it was decided to use it as a method to compute h_{cb}, due to the lack of alternative correlations developed for two-phase convective boiling in PHEs. Moreover, the authors noted a dominating effect of mass flux and vapour quality compared to heat flux on the heat transfer coefficient, thereby making two-phase convective boiling as the dominant heat transfer mechanism in their model. In-tube flow boiling correlations for mixtures were chosen as general correlations developed for tubular geometries. Both Gungor and Winterton [116, 117] models were considered with different choices on the correlation to use to compute the nucleate boiling contribution. Last, the PHE specific correlations chosen for the analysis were additionally corrected in order to account for the degradation of heat transfer in nucleate boiling. This was done by multiplying the boiling number Bo by the correction factor F_c in the correlations by Amalfi et al. [93] and Ayub et al. [113], which are enhancement models and the dependence on the heat flux was considered by the non-dimensional group Bo. In Longo et al. [112] and Hsieh and Lin [110], where two contributions are accounted for separately, F_c was directly multiplied to the nucleate boiling heat transfer coefficient h_{nb}.

The comparison between prediction methods was carried out by estimating the overall evaporator performance using the PHE model discretized in 1D. The correlations were implemented to compute the local values of heat transfer coefficient. The total heat flow rate calculated by the model was compared to the experimental value, with the model receiving as input the full PHE geometry and the inlet thermodynamic state of refrigerant and secondary fluid.

This section is structured as follow: subsection 3.3.1 presents the experimental test-rig and the data reduction procedure used for the analysis. Subsection 3.3.2 briefly explains the PHE model used for the analysis with related settings, subsection 3.3.3 introduces the main results, which are further discussed in subsection 3.3.5.

Table 3.3: Correlations chosen for further analysis

PHE specific correlations				
Hsieh and Lin [110]				
Longo et al. [112]				
Amalfi et al. [93]				
Ayub et al. [113]				
Theoretical models				
Method	h_{cb}	h_{nb}	F_c	h_{vo}
Silver [100]/Bell and Ghaly [101]	Amalfi et al. [93]	Cooper [107]	Thome and Shakir [119]	Martin [77]
Shah [126]	Gungor and Winterton [117]	Cooper [107]	Thome and Shakir [119]	Dittus and Boelter [111]
Shah [126]	Amalfi et al. [93]	Cooper [107]	Thome and Shakir [119]	Martin [77]
In-tube flow boiling correlations for mixtures				
Correlation		h_{nb}	F_c	
Gungor and Winterton [116]		Cooper [107]	Thome and Shakir [119]	
Gungor and Winterton [116]		Stephan and Abdelsalam [118]	Thome and Shakir [119]	
Gungor and Winterton [117]		Cooper [107]	Thome and Shakir [119]	
Gungor and Winterton [117]		Stephan and Abdelsalam [118]	Thome and Shakir [119]	
Jung et al. [89]				
Wettermann and Steiner [120]				
Zhang et al. [127]				
PHE specific correlations - corrected				
Correlation			F_c	
Hsieh and Lin [110]			Thome and Shakir [119]	
Longo et al. [112]			Thome and Shakir [119]	
Amalfi et al. [93]			Thome and Shakir [119]	
Ayub et al. [113]			Thome and Shakir [119]	

3.3.1 Experimental apparatus and data reduction

Fig.3.1 reports a sketch of the test-rig together with a picture of the experimental bench. It includes a variable speed scroll compressor, brazed PHE gas cooler, brazed PHE evaporator, internal HEX with liquid receiver and an electronic expansion valve. The measurements of temperatures were made using calibrated thermocouples, while pressure transmitters and Coriolis flow meters were used for pressure and mass flow rate measurements. The mixture composition was detected using gas chromatography analysis. Table 3.4 reports the values of all the geometrical parameters of the PHE used in the experimental apparatus as evaporator. The PHE was comprises by a total of 8 plates, with 3 refrigerant channels (upward flow) and 4 heat source channels (downward flow). The heat source was given by a mixture of ethylene glycol/water at (0.32/0.68) mass composition.

The experimental data were subsequently elaborated to obtain inlet and outlet conditions of the refrigerant at the evaporator, as well as the total heat flow rate. Since both refrigerant inlet and outlet may be in saturated conditions, the thermodynamic state points were estimated from the other components. The evaporator inlet was calculated by considering an isenthalpic expansion from the throttling valve. The thermodynamic state at the inlet of the throttling valve was in fact known by measured values of temperature and pressure. The outlet state was thus estimated using the pressure value measured at the evaporator inlet. The evaporator outlet was instead calculated by an energy balance on the internal HEX (IHEX) (see Fig. 3.1). The total heat flow rate at the evaporator

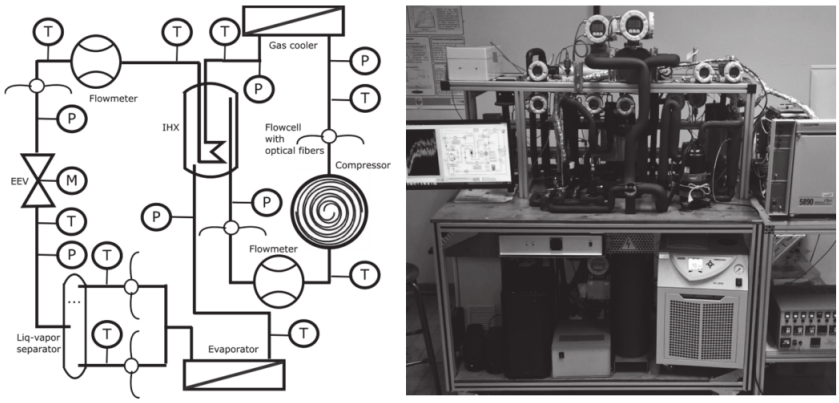

Figure 3.1: Schematic of the test facility and experimental bench [96]

was estimated by using the measured values of the ethylene glycol/water mixture, as:

$$\dot{Q}_{\mathrm{eva,exp}} = \dot{m}_{\mathrm{hs}} \bar{c}_{\mathrm{p,hs}} (T_{\mathrm{hs,in}} - T_{\mathrm{hs,out}}) \tag{3.36}$$

The data were collected at different conditions and mass fraction of CO_2/propane: 133 steady state measurements were considered in total. By varying the CO_2/propane composition, different temperature glides were obtained. Fig.3.2 shows the number of experimental data points included in three different ranges of temperature glide of the mixture. Mixtures experiencing lower glides, e.g. in the range 0 K - 5 K, are expected to behave more similarly to pure fluids compared to mixture having larger glides. In fact, for increasing glides, a larger amount of heat must be provided as sensible component to both liquid and vapour phases to increase the saturation temperature, as the more volatile component starts evaporating. The data included a larger number of data points in the lower range of glides.

Table 3.4: Geometrical data of the PHE

Parameter	Unit	Value
W	m	0.120
L_{ht}	m	0.329
t	mm	5.0
β	°	35
b	mm	2.0
Λ	mm	7.0
$N_{\mathrm{ch,ref}}$	-	3
D_h	mm	3.4
$A_{\mathrm{ht,tot}}$	m^2	0.28

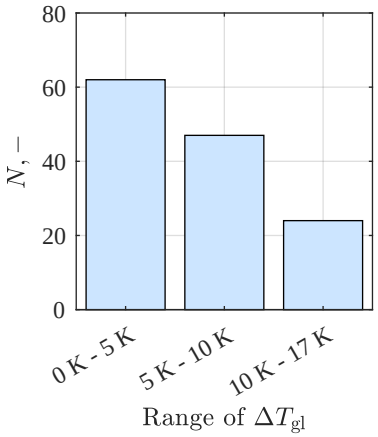

Figure 3.2: Distribution of ΔT_{gl} of the considered experimental points

The comparison between model and experimental data was carried out by comparing experimental and simulated heat flow rate, in terms of mean relative error and mean absolute error, previously introduced by Eq.(2.40) and (2.41).

3.3.2 PHE model

The comparison was carried out by using the PHE model discretized in 1D, presented in chapter 2.2. The model was run with $n = 100$ slices along the flow direction and tolerance set to 10^{-5}. The local values of heat transfer coefficient and pressure drop were estimated by following the approach presented in chapter 2.2.6. The single-phase heat transfer coefficient of the heat source was estimated by Martin [77]. The experimental data points contained also data with superheated refrigerant outlet. Therefore, the mixture heat transfer coefficient in the single-phase region was also estimated by Martin [77]. Frictional pressure drops were calculated by estimating the Fanning friction factor using Amalfi et al. [93] and Martin [77], for the two-phase and single-phase flow, respectively. The void fraction was estimated by Smith [84]. Note, that the discretized PHE model was validated first against experimental data of pure CO_2, collected at the same test-rig with the same evaporator geometry. The validation was presented in Chapter 2.5.4.

3.3.3 Results

Fig.3.3 reports the comparison between experimental and calculated total heat flow rate for all the 133 experimental points collected for CO_2/propane. The different sub-figures (a-e) illustrate the outcome for the different chosen prediction methods (see Table 3.3),

divided into different sub-categories: PHE specific correlations (a), theoretical methods (b), general correlations for mixture in-tube flow boiling (c-d) and PHE correlations with corrected nucleate boiling contribution (e). The values of mean relative and absolute errors for each method, including all the points, define the goodness of the match between the data and the models, and they are reported in Table 3.5 with bold values. Table 3.5 additionally reports the mean absolute error considering the data points included in the three different temperature glide intervals (see Fig.3.2).

Fig.3.3 (a), (b) and (e) prove that PHE specific correlations (corrected or not) and theoretical methods showed the best agreement with experimental data. Theoretical methods report slightly lower deviation, with Shah [126] (G&W) and Silver [100] and Bell and Ghaly [101] both resulting in the lowest mean absolute error of 3.4 %. In particular, using the Silver [100] and Bell and Ghaly [101] method leads to a a slight overestimation of the heat transfer coefficient, equal to +2.7 %. On the other hand, Amalfi et al. [93] resulted in the best match among the PHE specific correlations, with an absolute error equal to 3.7 % and a relative underestimation of -0.1 %. The slightly better performance of the former method is related to the mixture degradation of heat transfer, increasing for higher glides, which is not taken into account in the PHE correlations. In fact, looking at the relative errors reported in Table 3.5, all the PHE specific correlations showed increasing errors for increasing temperature glides. Amalfi et al. [93], for instance, starts with underestimating the heat flow rate at -2.5 % for mixtures with lower glides, e.g. with behaviour similar to pure fluids. If the glide is increased, the correlation is then slightly overestimating the performance, with a maximum of 5.5 % for the points with the highest glides. On the other hand, Silver [100] and Bell and Ghaly [101] always slightly overestimated the performance, with no particular trend found depending on the mixture glide. The Shah [126] method resulted in different behaviours depending on the correlation applied to compute the convective contribution: by applying Gungor and Winterton [117] the performance is underestimated, due to the fact the PHE geometry is not properly described by the model. By applying PHE specific correlation instead, the performance is slightly overestimated with a mean relative error equal to + 3.6 %.

PHE specific correlations were also considered if the nucleate boiling contribution is corrected by a factor F_c, and the match is reported in the last rows of the table. All correlations show anyway a good agreement with experimental data, and in this case no trend of increasing absolute deviation can be detected. Since the deviations remained low for all correlations, the convective contribution to heat transfer must be the dominating mechanism for these experimental data points, and correcting the nucleate boiling contribution does not lead to a better match.

Fig.3.3 (c) and (d) report the comparison for mixture general correlations. The general correlation by Gungor and Winterton [116] reported low mean absolute errors, respectively equal to 4.1 % and 9.3 %, depending on the use of Cooper [107] or Stephan and Abdelsalam [118] correlations for the computation of the nucleate boiling contribution to heat transfer. The better performance obtained by Cooper [107] well agrees with previous

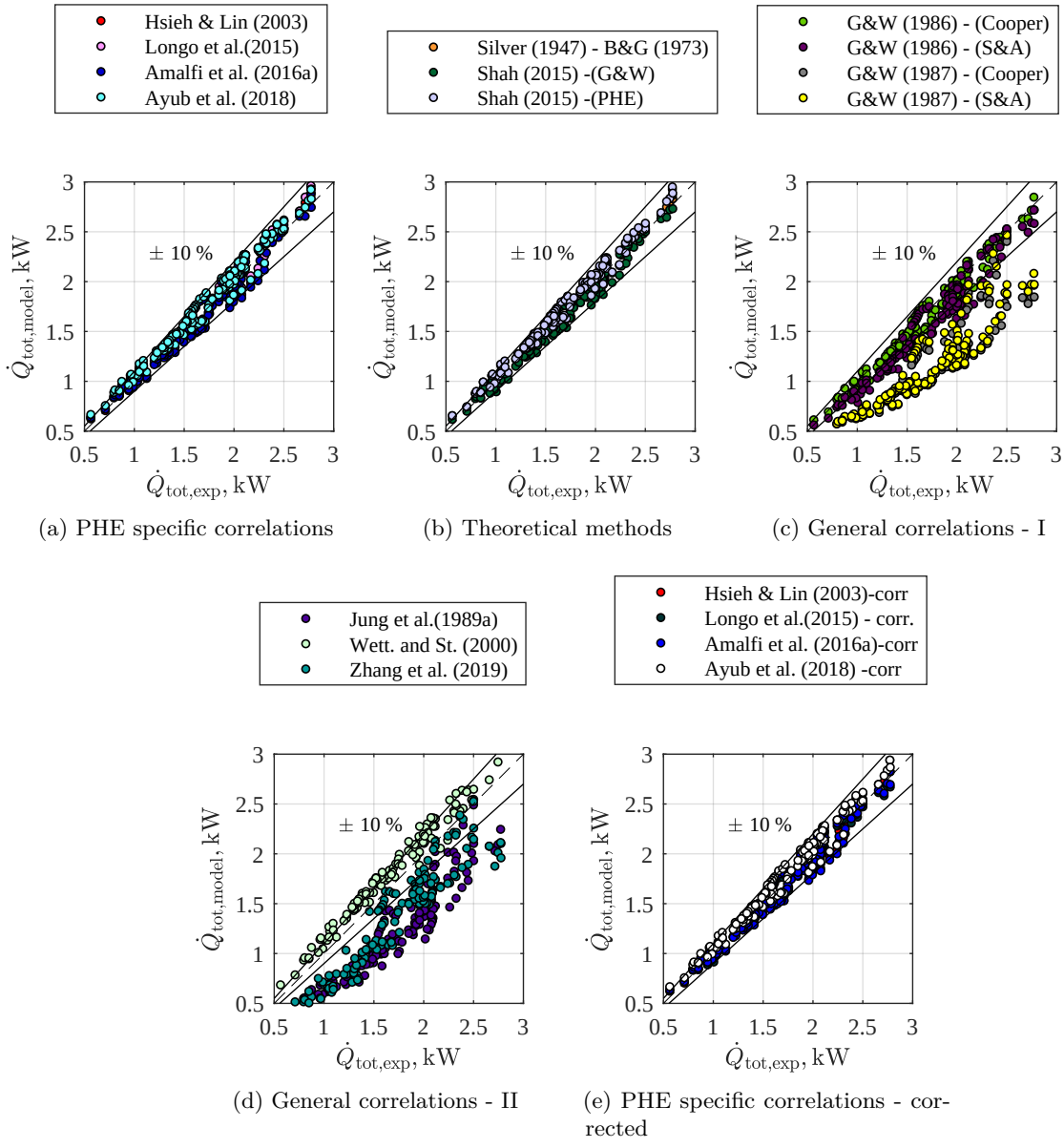

(a) PHE specific correlations (b) Theoretical methods (c) General correlations - I

(d) General correlations - II (e) PHE specific correlations - corrected

Figure 3.3: Comparison of experimental and measure heat flow rate for all the experimental data points of CO_2/propane, using the different prediction methods, divided in sub-groups

study recommending its use for PHEs [95]. Moreover, the mean relative errors equal to -2.2 % and -8.8 % shows a general underestimation of the heat transfer rate. This underestimation was found to be the same for all the correlations, with the exception

of Wettermann and Steiner [120], which instead overestimated the performance. The magnitude for the other correlations was found to be much higher, above 30 % for Gungor and Winterton [117], and equal to 29.7 % and 22.5 % for Jung et al. [89] and Zhang et al. [97], respectively. The interesting aspect is that such underestimation consistently decreases for increasing temperature glides. In fact, a considerable drop was calculated in the absolute error of the mixture points experiencing larger glides. Zhang et al. [97], as an example, resulted in a mean relative error of -22.4 % in the range 0 K - 5 K, which dropped down to -6.0 % for 10 K -17 K. Similar drops were found for all other correlations. This implies that, despite these methods do not characterize the PHE geometry and are thus experiencing larger deviations compared to PHE specific correlations and theoretical methods, they could predict with a sufficiently high degree of accuracy the heat transfer coefficient of those mixtures undergoing very large glides. The reason must be related to mixture effects, i.e. degradation of heat transfer having a dominant effect over the PHE geometry.

Table 3.5: Mean relative and absolute errors of the heat flow rate predicted by the different prediction methods. Bold values denote all data points

		PHE specific correlations		
	Hsieh and Lin [110]	Longo et al. [112]	Amalfi et al. [93]	Ayub et al. [113]
$\|\delta\|$	**4.1 %**	**4.4 %**	**3.7 %**	**4.8 %**
δ	**1.6 %**	**3.2 %**	**-0.1 %**	**3.7 %**
δ (0 K - 5 K)	-1.2 %	1.4 %	-2.5 %	2.3 %
δ (5 K - 10 K)	2.5 %	4.1 %	0.2 %	3.8 %
δ (10 K - 17 K)	6.8 %	6.1 %	5.5 %	7.0 %
		Theoretical methods		
	Silver [100] & Bell and Ghaly [101]	Shah [126] (G&W 87 [117])	Shah [126] (PHE)	
$\|\delta\|$	**3.4 %**	**3.4 %**	**4.2 %**	
δ	**2.7 %**	**-1.7 %**	**3.6 %**	
δ (0 K - 5 K)	2.4 %	-2.9 %	3.1 %	
δ (5 K - 10 K)	2.0 %	-2.1 %	3.5 %	
δ (10 K - 17 K)	4.5 %	2.4 %	5.5 %	
		In-tube flow boiling correlations for mixtures		
	Gungor and Winterton [116] (Cooper)	Gungor and Winterton [116] (S&A)	Gungor and Winterton [117] (Cooper)	Gungor and Winterton [117] (S& A)
$\|\delta\|$	**4.1 %**	**9.3 %**	**33.9 %**	**31.3 %**
δ	**-2.2 %**	**-8.8 %**	**-33.9 %**	**-31.3 %**
δ (0 K - 5 K)	-4.0 %	-12.7 %	-37.6 %	-36.4 %
δ (5 K - 10 K)	-2.4 %	-8.4 %	-35.0 %	-31.7 %
δ (10 K - 17 K)	3.1 %	0.6 %	-22.0 %	-17.4 %
	Jung et al. [89]	Wettermann and Steiner [120]	Zhang et al. [97]	
$\|\delta\|$	**29.7 %**	**10.2 %**	**22.5 %**	
δ	**-29.7 %**	**10.0 %**	**-22.4 %**	
δ (0 K - 5 K)	-33.4 %	10.6 %	-28.5 %	
δ (5 K - 10 K)	-31.4 %	10.3 %	-22.8 %	
δ (10 K - 17 K)	-17.0 %	7.9 %	-6.0 %	
		PHE specific correlations - corrected		
	Hsieh and Lin [110]	Longo et al. [112]	Amalfi et al. [93]	Ayub et al. [113]
$\|\delta\|$	**4.0 %**	**3.3 %**	**3.9 %**	**5.2 %**
δ	**0.4 %**	**-1.1 %**	**-0.8 %**	**4.1 %**
δ (0 K - 5 K)	-2.1 %	-1.4 %	-3.0 %	2.6 %
δ (5 K - 10 K)	0.7 %	-2.6 %	-0.9 %	4.5 %
δ (10 K - 17 K)	6.4 %	2.3 %	4.9 %	7.3 %

Note that very different results were obtained by applying the two correlations from the same authors Gungor and Winterton [116, 117] from different studies and years. While applying Cooper [107] correlation and the correction by Thome and Shakir [119] to the former led to a good match with experimental data, the latter [117] consistently underpredicted the data. The same correlation [117] applied to Shah [126] theoretical methods resulted in a good agreement. Therefore, depending on how the different contributions to heat transfer are integrated and how the correction is applied, the correlations might lead to completely different results.

Local variation of the heat transfer coefficient

The local values of heat transfer coefficient are presented for three experimental data points in Fig. 3.4 (a-c). The captions report the mass fraction of propane in the mixture, as well as the bubble point, the temperature glide and the outlet experimental vapour quality. The figure also reports, with a black dotted line, the heat transfer coefficient from the heat source side. It can be observed that the heat source gives the dominating thermal resistance depending on the chosen correlation. One reason for which larger differences between heat transfer coefficients do not lead to high deviations in the total heat flow rate is due to the contribution of the heat source side to the overall thermal resistance. The mixture data points subject to a larger temperature glide resulted in heat transfer coefficient values comparable to the heat source side. Therefore, the use of different correlations led to a larger impact on the estimation of the PHE evaporator performance.

Fig. 3.4 (a) corresponds to an experimental point experiencing a very low temperature glide, corresponding to a low mass fraction of propane and relatively high saturation temperature. Fig. 3.4 (b) and (c) were instead plotted for mixtures with higher propane fractions, thus undergoing higher temperature glides during the evaporation process. Note that the sudden drop in heat transfer coefficient at high values of cumulated heat flow rate in the two cases (b) and (c) is related to the superheated region.

Using a PHE specific correlation as Amalfi et al. [93] does not capture the degradation of heat transfer due to the increasing temperature glide of the mixture, and Fig.3.4 (a), (b) and (c) report similar values of heat transfer coefficients estimated by this correlation. However, if the mixture correction factor to the nucleate boiling contribution is applied, a slight degradation of the heat transfer coefficient is observed. This decrease was however lower compared to the use of theoretical methods or mixture specific correlations.

Applying theoretical methods like Silver [100] and Bell and Ghaly [101] and Shah [126] was found to be appropriate to catch the variation of the heat transfer coefficient in the three cases. The higher values depicted in Fig. 3.4 (a) were found to decrease in both Fig. 3.4 (b) and (c), consistently with the higher temperature glide experienced by the mixture.

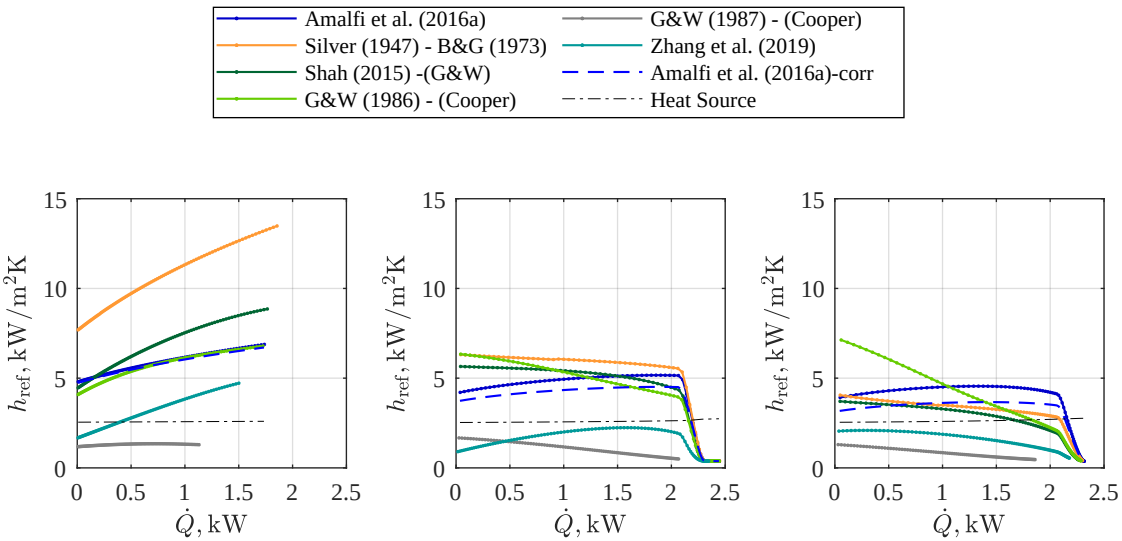

(a) $x_2 = 4.7$ %, $T_{\mathrm{bubble}} = 5.3$ °C, $\Delta T_{\mathrm{gl}} = 0.9$ K, $x_{\mathrm{out}} = 0.86$ (b) $x_2 = 15.3$ %, $T_{\mathrm{bubble}} = -8.0$ °C $\Delta T_{\mathrm{gl}} = 7.7$ K, $x_{\mathrm{out}} = 1$ (c) $x_2 = 24.5$ %, $T_{\mathrm{bubble}} = -10.7$ °C, $\Delta T_{\mathrm{gl}} = 17.0$ K, $x_{\mathrm{out}} = 0.99$

Figure 3.4: Heat transfer coefficient vs. cumulated heat flow rate for some prediction methods for three different experimental points in (a), (b) and (c)

On the other hand, by employing a general or specific correlation for mixtures, the case is different depending on the chosen correlation. Gungor and Winterton [116] presented a similar trend compared to Amalfi et al. [93] in Fig.3.4 (a) and a similar behaviour compared to Shah [126] in (b). Given the good agreement with experimental data previously discussed, this method was found to be a good choice to predict the heat transfer rate of the mixture. Gungor and Winterton [117], instead, entails an underestimation of the heat transfer coefficient compared to the other prediction methods and for Fig. 3.4 (a-c) the ranges were found to be similar. Last, Zhang et al. [97] correlation resulted in underestimation of the heat transfer coefficient in both Fig.3.4 (a) and (b), while comparable values to the theoretical methods are shown in Fig.3.4 (c), i.e. for larger glides. This is in agreement with the results previously presented: mixtures effects can become dominant over the PHE geometry for large glides, thereby making the use of specific mixtures correlations a possible alternative to predict the mixture heat transfer coefficient in PHEs.

3.3.4 Main finding and recommendations

In light of the results presented so far, the recommendations on the use of prediction methods to estimate the heat transfer coefficient of evaporating zeotropic mixtures in PHEs are summarized as follow.

- It is recommended to employ theoretical methods, e.g. Silver [100] and Bell and Ghaly [101] method or Shah [126], to estimate the heat transfer coefficient. These methods allow taking the degradation of heat transfer due to mixture effects into account, together with an appropriate representation of the geometry. The use of these methods is strongly advised for mixtures experiencing large temperature glides since they are subject to a higher degradation of heat transfer.
- PHE specific correlations, e.g. Amalfi et al. [93], resulted in an accurate estimation of the total heat flow rate, especially for mixtures experiencing lower temperature glides , due to the similar behaviour to pure fluids and the dominating resistance of the heat source. By correcting the nucleate boiling contribution of these correlations to account for mixture degradation did not lead to considerable improvements on the results. However, the latter approach can also be employed, since it showed a good agreement with the experimental data. For case studies in which the heat source thermal resistance does not play a significant role - differently from the case shown in this study - the correction might lead to better improvements.
- It is not recommended to use zeotropic mixtures specific correlations by substituting the tube diameter with PHE hydraulic diameter. Most prediction methods were found to underestimate the heat transfer coefficient, due to a poor characterization of the geometry. The use of these methods can only be justified with very large temperature glides, making mixture effects dominant over the geometrical representation.

3.3.5 Discussion

The experimental validation presented here was limited to the comparison against total evaporator heat flow rate, since no experimental measure of the heat transfer coefficient (local or global) was developed during the experimental campaign. Therefore, the recommendations derived in the present study must be merely seen as a guideline, particularly relevant for those interested in estimating the impact of PHE evaporators on integrated systems, or interested in understanding the sensitivity of the heat transfer coefficient to different correlations. More work must be carried out to understand the complex flow and heat transfer mechanism in PHEs for mixtures of refrigerants.

An additional aspect to consider is given by the thermal resistance of the heat source side, which resulted to have a significant impact in the present study. For mixtures experiencing a low temperature glide, with higher values of heat transfer coefficients, different methods presented a good agreement against the experimental data due to the dominating resistance of the ethylene/glycol water mixture compared to the refrigerant side. On the other hand, by looking at mixtures subject to large temperature glides, the relative weight of refrigerant and secondary fluid heat transfer coefficients was found to be similar, thus leading to a stronger impact of the correlation chosen to compute the mixture heat transfer coefficient.

Moreover, this study included data for mixtures of CO_2/propane only. The impact of fluid thermo-physical properties on heat transfer should also be included in future work, and more zeotropic mixtures should be investigated experimentally.

Last, the distribution of the collected experimental data with respect to temperature glide was shown. More investigation could be done in this respect, by collecting data for more mixtures undergoing a wide range of glides. In fact, limited data were included for mixtures experiencing glides larger than 15 K: it could be relevant to include data points up to 20 K - 25 K in the analysis.

3.4 Significance of the choice of the correlation to correct the nucleate boiling contribution

As reported in Section 3.2.2, different models can be chosen to compute the mixture degradation for the nucleate boiling contribution. The analysis presented in Section 3.3 illustrated the comparison of different methods, and the model proposed by Thome and Shakir [119] was used in all the cases to compute F_c. This section deals with the comparison of different correlations to compute the correction factor F_c in the Silver [100] and Bell and Ghaly [101] method. All the models presented in Table 3.2 are investigated and compared to the baseline choice of Thome and Shakir [119]. The comparison is carried out against the same experimental data used in the previous analysis, and by following a similar approach. The correlations by Amalfi et al. [93], Cooper [107] and Martin [77] were used as baseline combination to compute the other terms for the heat transfer coefficient formulation of the Silver [100] and Bell and Ghaly [101] method.

3.4.1 Results

The sensitivity analysis carried out on choosing different correlations in the Silver [100] and Bell and Ghaly [101] method, is first presented at a global level, i.e. by comparing the total heat flow rate estimated by the PHE model against the experimental values. Table 3.6 report the mean relative and absolute errors of the total heat flow rate obtained by changing the correlations for the computation of F_c. The errors were found to be equal to generally low values, regardless of the correlations chosen. The maximum deviation corresponded to the use of Schlunder [131] with a mean absolute error equal to 4.1 %, considering all the data points. Therefore, the choice of the correlation for the computation of the nucleate boiling correction was found not to be relevant when looking at the overall performance of the component for the considered case study.

The agreement with the experimental data was found to be low also when dividing the points according to the temperature glide range, despite a larger increase of the error was found in the interval 10 K - 17 K. This is related to the higher importance of the refrigerant heat transfer coefficient on the overall thermal resistance for increasing

Table 3.6: Mean relative and absolute errors of the heat flow rate predicted by the different correlations to compute F_c

Prediction method		δ, %	$\lvert\delta\rvert$, %
Thome and Shakir [119]	Overall	2.7	3.4
	0 K - 5 K	2.4	3.9
	5 K - 10 K	2.0	2.3
	10 K - 17 K	4.5	4.5
Stephan and Körner [129]	Overall	2.1	3.1
	0 K - 5 K	1.7	3.6
	5 K - 10 K	1.4	1.9
	10 K - 17 K	4.2	4.2
Jungnickel et al. [130]	Overall	1.6	3.0
	0 K - 5 K	1.5	3.6
	5 K - 10 K	0.7	1.6
	10 K - 17 K	3.9	3.9
Schlunder [131]	Overall	3.4	4.1
	0 K - 5 K	2.8	4.2
	5 K - 10 K	3.2	3.3
	10 K - 17 K	5.2	5.2
Fujita and Tsutsui [132]	Overall	1.5	2.8
	0 K - 5 K	1.4	3.4
	5 K - 10 K	0.5	1.5
	10 K - 17 K	3.7	3.7
Fujita and Tsutsui [133]	Overall	2.9	3.7
	0 K - 5 K	2.6	4.0
	5 K - 10 K	2.5	2.6
	10 K - 17 K	4.7	4.7
Inoue et al. [134]	Overall	1.3	2.7
	0 K - 5 K	1.2	3.4
	5 K - 10 K	0.2	1.4
	10 K - 17 K	3.6	3.6

mixture temperature glides. This aspect is shown in Fig.3.5: the heat transfer coefficient development in the evaporator is reported for three different experimental points, subject to very different temperature glides.

The mean relative error on the average heat transfer coefficient - with respect to the baseline case of Thome and Shakir [119] - is reported in the figure for the correlation deviating the most from the baseline, e.g. Schlunder [131]. The heat source is also reported in the plot. The figure shows that in the Silver [100] and Bell and Ghaly [101] method, the heat transfer coefficient of the refrigerant estimated for temperature glides up to 8 K is very large compared to the secondary fluid. It follows that deviations in the

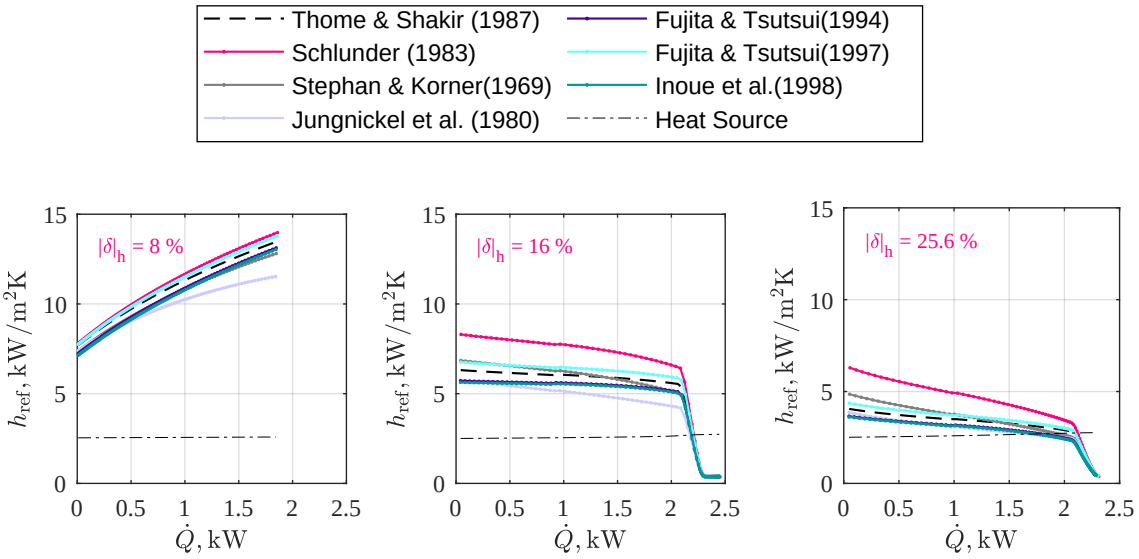

(a) x_2 = 4.7 %, T_{bubble} = 5.3 °C, ΔT_{gl} = 0.9 K, x_{out} = 0.86 (b) x_2 = 15.3 %, T_{bubble} = -8.0 °C, ΔT_{gl} = 7.7 K, x_{out} = 1 (c) x_2 = 24.5 %, T_{bubble} = -10.7 °C, ΔT_{gl} = 17.0 K, x_{out} = 0.99

Figure 3.5: Heat transfer coefficient vs. cumulated heat flow rate for the investigated correlations to compute F_c for three different experimental points in (a), (b) and (c)

computation of the refrigerant heat transfer coefficient do not lead to large deviations when looking at the match with the experimental heat flow rate. The deviations become more relevant in cases of larger glides, as shown in Fig.3.5 (c). Moreover, the differences between the correlations to compute F_c becomes more evident for mixtures undergoing larger glides. For instance, for the three chosen experimental point, Schlunder [131] overestimated the heat transfer coefficient of + 8% compared to Thome and Shakir [119] in (a), while deviation increased up to 25.6 % in (c). Note that, for experimental points included in the interval 10 K - 17 K, the agreement between the different correlations and the experimental data to compute the total heat flow rate, reported in Table 3.6, was found to be low in any case, with Schlunder [131] deviating the most with 5.2 %. This means that the use of Silver [100] and Bell and Ghaly [101] method to compute the mixture heat transfer coefficient is appropriate even for those cases in which the thermal resistance of the refrigerant is of the same order of magnitude of the water thermal resistance.

3.4.2 Discussion

This study was not able to identify a preferred correlation to compute the correction factor to nucleate boiling term, since all the methods resulted in very low deviations in terms of total heat flow rate. The agreement was particularly good for mixture

experiencing low glides, since the heat source resistance dominates the heat transfer. However, even for larger temperature glides - included in the interval 10 K - 17 K - the agreement was found to be low for any correlation, despite the refrigerant resistance to heat transfer was comparable to the one of water. The suitability of the method by Silver [100] and Bell and Ghaly [101] was thus confirmed by the good match obtained for these experimental points. However, the analysis resulted to yield larger deviations between estimation of local values of heat transfer coefficient, with increasing differences for increasing temperature glides. This aspect must be taken into account if a detailed characterization of the component is required, rather than PHE performance estimation aimed at system-level analysis.

3.5 Case study: impact of correlations on a performance problem

This section presents a comparison of correlation applied to a case study where a PHE evaporator is sized for different zeotropic mixtures of CO_2 and HCs, subject to different temperature glides from the heat source side. The study aims at evaluating the sensitivity of the results of a performance problem to the use of different correlations in the Silver [100] and Bell and Ghaly [101] method. The performance problem is formulated with the perspective of integrating the PHE evaporator in a heat pump cycle, and imposing defined control values for the refrigerant superheat and suction volume flow rate. The analysis is thus aimed at quantifying the impact on the output of a performance problem of choosing different correlations in the theoretical method.

3.5.1 Methods

The comparison was based on a case study of a single-stage vapor compression heat pump, presented in Zühlsdorf et al. [20] designed for delivering 2200 kW at the condenser, by heating up water from 40 °C to 80 °C. The inlet temperature of the heat source (water) was fixed to 40 °C, and different heat source temperature glides were assessed, namely 10 K, 15 K and 20 K, corresponding to Case I, II and III, respectively. Optimal zeotropic working fluid mixtures were found for the different temperature glides. These are reported in Table 3.7 with related mass composition, evaporation pressure, heat pump COP and heat load at the evaporator.

The impact of the chosen prediction methods was assessed in a relevant practical situation, in which the geometry of the PHE was entirely fixed and the suction volume of the refrigerant flow at the compressor inlet (corresponding to the evaporator outlet) and the super-heating were fixed by the control. The required number of channels was estimated for each working fluid with a preliminary evaporator sizing based on constant heat transfer coefficients in the different regions of evaporation and superheat. The other HEX parameters were defined according to an existing evaporator model (V65) manufactured

Table 3.7: Evaporator boundary conditions for the different working fluids [20]

Case I, ΔT_{gl} = 10 K				**Case II, ΔT_{gl} = 15 K**				**Case III, ΔT_{gl} = 20 K**			
Mixture	p_{eva} bar	COP -	$\dot{Q}_{eva,tot}$ kW	Mixture	p_{eva} bar	COP -	$\dot{Q}_{eva,tot}$ kW	Mixture	p_{eva} bar	COP -	$\dot{Q}_{eva,tot}$ kW
CO_2/DME (0.1/0.9)	7.5	5.62	1809	Propylene/butane (0.3/0.7)	4.0	5.4	1792	DME/pentane (0.3/0.7)	1.2	5.24	1780
DME/butane (0.5/0.5)	4.8	5.61	1807	Propane/butane (0.7/0.7)	3.9	5.38	1791	DME/iso-Pentane (0.3/0.7)	1.7	5.19	1776
Ethane/propane (0.1/0.9)	12.3	5.6	1807	CO_2/DME (0.1/0.9)	7.0	5.32	1787	Propylene/butane (0.5/0.5)	5.0	5.15	1773
Ethane/propylene (0.1/0.9)	14.5	5.57	1805	DME/iso-pentane (0.8/0.2)	4.5	5.31	1786				

by SWEP International AB [74], with design parameters reported in Table 3.8. The PHE was assumed to be constructed in stainless steel, with a thermal conductivity equal to 16.2 W/mK.

The performance of the PHE was assessed by using the evaporator 1D model, presented in chapter 2.2. The model was run with $n = 100$ slices along the flow direction and tolerance set to 10^{-5}. The local values of heat transfer coefficient and pressure drop were estimated by following the approach presented in chapter 2.2.6, choosing the different correlations included in the sensitivity study. The model was coupled with an external solver for the performance problem, i.e. to estimate the operating conditions of the evaporator to meet the control values. The solver was implemented following the Newton-Raphson method with a set tolerance of 10^{-3} on the relative residuals of the refrigerant suction volume and super-heating. It was assumed to employ a thermostatic expansion valve, thus calculating the refrigerant superheat in relation to inlet pressure. The refrigerant mass flow and saturation pressure were thus calculated in order to match the control values.

Table 3.8: Geometry of the SWEP Evaporator type V65 [74]

Parameter	Unit	Value
W	m	0.363
L_p	m	0.731
t	mm	5.0
β	°	35
b	mm	1.9
Λ	mm	7.0
D_p	m	0.1

Investigated correlations

The correlations chosen for investigation in the Silver [100] and Bell and Ghaly [101] method are reported in Table 3.9. The sensitivity study was carried out on the three terms of Eq.(3.21) to compute the two-phase convective contribution, the ideal nucleate boiling contribution and the vapour only heat transfer coefficient. The ideal nucleate boiling terms was subsequently corrected by Thome and Shakir [119]. The correlations by Hsieh and Lin [110] and Longo et al. [112] were used to compute both h_{cb} and h_{nb}. The former correlation is a superposition model, with distinct contributions for nucleate and convective boiling (see Eq.(3.2)), while the latter estimates the largest of both contributions (see Eq.(3.7)).. Therefore, each term of both correlations was considered in the appropriate category, as reported in Table 3.9. The remaining two-phase correlations were categorized as convective or nucleate boiling methods, depending on the related authors observations on the heat transfer, which could be dominated by heat flux (nucleate boiling) or by vapour quality and mass flow (convective boiling). All possible combinations of the three terms were analysed, leading to 75 different possibilities for each fluid.

Table 3.9: Investigated correlations for the case study

Two-phase convective boiling h_{cb}		Two-phase ideal nucleate boiling $h_{\mathrm{nb,id}}$		Single-phase h_{vo}
a	Danilova et al. [104]	A	Cooper [107]	Chisholm and Wanniarachchi [135]
b	Hsieh and Lin [110]	B	Hsieh and Lin [110]	Wanniarachchi et al. [136]
c	Han et al. [105]	C	Palm and Claesson [95]	Martin [77]
d	Longo et al. [112]	D	Gorenflo and Kenning [108]	
e	Amalfi et al. [93]	E	Longo et al. [112]	

3.5.2 Results

Fig.3.6, Fig. 3.7 and Fig. 3.8 show the heat transfer correlation sensitivity analysis results for Case I, II and III, respectively. Fig.3.6 (a), Fig. 3.7(a), and Fig.3.8 (a) report the mean UA value for all the combinations: the abscissa indicates different combination of nucleate and convective boiling correlations, while the three different marker styles represent the three single-phase correlations. Different colors represent the different working fluids of the three cases. Fig.3.6 (b), Fig. 3.7(b), and Fig.3.8 (b) represent the development of the UA value along the evaporator, as a function of the cumulated heat flow rate. The results are shown for only two correlation combinations for each fluid, represented by a continuous and a dotted line. The former characterizes the combination estimating the highest mean heat transfer coefficient for the specific fluid, while the latter represents the correlations giving the lowest mean heat transfer coefficient. The results are shown in terms of UA value to account for: (i) the impact of the heat source heat transfer coefficient, and (ii) the different heat transfer area related to the working fluids. In fact, the PHE evaporator was preliminarily sized for the different refrigerants using the same plate geometry, thereby leading to a different number of channels (and required

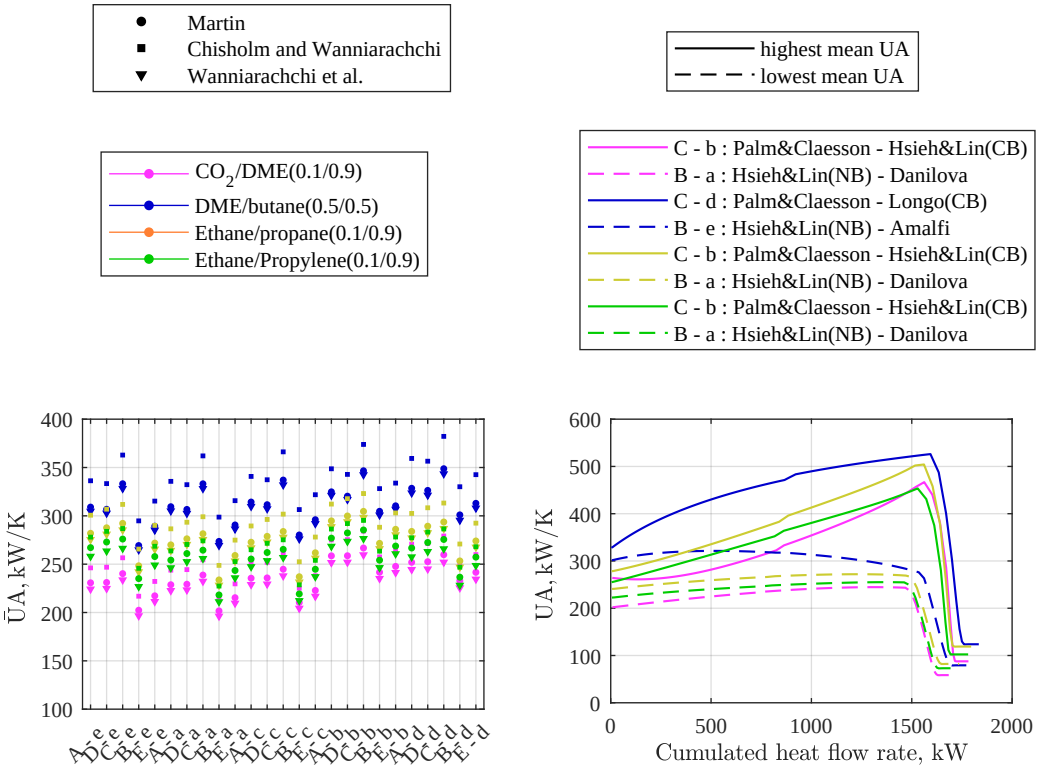

(a) Mean UA value

(b) UA value development in the evaporator

Figure 3.6: Case I results: (a) Impact of the different heat transfer correlations on the mean UA value; (b) UA as function of the cumulated heat flow rate in the evaporator

heat transfer area).

Better heat transfer performance was obtained for smaller temperature glides, with mean UA values up to 400 kW/K for Case I against values not higher than 300 kW/K for Case III. By looking at the UA distribution in the evaporator in Fig.3.6 (b), Fig.3.7 (b) and Fig.3.8 (b), Case I yields a steeper heat transfer growth for increasing vapour quality compared to Case II and III, for the best performing correlation combinations. This is due to the higher degradation of heat transfer for increasing temperature glide for both the case of nucleate and convective boiling due to the larger sensible heat flow rate needed for increasing the mixture temperature during phase change. The fluid ranking in terms of heat transfer performance remains the same in all cases, regardless of the correlation applied. By looking at Case I in Fig. 3.6 (b), the UA value of DME/butane(0.5/0.5) outperforms the other fluids for both the best and worst correlation combinations.

Similarities were found for the single-phase and nucleate boiling correlations. The

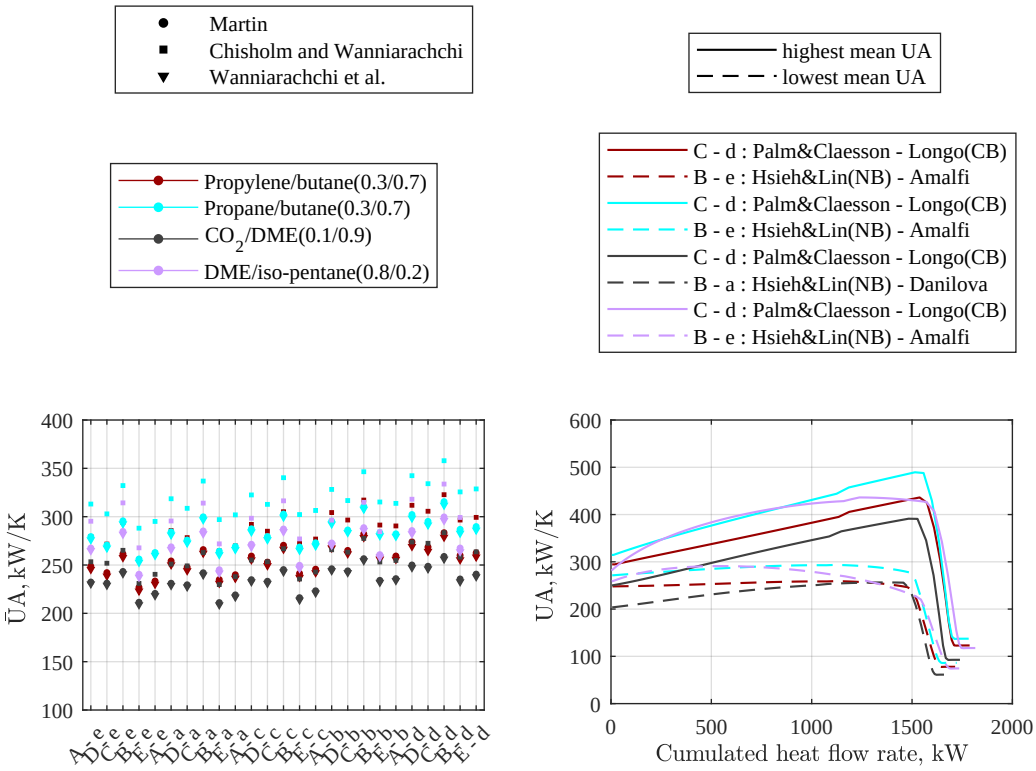

(a) Mean UA value

(b) UA value development in the evaporator

Figure 3.7: Case II results: (a) Impact of the different heat transfer correlations on the mean UA value; (b) UA as function of the cumulated heat flow rate in the evaporator

single-phase correlation by Chisholm and Wanniarachchi [135] led to higher heat transfer compared to Martin [77] and Wanniarachchi et al. [136], which yielded the lowest UA. This holds for all the mixtures, as shown by the different markers in Fig.3.6 (a), Fig. 3.7(a).

Hsieh and Lin [110] (B) underestimated the nucleate boiling contribution compared to the other correlations, while Palm and Claesson [95] (C) overestimated the nucleate boiling. The results, shown in Fig.3.6 (b), Fig.3.7 (b) and Fig.3.8 (b), are hence the same for all the fluids. By looking at convective boiling contributions, Hsieh and Lin [110] (b) correlation led to the best heat transfer coefficient for all the working fluids of Case I, whileLongo et al. [112] (d) yielded the best performances for Case II and III. The lowest convective boiling contribution to heat transfer was estimated by Amalfi et al. [93] (e) and Danilova et al. [104] (a), depending on the working fluid.

Fig.3.9 reports the percentage deviation from the mean of all correlation combinations of

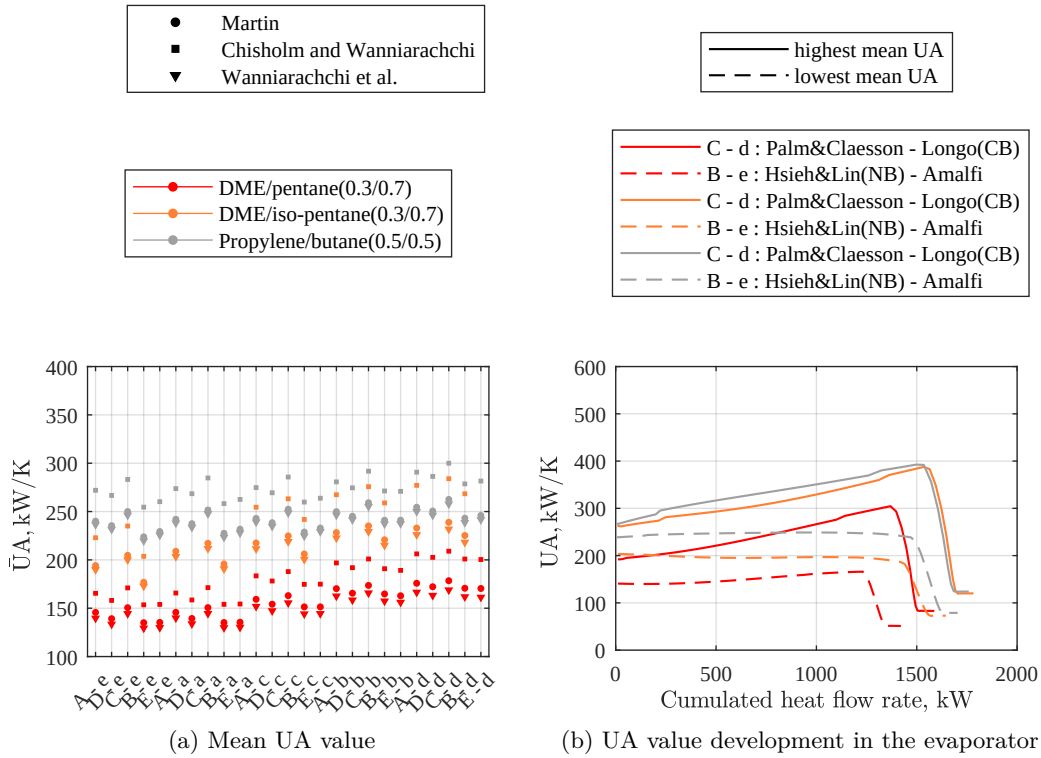

(a) Mean UA value

(b) UA value development in the evaporator

Figure 3.8: Case III results: (a) Impact of the different heat transfer correlations on the mean UA value; (b) UA as function of the cumulated heat flow rate in the evaporator

the most deviating correlation combinations for heat transfer, which were identified in Fig.3.6 (b), Fig.3.7 (b) and Fig.3.8 (b). The deviations are reported for the refrigerant mean heat transfer coefficient, for the mean UA value, and the consequent effect on the total heat flow rate at the evaporator, output of the performance model.

First of all, large deviations were obtained on the computation of the refrigerant heat transfer coefficients: a maximum value around 50 % was obtained in the case of DME/pentane (0.3/0.7). These large discrepancies were however compensated on the computation of the total UA value, taking the heat source thermal resistance and the heat transfer area into account. For the same refrigerant, this was translated in a + 30 % deviation on the mean UA value. Finally, a much lower deviation (lower than 10 %) was obtained on the output of the performance model, namely the total evaporator heat flow rate.

Case I and Case II presented maximum differences in mean refrigerant heat transfer coefficient around ±40%, mean UA values around ±20 %, while Case III reported slightly higher deviations, with a maximum around ±50% for the heat transfer coefficient and

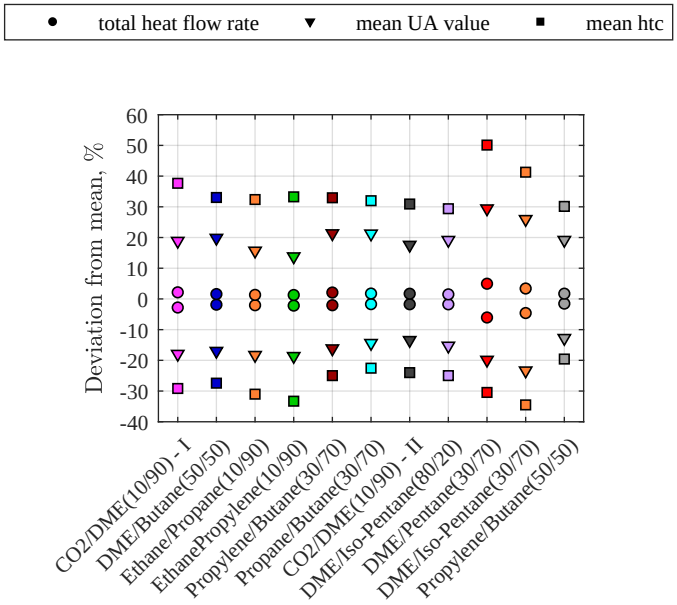

Figure 3.9: Highest and lowest deviations from the mean of the refrigerant heat transfer coefficient, UA value and of the total evaporator heat flow rate

±30% on the mean UA values. This means that very large discrepancies can be obtained between different correlations on the estimation of the refrigerant heat transfer coefficient. However, regarding the total heat flow rate, maximum deviations around ±2 % for Case I and II and ±6% for Case III, can be observed in Fig.3.9, much lower values compared to the heat transfer coefficients.

It can further be concluded that working fluids experiencing larger temperature glides presented a higher degradation of heat transfer, and a stronger dependence on the chosen prediction methods.

3.5.3 Discussion

The presented results suggest that the choice of the prediction method had a significant impact on the estimation of the heat transfer coefficients. The working fluids presented similarities in terms of correlations overestimating or underestimating the heat transfer coefficient compared to the mean results and this must be taken into account when choosing a certain prediction method for other mixtures of natural refrigerants.

Moreover, the results suggested that despite the large discrepancies on the absolute values of heat transfer coefficient and UA values, a much smaller deviation was obtained on the output of the performance model, i.e. the heat transfer rate at the evaporator. It must be therefore taken into account that different degrees of uncertainties are related

with the correlations choice depending on the scope of the analysis. For a user interested in analyzing the PHE performance impact on a thermodynamic cycle, the choice of the prediction method would not lead to large differences (max 6 % were obtained in Case III). On the other hand, it would be very relevant to consider the much larger differences between correlations for a user focusing on detailed heat transfer and pressure drop mechanisms in the component.

A typical practical situation was assessed in the present study, i.e. evaluating the performance of the evaporator (with fixed geometry) as the operating conditions were adjusted according to control. The design problem represents an additional situation in which experimental correlations are used. In this case, the operating conditions are fixed and the PHE heat transfer area must be found to meet the design thermal load. A sensitivity analysis to assess the prediction methods impact on the design problem will be therefore part of future work.

3.6 Summary

This chapter presented different studies aimed at evaluating the impact of choosing different prediction methods to evaluate the heat transfer coefficient of zeotropic mixtures in PHE evaporators.

First, a comparison between different types of correlations against experimental data of CO_2/propane at different mass compositions was presented. The comparison was carried out for mixtures subject to different temperature glides, and by using PHE specific correlations, theoretical models and mixture specific correlations developed for in-tube flow boiling. The best agreement with experimental data was obtained by using the theoretical methods by Silver [100] and Bell and Ghaly [101], and Shah [126], which matched the experimental data with a mean relative error equal to 3.4 %. PHE specific correlations resulted to predict the total heat flow rate with a good accuracy, especially at low temperature glides when the secondary fluid resulted to be the dominating thermal resistance. Larger deviations were instead found by employing mixture correlations developed for in-tube flow boiling.

Second, a sensitivity study on the correlations to compute the correction factor to the nucleate boiling contribution in theoretical methods was presented. The sensitivity was carried out by comparing the different correlations to the experimental data. It was found that larger deviations between the estimation of the local heat transfer coefficients are obtained at larger temperature glide. For a mixture undergoing 17 K temperature glide, the correlation by Schlunder [131] was found to deviate with a mean relative error of 25.6 % compared to the baseline correlation by Thome and Shakir [119]. However, similarly to what obtained previously, the goodness of the match to the experimental heat flow rate was not largely affected by the correlation.

Last, a sensitivity study on correlations to compute the different contributions of two-phase convective boiling, ideal nucleate boiling and vapour only heat transfer coefficients, was carried out for the Silver [100] and Bell and Ghaly [101] method, and a practical case study. Different mixtures were investigated, subject to heat source temperature glides of 10 K, 15 K and 20 K. It was found that despite deviations up to 50 % can be obtained on the estimation of the local heat transfer coefficient, the discrepancies were found to be lower on the mean UA value - accounting for both secondary fluid thermal resistance and geometry - and on the output heat flow rate, which was affected by 6 % in the worst case. It was again obtained that mixtures undergoing larger temperature glides are subject to a larger degradation of heat transfer.

To conclude, it was demonstrated that in-tube flow boiling correlations developed for mixtures are not a suitable approach to compute the heat transfer coefficient. Using theoretical models is instead strongly recommended, in order to model the PHE geometry and the degradation of heat transfer due to mixture effects. Different correlations were compared to compute the different terms in the theoretical models, and it was found that, in cases when the secondary fluid gives the dominating resistance, the choice of the methods is not relevant when looking at the total heat flow rate. However, larger discrepancies between methods are obtained on the local values of heat transfer coefficients. Therefore, depending on the focus of the analysis, e.g. detailed component characterization vs. system integration, different possible deviations resulting to different degrees of uncertainty must be taken into account.

4 Derivation of design guidelines

This chapter presents the research work carried out with the aim of deriving simplified guidelines to design the plate heat exchangers for heat pump cycles using both pure fluids and zeotropic mixtures of natural refrigerants. The chapter is based on [P1], [C1] and [C4].

4.1 Introduction

Optimal design of evaporators and condensers in heat pumps plays a key role for overall system thermodynamic and economic optimization. A common approach is to adopt design criteria based on heuristics, which possibly lead to suboptimal solutions depending on the working fluid. Moreover, the relative ranking of the refrigerants for both thermodynamic and economic indicators may be affected by the HEX design. This chapter aims at deriving design recommendations and guidelines for evaporators and condensers in heat pumps using pure fluids and zeotropic mixtures as refrigerants.

The chapter is structured as follows: section 4.2 presents general recommendations for PHE evaporator and condenser design in heat pumps using both pure fluids and mixtures. The derivation is illustrated based on a case study of heat pump integration in data centres for waste heat recovery purposes. In section 4.3, a methodology to derive simplified guidelines for optimal evaporator design is presented. The methodology is demonstrated by applying it to a case study of heat pump integration in a spray drying facility for waste heat recovery. Last, section 4.4 provides a summary of the main findings.

It is noted that, despite the approach could be theoretically extended to other HEX configurations, the chapter is based on the assumption that PHEs are used as both evaporator and condensing units.

4.2 Design recommendations for evaporator and condenser design

In this section, general recommendations for optimal evaporator and condenser design in heat pump systems are presented. The relative impact of each HEX component is assessed on both the cycle COP and the levelized cost of heat. Different designs, leading to different trade-offs of heat transfer area investment and pressure drop, are obtained for both components and different fluids for a case study.

4.2.1 Methods

A coupled PHE - heat pump simulation framework was used for design and off-design analysis of the cycle with different designs of PHE for both condenser and evaporator. First, the working fluid and the case study boundary conditions (BCs) were defined and used in a heat pump design model. The PHE evaporator and condenser designs were subsequently carried out, for different combinations of geometrical parameters. The aim of the parametric analysis was to obtain PHE designs with different heat transfer areas and pressure drop. The resulting configurations were finally used in an operating model. The model additionally received as inputs the control values chosen for the operation, namely a fixed superheat, subcooling and suction volume flow rate at the compressor inlet. The resulting heat pump operating conditions, affecting the compressor power requirement and the heat supply of the condenser, were used in an economic analysis to estimate the off-design COP, heat transfer area, and operating costs.

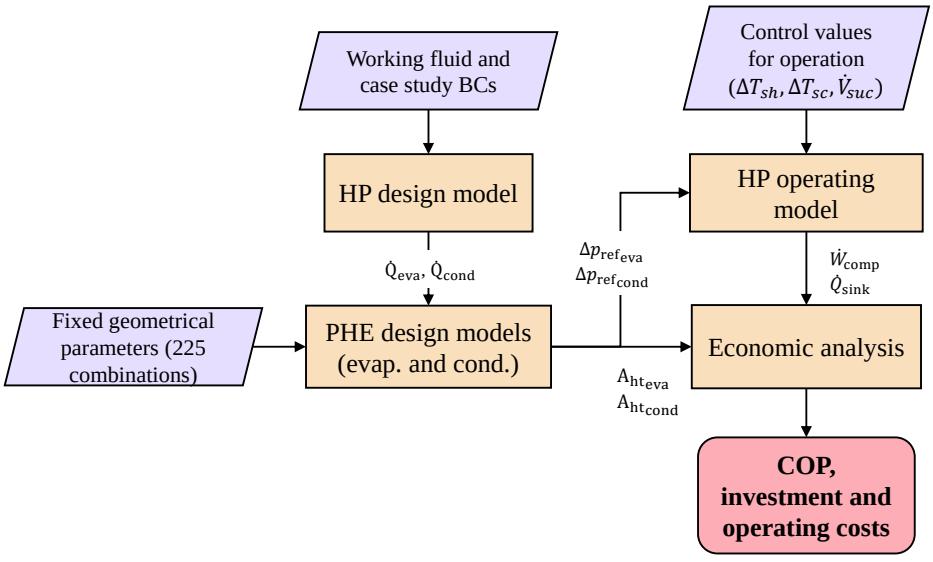

Figure 4.1: Work-flow of the overall procedure

The parametric study conducted on the geometry of both evaporator and condenser evaluated 225 different combinations of designs. It was decided to fix the corrugation geometry of the PHEs and to carry out a sensitivity study on the plate size and count. The plate width W and number of channels N_{ch} were varied for both the components, while the plate length L was estimated as an output of the design model. The values used in the parametric analysis are reported in Table 4.1.

Table 4.1: Plate width and number of channels values used in the parametric study

Paramter	Working fluid	Values	Unit
W_{eva}	All fluids	0.250 – 0.400 – 0.600	m
	Propane	50 – 100 – 150 – 200 – 250	
$N_{\text{ch,eva}}$	Butane	70 – 120 – 170 – 220 – 270	-
	Propylene/butane	80 – 130 – 180 – 230 – 280	
W_{cond}	All fluids	0.200 – 0.400 – 0.600	m
	Propane	50 – 100 – 150 – 200 – 250	
$N_{\text{ch,cond}}$	Butane	70 – 120 – 170 – 220 – 270	-
	Propylene/butane	50 – 100 – 150 – 200 – 250	

Numerical models

The numerical models used to run the different steps of the overall procedure shown in Fig.4.1, were presented in Chapter 2. The heat pump design model was described in Chapter 2.6.1. The PHE design models iterated on the plate length necessary to meet the required heat load, and they were based on a discretization of the component at constant enthalpy change steps, as described in Chapter 2.3. The PHE performance was instead estimated by the model presented in 2.2, while the coupled PHE - heat pump calculations during off-design operation used the framework presented in Chapter 2.6.2 and explained by Fig.2.14.

For the PHE model in both design and performance mode, a total of $n = 50$ number of CVs was used for the evaporator and $n = 110$ for the condenser discretization. The tolerance was set to 10^{-5}. The local values of heat transfer coefficient and pressure drop were estimated by following the approach presented in chapter 2.2.6. The evaporation heat transfer coefficient for pure fluids was estimated by Amalfi et al. [93] correlation. The Silver [100] and Bell and Ghaly [101] method was instead applied to account for mixture degradation of heat transfer during evaporation. In this method, Amalfi et al. [93] was applied for the two-phase convective contribution, Cooper [107] was used for the ideal nucleate boiling contribution, Thome and Shakir [119] correlation was used for estimating the mixture correction for the nucleate boiling term, and Martin [77] was applied for the single-phase vapour contribution. The Lockhart and Martinelli [78] method was applied to evaluate two-phase evaporation frictional pressure drop. The method was applied as

proposed by Palm and Claesson [95], i.e Martin [77] was used to estimate the single-phase frictional pressure drop and the correlation developed by Chisholm [80] estimated the two-phase multiplier with a Chisholm parameter equal to 4.67. Regarding pressure drop, no distinction was made between pure and mixed refrigerants, and the same method was applied. Yan et al. [137] was used for the condensation heat transfer coefficient of pure fluids, while the Silver [100] and Bell and Ghaly [101] method was applied to account for mixture degradation of heat transfer during condensation. The ideal heat transfer coefficient was computed using Zhang et al. [97], while Martin [77] was used for the vapour phase correction term. Condensation pressure drop was estimated by using the correlation for the Fanning friction factor proposed by Zhang et al. [97].

Case study

A case study previously published in Zühlsdorf et al. [13] was chosen for the analysis. A single-stage vapour compression heat pump was integrated in a data centre facility for waste heat recovery purposes, with the aim of supplying heat to the district heating network. Propane, butane and a mixture of propylene/butane at (0.5/0.5) mass composition were found among the best performing working fluids. The heat pump was sized by fixing the heat transfer rate at the evaporator, i.e. 500 kW to use as waste heat. Moreover, the heat source was considered to be water entering the evaporator at 50 °C and leaving at 25 °C, while the heat sink was considered to be water entering the condenser at 50 °C to be heated up to 75 °C, i.e. the temperature level required by the dostrict heating network. Table 4.2 reports the inputs used for the heat pump sizing, as well as the outputs, which determine the boundary conditions for evaporator and condenser sizing.

Table 4.2: Heat pump design and operating parameters for the selected working fluids

	Inputs					Outputs					
Working fluid	$\dot{Q}_{eva}$, kW	$T_{hs,in}$, °C	$T_{hs,out}$, °C	$T_{sink,in}$, °C	$T_{sink,out}$, °C	$\dot{Q}_{cond}$, kW	p_{cond}, bar	p_{eva}, bar	$\dot{V}_{out,eva}$, $m^3\ h^{-1}$	COP, -	c_h, €/MWh
Butane	500	50	25	50	75	630	9.5	2.2	1100	4.5	32.7
Propane	500	50	25	50	75	638	28.1	8.8	370	4.4	31.1
Propylene/Butane	500	50	25	50	75	600	16.4	5.6	460	5.6	25.8

4.2.2 Results

Impact of evaporator and condenser design on thermodynamic performance

Fig.4.2 shows how the refrigerant pressure drop of the evaporator affected the heat pump COP. Each point corresponds to one combination of the design variables reported in Table 4.1, e.g. different evaporator and condenser geometries. The different marker styles and colours represent the working fluid. The COP value was reported by scaling it with respect to the design value. The thermodynamic performance degradation due

to pressure drops for the different PHE evaporator designs was fitted linearly for each working fluid, and Fig.4.2 also reports the value of the slopes. For example, choosing a design with 30 kPa pressure drop entails around 4 % COP drop for butane, 3 % for propylene/butane, while it stays lower than 2 % for propane.

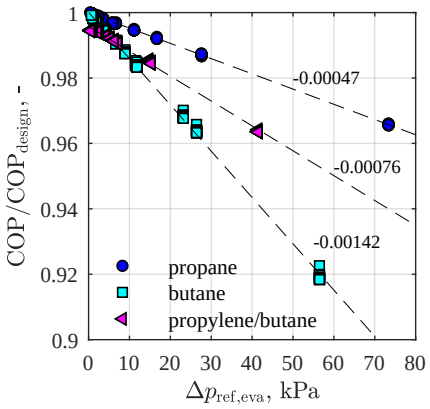

Figure 4.2: Normalized COP as a function of total refrigerant pressure drop in the evaporator

It must be noted that only few design points are visible in the figure compared to the 225 different combinations evaluated in the sensitivity study. This is due to the condenser design, which does not affect the COP, hence the points with the same evaporator geometry and different condenser designs overlap. Fig.4.3 (a) further illustrates this result, reporting the COP for the three working fluids as a function of the total refrigerant pressure drop in the condenser. There is no dependency between the COP and the condenser design, and the colour scale – indicating different normalized evaporator pressure drops – shows that maximum COP was obtained for minimum evaporator pressure drops in all the cases. Note that Fig.4.3 (a) shows that the relative ranking of the working fluids in terms of COP was slightly affected by the PHE designs. Propylene/butane remained the refrigerant with the highest COP regardless of the evaporator and condenser configuration, while butane and propane were found to overlap depending on the evaporator design (pressure drop).

The stronger dependence of the COP to the evaporator pressure drop was related to a number of reasons. First, a higher value of pressure drop entailed a decrease in the heat output of the condenser. This was due to the impact of evaporator operation on the operating parameters of the cycle, i.e. refrigerant mass flow rate and pressures. The mass flow rate was in fact diminished at fixed superheat and subcooling, and the HP operated at a lower pressure ratio, i.e. a lower compressor power was required. However, the decrease in total heat flow rate of the condenser affected the COP negatively to a larger extent, as shown in Fig.4.3(b): the condenser total heat flow rate – normalized

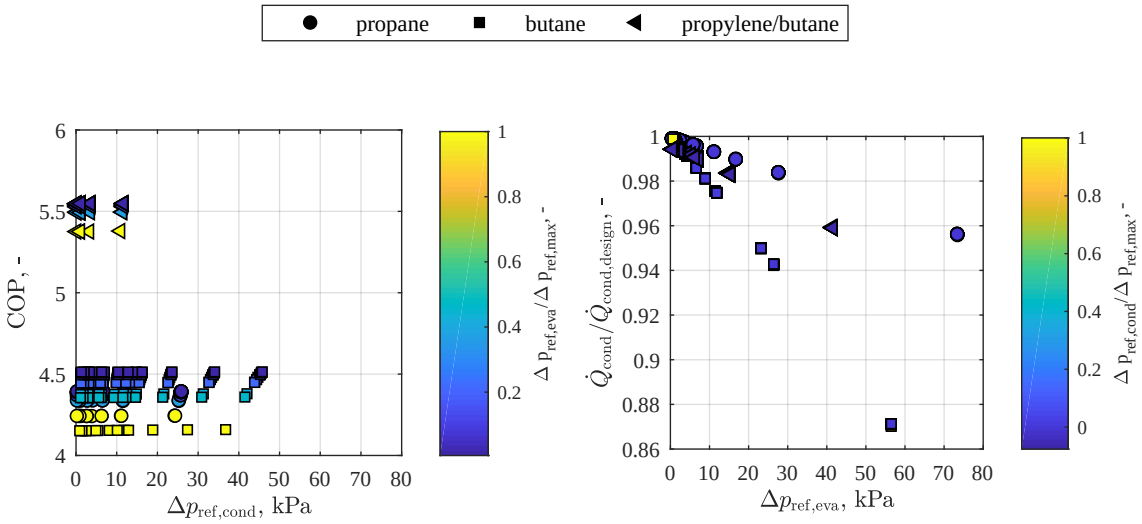

(a) (b)

Figure 4.3: (a) COP as a function of total refrigerant pressure drop in the condenser; (b) normalized condenser heat flow rate as function of total refrigerant pressure drop in the evaporator

by the design value – is plotted as a function of the evaporator pressure drop, with different colours representing different magnitudes of normalized condenser pressure drop. Similarly to the COP degradation reported in Fig.4.2, butane reports the steepest degradation, followed by propylene/butane and propane. The slopes of degradation were found to be similar to the COP drop plotted in Fig.4.2. Condenser pressure drop, represented by the different colour scale, was found not to affect the total heat flow rate at the condenser, and different condenser designs overlap in Fig.4.3 (b) similarly to Fig.4.2.

The higher drop of heat pump COP for butane compared to the other two fluids is due to another main reason: evaporator pressure drops also imply a saturation temperature drop, which increases the exergy destruction due to finite temperature differences in the evaporator component, thus contributing to the COP degradation. Depending on some relevant fluid thermo-physical properties, refrigerants can be more or less subject to this effect. Brignoli et al. [41] identified the ones characterizing refrigerants sensitivity to pressure drops, namely vapour density and saturation temperature drop due to pressure drop. These are reported in Table 4.3 for the three working fluids at design conditions. Lower vapour density implies higher pressure drops for the same mass flux and PHE geometry. Therefore, a design that is feasible for propane and propylene/butane, possibly enhancing the heat transfer coefficient, might entail too large pressure drops for butane, with vapour density much lower than the other two refrigerants. This was one of the reasons why the bounds for plate width and number of channels variation in the sensitivity

Table 4.3: Evaporating pressure and thermo-physical properties at the design point

Working fluid	p_{eva}, bar	ρ_v, kg/m^3	$\frac{dT_{\text{bubble}}}{dp}$, K/kPa
Propane	8.8	19.1	0.044
Butane	2.2	5.7	0.140
Propylene/butane (0.5/0.5)	5.6	13.6	0.054

study (see Table 4.1) were chosen differently for the working fluids, i.e. to ensure feasible PHE designs with similar values of pressure drop.

The refrigerant vapour density is thus a property that must be carefully taken into account when choosing the working fluid and subsequently selecting the HEX design. Higher saturation temperature drop due to pressure drop, estimated by the Clapeyron relation [138], entails a larger drop of the saturation temperature due to pressure drop, thereby increasing the exergy losses due to the temperature difference between the refrigerant and the heat source side in the evaporator. Table 4.3 shows how the ranking between the working fluids in terms of vapour density and dT_{bubble}/dp respects the slopes of the COP degradation reported in Fig.4.2. Therefore, despite both propane and propylene/butane reported similar slopes for the degradation of condenser heat flow rate, the mixture was found to be more sensitive to saturation temperature drop due to pressure drop, resulting in a steeper COP drop.

Impact of evaporator and condenser design on economic performance

The economic performance was evaluated by looking at the specific cost of heat, which is influenced by both condenser and evaporator design. The TCI is dependent on both HEX sizes (related to the heat transfer area), while the operating costs are strongly related to the heat pump COP. The economic performance indicator is reported in Fig.4.4 (a) for the three refrigerants as function of the pressure drop at the evaporator. The three working fluids present similar trends, with a trade-off and a minimum for a certain value of refrigerant pressure drop.

Fig.4.4 (a) reports a close-up for the case of propane, where the colours represent different values of condenser heat transfer area. The results show that evaporator and condenser have different types of impact on the specific cost of heat. For a fixed condenser design – thus a fixed value of heat transfer area shown by the colours of Fig.4.4 (b) – the economic performance was a trade-off between heat transfer area and pressure drop of the evaporator. The minimum cost was determined by a certain value of evaporator pressure drop, which was similar for all the different condenser designs.

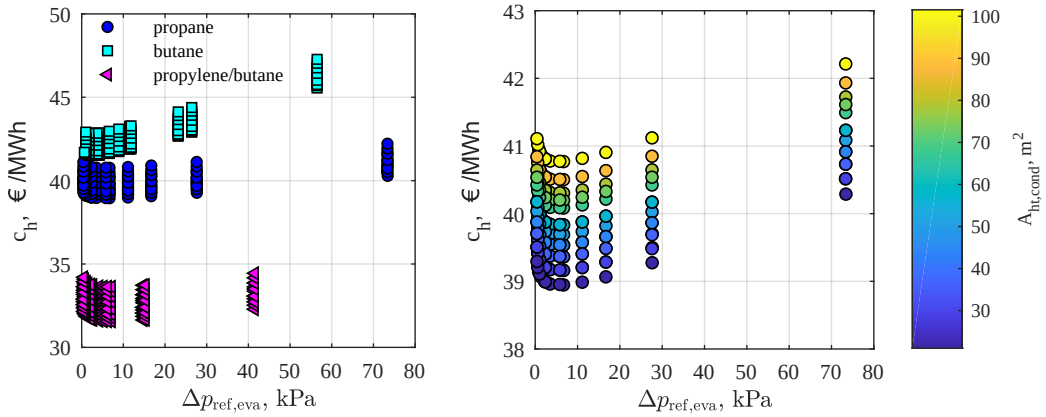

Figure 4.4: Specific cost of heat as function as a function of total refrigerant pressure drops in the evaporator for: (a) all fluids, (b) propane (close-up)

On the other hand, the condenser design influences the economic performance in a different manner: it was always desirable to employ condenser designs with minimum heat transfer area (shown by the darker blue colour in Fig.4.4). In fact, since the COP was not found to be affected by condenser pressure drop, the operating costs were not influenced by its design. The TCI was instead related to the heat transfer area, thereby suggesting a minimization of the condenser size. A relevant finding shown by Fig.4.4 is thus given by the fact that the evaporator and condenser geometry optimization, despite aimed at minimizing the cost of the overall system, could be considered as decoupled problems. The designer can choose to optimize the evaporator geometry and to find the design leading to the minimum cost, regardless of the condenser design (and the opposite holds).

One additional relevant aspect highlighted by Fig.4.4(a) is that all the refrigerants presented a minimum of specific cost of heat for similar values of refrigerant pressure drop. These values lie in the interval 5 – 10 kPa, which is relatively low, compared to usual manufacturer guidelines setting the limitation to around 50 kPa [74]. The results might therefore suggest that in this particular case study – regardless of the refrigerant chosen – an optimal value of pressure drop could be defined preliminarily to the refrigerant selection and HEX sizing. In this way, it is possible to define a guideline – based on optimal pressure drops – to design the PHE evaporators and condensers prior to the working fluid screening. This would enable the screening to avoid suboptimal solutions or the computational cost of optimizing the HEX design for all the working fluids, some of which the screening will in any case subsequently disregard.

This result might seem contradictory if one thinks about the different slopes of COP

degradation for the different fluids, previously shown in Fig.4.2. However, Fig.4.4 (a) reports an effective steeper increase of the specific cost of heat for butane rather than propane and propylene/butane. This increase started however after reaching the minimum specific cost of heat (after around 30 kPa), thus the different slopes of the working fluids for the COP degradation were not relevant to define the optimum. Moreover, since the optimal values of refrigerant pressure drops was found to be as low as 5 kPa to 10 kPa, the COP degradation (shown in Fig.4.2) admissible for this case was found to be lower than 2 %.

Economic optimum: PHE designs

Table 4.4 shows the geometrical specification of the PHE evaporator and condenser designs corresponding to the economic optimum shown in Fig.4.4. Moreover, heat transfer area, total refrigerant pressure drop and heat pump COP and specific cost of heat are reported. The designs minimizing the specific cost of heat are in agreements with the results presented above.

The PHE evaporator design was limited to pressure drops from 4.2 kPa for butane and 7.2 kPa for propylene/butane. The optimal values are thus close for all the working fluids. A similar plate size was found for propane and propylene/butane, while a plate with a lower aspect ratio (length-to-width ratio) was obtained for butane. Due to the lower vapour density, butane is in fact subject to higher pressure drop for the same velocity and channel geometry.

The condenser design was instead found to be similar for propane and butane, e.g. high pressure drops over 100 kPa were allowed. With similar channel geometry, the condenser design for propylene/butane led instead to low pressure drops, e.g. 11.5 kPa. This was likely due to the lower dependency of the total heat flow rate at the condenser on the pressure drops, as previously explained. Note that the condenser design corresponding to the economic optimum is an extreme design case of very high aspect ratio, due to the large bounds for variation of width and channels imposed in the sensitivity study. Such designs might be unrealistic compared to commercial plate size. The economic optimum would in any case correspond to the same evaporator design and a more realistic plate size for the condenser could be easily obtained by choosing solutions with higher condenser heat transfer area (e.g. going up in the parallel curves reported in Fig.4.4).

Table 4.4: PHE designs corresponding to the economic optimum

	Evaporator design					Condenser design						
Working fluid	W, m	L, m	N_{ch} -	A_{ht}, m^2	Δp_{ref}, kPa	W, m	L, m	N_{ch} -	A_{ht}, m^2	Δp_{ref}, kPa	COP, -	c_h €/MWh
Propane	0.250	0.460	150	20.5	6.7	0.200	1.768	50	21.1	113.3	4.4	38.9
Butane	0.400	0.447	170	36.0	4.2	0.200	1.472	80	28.1	140.2	4.5	41.5
Propylene/butane	0.250	0.655	180	35.1	7.1	0.200	1.774	100	42.3	11.5	5.5	31.6

General recommendations for design

The results presented so far led to the following findings, summarized as design recommendations for evaporator and condenser design in heat pump systems:

- Design criteria such as maximum allowable pressure drops and fixed velocities possibly lead to suboptimal solutions depending on the case study and the working fluid.
- Evaporator and condenser designs can be carried out as decoupled geometry optimization problems, e.g. the design of each component does not affect the other.
- Evaporator design influences the heat pump COP to a large extent, while the condenser design is not found to be relevant for the thermodynamic performance.
- Both components influence the economic performance: the minimum cost is found by defining optimal trade-offs between heat transfer area and pressure drop in the evaporator, while it is always desirable to minimize condenser heat transfer area.
- The economic optimum could be defined by a maximum allowable COP degradation, which theoretically corresponds to different allowable pressure drops for each refrigerant.
- The same optimal evaporator pressure drop was found for different refrigerants for this case study. This is not necessarily a general conclusion, given the very low allowable COP degradation and the dependence of the results from the economic boundary conditions.

4.2.3 Discussion

The results presented in this section were based on numerical modelling of PHE and heat pump, in both design and performance mode. The PHE models were based on a 1D discretization along the fluid-flow direction, thus neglecting the occurrence of channel-to-channel maldistribution effects. Chapter 5 will show that refrigerant pressure drops have a major impact on the heat transfer degradation due to maldistribution effects, causing an additional COP degradation. This implies that the optimal value of refrigerant pressure drop found in this study could be even lower for those refrigerants (like butane) that are particularly sensitive to maldistribution effects.

Moreover, the results of the economic analysis are strongly dependent on the boundary conditions assumed for the case study. The heat from the source was considered to come at no cost, and the COP degradation solely implied an increase of the compressor running cost. A COP decrease could also imply a reduction of the heat source utilization, which might partially counteract the cost increase in those cases where the heat source is not free (e.g. district heating applications).

Last, the importance of tailoring design criteria depending on the working fluid and application is stressed: designers must be aware that limiting inlet velocities or imposing allowable pressure drops can lead to suboptimal solutions, since the slope of COP degradation has a strong dependence on refrigerant properties. For example, for the economic analysis of propane shown in Fig.4.4 (b), choosing an evaporator design with pressure drops around 50 kPa would entail an increase of almost 1 €/MWh in the specific cost of heat.

4.3 A methodology to derive simplified guidelines to design plate heat exchanger evaporators in heat pumps using zeotropic mixtures

In this section, focus is given to evaporator design in heat pumps using zeotropic mixtures. The results of the previous section showed that the evaporator design impacts both thermodynamic and economic performance of heat pumps, while the condenser mainly affects the economic feasibility of the system. Moreover, Zühlsdorf et al. [20] showed that temperature glide matching in the evaporator has a dominating impact compared to the condenser for the optimization of heat pumps using zeotropic mixtures as working fluids, further stressing the importance of obtaining optimal evaporator configurations.

More specifically, this study presents a derivation of design guidelines for PHEs used for evaporation of zeotropic mixtures in heat pumps. A mapping of combined PHE and cycle calculations for different combinations of geometrical parameters and working fluids allows estimating the impact of heat transfer area and pressure drop on the thermodynamic and economic performance indicators of the cycle. By correlating the results with meaningful non-dimensional parameters describing the working fluid, the operating conditions and the PHE geometry, a design guideline is derived. The use of the proposed guideline is further illustrated for one of the optimal working fluids for the chosen case study, namely the mixture Propane/Iso-Pentane at (0.5/0.5) mass composition. The methodology presented in this section can be applied in different scenarios to develop similar guidelines, which are of paramount importance to avoid the cost of combined cycle and component optimization.

4.3.1 Methods

The methodology adopted in the present study is based on a parametric analysis on the main design parameters of a PHE to assess the impact of the different design configurations on the thermodynamic and economic performance indicators of a heat pump. Fig.4.5 shows the schematic of the work flow of the methodology. After the working fluid selection process, explained in section 4.3.1, the preliminary sizing of the heat pump was done and the design parameters were calculated, i.e. desired HEX capacity, mass flow rates,

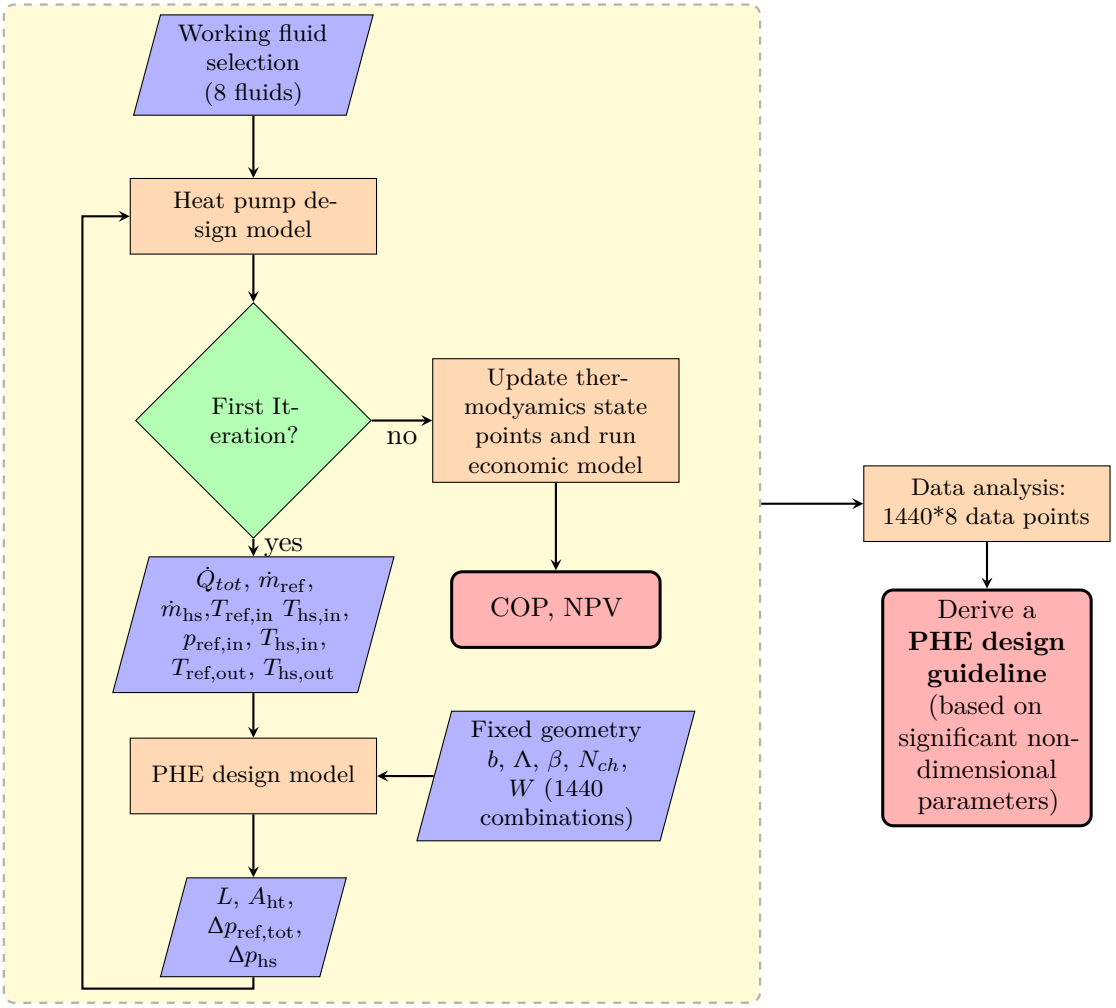

Figure 4.5: Work flow of the overall methodology

pressures and temperatures. The values were subsequently sent to the PHE design model, which additionally received as inputs the geometrical parameters from which the required heat transfer area and resulting pressure drop were estimated. The outputs were returned to the heat pump model, where the sizing of the cycle was re-evaluated. In this second iteration, the sizing process took into account the resulting heat exchanger size and pressure drops for the economic calculation, as it is briefly described in Section 4.3.1.

The process was repeated for all the combinations of geometrical parameters chosen for the parametric analysis, which is introduced in section 4.3.1. Moreover, the same process was repeated for all the eight working fluids considered in the case study, by considering the same combinations of PHE design parameters and calculating the COP and Net Present Value (NPV).

Table 4.5: Geometrical parameters of the PHE varied in the parametric study

Parameter	Value	Unit
W	0.15 - 0.25 - 0.35 - 0.45 - 0.55	m
N_{ch}	25 - 50 - 75 - 100 - 150 - 200	-
b	2 - 4 - 6 - 8	mm
Λ	2 - 4 - 6 - 8	mm
β	30 - 45 - 60	°
t	0.5	mm
D_{p}	0.03 - 0.06 - 0.1	mm

As shown in Fig.4.5, all the data points were collected and used as basis for deriving a general design guideline, valid for all the working fluids and the boundary conditions of the present case study. The aim was to correlate the point with optimal economic performances to the PHE design parameters. In order to generalize the results, non-dimensional parameters were employed as explained in section 4.3.1.

Parametric analysis and PHE geometry

The parametric analysis was carried out by varying the main design variables of the PHE. These were varied between the values reported in Table 4.5, investigating all the possible combinations between them, for a total of 1440 different PHE configurations. The plate thickness t was fixed to a value commonly found in literature [9]. The port diameter D_p was considered as fixed depending on the value of plate width W. The plate length L_{ht} was calculated as output of the PHE design model in order to match the evaporator capacity of the case study for all the combinations of PHE design variables. The plate were considered to be manufactured in stainless steel, with thermal conductivity equal to 16.2 W/(m K). In order to avoid unrealistic results and to ensure absence of maldistribution effects along the plate width, solutions with heat transfer length-to-width ratio lower than 2 were considered infeasible and excluded from further analysis.

Case study and working fluid selection

The framework of the analysis was given by a case study [139] assessing the integration of high temperature heat pumps in a spray drying facility. Waste heat was recovered by integrating a heat pump, with the aim of pre-heating air up to 120 °C. Different zeotropic mixtures were compared in terms of COP and NPV for a single-stage configuration of a vapor compression heat pump, in which the working fluid was varied based on binary mixtures formed by combinations of a number of natural refrigerants. The refrigerant screening included hydrocarbons, Dimethyl Ether (DME), Diethyl ether (DEE) and carbon dioxide CO_2, chosen for their low GWP and ODP, and being miscible between

each other for wide ranges of temperature and pressure without leading to any chemical reactions [20, 139]. Table 4.6 summarizes the best performing mixtures, with considered mass composition. It is noted that the evaporation pressures were found to be well below the maximum operating pressure for PHEs. The table also shows the ideal COP, calculated without accounting for pressure drop at the evaporator.

Table 4.6: Summary of the considered working fluids

Working fluid	p_{eva} , bar	COP, -
Propane/Iso-Pentane (0.5/0.5)	4.9	3.08
Propane/n-Pentane (0.8/0.2)	8.4	3.04
Propane/n-Pentane (0.4/0.6)	3.0	3.02
Butane/Hexane (0.9/0.1)	2.5	3.07
DME/n-Pentane (0.4/0.6)	2.6	3.26
DME/n-Pentane (0.7/0.3)	5.0	3.24
DME/Iso-Pentane (0.5/0.5)	4.0	3.15
Propylene/Iso-Pentane (0.4/0.6)	3.9	3.14

Heat pump cycle model

The thermodynamic cycle was modelled as presented in Chapter 2.6.1. Table 4.7 shows the design parameters of the cycle. The heat source side was completely defined by the boundary conditions, while the outlet temperature of the condenser was set as a free variable. The minimum superheat was imposed equal to 5 K.

Table 4.7: Boundary conditions for the heat pump

Evaporator			**Condenser**			**Compressor**		
Heat source	water		Heat sink	water		η_{is}	0.80	-
$T_{\text{hs,in}}$	65	°C	$T_{\text{sink,in}}$	75	°C	η_{motor}	0.95	-
$T_{\text{hs,out}}$	40	°C	$\dot{m}_{\text{sink,tot}}$	10.6	kg/s	ΔT_{sh}	5	K
$\dot{m}_{\text{hs,tot}}$	14.8	kg/s	ΔT_{pinch}	10	K			
$\dot{Q}_{\text{eva}}$	1544	kW						
ΔT_{pinch}	10	K						

PHE design model

The implemented PHE design model was described in Chapter 2.3, i.e. using the 1D discretization approach at constant enthalpy steps. A total number of $n = 50$ control volumes was chosen, while the tolerance was set to 10^{-2}. The Silver [100] and Bell and Ghaly [101] method was used to estimate the heat transfer coefficient, and the same correlations of section 4.2.1 were chosen. Martin [77] was applied for the single-phase heat transfer coefficient. All the contributions to pressure drop were accounted by the

model, as presented in Chapter 2.2.6. Frictional pressure drop was estimated by using the correlation by Amalfi et al. [93]. In the single-phase region, the friction factor correlation by Martin [77] was used for both the superheated refrigerant and the water flow. For the refrigerant flow, port pressure drop was considered only at the outlet control volume, since the inlet drop was included in the refrigerant expansion at the throttling valve. Both inlet and outlet pressure drops due to ports were evaluated for the heat source, thereby contributing to the total water pumping power.

Economic model

After the sizing of the PHE, the heat pump model was re-evaluated by taking the updated temperature and pressure at the evaporator outlet into account, as shown in Fig.4.5. Therefore, the COP was affected by the change in compressor power resulting from the mixture pressure drop. Different aspects of the HEX design influenced the value of the NPV of the heat pump. The NPV was calculated by considering different cost and revenue streams, by using Eq.(4.1) [139]. The considered costs were the Total Capital Investment (TCI), accounting for all the components of the system, the Operation and Maintenance Cost (OMC), the electricity cost(FC_{hp}) due to the compressor running and the required water pumping cost (FC_w). The revenue stream was considered as the natural gas saving(FC_{ng}), which otherwise would be necessary to produce the thermal energy output of the heat pump.

$$NPV = -TCI - OMC - \frac{FC_{hp}}{CRF} - \frac{FC_w}{CRF} + \frac{FC_{ng}}{CRF} \tag{4.1}$$

The interest and inflation rates were assumed equal to 7 % and 2 %, respectively, and then used for the estimation of the Capital Recovery Factor (CRF), with a plant economic lifetime of 20 years [98] [140]. Operation and Maintenance Costs were assumed to be the 20 % of the investment cost as one time cost at the time of the investment [140]. The saving of natural gas was calculated by estimating the useful thermal energy produced by the heat pump, equal to the heat sink capacity and by considering a boiler efficiency η_{boiler} equal to 0.9 [98]. The price of natural gas was considered as 0.0303 €/kWh [141].

The TCI accounted for the investment of condenser, compressor and evaporator. The sizing of the condenser was carried out by considering constant heat transfer coefficients and by using the logarithmic mean temperature difference methods for the three different sections of de-superheating, condensation and subcooling. The TCI of each individual component was calculated from the Purchased Equipment Cost (PEC), scaled according to the component size with scaling factors and reference values of PECs reported by Ommen et al. [98]. The TCI was increased by a factor 4.16 compared to the PEC, to account for the investment of the expansion of an existing facility[140].

The running cost of the compressor, given by FC_{hp} was adapted to the updated compressor power by considering an estimation of 7400 hr/yr [139] as annual operating time τ_h of

the heat pump and an electricity cost c_{el} of 0.0783 €/kWh [141]. The additional fuel cost term due to the water pressure drops, was calculated by using Eq.(4.2) as a function of the water mass flow rate, water density, total water pressure drops, and a pump efficiency η_{pump} equal to 0.95.

$$\mathrm{FC_w} = \frac{\dot{m}_{\mathrm{hs}}}{\rho_{\mathrm{hs}}} \frac{\Delta p_{\mathrm{hs,tot}}}{\eta_{\mathrm{pump}}} c_{\mathrm{el}} \tau_h \tag{4.2}$$

Fig.4.6 shows the log(p)-h diagram of the heat pump with and without pressure drops in the evaporator. It can be noticed how the outlet of the evaporator is affected by the pressure losses, thus changing the compressor power required as well as the investment cost, which is based on the suction line. The pressure drop also influences the evaporator inlet location in the diagram, but to a lower extent compared to the outlet. In order to compare the results for different working fluids, performing with different COP and maximum NPV, it was decided to normalize each NPV for the maximum value calculated for the specific fluid. The value of NPV of a certain design point of the HEX i for a given working fluid wf was therefore normalized as $\mathrm{NPV}^{\star}_{\mathrm{i-wf}}$, defined by Eq.(4.3).

$$\mathrm{NPV}^{*}_{\mathrm{i-wf}} = \frac{\mathrm{NPV}_{\mathrm{i-wf}}}{\max(\mathrm{NPV}_{\mathrm{wf}})} \tag{4.3}$$

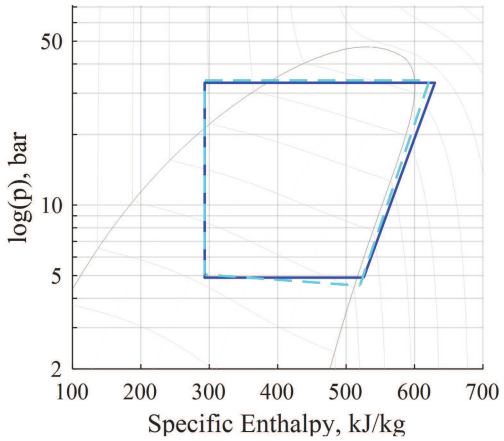

Figure 4.6: Example of log(p)-h diagram without pressure drops (blue) and with 50 kPa pressure losses in the evaporator (sky-blue)

Data analysis

The different HEX configurations and working fluids were compared based on dimensionless numbers, in order to derive a guideline describing the design points corresponding to maximum NPV. Non-dimensional parameters were chosen in order to describe the impact

of the fluid properties, of the boundary conditions imposed by the cycle (refrigerant evaporation pressure, mass flow and inlet quality) and of the PHE geometry. The main dimensionless numbers governing the heat transfer and pressure drop correlations for the two-phase flow of the mixture were used, and they are reported in Table 4.8.

The numbers were used to correlate the normalized net present value to the different heat exchanger designs. The parameters were evaluated at the refrigerant conditions at the evaporator inlet, since the scope was to derive guidelines applicable before the actual component design. The inlet conditions are fixed by the boundary conditions of the heat pump, thereby being known for all the fluids a priori. It was therefore decided to exclude the Boiling number from the data analysis, since it requires information on the heat flux distribution along the heat exchanger and a preliminary estimation of the heat transfer area is needed. Note that the Weber number We_m is defined by evaluating the two-phase momentum density (Eq.(2.20)).

Table 4.8: Non-dimensional parameters used for the analysis of the results

Symbol	Name	Formula
$\theta^\star$	Dimensionless inclination angle	$\frac{90-\beta}{70}$
Bd	Bond number	$\frac{gD_h^2(\rho_L-\rho_V)}{\sigma}$
We_m	Weber number	$\frac{G^2 D_h}{\sigma \rho_m}$
ρ^*	Liquid-to-vapour density ratio	$\frac{\rho_L}{\rho_V}$
$\mathrm{Re}_{\mathrm{LO}}$	Liquid only Reynolds number	$\frac{GD_h}{\mu_L}$
Re_V	Vapour alone Reynolds number	$\frac{GxD_h}{\mu_V}$

The correlation between the dimensionless parameters and the normalized NPV was obtained by adopting a power law of the form expressed by Eq.(4.4).

$$\mathrm{NPV}^* = a \cdot \theta^{*b} \cdot \mathrm{Bd}^c \cdot \mathrm{We}_m^d \cdot \mathrm{Re}_V^e \cdot {\mathrm{Re}_{\mathrm{LO}}}^f \cdot \rho^{*g} \tag{4.4}$$

The normalized NPV was first correlated as function of all the dimensionless parameters considered in Table 4.8. All the design points with positive NPV were considered in the fitting, and the results for all the working fluids were considered simultaneously in one fitting. After deriving the coefficient for Eq. (4.4), the most relevant parameters

were identified. This was done by evaluating the obtained exponent and by comparing different combinations of non-dimensional numbers. The correlation that best fitted the NPV trend for all the fluids, as well as leading to a similar optimal range for the different mixtures, was chosen and presented as design guideline.

Uncertainty analysis

For each correlation chosen for the PHE design model, for both heat transfer and pressure drop, a certain accuracy was reported by the authors. This measure represents an estimation of how well the prediction method fits the experimental database from which the correlation was derived. Therefore the accuracy does not necessarily indicate the uncertainty of the prediction methods when they are applied to different working fluids, geometry and operating conditions. It is however relevant to evaluate the change of the obtained results when a certain deviation is applied to the calculation of heat transfer coefficient and pressure drops. For this purpose the accuracy bounds of each correlations were considered as a source of uncertainty in an uncertainty analysis, with the aim of evaluating to which extent the results were dependent from likely errors in the inputs. The bounds are reported in Table 4.9, with the exception of h_V. Since Martin [77] expresses h_V as a a function of f_V, the uncertainty of h_V was directly included in by considering the accuracy bound for the vapour friction factor f_V.

Table 4.9: Input uncertainties for the uncertainty analysis

Parameter	Correlation	Bounds	Reference
h_C	Amalfi	± 22.1 %	Mean absolute error [93]
$h_{\mathrm{NB-id}}$	Cooper	± 59 %	Mean absolute error, reported in [28]
$\frac{h_{\mathrm{NB-mix}}}{h_{\mathrm{NB-id}}}$	Thome and Shackir	± 11.1 %	Mean absolute error, reported in [119]
f_{TP}	Amalfi	± 21.5 %	Mean absolute error [93]
f_{V}	Martin	- 50 % + 100 %	Accuracy bounds, reported in [9]

The Monte Carlo (MC) method [142] was applied in order to carry out the uncertainty analysis, with the aim of estimating the probability density of the model outputs, namely A_{ht}, $\Delta p_{\mathrm{r,tot}}$, $\Delta p_{\mathrm{s,tot}}$ and NPV. The inputs were assumed to be uniformly distributed between the uncertainty bounds reported in Table 4.9. A latin hypercube sampling (LHS) technique was adopted to create 500 different samples in the input space, proved to be more reliable compared to random sampling [143]. The Monte Carlo (MC) simulations

were performed following the approach by Sin and Gernaey [144], and the results were obtained as mean values, standard deviations and 95 % coverage intervals. The analysis was applied to Propane/Iso-Pentane (0.5/0.5), by fixing the PHE geometry to one of the optimal designs found by applying the derived design guideline.

4.3.2 Results

In this section the main results are presented. First, the trade-off between heat transfer area and pressure drops and the impact on the different revenue and cost streams is reported. Next, the fitting with the non-dimensional parameters and the derivation of the final design guideline is illustrated for the case study.

Heat transfer area and pressure drops

Fig.4.7 shows the NPV as function of the heat transfer area (a) and total refrigerant pressure drops (b) for all the fluids considered in the analysis. It is shown that both heat transfer area and pressure drops have an impact on the economic performance of the heat pump. However, the NPV decreases to a lower extent for higher values of A_{ht} compared to an increase of the refrigerant pressure drops. Fig 4.7(b) shows that for

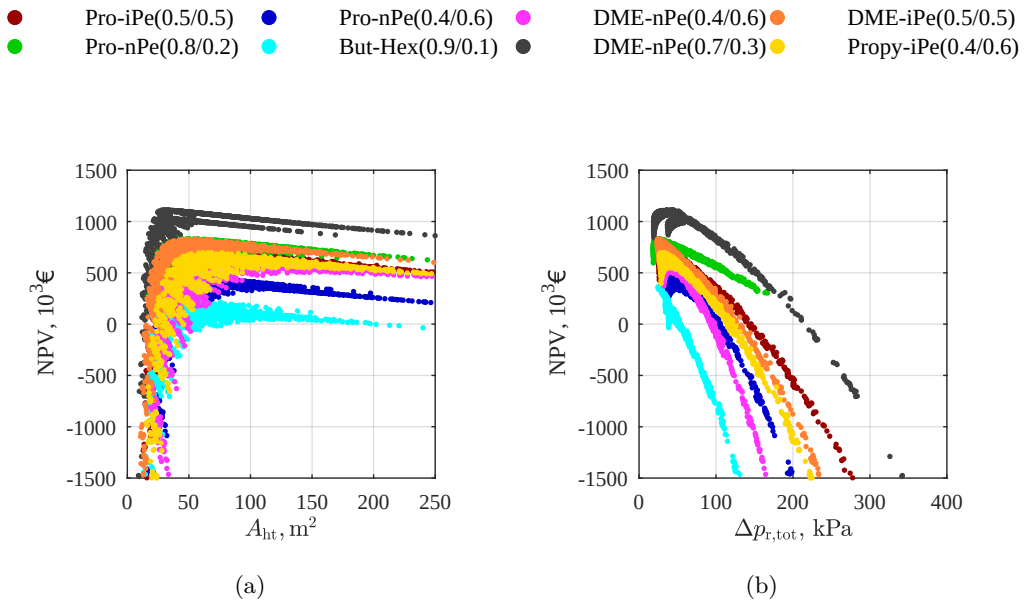

Figure 4.7: Effect of heat transfer area of the evaporator (a) and refrigerant total pressure losses (b) on the non-dimensional NPV for all the working fluids

all the eight cases there is a trade-off which coincides with minimizing the refrigerant pressure drops to a very low value. Moreover, Fig 4.7(b) shows that the pressure drops impact is different depending on the fluid: the mixtures Butane/Hexane (0.9/0.1) and DME/n-Pentane (0.4/0.6) are the most sensitive to pressure drops, performing with negative NPVs at 60 kPa and 120 kPa, respectively. On the contrary,Propane/n-Pentane (0.4/0.6) shows a weaker dependence, with NPV values always positive in the considered pressure drop range.

Cost breakdown

Fig.4.8 shows the breakdown of the NPV as calculated by Eq.4.1. The abscissa reports the refrigerant total pressure drop, and the obtained trends are similar for all the working fluids. The blue line indicates the revenue stream, positively contributing to the NPV and determined by the natural gas saving. The black line represents the cost stream, negatively impacting on the NPV and estimated as the sum of the different cost terms. The breakdown of the cost is indicated by the different filling colors of the cost line.

The dominant contribution to the cost stream was given by the compressor running cost (grey area), negatively affected by the refrigerant pressure drops, which caused an increase of the compressor work. This is explained by Fig.4.9, where the COP of the heat pump is plotted against the total refrigerant pressure drops. For a fixed design thermal load of the heat pump, a lower COP entails a higher required compressor work, as shown by Eq.(2.42). A sharp decrease is observed for all the fluids, with different slopes, similarly to the trends found in Fig.4.7 (b). The different trends for the different fluids found in the cost breakdown of Fig.4.8 can be therefore explained by a different sensitivity of the COP to the pressure drop. The mixture Propane/n-Pentane (0.8/0.2) was found to be the least affected by pressure drop, while Butane/Hexane (0.9/0.1) presented the steepest slope.

In the cost breakdown of Fig.4.8, the TCI is the second highest contribution, indicated by the light-blue area. The TCI undergoes a slight increase for low values of refrigerant pressure drop, and then increases more sharply for higher pressure drop. Since operation and maintenance was considered as a fixed share of the capital investment, OMC undergoes the same trend. An explanation for the TCI behaviour can be found in Fig.4.10(a) and (b), showing the capital investment of the evaporator, condenser and compressor as functions of the total refrigerant pressure drop. All the working fluids are reported in the same plot with different marker colors. The evaporator and condenser investment costs, directly related to the heat transfer area, are one order of magnitude lower than the compressor investment if the pressure drops are not minimized. When the evaporator investment increases at lower pressure drops (entailing a higher investment due to the larger heat transfer area), the CI of the HEX reaches the same order of magnitude of the lower investment entailed by the compressor. The change in HEX CI due to varying heat transfer area is similar for all the fluids, with an overlap of the different curves.

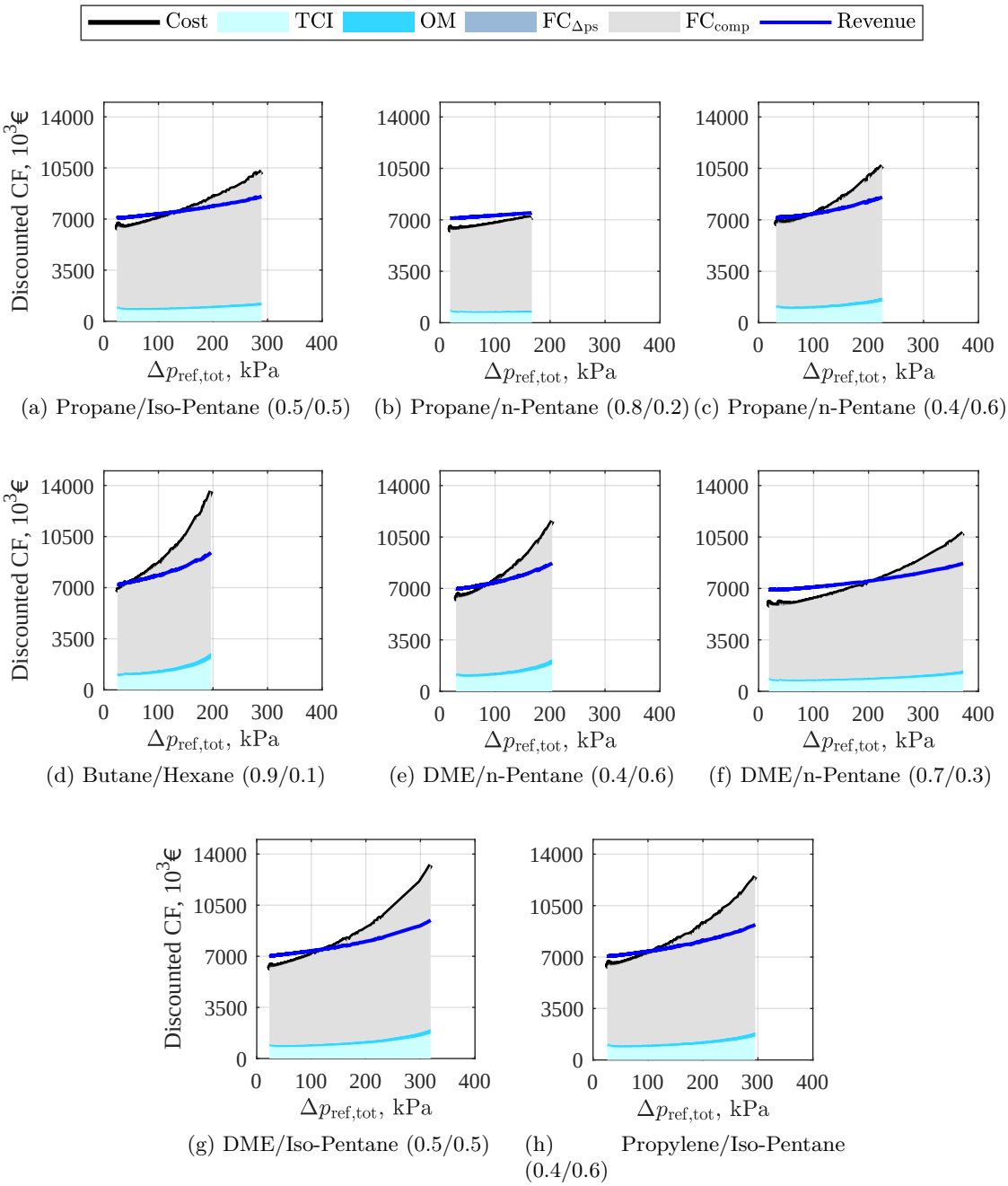

(a) Propane/Iso-Pentane (0.5/0.5) (b) Propane/n-Pentane (0.8/0.2) (c) Propane/n-Pentane (0.4/0.6)

(d) Butane/Hexane (0.9/0.1) (e) DME/n-Pentane (0.4/0.6) (f) DME/n-Pentane (0.7/0.3)

(g) DME/Iso-Pentane (0.5/0.5) (h) Propylene/Iso-Pentane (0.4/0.6)

Figure 4.8: Breakdown of the contributions to the NPV, divided in cost and revenue. The colours indicate the different shares of the terms contributing to the cost stream

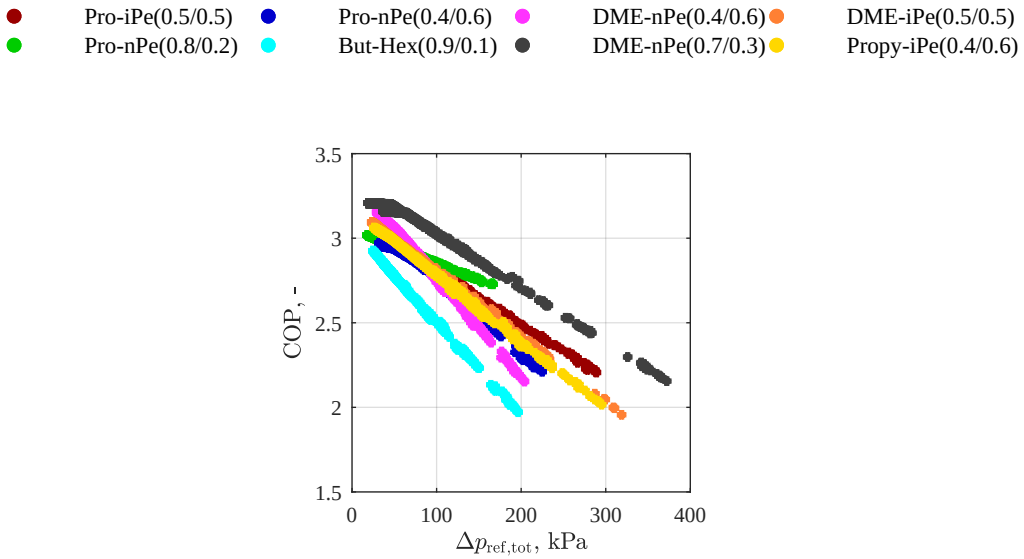

Figure 4.9: COP as function of the total refrigerant pressure drops for all the working fluids

On the other hand, the compressor CI in Fig.4.10 (b) undergoes a steep increase for higher values of pressure drop and presents different trends depending on the mixture. The sharp increase is due to the change in the compressor suction line, affected by the true evaporator outlet. In fact, for higher refrigerant pressure drops, a lower refrigerant outlet density is obtained, entailing a higher volume flow rate, which is directly proportional to the compressor size. The different slopes for the different fluids must be instead related to a different sensitivity of the refrigerant properties, in particular density, to the change in evaporator outlet pressure. The trends of the fluids follow the results found for COP in Fig.4.9, with Propane/n-Pentane (0.8/0.2) showing the weakest dependence on the pressure drops and opposite trends for mixtures Propane/n-Pentane (0.4/0.6) and Butane/Hexane (0.9-0.1), where the pressure drops have a major influence on both the compressor running cost and TCI.

One very relevant aspect to highlight is the intersection point between revenue and costs streams, in Fig.4.8, representing the pressure drop limit above which the design of the PHE leads to infeasible solutions, i.e. with negative NPV. This limit value is not the same for all the working fluids, supporting the thesis that it is not necessarily optimal to design HEXs by imposing a maximum allowable pressure drop regardless of the working fluid or boundary conditions.

The water pumping cost was found to be negligible compared to the all the other contributions. No clear relation is therefore expected between heat source pressure drops and NPV.

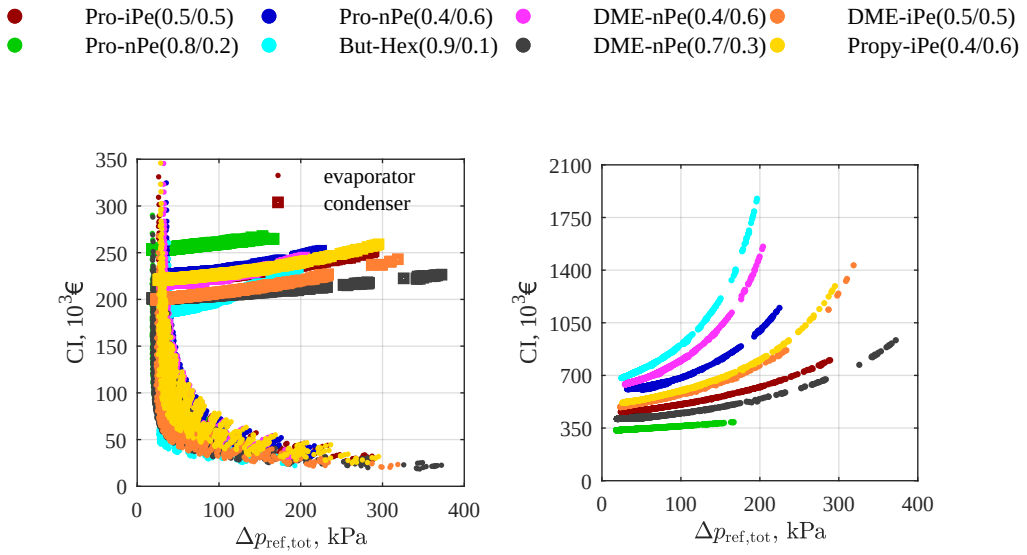

(a) heat exchangers (b) compressor

Figure 4.10: Capital investment of the heat exchangers (a) and compressor (b), as function of the total refrigerant pressure drops for all the working fluids

Last, it must be noted that such analysis highlights considerations, which might be useful when choosing a optimal working fluid for a specific case study. In fact, by looking at Fig.4.7 (a) and Fig.4.9, the mixture DME/-Pentane (0.7/0.3) outperforms the other fluids both in terms of maximum NPV and COP found in the mapping, thereby suggesting the choice of such fluid as optimal. However, the mixture Propane/n-Pentane (0.8/0.2) resulted to have the weakest dependence from refrigerant pressure drops, thus offering an additional flexibility during the evaporator design process. It would be therefore up to the designer to evaluate and prioritize the different aspects.

Correlation between NPV and non-dimensional parameters

By exponentially correlating the design points by means of Eq.(4.4) to the chosen non-dimensional parameters, the NPV* is found to be proportional to the combinations of dimensionless numbers reported by Eq.(4.5), indicated by K.

$$K = \theta^{*0.045}\mathrm{Bd}^{0.051}\mathrm{We}_m^{-0.011}\rho^{*-0.066}\mathrm{Re}_{LO}^{0.009}\mathrm{Re}_V^{-0.12} \tag{4.5}$$

Fig.4.11 reports the normalized net present value as function of K, for Propane/Iso-Pentane (0.5/0.5). The different colors represent the chevron angle of the PHE, namely 30°, 45° and 60° corresponding to a value of non-dimensional inclination angle of 0.86,

0.64 and 0.43, respectively. The trends for the other working fluids are not shown in the paper, but they are similar. The obtained design points are well correlated by K, and it is recommended to employ HEXs with $K = [0.4 - 0.6]$ at the evaporator inlet, in order to obtain solutions with NPV in the best 20 %. By increasing the value of K, the economic performance is negatively affected by the increase in heat transfer area, while for $K < 0.4$ an increase of refrigerant pressure losses entails a steep decrease of NPV.

The use of a design guideline based on K, which depends on six different parameters, might however lead to have redundant information on the boundary conditions and the fluids in the parameters. The problem was therefore simplified by relating the NPV* to a selected number of non-dimensional parameters only. In order to do so, the results were assessed based on the coefficients and on additional considerations.

First, the dependence of the NPV on the liquid only Reynolds number $\mathrm{Re_{LO}}$ is weak, since its exponent in Eq.(4.5) is two orders of magnitude lower than the vapour alone Reynolds number and one order of magnitude lower compared to the other parameters, thereby suggesting that a good fitting could be obtained by neglecting the influence of this non-dimensional number. Furthermore, it was decided to exclude the liquid to vapour density ratio ρ^*, since it contains information solely depending on the inlet densities and other dimensionless number, as the Reynolds numbers, the Weber number and the Bond number already contain the density characteristics of both vapour and liquid phases.

Lastly, by looking at the impact of the dimensionless inclination angle θ^* in Fig.4.11, the plot suggests that it is always optimal to minimize the chevron angle (hence enhancing the degree of turbulence of the fluid flow in the channels) if the PHE design is carried out in the optimal region or else for high value of K, i.e. designs with higher heat

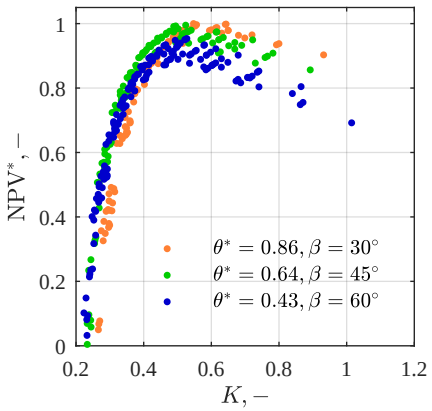

Figure 4.11: Normalized NPV as function of all the dimensionless parameters correlated exponentially for Propane/Iso-Pentane (0.5/0.5). The different colors represent the different chevron angles adopted

transfer area. On the contrary, with refrigerant dominant pressure losses ($K < 0.4$), it is slightly better to employ higher chevron angles for reaching less turbulent flow, thereby decreasing the pressure losses. It is therefore unnecessary to include the chevron angle into the design guideline, since it is possible to tune the other PHE design parameters in order to be in the optimal design region, where it is recommended to employ low values of β.

Correlation between NPV and selected dimensionless numbers

The results are presented as function of the three remaining dimensionless numbers, namely the Bond number Bd, the Weber number We_m and the Reynolds number of the vapour flowing alone Re_V. Table 4.10 shows the coefficients obtained by fitting the normalized net present values with different combinations of the three dimensionless parameters. Four different cases were assessed by combining the three parameters all at once and by considering combinations of only two of them. The aim was to find which correlation attained the best representation of NPV*, thereby being appropriate for deriving the design guideline. The values reported in the first row of the table (Case I), obtained by considering all the three non-dimensional numbers, suggest that there is not a predominant contribution of one of them, since the coefficients lie in a similar range.

Table 4.10: Coefficients obtained by fitting the NPV* to different combinations of dimensionless parameters

Case	Parameters combination	a	b	c
Case I	$\mathrm{Re}_V^a \cdot \mathrm{Bd}^b \cdot \mathrm{We}_m^c$	1.21	-0.19	-0.87
Case II	$\mathrm{Bd}^b \cdot \mathrm{We}_m^c$	0.14	-0.25	
Case III	$\mathrm{Re}_V^a \cdot \mathrm{We}_m^c$	0.74	-	-0.62
Case IV	$\mathrm{Re}_V^a \cdot \mathrm{Bd}^b$	-0.42	0.26	-

Fig.4.12 shows the NPV* as a function of the different exponential combinations of dimensionless numbers, with the ordinate axis reporting the design points of all the working fluids. It can be observed that the normalized net present value presents a clear trend for all of the combinations. This is possibly related to the redundancy of information on geometry, fluid properties and boundary conditions contained in the three parameters.

By looking at the formulas reported in Table 4.8, We_m and Re_V are dependent on the hydraulic diameter D_h and on the free flow area A_0, while the Bond number Bd solely

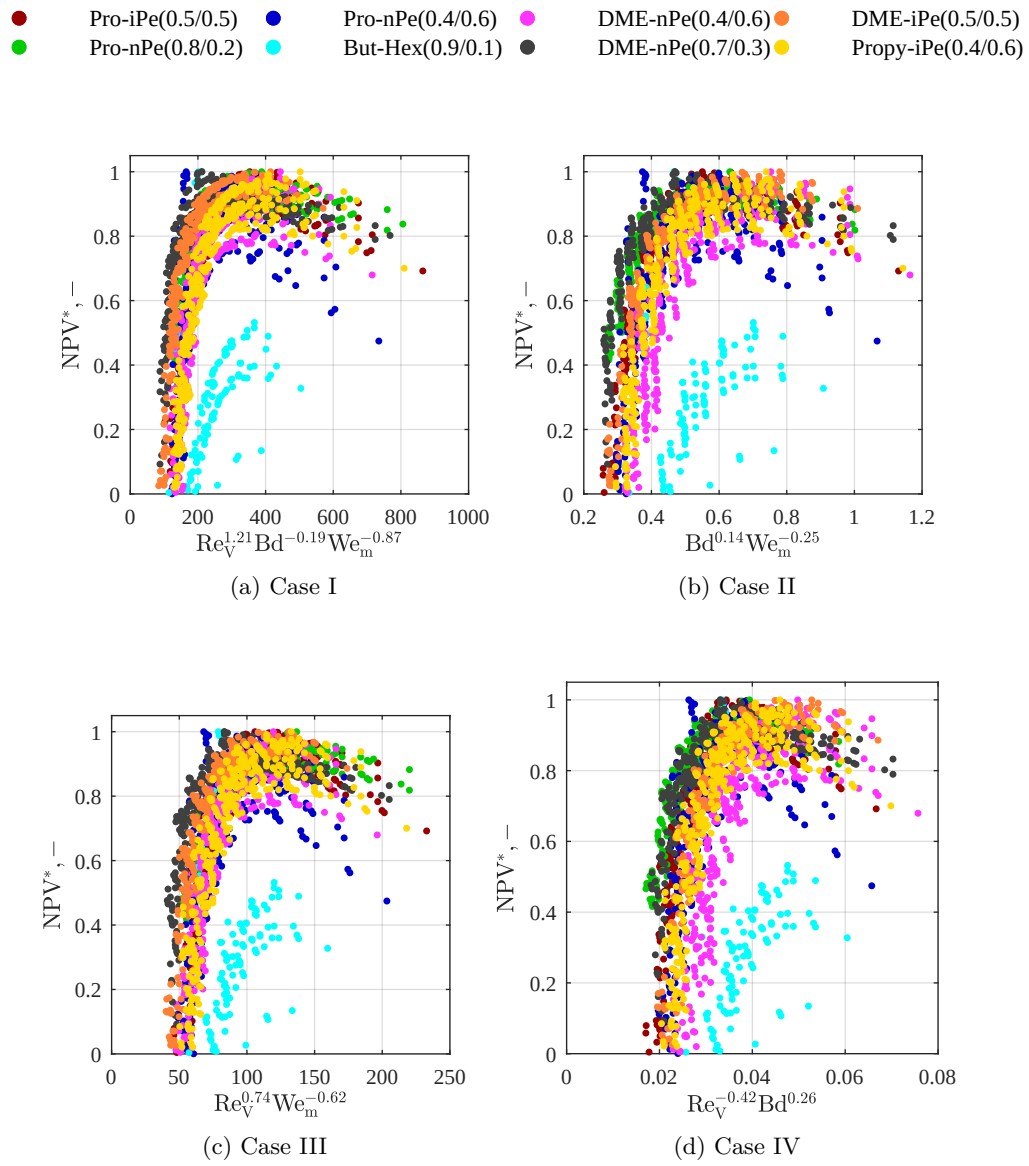

(a) Case I (b) Case II

(c) Case III (d) Case IV

Figure 4.12: Normalized NPV as function of different combinations of non-dimensional numbers for all the working fluids reported in Table 4.10; (a)Case I; (b)Case II; (c)Case III; (d)Case IV

depends on D_h. Any combinations of the parameters therefore contain all the information regarding the PHE geometry, i.e. the corrugation geometry, plate width and number of channel, with the exception of plate length (estimated by the PHE sizing for matching the thermal load and thus not needed to be included in the guideline) and chevron angle, excluded from the guideline.

Moreover, by looking at the fluid properties of the three non-dimensional numbers, it can be seen that surface tension σ and the liquid and vapour phase densities ρ_L and ρ_V are contained in any of considered combinations, together with the inlet vapour quality x and mass flow $\dot{m}_r$.

In order to choose which combination of parameters to consider for the final design guideline, the position of the optimal values of the different coefficients was compared for the different working fluids. The aim was to understand which design guideline resulted in a recommendation which was narrower to describe the optimal NPV* for all the working fluids.

Table 4.11 reports the minimum, maximum and mean values of the different cases for the best solutions, which were selected as NPV* deviating at most 5 % from each best solution. The results are reported for all the working fluids, as well as the overall maximum, minimum and mean value. The deviation (last row) was estimated by considering how far the minimum and maximum value were from the overall mean.

The results suggest that the best agreement between the different mixtures is obtained by the combination of Re_V and Bd, whose deviations are -34 % and 48 % for the minimum and maximum value, respectively. The interval covered by Butane/Hexane(0.9/0.1) is shifted towards the left compared to the other working fluids.

Fig.4.13 shows the positive solutions of NPV for all the working fluids as function of the obtained parameter $\mathrm{Re_V}^{-0.42}\mathrm{Bd}^{0.26}$. The red line represents the mean value, equal to 0.040, while the dotted black lines represent the minimum (0.026) and maximum value (0.059). The plots show that all the fluids, except Butane/Hexane (0.91/0.1), present a

Table 4.11: Minimum, maximum and average values of different combinations of dimensionless numbers for the best results (5 % NPV*), for each working fluid and overall

	Case I $\mathrm{Re}_V^{1.21}\cdot\mathrm{Bd}^{-0.19}\cdot\mathrm{We}_m^{-0.87}$			Case II $\mathrm{Bd}^{0.14}\cdot\mathrm{We}_m^{-0.25}$			Case III $\mathrm{Re}_V^{0.74}\cdot\mathrm{We}_m^{-0.62}$			Case IV $\mathrm{Re}_V^{-0.42}\cdot\mathrm{Bd}^{0.26}$		
Working fluid	min	max	mean	min	max	mean	min	max	mean	min	max	mean
Propane/Iso-Pentane (0.5/0.5)	2110	3310	2620	0.48	0.75	0.59	91.4	152	118	0.030	0.047	0.038
Propane/n-Pentane (0.8/0.2)	2240	3800	2900	0.48	0.77	0.60	104	166	128	0.031	0.046	0.037
Propane/n-Pentane (0.4/0.6)	1420	2780	2130	0.37	0.70	0.54	68	129	99	0.026	0.045	0.036
Butane/Hexane (0.9/0.1)	1560	1570	1560	0.47	0.47	0.47	78.9	80.9	79.8	0.034	0.034	0.034
DME/n-Pentane (0.4/0.6)	2150	2800	2380	0.65	0.86	0.72	103	144	118	0.044	0.058	0.049
DME/n-Pentane (0.7/0.3)	1640	2430	1930	0.46	0.67	0.53	81.3	121	96	0.032	0.045	0.037
DME/Iso-Pentane (0.5/0.5)	1810	2920	2190	0.55	0.88	0.66	88	151	111	0.038	0.059	0.046
Propylene/Iso-Pentane (0.4/0.6)	2100	3330	2670	0.52	0.84	0.67	93	160	124	0.034	0.054	0.043
Overall	1420	3800	2300	0.37	0.88	0.60	68	166	109	0.026	0.059	0.040
Deviation in %	-38%	65%		-38%	46%		-38%	-52%		**-34**%	**-48**%	

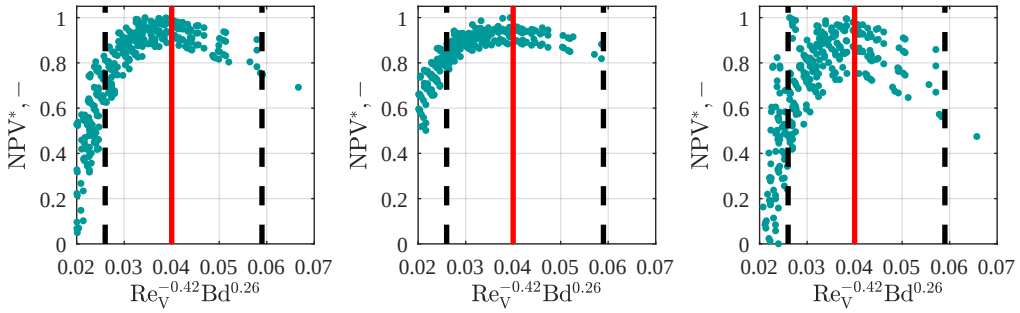

(a) Propane/Iso-Pentane (0.5/0.5) (b) Propane/n-Pentane (0.8/0.2) (c) Propane/n-Pentane (0.4/0.6)

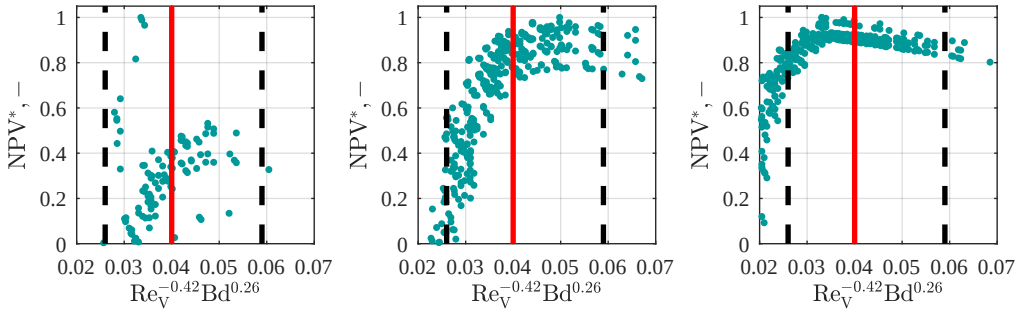

(d) Butane/Hexane (0.9/0.1) (e) DME/n-Pentane (0.4/0.6) (f) DME/n-Pentane (0.7/0.3)

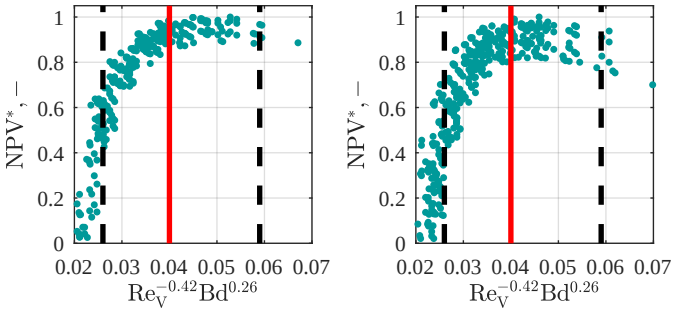

(g) DME/Iso-Pentane (0.5/0.5) (h) Propylene/Iso-Pentane (0.4/0.6)

Figure 4.13: Normalized NPV as function of $\mathrm{Re_V}^{-0.42}\mathrm{Bd}^{0.26}$ for all the working fluids. The red line represents the mean value $\mathrm{Re}_V^{-0.42}\mathrm{Bd}^{0.26} = 0.04$, while the dotted lines represent max and min, 0.059 and 0.026 respectively.

good agreement with the obtained guideline: the optimal NPV points are all included

in the interval [0.040-0.059], with the peak lying around 0.040 for almost all the fluids. DME/n-Pentane (0.4/0.6) and DME/Iso-Pentane (0.5/0.5) have the maximum slightly shifted towards 0.050. They perform however with NPV* very close to the optimum for 0.040 (equal or above 80 % of the optimal value). Propane/n-Pentane(0.4/0.6) shows solutions with NPV* going down to -30 % for the optimal value for 0.040.

The worst performing points are probably related to higher values of chevron angle (see Fig.4.11), thus optimal designs can be achieved as well with the proposed guideline. In agreement with the numbers reported in Table 4.11, Butane/Hexane (0.91/0.1) is slightly shifted towards the left compared to the other fluids, i.e. with optimal points in the interval [0.026-0.040]. Nonetheless it has been decided not to shift the design interval towards values optimal for this fluid, since it was shown that this mixture performed with mostly negative NPV in the mapping compared to all the other fluids (see Fig.4.8).

After the assessment of the results from Table 4.11 and Fig.4.13, it was decided to propose the guideline presented by Eq.4.6 as design recommendation.

$$\mathrm{Re}_V^{-0.42}\mathrm{Bd}^{0.26} \approx 0.040 \tag{4.6}$$

If a higher value is obtained, the PHE design is expected to lead to higher equipment investment (related to the heat transfer area), while a lower value will lead to high refrigerant pressure losses, resulting in a steep decrease of the NPV.

4.3.3 Discussion

Section 4.3.3 presents the discussion of an application of the derived guideline, Section 4.3.3 reports the results of the uncertainty analysis while Section 4.3.3 briefly comments on the deviation of the obtained guideline if an alternative prediction method is used for the refrigerant pressure drop estimation, which resulted to have the largest impact on the heat pump economic performance. Section 4.3.3 highlights on the limitation of the study and potential future work.

Application of the derived design recommendation

The case of the first working fluid mixture was considered, namely Propane/Iso-Pentane (0.5/0.5). The design, based on the derived guideline consists of the following steps:

1. Fix the boundary conditions of the thermodynamic cycle and estimate the inlet condition at the evaporator (quality, mass flow, evaporation pressure).
2. Calculate the following fluid properties at the inlet condition: ρ_L, ρ_V, σ, μ_V.
3. Choose a value for the chevron angle β. It is recommended to employ low values (e.g. $30-35°$), if the design parameter is not constrained.

4. Decide which design parameters are fixed by external boundaries (fixed plate size and/or numbers and/or corrugation geometry).

5. Tune the remaining free design parameters in order to obtain $\mathrm{Re}_V^{-0.42}\mathrm{Bd}^{0.26} \approx 0.040$. Calculate the required plate length by using the evaporator heat flow rate, fixed by the cycle.

Table 4.12 shows different combinations of geometrical parameters, each line corresponding to a different PHE design. Some geometrical parameters were fixed a priori, while other were calculated by means of the design guideline using the methodology presented above. The goal of fixing and releasing different geometrical parameters was to show the different possible scenarios of a designer, which might be constrained in some of the design variables. The plate length was estimated by the sizing model, matching the case study thermal load.
In the first three rows of the table, the corrugation geometry, namely pitch Λ and height b, were fixed together with the corrugation angle. The number of channels N_{ch} and plate width W were found in order to obtain values of $\mathrm{Re}_V^{-0.42}\mathrm{Bd}^{0.26}$ equal to 0.040. It can be noticed that by respecting the proposed design guideline, the NPV deviates maximum -4.4 % from the best value of the parametric analysis. The COP in the third design point is slightly lower due the the higher pressure drops of the refrigerant.

The forth and fifth rows of Table 4.12 report two PHE design which were obtained by fixing the plate width and the number of plates, as well as the chevron angle. The corrugation geometry was found in order to match the design guideline and it was found that also in this case the two solutions deviate of only -1.9 % and -1.5 % from the best NPV, thereby lying in an optimal region for the PHE design. It can be noticed that all the five solutions proposed have the same magnitude of refrigerant pressure drops, ranging from 30 kPa to 35 kPa. This is the same range shown in Fig.4.8(a) for the same working fluid.

Table 4.12: Some examples of PHE design points for the mixture Propane/Iso-Pentane (0.5/0.5)

Design	W, m	N_{ch}, -	β, °	b, m	Λ, m	L_{ht}, m	A_{ht}, m^2	$\Delta p_{\mathrm{ref,tot}}$, kPa	NPV, €	ΔNPV, %	COP, -	$\mathrm{Re}_V^{-0.42}\mathrm{Bd}^{0.26}$, -
	Free variables		Fixed geometry									
I	0.20	188	45	0.005	0.007	0.66	92.0	31.0	696960	-3.6	3.02	0.040
II	0.19	196	35	0.005	0.007	0.57	80.1	31.3	711620	-1.5	3.02	0.040
III	0.44	59	35	0.007	0.007	0.65	80.7	36.0	690990	-4.4	3.01	0.040
	Fixed geometry			Free variables								
IV	0.20	100	35	0.009	0.008	0.77	82.1	32.6	708580	-1.9	3.02	0.040
V	0.18	150	35	0.007	0.006	0.54	79.8	31.0	712180	-1.5	3.02	0.040

Uncertainty analysis

The uncertainty analysis on the values of heat transfer coefficients and pressure drops was carried out for the design I reported in Table 4.12 for Propane/Iso-Pentane (0.5/0.5), performing with a NPV -3.6 % lower than the best solution found in the mapping. The mean values, standard deviation and 95 % coverage interval are reported in Table 4.13. The input uncertainties assigned to the heat transfer and pressure drops correlations resulted in a standard deviation of 10.6 % and 5.0 % for heat transfer area and refrigerant pressure drops, respectively. However, the overall impact on the heat pump NPV resulted to be only equal to a 1.8 % standard deviation. This was also translated in 95 % of all the solutions deviating maximum 3.5 % from the mean. Moreover, it can be observed that the PHE design I obtained in Table 4.12 deviated of only +0.3 % compared to the mean value estimated performing 500 simulations from the uncertainty input space. The heat source pressure drop are not reported, since the results showed a negligible impact on the NPV.

Table 4.13: MC uncertainty analysis results for PHE design I for Propane/Iso-Pentane (0.5/0.5) performed with a sample population of 500 elements

	A_{ht}, m^2	$\Delta p_{\mathrm{ref,tot}}$, kPa	NPV, €
Mean value	93.2	33.2	694780
Absolute standard deviation	9.9	1.7	12370
Percentage standard deviation	10.6 %	5.0 %	1.8 %
95 % coverage interval	20.7 %	9.8 %	3.5%
Design I	92.0	31.0	696960
Deviation from the mean	-1.3 %	-6.8 %	+0.3%

It must be stressed again that the input uncertainties were taken from the reference papers for the experimental correlations, and they were estimated by the authors as accuracy referred to experimental database not containing the present working fluids and operating conditions. This analysis ensures however that, despite very large deviations assigned to the heat transfer and pressure drop calculations, such as the wide interval of [-50%, +100%] given as input for the estimation of f_V in Table 4.9,a much smaller impact was obtained on the NPV estimation, equal to only 1.8 % standard deviation.

It is nevertheless very relevant to focus future work on validating the use of the chosen prediction methods for similar case studies, by conducting experiments for flow boiling of zeotropic mixtures in PHEs. Moreover, despite small uncertainties were obtained on the NPV for PHE design I, the input uncertainties might lead to exclude some of the optimal solutions for a possible underestimation of the NPV.

Significance of the choice of the pressure drop correlation

From the analysis of the results, the refrigerant pressure drops were found to have the largest impact on the NPV. Therefore, it was decided to carry out a sensitivity analysis on the prediction method chosen to evaluate the two-phase frictional contribution, constituting the major contribution to the refrigerant total pressure loss. The same parametric study was carried out, i.e. considering the same design points, yet by employing an alternative prediction method.

The Lockhart-Martinelli [78] method was applied, for which the Martinelli parameter was estimated from the ratio of the singe-phase vapour and liquid pressure drops. Martin correlation [77] was used in order to estimate the single-phase contributions, and the two-phase multiplier was calculated by using the fitting to the Martinelli's parameter developed by Chisholm [80] with a multiplication coefficient $C = 4.67$, as proposed by Palm and Claesson [95].

By using the same fitting coefficients obtained using the previous data set, i.e. -0.42 and 0.26 for Re_V and Bd respectively, the mean value was calculated for the best results, namely PHE designs based on the best 5 % NPV. A good agreement was obtained between the two different data sets, since the mean value of the guideline $\mathrm{Re}_V^{-0.42}\mathrm{Bd}^{0.26}$ was found equal to 0.044, thereby being +9.5 % higher than the base case.

Limitations of the study

The methodology presented in this work is based on a number of boundary conditions and assumptions. First and foremost, the methodology is based on numerical calculations and has not been documented experimentally. The study has only been applied to a limited number of cases. The work should be seen as a suggestion and exemplification of a method, not as a complete guideline.

The methodology was indeed derived for eight different working fluids integrated in the same heat pump, with fixed heat source temperature glide of $25°C$. Therefore, the influence of having different glides along the evaporator might be investigated as part of future work. Moreover, the economic analysis showed that the refrigerant total pressure drops have a major impact on the NPV of the heat pump. In order to estimate the NPV, a number of economic boundaries were assumed, and the price of electricity and natural gas were based on the data available for the Danish energy sector. Therefore, the results must be generalized by taking into consideration the sensitivity of the proposed correlation to such assumptions. The cost analysis showed that a major influence was given by the running cost of the compressor, which was mainly affected by COP and cost of electricity. Understanding the relative impact of the electricity cost is therefore a relevant suggestion for further work.

Last, two limitations were entailed by the utilization of the PHE sizing model. Flow

maldistribution is not taken into consideration, neither along the plate width nor among the different HEX channels. This aspect might lead to different results concerning some design variables, e.g. plate length-to-width ratio, since it does not take into account that the flow might not be perfectly counter-current if low values of such ratio are employed. In order to avoid unrealistic results, a minimum ratio was assumed in the present analysis.

4.4 Summary

This chapter presented different approaches to derive recommendations for PHE design in heat pumps using pure and mixed refrigerants. In the first part, a sensitivity study was carried out by simultaneously varying plate size and count for both evaporator and condenser, and PHE geometrical configurations with different trade-offs between heat transfer area and pressure drops were obtained. This study constituted an attempt to derive design guidelines during a preliminary cycle design phase, where a full component optimization is computationally expensive, and adopting heuristics criteria might lead to suboptimal solutions. The results showed that only evaporator pressure drop affected the COP, and the different refrigerants were subject to different degradation slopes. Butane, with lowest vapour density and higher saturation temperature drop due to pressure drop, resulted in the steepest drop, with 30 kPa generating a 4 % COP drop. Condenser design solely influenced the economic performance, thus a minimization of the size was always preferable. The trade-off between evaporator size and pressure drops was found to be independent from the condenser design, and the analysed case study resulted in optimal COP degradation of maximum 2 % for all the working fluids, thereby defining optimal pressure drop values in a narrow range, around 5 kPa.

In the second part of the chapter, a methodology to derive simplified design guidelines for PHE evaporators was derived. The methodology was demonstrated by applying it to a case study of heat pumps using zeotropic mixtures. The analysis showed that there is an economic trade-off between heat transfer area and refrigerant pressure drop, with the latter having a larger impact on the results. Higher refrigerant pressure drops resulted in a COP degradation, subsequent increase of the compressor running costs, as well as higher investment required for the compressor. Different working fluids presented different sensitivity to pressure drops, thus the trade-off could not be uniquely defined in terms of a maximum allowable pressure drop. The results were therefore assessed with the aim of deriving a general design guideline, applicable for all the fluids. Different non-dimensional parameters were correlated to the normalized NPV, and it was shown that Re_V, Bd and We_m are the parameters mostly influencing the results. Moreover, an optimal value was identified for the dimensionless factor $\mathrm{Re}_V^{-0.42}\mathrm{Bd}^{0.26}$ for the best solutions in terms of NPV, deviating no more than 5 % from the highest NPV. It was shown that for most of the mixtures values above 80 % of the best NPV were found for $\mathrm{Re}_V^{-0.42}\mathrm{Bd}^{0.26} \approx 0.040$.

Regarding the analysed working fluids, Butane/Hexane(0.9/0.1) presented non-favourable

design points, with an optimal region shifted towards the left of the obtained guideline. Moreover, Propane/n-Pentane at (0.4/0.6) reported values of NPV above 70% of the best solution for the suggested guideline, performing slightly worse than the other working fluids for some of the designs. This was related to the effect of the chevron angle, and it was therefore recommended to employ low values of β in the optimal region.

The design steps, based on applying the aforementioned guideline, were summarized and applied to the case of for the Propane/Iso-Pentane (0.5/0.5). It was illustrated that different configurations respecting $\mathrm{Re}_V^{-0.42}\mathrm{Bd}^{0.26} \approx 0.040$ yielded close to optimal NPVs. These were obtaining by tuning differently plate corrugation geometry, size and number of plates.

5 Flow maldistribution

This chapter presents the main results of research work carried out with the aim of estimating the impact of flow maldistribution in plate heat exchanger evaporators, and the subsequent effect on the heat pump thermodynamic and economic performance indicators. Part of this chapter was published in [P2] and [C3].

5.1 Introduction

As highlighted in the literature review in Chapter 1, flow maldistribution can negatively impact the performance of multiple channels HEXs. A study on the impact of maldistribution effects in PHE evaporators is here presented. By using the 2D evaporator model coupled with the heat pump off-design model presented in Chapter 2, the effect of end-plates and liquid/vapour maldistribution can be estimated at both component and cycle level.

First, a study on evaporator performance is carried out for four different refrigerants, namely the pure fluids butane and propane, and the zeotropic mixtures propylene/butane at (0.5,0.5) mass composition and CO_2/dimethyl ether (DME) (0.2,0.8). The impact at component level was assessed for a prescribed geometry for all the working fluids, while the operating conditions were assumed from a case study. Moreover, the significance of choosing a different correlation to compute the frictional contribution to pressure drop is assessed. Last, the sensitivity of the impact of maldistribution with respect to the plate size and count is investigated for one of the refrigerants.

In the second part of the chapter, the impact of maldistribution effects is assessed on the thermodynamic performance of heat pumps. A case study is presented with the aim of demonstrating the utilization of the integrated simulation framework presented in Chapter 2.6.3. An economic analysis was additionally carried out with the aim of showing the potential impact of evaporator performance degradation due to maldistribution effects on the economic feasibility of heat pumps.

The chapter is structured as follows: section 5.2 presents the case study and results of the study on the impact of flow maldistribution on the evaporator performance. Section 5.3 illustrates the results of the study on impact of maldistribution on cycle performance, while sections 5.4 presents a discussion of the main findings of both studies. Finally, section 5.5 presents a short summary of the chapter.

5.2 Impact on evaporator performance

This section presents a study aimed at estimating the performance degradation of evaporators due to maldistribution effects. The aim was to understand the impact of end plates and liquid/vapour maldistribution on the performance of PHE evaporators using different refrigerants. Four different working fluids were chosen, namely the two pure fluids butane and propane, and the two zeotropic mixtures of natural refrigerant propylene/butane at (0.5/0.5) mass composition and CO_2/dimethyl ether (DME) (0.2/0.8). The working fluids were chosen as among the best performing refrigerants in terms of COP for two different heat pumps applications in the work by Zühlsdorf et al. [13, 21]. Moreover, the refrigerants were chosen with the additional purpose of assessing the impact of maldistribution for a diverse range of refrigerants, with different thermo-physical properties and at different operating pressures. The geometry was prescribed for all the fluids, in order to make the comparison independent from the specific PHE design, and with the aim of focusing on the refrigerants sensitivity to maldistribution.

5.2.1 Methods

The refrigerant operating conditions at the evaporator were fixed to the design values of a booster heat pump case study, published in [21]. A single-stage vapor compression heat pump was suggested for increasing the temperature of one part of the district heating forward water stream from 40 °C up to 60 °C, with a total thermal load of 13.9 kW at the condenser. The design of the heat pump with the four different working fluids resulted in the operating conditions reported in Table 5.1 for the evaporator. The secondary fluid at the evaporator was defined as water.

Table 5.1: Working fluids and evaporator inlet conditions

Working fluid	$p_{\mathrm{ref,in}}$, bar	$T_{\mathrm{ref,in}}$, °C	$x_{\mathrm{ref,in}}$, -	$\dot{m}_{\mathrm{ref,tot}}$, kg/s	$p_{\mathrm{hs,in}}$, bar	$T_{\mathrm{hs,in}}$, °C	$\dot{m}_{\mathrm{hs,tot}}$, kg/s
Butane	2.25	22.5	0.14	0.0360	3.00	40.0	0.186
Propane	8.93	22.5	0.16	0.0394	3.00	40.0	0.185
Propylene/butane (0.5/0.5)	5.54	17.9	0.17	0.0361	3.00	40.0	0.193
CO_2/DME (0.2/0.8)	9.07	17.6	0.18	0.0345	3.00	40.0	0.191

As a first step to evaluate the impact of maldistribution effects on the evaporator

performance only, and to evaluate the differences between the refrigerants, the PHE geometry was fixed to a typical dimensions from a commercial manufacturer, reported in Table 5.2 [74].

Table 5.2: PHE evaporator geometry [74]

W, m	L_{ht}, m	L_p, m	L_p/W, -	$N_{\mathrm{ch,tot}}$, -	b, mm	Λ, mm	β, °	t, mm
0.117	0.524	0.524	4.5	21	1.8	7.0	35	0.5

The comparison was carried out by using the PHE model with both 1D and 2D discretization approaches presented in Chapter 2.2. The 2D model was coupled with the flow distribution solver presented in Chapter 2.4, with imposed liquid/vapour maldistribution. The model was run with $n = 50$ CVs along the flow direction and tolerance set to 10^{-5}. Given the monotonic trend observed experimentally by Vist and Pettersen [62], a linear variation of the inlet vapour quality was imposed between the first and last channel. The slope of the variation was defined by the parameter Δx, indicating the difference between the vapour quality of the first and last channel of the PHE, presented explained in Chapter 2.4. The parameter Δx (Eq.(2.38)) was varied between 0 (for even distribution) and 0.25 by steps of 0.05. The effect of end plates corresponded to the case of $\Delta x = 0$. In this last case, an even distribution of the vapour quality was imposed at the inlet of the PHE channels. The difference between the 1D evaporator model and the 2D evaporator model with $\Delta x = 0$ allowed quantifying this effect.

The local values of heat transfer coefficient and pressure drop were estimated by following the approach presented in Chapter 2.2.6. The evaporation heat transfer coefficient for pure fluids was estimated by the Amalfi et al. [93] correlation. The Silver [100] and Bell-Ghaly[101] method was instead applied to account for mixture degradation of heat transfer during evaporation. In this method, Amalfi et al.[93] was applied for the two-phase convective contribution, Cooper [107] was used for the ideal nucleate boiling contribution, the Thome and Shakir [119] correlation was used for estimating the mixture correction for the nucleate boiling term, and Martin [77] was applied for the single-phase vapour contribution.

The Lockhart and Martinelli [78] method was used to evaluate two-phase evaporation frictional pressure drop. The method was applied as proposed by Palm and Claesson [95], i.e. Martin [77] was used to estimate the single-phase frictional pressure drop and the correlation developed by Chisholm [80] estimated the two-phase multiplier with a multiplication parameter equal to 4.67. Regarding pressure drop, no distinction was made between pure and mixed refrigerants, and the same method was applied. The variation of the local saturation properties for mixtures was however taken into account by evaluating the value in each cell.

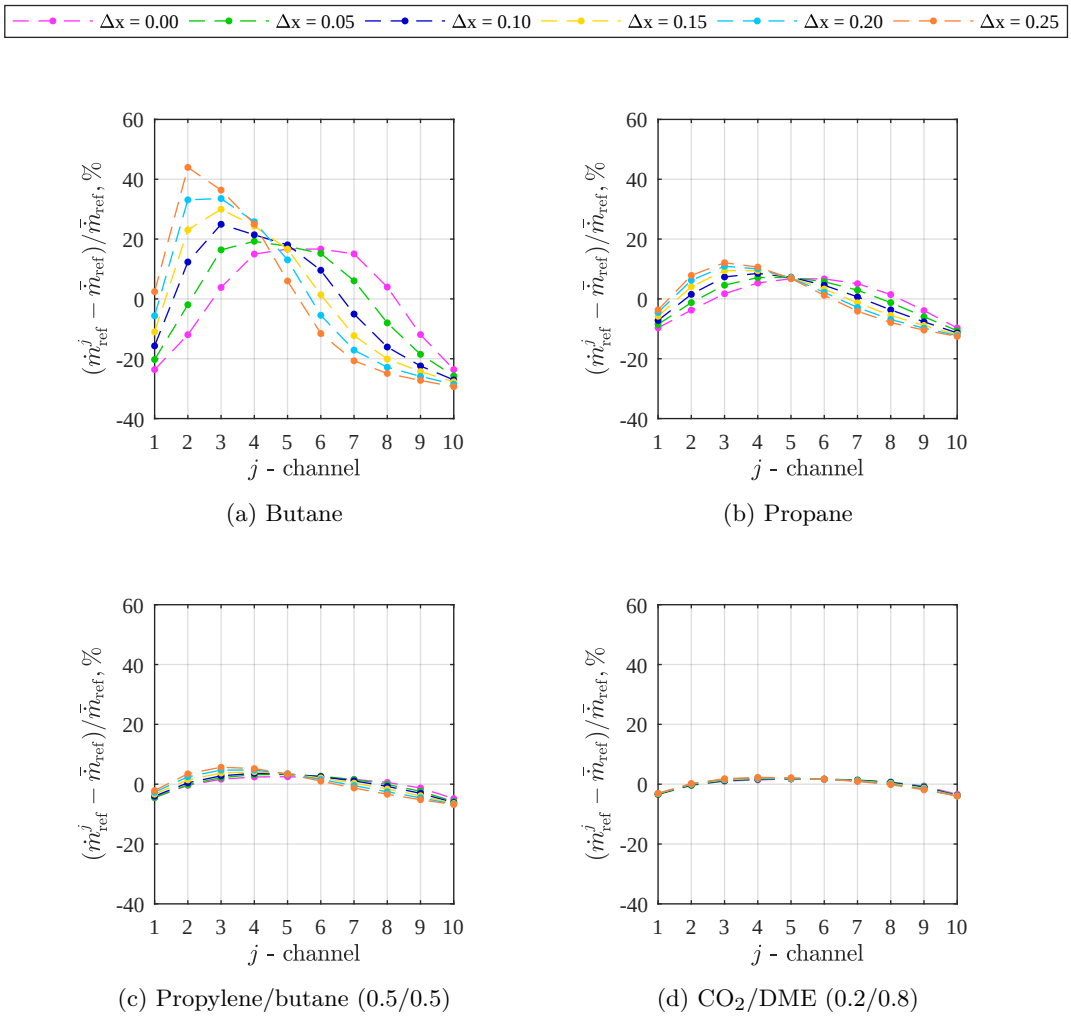

(a) Butane

(b) Propane

(c) Propylene/butane (0.5/0.5)

(d) CO_2/DME (0.2/0.8)

Figure 5.1: Mass flow distribution of the refrigerants in the different evaporator channels, shown as percentage deviation from the average value

5.2.2 Results

Fig.5.1 shows the mass flow rate distribution of the refrigerant into the different channels of the evaporator. The different colors represent the degree of maldistribution imposed by the model. $\Delta x = 0$ corresponds to a uniform vapour quality distribution, thus indicating the effect of end plates on the channel-to-channel mass flow distribution. $\Delta x = 0.25$ corresponds instead to the most severe maldistribution imposed by the model, namely an absolute difference of vapour quality at the inlet of the outermost channels of 0.25. The results are reported in terms of percentage deviation from the average mass flow rate, e.g. the mass flow rate in each channel if an equal distribution was attained.

The obtained trends were similar for all fluids: a larger mass flow rate resulted to flow in those channels with lower inlet vapour quality (see Fig.2.6, e.g channels with lower numbering). In fact, the higher pressure drop entailed by the vapour phase leads to a reduction of the mass flow rate in those channels where complete evaporation is reached earlier, in order to equalize the pressure drops. Butane showed the largest sensitivity to maldistribution, with mass flow rate deviation of up to 50 % for $\Delta x = 0.25$, followed by propane with maximum deviation around 15 %. The two zeotropic mixtures reported instead a much lower impact on the mass flow rate distribution. Propylene/butane resulted in deviations smaller than 10 %, while CO_2/DME reported trends with very small differences between the different cases, all below 5 %.

The higher sensitivity to maldistribution of the pure fluids can further be observed in the temperature distribution of the refrigerant, heat source and wall temperature in the different channels, shown in Fig.5.2 for the case of severe maldistribution ($\Delta x = 0.25$). The refrigerant flows upward in the even channels, while the water flows downward in the odd ones. Fig.5.2 (a) and (b) shows the results for butane and propane, respectively. The channels with a low refrigerant mass flow rate experienced a large region of superheat, where the temperature level of the refrigerant outlet reached the inlet heat source temperature. Note, that the effect on the overall outlet superheat can in any case be compensated by the channels with lower outlet temperature.

Fig.5.2 (c) and (d) shows the same temperature distribution for the case of propylene/butane and CO_2/DME . Compared to the pure fluids, a refrigerant temperature rise can be observed during the evaporation process, due to the characteristic temperature glides experienced by zeotropic mixtures during phase-change. The effect of maldistribution, which resulted in large non-uniformities in temperature between channels the two pure fluids, is only slightly detectable for propylene/butane. CO_2/DME resulted instead to be unaffected by the liquid/vapour maldistribution. Only the effect of end plates can be noticed in the outermost refrigerant channels, resulting in a slightly higher temperature compared to the inner channels - due to the lower mass flow rates (see Fig. 5.1 (d)).

Maldistribution effects implied a degradation of the heat transfer performance of the PHE evaporator, which was quantified in terms of total heat flow rate. Fig.5.3 (a) reports the total heat flow rate as a function of the maldistribution parameter Δx for all the working fluids. The value of the heat flow rate was normalized with respect to the ideal value obtained by using the PHE model discretized in 1D, i.e. assuming an equal distribution of the refrigerant in all the channels. Table 5.3 reports the reference value obtained in the 1D case, and the degradation in percentage point due to effect of end plates, liquid/vapour maldistribution and overall. Accordingly to the results of mass flow rate distribution, butane resulted to be the refrigerant affected to the largest extent, with -8.8 % and -5.8 % degradation due to effect of end plates and liquid/vapour non-uniformities, respectively. Propane presented similar trends, with lower magnitude of deviation. The two zeotropic mixtures resulted to be slightly affected by both effects. CO_2/DME did not experience a performance drop for liquid/vapour maldistribution, yet - 1.4 % drop in

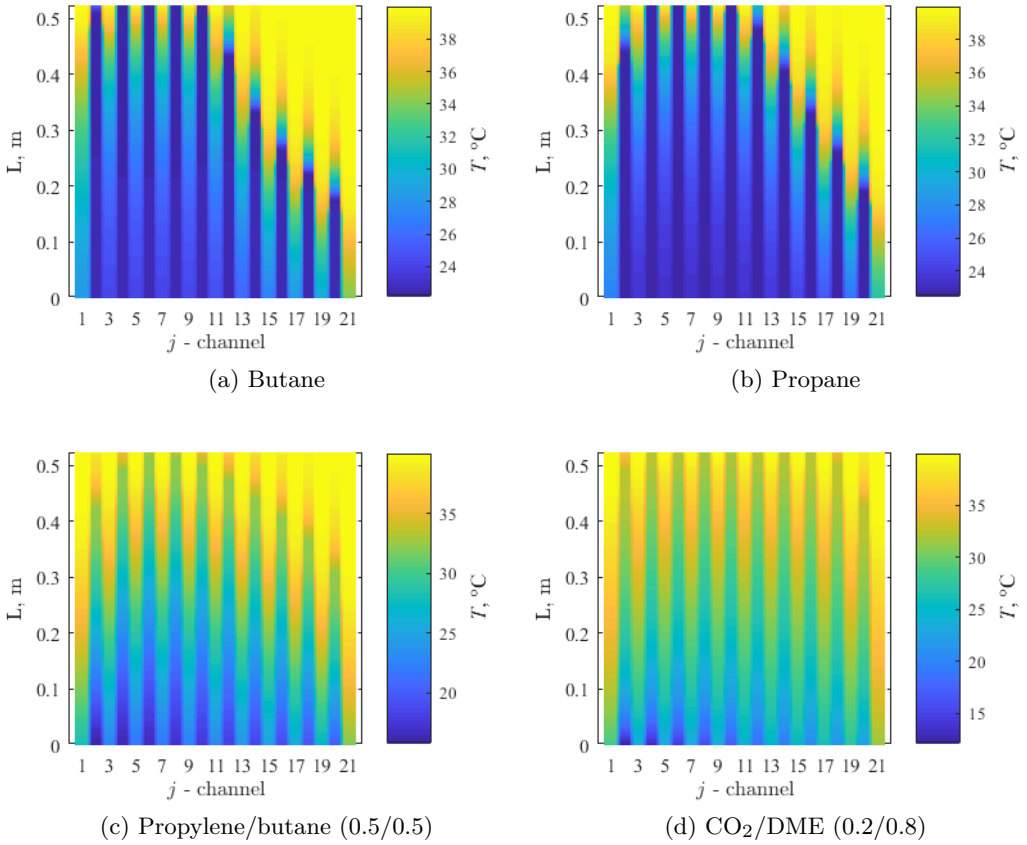

(a) Butane (b) Propane

(c) Propylene/butane (0.5/0.5) (d) CO_2/DME (0.2/0.8)

Figure 5.2: Temperature distribution in the PHE evaporator for the case of severe maldistribution rate $\Delta x = 0.25$

heat flow rate was due to the effect of end plates. Propylene/butane resulted to be the fluid with the lowest overall degradation (-0.9 %), due to the lowest end plates effect.

The results of this study must however be assessed in relation to relevant fluid thermophysical properties and design of the HEX. Fig.5.3 (b) reports the total pressure drop experienced by the refrigerant in the different maldistribution cases. The right-hand side of Table 5.3 reports instead the refrigerant mass flux and superheat for the different fluids, as well as the value of vapour density at the bubble point and dT_{bubble}/dp, i.e. the saturation temperature decrease due to pressure drop - estimated by the Clapeyron relation [138].

Fig.5.3 (b) shows that butane experienced the higher pressure drop, followed by propylene/butane. This is mainly related to the lower vapour density of these fluids, which - as pinpointed by Brignoli et al. [41] - entail higher refrigerant pressure drops. Moreover,

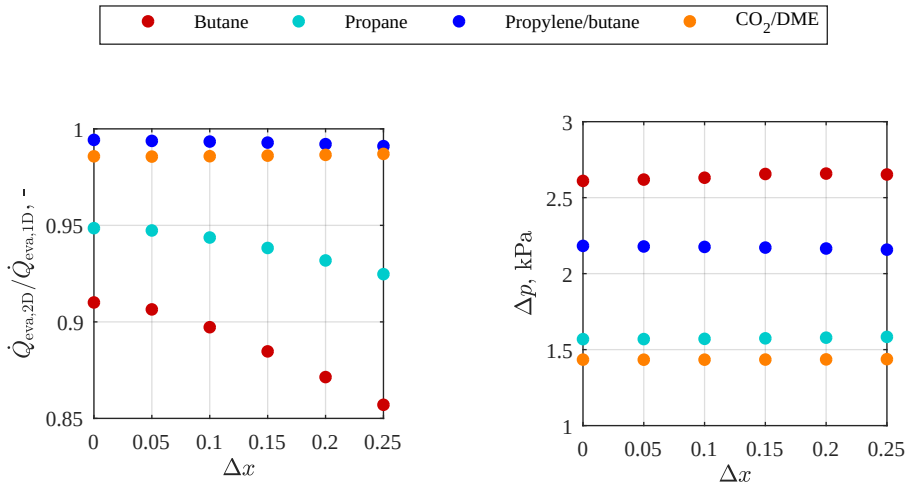

(a) Heat flow rate

(b) Pressure drop

Figure 5.3: Impact of maldistribution effects on (a) total heat flow rate of the evaporator and (b) total refrigerant pressure drop

Table 5.3: Heat flow rate degradation due to maldistribution effects and working fluid thermo-physical properties at saturation pressure

Working fluid	$\dot{Q}_{\text{eva,1D}}$, kW	effect of end plates $\frac{\dot{Q}_{\Delta x=0}-\dot{Q}_{\text{1D}}}{\dot{Q}_{\text{1D}}}$, %	liquid/vapour maldistribution $\frac{\dot{Q}_{\Delta x=0.25}-\dot{Q}_{\Delta x=0}}{\dot{Q}_{\Delta x=0}}$, %	overall effect $\frac{\dot{Q}_{\Delta x=0.25}-\dot{Q}_{\text{1D}}}{\dot{Q}_{\text{1D}}}$, %	G_{ref}, kg m^{-2} s^{-1}	ΔT_{sh}, K	ρ_{V}, kg m^{-3}	$\frac{dT_{\text{bubble}}}{dp}$, K kPa^{-1}
Butane	11.9	-8.8	-5.8	-14.2	17.1	0.0	5.7	0.140
Propane	12.4	-5.1	-2.5	-7.5	18.7	7.2	19.3	0.043
Propylene/butane	12.4	-0.6	-0.3	-0.9	17.2	5.4	12.0	0.060
CO_2/DME	11.7	-1.4	0.1	-1.3	16.4	0.0	18.8	0.035

dT_{bubble}/dp affects the drop in the refrigerant temperature due to pressure drop during the evaporation process, negatively impacting the performance of the PHE evaporator. Butane reported the highest value among all fluids. Therefore, despite the degree of superheat equal to zero, and a mass flux in the same range compared to the other working fluids, butane was found to be the most sensitive to both pressure drops and maldistribution effects. Propylene/butane resulted in the second highest pressure drop, yet only slightly affected by the maldistribution effects. Propane, despite comparable values of vapour density, dT_{bubble}/dp, and mass flux, resulted in a higher degradation compared to both mixtures. The use of the two zeotropic mixtures investigated in this study resulted to experience a consistently lower impact of maldistribution effects in terms of mass flow rate distribution, temperature profiles and heat flow rate degradation. Note, that the overall pressure drop was found to be low for all the refrigerants, well below 3 kPa, which is a reasonable result for the low mass fluxes in the present case study.

5.2.3 Significance of the prediction method to compute pressure drop

The results of the study for the pure fluid butane and for the mixture propylene/butane were compared to the results obtained by using an alternative method to compute the frictional pressure drop. The comparison aimed at demonstrating the independence of the obtained results with respect to the choice of the correlation, since different prediction methods can be chosen from literature. The comparison was carried out for the pressure drop correlation, since it affects the results to the largest extent due to the identical pressure drop governing equations imposed to the model. Moreover, frictional pressure drop are the largest contribution to the total losses compared to gravity and acceleration.

The qualitative comparison is reported in Fig.5.4. As stated in subsection 5.2.1, the Lockhart and Martinelli [78] method was applied in the case study. The computation of frictional pressure drop using the Fanning friction factor proposed by Amalfi et al. [93] was used as an alternative method. The figure shows that the degradation trend is kept with similar slopes to the base case for both fluids. The magnitude of the degradation was found to be slightly modified, yet with differences lower than 5 % for butane, showing the highest deviation. Therefore, the outputs of the maldistribution studies were found to be independent from the choice of the correlation, and the relative ranking of the refrigerants in terms of sensitivity to maldistribution effects is not expected to change if a different prediction method is applied to compute the frictional pressure drop.

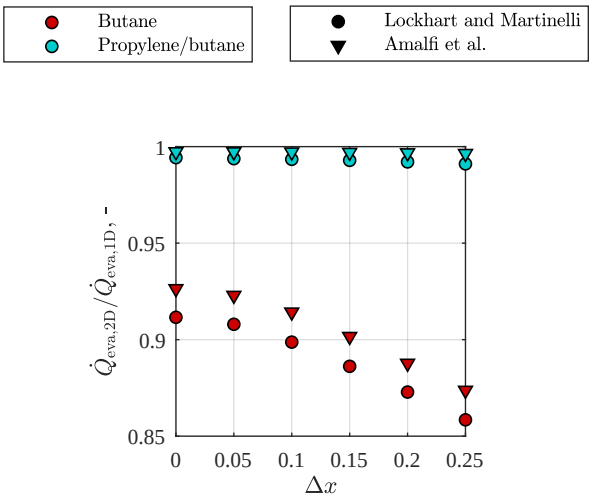

Figure 5.4: Impact of maldistribution effects on total heat flow rate of using two different methods for frictional pressure drop for butane and propylene/butane

5.2.4 Significance of plate size and count

In this section, a sensitivity study is performed for butane, with the aim of evaluating the dependence of the results on some relevant geometrical parameters. The corrugation geometry of the PHE was fixed to the values of the previous analysis, reported in Table 5.2. On the other hand, the plate size and count were modified to investigate the effect of the length-to-width ratio and of the total number of channels on the sensitivity to maldistribution effects. In particular, Jin and Hrnjak [56] found an increasing effect of end plates for decreasing number of channels. Therefore, it is expected that the degradation of the total heat flow rate due to this effect increases for configurations with lower number of channels.

Table 5.4: PHE size and count for the three considered case (plate dimensions from [74])

	W, m	L_{ht}, m	L_p, m	L_p/W, -	$N_{\mathrm{ch,tot}}$, -	G_{ref}, kg/(m^{2}s)
Case I	0.117	0.524	0.524	4.5	21	17.1
Case II	0.243	0.393	0.393	1.6	21	8.2
Case III	0.117	0.524	0.524	4.5	11	34.2

Table 5.4 reports the three PHE geometries considered in this study. Case I corresponds to the same geometry previously used for the comparison between the four working fluids. Case II corresponds to a case in which the same number of channels is used, but the plate size is modified to another commercial model from [74], resulting to a lower lenght-to-width ratio. Case III corresponds instead to the same plate size of Case I, but with half number of channels. In the table, the mass flux is also reported, giving a preliminary estimation of the relative magnitude of the pressure drop entailed by each design.

The results of the study are reported in Fig.5.5 and Table 5.5, where the degradation is divided between effect of end plate and liquid/vapour maldistribution. Case II reports an overall degradation equal to around half of Case I, namely -7.6 % against -14.2 %. Despite the number of channels was kept as constant compared to Case I, the effect of end plates was found to be lower (3.8 % points below). This is likely to be related to the lower pressure drop entailed by this design, reported in the third column of Table 5.5. Moreover, the liquid/vapour maldistribution effect resulted to account for only -2.7 % of the total degradation, thus being equal to around half of the original effect. Therefore, a higher length-to-width ratio, related to higher pressure drop for the same number of channels, entails a higher effect of end plates as well as liquid/vapour maldistribution.

On the other hand, Case III resulted to perform with an overall degradation higher than Case I, equal to -21.2 %. The overall drop was largely due to the effect of end plates, contribution with -16.9 % to the overall degradation. It was found that by employing

Table 5.5: Heat flow rate degradation due to effect of end plates and liquid/-vapour maldistribution for butane and different geometries

PHE geometry	$\dot{Q}_{\mathrm{eva,1D}}$, kW	$\Delta p_{\mathrm{ref,tot-1D}}$, kPa	effect of end plates $\frac{\dot{Q}_{\Delta x=0}-\dot{Q}_{1D}}{\dot{Q}_{1D}}$, %	liquid/vapour maldistribution $\frac{\dot{Q}_{\Delta x=0.25}-\dot{Q}_{\Delta x=0}}{\dot{Q}_{\Delta x=0}}$, %	overall effect $\frac{\dot{Q}_{\Delta x=0.25}-\dot{Q}_{1D}}{\dot{Q}_{1D}}$, %
Case I	11.9	2.5	-8.8	-5.8	-14.2
Case II	12.0	0.7	-5.0	-2.7	-7.6
Case III	11.0	7.8	-16.9	-5.2	-21.2

half number of channels, the effect of end plates was two times larger. The liquid/vapour maldistribution effect was instead found to be almost equal to the original value of Case I. The results shown in this section highlights the importance of taking the PHE design into account when comparing different working fluids using different PHE geometries. In fact, as previously shown, both effect of end plates and liquid/vapour maldistribution impact are related to refrigerant thermo-phyisical properties. However, a strong dependence on the chosen PHE design was also found in this study, with pressure drop being a relevant aspect to take into consideration.

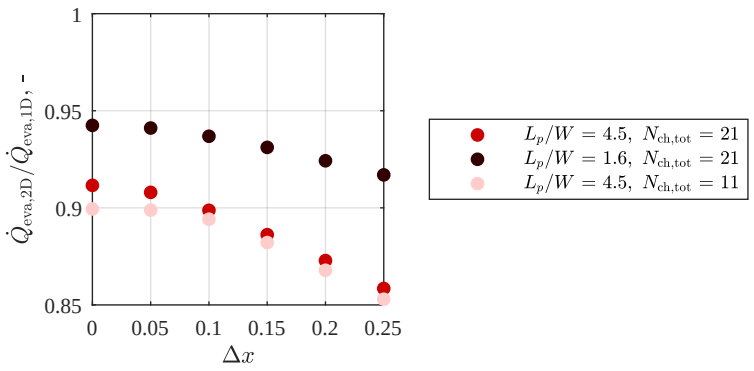

Figure 5.5: Impact of maldistribution effects on total heat flow rate for butane and three evaporator geometries

5.3 Impact on cycle performance

The impact of maldistribution on the thermodynamic performance of heat pumps was assessed for a case study. The objective of the work was to estimate the effect of end plates and liquid/vapour non-uniformities on the COP of a heat pump for a case study of waste heat recovery from data centres. The coupled heat pump-PHE simulation framework, presented in Chapter 2.6, was used for the integrated analysis, including design and

off-design calculations of both cycle and components, considering the evaporator with and without maldistribution effects. This study aimed at demonstrating the utilization of the integrated framework for the design and off-design analysis of heat pumps using PHE as evaporator and condenser unit, with and without maldistribution effects.

5.3.1 Methods

The case study was previously published in Zühlsdorf et al. [13], without considering detailed HEX design and maldistribution effects in evaporators. The present section presents the choice of the working fluids and the heat pump boundary condition, together with the inputs adopted for the cycle and PHEs design. Moreover, the economic boundary conditions considered for the analysis are introduced.

Working fluids and boundary conditions

The case study aimed at integrating heat pumps in data centre facilities for excess heat recovery purposes, for supplying heat to a district heating (DH) network. Zühlsdorf et al. [13] carried out a screening of working fluids, including both pure and mixed refrigerants, aiming at maximizing the cycle COP. Table 5.6 reports four working fluids that were found among the most promising from both thermodynamic and economic standpoints, namely the two pure fluids butane and propane, and the two zeotropic mixtures propylene/butane and CO_2/DME at (0.5/0.5) and (0.2/0.8) mass compositions, respectively. The heat pump design parameters and resulting operating pressures, suction volume flow rate, COP and specific cost of heat are also reported in the table. Note, that the two zeotropic mixtures outperform both pure fluids with higher COP at a lower specific cost of heat. The sizing was carried out by fixing the heat source side, since a nominal cooling load must be provided to the data centre and the heat released to the sink (DH network) was considered as a subsequent revenue. A minimum superheat was ensured at the evaporator outlet, e.g. the temperature of the refrigerant was increased of ΔT_{SH} in order to avoid refrigerant liquid droplets at the compressor inlet. The subcooling was defined to reach the highest possible COP by maximizing it and reaching the imposed pinch point temperature difference at the liquid outlet of the condenser. For a more detailed description of the heat pump cycle design, the reader is referred to [13].

Table 5.6: Heat pump design and operating parameters for the selected working fluids

	Inputs					Outputs						
Working fluid	$\dot{Q}_{\mathrm{eva}}$, kW	$T_{\mathrm{hs,in}}$, °C	$T_{\mathrm{hs,out}}$, °C	$T_{\mathrm{sink,in}}$, °C	$T_{\mathrm{sink,out}}$, °C	$\dot{Q}_{\mathrm{cond}}$, kW	p_{cond}, bar	p_{eva}, bar	$\dot{m}$, kg s^{-1}	$\dot{V}_{\mathrm{out,eva}}$, m^3 h^{-1}	COP, -	c_h, €/MWh
Butane	500	50	25	50	75	630	9.5	2.2	1.69	1100	4.5	32.7
Propane	500	50	25	50	75	638	28.1	8.8	1.90	370	4.4	31.1
Propylene/Butane	500	50	25	50	75	600	16.4	5.6	1.62	460	5.6	25.8
CO_2/DME	500	50	25	50	75	600	25.3	9.7	1.56	290	5.6	25.4

Heat exchangers design

The PHE design for both evaporator and condenser was carried out by using the design solver presented in Chapter 2.2.8, considering typical plate dimensions from commercial manufacturers [74, 145]. The plate size and models are reported in Table 5.7. Note that different plate geometries were assumed for the different working fluids, due to the large differences in required heat transfer area. Mixtures usually require a larger area and hence investment, due to the lower temperature differences in the HEXs and the degradation of heat transfer coefficients compared to pure fluids. Therefore, plates with the larger area were selected for both propylene/butane and CO_2/DME for the evaporator and condenser side. For the evaporator, a plate size with a lower aspect ratio (L_p/W) was chosen for the pure fluids, due to the larger sensitivity of butane to pressure drop - already shown in the results of this section. On the other hand, the two condenser sizes were chosen with similar length-to-width ratios.

Table 5.7: Evaporator and condenser plate geometry, input for the design models [74, 145]

Working fluid	Evaporator				Condenser			
	HEX model	W, m	L_p, m	L_p/W, -	HEX model	W, m	L_p, m	L_p/W, -
Butane	SWEP B633	0.537	0.593	1.1	SWEP V65	0.363	0.731	2.0
Propane	SWEP B633	0.537	0.593	1.1	SWEP V65	0.363	0.731	2.0
Propylene/Butane	SWEP B649	0.537	0.995	1.9	AQ6-FG	0.650	1.390	2.1
CO_2/DME	SWEP B649	0.537	0.995	1.9	AQ6-FG	0.650	1.390	2.1

PHE model settings and correlations

In order to use the integrated simulation framework, some model specifications were fixed. Table 5.8 reports the discretization details for both the evaporator and condenser models. A higher number of CVs was applied in the condenser case as a result of the grid independence study.

Table 5.8: Discretization and tolerances adopted for the PHE models

	Design models		Performance models	
	Evaporator	Condenser	Evaporator	Condenser
Type of discretization	1D	1D	1D/2D	1D
Number of CVs	50	110	50 / 50 x ($N_{\text{ch,ref}} + N_{\text{ch,hs}}$)	110
Tolerance	10^{-5}	10^{-5}	10^{-5}	10^{-5}

Moreover, experimental correlations were selected to compute local heat transfer coefficients and frictional pressure drop of both evaporator and condenser, for both design and off-design analysis. The same evaporator correlations chosen for the case study on

evaporator performance - presented in section 5.2.1 of the present chapter - were selected for the analysis.

Yan and Lin [137] was used for the condensation heat transfer coefficient of pure fluids, while the Silver [100] and Bell-Ghaly [101] method was applied to account for mixture degradation of heat transfer during condensation. The ideal heat transfer coefficient was computed using Yan and Lin [137], while Martin [77] was used for the vapour phase correction term. Condensation pressure drop was estimated by using the correlation for the Fanning friction factor proposed by Yan and Lin [94]. Similarly to the evaporation case, no distinction was made between pure and mixed refrigerants with respect to pressure drop calculations.

Economic boundary conditions

As the design of the HEXs and compressor was fixed by the nominal heat pump conditions, the total capital investment of the heat pump was not affected by the off-design operation. The assumptions and cost correlations used in order to estimate the TCI are described in [13].

The operating cost and revenue streams were on the other hand influenced by maldistribution. The different boundary conditions adopted for the calculations are reported in Table 5.9. A fixed number of yearly OH was assumed, since the heat pump was designed for waste heat recovery and the income from the supplied heat to the DH was considered as an additional benefit of the heat pump integration. The specific revenue from the heat source was assumed equal to zero.

Table 5.9: Economic boundary conditions for the case study [21]

Description	Parameter	Value	Unit
Lifetime	n_{hp}	20	y
Operating hours	OH	8000	h y^{-1}
Effective interest rate	i_{eff}	5	%
Specific cost of electricity	c_{el}	120	€ MWh^{-1}
Specific revenue of heat source	c_{hs}	0	€ MWh^{-1}
Specific income per supplied heat	c_{sink}	40	€ MWh^{-1}

5.3.2 Results

This section presents the results obtained by applying the simulation framework to the case study. First, the results of the PHE sizing for both evaporator and condenser are introduced, as a basis for the subsequent off-design analysis. The impact of the imposed maldistribution on the working fluid mass flow distribution and evaporator performance is subsequently presented, followed by the impact on the thermodynamic cycle performance.

Last, the results of the economic analysis for one of the working fluids are given.

Evaporator and condenser designs

Table 5.10 shows the output of the design models. The total number of channels and heat transfer area was estimated, which gives an indication of the size of the components for each case and refrigerant. The effective heat flow rate, the mass flux, and the total refrigerant pressure drop were additional outputs of the design process. These results are dependent on the plate base design that was chosen for the working fluids. Commercial plates from manufacturers were considered, hence the PHE design was not based on a full optimization of the geometry but it was in fact based on heuristics in accordance with typically accepted values of refrigerant pressure drop. This approach resulted in designs with a different number of channels for the four refrigerants. A full optimization of the PHE geometry was considered as outside the scope of the present work.

The evaporator design for the two pure fluids butane and propane led to refrigerant pressure drop within the usual 50 kPa limit adopted by commercial manufacturers [74]. Despite the evaporator for butane was designed with a mass flux (G_{ref}) equal to around half of the case of propane, similar pressure drops were obtained for the two fluids. This constitutes a first indication of the higher sensitivity to pressure drop of butane, i.e. a higher degradation of the PHE performance due to pressure drop is expected even if no maldistribution effect is accounted for. This will be further explained in section 5.3.2.

The two zeotropic mixtures led to opposite PHE designs, despite the same plate geometry was assumed in both cases. The design for propylene/butane entailed higher pressure drop (equal to 63.5 kPa) and a lower heat transfer area, whereas low pressure drop and bigger heat transfer area was obtained for the case of CO_2/DME. This is likely to lead to different impact of maldistribution for the two working fluids.

It is noted, that the condenser pressure drop predicted using the correlation by Yan and Lin [94] is very low for all the working fluids, and in the case of propane equal to -0.86 kPa. The design of the condenser presented in this case study corresponds however to a case with a large refrigerant sub-cooling, equal to 24.3 K and 21.3 K at the design point for butane and propane, respectively, and 8.7 K and 2.0 K for propylene/butane and CO_2/DME. The large sub-cooling results in a dominant contribution of gravity pressure drop, which in turn, for downward-flow condensers, negatively contributes to the total value (i.e. results in a pressure recovery). Note that the dominant contribution of gravity pressure drop was obtained as a consequence of using the correlation by Yan and Lin [94](due to the low values of friction factor), and the choice of other prediction methods might change the result.

Though not the focus of the present study, it is important to point out one aspect of condenser design and pressure drop prediction. The results of Table 5.10 showed that

the frictional pressure drop evaluated using the Yan et al. [137] correlation resulted in very low values of the frictional contribution. This led, for the case of propane, to have a dominant effect of gravity pressure recovery. However, it is again stressed that the conclusion on the dominating effect of gravity pressure recovery is strictly related to the chosen prediction method for frictional pressure drop, and using correlations recently published by Tao and Ferreira [146] or Zhang et al. [97] could lead to opposite results. However, the results of Chapter 4 showed that the influence of condenser pressure drop is not relevant for the heat pump COP of the same case study and fluids considered in the present paper. The results on evaporator maldistribution effects presented in this paper are thus not sensitive to the chosen prediction method and to the resulting condenser design.

Table 5.10: Results of design model for evaporator and condenser

	Evaporator					Condenser				
Working fluid	$N_{ch,tot}$, -	A_{ht}, m^2	$\dot{Q}$, kW	G_{ref}, kg m^{-2} s^{-1}	$\Delta p_{ref,tot}$, kPa	$N_{ch,tot}$, -	A_{ht}, m^2	$\dot{Q}$, kW	G_{ref}, kg m^{-2} s^{-1}	$\Delta p_{ref,tot}$, kPa
Butane	61	22.3	501	57.4	28.8	161	49.2	633	29.0	0.01
Propane	39	14.3	502	100.8	34.0	210	65.8	638	23.2	-0.86
Propylene/Butane	33	20.8	501	91.2	63.5	51	55.3	603	47.6	2.32
CO_2/DME	65	41.0	500	44.6	10.9	51	55.3	602	45.8	0.55

Impact on evaporator performance

Fig.5.6 shows the mass flow rate distribution of the refrigerant into the different channels of the evaporator. The results are presented and plotted similarly to the previous case study shown in Fig.5.1. The trends were found to be similar compared to the ones obtained with the previous study. However, the magnitude of maldistribution effects increased for propane, propylene/butane and CO_2/DME, reaching maximum deviation values around 20 % to 30 %. Butane resulted to be the fluid most affected by non-uniformities, similarly to the previous case, with mass flow rate deviation of up to 50 % for $\Delta x = 0.25$.

Since the PHE model was coupled with off-design calculation of the heat pump, the total mass flow rate of the working fluid was modified for each value of maldistribution rate, in order to ensure the defined control values of superheat and suction volume flow rate. Therefore, Fig. 5.7(a) reports the total refrigerant mass flow rate as a function of the maldistribution parameter Δx. The total evaporator heat flow rate (b) and the total refrigerant pressure drop are plotted in Fig. 5.7 (b) and (c), respectively. The values of mass flow rate and heat flow rate were normalized with respect to the design point, presented in Table 5.6, while the refrigerant pressure drop in Fig.5.7 (c) was plotted using absolute values in order to show the ranking of the working fluids.

The dashed lines in Fig. 5.7 represent the results of an evaporator 1D performance model, where the flow was assumed to distribute perfectly uniformly between the different

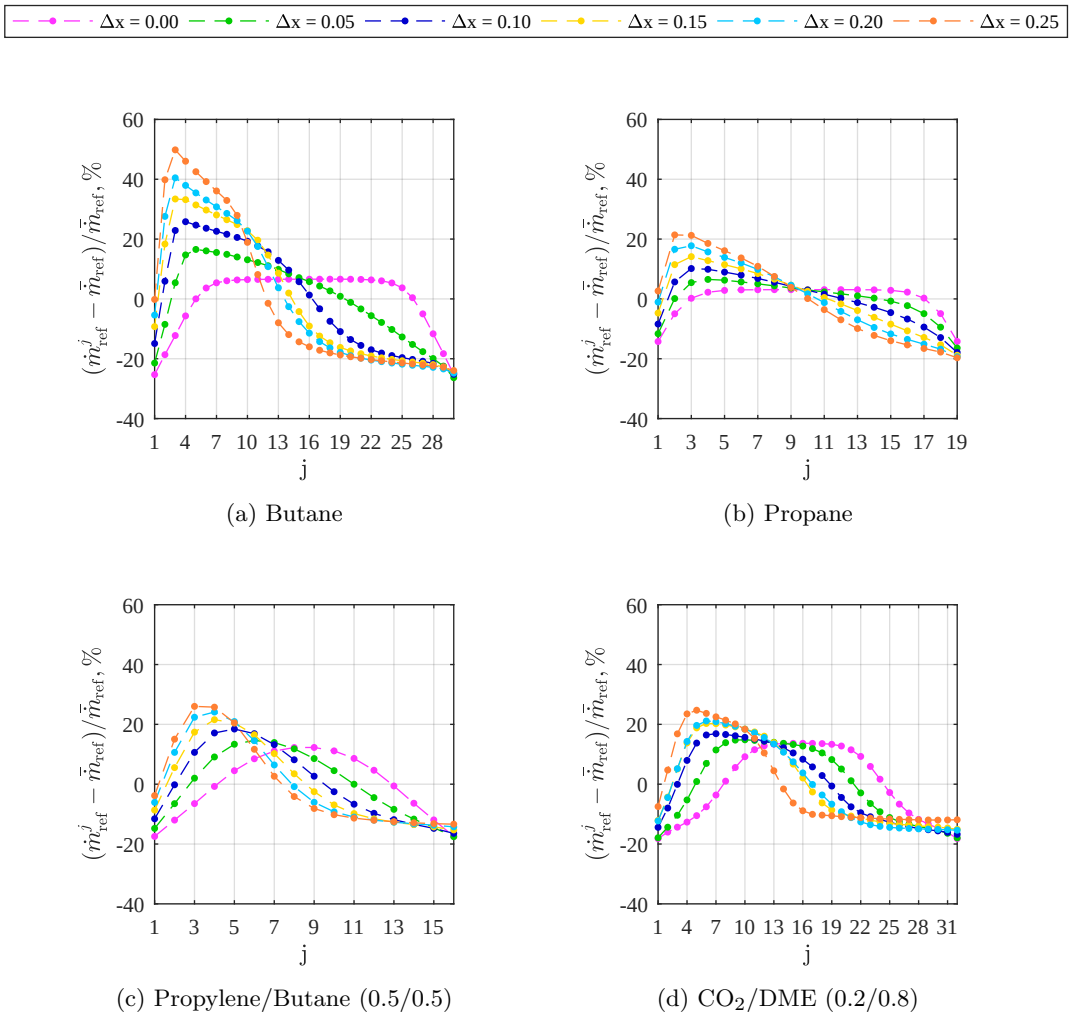

(a) Butane

(b) Propane

(c) Propylene/Butane (0.5/0.5)

(d) CO_2/DME (0.2/0.8)

Figure 5.6: Mass flow distribution of the refrigerant in the different evaporator channels, shown as percentage deviation from the average value

channels. Therefore, the difference between the design value and the 1D performance model accounts for the real operation of the heat pump, in which pressure drops of both evaporator and condenser affect the operating conditions, i.e. pressure levels and mass flow rate, due to the imposed control parameters, which were set as a fixed superheat, subcooling and compressor suction volume flow rate. On the other hand, the difference between the dashed line and the point marker at $\Delta x = 0$ quantifies the effect of end plates. The third and fourth columns of Table 5.11 report these differences in terms of percentage deviation for the evaporator heat flow rate. The trend outlined by the point markers in Fig. 5.7 represent instead the effect of liquid/vapour maldistribution. The last two columns of Table 5.11 report the degradation of heat flow rate in the most severe

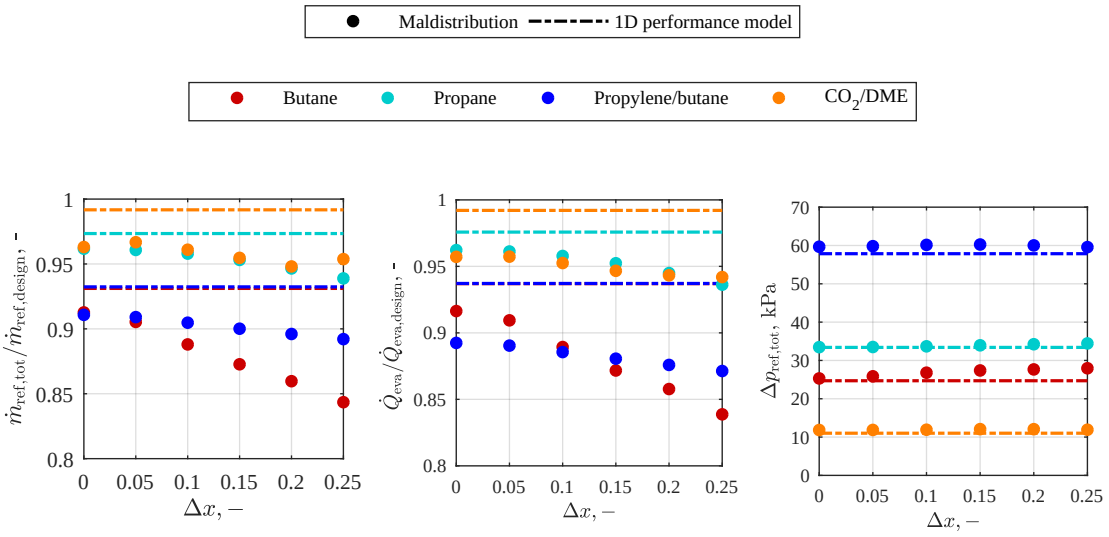

(a) Total mass flow rate (b) Evaporator load (c) Refrigerant pressure drop

Figure 5.7: Impact of maldistribution effects on (a) total refrigerant mass flow rate, (b) evaporator heat flow rate and (c) total refrigerant pressure drop

case of maldistribution ($\Delta x = 0.25$), compared to the case of uniform vapour quality distribution ($\Delta x = 0$) and to the results of the 1D model, respectively. The former solely quantifies the effect of liquid/vapour maldistribution, i.e. the slope of the degradation, while the latter reports the overall degradation due to end plates and liquid/vapour non-uniformity effects altogether.

Fig. 5.7(a) shows that both pure fluids – butane and propane – and the mixture propylene/butane report an evident decrease of the total mass flow rate with increasing Δx, whereas the zeotropic mixture CO_2/DME does not follow a clear trend. Moreover, the reduction of mass flow rate in the case of operation with no maldistribution (dotted line) was found to be very small (around 1 %) for CO_2/DME, slightly higher for propane (around 2.5 %) and similar for butane and propylene/butane, around 8 % to 9 %. The impact of real system operation on the evaporator heat flow rate was analogous, as shown in Fig.5.7(b). Real operation is strongly dependent on the effect of refrigerant pressure drop (in both evaporator and condenser) on the cycle operating conditions, and Fig. 5.7(c) shows that higher pressure drop resulted in higher degradation of the mass flow and evaporator heat flow rate. Butane was found to be the only exception, with pressure drop being the second lowest after CO_2/DME, yet entailing a higher degradation of performance.

Regarding the effect of end plates, propylene/butane resulted to be the fluid most influenced, with a deviation of 4.8 %. CO_2/DME follows with a deviation of 3.5 %,

Table 5.11: Evaporator heat flow rate degradation due to effect of end plates and liquid/vapour maldistribution

Working fluid	$\dot{Q}_{\text{eva,design}}$, kW	$\dot{Q}_{\text{eva,1D}}$, kW	real operation $\frac{\dot{Q}_{\text{1D}}-\dot{Q}_{\text{design}}}{\dot{Q}_{\text{design}}}$, %	end plates effect $\frac{\dot{Q}_{\Delta x=0}-\dot{Q}_{\text{1D}}}{\dot{Q}_{\text{1D}}}$, %	liquid/vapour maldistribution $\frac{\dot{Q}_{\Delta x=0.25}-\dot{Q}_{\Delta x=0}}{\dot{Q}_{\Delta x=0}}$, %	overall effect $\frac{\dot{Q}_{\Delta x=0.25}-\dot{Q}_{\text{1D}}}{\dot{Q}_{\text{1D}}}$, %
Butane	500	468	-6.7	-2.2	-8.5	-10.5
Propane	500	488	-2.5	-1.4	-2.7	-4.1
Propylene/Butane	500	469	-6.7	-4.8	-2.4	-7.0
CO_2/DME	500	496	-0.8	-3.5	-1.6	-5.1

Table 5.12: Refrigerant saturation pressure and thermo-physical properties at evaporator design conditions

Working fluid	$p_{\text{eva,design}}$, bar	T_{bubble}, °C	T_{dew}, °C	ρ_V, kg m^{-3}	$\frac{dT_{\text{bubble}}}{dp}$, K kPa^{-1}
Butane	2.2	22.5	22.5	5.7	0.140
Propane	8.8	22.0	22.0	19.1	0.044
Propylene/Butane	5.6	19.8	37.0	13.6	0.054
CO_2/DME	9.7	11.2	34.9	20.1	0.033

while the two pure fluids report smaller degradations. This was already shown in Fig. 5.6, where the mass flow distribution into the different channels was reported for the working fluids. It may be seen that the line corresponding to $\Delta x = 0$ reports a lower deviation from the average mass flow rate for both butane and propane compared to the mixtures. The deviation increases then more sharply for both pure fluids with increasing $\Delta x0$, compared to the mixtures. Fig. 5.6 shows indeed that the end plates affect the mixtures to a higher extent than both pure fluids, which instead resulted to be more sensitive to vapour quality maldistribution. Part of the higher effect of end plates for propylene/butane was due to the lowest number of channels used in the PHE evaporator design, namely 16 refrigerant channels.

Liquid/vapour maldistribution impacted butane to the largest extent, leading to an overall degradation of the heat flow rate of 10.5 % compared to the performance estimated by the 1D model. Non-uniform quality distribution contributed with 8.5 % degradation. Propane resulted to be the second most affected fluid with a degradation of 2.7 %. This is also shown by the slope of the point markers in Fig.5.7 (b), which is steeper for the two pure fluids. Despite the lower degradation due to vapour quality non-uniformity experienced by propylene/butane, equal to 2.4 %, a high impact was found for end plates effects, leading to an overall higher evaporator performance degradation of 7.0 %. The mixture CO_2/DME resulted to be only slightly affected by liquid/vapour maldistribution, with an overall degradation of 5.1 % mostly due to end plates effect.

The differences between working fluids shown for this case study were found to be related to system operation (refrigerant pressure drop), PHE design and fluid thermo-physical properties, contrarily to the previous case study where the same PHE evaporator geometry was used for all fluids. Here, the PHE design led to different trade-offs in terms of heat transfer area and pressure drop, and the pressure drop range resulted to be very different (see Fig. 5.7 (c)). The refrigerant pressure drop trends are highlighted in Fig.5.7 (c), with butane clearly showing an increase in pressure drop with increasing Δx. Table 5.12 reports some relevant fluid thermo-physical properties, evaluated at the evaporator design conditions. Accordingly to the previous case study, butane reports vapour density nearly one third lower than propylene/butane and one forth lower than both propane and CO_2/DME. Moreover, dT_{bubble}/dp for butane is one order of magnitude higher than for the other working fluids, which instead present similar values. This means that, despite the lower pressure drop related to the PHE design for butane, the evaporator is more affected compared to the other working fluids. This explains why butane reports the higher degradation of evaporator performance due to real system operation, as well as a higher sensitivity to vapour quality non-uniformities. On the other hand, the change in ranking between propane and propylene/butane was found to be related to the design of the PHE: in this case study, propylene/butane resulted in an evaporator design with large pressure drops compared to the other fluids, i.e. six times higher than CO_2/DME. Therefore, a large share of the maldistribution effects must be related to the PHE design: this can be clearly shown by looking at the relative share of overall degradation due to the real operation and effect of end plates, rather than liquid/vapour maldistribution. CO_2/DME was found to be the least affected fluid for a combined effect of PHE design (low pressure drops and higher heat transfer area) and fluid properties.

Impact on cycle thermodynamic performance

A degradation of evaporator performance due to maldistribution effects influences the performance of the overall thermodynamic cycle. Fig. 5.8 shows the effect of the different rates of imposed vapour quality non-uniformity on total condenser heat flow rate (a), on the power required by the compressor (b) and the COP (c), defining the heat pump thermodynamic performance.

The condenser load estimated by the 1D performance model, thereby accounting for pressure drops of both evaporator and condenser, was found to be lower than the design value for all working fluids. Similarly to the evaporator case, the decrease for butane and propylene/butane was found to be higher, around 5 % vs. a decrease of around 1 % to 2 % for propane and nearly negligible for CO_2/DME. This was due to the higher sensitivity of butane to pressure drop and the highest value of pressure drop for propylene/butane as already presented in the previous section. The end plate effects in the evaporator for both butane and propylene/butane translate into similar values of condenser load reduction, yet the slope of butane was the steepest among all the working fluids. This is consistent with the results presented in Table 5.11, which showed butane being the

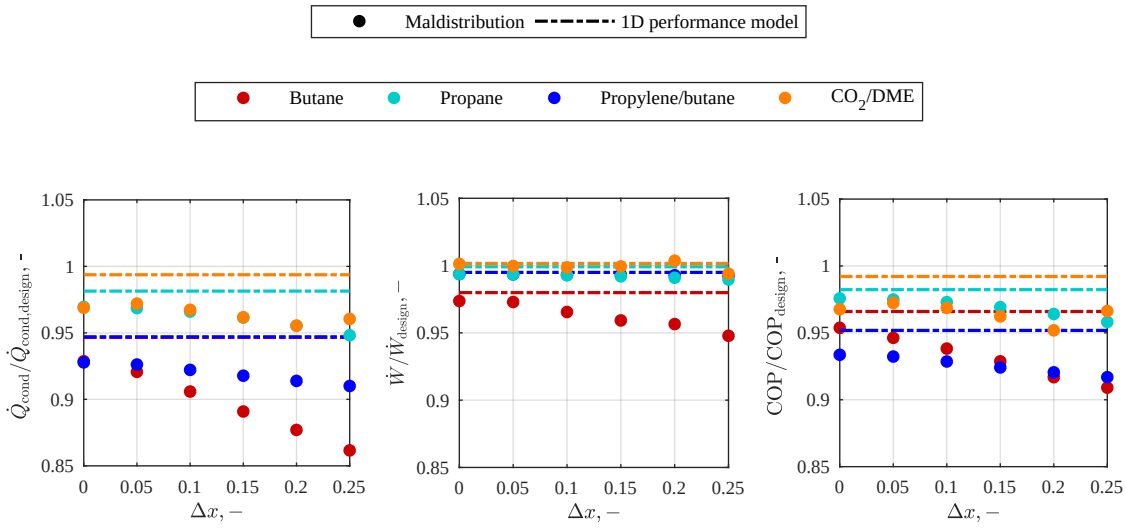

(a) Condenser load (b) Compressor power (c) COP

Figure 5.8: Impact of maldistribution effects on (a) condenser heat flow rate, (b) compressor power and (c) heat pump COP

Table 5.13: COP degradation due to effect of end plates and liquid/vapour maldistribution

Working fluid	COP_{design}, -	COP_{1D}, -	real operation $\frac{COP_{1D}-COP_{design}}{COP_{design}}$, %	end plates effect $\frac{COP_{\Delta x=0}-COP_{1D}}{COP_{1D}}$, %	liquid/vapour maldistribution $\frac{COP_{\Delta x=0.25}-COP_{\Delta x=0}}{COP_{\Delta x=0}}$, %	overall effect $\frac{COP_{\Delta x=0.25}-COP_{1D}}{COP_{1D}}$, %
Butane	4.52	4.37	-3.4	-1.3	-4.7	-5.9
Propane	4.40	4.32	-1.8	-0.7	-1.8	-2.5
Propylene/Butane	5.58	5.31	-4.8	-1.9	-1.8	-3.7
CO_2/DME	5.63	5.59	-0.7	-2.5	-0.1	-2.6

most affected fluid regarding liquid/vapour maldistribution. CO_2/DME does not follow a clearly decreasing trend, similarly to what was found for the total refrigerant mass flow rate in Fig. 5.7 (a).

The effect of maldistribution on the power required by the compressor in Fig. 5.8 (b) shows that propane, propylene/butane and CO_2/DME were negligibly affected by maldistribution, while butane underwent a visible decrease (2 % to 3 %). This is due to the opposite effects of the mass flow reduction (shown in Fig. 5.7 (a)) and an increase of pressure ratio and reduction of isentropic efficiency during off-design operation. The mass flow rate reduction is the dominating effect for butane, thus entailing a lower compressor power, whereas the other working fluids resulted to have a counteracting effect from mass flow rate and pressure ratio/efficiency, thereby having nearly constant compressor power.

The condensation heat flow rate reduction together with the different trends from the

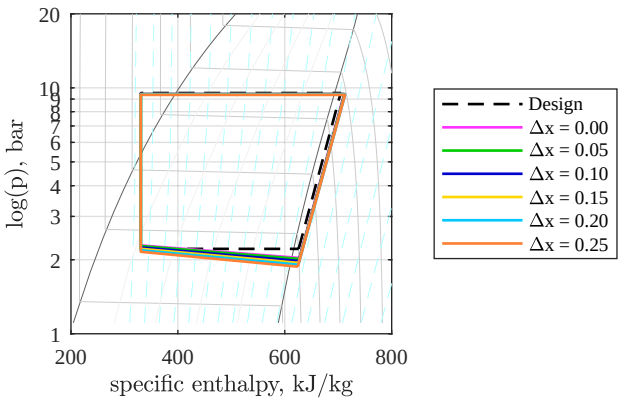

Figure 5.9: Impact of maldistribution effects on the heat pump cycle for butane

compressor power affected the resulting heat pump COP, shown in Fig. 5.8 (c). The percentage deviations are reported in Table 5.13, similarly to the evaporator case, i.e. by estimating the effect of real operation, end plates and vapour quality non-uniformity separately and altogether.

The effect of maldistribution on COP follows the same trend as the condenser heat flow rate for propane, propylene/butane and CO_2/DME, since the compressor power was not affected. The decrease of condenser heat flow rate was found to be dominating over the reduction of power consumption for butane, thereby entailing a COP reduction. The effect of end plates was however reduced compared to the evaporator, and the slope of the maldistribution rates (increasing Δx) is less steep.

By comparing the last columns of Tables 5.11 and 5.13, it may be observed that the PHE evaporator degradation was translated into a lower effect on the COP for all the working fluids, comparable to half of the evaporator degradation. The difference between the design and 1D model was reduced, as well as the effect of end plates, compared to the evaporator performance degradation. The relative ranking of the fluids with respect to each other was maintained, hence butane experienced the largest reduction of COP equal to 5.9 %, followed by propylene/butane, CO_2/DME and propane.

The effect of maldistribution on the cycle thermodynamic performance is additionally presented in Fig. 5.9 by the log(p)-h diagram of the heat pump cycle at the design point compared to the different cases of maldistribution. Fig. 5.9 shows the case of butane, since it resulted as the most sensitive fluid to maldistribution. The trends for the other refrigerants were found to be similar. In agreement with the results shown in Fig. 5.7 (c), increasing Δx entails an increase of refrigerant pressure drop at the evaporator, as clearly shown by the evaporator outlet state point reported in the log(p)-h diagram.

Fig. 5.9 shows that the cycle operation is significantly affected by the occurrence of maldistribution effects.

Economic analysis

The results of the economic analysis are presented solely for butane. The other working fluids showed similar trends yet with different magnitude of the impact. Moreover, the results of the economic analysis serve as a mere indication of the utilization of the simulation framework presented in this thesis, since they are dependent on the assumptions made for the specific case study.

The economic performance indicator introduced by Eq.(2.44), namely the specific cost of heat, is shown in Fig. 5.10(a), while the two different revenue and cost streams associated with the chosen case study are reported in Fig. 5.10(b), for design case, the heat pump real operation and the different maldistribution rates. Since the heat pump was assumed to be operated for a fixed number of hours, the specific cost of heat was found to increase due to maldistribution effects. The heat load of the condenser (presented in Fig. 5.8 (a)) resulted to be decreasing with increasing Δx, and had a dominating effect compared to the decrease in operating costs associated to the compressor. The heat source was considered to be free excess heat from a data centre, while the TCI was fixed in all the

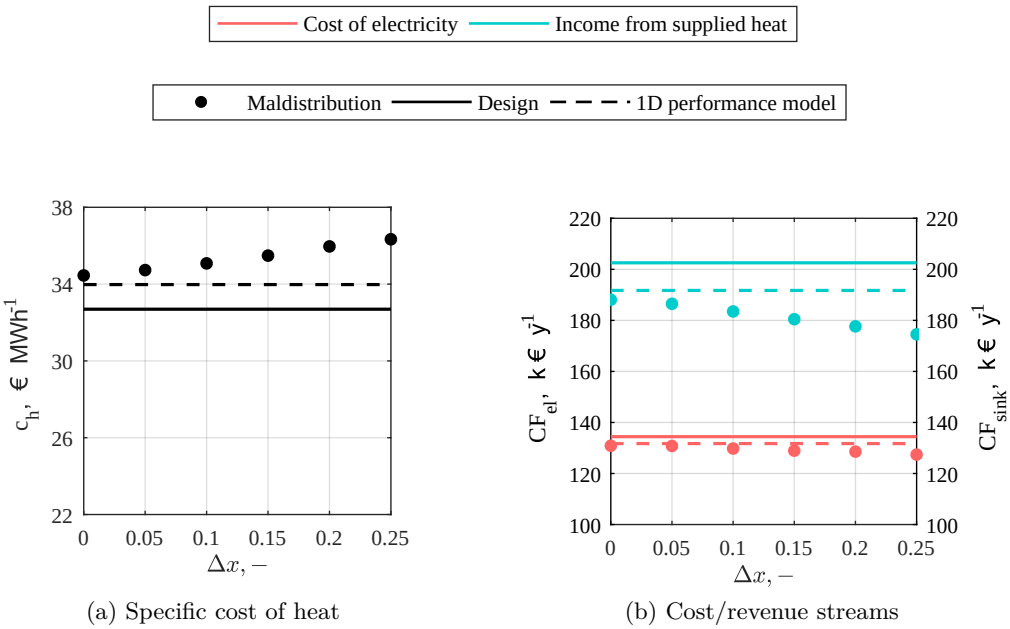

(a) Specific cost of heat

(b) Cost/revenue streams

Figure 5.10: (a) Specific cost of heat and (b) yearly cost and revenue streams as function of Δx for butane

cases, hence constituting the heat sink and compressor costs to be the only influencing factors. Fig.5.10(b) shows the yearly electricity cost of the compressor compared to the revenue stream (which is not considered for the computation of c_h). The revenue stream was determined by the heat of the condenser, which was supplied to the DH network. In agreement with the increasing trend of the specific cost of heat, the revenue stream was found to decrease with a steeper slope compared to the compressor running costs, thereby leading to an increase in the operation cost of the heat pump when maldistribution affects the operation of the evaporator.

5.4 Discussion

The results presented in this chapter showed a general degradation of the evaporator and cycle performance both due to the effects of end plates and liquid/vapour maldistribution. The differences between working fluids were presented in light of several aspects contributing to such discrepancies, namely PHE design, obtained pressure drop and fluid properties.

In the first part of the chapter, the PHE design was prescribed, and two alternative geometries were investigated for butane, by changing the length-to-width ratio and number of channels. A more thorough understanding of the influence of PHE geometry would however required a more systematic sensitivity analysis on different PHE geometrical parameters, for example using statistical methods [147] to explore the entire design space and to capture the variance of the outputs with respect to the inputs - also including potential interrelations.

In the second part of the paper, the PHE design was carried out by fixing the plate geometry to typical dimensions available from suppliers, and no numerical optimization was carried out for any working fluids and the designs were chosen to respect typical allowable limits for pressure drop. Since the pressure drop, which is strongly influenced by the geometry, was found to affect the refrigerant sensitivity to maldistribution effects, the results should not be taken as a final ranking of the different refrigerants. The results were instead presented as a way to use the simulation framework and to understand the different aspects to take into consideration during design and analysis of both evaporator and cycle. For instance, by looking at the results for PHE design for the two mixtures propylene/butane and CO_2/DME in Table 5.10, it can be observed that opposite evaporator designs were obtained: propylene/butane resulted in a configuration with a low number of channels, thereby higher pressure drop and low heat transfer area, whereas for CO_2/DME a higher plates number was employed, entailing higher heat transfer area and low pressure drop. It was therefore found that a lower evaporator investment could be required for propylene/butane. The maldistribution study showed however that propylene/butane, with this particular PHE design, experienced evaporator heat flow rate reduction of up 7 %, leading to a 3.7 % decrease of the system COP. The design for CO_2/DME was instead found to entail lower effects of maldistribution, leading

to maximum 2.6 % reduction of COP, almost entirely due to end plates. This means that, case by case, the trade-off between pressure drop and area investment must be decided also taking maldistribution effects into account, since they may impact the evaporator and cycle performance considerably, depending on the PHE geometry and pressure drop limit chosen during the design phase.

Moreover, the results of the study showed that the thermo-physical properties of the refrigerant are a relevant aspect to consider. Brignoli et al. [41] already stressed the importance of taking fluid characteristics into account to discriminate when combined optimization of cycle and HEX design leads to an effective increase of the cycle thermodynamic performance. They showed how a higher margin of COP improvement was obtained for those fluids for which increasing mass fluxes entailed a higher increase of heat transfer coefficient compared to pressure drop. They additionally discussed how some fluid properties, such as vapour density and refrigerant temperature drop due to pressure drop, were influencing the trends. Maldistribution is another aspect to consider, since non-favourable thermo-physical properties (like the ones showed for butane in Table 5.12) implied higher performance degradation due to such effects. Choosing a PHE design leading to a lower impact of both end plates and liquid/vapour maldistribution is therefore particularly relevant for fluids with higher pressure drop sensitivity. For example optimizing the PHE design for butane for given applications, would likely lead to higher benefits in terms of performance improvement compared to the other working fluids. This must also be considered when choosing empirical design criteria to size PHE, e.g. limiting velocities or pressure drop. In Chapter 4, it was shown how the typical design approaches do not necessarily lead to an optimal design for different working fluids, since different refrigerants are differently sensitive to pressure drop. This is in agreement with the findings of this chapter, which further stresses the importance of understanding maldistribution effects and of discriminating if it is relevant to consider them or to optimize the PHE design.

It is relevant to mention that the application of the simulation framework consisted of an economic analysis to study the effect of maldistribution on the operating costs of the heat pump. The results are strongly dependent on the assumption of this particular case study, especially regarding the values chosen for electricity cost and revenue from selling heat. Moreover, it was considered that the heat source comes at no cost from internal excess heat recovery from the data centre. These assumptions might completely change for different applications of heat pump integration, thereby stressing again that the economic analysis must be solely taken as an explanatory example of the procedure presented in the paper.

This study was focused on maldistribution effects in PHE evaporators only, thus neglecting potential maldistribution issues related to condenser design. Specifically, no liquid/vapour non-uniform distribution can occur at the condenser inlet, since the refrigerant is superheated vapour, hence only the effect of end plates may potentially be considered. Previous study by Zühlsdorf et al. [20] showed however that evaporator

design affects the performance of heat pumps using mixed refrigerant to a larger extent compared to the condenser. Moreover, the results of Chapter 4 confirmed the relevant impact of evaporator design on the cycle COP, while the condenser design was found to solely impact the levelized cost of heat.

Note that liquid/vapour maldistribution was evaluated by carrying out a sensitivity study on different slopes of vapour quality variation at the channel inlets. This was based on the assumption of linear vapour quality profiles, as experimentally shown for tubular manifolds for compact HEXs in Vist and Pettersen [62], and confirmed by Mahvi and Garimella [63]. Moreover, a maximum variation of 0.25 was imposed as input to the model. Further experiments should therefore be carried out in order to validate the linear assumptions, as well as the slope of the distribution. Both evaporator and heat pump COP resulted to be largely affected, by limiting the maximum difference of the inlet vapour quality to 0.25, with maximum deviations due to liquid/vapour maldistribution obtained for butane of -8.5 % and 4.7 %, respectively. For a higher degree of maldistribution, it is thus expected to obtain even larger degradation of both PHE and heat pump performance.

5.5 Summary

In this chapter different maldistribution studies were carried out with the aim of quantifying the effect of end plates and liquid/vapour maldistribution on evaporator and heat pump thermodynamic performance, for pure fluids and zeotropic mixtures of natural refrigerants, and different PHE designs. First, a comparison between butane, propane, propylene/butane (0.5/0.5), and CO_2/DME (0.2,0.8) and a fixed PHE geometry was carried out.

- Butane was the most sensitive fluid to both effect of end plates and liquid/vapour non-uniformities. A total heat flow rate degradation of -14.2 % was found, with -8.8 % due to the former effect and -5.8 % due to the latter.
- Propane was the fluid with the second highest degradation, while the two zeotropic mixtures were found to be only slightly affected by both effects.
- Refrigerant vapour density, impacting the total pressure drop, and saturation temperature drop due to pressure drop were identified as fluid properties influencing the results to a large extent.
- Despite propylene/butane resulted in higher pressure drop compared to propane, the degradation of performance was lower.
- The choice of the correlation to compute frictional pressure drop was found not to influence the results and relative ranking of the fluids.

- By decreasing the number of channels to half of the value for butane, the evaporator heat flow rate was subject to a degradation two times larger due to effect of end plates.
- By decreasing the length-to-width ratio for butane, a lower pressure drop was obtained, thus reducing the degradation of the total heat flow rate due to both effects.

Second, an integrated PHE - heat pump design and off-design analysis, accounting for maldistribution effects, was carried out. Four different PHE geometries were obtained for all the fluids, thereby leading to a combined effect of fluid properties, real operation and maldistribution effects influencing the performance of the heat pump.

- All working fluids resulted in a reduction of the evaporator heat flow rate due to end plate effects. Propylene/butane (with the lowest number of channels equal to 33) was found as the working fluid that was most sensitive to end plates, with a 4.8 % reduction of evaporator heat flow rate, followed by CO_2/DME and the two pure fluids. The results did not follow the trend of number of channels: the effect of end plates is thus simultaneously related to both number of channels and fluid properties.
- Butane was the most sensitive fluid to liquid/vapour maldistribution, with an impact equal to -8.5 %, leading to an overall evaporator performance reduction of -10.5 %. The high sensitivity was found to be related to the PHE design, and especially to the low working fluid vapour density, the higher temperature drop due to pressure drop and low evaporation pressure.
- The impact of maldistribution effects was also translated into an estimation of COP degradation. The relative ranking of the working fluids was shown to be similar to the ones for the evaporator, i.e. with butane as the most sensitive fluid, with -5.9 % due to end plates and vapour quality non-uniformity effects altogether and propane the least affected (-2.5 %). The reduction of COP was lower compared to the evaporator performance degradation, around half of the value of all the working fluids.
- The economic analysis showed the impact of COP reduction on the specific cost of heat, compressor running costs and revenue from the heat sink. It was shown that, despite a decrease in the electricity needed to run the compressor during off-design operation due to maldistribution, a lower yearly production of energy was achieved for a fixed number of operating hours. Therefore, an increase of the cost of heat was obtained, together with a steep drop in the revenue from selling the heat to the DH network. The economic analysis was highly dependent on the case study and related assumptions.

6 Conclusions

6.1 Summary of findings

Heat pumps are envisioned to contribute to the decarbonisation of the Danish energy sector, and the use of zeotropic mixtures as working fluids is a possibility to optimize the thermodynamic performance of these systems. Heat exchangers are core-components in heat pumps, thus ensuring their optimal design is of paramount importance for the thermodynamic and economic performance of the cycle. Plate heat exchangers constitute a promising solution due to the high effectiveness within a compact design, and were thus investigated in this thesis.

The objectives of this PhD project were defined in relation to three main research questions. First, the thesis attempted at identifying suitable prediction methods to evaluate the heat transfer coefficient of zeotropic mixtures during evaporation in PHEs. The accurate prediction of the heat transfer performance is, in fact, essential to correctly design the component and to estimate its impact on the cycle performance. Second, the thesis aimed at deriving simplified guidelines for evaporator and condenser design in heat pumps using zeotropic mixtures. The guidelines were obtained with the aim of avoiding the computational cost of combined cycle-component optimization, during the preliminary design phase, when many different working fluids at different compositions are screened and ranked. Last, the impact of liquid/vapour maldistribution and effect of end plates on the evaporator performance was evaluated, and the subsequent degradation of the heat pump thermodynamic performance was quantified.

In order to answer the defined research questions, detailed numerical models of PHEs were implemented, validated, and integrated with a heat pump simulation framework, for design and off-design analysis at both component and system level.

6.1.1 Recommendations on heat transfer correlations for evaporation of zeotropic mixtures in PHEs

Different prediction methods to evaluate the local heat transfer coefficient of zeotropic mixtures were compared against experimental data of CO_2/propane at different mass compositions. Theoretical models for mixtures, as the Silver [100] and Bell and Ghaly [101] method, and the Shah [126] method, reported the lowest deviation with the experimental heat flow rate, matching the data with a mean relative error of 3.4 %. Moreover, due to the dominant thermal resistance of the secondary fluid at low temperature glides, the experimental heat flow rate was matched with generally low deviations when using both PHE specific correlations (e.g. Amalfi et al. [93]) and theoretical models for mixtures. Larger deviations were obtained by using mixture correlations developed for in-tube flow boiling, since the methods were not able to accurately characterize the PHE geometry. However, the deviation with experimental data was smaller for mixture subject to large temperature glides, due to a dominating effect of the mixture degradation of heat transfer compared to a correct representation of the geometry. It is thus recommended to use theoretical methods for mixtures to evaluate the heat transfer coefficient of zeotropic mixtures in PHEs, since both geometry and mixture degradation of heat transfer are taken into account, regardless of the magnitude of the temperature glide.

Furthermore, different sensitivity studies on applying different correlations in the Silver [100] and Bell and Ghaly [101] method were carried out with the aim of evaluating the impact on the PHE performance. Correlations to compute the following contributions were included in the analysis: (i) two-phase convective, (ii) ideal nucleate boiling, (iii) vapour-only heat transfer coefficients, and (iv) correction factors for the nucleate boiling contribution. It was found that the choice of the correlations has a large impact on the value of local heat transfer coefficient, leading to deviations up to 50 %. However, depending on the magnitude of the secondary fluid thermal resistance, these deviations are reduced in the computation of the UA-value, and further reduced in the computation of the total heat flow rate. Therefore, the user must account for different deviations and uncertainties depending on the scope of the analysis. To conclude, if the work focuses on analyzing the PHE performance impact on a thermodynamic cycle, the choice of the prediction method does not lead to large differences. On the other hand, if the work focuses on a detailed characterization of the heat transfer mechanism in the component, the larger discrepancies between correlations become a relevant aspect to consider.

6.1.2 Simplified design guidelines of evaporator and condenser design in heat pumps

A parametric study on the main geometrical parameters of both evaporator and condenser was carried out with the aim of defining design guidelines for both components. A first case study served as a basis to evaluate the relative impact of evaporator and condenser design, and two pure fluids and a zeotropic mixture were included in the analysis. It

was found that the condenser design solely impacted the economy, while the evaporator design affected both the cycle COP and levelized cost of heat. An optimal trade-off between evaporator heat transfer area and pressure drop can be thus defined, yet the optimal value of pressure drop highly depends on the considered refrigerant. In fact, depending on the working fluid sensitivity to pressure drop, different degradation of the heat pump COP were obtained. Therefore, it is suggested to define a guideline based on a maximum COP degradation, rather than a maximum allowable pressure drop, in order to ensure a consistent comparison between fluids.

Moreover, focus was given to evaporator design, due to the higher impact on the thermodynamic performance of the heat pump system. A methodology to derive simplified guidelines for evaporator design was presented and applied to a case study. Eight different mixtures of natural refrigerants were compared as suitable candidates for a heat pump integration in a spray drying facility for waste heat recovery purposes. A parametric study on the PHE geometrical parameters was carried out with the aim of mapping the COP and the NPV with respect to the evaporator design. By considering all the working fluids and PHE evaporator design, the economic performance indicator, namely NPV, was correlated to non-dimensional numbers, describing both refrigerant properties and the evaporator geometry. For the considered case study, it was found that evaporator optimal design could be obtained for $\mathrm{Re}_V^{-0.42}\mathrm{Bd}^{0.26} \approx 0.040$, evaluated at the evaporator inlet. The presented methodology offers the possibility of deriving guidelines for different applications, where different configurations of HEXs are integrated in a thermodynamic cycle and different working fluids are compared, avoiding computationally expensive combined cycle and component optimization to obtain feasible designs.

6.1.3 Impact of flow maldistribution on evaporator and cycle performance

Effect of end plates and liquid/vapour maldistribution in PHE evaporators integrated in vapour compression heat pumps were investigated. First, maldistribution effects were quantified for four different refrigerants (butane, propane, propylene/butane (0.5/0.5) and CO_2/DME(0.2/0.8)), and a prescribed PHE geometry. The refrigerant sensitivity to maldistribution effects was found to be related to the refrigerant sensitivity to pressure drop, and fluid thermo-physical properties. Butane resulted to be the most sensitive among the investigated working fluids, with a total heat flow rate degradation of -8.8 % due to effect of end plates and -5.5 % due to liquid/vapour maldistribution. Moreover, by varying the PHE geometry, it was found that a higher effect of end plates occurs for lower number of channels, while a lower plate length-to-width ratio reduces both maldistribution effects.

An integrated cycle - PHE simulation framework to assess the impact of maldistribution on the heat pump thermodynamic and economic performance indicators was implemented and applied to a case study. The impact of maldistribution was thus translated into a

COP degradation. An overall evaporator heat flow rate degradation of -10.5 % led to a COP drop equal to -5.9 % for butane. Moreover, the COP drop entailed an increase of the levelized cost of heat, due to increasing operating costs due to maldistribution effects. The results were mainly affected by working fluid thermo-physical properties and sensitivity to pressure drop, and PHE geometry, more specifically number of channels and length-to-width ratio. This highlights the importance of choosing a PHE design leading to a lower impact of both end plates and liquid/vapour maldistribution for fluids with higher pressure drop sensitivity.

6.2 Recommendations for future work

The work presented in this thesis was based on detailed numerical models of PHE evaporators and condensers. The study attempted to carry out validation against available experimental data, and Chapter 3 was devoted to compare experimental heat flow rate vs. model results for zeotropic mixtures of CO_2/propane. However, the comparison with experimental data was carried out solely at global level, i.e. by comparing the overall PHE heat transfer performance. This limitation was assumed to be acceptable, since the work mostly focused on integration of PHEs in thermodynamic cycles, rather than a detailed characterization of the component performance. The different correlations were in fact compared with respect to the total heat flow rate, and the local values of heat transfer coefficient could not be directly compared to experimental data. Therefore, further efforts should be directed towards a complete understanding of the heat transfer mechanism in PHEs, and a characterization of the heat transfer performance of zeotropic mixtures of natural refrigerant. This aspect can be addressed by conducting experimental campaigns on evaporation and condensation of different mixtures in PHEs, with the aim of measuring local values of heat transfer coefficient.

Chapter 4 presented a methodology to derive simplified guidelines. The work was mostly related to the need of simple criteria during the preliminary design phase of thermodynamic cycles, when a complete component optimization for several refrigerant choices is too computationally demanding. The presented methodology was applied to a case study, and it could be theoretically applied to different cases. Future work can focus on demonstrating the methodology for other studies, and validating the results with practical implementation of the solutions.

The study on flow maldistribution presented in Chapter 5 was limited to investigate four refrigerants and a limited number of PHE geometries. A more extensive sensitivity study should be carried out in order to fully describe the influence of all PHE geometrical parameters on the relevance of both effect of end plates and liquid/vapour maldistribution. For example, statistical methods as suggested by Saltelli et al. [147] can be used to ensure the coverage of all possible geometries, as well as to capture the mutual influence of parameters. Moreover, the imposed linear profile assumed to model liquid/vapour maldistribution should be validated experimentally.

Last, it is relevant to mention that the findings of Chapters 4 and 5 put the focus on the importance of HEX design when screening and comparing different refrigerants for a given application. In fact, the thermodynamic performance of the cycle was found to be strongly affected by the HEX design, and maldistribution effects were found to entail a different degradation of COP depending on the working fluid. Therefore, an optimized design of the HEX for all the screened refrigerants is imperative to ensure a consistent and meaningful comparison with respect to the cycle COP. In fact, a PHE design that is optimal for one fluid was found to lead to suboptimal solutions for others, especially in relation to pressure drop and maldistribution. Moreover, a higher COP improvement margin is expected to be obtained with optimized HEX designs, for those fluids that are more sensitive to pressure drop and maldistribution effects. Future work should thus be focused on deriving simplified methods to account for the different behaviours of refrigerants in relation to HEX design, in order to take both refrigerant sensitivity to pressure drop and maldistribution effects into consideration during the screening process of promising working fluid candidates.

Bibliography

[1] United Nations Framework Convention on Climate Change. Paris Agreement: Conference of the Parties on Its Twenty-First Session. 2015. doi: FCCC/CP/2015/L.9/Rev.1.

[2] International Energy Agency (IEA). Energy Technology Perspectives 2017 - Catalysing Energy Technology Transformation. 2017. URL https://webstore.iea.org/energy-technology-perspectives-2017.

[3] International Energy Agency (IEA). Energy Technology Perspectives 2016 - Towards Sustainable Urban Energy Systems. 2016. URL https://webstore.iea.org/energy-technology-perspectives-2016.

[4] B. Huang, F. Bühler, and F.H. Müller. Industrial Energy Mapping: THERMCYC WP6. Technical report, 2015.

[5] Fabian Bühler, Stefan Petrovic, Kenneth Karlsson, Brian Elmegaard, and Denmark West. Industrial excess heat for district heating in Denmark. 205(August):991–1001, 2017. doi: 10.1016/j.apenergy.2017.08.032.

[6] Brian Elmegaard - project manager. THERMCYC - Advanced Thermodynamic Cycles Utilizing Low Temperature Heat Sources. URL http://www.thermcyc.mek.dtu.dk/. Accessed 01-05-2019.

[7] United Nations Environmental Programme. Report of the Twenty-Eighth Meeting of the Parties to the Montreal Protocol on Substances that Deplete the Ozone Layer. *Kigali, Rwanda*, 2016. doi: doi:10.1002/9780470670590.wbeog931.

[8] Danfoss 2019. Sondex AS. URL https://heatexchangers.danfoss.com/. Accessed 01-05-2019.

[9] Ramesh K. Shah and Dusan P. Sekulic. *Fundamentals of Heat Exchanger Design*. Wiley, 2002. ISBN 9780470172605. doi: 10.1002/9780470172605.

[10] L. Wang, B. Sundén, and R.M. Manglik. *Plate Heat Exchangers: Design, Applications and Performance*. Developments in heat transfer. WIT Press, 2007. ISBN 9781853127373. URL https://books.google.dk/books?id=P3gTR8YHLHgC.

[11] Sotirios Karellas, Georgios Panousis, and Aris-Dimitrios Leontaritis. Heat Transfer In Organic Rankine Cycle Applications. In Alina A. Minea, editor, *Advances in Industrial Heat Transfer*, pages 339–390. Taylor and Francis, 2012. ISBN 9781138072930.

[12] A. Cavallini. Heat transfer and heat exchangers. In Ennio Macchi and Marco Astolfi, editors, *Organic Rankine Cycle (ORC) Power Systems: Technology and Applications*, pages 397–470. Elsevier Ltd, 2016. ISBN 9780081005101. doi: 10.1016/B978-0-08-100510-1.00013-2. URL http://dx.doi.org/10.1016/B978-0-08-100510-1.00013-2.

[13] Benjamin Zühlsdorf, Jonas Kjær Jensen, and B. Elmegaard. Heat pump working fluid selection – Economic and thermodynamic comparison of criteria and boundary conditions. *International Journal of Refrigeration*, 2019. ISSN 01407007. doi: 10.1016/j.ijrefrig.2018.11.034.

[14] Eric Granryd. Hydrocarbons as refrigerants - an overview. 24(1):15–24, 2001. doi: /10.1016/S0140-7007(00)00065-7.

[15] Ju Hyok Kim, Jin Min Cho, and Min Soo Kim. Cooling performance of several CO2/propane mixtures and glide matching with secondary heat transfer fluid. *International Journal of Refrigeration*, 31:800–806, 2008. ISSN 01407007. doi: 10.1016/j.ijrefrig.2007.11.009.

[16] Jahar Sarkar and Souvik Bhattacharyya. Assessment of blends of CO2 with butane and isobutane as working fluids for heat pump applications. *International Journal of Thermal Sciences*, 48(7):1460–1465, 2009. ISSN 12900729. doi: 10.1016/j.ijthermalsci.2008.12.002.

[17] Xianping Zhang, Fang Wang, Xiaowei Fan, Huanlin Duan, and Feiyu Zhu. An investigation of a heat pump system using CO2/propane mixture as a working fluid. *International Journal of Green Energy*, 14(1):105–111, 2017. ISSN 15435083. doi: 10.1080/15435075.2016.1253577.

[18] Binbin Yu, Jingye Yang, Dandong Wang, Junye Shi, and Jiangping Chen. Modeling and theoretical analysis of a CO2-propane autocascade heat pump for electrical vehicle heating. *International Journal of Refrigeration*, 95:146–155, 2018. ISSN 01407007. doi: 10.1016/j.ijrefrig.2018.07.030.

[19] Fujun Ju, Xiaowei Fan, Yaping Chen, Tuanjie Wang, Xiangyang Tang, Amin Kuang, and Shengfei Ma. Experimental investigation on a heat pump water heater using R744/R290 mixture for domestic hot water. *International Journal of Thermal Sciences*, 132:1–13, 2018. ISSN 12900729. doi: 10.1016/j.ijthermalsci.2018.05.043.

[20] Benjamin Zühlsdorf, Jonas Kjaer Jensen, Stefano Cignitti, Claus Madsen, and Brian Elmegaard. Analysis of temperature glide matching of heat pumps with

zeotropic working fluid mixtures for different temperature glides. *Energy*, 153: 650–660, 2018. doi: 10.1016/j.energy.2018.04.048.

[21] Benjamin Zühlsdorf, Wiebke Meesenburg, Torben Ommen, J.E. Thorsen, Wiebke Brix Markussen, and Brian Elmegaard. Improving the performance of booster heat pumps using zeotropic mixtures. *Energy*, 154:390–402, 2018. doi: 10.1016/j.energy.2018.04.137.

[22] Paul Bouteiller, Marie France Terrier, and Pascal Tobaly. Experimental study of heat pump thermodynamic cycles using CO2based mixtures - Methodology and first results. *AIP Conference Proceedings*, 1814, 2017. ISSN 15517616. doi: 10.1063/1.4976271.

[23] Pascal Tobaly, Marie-france Terrier, and Paul Bouteiller. CO2 + Propane mixture as working fluid for refrigeration in hot climates. Experimental results of energy efficiency tests. In *Proceedings of the 13th IIR-Gustav Lorentzen Conference on Natural Refrigerants*, 2018. doi: 10.18462/iir.gl.2018.1276.

[24] Pardeep Garg, Pramod Kumar, Kandadai Srinivasan, and Pradip Dutta. Evaluation of carbon dioxide blends with isopentane and propane as working fluids for organic Rankine cycles. *Applied Thermal Engineering*, 52(2):439–448, 2013. ISSN 13594311. doi: 10.1016/j.applthermaleng.2012.11.032.

[25] J. G. Collier and J.R. Thome. *Convective boiling and condensation*. 1994. ISBN 0191591262. doi: 10.1016/0923-0467(95)80021-2.

[26] RL Amalfi, F Vakili-Farahani, and JR Thome. Flow boiling and frictional pressure gradients in plate heat exchangers. Part 1: Review and experimental database. *International Journal of Refrigeration*, 61:166–184, 2016. ISSN 01407007. doi: 10.1016/j.ijrefrig.2015.07.010. URL http://dx.doi.org/10.1016/j.ijrefrig.2015.07.010.

[27] F. Táboas, M. Vallès, M. Bourouis, and A. Coronas. Assessment of boiling heat transfer and pressure drop correlations of ammonia/water mixture in a plate heat exchanger. *International Journal of Refrigeration*, 35(3):633–644, 2012. ISSN 01407007. doi: 10.1016/j.ijrefrig.2011.10.003.

[28] Farzad Vakili-Farahani, Raffaele L Amalfi, and John R Thome. Two-Phase Heat Transfer and Pressure Drop within Plate Heat Exchangers. In John R. Thome and Jungho Kim, editors, *Encyclopedia of Two-Phase Heat Transfer and Flow II : Special topics and applications. Volume 2: Boiling Using Enhanced Surfaces, Plate Heat Exchangers and Two-Phase Devices. Chapter 4.*, chapter Chapter 4, pages 145–215. World Scientific Publishing, 2015. ISBN 978-981-4623-29-2. doi: https://doi.org/10.1142/9789814623285_0011.

[29] VDI-Gesellschaft. *VDI Heat Atlas*, volume 1. 2015. ISBN 978-3-540-77877-6. doi: 10.1007/978-3-540-77877-6.

[30] Jorge Gut and José M. Pinto. Optimal configuration design for plate heat exchangers. *International Journal of Heat and Mass Transfer*, 47(22):4833–4848, 2004. ISSN 00179310. doi: 10.1016/j.ijheatmasstransfer.2004.06.002.

[31] F.O. Jegede and G.T. Polley. Optimum heat exchanger design. *Chemical Engineering Research and Design*, 70(A2):133–141, 1992.

[32] A. Unuvar and S. Kargici. An approach for the optimum design of heat exchangers. *International Journal of Energy Research*, 28(15):1379–1392, 2004. ISSN 0363907X. doi: 10.1002/er.1080.

[33] K. Muralikrishna and U.V. Shenoy. Heat Exchanger Design Targets for Minimum Area and Cost. *Chemical Engineering Research and Design*, 78(2):161–167, 2000. ISSN 02638762. doi: 10.1205/026387600527185.

[34] E. Jarzebeski and E. Wardas-Koziel. Dimensioning plate heat exchangers giving minimum annual operating costs. *Chemical Engineering Research and Design*, 63 (4):211–218, 1985.

[35] Lieke Wang and Bengt Sundén. Optimal design of plate heat exchangers with and without pressure drop specifications. *Applied Thermal Engineering*, 23(3):295–311, 2003. ISSN 13594311. doi: 10.1016/S1359-4311(02)00195-3.

[36] Sotirios Karellas, Andreas Schuster, and Aris-Dimitrios Leontaritis. Influence of supercritical ORC parameters on plate heat exchanger design. *Applied Thermal Engineering*, 33-34:70–76, 2012. ISSN 13594311. doi: 10.1016/j.applthermaleng.2011.09.013.

[37] Nur Rohmah, Ghalya Pikra, Andri Joko Purwanto, and Rakhmad Indra Pramana. The Effect of Plate Spacing in Plate Heat Exchanger Design as a Condenser in Organic Rankine cycle for Low Temperature Heat Source. *Energy Procedia*, 68: 87–96, 2015. ISSN 18766102. doi: 10.1016/j.egypro.2015.03.236.

[38] Daniel Walraven, Ben Laenen, and William D'Haeseleer. Comparison of shell-and-tube with plate heat exchangers for the use in low-temperature organic Rankine cycles. *Energy Conversion and Management*, 87:227–237, 2014. ISSN 01968904. doi: 10.1016/j.enconman.2014.07.019.

[39] Muhammad Imran, Muhammad Usman, Byung-Sik Park, Hyouck-Ju Kim, and Dong-Hyun Lee. Multi-objective optimization of evaporator of organic Rankine cycle (ORC) for low temperature geothermal heat source. *Applied Thermal Engineering*, 80:1–9, 2015. ISSN 13594311. doi: 10.1016/j.applthermaleng.2015.01.034.

[40] Junjun Xu, Xianglong Luo, Ying Chen, and Songping Mo. Multi-criteria Design Optimization and Screening of Heat Exchangers for a Subcritical ORC. *Energy Procedia*, 75:1639–1645, 2015. ISSN 18766102. doi: 10.1016/j.egypro.2015.07.397.

[41] Riccardo Brignoli, J. Steven Brown, Harrison M. Skye, and Piotr A. Domanski. Refrigerant performance evaluation including effects of transport properties and optimized heat exchangers. *International Journal of Refrigeration*, 80:52–65, 2017. ISSN 01407007. doi: 10.1016/j.ijrefrig.2017.05.014. URL http://dx.doi.org/10.1016/j.ijrefrig.2017.05.014.

[42] Alberto Cavallini, J. Steven Brown, Davide Del Col, and Claudio Zilio. In-tube condensation performance of refrigerants considering penalization terms (exergy losses) for heat transfer and pressure drop. *International Journal of Heat and Mass Transfer*, 53(13-14):2885–2896, 2010. ISSN 00179310. doi: 10.1016/j.ijheatmasstransfer.2010.02.007.

[43] J. Steven Brown, Claudio Zilio, Riccardo Brignoli, and Alberto Cavallini. Heat transfer and pressure drop penalization terms (exergy losses) during flow boiling of refrigerants. *International journal of energy research*, 37:1669–1679, 2013. doi: 10.1002/er.2989.

[44] J. Steven Brown, Claudio Zilio, Riccardo Brignoli, and Alberto Cavallini. Thermophysical properties and heat transfer and pressure drop performance potentials of hydrofluoro-olefins, hydrochlorofluoro-olefins, and their blends. *HVAC and R Research*, 2014. ISSN 10789669. doi: 10.1080/10789669.2013.854146.

[45] A. C. Mueller and J. P. Chiou. Review of various Types of Flow Maldistribution in Heat Exchangers. *Heat Transfer Engineering*, 9:36–50, 1988. ISSN 0145-7632. doi: 10.1080/01457638808939664.

[46] M.K. Bassiouny and H. Martin. Flow distribution and pressure drop in plate heat exchangers—I U-type arrangement. *Chemical Engineering Science*, 39(4):693–700, 1984. ISSN 00092509. doi: 10.1016/0009-2509(84)80176-1.

[47] M.K. Bassiouny and H. Martin. Flow distribution and pressure drop in plate heat exchangers—II Z-type arrangement. *Chemical Engineering Science*, 39(4):701–704, 1984.

[48] N. Srihari, B. Prabhakara Rao, Bengt Sunden, and Sarit K. Das. Transient response of plate heat exchangers considering effect of flow maldistribution. *International Journal of Heat and Mass Transfer*, 48(15):3231–3243, 2005. ISSN 00179310. doi: 10.1016/j.ijheatmasstransfer.2005.02.032.

[49] N. Srihari and Sarit K. Das. Transient response of multi-pass plate heat exchangers considering effect of flow maldistribution. *Chemical Engineering and Processing*, 47 (4):695–707, 2006. ISSN 18733204, 02552701, 15732991, 02511088. doi: 10.1016/j.cep.2006.12.011.

[50] Wenzhe Li and Pega Hrnjak. Single Phase Pressure Drop and Flow Distribution in Brazed Plate Heat Exchangers. In *International Refrigeration and Air Conditioning*

Conference, page Paper 1812, Purdue university, 2016. URL http://docs.lib.purdue.edu/iracc/1812.

[51] B. Prabhakara Rao and Sarit K. Das. An Experimental Study on the Influence of Flow Maldistribution on the Pressure Drop Across a Plate Heat Exchanger. *Journal of Fluids Engineering - Transaction of ASME*, 126:680–691, 2004. doi: 10.1115/1.1779664.

[52] B Prabhakara Rao, Bengt Sunden, and Sarit K Das. An Experimental and Theoretical Investigation of the Effect of Flow Maldistribution on the Thermal Performance of Plate Heat Exchangers. *Journal of Heat Transfer-transactions of the Asme*, 127, 2005. doi: 10.1115/1.1860568.

[53] Prabhakara Rao Bobbili, Bengt Sunden, and Sarit K. Das. An experimental investigation of the port flow maldistribution in small and large plate package heat exchangers. *Applied Thermal Engineering*, 26(16):1919–1926, 2006. ISSN 13594311. doi: 10.1016/j.applthermaleng.2006.01.015.

[54] Fantu A. Tereda, N. Srihari, Bengt Sunden, and Sarit K. Das. Experimental investigation on port-to-channel flow maldistribution in plate heat exchangers. *Heat Transfer Engineering*, 28(5):435–443, 2007. ISSN 01457632. doi: 10.1080/01457630601163769.

[55] Wenzhe Li and Pega Hrnjak. An experimentally validated model of single-phase flow distribution in brazed plate heat exchanger. In *17th International Refrigeration and Air Conditioning Conference at Purdue*, 2018.

[56] Shenghan Jin and Pega Hrnjak. Effect of end plates on heat transfer of plate heat exchanger. *International Journal of Heat and Mass Transfer*, 108:740–748, 2017. ISSN 00179310. doi: 10.1016/j.ijheatmasstransfer.2016.11.106.

[57] Martin Ryhl Kærn, Brian Elmegaard, and Lars Finn Sloth Larsen. Comparison of fin-and-tube interlaced and face split evaporators with flow maldistribution and compensation. *International Journal of Refrigeration*, 36(1):203–214, 2012. ISSN 0140-7007. doi: 10.1016/j.ijrefrig.2012.10.006.

[58] Wiebke Brix, Martin Ryhl Kærn, and Brian Elmegaard. Modelling refrigerant distribution in microchannel evaporators. *International Journal of Refrigeration*, 32(7):1736–1743, 2009. doi: 10.1016/j.ijrefrig.2009.05.006.

[59] Wiebke Brix, Martin Ryhl Kærn, and Brian Elmegaard. Modelling distribution of evaporating CO2 in parallel minichannels. *International Journal of Refrigeration*, 33(6):1086–1094, 2010. ISSN 01407007. doi: 10.1016/j.ijrefrig.2010.04.012.

[60] K.K. Nielsen, K. Engelbrecht, and C.R.H. Bahl. The influence of flow maldistribution on the performance of inhomogeneous parallel plate heat exchangers. *International Journal of Heat and Mass Transfer*, 60:432–439, 2013. ISSN 00179310. doi: 10.1016/j.ijheatmasstransfer.2013.01.018.

[61] Shenghan Jin and Pega Hrnjak. A new method to simultaneously measure local heat transfer and visualize flow boiling in plate heat exchanger. *International Journal of Heat and Mass Transfer*, 113:635–646, 2017. ISSN 00179310. doi: 10.1016/j.ijheatmasstransfer.2017.04.116.

[62] Sivert Vist and Jostein Pettersen. Two-phase flow distribution in compact heat exchanger manifolds. *Experimental Thermal and Fluid Science*, 28:209–215, 2004. ISSN 08941777. doi: 10.1016/S0894-1777(03)00041-4.

[63] Allison J. Mahvi and Srinivas Garimella. Modeling Framework To Predict Two-Phase Flow Distribution in Heat Exchanger Headers. *International Journal of Refrigeration*, 2019. ISSN 01407007. doi: 10.1016/j.ijrefrig.2019.04.031.

[64] Jonas Kjær Jensen, Martin Ryhl Kærn, Torben Schmidt Ommen, Wiebke Brix, Lars Reinholdt, and Brian Elmegaard. Effect of liquid/vapour maldistribution on the performance of plate heat exchanger evaporators. In *Proceedings of the 24th IIR International Congress of Refrigeration*, 2015.

[65] Martin Ryhl Kærn, Wiebke Brix, Brian Elmegaard, and Lars Finn Sloth Larsen. Performance of residential air-conditioning systems with flow maldistribution in fin-and-tube evaporators. *International Journal of Refrigeration*, 34(3):696–706, 2011. ISSN 01407007. doi: 10.1016/j.ijrefrig.2010.12.010.

[66] Jianying Gong, Tieyu Gao, Xiuling Yuan, and Dong Huang. Effects of air flow maldistribution on refrigeration system dynamics of air source heat pump chiller under frosting conditions. *Energy Conversion and Management*, 49(6):1645–1651, 2008. ISSN 01968904. doi: 10.1016/j.enconman.2007.11.004.

[67] Gunda Mader, Björn Palm, and Brian Elmegaard. Maldistribution in air-water heat pump evaporators. Part 1: Effects on evaporator, heat pump and system level. *International Journal of Refrigeration*, 50:207–216, 2015. ISSN 01407007. doi: 10.1016/j.ijrefrig.2014.07.006.

[68] José M Corberán, P. Fernández de Córdoba, S. Ortuno, V. Ferri, and P. Montes. Modelling of compact evaporators and condensers. *Computational Studies*, 3: 487–496, 2000.

[69] José M. Corberán, P. F. De Córdoba, José Gonzálvez, and Francisco Alias. Semiexplicit method for wall temperature linked equations (SEWTLE): A general finite-volume technique for the calculation of complex heat exchangers. *Numerical Heat Transfer, Part B: Fundamentals*, 40(1):37–59, 2001. ISSN 15210626. doi: 10.1080/104077901300233596.

[70] Hongtao Qiao, Vikrant Aute, Hoseong Lee, Khaled Saleh, and Reinhard Radermacher. A new model for plate heat exchangers with generalized flow configurations and phase change. *International Journal of Refrigeration*, 36

(2):622–632, 2013. ISSN 01407007. doi: 10.1016/j.ijrefrig.2012.11.020. URL http://dx.doi.org/10.1016/j.ijrefrig.2012.11.020.

[71] Radia Eldeeb, Vikrant Aute, and Reinhard Radermacher. An Improved Approach for Modeling Plate Heat Exchangers Based on Successive Substitution in Alternating Flow Directions. In *Proceedings of the International Refrigeration and Air Conditioning Conference, Purdue university, US*, 2016. ISBN 3014058726. URL http://docs.lib.purdue.edu/iracc/1684.

[72] Vijaya Sekhar Gullapalli. *Estimation of Thermal and Hydraulic Characteristics of Compact Brazed Plate Heat Exchangers*. Phd thesis, Lund University, 2013. URL http://lup.lub.lu.se/search/ws/files/5818132/3799358.pdf.

[73] Vijaya S Gullapalli. Modeling of brazed plate heat exchangers for ORC systems. In *Energy Procedia - IV International Seminar on ORC Power Systems*, volume 129, pages 443–450, 13-15 September 2017, Milano, Italy, 2017. doi: 10.1016/j.egypro.2017.09.207.

[74] SWEP International AB. SSP G8 calculation software, 2019. URL https://www.swep.net/support/ssp-calculation-software/. Accessed 01-05-2019.

[75] Raffaele L Amalfi and John R Thome. Two-Phase Flow Simulations within Plate Heat Exchangers. In *Proceedings of 17th IEEE Intersociety Conference on Thermal and Thermomechanical Phenomena in Electronic Systems (ITherm)*, pages 487–496. IEEE, 2018. ISBN 9781538612729.

[76] Mathworks. Matlab R2017b, 2017. URL https://www.mathworks.com/products/new{_}products/latest{_}features.html. Accessed 01-05-2019.

[77] Holger Martin. A theoretical approach to predict the performance of chevron-type plate heat exchangers. *Chemical Engineering and Processing: Process Intensification*, 35(4):301–310, 1996. ISSN 02552701. doi: 10.1016/0255-2701(95)04129-X.

[78] R.W. Lockhart and R.C. Martinelli. Proposed correlation of data for isothermal two-phase, two-component flow in pipes. *Chemical engineering progress*, 45(1): 39–48, 1949.

[79] John R. Thome and Andrea Cioncolini. Two-Phase Pressure Drop. In John R. Thome, editor, *Encyclopedia of Two-Phase Heat Transfer and Flow I: Fundamentals and methods. Volume 3: Flow boiling in Macro and Microchannels*, chapter 6, pages 143–176. World Scientific Publishing, 2015.

[80] D Chisholm. A Theoretical Basis for the Lockhart-Martinelli Correlation for Two-Phase Flow. *lnternational Journal of Heat and Mass Transfer*, 10(18):1767–1778, 1967. ISSN 00179310. doi: http://dx.doi.org/10.1016/0017-9310(67)90047-6.

[81] G A Longo and A Gasparella. Heat transfer and pressure drop during HFC refrigerant vaporisation inside a brazed plate heat exchanger. *International Journal of Heat and Mass Transfer*, 50(25-26):5194–5203, 2007. ISSN 00179310. doi: 10.1016/j.ijheatmasstransfer.2007.07.001.

[82] Giovanni A Longo. Heat transfer and pressure drop during hydrocarbon refrigerant condensation inside a brazed plate heat exchanger. *International Journal of Refrigeration*, 33(5):944–953, 2010. ISSN 0140-7007. doi: 10.1016/j.ijrefrig.2010.02.007.

[83] John R Thome and Andrea Cioncolini. Void fraction. In John R Thome, editor, *Encyclopedia of Two-Phase Heat Transfer and Flow I, Volume 3: Flow boiling in Macro and Microchannels*, chapter 4, pages 85–112. doi: 10.1142/9789814623216_0021. URL https://www.worldscientific.com/doi/abs/10.1142/9789814623216_0021.

[84] S. L. Smith. Void fractions in two-phase flow: a correlation based upon an equal velocity head model. *Proceedings of the Institution of Mechanical Engineers*, 184(1):647–664, 1969. ISSN 0020-3483. doi: 10.1243/PIME_PROC_1969_184_051_02.

[85] Pranav V. Godbole, Clement C. Tang, and Afshin J. Ghajar. Comparison of void fraction correlations for different flow patterns in upward vertical two-phase flow. *Heat Transfer Engineering*, 32(10):843–860, 2011. ISSN 01457632. doi: 10.1080/01457632.2011.548285.

[86] R.K. Shah and W.W. Focke. Plate heat exchangers and their design theory. In R.K. Shah, E.C. Subbarao, and R.A. Mashelkar, editors, *Heat transfer equipment design*, pages 227–254. Hemisphere Publishing, Washington DC, 1988.

[87] E.W. Lemmon, Ian H. Bell, M. Huber, and M.O. McLinden. NIST Standard Reference Database 23: Reference Fluid Thermodynamic and Transport Properties - REFPROP, version 10.0, 2018. URL https://media.readthedocs.org/pdf/refprop-docs/latest/refprop-docs.pdf.

[88] Ian H. Bell, Jorrit Wronski, Sylvain Quoilin, and Vincent Lemort. Pure and pseudo-pure fluid thermophysical property evaluation and the open-source thermophysical property library coolprop. *Industrial and Engineering Chemistry Research*, 53(6):2498–2508, 2014. ISSN 08885885. doi: 10.1021/ie4033999.

[89] D.S. Jung, M. McLinden, R. Radermacher, and D. Didion. A study of flow boiling heat transfer with refrigerant mixtures. *International Journal of Heat and Mass Transfer*, 32(9):1751–1764, 1989a. ISSN 00179310. doi: 10.1016/0017-9310(89)90057-4.

[90] D. S. Jung, M. McLinden, R. Radermacher, and D. Didion. Horizontal flow boiling heat transfer experiments with a mixture of R22/R114. *International*

Journal of Heat and Mass Transfer, 32(1):131–145, 1989b. ISSN 00179310. doi: 10.1016/0017-9310(89)90097-5.

[91] Mathworks. fsolve - solve system of nonlinear equations, Matlab 2017b, 2017. URL https://se.mathworks.com/help/optim/ug/fsolve.html. Accessed 01-05-2019.

[92] Ji Zhang, Adriano Desideri, Martin Ryhl Kærn, Torben Schmidt Ommen, Jorrit Wronski, and Fredrik Haglind. Flow boiling heat transfer and pressure drop characteristics of R134a, R1234yf and R1234ze in a plate heat exchanger for organic Rankine cycle units. *International Journal of Heat and Mass Transfer*, 108:1787–1801, 2017. ISSN 00179310. doi: https://doi.org/10.1016/j.ijheatmasstransfer.2017.01.026.

[93] RL Amalfi, F Vakili-Farahani, and JR Thome. Flow boiling and frictional pressure gradients in plate heat exchangers . Part 2: Comparison of literature methods to database and new prediction methods. *International Journal of Refrigeration*, 61:185–203, 2016. ISSN 0140-7007. doi: 10.1016/j.ijrefrig.2015.07.009. URL http://dx.doi.org/10.1016/j.ijrefrig.2015.07.009.

[94] Y Yan and T.F. Lin. Evaporation heat transfer and pressure drop of refrigerant R134a in Plate Heat Exchanger. *Journal of Heat Transfer-Transactions of the Asme*, 121(1):118–127, 1999. doi: 10.1115/1.2825924.

[95] Björn Palm and Joachim Claesson. Plate Heat Exchangers: Calculation Methods for Single and Two-Phase Flow. *Heat Transfer Engineering*, 27(4):88–98, 2006. ISSN 0145-7632. doi: 10.1080/01457630500523949.

[96] Paul Bouteiller, Marie France Terrier, and Pascal Tobaly. Experimental study of heat pump thermodynamic cycles using CO2based mixtures - Methodology and first results. *AIP Conference Proceedings*, 1814, 2017. ISSN 15517616. doi: 10.1063/1.4976271.

[97] Ji Zhang, Martin Ryhl Kærn, Torben Ommen, Brian Elmegaard, and Fredrik Haglind. Condensation heat transfer and pressure drop characteristics of R134a, R1234ze(E), R245fa and R1233zd(E) in a plate heat exchanger. *International Journal of Heat and Mass Transfer*, 128:136–149, 2019. ISSN 00179310. doi: 10.1016/j.ijheatmasstransfer.2018.08.124.

[98] Torben Ommen, Jonas K. Jensen, Wiebke B. Markussen, Lars Reinholdt, and Brian Elmegaard. Technical and economic working domains of industrial heat pumps: Part 1 - Single stage vapour compression heat pumps. *International Journal of Refrigeration*, 55:168–182, 2015. ISSN 01407007. doi: 10.1016/j.ijrefrig.2015.02.011.

[99] Eric Granryd, Ingvar Ekroth, Per Lundqvist, Åke Melinder, Björn Palm, and Peter Rohlin. *Refrigerating engineering*. Royal Institute of Technology, KTH, Department of Energy Technology, Division of Applied Thermodynamics and Refrigeration, 2009. ISBN 9789174154153.

[100] L Silver. Gas cooling with aqueous condensation. *Industrial Chemist and Chemical Manufacturer*, 23(269):380–386, 1947.

[101] KJ Bell and MA Ghaly. An approximate generalized design method for multicomponent/partial condenser. *AIChE Symposium Series*, 69:72–79, 1973.

[102] John C. Chen. Correlation for boiling heat transfer to saturated fluids in convective flow. *Industrial and Engineering Chemistry Process Design and Development*, 5(3): 322–329, 1966. ISSN 01964305. doi: 10.1021/i260019a023.

[103] Radia Eldeeb, Vikrant Aute, and Reinhard Radermacher. A Survey of Correlations for Heat Transfer and Pressure Drop for Evaporation and Condensation in Plate Heat Exchangers. *International Journal of Refrigeration*, 65:12–26, 2015. ISSN 0140-7007. doi: 10.1016/j.ijrefrig.2015.11.013. URL http://linkinghub.elsevier.com/retrieve/pii/S0140700715003758.

[104] G N Danilova, V M Azarskov, and B B Zemskov. Teploobmen V plastinchatihispariteljan razichnole geometri (in Russian) - heat transfer in plates of different geometry. *Kholodilnaya Tekhnika*, 4:25–31, 1981.

[105] Dong Hyouck Han, Kyu Jung Lee, and Yoon Ho Kim. Experiments on the characteristics of evaporation of R410A in brazed plate heat exchangers with different geometric configurations. *Applied Thermal Engineering*, 23(10):1209–1225, 2003. ISSN 13594311. doi: 10.1016/S1359-4311(03)00061-9.

[106] W. W Akers, H. A. Deans, and O. K. Crosser. Condensing heat transfer within horizontal tubes. *Chemical Engineering Progress Symposium Series*, 55(29):171–176, 1959.

[107] M.G. Cooper. Heat flow rates in saturated nucleate pool boiling - a wide ranging examination using reduced properties. *Advances in Heat Transfer*, 16:59–156, 1984.

[108] Dieter Gorenflo and David Kenning. Pool boiling. In Peter Stephan, editor, *VDI Heat Atlas Second Edition*, chapter H2, pages 757–792. Springer Berlin Heidelberg, 2010. ISBN 978-3-540-77877-6.

[109] Jianchang Huang, Thomas J. Sheer, and Michael Bailey-Mcewan. Heat transfer and pressure drop in plate heat exchanger refrigerant evaporators. *International Journal of Refrigeration*, 35(2):325–335, 2012. ISSN 01407007. doi: 10.1016/j.ijrefrig.2011.11.002.

[110] Y.Y. Hsieh and T.F. Lin. Evaporation Heat Transfer and Pressure Drop of Refrigerant R-410A Flow in a Vertical Plate. *Journal of Heat Transfer-Transactions of the Asme*, 125(5):852–857, 2003. doi: 10.1115/1.1518498.

[111] W. Dittus and L. M. K. Boelter. Heat transfer in automobile radiators od tubular type. *University of California - Publications in Engineering*, 2(13):443–461, 1930. ISSN 00969311.

[112] Giovanni A. Longo, Simone Mancin, Giulia Righetti, and Claudio Zilio. A new model for refrigerant boiling inside Brazed Plate Heat Exchangers (BPHEs). *International Journal of Heat and Mass Transfer*, 91:144–149, 2015. ISSN 00179310. doi: 10.1016/j.ijheatmasstransfer.2015.07.078.

[113] Zahid H. Ayub, Tariq S. Khan, Saqib Salam, Kashif Nawaz, Adnan H. Ayub, and M.S. Khan. Literature Survey and a Universal Evaporation Correlation for Plate type Heat Exchangers. *International Journal of Refrigeration*, 99:408–418, 2018. ISSN 01407007. doi: 10.1016/j.ijrefrig.2018.09.008.

[114] R. Radermacher and Y. Hwang. Heat Transfer of Refrigerant Mixturers. In *Vapor Compression Heat Pumps with Refrigerant Mixtures*, chapter 8, pages 237–278. CRC Press 2005, 2005. ISBN 978-0-8493-3489-4. doi: doi:10.1201/9781420037579.ch8.

[115] John R Thome. Boiling of new refrigerants: a state-of-the-art review. *International Journal of Refrigeration*, 19(7):435–457, 1996. ISSN 01407007. doi: 10.1016/S0140-7007(96)00004-7.

[116] E Gungor and R H S Winterton. A general correlation for flow and annuli boiling in tubes. *International Journal of Heat and Mass transfer*, 29(3):351–358, 1986.

[117] E Gungor and R H S Winterton. Simplified general correlation for saturated flow boiling and comparisons of correlations with data. *Chemical Engineering Research and Design*, 65(2):148–156, 1987.

[118] K. Stephan and M. Abdelsalam. Heat-transfer correlations for natural convection boiling. *International Journal of Heat and Mass Transfer*, 23(1):73–87, 1980. ISSN 00179310. doi: 10.1016/0017-9310(80)90140-4.

[119] John R. Thome and S. Shakir. A new correlation for nucleate pool boiling of aqueous mixtures. *AIChE Symposium Series*, 83(257):46–51, 1987.

[120] Matthias Wettermann and Dieter Steiner. Flow boiling heat transfer characteristics of wide-boiling mixtures. *International Journal of Thermal Sciences*, 39(2):225–235, 2000. ISSN 12900729. doi: 10.1016/S1290-0729(00)00241-6.

[121] H.C. Ünal. Prediction of nucleate pool boiling heat transfer coefficients for binary mixtures. *International Journal of Heat and Mass Transfer*, 29(4):637–640, 1986. doi: 10.1016/0017-9310(86)90096-7.

[122] S. Grauso, R. Mastrullo, A. W. Mauro, and G. P. Vanoli. CO2 and propane blends: Experiments and assessment of predictive methods for flow boiling in horizontal tubes. *International Journal of Refrigeration*, 34(4):1028–1039, 2011. ISSN 01407007. doi: 10.1016/j.ijrefrig.2011.03.001.

[123] Jin Min Cho, Yong Jin Kim, and Min Soo Kim. Experimental studies on the characteristics of evaporative heat transfer and pressure drop of CO2/propane

mixtures in horizontal and vertical smooth and micro-fin tubes. *International Journal of Refrigeration*, 33(1):170–179, 2010. ISSN 0140-7007. doi: 10.1016/j.ijrefrig.2009.09.009.

[124] Dieter Steiner and Matthias Kind. Flow boiling - an introduction. In Peter Stephan, editor, *VDI Heat Atlas Second Edition*, chapter H3, pages 793–800. Springer Berlin Heidelberg, 2010. ISBN 9783540778769.

[125] R. G. Sardesai, R. A.W. Shock, and D. Butterworth. Heat and mass transfer in multicomponent condensation and boiling. *Heat Transfer Engineering*, 3(3-4): 104–114, 1982. ISSN 15210537. doi: 10.1080/01457638108939589.

[126] Mirza M. Shah. A method for predicting heat transfer during boiling of mixtures in plain tubes. *Applied Thermal Engineering*, 89:812–821, 2015. ISSN 13594311. doi: 10.1016/j.applthermaleng.2015.06.047.

[127] Ji Zhang, Maria E. Mondejar, and Fredrik Haglind. General heat transfer correlations for flow boiling of zeotropic mixtures in horizontal plain tubes. *Applied Thermal Engineering*, 150(January):824–839, 2019. ISSN 13594311. doi: 10.1016/j.applthermaleng.2019.01.036.

[128] M.R. Kærn, A. Modi, J.K. Jensen, J.G. Andreasen, and F. Haglind. An assessment of in-tube flow boiling correlations for ammonia-water mixtures and their influence on heat exchanger size. *Applied Thermal Engineering*, 93:623–638, 2015. ISSN 13594311. doi: 10.1016/j.applthermaleng.2015.09.106. URL http://dx.doi.org/10.1016/j.applthermaleng.2015.09.106.

[129] K. Stephan and M. Körner. Berechnung des wärmeübergangs verdampfender binärer flüssigkeitsgemische. *Chemie Ingenieur Technik*, 41(7):409–417, 1969. doi: 10.1002/cite.330410702. URL https://onlinelibrary.wiley.com/doi/abs/10.1002/cite.330410702.

[130] H Jungnickel, P Wassilew, and W E Kraus. Investigations on the heat transfer of boiling binary refrigerant mixtures. *International Journal of Refrigeration*, 3(3):129–133., 1980. ISSN 0140-7007. doi: https://doi.org/10.1016/0140-7007(80)90092-4.

[131] E.U. Schlunder. Heat transfer in nucleate boiling of mixtures. *Int. Chem. Eng.*, 23 (4):589–599, 1983.

[132] Yasunobu Fujita and Masayuki Tsutsui. Heat transfer in nucleate pool boiling of binary mixtures. *International Journal of Heat and Mass Transfer*, 37(1):291–302, 1994. ISSN 18792189 and 00179310. doi: 10.1016/0017-9310(94)90030-2.

[133] Yasunobu Fujita and Masayuki Tsutsui. Heat transfer in nucleate boiling of binary mixtures (development of a heat transfer correlation). *JSME International Journal Series B Fluids and Thermal Engineering*, 40(1):134–141, 1997. ISSN 09168451. doi: 10.1299/jsmeb.40.134.

[134] T Inoue, N Kawae, and M Monde. Characteristics of heat transfer coefficient during nucleate pool boiling of binary mixtures - Improvement of correlation and its physical meaning. *Heat and Mass Transfer*, 33:337–344, 1998. ISSN 09477411. doi: 10.1007/s002310050199.

[135] D. Chisholm and A. S. Wanniarachchi. Layout of plate heat exchangers. *ASME/JSME Thermal Engineering Proceedings*, 4:433–438, 1991.

[136] A S Wanniarachchi, U Ratnam, B E Tilton, and K Dutta-Roy. Approximate correlation for chevron-type plate heat exchangers. In *30th National heat transfer conference*, volume 12, 1995. ISBN 079181713X.

[137] Yi-Yie Yan, Hsiang-Chao Lio, and Tsing-Fa Lin. Condensation heat transfer and pressure drop of refrigerant R-134a in a plate heat exchanger. *International Journal of Heat and Mass Transfer*, 42(6):993–1006, 1999. ISSN 00179310. doi: 10.1016/S0017-9310(98)00217-8.

[138] M.J. Moran, H.N. Shapiro, D.D. Boettner, and M.B. Bailey. *Fundamentals of Engineering Thermodynamics*. Wiley, 2018. ISBN 9781119391425. URL https://books.google.dk/books?id=QHJlDwAAQBAJ.

[139] Benjamin Zühlsdorf, Fabian Bühler, Roberta Mancini, Stefano Cignitti, and Brian Elmegaard. High Temperature Heat Pump Integration using Zeotropic Working Fluids for Spray Drying Facilities. In *Proceedings of the 12th IEA Heat pump conference*, Rotterdam, 2017.

[140] Adrian Bejan, George Tsatsaronis, and Michael Moran. *Thermal design and optimization*. John Wiley and Sons, Inc., 1996. ISBN 0471584673. doi: 10.1016/S0140-7007(97)87632-3.

[141] Danish Energy Agency. Data, Tables, Statistics and Maps, Energy in Denmark, 2015.

[142] Nicholas Metropolis and S. Ulam. The Monte Carlo Method. *Journal of the americal statistical association*, 44(247):335–341, 1949.

[143] J. C. Helton and F. J. Davis. Latin hypercube sampling and the propagation of uncertainty in analyses of complex systems. *Reliability Engineering and System Safety*, 81(1):23–69, 2003. ISSN 09518320. doi: 10.1016/S0951-8320(03)00058-9.

[144] Gurkan Sin and Krist V. Gernaey. Data Handling and Parameter Estimation. In Damir Brdjanovic Mark C.M. van Loosdrecht, P.H. Nielsen, C.M. Lopez-Vazquez, editor, *Experimental Methods in Wastewater Treatment*, pages 201–234. London, UK, iwa publis edition, 2016. ISBN 9781780404752.

[145] ALFA LAVAL. Alfa Laval, AlfaQ series, 2018. URL https://www.alfalaval.com/products/heat-transfer/plate-heat-exchangers/gasketed-plate-and-frame-heat-exchangers/alfaq/. Accesed on 25-10-2018.

[146] Xuan Tao and Carlos A Infante Ferreira. Heat transfer and frictional pressure drop during condensation in plate heat exchangers : Assessment of correlations and a new method. *International Journal of Heat and Mass Transfer*, 135:996–1012, 2019. ISSN 0017-9310. doi: 10.1016/j.ijheatmasstransfer.2019.01.132. URL https://doi.org/10.1016/j.ijheatmasstransfer.2019.01.132.

[147] Andrea Saltelli, Ksenia Aleksankina, William Becker, Pamela Fennell, Federico Ferretti, Niels Holst, Sushan Li, and Qiongli Wu. Why so many published sensitivity analyses are false: A systematic review of sensitivity analysis practices. *Environmental Modelling and Software*, 114(January):29–39, 2019. ISSN 13648152. doi: 10.1016/j.envsoft.2019.01.012.

List of Figures

1.1 Working principle of a Sondex AS [8] gasketed PHE 3

1.2 Operability limit of different PHE designs (adapted from [11, 12]) 4

1.3 (a) Flow sheet of a single-stage vapour compression heat pump, and (b) Temperature - heat diagram for a case study with propylene/butane (0.5/0.5) as working fluid (adapted from [13]) 5

1.4 Mass flow rate distribution for upward (a) and downward (b) flow [62] . 10

2.1 Chevron PHE geometry 18

2.2 PHE model discretization approaches:(a) 1D ; (b) 2D 20

2.3 Detailed discretization schemes: (a) 1D, (b) 2D 21

2.4 Work flow of the solver for heat transfer and fluid flow 24

2.5 Work flow of the design solver 29

2.6 Vapour quality variation in different PHE channels for different values of Δx 34

2.7 Comparison between the results of the present model and the results of the model by Li and Hrnjak [55] 36

2.8 Comparison of simulated data points vs. experimental data for the (a), (b) total heat flow rate, and (c), (d) total refrigerant pressure drop 38

2.9 Comparison of simulated data points vs. experimental data for the estimation of (a) total heat flow rate, (b) total pressure drop of ammonia, and (c) total pressure drop of the brine 40

2.10 Comparison of simulated data points vs. experimental data for the estimation of total heat flow rate 42

2.11 Comparison of simulated data points vs. experimental data for the (a) total heat flow rate and (b) total refrigerant pressure drop 43

2.12 Work flow of the overall procedure. Rectangles represent a numerical model; parallelepipeds represent input/output; rounded bold rectangles represent main output 44

2.13 Schematic of the heat pump cycle (adapted from [13]) 45

2.14 Work flow of the coupled off-design heat pump model and PHE performance models without maldistribution effects (1D evaporator model) . . 47

2.15 Work flow of the coupled off-design heat pump model and PHE performance models with maldistribution effects (2D evaporator model) 49

3.1 Schematic of the test facility and experimental bench [96] 63

3.2 Distribution of ΔT_{gl} of the considered experimental points 64

3.3 Comparison of experimental and measure heat flow rate for all the experimental data points of CO_2/propane, using the different prediction methods, divided in sub-groups 66

3.4 Heat transfer coefficient vs. cumulated heat flow rate for some prediction methods for three different experimental points in (a), (b) and (c) 69

3.5 Heat transfer coefficient vs. cumulated heat flow rate for the investigated correlations to compute F_c for three different experimental points in (a), (b) and (c) 73

3.6 Case I results: (a) Impact of the different heat transfer correlations on the mean UA value; (b) UA as function of the cumulated heat flow rate in the evaporator 77

3.7 Case II results: (a) Impact of the different heat transfer correlations on the mean UA value; (b) UA as function of the cumulated heat flow rate in the evaporator 78

3.8 Case III results: (a) Impact of the different heat transfer correlations on the mean UA value; (b) UA as function of the cumulated heat flow rate in the evaporator 79

3.9 Highest and lowest deviations from the mean of the refrigerant heat transfer coefficient, UA value and of the total evaporator heat flow rate . 80

4.1 Work-flow of the overall procedure 84

4.2 Normalized COP as a function of total refrigerant pressure drop in the evaporator 87

4.3 (a) COP as a function of total refrigerant pressure drop in the condenser; (b) normalized condenser heat flow rate as function of total refrigerant pressure drop in the evaporator 88

4.4 Specific cost of heat as function as a function of total refrigerant pressure drops in the evaporator for: (a) all fluids, (b) propane (close-up) 90

4.5 Work flow of the overall methodology 94

4.6 Example of log(p)-h diagram without pressure drops (blue) and with 50 kPa pressure losses in the evaporator (sky-blue) 98

4.7 Effect of heat transfer area of the evaporator (a) and refrigerant total pressure losses (b) on the non-dimensional NPV for all the working fluids 101

4.8 Breakdown of the contributions to the NPV, divided in cost and revenue. The colours indicate the different shares of the terms contributing to the cost stream 103

4.9 COP as function of the total refrigerant pressure drops for all the working fluids 104

4.10 Capital investment of the heat exchangers (a) and compressor (b), as function of the total refrigerant pressure drops for all the working fluids . 105

4.11 Normalized NPV as function of all the dimensionless parameters correlated exponentially for Propane/Iso-Pentane (0.5/0.5). The different colors represent the different chevron angles adopted 106

4.12 Normalized NPV as function of different combinations of non-dimensional numbers for all the working fluids reported in Table 4.10; (a)Case I; (b)Case II; (c)Case III; (d)Case IV 108

4.13 Normalized NPV as function of $\mathrm{Re_V}^{-0.42}\mathrm{Bd}^{0.26}$ for all the working fluids. The red line represents the mean value $\mathrm{Re}_V^{-0.42}\mathrm{Bd}^{0.26} = 0.04$, while the dotted lines represent max and min, 0.059 and 0.026 respectively. 110

5.1 Mass flow distribution of the refrigerants in the different evaporator channels, shown as percentage deviation from the average value 120

5.2 Temperature distribution in the PHE evaporator for the case of severe maldistribution rate $\Delta x = 0.25$ 122

5.3 Impact of maldistribution effects on (a) total heat flow rate of the evaporator and (b) total refrigerant pressure drop 123

5.4 Impact of maldistribution effects on total heat flow rate of using two different methods for frictional pressure drop for butane and propylene/butane 124

5.5 Impact of maldistribution effects on total heat flow rate for butane and three evaporator geometries 126

5.6 Mass flow distribution of the refrigerant in the different evaporator channels, shown as percentage deviation from the average value 132

5.7 Impact of maldistribution effects on (a) total refrigerant mass flow rate, (b) evaporator heat flow rate and (c) total refrigerant pressure drop . . . 133

5.8 Impact of maldistribution effects on (a) condenser heat flow rate, (b) compressor power and (c) heat pump COP 136

5.9 Impact of maldistribution effects on the heat pump cycle for butane . . . 137

5.10 (a) Specific cost of heat and (b) yearly cost and revenue streams as function of Δx for butane 138

List of Tables

2.1 Geometrical parameters 18

2.2 Deviations between experimental data and results of the evaporator model using 1D and 2D discretization (DTU data) 39

2.3 Deviations between experimental data and results of the evaporator model (Sondex data) 41

2.4 Deviations between experimental data and results of the model 42

3.1 Some relevant PHE flow boiling correlations 54

3.2 Nucleate boiling correction factors for mixtures $F_c = h_{\mathrm{nb}}/h_{\mathrm{nb,id}}$ 60

3.3 Correlations chosen for further analysis 62

3.4 Geometrical data of the PHE 63

3.5 Mean relative and absolute errors of the heat flow rate predicted by the different prediction methods. Bold values denote all data points 67

3.6 Mean relative and absolute errors of the heat flow rate predicted by the different correlations to compute F_c 72

3.7 Evaporator boundary conditions for the different working fluids [20] . . . 75

3.8 Geometry of the SWEP Evaporator type V65 [74] 75

3.9 Investigated correlations for the case study 76

4.1 Plate width and number of channels values used in the parametric study . 85

4.2 Heat pump design and operating parameters for the selected working fluids 86

4.3 Evaporating pressure and thermo-physical properties at the design point . 89

4.4 PHE designs corresponding to the economic optimum 91

4.5 Geometrical parameters of the PHE varied in the parametric study 95

4.6 Summary of the considered working fluids 96

4.7 Boundary conditions for the heat pump 96

4.8 Non-dimensional parameters used for the analysis of the results 99

4.9 Input uncertainties for the uncertainty analysis 100

4.10 Coefficients obtained by fitting the NPV* to different combinations of dimensionless parameters 107

4.11 Minimum, maximum and average values of different combinations of dimensionless numbers for the best results (5 % NPV*), for each working fluid and overall 109

4.12 Some examples of PHE design points for the mixture Propane/Iso-Pentane (0.5/0.5) 112

4.13 MC uncertainty analysis results for PHE design I for Propane/Iso-Pentane (0.5/0.5) performed with a sample population of 500 elements 113

5.1 Working fluids and evaporator inlet conditions 118

5.2 PHE evaporator geometry [74] 119

5.3 Heat flow rate degradation due to maldistribution effects and working fluid thermo-physical properties at saturation pressure 123

5.4 PHE size and count for the three considered case (plate dimensions from [74]) 125

5.5 Heat flow rate degradation due to effect of end plates and liquid/vapour maldistribution for butane and different geometries 126

5.6 Heat pump design and operating parameters for the selected working fluids 127

5.7 Evaporator and condenser plate geometry, input for the design models [74, 145] 128

5.8 Discretization and tolerances adopted for the PHE models 128

5.9 Economic boundary conditions for the case study [21] 129

5.10 Results of design model for evaporator and condenser 131

5.11 Evaporator heat flow rate degradation due to effect of end plates and liquid/vapour maldistribution 134

5.12 Refrigerant saturation pressure and thermo-physical properties at evaporator design conditions 134

5.13 COP degradation due to effect of end plates and liquid/vapour maldistribution 136

Papers

Energy 156 (2018) 492–508

Contents lists available at ScienceDirect

Energy

journal homepage: www.elsevier.com/locate/energy

Deriving guidelines for the design of plate evaporators in heat pumps using zeotropic mixtures

Roberta Mancini*, Benjamin Zühlsdorf, Jonas Kjær Jensen, Wiebke Brix Markussen, Brian Elmegaard

Technical University of Denmark, Department of Mechanical Engineering, Nils Koppels Allé, Building 403, 2800 Kongens Lyngby, Denmark

ARTICLE INFO

Article history:
Received 1 December 2017
Received in revised form
25 April 2018
Accepted 3 May 2018
Available online 8 May 2018

Keywords:
Plate heat exchanger
Zeotropic mixture
Economic analysis
Design guideline
Dimensionless numbers
Pressure drops
Heat transfer area

ABSTRACT

This paper presents a derivation of design guidelines for plate heat exchangers used for evaporation of zeotropic mixtures in heat pumps. A mapping of combined heat exchanger and cycle calculations for different combinations of geometrical parameters and working fluids allowed estimating the trade-off between heat transfer area and pressure drops on the thermodynamic and economic performance indicators of the cycle. Compressor running costs constituted the largest cost share, and increased due to a steep decrease of the heat pump coefficient of performance at high refrigerant pressure drops. It was found that the pressure drop limit leading to infeasible designs was dependent on the working fluid, thereby making it impossible to define a guideline based on maximum allowable pressure drops. It was found that economically feasible designs could be obtained by correlating the vapour Reynolds number and the Bond number at the evaporator inlet as $Re_V^{-0.42} Bd^{0.26} \approx 0.040$. The use of the proposed guideline was illustrated for the mixture Propane/Iso-Pentane (0.5/0.5), leading to evaporator designs with net present values deviating maximum −4.4% from the best value found in the mapping. The presented methodology can be applied in different scenarios to develop similar guidelines, thereby decreasing the cost of combined cycle and component optimizations.

© 2018 Elsevier Ltd. All rights reserved.

1. Introduction

Zeotropic mixtures are blends of two or more components, with different mass fractions of the liquid and vapour phases at thermodynamic phase equilibrium. Therefore, the temperature at bubble and dew points differ at any saturation pressure and the mixture undergoes a temperature glide during phase change. The use of zeotropic mixtures as working fluids for thermodynamic cycles offers a possibility of optimizing the cycle efficiency by reducing the thermodynamic irreversibility in the heat exchangers (HEXs). Due to non-isothermal evaporation and condensation, the exergy destruction in the HEXs can be reduced by matching the working fluid temperature glide with the heat source and heat sink temperature profiles.

Zühlsdorf et al. [1–3] demonstrated the advantage of using zeotropic mixtures in heat pumps for different applications. A good glide match between the evaporating fluid and the heat source resulted in a beneficial influence on the cycle thermodynamic performance and better improvements were obtained for larger heat source temperature glides [2]. The improvement of using mixtures in a booster heat pump for a district heating system was estimated equal to up 30% compared to pure working fluids. A larger overall improvement up to 40% was achieved for a reduced degree of required superheat imposed in the case of mixtures [3].

One drawback of using zeotropic mixtures is the degradation of the heat transfer coefficient compared to pure fluids, which was observed during both evaporation and condensation in different experimental campaigns, as reported in Refs. [4,5]. In the case of evaporation, several reasons contribute to the heat transfer degradation: (i) an earlier suppression of the nucleate boiling contribution due to an additional mass diffusion resistance created by the more readily evaporation of the more volatile component [6,7]; (ii) large variation of the refrigerant physical properties during evaporation, due to variable compositions of liquid and vapour phases, which, according to Jung et al. [8,9], accounts for the 80% of the total heat transfer degradation; (iii) worse transport properties of mixtures compared to pure fluids [5]. A number of

* Corresponding author.
E-mail addresses: robman@mek.dtu.dk (R. Mancini), bezuhls@mek.dtu.dk (B. Zühlsdorf), jkjje@mek.dtu.dk (J. Kjær Jensen), wb@mek.dtu.dk (W. Brix Markussen), be@mek.dtu.dk (B. Elmegaard).

https://doi.org/10.1016/j.energy.2018.05.026
0360-5442/© 2018 Elsevier Ltd. All rights reserved.

studies quantified the heat transfer degradation differently: Ross et al. [6] observed a reduction of up to 50% compared to pure fluids, Jung et al. [8,9] reported varying reduction rates between 19% and 36% depending on the mixture composition, while Torikoshi and Ebisu [10] calculated a degradation of 20% and 30% compared to the heat transfer coefficient estimated by the ideal mixing rule. It is therefore of paramount importance to optimize the design of the heat transfer equipment when zeotropic mixtures are employed, in order to avoid investing in higher heat transfer areas for the heat exchangers.

Plate Heat Exchangers (PHEs) offer a modular and flexible solution for such applications, since it is possible to achieve high heat transfer coefficients within a compact design due to the flow turbulence generated by the characteristic plate corrugation patterns. PHEs are comprised of thin parallel plates stacked together in order to form channels for fluid flow, which can also be arranged in a counter-current manner for achieving a temperature glide match between the mixture and the secondary fluid. Gasketed-type PHEs consist of plates sealed by gaskets and held together by a frame. For higher operating temperature and pressure, the plates can be sealed together by brazing. At the current state-of-the-art, the operating conditions of gasketed-type PHEs are limited to 20.4 bar and 150 °C, whilst brazed heat exchangers can be operated up to 40 bar [11,12], thereby offering a reasonable range of operation at typical heat pump working conditions.

When designing heat exchangers for a given application, different criteria can be adopted to select the geometrical configuration. The pressure drop of one or both fluids can be limited to a maximum allowable value [11,12], and the heat transfer area can be minimized for a full utilization of the available pressure loss, as applied in Ref. [13]. For single phase HEXs, such pressure drop limitations could also be translated into maximum gas and liquid phase velocities at the inlet, and typical design values can be found in literature for a number of heat exchanger configurations [12]. These values are often based on heuristics from manufacturers and the extension to other types of applications (e.g. zeotropic mixtures and/or phase change) is not trivial.

Following other design approaches, the heat exchanger can be optimized by carrying out a cost minimization problem without a maximum pressure drop limitation, and evaluating the trade-off between heat transfer area and pressure drops. Different previous studies have approached the problem by considering solely the cost related to the heat exchanger, namely the investment cost and the pumping and compression costs related to the two streams, for a general heat exchanger configuration [14,15], for shell and tube heat exchangers [16] and for plate heat exchangers [17,18]. However, the economic analysis lacked assessment of the impact of the heat exchanger pressure drops on the other components, as well as on the overall cycle thermodynamic performance.

In literature a number of studies can be found on simultaneous optimization of plate heat exchangers used as evaporators and/or condensers and thermodynamic cycle design, mostly focusing on low temperature applications and pure fluids. Some of the works are related to the assessment of the impact of some specific cycle parameters on the PHE design [19,20], whilst other studies performed combined cycle-PHE optimization procedures with the aim of maximizing the cycle efficiency [21], and by including also an economic analysis [22,23]. The pressure drops were mostly considered as pumping cost on the heat source/sink side, and none of the studies assessed the impact of the working fluid pressure drops on the outlet condition of the evaporator. Moreover, a complete and combined component-cycle optimization comes at a demanding computational cost, especially during the preliminary design phase, when many different working fluids are usually compared and ranked.

The study presented in this paper addresses the following aspects: (i) It presents a methodology for deriving design guidelines for plate heat exchangers integrated in a thermodynamic cycle, namely a heat pump. (ii) The methodology is based on assessing the impact of both plate heat exchanger size and pressure drops on the thermodynamic and economic performance of the heat pump; the pressure losses are not only included as pumping cost of the heat source side, but also imply a modification of the thermodynamic state points of the cycle at the evaporator outlet, which accordingly affects the heat pump design, investment and operating cost. (iii) It utilizes the aforementioned methodology to derive design guidelines for PHE evaporator design in heat pumps using zeotropic mixtures as working fluids. The obtained results are intended for employment in practical engineering during the process of component selection for similar applications, hence avoiding the cost of combined cycle and component analysis.

The methodology is based on complementing a vapour compression heat pump sizing model together with a detailed numerical model of the evaporator, accounting for the variation of the heat transfer coefficient and fluid properties during the evaporation process and estimating the impact of heat transfer area and pressure drops on the cycle thermodynamic and economic performance indicators. The methodology was applied to the case of evaporator design for a heat pump, and eight different working fluids were selected based on a previous study [1], which demonstrated the thermodynamic and economic feasibility of using zeotropic mixtures in heat pumps for waste heat recovery in a spray drying facility.

2. Methods

The methodology adopted in the present study is based on a parametric analysis on the main design parameters of a plate heat exchanger to assess the impact of the different design configurations on the thermodynamic and economic performance indicators of a thermodynamic cycle, namely a heat pump. Fig. 1 shows the schematic of the work flow of the methodology. Two different models were built and integrated in the Matlab environment [24], i.e. a cycle simulation model for a heat pump, explained in details in Section 2.3, and a detailed PHE model, presented in Section 2.4. After the working fluid selection process, explained in Section 2.2, the preliminary sizing of the heat pump was done and the design parameters were calculated, i.e. desired heat exchanger capacity, mass flow rates, pressures and temperatures. The values were subsequently sent to the plate heat exchanger model, which additionally received as inputs the geometrical parameters from which the required heat transfer area and resulting pressure losses were estimated. The outputs were returned to the heat pump model, where the sizing of the cycle was re-evaluated. In this second iteration, the sizing process took into account the resulting heat exchanger size and pressure drops for the economic calculation, as it is briefly described in Section 2.6. The process was repeated for all the combinations of geometrical parameters chosen for the parametric analysis, which is introduced in Section 2.1. Moreover, the same process was repeated for all the eight working fluids considered in the case study, by considering the same combinations of PHE design parameters and calculating the Coefficient of Performance (COP) and Net Present Value (NPV). As shown in Fig. 1, all the data points were collected and used as basis for deriving a general design guideline, valid for all the working fluids and the boundary conditions of the present case study. The aim was to correlate the point with optimal economic performances to the PHE design parameters. In order to generalize the results, non-dimensional parameters were employed as explained in Section 2.8.

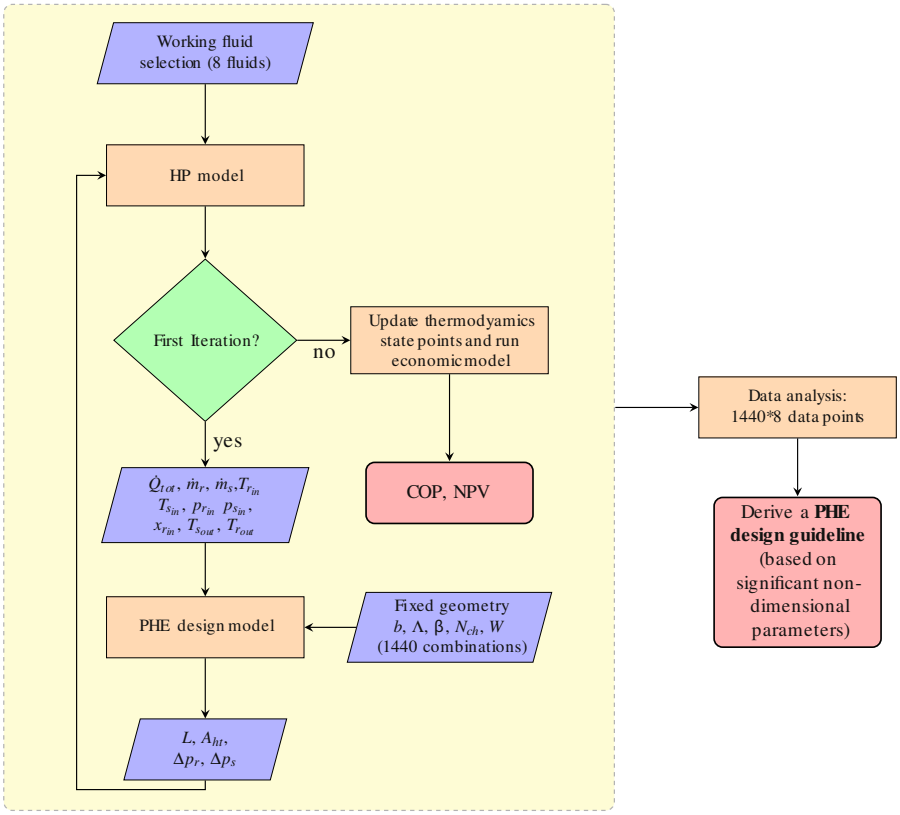

Fig. 1. Work flow of the overall methodology.

2.1. Parametric analysis and PHE geometry

The parametric analysis was carried out by varying the main design variables of a PHE. Fig. 2 shows the main geometrical parameters, namely plate size, number and corrugation geometry. The plate size is given by the width W and the length L; L_{HT} defines the effective length for heat transfer and the total heat transfer area depends on the number of channels N_{ch} employed. The corrugation characteristics are determined by the corrugation pitch Λ, the corrugation height b and the chevron angle β. The corrugation thickness t is a trade-off between mechanical resistance to stresses and conductive thermal resistance. The corrugation parameters determine the hydraulic diameter of the channels, thereby defining the flow conditions of the working fluid. The hydraulic diameter was estimated by using Eq. (1) [11], where Φ is the enlargement factor.

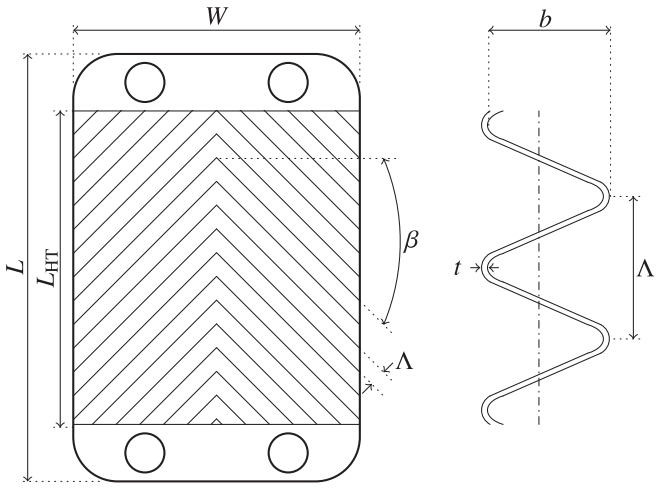

Fig. 2. Schematic view of a chevron type PHE [25].

$$D_h = \frac{2b}{\Phi} \tag{1}$$

The enlargement factor represents the ratio between the actual heat transfer area and the projected area of the plate (without corrugation), and it is expressed by Eq. (2) [11] as function of corrugation height and pitch.

$$\Phi = \frac{1}{6}\left(1 + \sqrt{1 + \left(\frac{\pi b}{\Lambda}\right)^2} + \sqrt{1 + \frac{1}{2}\left(\frac{\pi b}{\Lambda}\right)^2}\right) \tag{2}$$

The port diameter D_p determines the inlet/outlet velocities of the refrigerant and the heat source, mainly affecting the port pressure losses; the PHE can be manufactured with different values of the diameter for the two working fluids, depending on the desired velocity and the phase.

In the parametric study, the design variables were varied among the values reported in Table 1, investigating all the possible combinations between them, for a total of 1440 different PHE configurations. The thickness was fixed to a value commonly found in literature [11]. The port diameter was considered as fixed depending on the magnitude of the plate width. The plate length was calculated as output of the plate heat exchanger design model in order to match the evaporator capacity of the case study for all the combinations of PHE design variables. The plates were considered to be manufactured in stainless steel, with thermal

Table 1
Geometrical parameters of the PHE varied in the parametric study.

Parameter	Value	Unit
W	0.15, 0.25, 0.35, 0.45, 0.55	m
N_{ch}	25, 50, 75, 100, 150, 200	–
b	2, 4, 6, 8	mm
Λ	2, 4, 6, 8	mm
β	30, 45, 60	°
t	0.5	mm
D_p	0.03, 0.06, 0.1	mm

conductivity equal to 16.2 W/(m K). The free flow area and the heat transfer area were calculated as function of the design parameters, as reported in Eqs. (3) and (4) [11], respectively.

$$A_0 = bN_{ch}W \tag{3}$$

$$A_{ht} = 2(W \cdot L_{HT} + b \cdot L_{HT}) \cdot N_{ch}\Phi \tag{4}$$

The effective length L_{ht} was employed for heat transfer calculations, while the port-to-port length was used in order to calculate the frictional pressure losses. The relation between port-to-port length and effective length is given by Eq. (5) [11].

$$L_p = L_{HT} + \frac{D_{p-in}}{2} + \frac{D_{p-out}}{2} \tag{5}$$

In order to avoid unrealistic results and to minimize maldistribution effects along the plate width, solutions with length to width ratio lower than 2 were considered infeasible and excluded from further analysis.

2.2. Case study and working fluid selection

The framework of the analysis was given by a case study [1] assessing the integration of high temperature heat pumps in a spray drying facility. Waste heat was recovered by integrating a heat pump, with the aim of pre-heating air up to 120 °C. Different zeotropic mixtures were compared in terms of COP and NPV for a single-stage configuration of a vapour compression heat pump, in which the working fluid was varied based on binary mixtures formed by combinations of a number of natural refrigerants. The refrigerant screening included hydrocarbons, Dimethyl Ether (DME), Diethyl ether (DEE) and carbon dioxide CO_2, chosen for their low Global Warming Potential (GWP) and Ozone Depletion Potential (ODP), and being miscible between each other for wide ranges of temperature and pressure without leading to any chemical reactions [1,2]. Table 2 summarizes the best performing mixtures, with considered mass composition and all the evaporation pressures were found to be well below the maximum operating pressure for PHEs. The table also shows the preliminary COP, calculated without accounting for pressure losses of the evaporator.

Table 2
Summary of the considered working fluids.

Working fluid	p_{ev}, bar	COP, –
Propane/Iso-Pentane (0.5/0.5)	4.9	3.08
Propane/n-Pentane (0.8/0.2)	8.4	3.04
Propane/n-Pentane (0.4/0.6)	3.0	3.02
Butane/Hexane (0.9/0.1)	2.5	3.07
DME/n-Pentane (0.4/0.6)	2.6	3.26
DME/n-Pentane (0.7/0.3)	5.0	3.24
DME/Iso-Pentane (0.5/0.5)	4.0	3.15
Propylene/Iso-Pentane (0.4/0.6)	3.9	3.14

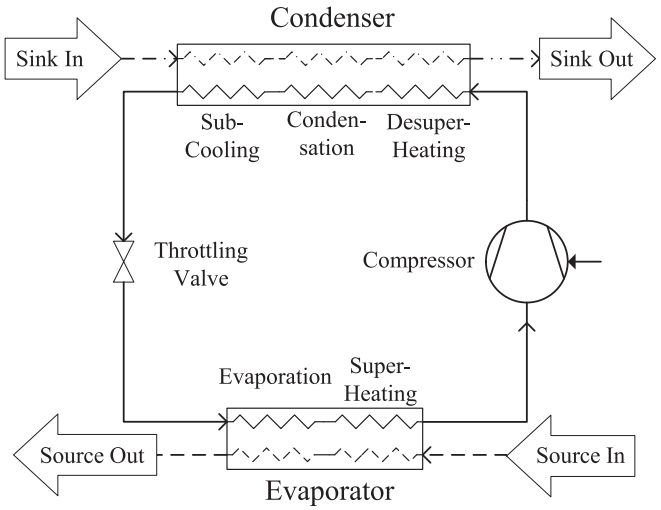

Fig. 3. Schematic of the heat pump model.

2.3. Heat pump cycle model

The thermodynamic cycle was modelled in steady state and it consists of a single-stage configuration of a vapour compression heat pump. Fig. 3 shows the sketch of the unit, with the different components integrated in the cycle, namely compressor, condenser, throttling valve and evaporator.

Table 3 shows the design parameters of the cycle. The heat source side was completely defined by the boundary conditions, while the outlet temperature of the condenser was set as a free variable. The evaporation and condensation pressures of the working fluid were defined by the minimum required pinch point temperature difference between the working fluid and the fluid at the secondary side. The amount of subcooling was defined by the pinch point temperature difference and the sink inlet temperature in order to obtain the maximum efficiency. A minimum superheating of 5 K was included in the evaporator, in order to ensure a dry compression for all the fluids. The compressor was modelled by assuming a constant isentropic efficiency, while the motor efficiency accounted for the power generation losses [26]. The thermodynamic performance was evaluated by estimating the COP, defined in Eq. (6), as the ratio between the thermal energy provided to the heat sink and the compressor power.

Table 3
Boundary conditions for the heat pump.

Parameter	Value	Unit
Heat source		
Medium	Water	
T_{in}	65	°C
T_{out}	40	°C
$\dot{m}$	14.8	kg/s
$\dot{Q}$	1544	W
Heat sink		
Medium	Water	
T_{in}	75	°C
$\dot{m}$	10.6	kg/s
Compressor		
η_{is}	0.8	–
η_{motor}	0.95	–
ΔT_{sh}	5	K
Heat exchangers		
ΔT_{pinch}	10	°C

$$\mathrm{COP} = \frac{\dot{Q}_{\mathrm{sink}}}{\dot{W}_{\mathrm{comp}}} \tag{6}$$

The working fluid properties were calculated by Refprop [27], using recommended standard equation of states and mixing parameters, while heat sink and source properties were computed using CoolProp [28].

2.4. PHE design model

The PHE design model was based on a one-dimensional discretization of the heat exchanger along the flow direction, at constant enthalpy steps, hence with constant heat flow rate for each control volume (CV). The heat exchanger solver was based on a successive substitution approach, with heat transfer area and pressure drops set as unknown. A total number of n=50 control volumes was chosen, as trade-off between accuracy and computational cost of the design model. The internal solver iterated on the length of each CV, as well as on the pressure drops of both refrigerant and heat source, with a tolerance set on the relative residuals equal to 10^{-2}.

The PHE model was solved by imposing steady-state mass, momentum and energy conservation equations, which were solved for each CV and both fluids. The logarithmic mean temperature difference method was applied locally, for the computation of the UA value in each CV. Counter-current flow of the refrigerant and heat source was imposed, longitudinal conduction through the walls and heat loss to the external environment were neglected. Thermodynamic state variables and fluid properties were computed for each CV based on a first order linear interpolation of the values at the nodes. The local heat transfer coefficients and pressure drops were estimated using experimental correlations. The choice of appropriate prediction methods for the considered case study is discussed in Section 2.5.

2.5. Choice of prediction methods

The local heat transfer coefficient and frictional pressure drops were computed for both fluids using experimental correlations, thereby conveying focus on the choice of suitable prediction methods for the working fluids and the boundary conditions of the case study. Literature presents several correlations developed for the estimation of the heat transfer coefficient for refrigerant flow boiling in PHEs. There is however a lack of a suitable prediction method for the evaporation heat transfer coefficient in PHEs for zeotropic mixtures of natural refrigerants. Amalfi et al. [29] developed a flow boiling correlation based on an extensive database collected from several studies in literature, claiming to have a better agreement than other existing correlations. The only zeotropic mixture included in the database was the near-azeotropic mixture R410a, which presents a small temperature glide during evaporation. Such correlation is therefore not directly applicable to the estimation of the heat transfer coefficient of mixtures. Moreover, it does not take the mixture degradation of heat transfer into account.

Mixture degradation of heat transfer was estimated by a number of experimental studies focusing on in-tube flow boiling of different zeotropic mixtures, including ammonia-water. An extensive literature review can be found in [30]. The developed correlations were however derived for tubular geometry, with a different flow mechanism compared to PHEs. In order for a correlation to be fully applicable, the effect of the geometry must be included as well. It was therefore decided to apply a theoretical method, which was first developed for mixture condensation by Silver [31] and Bell-Ghaly [32]. Sardesai et al. [33] extended the theoretical derivation to convective boiling heat transfer, deriving the formulation expressed by Eq. (7) [33].

$$h_{\mathrm{TP}} = \frac{1 + h_{\mathrm{NB-mix}}/h_C}{1/h_C + \bar{z}/h_V} \tag{7}$$

Here, $h_{\mathrm{NB-mix}}$ is the nucleate boiling contribution of the mixture, h_C is the convective two-phase contribution and h_V is the single-phase vapour heat transfer coefficient estimated for the vapour flowing alone in the channel. $\bar{z}$ is a correction term taking into account the ratio of sensible over latent heat transfer, and it is evaluated by Eq. (8) [32].

$$\bar{z} = x \cdot \frac{dT}{dh} \cdot c_{p,V} \tag{8}$$

In the estimation of $h_{\mathrm{NB-mix}}$, the mixture effects on degradation of nucleate boiling and loss of effective wall superheat is accounted for by applying a suitable correction factor. Thome and Shakir [34] approach was used for this purpose, expressing the relation between ideal and mixture heat transfer coefficient as [34]:

$$\frac{h_{\mathrm{NB-mix}}}{h_{\mathrm{NB-id}}} = \left\{ 1 + \frac{h_{\mathrm{NB-id}}}{\dot{Q}''} \left(T_{\mathrm{dew}} - T_{\mathrm{bubble}}\right) \left[1 - \exp\left(\frac{\dot{Q}''}{\rho_L h_{\mathrm{lat}} \beta_L} \right) \right] \right\}^{-1} \tag{9}$$

By using the theoretical method proposed by Sardesai [33], it was possible to choose prediction methods specifically developed for chevron-type PHEs for the estimation of the different terms $h_{\mathrm{NB-id}}$, h_C and h_V. The method by Amalfi et al. [29] was used to estimate the contribution of convective boiling, while Cooper [35] was employed for the nucleate boiling term. Martin [36] correlation was employed for the single-phase heat transfer coefficient of the vapour flowing alone. The same correlation was used for the refrigerant heat transfer coefficient in the superheated region, as well as for the water single-phase heat transfer coefficient along the whole heat exchanger.

Pressure drops were computed by considering all the contributions to the steady state momentum equation, i.e. friction, gravity (static), acceleration and inlet/outlet ports terms:

$$\Delta p_{\mathrm{tot}} = \Delta p_{\mathrm{fr}} + \Delta p_{\mathrm{gr}} + \Delta p_{\mathrm{acc}} + \Delta p_{\mathrm{ports}} \tag{10}$$

The pressure drop over the total length of the HEX was calculated by considering each control volume separately. In the two-phase region, the acceleration and static contributions were calculated by the homogeneous model, thereby using Eq. (11) and Eq. (12) for each CV, respectively [37].

$$\Delta p_{\mathrm{acc}} = G^2 \left[\left(\frac{x}{\rho_V} + \frac{1-x}{\rho_L} \right)_{\mathrm{OUT}} - \left(\frac{x}{\rho_V} + \frac{1-x}{\rho_L} \right)_{\mathrm{IN}} \right] \tag{11}$$

$$\Delta p_{\mathrm{gr}} = \rho_m g \Delta L \tag{12}$$

The two-phase mean density was determined by:

$$\rho_m = \left[\frac{x}{\rho_V} + \frac{1-x}{\rho_L} \right]^{-1} \tag{13}$$

Eq. (13) was also used for the computation of the frictional pressure drop in the two-phase region. The frictional contribution was calculated by means of the two-phase Fanning friction factor, as expressed by Eq. (14) [37].

$$\Delta p_{\mathrm{fr}} = 2 f_{\mathrm{TP}} \frac{\Delta L G^2}{D_h \rho_m} \tag{14}$$

The friction factor was computed by using the correlation by Amalfi et al. [29]. In the single-phase region, the friction factor correlation by Martin [36] was used for both the refrigerant superheating and the water flow. Last, the port pressure drops were computed using the Shah and Focke [38] correlation, as expressed by Eq. (15), where G_p indicates the mass flux at the ports, depending on the port diameter.

$$\Delta p_{\text{ports}} = 0.75\left[\left(\frac{G_p^2}{2\rho}\right)_{\text{IN}} + \left(\frac{G_p^2}{2\rho}\right)_{\text{OUT}}\right] \tag{15}$$

For the refrigerant flow, port pressure losses were considered only at the outlet control volume, since the inlet loss was included in the refrigerant expansion at the throttling valve. Both inlet and outlet pressure drops due to ports were evaluated for the heat source, thereby contributing to the pumping power.

2.6. Economic model

After the sizing of the PHE, the heat pump model was re-evaluated by taking the updated temperature and pressure at the evaporator outlet into account, as shown in Fig. 1. Therefore, the COP was slightly affected by the change in compressor power resulting from the mixture pressure drop. Different aspects of the HEX design influenced the value of the NPV of the heat pump. The NPV was calculated by considering different cost and revenue streams, by using Eq. (16) [1]. The considered costs were the Total Capital Investment (TCI), accounting for the Capital Investment (CI) of each system component, the Operation and Maintenance Cost (OMC), the electricity cost (FC_{hp}) due to the compressor running and the required water pumping cost (FC_w). The revenue stream was considered as the natural gas saving (FC_{ng}), which otherwise would be necessary to produce the thermal energy output of the heat pump.

$$\text{NPV} = -\text{TCI} - \text{OMC} - \frac{\text{FC}_{hp}}{\text{CRF}} - \frac{\text{FC}_w}{\text{CRF}} + \frac{\text{FC}_{ng}}{\text{CRF}} \tag{16}$$

The interest and inflation rates were assumed equal to 7% and 2%, respectively, and then used for the estimation of the Capital Recovery Factor (CRF), with a plant economic lifetime of 20 years [26,39]. Operation and Maintenance Costs were assumed to be the 20% of the investment cost as one time cost at the time of the investment [39]. The saving of natural gas was calculated by estimating the useful thermal energy produced by the heat pump, equal to the heat sink capacity and by considering a boiler efficiency η_{boiler} equal to 0.9 [26]. The price of natural gas was considered as 0.0303 €/kWh [40].

The TCI accounted for the investment of condenser, compressor and evaporator. The sizing of the condenser was carried out by considering constant heat transfer coefficients and by using the logarithmic mean temperature difference methods for the three different sections of desuperheating, condensation and subcooling. The TCI of each individual component was calculated from the Purchased Equipment Cost (PEC), scaled according to the component size with scaling factors and reference values of PECs reported by Ommen et al. [26]. The TCI was increased by a factor 4.16 compared to the PEC, to account for the investment of the expansion of an existing facility [39].

The running cost of the compressor, given by FC_{hp} was adapted to the updated compressor power by considering an estimation of 7400 h/yr [1] as annual operating time τ_h of the heat pump and an electricity cost c_{el} of 0.0783 €/kWh [40]. The additional fuel cost term due to the water pressure drops, was calculated by using Eq. (17) as a function of the water mass flow rate, water density, total water pressure drops, and a pump efficiency η_{pump} equal to 0.95.

$$\text{FC}_w = \frac{\dot{m}_s}{\rho_s}\frac{\Delta p_{s-\text{tot}}}{\eta_{\text{pump}}} c_{el}\tau_h \tag{17}$$

Fig. 4 shows the log(p)-h diagram of the heat pump with and without pressure drops in the evaporator. It can be noticed how the outlet of the evaporator is affected by the pressure losses, thus changing the compressor power required as well as the investment cost, which is based on the suction line. The pressure drop also influences the evaporator inlet location in the diagram, but to a lower extent compared to the outlet. In order to compare the results for different working fluids, performing with different COP and maximum NPV, it was decided to normalize each NPV for the maximum value calculated for the specific fluid. The value of NPV of a certain design point of the HEX i for a given working fluid wf was therefore normalized as $\text{NPV}^{\star}_{i-wf}$, defined by Eq. (18).

$$\text{NPV}^{*}_{i-wf} = \frac{\text{NPV}_{i-wf}}{max\left(\text{NPV}_{wf}\right)} \tag{18}$$

2.7. Data analysis

The different HEX configurations and working fluids were compared based on dimensionless numbers, in order to derive a guideline describing the design points corresponding to maximum NPV. Non-dimensional parameters were chosen in order to describe the impact of the fluid properties, of the boundary conditions imposed by the cycle (refrigerant evaporation pressure, mass flow and inlet quality) and of the PHE geometry. The main dimensionless numbers governing the heat transfer and pressure drop correlations for the two-phase flow of the mixture were used (see Section 2.4), and they are reported in Table 4.

The numbers were used to correlate the normalized net present value to the different heat exchanger designs. The parameters were evaluated at the refrigerant conditions at the evaporator inlet, since the scope was to derive guidelines applicable before the actual

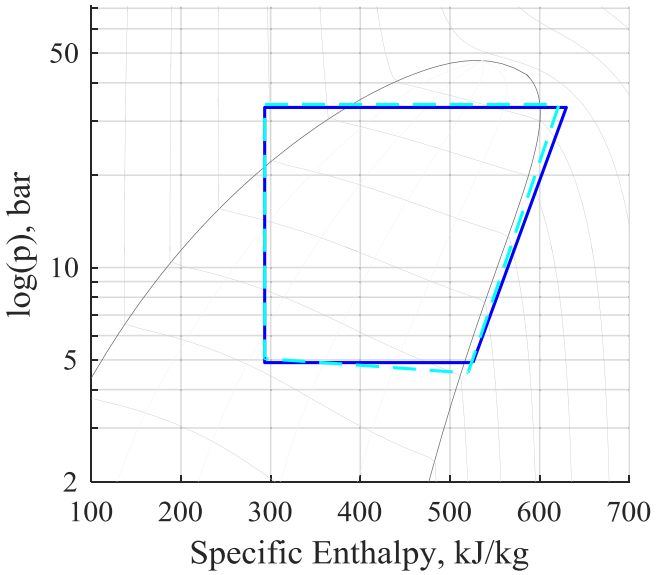

Fig. 4. Example of log(p)-h diagram without pressure drops (blue) and with 50 kPa pressure losses in the evaporator (sky-blue). (For interpretation of the references to color in this figure legend, the reader is referred to the Web version of this article.)

Table 4
Non-dimensional parameters used for the analysis of the results.

Symbol	Name	Formula
$\theta^{\star}$	Dimensionless inclination angle	$\frac{90-\beta}{70}$
Bd	Bond number	$\frac{gD_h^2(\rho_L-\rho_V)}{\sigma}$
We_m	Weber number	$\frac{G^2 D_h}{\sigma \rho_m}$
ρ^*	Liquid-to-vapour density ratio	$\frac{\rho_L}{\rho_V}$
Re_{LO}	Liquid only Reynolds number	$\frac{GD_h}{\mu_L}$
Re_V	Vapour alone Reynolds number	$\frac{GxD_h}{\mu_V}$

component design. The inlet conditions are fixed by the boundary conditions of the heat pump, thereby being known for all the fluids a priori. It was therefore decided to exclude the Boiling number from the data analysis, since it requires information on the heat flux distribution along the heat exchanger and a preliminary estimation of the heat transfer area is needed. The Weber number We_m is defined by evaluating the equivalent two-phase density, expressed by Eq. (13).

The correlation between the dimensionless parameters and the normalized NPV was obtained by adopting a power law of the form expressed by Eq. (19).

$$NPV^* = a \cdot \theta^{*b} \cdot Bd^c \cdot We_m^d \cdot Re_V^e \cdot Re_{LO}^f \cdot \rho^{*g} \quad (19)$$

The normalized NPV was first correlated as function of all the dimensionless parameters considered in Table 4. All the design points with positive NPV were considered in the fitting, and the results for all the working fluids were considered simultaneously in one fitting. After deriving the coefficient for Eq. (19), the most relevant parameters were identified. This was done by evaluating the obtained exponent and by comparing different combinations of non-dimensional numbers. The correlation that best fitted the NPV trend for all the fluids, as well as leading to a similar optimal range for the different mixtures, was chosen and presented as design guideline.

2.8. Uncertainty analysis

For each correlation chosen for the PHE design model, for both heat transfer and pressure drop, a certain accuracy was reported by the authors. This measure represents an estimation of how well the prediction method fits the experimental database from which the correlation was derived. Therefore the accuracy does not necessarily indicate the uncertainty of the prediction methods when they are applied to different working fluids, geometry and operating conditions. It is however relevant to evaluate the change of the obtained results when a certain deviation is applied to the calculation of heat transfer coefficient and pressure drops. For this purpose the accuracy bounds of each correlations were considered as a source of uncertainty in an uncertainty analysis, with the aim of evaluating to which extent the results would change for similar variations in the inputs. The bounds are reported in Table 5, with the exception of h_V. Since Martin [36] expresses h_V as a function of f_V, the uncertainty of h_V was directly included by considering the accuracy bound for the vapour friction factor f_V.

The Monte Carlo (MC) method [42] was applied in order to carry out the uncertainty analysis, with the aim of estimating the probability density of the model outputs, namely A_{ht}, $\Delta p_{r,tot}$, $\Delta p_{s,tot}$ and NPV. The inputs were assumed to be uniformly distributed between

Table 5
Input uncertainties for the uncertainty analysis.

Parameter	Correlation	Bounds	Reference
h_C	Amalfi	±22.1%	Mean absolute error [29]
h_{NB-id}	Cooper	±59.0%	Mean absolute error, reported in Ref. [37]
$\frac{h_{NB-mix}}{h_{NB-id}}$	Thome and Shakir	±11.1%	Mean absolute error, reported in Ref. [41]
f_{TP}	Amalfi	±21.5%	Mean absolute error [29]
f_V	Martin	−50.0% + 100%	Accuracy bounds, reported in Ref. [11]

the uncertainty bounds reported in Table 5. A latin hypercube sampling (LHS) technique was adopted to create 500 different samples in the input space, proved to be more reliable compared to random sampling [43]. The MC simulations were performed following the approach by Sin and Gernaey [44], and the results were obtained as mean values, standard deviations and 95% coverage intervals. The analysis was applied to Propane/Iso-Pentane (0.5/0.5), by fixing the PHE geometry to one of the optimal designs found by applying the derived design guideline.

3. Results

In this section, the main results are presented. Sections 3.1 and 3.2 present the trade-off between heat transfer area and pressure drops and the impact on the different revenue and cost streams. Sections 3.3 and 3.4 report the fitting with the non-dimensional parameters and the derivation of the final design guideline.

3.1. Heat transfer area and pressure drops

Fig. 5 shows the NPV as function of the heat transfer area (a) and total refrigerant pressure drops (b) for all the fluids considered in the analysis. It is shown that both heat transfer area and pressure drops have an impact on the economic performance of the heat pump. However, the NPV decreases to a lower extent for higher values of A_{ht} compared to an increase of the refrigerant pressure drops. Fig. 5(b) shows that for all the eight cases there is a trade-off which coincides with minimizing the refrigerant pressure drops to a very low value. Moreover, Fig. 5(b) shows that the pressure drops impact is different depending on the fluid: the mixtures Butane/Hexane (0.9/0.1) and DME/n-Pentane (0.4/0.6) are the most sensitive to pressure drops, performing with negative NPVs at 60 kPa and 120 kPa, respectively. On the contrary, Propane/n-Pentane (0.8/0.2) shows a weaker dependence, with NPV values always positive in the considered pressure drop range.

3.2. Cost breakdown

Fig. 6 shows the breakdown of the NPV as calculated by Eq. (16). The abscissa reports the refrigerant total pressure drop, with trends similar for all the working fluids. The blue line indicates the revenue stream, which contributed positively to the NPV and was determined by the natural gas saving. The black line represents the sum of all the expenses, which impacted negatively the NPV. The breakdown of the different terms of the total cost is indicated by the filling colors of the cost line.

The dominant contribution was given by the compressor running cost (grey area), which was negatively affected by the refrigerant pressure drop, causing an increase of the required compressor work. This is explained by Fig. 7, where the COP of the heat pump is plotted against the total refrigerant pressure drop. For a fixed design thermal load of the heat pump, a lower COP entails a

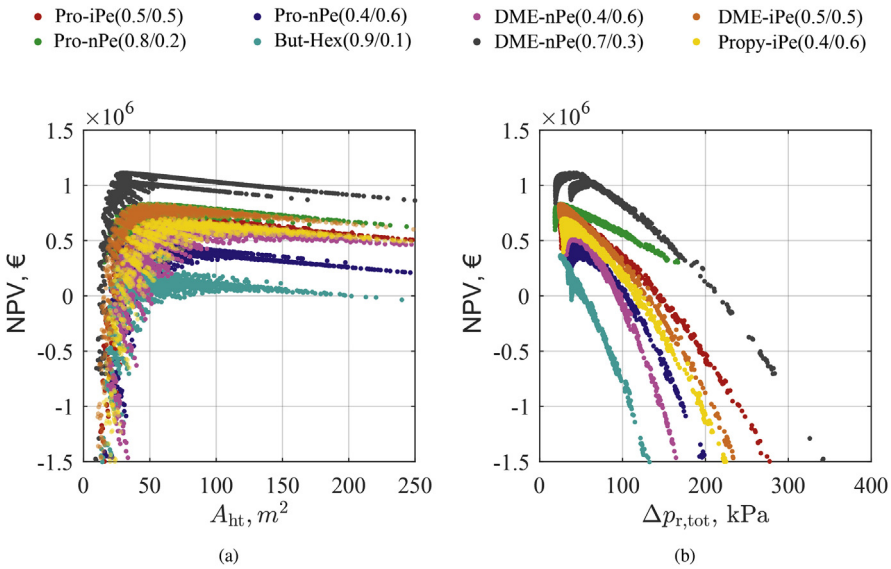

Fig. 5. Effect of heat transfer area of the evaporator (a) and refrigerant total pressure losses (b) on the non-dimensional NPV for all the working fluids.

higher required compressor work, as shown by Eq. (6). A sharp decrease is observed for all the fluids, with different slopes, similarly to the trends found in Fig. 5(b). The different trends for the different fluids found in the cost breakdown of Fig. 6 can therefore be explained by a different sensitivity of the COP to the pressure drop. The mixture Propane/n-Pentane (0.8/0.2) was found to be least affected by pressure drop, while Butane/Hexane (0.9/0.1) presented the steepest slope.

In the cost breakdown of Fig. 6, the TCI is the second highest contribution, indicated by the light-blue area. The TCI undergoes a slight increase for low values of refrigerant pressure drop, and then increases more sharply for higher pressure drop. Since operation and maintenance was considered as a fixed share of the capital investment, OMC undergoes the same trend. An explanation for the TCI behaviour can be found in Fig. 8(a) and (b), showing the capital investment of the evaporator, condenser and compressor as functions of the total refrigerant pressure drop. All the working fluids are reported in the same plot with different marker colors. The evaporator and condenser investment costs, directly related to the heat transfer area, are one order of magnitude lower than the compressor investment if the pressure drops are not minimized. When the evaporator investment increases at lower pressure drops (entailing a higher investment due to the larger heat transfer area), the CI of the HEX reaches the same order of magnitude of the lower investment entailed by the compressor. The change in HEX CI due to varying heat transfer area is similar for all the fluids, with an overlap of the different curves.

On the other hand, the compressor CI in Fig. 8(b) undergoes a steep increase for higher values of pressure drop and presents different trends depending on the mixture. The sharp increase is due to the change in the compressor suction line, which is affected by the evaporator outlet. In fact, for higher refrigerant pressure drops, a lower refrigerant outlet density is obtained, entailing a higher volume flow rate, which is directly proportional to the compressor size and cost. The different slopes for the different fluids are related to a different sensitivity of the refrigerant properties to the change in evaporator outlet pressure. The trends of the fluids follow the results found for COP in Fig. 7, with Propane/n-Pentane (0.8/0.2) showing the weakest dependence on the pressure drops and opposite trends for mixtures Propane/n-Pentane (0.4/0.6) and Butane/Hexane (0.9/0.1), where the pressure drops have a major influence on both the compressor running cost and TCI.

One very relevant aspect to highlight is the intersection point between revenue and costs streams, in Fig. 6, representing the pressure drop limit above which the design of the PHE leads to infeasible solutions, i.e. with negative NPV. This limit value is not the same for all the working fluids, supporting the thesis that it is not necessarily optimal to design HEXs by imposing a maximum allowable pressure drop regardless of the working fluid or boundary conditions.

The water pumping cost was found to be negligible compared to the all the other contributions. No clear relation is therefore expected between heat source pressure drops and NPV.

Last, it must be noted that such analysis highlights considerations, which might be useful when choosing an optimal working fluid for a specific case study. In fact, by looking at Figs. 5 (a) and Fig.7, the mixture DME/-Pentane (0.7/0.3) outperforms the other fluids both in terms of maximum NPV and COP found in the mapping, thereby suggesting the choice of such fluid as preferred option. However, the mixture Propane/n-Pentane (0.8/0.2) showed the weakest dependence on refrigerant pressure drops, thus offering an additional flexibility during the evaporator design process. It would therefore be up to the designer to evaluate and prioritize the different aspects.

3.3. Correlation between NPV and non-dimensional parameters

By exponentially correlating the design points by means of Eq. (19) to the chosen non-dimensional parameters, the NPV* is found to be proportional to the combinations of dimensionless numbers reported by Eq. (20), indicated by K.

$$K = \theta^{*0.045}\mathrm{Bd}^{0.051}\mathrm{We}_m^{-0.011}\rho^{*-0.066}\mathrm{Re}_{LO}^{0.009}\mathrm{Re}_V^{-0.12} \tag{20}$$

Fig. 9 reports the normalized net present value as function of K, for Propane/Iso-Pentane (0.5/0.5). The different colors represent the chevron angle of the PHE, namely 30°, 45° and 60° corresponding to a value of non-dimensional inclination angle of 0.86, 0.64 and 0.43, respectively. The trends for the other working fluids are not shown in the paper, but they are similar. The obtained design points are well correlated by K, and it is recommended to

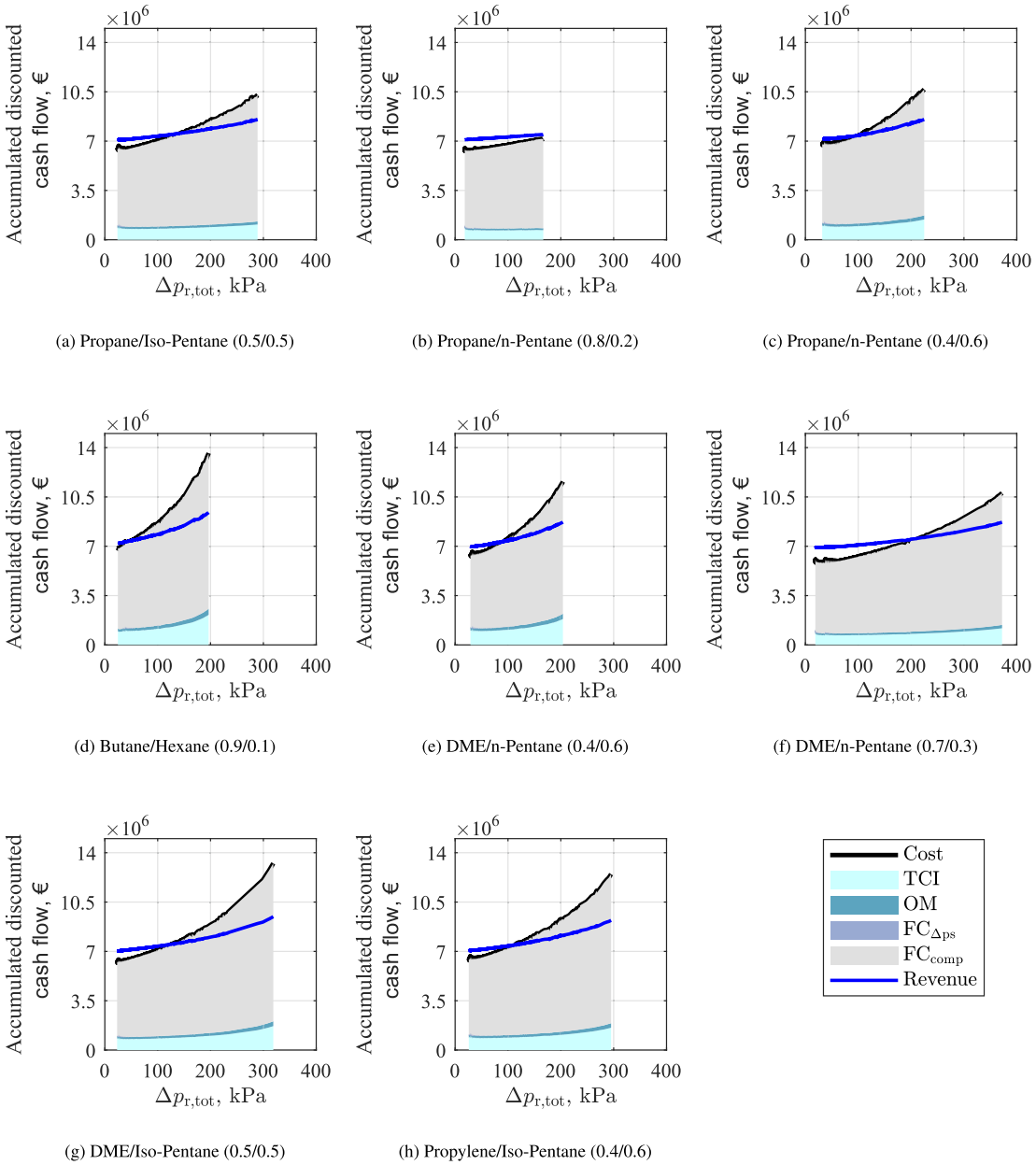

(a) Propane/Iso-Pentane (0.5/0.5)
(b) Propane/n-Pentane (0.8/0.2)
(c) Propane/n-Pentane (0.4/0.6)
(d) Butane/Hexane (0.9/0.1)
(e) DME/n-Pentane (0.4/0.6)
(f) DME/n-Pentane (0.7/0.3)
(g) DME/Iso-Pentane (0.5/0.5)
(h) Propylene/Iso-Pentane (0.4/0.6)

Fig. 6. Breakdown of the contributions to the NPV, divided in cost and revenue. The colours indicate the different shares of the terms contributing to the cost stream. (For interpretation of the references to color in this figure legend, the reader is referred to the Web version of this article.)

employ HEXs with K=[0.4–0.6] at the evaporator inlet, in order to obtain solutions with NPV in the best 20%. By increasing the value of K, the economic performance is negatively affected by the increase in heat transfer area, while for K<0.4 an increase of refrigerant pressure losses entails a steep decrease of NPV.

The use of a design guideline based on K, which depends on six different parameters, might however lead to have redundant information on the boundary conditions and the fluids in the parameters. The problem was therefore simplified by relating the NPV* to a selected number of non-dimensional parameters only. In order to do so, the results were assessed based on the coefficients and on additional considerations.

First, the dependence of the NPV on the liquid only Reynolds number Re_{LO} is weak, since its exponent in Eq. (20) is two orders of magnitude lower than the vapour alone Reynolds number and one order of magnitude lower compared to the other parameters, thereby suggesting that a good fitting could be obtained by neglecting the influence of this non-dimensional number. Furthermore, it was decided to exclude the liquid to vapour density ratio ρ^*, since it contains information solely depending on the inlet densities and other dimensionless number, as the Reynolds numbers, the Weber number and the Bond number already contain the density characteristics of both vapour and liquid phases.

Lastly, by looking at the impact of the dimensionless inclination angle θ^* in Fig. 9, the plot suggests that it is always optimal to minimize the chevron angle (hence enhancing the degree of turbulence of the fluid flow in the channels) if the PHE design is carried out in the optimal region or else for high value of K, i.e. designs with higher heat transfer area. On the contrary, with refrigerant dominant pressure losses (K<0.4), it is slightly better to employ

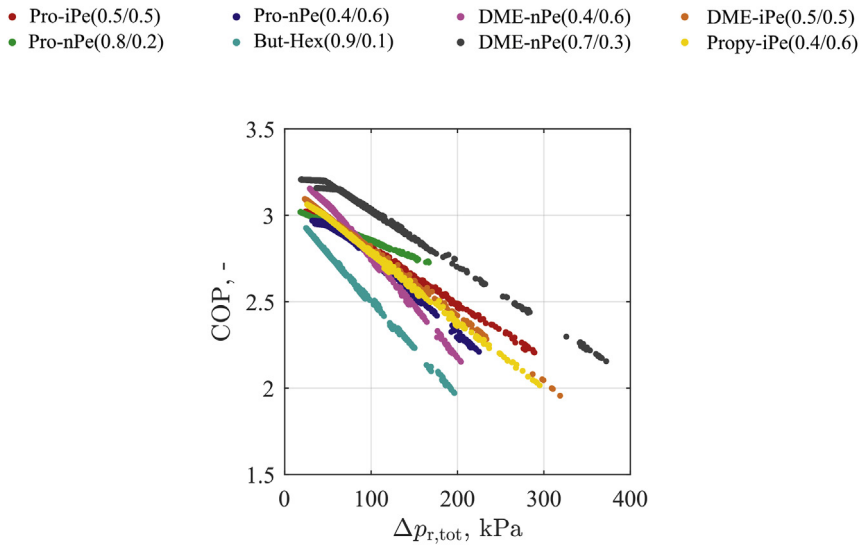

Fig. 7. COP as function of the total refrigerant pressure drops for all the working fluids.

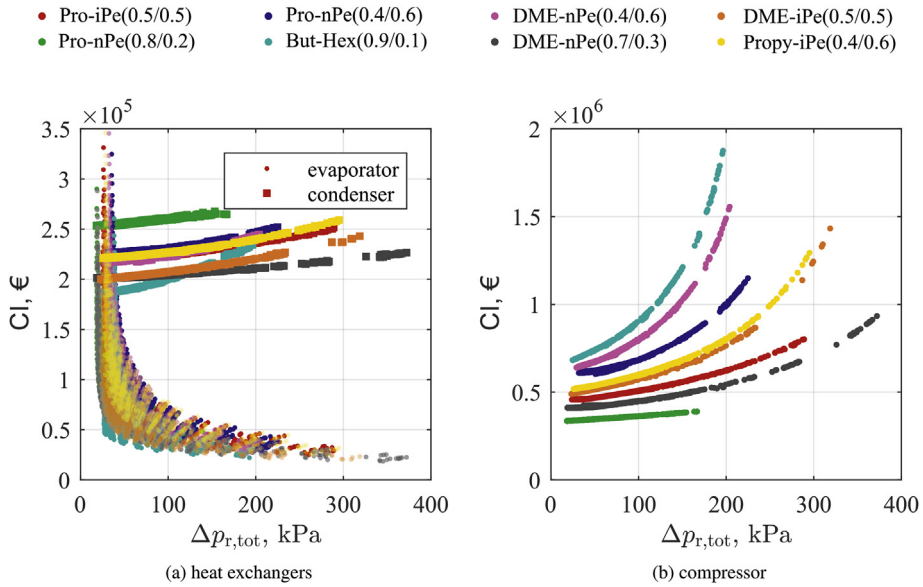

(a) heat exchangers (b) compressor

Fig. 8. Capital investment of the heat exchangers (a) and compressor (b), as function of the total refrigerant pressure drops for all the working fluids.

higher chevron angles for reaching less turbulent flow, thereby decreasing the pressure losses. It is therefore unnecessary to include the chevron angle into the design guideline, since it is possible to tune the other PHE design parameters in order to be in the optimal design region, where it is recommended to employ low values of β.

3.4. Correlation between NPV and selected dimensionless numbers

The results are presented as function of the three remaining dimensionless numbers, namely the Bond number Bd, the Weber number We_m and the Reynolds number of the vapour flowing alone Re_V. Table 6 shows the coefficients obtained by fitting the normalized net present values with different combinations of the three dimensionless parameters. Four different cases were assessed by combining the three parameters all at once and by considering combinations of only two of them. The aim was to find which correlation attained the best representation of NPV^*, thereby being appropriate for deriving the design guideline. The values reported in the first row of the table (Case I), obtained by considering all the three non-dimensional numbers, suggest that there is not a predominant contribution of one of them, since the coefficients lie in a similar range.

Fig. 10 shows the NPV^* as a function of the different exponential combinations of dimensionless numbers, with the ordinate axis reporting the design points of all the working fluids. It can be observed that the normalized net present value presents a clear trend for all of the combinations. This is possibly related to the redundancy of information on geometry, fluid properties and boundary conditions contained in the three parameters.

By looking at the formulas reported in Table 4, We_m and Re_V are dependent on the hydraulic diameter D_h and on the free flow area A_0, while the Bond number Bd solely depends on D_h. Any combinations of the parameters therefore contain all the information regarding the PHE geometry, i.e. the corrugation geometry, plate width and number of channel, with the exception of plate length

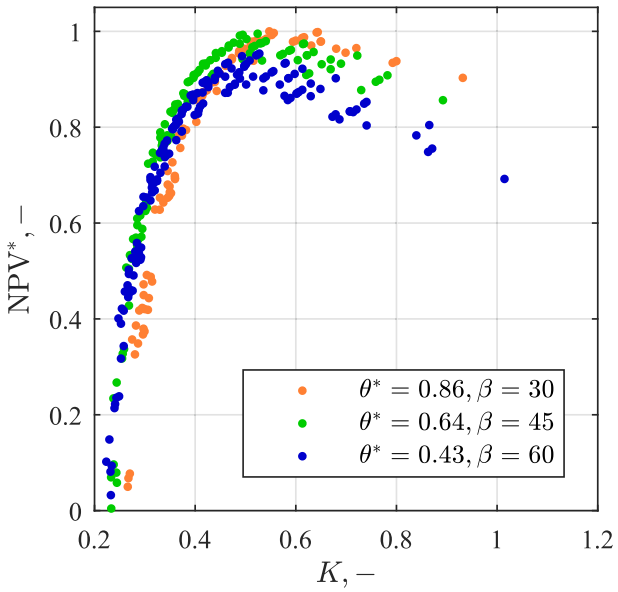

Fig. 9. Normalized NPV as function of all the dimensionless parameters correlated exponentially for Propane/Iso-Pentane (0.5/0.5). The different colors represent the different chevron angles adopted. (For interpretation of the references to color in this figure legend, the reader is referred to the Web version of this article.)

Table 6
Coefficients obtained by fitting the NPV* to different combinations of dimensionless parameters.

Case	Parameters combination	a	b	c
Case I	$Re_V^a \cdot Bd^b \cdot We_m^c$	1.21	−0.19	−0.87
Case II	$Bd^b \cdot We_m^c$	0.14	−0.25	
Case III	$Re_V^a \cdot We_m^c$	0.74	–	−0.62
Case IV	$Re_V^a \cdot Bd^b$	−0.42	0.26	–

(estimated by the PHE sizing for matching the thermal load and thus not needed to be included in the guideline) and chevron angle, excluded from the guideline.

Moreover, by looking at the fluid properties of the three non-dimensional numbers, it can be seen that surface tension σ and the liquid and vapour phase densities ρ_L and ρ_V are contained in any of considered combinations, together with the inlet vapour quality x and mass flow m_r.

In order to choose which combination of parameters to consider for the final design guideline, the position of the optimal values of the different coefficients was compared for the different working fluids. The aim was to understand which design guideline resulted in a recommendation which was narrower to describe the optimal NPV* for all the working fluids.

Table 7 reports the minimum, maximum and mean values of the different cases for the best solutions, which were selected as NPV* deviating at most 5% from each best solution. The results are reported for all the working fluids, as well as the overall maximum, minimum and mean value. The deviation (last row) was estimated by considering how far the minimum and maximum value were from the overall mean.

The results suggest that the best agreement between the different mixtures is obtained by the combination of Re_V and Bd, whose deviations are −34% and 48% for the minimum and maximum value, respectively. The interval covered by Butane/Hexane (0.9/0.1) is shifted towards the left compared to the other working fluids.

Fig. 11 shows the positive solutions of NPV for all the working fluids as function of the obtained parameter $Re_V^{-0.42}Bd^{0.26}$. The red line represents the mean value, equal to 0.040, while the dotted black lines represent the minimum (0.026) and maximum value (0.059). The plots show that all the fluids, except Butane/Hexane (0.91/0.1), present a good agreement with the obtained guideline: the optimal NPV points are all included in the interval [0.040–0.059], with the peak lying around 0.040 for almost all the fluids. DME/n-Pentane (0.4/0.6) and DME/Iso-Pentane (0.5/0.5) have the maximum slightly shifted towards 0.050. They perform however with NPV* very close to the optimum for 0.040 (equal or above 80% of the optimal value). Propane/n-Pentane (0.4/0.6) shows solutions with NPV* going down to −30% for the optimal value for 0.040. The worst performing points are probably related to higher values of chevron angle (see Fig. 9), thus optimal designs can be achieved as well with the proposed guideline. In agreement with the numbers reported in Table 7, Butane/Hexane (0.91/0.1) is slightly shifted towards the left compared to the other fluids, i.e. with optimal points in the interval [0.026–0.040]. Nonetheless it has been decided not to shift the design interval towards values optimal for this fluid, since it was shown that this mixture performed with generally lower NPV in the mapping compared to all the other fluids (see Fig. 6).

After the assessment of the results from Table 7 and Fig. 11, it was decided to propose the guideline presented by Eq. (21) as design recommendation.

$$Re_V^{-0.42}Bd^{0.26} \approx 0.040 \tag{21}$$

If a higher value is obtained, the PHE design is expected to lead to higher equipment investment (related to the heat transfer area), while a lower value will lead to high refrigerant pressure drop, resulting in a steep decrease of both COP and NPV.

4. Discussion

Section 4.1 presents the discussion of an application of the derived guideline, Section 4.2 reports the results of the uncertainty analysis while Section 4.3 briefly comments on the deviation of the obtained guideline if an alternative prediction method is used for the refrigerant pressure drop estimation, which resulted to have the largest impact on the heat pump economic performance. Section 4.4 highlights the limitation of the study and potential future work.

4.1. Application of the derived design recommendation

The case of the first working fluid mixture was considered, namely Propane/Iso-Pentane (0.5/0.5). The design, based on the derived guideline consists of the following steps:

1. Fix the boundary conditions of the thermodynamic cycle and estimate the inlet condition at the evaporator (quality, mass flow, evaporation pressure).
2. Calculate the following fluid properties at the inlet condition: ρ_L, ρ_V, σ, μ_V.
3. Choose a value for the chevron angle β. It is recommended to employ low values (e.g. 30–35°), if the design parameter is not constrained.
4. Decide which design parameters are fixed by external boundaries (fixed plate size and/or numbers and/or corrugation geometry).
5. Tune the remaining free design parameters in order to obtain $Re_V^{-0.42}Bd^{0.26} \approx 0.040$. Calculate the required plate length by using the evaporator heat flow rate, fixed by the cycle.

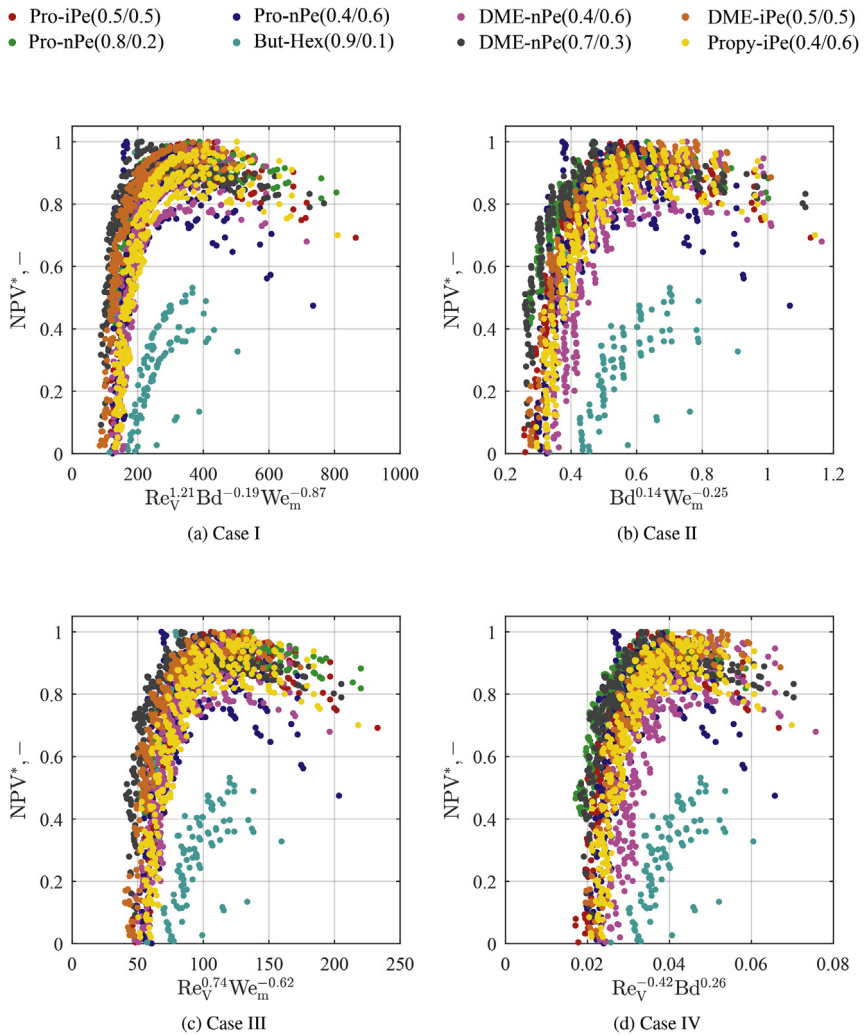

Fig. 10. Normalized NPV as function of different combinations of non-dimensional numbers for all the working fluids reported in Table 6; (a) Case I; (b) Case II; (c) Case III; (d) Case IV.

Table 7
Minimum, maximum and average values of different combinations of dimensionless numbers for the best results (5 % NPV*), for each working fluid and overall. Bold values represent the results for the dimensionless number combination chosen as guideline.

Working fluid	Case I			Case II			Case III			Case IV		
	$Re_V^{1.21} \cdot Bd^{-0.19} \cdot We_m^{-0.87}$			$Bd^{0.14} \cdot We_m^{-0.25}$			$Re_V^{0.74} \cdot We_m^{-0.62}$			$Re_V^{-0.42} \cdot Bd^{0.26}$		
	min	max	mean	min	max	mean	min	max	mean	min	max	mean
Propane/Iso-Pentane (0.5/0.5)	2110	3310	2620	0.48	0.75	0.59	91.4	152	118	0.030	0.047	0.038
Propane/n-Pentane (0.8/0.2)	2240	3800	2900	0.48	0.77	0.60	104	166	128	0.031	0.046	0.037
Propane/n-Pentane (0.4/0.6)	1420	2780	2130	0.37	0.70	0.54	68	129	99	0.026	0.045	0.036
Butane/Hexane (0.9/0.1)	1560	1570	1560	0.47	0.47	0.47	78.9	80.9	79.8	0.034	0.034	0.034
DME/n-Pentane (0.4/0.6)	2150	2800	2380	0.65	0.86	0.72	103	144	118	0.044	0.058	0.049
DME/n-Pentane (0.7/0.3)	1640	2430	1930	0.46	0.67	0.53	81.3	121	96	0.032	0.045	0.037
DME/Iso-Pentane (0.5/0.5)	1810	2920	2190	0.55	0.88	0.66	88	151	111	0.038	0.059	0.046
Propylene/Iso-Pentane (0.4/0.6)	2100	3330	2670	0.52	0.84	0.67	93	160	124	0.034	0.054	0.043
Overall	1420	3800	2300	0.37	0.88	0.60	68	166	109	0.026	0.059	0.040
Deviation in %	−38%	65%		−38%	46%		−38%	−52%		**−34%**	**−48%**	

Table 8 shows different combinations of geometrical parameters, each line corresponding to a different PHE design. Some geometrical parameters were fixed a priori, while other were calculated by means of the design guideline using the methodology presented above. The goal of fixing and releasing different geometrical parameters was to show the different possible scenarios of a designer, which might be constrained in some of the design variables. The plate length was estimated by the sizing

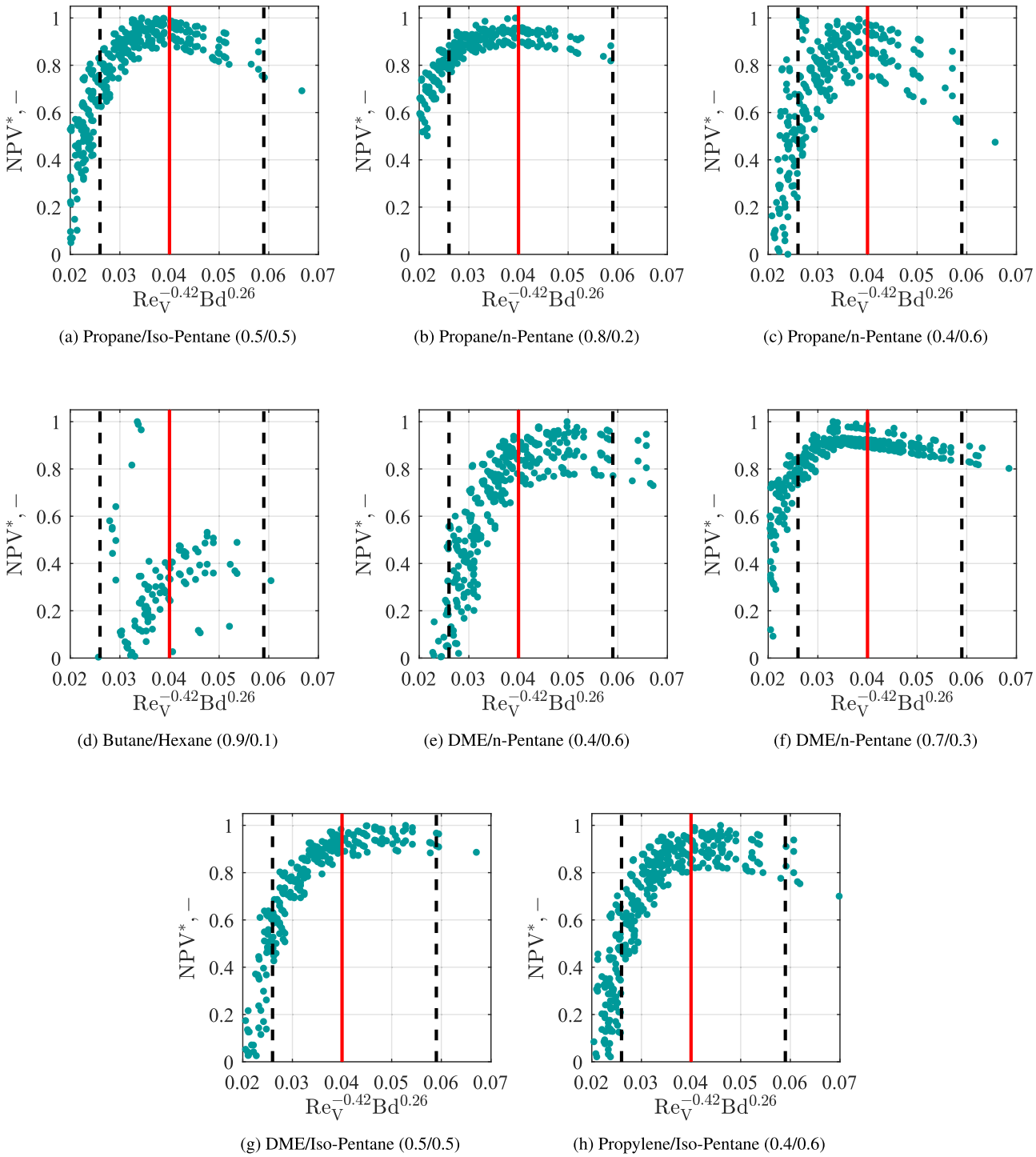

(a) Propane/Iso-Pentane (0.5/0.5)

(b) Propane/n-Pentane (0.8/0.2)

(c) Propane/n-Pentane (0.4/0.6)

(d) Butane/Hexane (0.9/0.1)

(e) DME/n-Pentane (0.4/0.6)

(f) DME/n-Pentane (0.7/0.3)

(g) DME/Iso-Pentane (0.5/0.5)

(h) Propylene/Iso-Pentane (0.4/0.6)

Fig. 11. Normalized NPV as function of $Re_V^{-0.42}Bd^{0.26}$ for all the working fluids. The red line represents the mean value $Re_V^{-0.42}Bd^{0.26} = 0.04$, while the dotted lines represent max and min, 0.059 and 0.026 respectively. (For interpretation of the references to color in this figure legend, the reader is referred to the Web version of this article.)

model, matching the case study thermal load.

In the first three rows of the table, the corrugation geometry, namely pitch Λ and height b, were fixed together with the corrugation angle. The number of channels N_{ch} and plate width W were found in order to obtain values of $Re_V^{-0.42}Bd^{0.26}$ equal to 0.040. It can be noticed that by respecting the proposed design guideline, the NPV deviates maximum −4.4% from the best value of the parametric analysis. The COP in the third design point is slightly lower due the higher pressure drops of the refrigerant.

The forth and fifth rows of Table 8 report two PHE design which were obtained by fixing the plate width and the number of plates, as well as the chevron angle. The corrugation geometry was found in order to match the design guideline and it was found that also in this case the two solutions deviate of only −1.9% and −1.5% from

Table 8
Some examples of PHE design points for the mixture Propane/Iso-Pentane (0.5/0.5).

Design	W [m]	N_{ch} [−]	β [°]	b [m]	Λ [m]	L_{HT} [m]	A_{ht} [m]2	Δp_{r-tot} [kPa]	NPV [€]	ΔNPV [%]	COP [−]	$Re_V^{-0.42}Bd^{0.26}$ [−]
	Free variables		Fixed geometry									
I	0.20	188	45	0.005	0.007	0.66	92.0	31.0	696,960	−3.6	3.02	0.040
II	0.19	196	35	0.005	0.007	0.57	80.1	31.3	711,620	−1.5	3.02	0.040
III	0.44	59	35	0.007	0.007	0.65	80.7	36.0	690,990	−4.4	3.01	0.040
	Fixed geometry		Free variables									
IV	0.20	100	35	0.009	0.008	0.77	82.1	32.6	708,580	−1.9	3.02	0.040
V	0.18	150	35	0.007	0.006	0.54	79.8	31.0	712,180	−1.5	3.02	0.040

the best NPV, thereby lying in an optimal region for the PHE design. It can be noticed that all the five solutions proposed have the same magnitude of refrigerant pressure drops, ranging from 30 kPa to 35 kPa. This is the same range shown in Fig. 6(a) for the same working fluid.

4.2. Uncertainty analysis

The uncertainty analysis of the values of heat transfer coefficients and pressure drops was carried out for the design I reported in Table 8 for Propane/Iso-Pentane (0.5/0.5), performing with a NPV −3.6% lower than the best solution found in the mapping. The mean values, standard deviation and 95% coverage interval are reported in Table 9. The input uncertainties assigned to the heat transfer and pressure drop correlations resulted in a standard deviation of 10.6% and 5.0% for heat transfer area and refrigerant pressure drops, respectively. However, the overall impact on the heat pump NPV resulted to be only equal to a 1.8% standard deviation. This was also translated to 95% of all the solutions deviating maximum 3.5% from the mean. Moreover, it can be observed that the PHE design I obtained in Table 8 deviated only 0.3% compared to the mean value estimated performing 500 simulations from the uncertainty input space. The heat source pressure drop is not reported, since the results showed a negligible impact on the NPV.

It must be stressed again that the input uncertainties were taken from the reference papers for the experimental correlations, and they were estimated by the authors as accuracy referred to experimental database not containing the present working fluids and operating conditions. This analysis ensures however that, despite large deviations assigned to the heat transfer and pressure drop calculations, such as the wide interval of [−50%, +100%] given as input for the estimation of f_V in Table 5, a much smaller impact was obtained on the NPV estimation, equal to only 1.8% standard deviation.

It is nevertheless relevant to focus future work on validating the use of the chosen prediction methods for similar case studies by conducting experiments for flow boiling of zeotropic mixtures in PHEs. Moreover, despite the small uncertainties obtained on the NPV for PHE design I, the input uncertainties might lead to exclude some of the optimal solutions due to possible underestimations of the NPV.

Table 9
MC uncertainty analysis results for PHE design I for Propane/Iso-Pentane (0.5/0.5) performed with a sample population of 500 elements.

	A_{ht}	$\Delta p_{r,tot}$	NPV
Mean value	93.2 m^2	33.2 kPa	694,780 €
Absolute standard deviation	9.9 m^2	1.7 kPa	12,370 €
Percentage standard deviation	10.6%	5.0%	1.8%
95% coverage interval	20.7%	9.8%	3.5%
Design I	92.0 m^2	31.0 kPa	696,960 €
Deviation from the mean	−1.3%	−6.8%	+0.3%

4.3. Sensitivity to pressure drop correlation

From the analysis of the results, the refrigerant pressure drop was found to have the largest impact on the NPV. Therefore, it was decided to carry out a sensitivity analysis on the prediction method chosen to evaluate the two-phase frictional contribution, constituting the major contribution to the refrigerant total pressure loss. The same parametric study was carried out, i.e. considering the same design points, yet by employing an alternative prediction method.

The Lockhart-Martinelli [45] method was applied, for which the Martinelli parameter was estimated from the ratio of the singe-phase vapour and liquid pressure drops. The Martin correlation [36] was used in order to estimate the single-phase contributions, and the two-phase multiplier was calculated by using the fitting to the Martinelli's parameter developed by Chisholm [46] with a multiplication coefficient C=4.67, as proposed by Palm and Claesson [47].

By using the same fitting coefficients obtained using the previous data set, i.e. −0.42 and 0.26 for Re_V and Bd respectively, the mean value was calculated for the best results, namely PHE designs based on the best 5% NPV. A good agreement was obtained between the two different data sets, since the mean value of the guideline $Re_V^{-0.42}Bd^{0.26}$ was found equal to 0.044, thereby being +9.5% higher than the base case.

4.4. Limitations and future work

The methodology presented in this work is based on a number of boundary conditions and assumptions. First and foremost, the methodology is based on numerical calculations and has not been documented experimentally. The study has only been applied to a limited number of cases. The work should be seen as a suggestion and exemplification of a method, rather than a complete guideline. The methodology was indeed derived for eight different working fluids integrated in the same heat pump, with fixed heat source temperature glide of 25 °C. The influence of having different glides along the evaporator might be investigated as part of future work.

The economic analysis showed that the refrigerant total pressure drops have a major impact on the NPV of the heat pump. In order to estimate the NPV, a number of economic boundaries were assumed, and the price of electricity and natural gas were based on the data available for the Danish energy sector. Furthermore, the case study was based on a waste heat recovery application, where the heat source comes at zero cost. The COP decrease, entailing a higher compressor running cost, could be partially balanced by a reduced utilization of the heat source. The economic boundaries are therefore dependent on the specific case study, and the application of the presented methodology should be adapted to the

specific boundary conditions.

Last, it is worth it mentioning two limitations imposed by the PHE sizing model. Flow maldistributions are not taken into consideration, neither along the plate width nor among the different HEX channels. This aspect might lead to different results concerning some design variables, e.g. plate length-to-width ratio, since it does not take into account that the flow might not be perfectly counter-current if low values of such ratio are employed. In order to avoid unrealistic results, a minimum ratio was assumed in the present analysis.

5. Conclusions

This paper presented a methodology to derive design guidelines for plate heat exchangers. The methodology was demonstrated by applying it to a case study of plate heat exchanger evaporators in heat pumps using zeotropic mixtures. The basis for the derivation was a numerical model used for simultaneous sizing of the thermodynamic cycle and of the heat exchanger, with heat transfer area and pressure drops being considered for both the calculation of the cycle COP and NPV.

The analysis showed that there is an economic trade-off between heat transfer area and refrigerant pressure drop, with the latter having a larger impact on the results. Higher refrigerant pressure drops resulted in a COP degradation, subsequent increase of the compressor running costs, as well as higher investment required for the compressor. Different working fluids presented different sensitivity to pressure drops, thus the trade-off could not be uniquely defined in terms of a maximum allowable pressure drop.

The results were therefore assessed with the aim of deriving a general design guideline, applicable for all the fluids. Different non-dimensional parameters were correlated to the normalized net present value, and it was shown that Re_V, Bd and We_m are the parameters mostly influencing the results. Moreover, an optimal value was identified for the dimensionless factor $Re_V^{-0.42}Bd^{0.26}$ for the best solutions in terms of NPV, deviating no more than 5% from the highest NPV. It was shown that for most of the mixtures values above 80% of the best NPV were found for $Re_V^{-0.42}Bd^{0.26} \approx 0.040$.

Butane/Hexane (0.9/0.1) presented non-favourable design points, with an optimal region shifted towards the left of the obtained guideline. Moreover, Propane/n-Pentane at (0.4/0.6) reported values of NPV above 70% of the best solution for the suggested guideline, performing slightly worse than the other working fluids for some of the designs. This was related to the effect of the chevron angle, and it was therefore recommended to employ low values of β in the optimal region.

The design steps, based on applying the aforementioned guideline, were summarized and applied to the case of for the Propane/Iso-Pentane (0.5/0.5). It was illustrated that different configurations respecting $Re_V^{-0.42}Bd^{0.26} \approx 0.040$ yielded close to optimal NPVs. These were obtaining by tuning differently plate corrugation geometry, size and number of plates.

Moreover, an uncertainty analysis of the heat transfer coefficients and pressure drops estimated by experimental correlations was carried out for one of the optimal designs of Propane/Iso-Pentane (0.5/0.5), using the MC method on a population sample of 500 elements obtained using LHS. The NPV mean value was found to be 0.3% higher than the design point, with a standard deviation of 1.8%.

The presented methodology offers the possibility of deriving guidelines for different applications, where HEXs are integrated in a thermodynamic cycle and different working fluids are compared, avoiding computationally expensive combined cycle and component optimization to obtain feasible designs.

Acknowledgments

The research work was conducted within the frame of the THERMCYC project (Advanced thermodynamic cycles utilizing low temperature heat sources) funded by Innovations Fund Denmark: The Danish Council for Strategic Research in Sustainable Energy and Environment. The support is gratefully acknowledged.

Nomenclature

A_0	free flow area [m^2]
D_h	hydraulic diameter [m]
D_p	port diameter [m]
G	mass flux [kg/(s m^2)]
L	plate length [m]
N_{ch}	number of channels [−]
T	temperature [°C]
U	overall heat transfer coefficient [W/(m^2 K)]
W	plate width [m]
$\bar{z}$	Silver and Bell-Ghaly correction [−]
$\dot{Q}$	heat load [W]
$\dot{W}$	work [W]
$\dot{m}$	mass flow [kg/s]
b	corrugation height [m]
c_{el}	specific cost of electricity [€/kWh]
f	Fanning friction factor [−]
g	gravitational acceleration [m/s^2]
h	heat transfer coefficient [W/(m^2 K)]
n	number of control volumes [−]
p	pressure [Pa]
t	plate thickness [m]
x	vapour quality [−]
Bd	Bond number [−]
COP	coefficient of performance [−]
CRF	capital recovery factor [1/a]
FC	fuel cost [€/a]
NPV	net present value [€]
OMC	operation and maintenance cost [€]
PEC	purchased equipment cost [€]
Re	Reynolds number [−]
TCI	total capital investment [€]
We	Weber number [−]

Abbreviations and acronyms

CI	capital investment
CV	control volume
HEX	heat exchanger
LHS	latin hypercube sampling
MC	Monte Carlo
PHE	plate heat exchanger

Greek letters

β	chevron angle [°]
Δ	difference [−]
η	efficiency [−]
Λ	corrugation thickness [m]
μ	viscosity [Pa s]
Φ	enlargement factor [−]
ρ	density [kg/m^3]
σ	surface tension [N/m]
τ	time [h]
θ	inclination angle ($90-\beta$) [°]

Superscripts

"	per unit area
*	normalized
i	control volume i
j	solver iteration j

Subscripts

acc	acceleration
C	convective
comp	compressor
ev	evaporation
fr	friction
gr	gravity
hp	heat pump
ht, HT	heat transfer
id	ideal
id	mixture
in	inlet
is	isentropic
L	liquid
lat	latent
LO	liquid only
m	mean
NB	nucleate boiling
ng	natural gas
out	outlet
p	port-to-port
r	refrigerant
s	heat source
sh	super-heating
tot	total
TP	two-phase
V	vapour
w	water
wf	working fluid

References

[1] Zühlsdorf B, Bühler F, Mancini R, Cignitti S, Elmegaard B. High temperature heat pump integration using zeotropic working fluids for spray drying facilities. In: Proceedings of the 12th IEA heat pump conference, Rotterdam; 2017.

[2] Zühlsdorf B, Kjaer Jensen J, Cignitti S, Madsen C, Elmegaard B. Analysis of temperature glide matching of heat pumps with zeotropic working fluid mixtures for different temperature glides. Energy 2018;153:650–60. https://doi.org/10.1016/j.energy.2018.04.048.

[3] Zühlsdorf B, Meesenburg W, Ommen T, Thorsen J, Brix Markussen W, Elmegaard B. Improving the performance of booster heat pumps using zeotropic mixtures. Energy 2018;154:390–402. https://doi.org/10.1016/j.energy.2018.04.137.

[4] Collier JG, Thome J. Convective boiling and condensation. 1994. https://doi.org/10.1016/0923-0467(95)80021-2. arXiv:arXiv:1011.1669v3.

[5] Radermacher R, Hwang Y. Heat transfer of refrigerant mixturers. In: Vapor compression heat pumps with refrigerant mixtures. CRC Press; 2005. p. 237–78. https://doi.org/10.1201/9781420037579.ch8. 2005, Ch. 8.

[6] Ross H, Radermacher R, di Marzo M, Didion D. Horizontal flow boiling of pure and mixed refrigerants. Int J Heat Mass Tran 1987;30:979–92. https://doi.org/10.1016/0017-9310(87)90016-0.

[7] Wattelet P, Chato C, Souza AL, Christofferson B. Initial evaporative comparison of R-22 with alternative refrigerants R-134a and R-32/R-125. Tech. rep. University of Illinois; 1993.

[8] Jung D, McLinden M, Radermacher R, Didion D. A study of flow boiling heat transfer with refrigerant mixtures. Int J Heat Mass Tran 1989a;32:1751–64. https://doi.org/10.1016/0017-9310(89)90057-4.

[9] Jung DS, McLinden M, Radermacher R, Didion D. Horizontal flow boiling heat transfer experiments with a mixture of R22/R114. Int J Heat Mass Tran 1989b;32(1):131–45. https://doi.org/10.1016/0017-9310(89)90097-5.

[10] Torikoshi K, Ebisu T. Heat transfer and pressure drop of R134a R32 and a mixture of R32 R134a. ASHRAE Trans 1993;99(2):90–3.

[11] Shah RK, Sekulic DP. Fundamentals of heat exchanger design. 2002. https://doi.org/10.1002/9780470172605.

[12] VDI-Gesellschaft, VDI heat Atlas, vol. 1; 2015. https://doi.org/10.1007/978-3-540-77877-6.

[13] Gut JAW, Pinto JM. Optimal configuration design for plate heat exchangers. Int J Heat Mass Tran 2004;47(22):4833–48. https://doi.org/10.1016/j.ijheatmasstransfer.2004.06.002.

[14] Jegede F, Polley G. Optimum heat exchanger design. Chem Eng Res Des 1992;70(A2):133–41.

[15] Unuvar A, Kargici S. An approach for the optimum design of heat exchangers. Int J Energy Res 2004;28(15):1379–92. https://doi.org/10.1002/er.1080.

[16] Muralikrishna K, Shenoy U. Heat exchanger design targets for minimum area and cost. Chem Eng Res Des 2000;78(2):161–7. https://doi.org/10.1205/026387600527185.

[17] Jarzebeski E, Wardas-Koziel E. Dimensioning plate heat exchangers giving minimum annual operating costs. Chem Eng Res Des 1985;63(4):211–8.

[18] Wang L, Sundén B. Optimal design of plate heat exchangers with and without pressure drop specifications. Appl Therm Eng 2003;23(3):295–311. https://doi.org/10.1016/S1359-4311(02)00195-3.

[19] Karellas S, Schuster A, Leontaritis A-D. Influence of supercritical ORC parameters on plate heat exchanger design. Appl Therm Eng 2012;33–34:70–6. https://doi.org/10.1016/j.applthermaleng.2011.09.013.

[20] Rohmah N, Pikra G, Purwanto AJ, Pramana RI. The effect of plate spacing in plate heat exchanger design as a condenser in organic rankine cycle for low temperature heat source. Energy Procedia 2015;68:87–96. https://doi.org/10.1016/j.egypro.2015.03.236.

[21] Walraven D, Laenen B, D'Haeseleer W. Comparison of shell-and-tube with plate heat exchangers for the use in low-temperature organic Rankine cycles. Energy Convers Manag 2014;87:227–37. https://doi.org/10.1016/j.enconman.2014.07.019.

[22] Imran M, Usman M, Park B-S, Kim H-J, Lee D-H. Multi-objective optimization of evaporator of organic Rankine cycle (ORC) for low temperature geothermal heat source. Appl Therm Eng 2015;80:1–9. https://doi.org/10.1016/j.applthermaleng.2015.01.034.

[23] Xu J, Luo X, Chen Y, Mo S. Multi-criteria design optimization and screening of heat exchangers for a subcritical ORC. Energy Procedia 2015;75:1639–45. https://doi.org/10.1016/j.egypro.2015.07.397.

[24] Mathworks, Matlab R. 2017. https://www.mathworks.com/help/matlab/.

[25] Jensen JK, Kaern MR, Ommen TS, Brix W, Reinholdt L, Elmeegard B. Effect of liquid/vapour maldistribution on the performance of plate heat exchanger evaporators. In: Proceedings of the 24th IIR international congress of Refrigeration; 2015.

[26] Ommen T, Jensen JK, Markussen WB, Reinholdt L, Elmegaard B. Technical and economic working domains of industrial heat pumps: Part 1-Single stage vapour compression heat pumps. Int J Refrig 2015;55:168–82. https://doi.org/10.1016/j.ijrefrig.2015.02.011.

[27] Lemmon E, Huber M, McLinden M. IST standard reference database 23: reference fluid thermodynamic and transport properties-REFPROP. 2013., Version 9.1. .

[28] Bell IH, Wronski J, Quoilin S, Lemort V. Pure and pseudo-pure fluid thermophysical property evaluation and the open-source thermophysical property library coolprop. Ind Eng Chem Res 2014;53(6):2498–508. https://doi.org/10.1021/ie4033999. arXiv:http://pubs.acs.org/doi/pdf/10.1021/ie4033999.

[29] Amalfi RL, Vakili-Farahani F, Thome JR. Flow boiling and frictional pressure gradients in plate heat exchangers. Part 2 : comparison of literature methods to database and new prediction methods. Int J Refrig 2016;61:185–203. https://doi.org/10.1016/j.ijrefrig.2015.07.009.

[30] Kærn M, Modi A, Jensen J, Andreasen J, Haglind F. An assessment of in-tube flow boiling correlations for ammonia-water mixtures and their influence on heat exchanger size. Appl Therm Eng 2015;93:623–38. https://doi.org/10.1016/j.applthermaleng.2015.09.106.

[31] Silver L. Gas cooling with aqueous condensation. Ind Chem Chem Manuf 1947;23(269):380–6.

[32] Bell K, Ghaly M. An approximate generalized design method for multicomponent/partial condenser. AICHE Symp Ser 1973;69:72–9.

[33] Sardesai RG, Shock RA, Butterworth D. Heat and mass transfer in multicomponent condensation and boiling. Heat Tran Eng 1982;3(3–4):104–14. https://doi.org/10.1080/01457638108939589.

[34] Thome J, Shakir S. A new correlation for nucleate pool boiling of aqueous mixtures. AICHE Symp Ser 1987;83(257):46–51.

[35] Cooper M. Heat flow rates in saturated nucleate pool boiling - a wide ranging examination using reduced properties. Adv Heat Tran 1984;16:59–156.

[36] Martin H. A theoretical approach to predict the performance of chevron-type plate heat exchangers. Chem Eng Process 1996;35(4):301–10. https://doi.org/10.1016/0255-2701(95)04129-X.

[37] Vakili-Farahani F, Amalfi RL, Thome JR. Two-phase heat transfer and pressure drop within plate heat exchangers. In: Thome JR, Kim J, editors. Encyclopedia of two-phase heat transfer and flow II : special topics and applications. Volume 2: boiling using enhanced surfaces, plate heat exchangers and two-phase devices. Chapter 4. World Scientific Publishing; 2015. p. 145–215. https://doi.org/10.1142/9789814623285_0011. Ch. Chapter 4.

[38] Shah R, Focke W. Plate heat exchangers and their design theory. In: Shah R, Subbarao E, Mashelkar R, editors. Heat transfer equipment design. Washington DC: Hemisphere Publishing; 1988. p. 227–54.

[39] Bejan A, Tsatsaronis G, Moran M. Thermal design and optimization. John Wiley and Sons, Inc; 1996. https://doi.org/10.1016/S0140-7007(97)87632-3.

[40] Danish Energy Agency. Data, tables, statistics and maps, energy in Denmark. 2015.

[41] Thome JR. Prediction of the mixture effect on boiling in vertical thermysyphon reboilers. Heat Tran Eng 1989;10(2):29–38. https://doi.org/10.1080/

01457638908939696.
[42] Metropolis N, Ulam S. The Monte Carlo method. J Am Stat Assoc 1949;44(247):335–41.
[43] Helton JC, Davis FJ. Latin hypercube sampling and the propagation of uncertainty in analyses of complex systems. Reliab Eng Syst Saf 2003;81(1):23–69. https://doi.org/10.1016/S0951-8320(03)00058-9. arXiv:0511236.
[44] Sin G, Gernaey KV. Data handling and parameter estimation. In: Mark DB, van Loosdrecht CM, Nielsen PH, Lopez-Vazquez CM, editors. Experimental methods in wastewater treatment. London, UK: iwa publis Edition; 2016. p. 201–34.
[45] Lockhart R, Martinelli R. Proposed correlation of data for isothermal two-phase, two-component flow in pipes. Chem Eng Prog 1949;45(1):39–48.
[46] Chisholm D. A theoretical basis for the Lockhart-Martinelli correlation for two-phase flow. Int J Heat Mass Trans 1967;10(18):1767–78. https://doi.org/10.1016/0017-9310(67)90047-6.
[47] Palm B, Claesson J. Plate heat exchangers: calculation methods for single and two-phase flow. Heat Tran Eng 2006;27(4):88–98. https://doi.org/10.1080/01457630500523949.

International Journal of Refrigeration 104 (2019) 390–403

Contents lists available at ScienceDirect

International Journal of Refrigeration

journal homepage: www.elsevier.com/locate/ijrefrig

Performance of heat pumps using pure and mixed refrigerants with maldistribution effects in plate heat exchanger evaporators

Roberta Mancini[a,*], Benjamin Zühlsdorf[a], Vikrant Aute[b], Wiebke Brix Markussen[a], Brian Elmegaard[a]

[a] Department of Mechanical Engineering, Technical University of Denmark, Nils Koppels Allé, Building 403, Kongens Lyngby, 2800, Denmark
[b] Department of Mechanical Engineering, University of Maryland, 4164 Glenn L. Martin Hall, College Park, MD 20742, United States

ARTICLE INFO

Article history:
Received 11 January 2019
Revised 8 May 2019
Accepted 16 May 2019
Available online 21 May 2019

Keywords:
Plate heat exchanger
Liquid-vapour maldistribution
End plates
Pressure drop
Zeotropic mixtures
Economic analysis

ABSTRACT

This paper presents a combined plate heat exchanger (PHE) - heat pump simulation framework for the evaluation of flow maldistribution in PHE evaporators and its effect on the cycle thermodynamic and economic performance. A case study of heat pump integration for waste heat recovery purposes in data centres was chosen to demonstrate the utilization of the simulation tool. The analyses were made for the pure fluids butane and propane, and for the zeotropic mixtures propylene/butane at (0.5,0.5) mass composition and CO_2/dimethyl ether (DME) (0.2,0.8) as refrigerants. Both liquid/vapour maldistribution and the effect of end plates were considered in the heat exchanger models. Results show that butane is most sensitive to maldistribution, with a maximum Coefficient of Performance (COP) reduction of 5.9%, while propane experiences the lowest reduction of 2.5%. The different sensitivity of the working fluids to maldistribution was found to be related to the evaporator design, refrigerant pressure drop, and fluid properties. Last, the results of the economic analysis show that a higher specific cost of heat is obtained when considering maldistribution effects.

© 2019 Elsevier Ltd and IIR. All rights reserved.

Performances des pompes à chaleur utilisant des frigorigènes purs et mélangés avec des effets de mauvaise distribution dans les évaporateurs des échangeurs de chaleur à plaques

Mots-clés: Échangeurs de chaleur à plaques; Mauvaise distribution de liquide-vapeur; Plaques d'extrémité; Chute de pression; Mélanges zéotropiques; Analyse économique

1. Introduction

Flow maldistribution implies a degradation in heat transfer performance for heat exchangers (HEXs) with multiple parallel channels. Mueller and Chiou (1988) published a work defining maldistribution within the context of HEX design, namely as non-uniform mass flow distribution entailing a degradation of heat transfer between the working fluids. Three main causes were identified, i.e. entry problems due to improper nozzle design, self-induced maldistribution by fluid flow characteristics, e.g. viscous or two-phase flow, and fouling and corrosion effects.

Plate heat exchangers (PHEs) are one kind of multi-channel HEX, which is used extensively in a number of sectors. By stacking thin corrugated plates together, co- or counter-current flow channels are formed, and high heat transfer coefficients are achieved in a compact design.

Maldistribution in PHEs can be related to three main effects: (i)uneven channel-to-channel mass flow rate distribution, (ii) uneven in-channel mass flow rate distribution, and (iii) effect of end plates, i.e. the different heat transfer area of the outer-most PHE channels causes a modification of the mass flow distribution.

Single-phase channel-to-channel maldistribution in PHEs has been described analytically (Bassiouny and Martin, 1984a; 1984b;

* Corresponding author.
E-mail addresses: robman@mek.dtu.dk (R. Mancini), bezuhls@mek.dtu.dk (B. Zühlsdorf), vikrant@umd.edu (V. Aute), wb@mek.dtu.dk (W.B. Markussen), be@mek.dtu.dk (B. Elmegaard).

https://doi.org/10.1016/j.ijrefrig.2019.05.023
0140-7007/© 2019 Elsevier Ltd and IIR. All rights reserved.

Nomenclature

1D	one dimensional
2D	two-dimensional
CV	control volume
DH	district heating
DME	dimethyl ether
HEX	heat exchanger
PHE	plate heat exchanger

Roman letters

A_{ht}	heat transfer area [m^2]
b	corrugation height [m]
CF	annual cash flow [€ y^{-1}]
COP	coefficient of performance [-]
CRF	capital recovery factor [y^{-1}]
C	yearly cost [€ y^{-1}]
c	specific cost/income [€ MWh^{-1}]
G	mass flux [kg s^{-1} m^{-2})]
i	interest rate [%]
k_{wall}	wall conductivity [W m^{-1} K^{-1}]
L_p	plate port-to-port length [m]
$\dot{m}$	mass flow rate [kg s^{-1}]
n	number of control volumes [-]
N_{ch}	number of channels [-]
n_{hp}	lifetime [y]
OH	operating hours [h y^{-1}]
p	pressure [bar]
$\dot{Q}$	heat flow rate [W]
TCI	total capital investment [€]
T	temperature [°C]
t	plate thickness[m]
$\dot{W}$	power [W]
W	plate width [m]
x	vapour quality [-]
$\dot{V}$	volumetric flow rate [m^3 h^{-1}]

Greek letters

α	void fraction [-]
β	chevron angle [°]
Δ	difference [-]
η	efficiency [-]
Λ	corrugation pitch [m]
ρ	density [kg m^{-3}]

Superscripts

i	index discretization along flow direction
j	index discretization number of channel

Subscripts

bubble	bubble
cond	condenser
design	design
dew	dew
eff	effective
el	electricity
eva	evaporator
gen	generation
h	heat
hg	heat generation
hs	heat source
HT	heat transfer
in	inlet
is	isentropic
min	minimum
out	outlet
Δp	pressure drop
pinch	pinch
ref	refrigerant
SH	superheat
sink	sink
tot	total
V	vapour

Srihari and Das, 2006; Srihari et al., 2005), numerically (Li and Hrnjak, 2016) and experimentally (Bobbili et al., 2006; Li and Hrnjak, 2018; Rao and Das, 2004; Rao et al., 2005; Tereda et al., 2007). A higher PHE performance degradation was found to occur for smaller manifold port diameters, higher mass flow rates and a higher number of channels. The effect of end plates in single-phase flow was studied by Jin and Hrnjak (2017b). They found that an overestimation of the overall heat transfer coefficient occurs by neglecting the effect of end plates, due to an underestimation of the effective heat transfer area. Li and Hrnjak (2018) developed a validated model for single-phase flow distribution in PHEs, showing that plates with higher length-to-width ratios are less affected by maldistribution.

Two-phase flow maldistribution in PHEs was addressed by a few studies. Jin and Hrnjak (2017a) investigated the in-channel distribution of R245fa experimentally. Large non-uniformities of the refrigerant mass flow rate were observed, with the occurrence of dry-out zones. Channel-to-channel flow maldistribution is particularly relevant for PHE evaporators in vapour compression systems. Since the refrigerant inlet is in two-phase, a non-uniform mass flow rate distribution entails uneven liquid/vapour distribution. Vist and Pettersen (2004) observed this phenomenon experimentally in a HEX manifold distributing saturated refrigerant mass flow into ten channels. They observed a monotonic decrease/increase of the inlet vapour phase with increasing distance from the inlet, for upward/downward flow, respectively. Madanan et al. (2018) investigated the two-phase flow distribution of an air/water mixture from a U-type manifold into six and eight parallel horizontal mini-channels. The vapour phase distribution resulted to be dependent on the flow regime. A monotonic decrease was observed in case of slug flow and six channels, while oscillations occurred for the experiments with eight channels and plug flow.

By taking the experimental results observed by Vist and Pettersen (2004) into account, Jensen et al. (2015) imposed different linear profiles of vapour quality at the PHE evaporator inlet by means of a numerical model with R134a used as a refrigerant and two different plate geometries. Mancini et al. (2018a) extended the work by comparing the degradation of heat transfer performance due to this kind of uneven liquid/vapour maldistribution for pure fluids and zeotropic mixtures. The use of a zeotropic mixture was demonstrated to increase the thermodynamic performance of heat pumps with respect to pure fluids by reducing the irreversibility in the HEXs (Zühlsdorf et al., 2019; 2018a; 2018b). Zühlsdorf et al. (2018a) further showed that the temperature glide match in the evaporator has a dominating effect compared to the condenser, which suggests that major attention should be given to the optimal design and operation of the evaporator.

Mancini et al. (2018a) showed that a mixture of propylene/butane at 0.5/0.5 mass composition is only slightly affected by maldistribution effects. The refrigerant temperature distribution in the different channels was shown to remain unchanged for different rates of liquid/vapour non-uniformity at the inlet, resulting in no changes for the temperature glide match. The pure fluid butane is on the other hand subject to a degradation in total heat transfer of up to 11.2%. The results were however limited to a particular

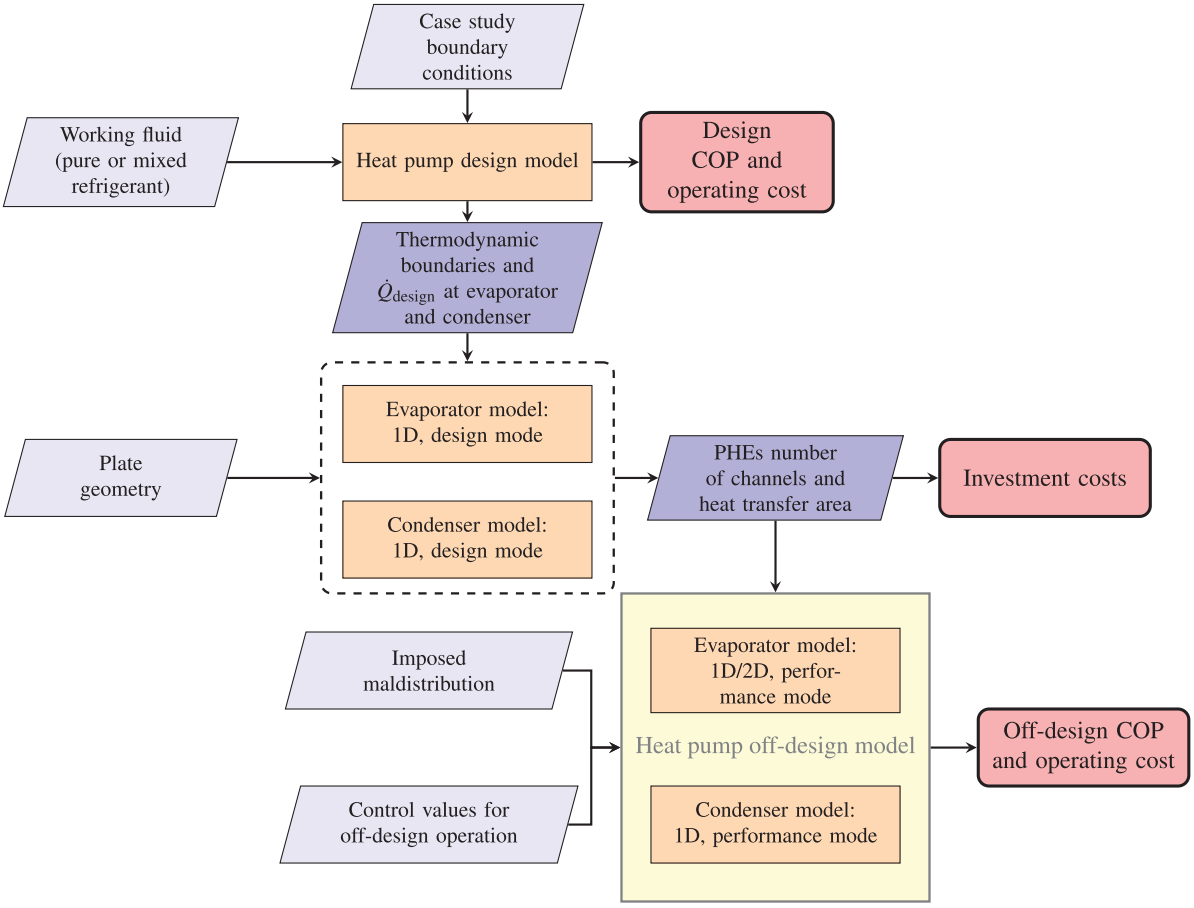

Fig. 1. Work-flow of the overall procedure.

case study (Zühlsdorf et al., 2018b), and the impact on the overall cycle performance was not estimated.

It is in fact of paramount importance to evaluate how the heat transfer degradation in evaporators affects the thermodynamic performance of the cycle. Previous works address the analysis of flow maldistribution effects in air conditioning systems (Kærn et al., 2011) and heat pumps (Gong et al., 2008; Mader et al., 2015) for fin-and-tube evaporators.

This paper presents a combined cycle and PHE simulation framework, which can be used in order to assess the impact on the Coefficient of Performance (COP) of heat pumps caused by end plates and liquid/vapour maldistribution at the inlet of PHE evaporators. The procedure is demonstrated by applying it to a relevant case study (Zühlsdorf et al., 2019), evaluating four different working fluids among pure and mixed refrigerants. The case study is also used as an explanatory example to estimate the impact on the system operating costs, thereby highlighting the importance of taking the heat transfer degradation in evaporators due to flow maldistribution into account when assessing the techno-economic feasibility of heat pump systems, as well as it allows comparing different refrigerants.

2. Methods

This section presents the procedure that was developed for evaluating the impact of maldistribution on the heat pump COP. The models were published in Mancini (2018), where the scripts utilized for the case study analysis can be accessed together with a detailed documentation. The numerical models were built and integrated in the Matlab simulation environment (Mathworks, 2017b).

2.1. Integrated framework for coupled cycle-PHE analysis

Fig. 1 shows the schematic of the procedure developed in this study. The work addressed the estimation of the off-design performance of both evaporator and cycle due to flow maldistribution. It was however coupled with preliminary cycle and HEX design.

First, the boundary conditions for the heat pump sizing and the working fluid were defined. The heat pump design model allowed estimating the COP and the operating cost at design conditions. The refrigerant design mass flow rate, together with the thermodynamic state of the refrigerant, heat source and heat sink at evaporator and condenser inlet and outlet were obtained as additional outputs and used in order to size the HEXs. The PHE evaporator and condenser models in design mode estimated the number of channels for a given plate geometry, thereby allowing the calculation of the total investment required for the heat pump. In order to evaluate the effect of maldistribution, a two-dimensional (2D) evaporator model was developed and integrated with a heat pump model, containing off-design calculations for the remaining components and the condenser model in performance mode, based on a one-dimensional (1D) discretization. The overall off-design analysis was carried out for different imposed liquid/vapour maldistribution rates, which allowed estimating the impact on the heat pump COP and operating cost. The off-design model was additionally implemented by using an evaporator model in 1D. The aim was to assess the difference between an ideal distribution of the mass flow rate (equal to using the 1D model) and the 2D model with a uniform

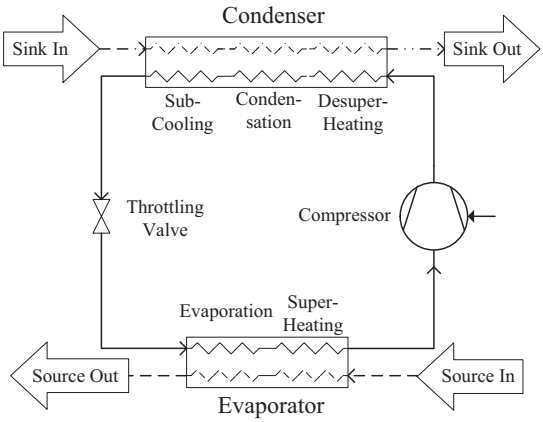

Fig. 2. Schematic of the heat pump model.

quality distribution at the inlet, thereby quantifying the effect of end plates. This will be futher explained in Section 2.4. The following subsections present in details the different submodels, base of the overall procedure. More focus is given to the PHE modelling, since the heat pump cycle modelling approach was based on the work by Zühlsdorf et al. (2019) with a more detailed characterization of the HEX components for both design and performance calculations.

2.2. Heat pump design model

The thermodynamic cycle was modelled in steady-state operation as a single-stage vapour compression heat pump with four components, as shown in Fig. 2. The design procedure was based on a fixed load at the evaporator or the condenser depending on the constraints of the specific case study. The design parameters were given by minimum pinch temperature differences in the HEXs, minimum superheat and fixed subcooling. The compressor was modelled by defining isentropic and motor efficiencies, while an isenthalpic operation of the expansion valve was assumed. The design model was developed for both pure and mixed refrigerants. The thermodynamic performance of the heat pump was evaluated by means of the COP, as expressed by Eq. (1).

$$\mathrm{COP} = \frac{\dot{Q}_{\mathrm{sink}}}{\dot{W}_{\mathrm{comp}}} \tag{1}$$

2.3. Heat exchangers models

The simulation framework comprises HEX models, which can be run in either design or performance mode, to respectively solve the design and performance problems. The design mode aims at calculating the physical size of the HEX for a given heat load, mass flow rates and inlet and outlet temperatures and pressures. The performance mode aims at estimating the heat transfer and pressure drop of an already sized HEX, thereby using the full HEX geometry, inlet thermodynamics, and mass flow rates as input and calculating heat flow rate, pressure drop and outlet temperatures and pressures (Shah and Sekulic, 2002).

The models were based on an internal solver for the solution of heat transfer and fluid flow, presented in Section 2.3.1. Different external solvers were employed for the solution of the design problem and of the performance problem, as described respectively in Sections 2.3.3 and 2.4. Note that the two performance solvers for evaporator and condenser were directly coupled with the equations for off-design operation of the heat pump.

The following assumptions were employed in all the models: (i) steady-state operating conditions, (ii) adiabatic end plates, i.e. no heat loss to the environment (iii) no longitudinal conduction through the plates, (iv) separated flow model for liquid and vapour phases, and (v) no pressure drop in the PHE manifolds. The manifold pressure drop can in some cases constitute a relevant contribution to the total pressure drop. It was however decided to neglect it since it is a term highly impacted by the real design of the HEX from specific manufacturers. Moreover, Li and Hrnjak (2018) showed that manifold pressure drop decreases with decreasing number of channels and increasing length-to-width ratios of the plates, thereby becoming negligible compared to channel pressure drop for PHE channels number lower than 100 and typically manufactured length-to-width ratios.

Table 1
Discretization and tolerances adopted for the PHE models.

	Design models		Performance models	
	Evaporator	Condenser	Evaporator	Condenser
Type of discretization	1D	1D	1D/2D	1D
Number of CVs	50	110	50 / 50 x $(N_{\mathrm{ch,ref}} + N_{\mathrm{ch,hs}})$	110
Tolerance	10^{-5}	10^{-5}	10^{-5}	10^{-5}

2.3.1. Solver for heat transfer and fluid flow

The solver for heat transfer and fluid flow was implemented to solve the PHE model in performance mode, i.e. with the full geometry and inlet thermodynamics and mass flow rates specified as inputs. The solver iterated on wall temperatures and pressure drops of both fluids, i.e. refrigerant and secondary fluid, following a successive substitution approach, in order to estimate the total heat flow rate and pressure drops of both fluids. Based on a start guess of linear wall temperature profile and pressure drop distributed evenly in the control volumes (CVs) along the flow direction for both fluids, the mass, momentum, and energy conservation equations were solved iteratively for each CV. An alternate iteration approach, as suggested by Eldeeb et al. (2016), was implemented in order to accelerate the model convergence.

The evaporator model in performance mode was based on both 1D and 2D discretization approaches. The latter was used in order to describe maldistribution effects. The discretization schemes and iteration variables are shown in Fig. 3 (a) for the 1D case and (b) for the 2D case. A 1D discretization approach - similar to the one shown for the evaporator in Fig. 3(a) - was applied for the condenser model. In this last case, the mass flow of both fluids was assumed to distribute uniformly, thereby applying the discretization solely along the fluid flow direction with uniform steps of heat transfer area.

Table 1 reports the discretization details for the solvers. The convergence criterion was defined based on the l^2-norm of the relative residuals of the wall temperature and refrigerant and secondary fluid pressure drop. A higher number of CVs was applied in the condenser case as a result of the grid independence study. Fluid thermo-physical properties were estimated by means of REFPROP 10 (Lemmon et al., 2018) for the refrigerants and CoolProp (Bell et al., 2014) for water.

2.3.2. Correlations for heat transfer coefficients and pressure drop

Correlations were used for the computation of heat transfer coefficients, frictional pressure drop and void fraction for each control volume in both two-phase and single-phase flow.

The evaporation and condensation heat transfer coefficients for pure fluids were estimated by Amalfi et al. (2016) and Yan et al. (1999), respectively. The Silver (1947) and Bell and Ghaly (1973) method was instead applied to account for mixture degradation of heat transfer during both evaporation and condensation. The method was initially developed for mixture condensation and

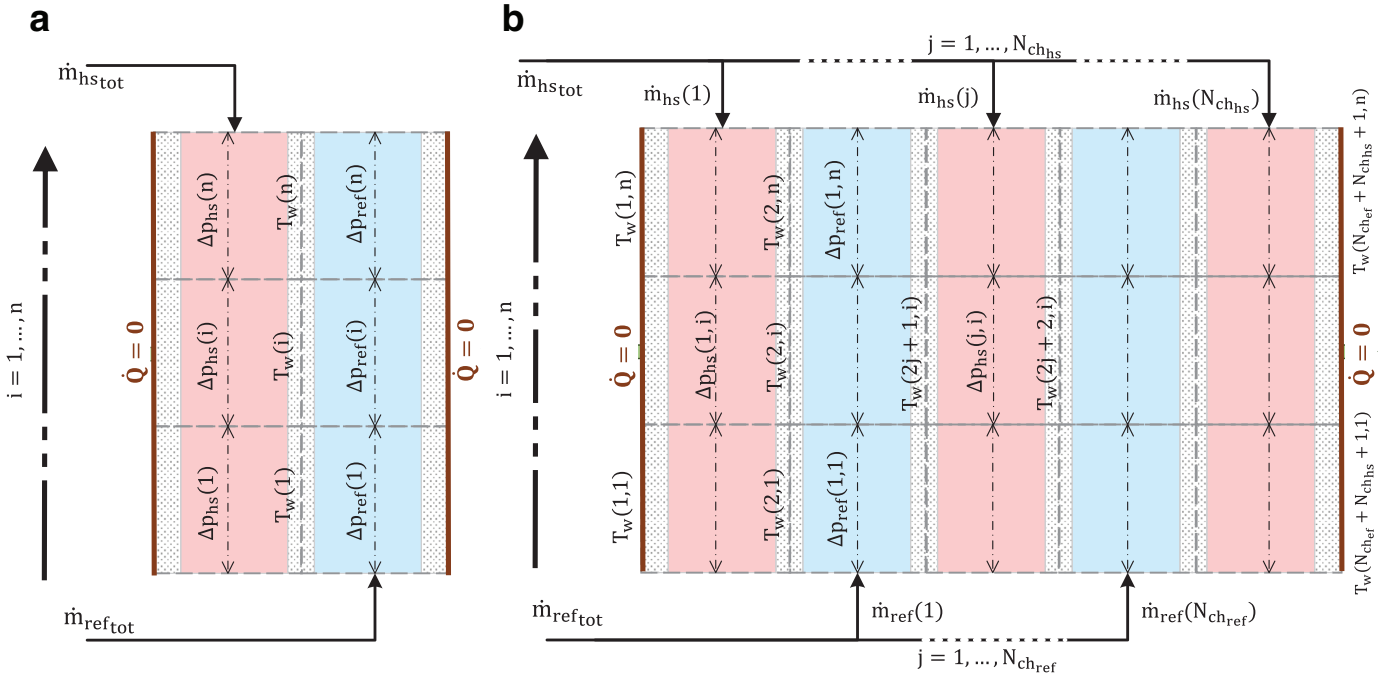

Fig. 3. Discretization approaches for evaporator: 1D (a); 2D (b).

was later extended to evaporation by Sardesai et al. (1982). For mixture condensation, the ideal heat transfer coefficient was computed using (Yan et al., 1999), while (Martin, 1996) was used for the vapour phase correction term. For the evaporation heat transfer coefficient of mixtures, Mancini et al. (2018b) showed that small deviations on the total heat flow rate are obtained regardless of the combination of heat transfer correlations chosen for the method. Therefore, Amalfi et al. (2016) was applied for the two-phase convective contribution, Cooper (1984) was used for the ideal nucleate boiling contribution, Thome and Shakir (1987) was used for estimating the mixture correction for the nucleate boiling term and Martin (1996) was applied for the single-phase vapour contribution.

The Lockhart and Martinelli (1949) method was applied to evaluate two-phase evaporation frictional pressure drop. The method was applied as proposed by Palm and Claesson (2006), i.e. Martin (1996) was used to estimate the single-phase frictional pressure drop and the correlation developed by Chisholm (1967) estimated the two-phase multiplier with a Chisholm parameter equal to 4.67. The Fanning friction factor correlation proposed by Yan et al. (1999) was instead used for condensation frictional pressure drop. Regarding pressure drop, no distinction was made between pure and mixed refrigerants and the same methods were applied for both evaporation and condensation.

Since no void fraction correlation is available in literature for PHEs, the widely used correlation presented by Smith (1969) was used to estimate the cross-sectional average density and the momentum density, which respectively are needed to compute the gravitational and acceleration contributions to pressure drop. The correlation was chosen since it was proven to well correlate data for two-phase upward annular flow (Godbole et al., 2011), which is a reasonable assumption in PHE evaporators (Vakili-Farahani et al., 2015).

A smooth transition was ensured between two-phase and single-phase in both superheated and subcooled regions for both evaporator and condenser, to avoid discontinuities. This was carried out by calculating the refrigerant heat transfer coefficient and frictional pressure drop by interpolating the two-phase and single-phase contributions at the interface. The smoothing was applied to the CVs with local vapour quality included in the intervals [0, 0.1] and [0.9, 1.0].

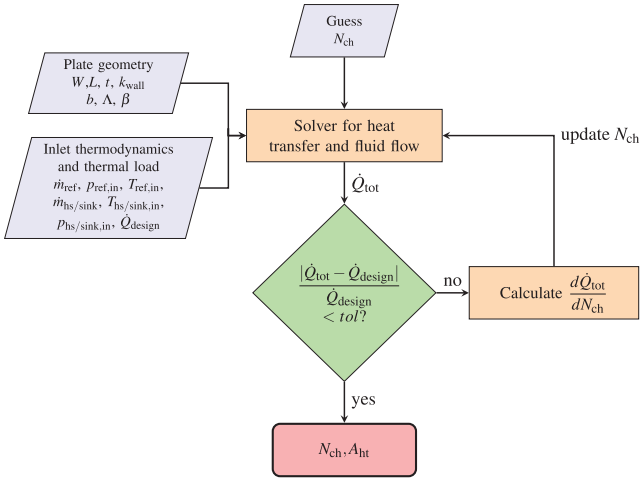

Fig. 4. Work-flow of the solver for the design problem.

2.3.3. Solver for the design problem

The evaporator and condenser models in design mode were solved based on an external solver iterating on the total number of channels in order to meet a dimensioning thermal load for a given plate geometry, following the Newton-Raphson method. The work-flow of the implemented solver is shown in Fig. 4. The plate size (given by width W, length L and thickness t) were defined together with the characteristic chevron-PHE corrugation height b, corrugation pitch Λ and chevron angle β. The inlet states and the mass flow rates of both working fluids were also fixed. An initial guess of the total number of channels N_{ch} was provided to the solver for heat transfer and fluid flow. The solver estimated the total heat flow rate, and the first derivative with respect to N_{ch}, subsequently used to update the guess value. The tolerance on the relative

Table 2
Operating conditions equations for off-design operation.

Evaporator	Condenser
$\bar{T}_{\text{ref,out}} - T_{\text{dew}} = \Delta T_{\text{SH}}$	$\bar{T}_{\text{ref,out}} = T_{\text{sink,in}} + \Delta T_{\text{pinch,min}}$
$\dot{m}_{\text{ref,tot}} \cdot \bar{\rho}_{\text{ref,out}} = \dot{V}_{\text{ref,out}}$	$T_{\text{sink,out}} = T_{\text{sink,out-design}}$

Table 3
Evaporator flow distribution equations.

Mass conservation in manifold		
Refrigerant	*Heat source*	*Refrigerant vapour*
$\sum_{j=1}^{N_{\text{ch,ref}}} \dot{m}_{\text{ref}}^{(j)} = \dot{m}_{\text{ref,tot}}$	$\sum_{j=1}^{N_{\text{ch,hs}}} \dot{m}_{\text{hs}}^{(j)} = \dot{m}_{\text{hs,tot}}$	$\sum_{j=1}^{N_{\text{ch,ref}}} \dot{m}_{\text{ref}}^{(j)} \cdot x_{\text{ref,in}}^{(j)} = \dot{m}_{\text{ref,tot}} \cdot x_{\text{ref,in}}$
Outlet pressure equalization		
Refrigerant		*Heat source*
$\sum_{i=1}^{n} \Delta p_{\text{ref}}^{(j,i)} = \sum_{i=1}^{n} \Delta p_{\text{ref}}^{(j+1,i)}$, $j = 1, \ldots, N_{\text{ch,ref}} - 1$		$\sum_{i=1}^{n} \Delta p_{\text{hs}}^{(j,i)} = \sum_{i=1}^{n} \Delta p_{\text{hs}}^{(j+1,i)}$, $j = 1, \ldots, N_{\text{ch,hs}} - 1$

residual of the total heat flow rate was fixed to 10^{-3}. The required heat transfer area was calculated as the output of the solver.

2.4. Off-design conditions: coupled cycle and PHE models in performance mode

The off-design conditions were solved by creating an overall solver for the cycle, the PHE condenser and the PHE evaporator with and without liquid/vapour maldistribution. The solver was based on the *fsolve* algorithm (Mathworks, 2017a) coupled with the solver for heat transfer and fluid flow of condenser and evaporator and calculations for off-design compressor performance. The solver for heat transfer and pressure drop of both evaporator and condenser was presented in Section 2.3.1. The compressor performance during off-design operation was evaluated by using the correlation presented in Granryd et al. (2009), relating the isentropic efficiency to the deviating pressure ratio. This correlation is valid for volumetric compressors with built-in volume ratios, which are typically used in many heat pump applications. A full description of all the governing equations for all the components can be found in the model documentation available in Mancini (2018).

In the off-design model without maldistribution effects, the unknowns were defined as the heat pump operating conditions, while for the off-design model with maldistribution effect the unknowns were given by the operating conditions and the mass flow rate distribution inside the evaporator. More specifically, the total mass flow rate of the refrigerant $\dot{m}_{\text{ref,tot}}$ and of the heat sink $\dot{m}_{\text{sink,tot}}$, the evaporation pressure p_{eva} and condensation pressure p_{cond} were chosen as the four variables describing the cycle operation. For the off-design model with maldistribution effects, where the evaporator was discretized based on a 2D approach, the vectors containing the mass flow rate distribution of the refrigerant and heat source in the different channels, namely $\dot{m}_{\text{ref}}$ and $\dot{m}_{\text{hs}}$, constituted by $N_{\text{ch,ref}}$ and $N_{\text{ch,hs}}$ elements each, were set as additional unknowns, together with the inlet vapour quality $x_{\text{ref,in}}$.

The equations implemented are reported in Table 2 for the off-design model without maldistribution effects. The four equations describe the operating strategy of the heat pump, thus dependent on the boundary conditions for the specific case study. In this case, the refrigerant superheat at the evaporator outlet, the suction volume flow rate at the compressor inlet, the refrigerant subcooling, and the sink outlet temperature were chosen as control values, thus fixed to the values at the design point.

Table 3 reports instead the additional equations needed for the off-design model with maldistribution effects, describing the mass flow rate distribution of refrigerant and heat source in the different PHE evaporator channels. Table 3 shows a total of $N_{\text{ch,ref}} + N_{\text{ch,hs}} + 1$ governing equations, since the outlet pressure equalization equations for both refrigerant and heat source (reported in the second row) consisted of $N_{\text{ch,ref}} - 1$ and $N_{\text{ch,hs}} - 1$ equations, respectively.

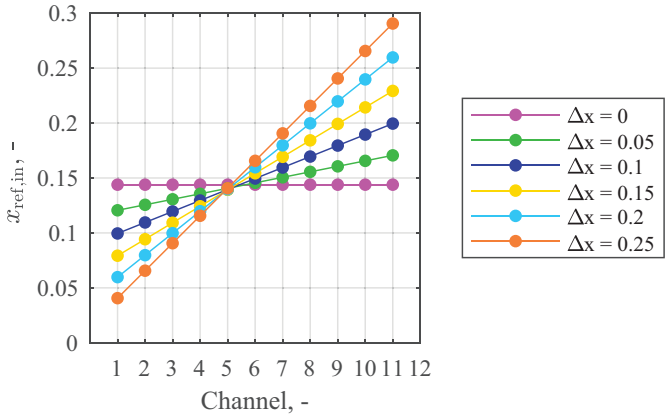

Fig. 5. Imposed vapour quality maldistribution for a PHE with 11 refrigerant channels.

As indicated in Fig. 1, the maldistribution rate was an input to the off-design model with maldistribution effects. A linear vapour quality variation was therefore imposed to the channels at the PHE inlet, similarly to Mancini et al. (2018a). The variation was calculated as function of a parameter Δx, representing the difference in vapour quality between the outer-most PHE refrigerant channels. The inlet quality at the jth channel was thus estimated as function of the quality at the first channel, as expressed by Eq. (2).

$$x_{\text{in}}^{(j)} = x_{\text{in}}^{(1)} + \frac{j-1}{N_{\text{ch,ref}} - 1} \Delta x \tag{2}$$

The parameter Δx was varied between zero (for even distribution) and 0.25 by steps of 0.05. An example of the imposed variation of vapour quality for a case of 11 refrigerant channels is shown in Fig. 5, where each colour represents a different maldistribution rate and therefore a different off-design operation point of both evaporator and heat pump.

The effect of end plates corresponded to the case of $\Delta x = 0$. In this last case, an even distribution of the vapour quality was imposed at the inlet of the PHE channels. The mass flow distribution of both refrigerant and heat source is however non-uniform, since it is affected by the outer-most channels that are assumed perfectly adiabatic towards the outer environment. The difference between the 1D evaporator model and the 2D evaporator model with $\Delta x = 0$ allowed quantifying this effect on both evaporator and heat pump performance.

2.5. Economic analysis

The impact of maldistribution on the economic performance of the heat pump was evaluated using the integrated framework presented above. The degradation of COP in off-design conditions entails a drop of economic performance. By considering the economic boundary conditions case by case, the change in operating costs and revenue streams can be evaluated. The reader is referred to Zühlsdorf et al. (2019) for a comprehensive discussion about evaluating costs and revenues for heat pumps in different applications. A common indicator is given by the (levelized) specific cost of heat, calculated in € /MWh by Eq. (3). It is function of the different cash flow (CF) terms: the cost of electricity CF_{el} and the income of supplying cold by cooling the heat source CF_{hs}. Moreover, it depends

Table 4
Heat pump design and operating parameters for the selected working fluids.

Working fluid	Inputs					Outputs						
	$\dot{Q}_{eva}$, kW	$T_{hs,in}$, °C	$T_{hs,out}$, °C	$T_{sink,in}$, °C	$T_{sink,out}$, °C	$\dot{Q}_{cond}$, kW	p_{cond}, bar	p_{eva}, bar	$\dot{m}$, kg s^{-1}	$\dot{V}_{out,eva}$, m^3 h^{-1}	COP, -	c_h, € /MWh
Butane	500	50	25	50	75	630	9.5	2.2	1.69	1100	4.5	32.7
Propane	500	50	25	50	75	638	28.1	8.8	1.90	370	4.4	31.1
Propylene/Butane(0.5/0.5)	500	50	25	50	75	600	16.4	5.6	1.62	460	5.6	25.8
CO_2/DME(0.2/0.8)	500	50	25	50	75	600	25.3	9.7	1.56	290	5.6	25.4

on the Total Capital Investment (TCI), Capital Recovery Factor (CRF) and the yearly production of heat, evaluated by multiplying the condenser load ($\dot{Q}_{sink}$) by the yearly operating hours (OH).

$$c_h = \frac{CF_{el} - CF_{hs} + TCI \cdot CRF}{\dot{Q}_{sink} \cdot OH} \quad (3)$$

2.6. Case study

The present section aims at introducing the case study chosen to demonstrate the utilization of the coupled cycle-PHE analysis procedure. The case was previously published in Zühlsdorf et al. (2019), without considering detailed HEX design and maldistribution effects in evaporators. Section 2.6.1 presents the choice of the working fluids and the heat pump boundary conditions. Sections 2.6.2 and 2.6.3 highlight the assumptions and criteria adopted for the cycle and PHEs design, respectively. Last, Section 2.6.4 describes the economic boundary conditions.

2.6.1. Working fluids and boundary conditions

The case study aims at integrating heat pumps in data centre facilities for excess heat recovery purposes, for supplying heat to a district heating (DH) network. Zühlsdorf et al. (2019) carried out a screening of working fluids, including both pure and mixed refrigerants, aiming at maximizing the cycle COP. Table 4 reports four working fluids that were found among the most promising from both thermodynamic and economic standpoints, namely the two pure fluids butane and propane, and the two zeotropic mixtures propylene/butane and CO_2/dimethyl ether (DME) at (0.5/0.5) and (0.2/0.8) mass compositions, respectively. The heat pump design parameters and resulting operating pressures, suction volume flow rate, COP and specific cost of heat are also reported in the table. Note, that the two zeotropic mixtures outperform both pure fluids with higher COP at a lower specific cost of heat. The working fluids to include in the present study were selected with the purpose of assessing the impact of maldistribution for a diverse range of refrigerants, with different thermo-physical properties and operating pressures.

2.6.2. Heat pump design

The design parameters and assumptions are reported in Table 5. The sizing was carried out by fixing the heat source side, since a nominal cooling load must be provided to the data centre and the heat released to the sink (DH network) was considered as a subsequent revenue. A minimum superheat was ensured at the evaporator outlet, e.g. the temperature of the refrigerant was increased of ΔT_{SH} in order to avoid refrigerant liquid droplets at the compressor inlet. The subcooling was defined to reach the highest possible COP by maximizing it and reaching the imposed pinch point temperature difference at the liquid outlet of the condenser. The compressor was assumed to have no heat losses to the environment, and typical values of isentropic and motor efficiencies were considered.

Table 5
Assumptions and design parameters for the case study.

Description	Parameter	Value	Unit
Evaporator			
Medium source		water	–
Pinch point temperature difference	ΔT_{pinch}	3	K
Minimum superheat	ΔT_{SH}	5	K
Design load	$\dot{Q}$	500	kW
Condenser			
Medium sink		water	–
Pinch point temperature difference	ΔT_{pinch}	3	K
Subcooling	$T_{ref,out}$	$T_{sink,in} + \Delta T_{pinch}$	K
Compressor			
Isentropic efficiency	η_{is}	0.75	–
Motor efficiency	η_{motor}	0.95	–

2.6.3. Heat exchangers design

The PHE design for both evaporator and condenser was carried out by considering typical plate dimensions from commercial manufacturers (ALFA LAVAL, 2018; SWEP International AB, 2015). The plate size and models are reported in Table 6. Note that different plate geometries were assumed for the different working fluids, due to the large differences in required heat transfer area. Mixtures usually require a larger area and hence investment, due to the lower temperature differences in the HEXs and the degradation of heat transfer coefficients compared to pure fluids. Therefore, plates with the larger area were selected for both propylene/butane and CO_2/DME for the evaporator and condenser side. For the evaporator, a plate size with a lower aspect ratio (L_p/W) was chosen for the pure fluids, due to the larger sensitivity of butane to pressure drop. On the other hand, the two condenser sizes were chosen with similar length-to-width ratios.

2.6.4. Economic boundary conditions

As the design of the HEXs and compressor was fixed by the nominal heat pump conditions, the total capital investment of the heat pump was not affected by the off-design operation. The

Table 6
Evaporator and condenser plate geometry, input for the design models (ALFA LAVAL, 2018; SWEP International AB, 2015).

Working fluid	Evaporator				Condenser			
	HEX model	W, m	L_p, m	L_p/W, –	HEX model	W, m	L_p, m	L_p/W, –
Butane	SWEP B633	0.537	0.593	1.1	SWEP V65	0.363	0.731	2.0
Propane	SWEP B633	0.537	0.593	1.1	SWEP V65	0.363	0.731	2.0
Propylene/Butane (0.5/0.5)	SWEP B649	0.537	0.995	1.9	AQ6-FG	0.650	1.390	2.1
CO_2/DME(0.2/0.8)	SWEP B649	0.537	0.995	1.9	AQ6-FG	0.650	1.390	2.1

Table 7
Economic boundary conditions for the case study (Zühlsdorf et al., 2019).

Description	Parameter	Value	Unit
Lifetime	n_{hp}	20	y
Operating hours	OH	8000	h y^{-1}
Effective interest rate	i_{eff}	5	%
Specific cost of electricity	c_{el}	120	€ MWh^{-1}
Specific revenue of heat source	c_{hs}	0	€ MWh^{-1}
Specific income per supplied heat	c_{sink}	40	€ MWh^{-1}

assumptions and cost correlations used in order to estimate the TCI are described in Zühlsdorf et al. (2019).

The operating cost and revenue streams were on the other hand influenced by maldistribution. The different boundary conditions adopted for the calculations are reported in Table 7. A fixed number of yearly OH was assumed, since the heat pump was designed for waste heat recovery and the income from the supplied heat to the DH was considered as an additional benefit of the heat pump integration. The specific revenue from the heat source was assumed equal to zero.

3. Results

This section presents the results obtained by applying the simulation framework to the case study. Section 3.1 presents the results of the PHE sizing for both evaporator and condenser, as a basis for the subsequent off-design analysis. Section 3.2 presents the impact of the imposed maldistribution on the working fluid mass flow distribution and evaporator performance, while Section 3.3 explains the impact on the thermodynamic cycle performance. Last, Section 3.4 reports the results of the economic analysis for one of the working fluids.

3.1. Evaporator and condenser designs

Table 8 shows the output of the design models. The total number of channels and heat transfer area was estimated, which gives an indication of the size of the components for each case and refrigerant. The effective heat flow rate, the mass flux, and the total refrigerant pressure drop were additional outputs of the design process. These results are dependent on the plate base design that was chosen for the working fluids. Commercial plates from manufacturers were considered, hence the PHE design was not based on a full optimization of the geometry but it was in fact based on heuristics in accordance with typically accepted values of refrigerant pressure drop. This approach resulted in designs with a different number of channels for the four refrigerants. A full optimization of the PHE geometry was considered as outside the scope of the present work.

The evaporator design for the two pure fluids butane and propane led to refrigerant pressure drop within the usual 50 kPa limit adopted by commercial manufacturers (SWEP International AB, 2015). Despite the evaporator for butane was designed with a mass flux (G_{ref}) equal to around half of the case of propane, similar pressure drops were obtained for the two fluids. This constitutes a first indication of the higher sensitivity to pressure drop of butane, i.e. a higher degradation of the PHE performance due to pressure drop is expected even if no maldistribution effect is accounted for. This will be further explained in Section 3.2.

The two zeotropic mixtures led to opposite PHE designs, despite the same plate geometry was assumed in both cases. The design for propylene/butane entailed higher pressure drop (equal to 63.5 kPa) and a lower heat transfer area, whereas low pressure drop and bigger heat transfer area was obtained for the case of CO_2/DME. This is likely to lead to different impact of maldistribution for the two working fluids.

It is noted, that the condenser pressure drop predicted using the correlation by Yan et al. (1999) is very low for all the working fluids, and in the case of propane equal to -0.86 kPa. The design of the condenser presented in this case study corresponds however to a case with a large refrigerant sub-cooling, equal to 24.3 and 21.3 K at the design point for butane and propane, respectively, and 8.7 and 2.0 K for propylene/butane and CO_2/DME. The large sub-cooling results in dominant contribution of gravity pressure drop, which in turn, for downward-flow condensers, negatively contributes to the total value (i.e. results in a pressure recovery). Note that the dominant contribution of gravity pressure drop was obtained as a consequence of using the correlation by Yan et al. (1999)(due to the low values of friction factor), and the choice of other prediction methods might change the result. This point is further discussed in Section 4.

3.2. Impact on evaporator performance

Fig. 6 shows the mass flow rate distribution of the refrigerant into the different channels of the evaporator. The different colors represent the degree of maldistribution imposed by the model. $\Delta x = 0$ corresponds to a uniform vapour quality distribution, thus indicating the effect of end plates on the channel-to-channel mass flow distribution. $\Delta x = 0.25$ corresponds instead to the most severe maldistribution imposed by the model, namely an absolute difference of vapour quality at the inlet of the outer-most channels of 0.25. The results are reported in terms of percentage deviation from the average mass flow rate, e.g. the mass flow rate in each channel if an equal distribution was attained.

The trends were similar for both pure fluids and mixtures, with larger mass flow rates flowing in those channels with lower inlet vapour quality (see Fig. 5). The higher pressure drop entailed by the vapour phase leads to a reduction of the mass flow rate in those channels where complete evaporation is reached earlier, in order to equalize the pressure drops. Butane showed the largest sensitivity to maldistribution, with mass flow rate deviation of up to 50% for $\Delta x = 0.25$. The maximum deviation of the other working fluids resulted to be similar, with maximum values around 20% to 30%.

Fig. 7 reports the total refrigerant mass flow rate (a), the total evaporator heat flow rate (b) and the total refrigerant pressure drop (c), as a function of the maldistribution parameter Δx. In Fig. 7 (a) and (b), the values were normalized with respect to the design point, which were presented in Table 4. The refrigerant

Table 8
Results of design model for evaporator and condenser.

Working fluid	Evaporator					Condenser				
	$N_{ch,tot}$, –	A_{ht}, m^2	$\dot{Q}$, kW	G_{ref}, kg m^{-2} s^{-1}	$\Delta p_{ref,tot}$, kPa	$N_{ch,tot}$, –	A_{ht}, m^2	$\dot{Q}$, kW	G_{ref}, kg m^{-2} s^{-1}	$\Delta p_{ref,tot}$, kPa
Butane	61	22.3	501	57.4	28.8	161	49.2	633	29.0	0.01
Propane	39	14.3	502	100.8	34.0	210	65.8	638	23.2	-0.86
Propylene/Butane (0.5/0.5)	33	20.8	501	91.2	63.5	51	55.3	603	47.6	2.32
CO_2/DME (0.2/0.8)	65	41.0	500	44.6	10.9	51	55.3	602	45.8	0.55

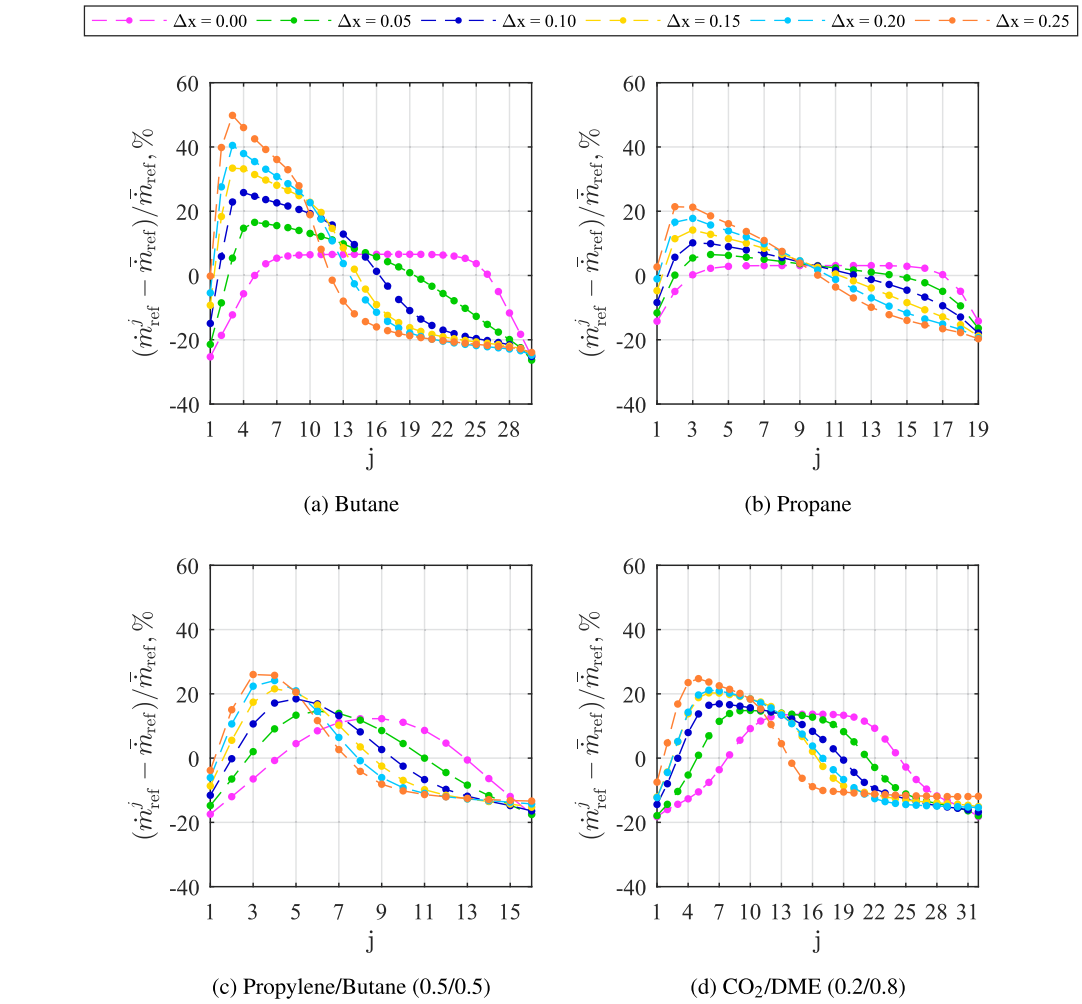

Fig. 6. Mass flow distribution of the refrigerant in the different evaporator channels, shown as percentage deviation from the average value.

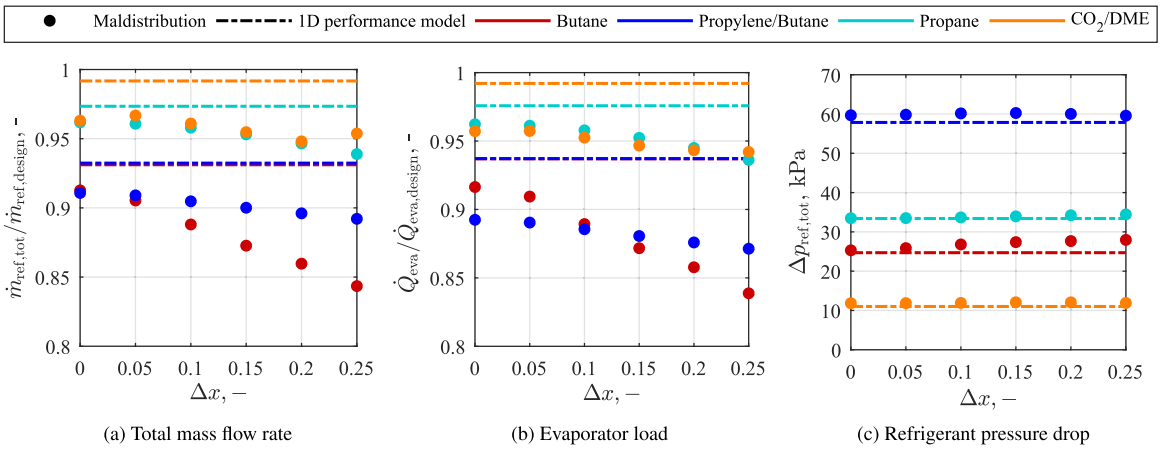

Fig. 7. Impact of maldistribution effects on (a) total refrigerant mass flow rate, (b) evaporator heat flow rate and (c) total refrigerant pressure drop.

pressure drop in Fig. 7 (c) was instead plotted as absolute values in order to show the ranking of the working fluids.

The dashed lines in Fig. 7 represent the results of an evaporator 1D performance model, where the flow was assumed to distribute perfectly uniformly between the different channels. Therefore, the difference between the design value and the 1D performance model accounts for the real operation of the heat pump, in which pressure drops of both evaporator and condenser affect the operating conditions, i.e. pressure levels and mass flow rate, due to the imposed control parameters, which were set as a fixed superheat, subcooling and compressor suction volume flow rate. On the other hand, the difference between the dashed line and the point marker at $\Delta x = 0$ quantifies the effect of end plates. The third and fourth columns of Table 9 report these differences in terms of percentage deviation for the evaporator heat flow rate. The trend outlined by the point markers in Fig. 7 represent instead the effect of

Table 9
Evaporator heat flow rate degradation due to effect of end plates and liquid/vapour maldistribution.

Working fluid	$\dot{Q}_{eva,design}$, kW	$\dot{Q}_{eva,1D}$, kW	Real operation $\frac{\dot{Q}_{1D}-\dot{Q}_{design}}{\dot{Q}_{design}}$, %	End plates effect $\frac{\dot{Q}_{\Delta x=0}-\dot{Q}_{1D}}{\dot{Q}_{1D}}$, %	Liquid/vapour maldistribution $\frac{\dot{Q}_{\Delta x=0.25}-\dot{Q}_{\Delta x=0}}{\dot{Q}_{\Delta x=0}}$, %	Overall effect $\frac{\dot{Q}_{\Delta x=0.25}-\dot{Q}_{1D}}{\dot{Q}_{1D}}$, %
Butane	500	468	−6.7	−2.2	−8.5	−10.5
Propane	500	488	−2.5	−1.4	−2.7	−4.1
Propylene/Butane (0.5/0.5)	500	469	−6.7	−4.8	−2.4	−7.0
CO_2/DME (0.2/0.8)	500	496	−0.8	−3.5	−1.6	−5.1

liquid/vapour maldistribution. The last two columns of Table 9 report the degradation of heat flow rate in the most severe case of maldistribution ($\Delta x = 0.25$), compared to the case of uniform vapour quality distribution ($\Delta x = 0$) and to the results of the 1D model, respectively. The former solely quantifies the effect of liquid/vapour maldistribution, i.e. the slope of the degradation, while the latter reports the overall degradation due to end plates and liquid/vapour non-uniformity effects altogether.

Fig. 7(a) shows that both pure fluids – butane and propane – and the mixture propylene/butane report an evident decrease of the total mass flow rate with increasing Δx, whereas the zeotropic mixture CO_2/DME does not follow a clear trend. Moreover, the reduction of mass flow rate in the case of operation with no maldistribution (dotted line) was found to be very small (around 1%) for CO_2/DME, slightly higher for propane (around 2.5%) and similar for butane and propylene/butane, around 8% to 9%. The impact of real system operation on the evaporator heat flow rate was analogous, as shown in Fig. 7(b). Real operation is strongly dependent on the effect of refrigerant pressure drop (in both evaporator and condenser) on the cycle operating conditions, and Fig. 7(c) shows that higher pressure drop resulted in higher degradation of the mass flow and evaporator heat flow rate. Butane was found to be the only exception, with pressure drop being the second lowest after CO_2/DME, yet entailing a higher degradation of performance.

Regarding the effect of end plates, propylene/butane resulted to be the fluid most influenced, with a deviation of 4.8%. CO_2/DME follows with a deviation of 3.5%, while the two pure fluids report smaller degradations. This was already shown in Fig. 6, where the mass flow distribution into the different channels was reported for the working fluids. It may be seen that the line corresponding to $\Delta x = 0$ reports a lower deviation from the average mass flow rate for both butane and propane compared to the mixtures. The deviation increases then more sharply for both pure fluids with increasing $\Delta x = 0$, compared to the mixtures. Fig. 6 shows indeed that the end plates affect the mixtures to a higher extent than both pure fluids, which instead resulted to be more sensitive to vapour quality maldistribution.

Liquid/vapour maldistribution in fact impacted butane to the largest extent, leading to an overall degradation of the heat flow rate of 10.5% compared to the performance estimated by the 1D model. Non-uniform quality distribution contributed with 8.5% degradation. Propane resulted to be the second most affected fluid with a degradation of 2.7%. This is also shown by the slope of the point markers in Fig. 7 (b), which is steeper for the two pure fluids. Despite the lower degradation due to vapour quality non-uniformity experienced by propylene/butane, equal to 2.4%, a high impact was found for end plates effects, leading to an overall higher evaporator performance degradation of 7.0%. The mixture CO_2/DME resulted to be only slightly affected by liquid/vapour maldistribution, with an overall degradation of 5.1% mostly due to end plates effect.

The different sensitivity of the working fluids to real system operation, the effect of end plates and liquid/vapour maldistribution can be related to the PHE design, as well as to the different working fluid properties. The refrigerant pressure drop trends are highlighted in Fig. 7 (c), with butane clearly showing an increase in pressure drop with increasing Δx. Table 10 reports some relevant fluid thermo-physical properties, evaluated at the evaporator design conditions. These were used to analyze any possible correlations between maldistribution and fluid characteristics. Brignoli et al. (2017) discussed about the effect of refrigerant thermo-physical properties on two-phase heat transfer and pressure drop. The authors highlighted how high refrigerant vapour density impacts the total refrigerant pressure drop by lowering the saturation temperature decrease due to pressure drop. This is

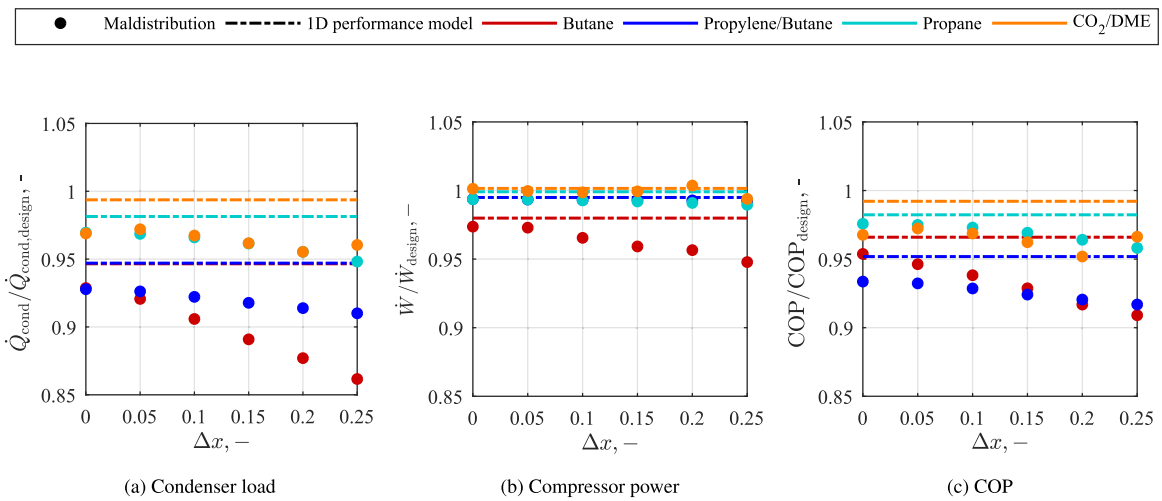

(a) Condenser load (b) Compressor power (c) COP

Fig. 8. Impact of maldistribution effects on (a) condenser heat flow rate, (b) compressor power and (c) heat pump COP.

Table 10
Refrigerant saturation pressure and thermo-physical properties at evaporator design conditions.

Working fluid	$p_{eva,design}$, bar	T_{bubble}, °C	T_{dew}, °C	ρ_V, kg m^{-3}	$\frac{dT_{bubble}}{dp}$, K kPa^{-1}
Butane	2.2	22.5	22.5	5.7	0.140
Propane	8.8	22.0	22.0	19.1	0.044
Propylene/Butane (0.5/0.5)	5.6	19.8	37.0	13.6	0.054
CO_2/DME (0.2/0.8)	9.7	11.2	34.9	20.1	0.033

quantified by dT_{bubble}/dp, which can be estimated using the Clapeyron relation (Moran et al., 2018). Table 10 shows that butane reports vapour density nearly one third lower than propylene/butane and one forth lower than both propane and CO_2/DME. Moreover, dT_{bubble}/dp for butane is one order of magnitude higher than for the other working fluids, which instead present similar values. This means that, despite the lower pressure drop related to the PHE design for butane, the evaporator is more affected compared to the other fluids. This explains why butane reports the higher degradation of evaporator performance due to real system operation, as well as a higher sensitivity to vapour quality non-uniformities.

3.3. Impact on cycle thermodynamic performance

A degradation of evaporator performance due to maldistribution effects influences the performance of the overall thermodynamic cycle. Fig. 8 shows the effect of the different rates of imposed vapour quality non-uniformity on total condenser heat flow rate (a), on the power required by the compressor (b) and the COP (c), defining the heat pump thermodynamic performance.

The condenser load estimated by the 1D performance model, thereby accounting for pressure drops of both evaporator and condenser, was found to be lower than the design value for all working fluids. Similarly to the evaporator case, the decrease for butane and propylene/butane was found to be higher, around 5% vs. a decrease of around 1% to 2% for propane and nearly negligible for CO_2/DME. This was due to the higher sensitivity of butane to pressure drop and the highest value of pressure drop for propylene/butane as already presented in the previous section. The end plate effects in the evaporator for both butane and propylene/butane translate into similar values of condenser load reduction, yet the slope of butane was the steepest among all the working fluids. This is consistent with the results presented in Table 9, which showed butane being the most affected fluid regarding liquid/vapour maldistribution. CO_2/DME does not follow a clearly decreasing trend, similarly to what was found for the total refrigerant mass flow rate in Fig. 7 (a).

The effect of maldistribution on the power required by the compressor in Fig. 8 (b) shows that propane, propylene/butane and CO_2/DME were negligibly affected by maldistribution, while butane underwent a visible decrease (2% to 3%). This is due to the opposite effects of the mass flow reduction (shown in Fig. 7 (a)) and an increase of pressure ratio and reduction of isentropic efficiency during off-design operation. The mass flow rate reduction is the dominating effect for butane, thus entailing a lower compressor power, whereas the other working fluids resulted to have a counteracting effect from mass flow rate and pressure ratio/efficiency, thereby having nearly constant compressor power.

The condensation heat flow rate reduction together with the different trends from the compressor power affected the resulting heat pump COP, shown in Fig. 8 (c). The percentage deviations are reported in Table 11, similarly to the evaporator case, i.e. by estimating the effect of real operation, end plates and vapour quality non-uniformity separately and altogether.

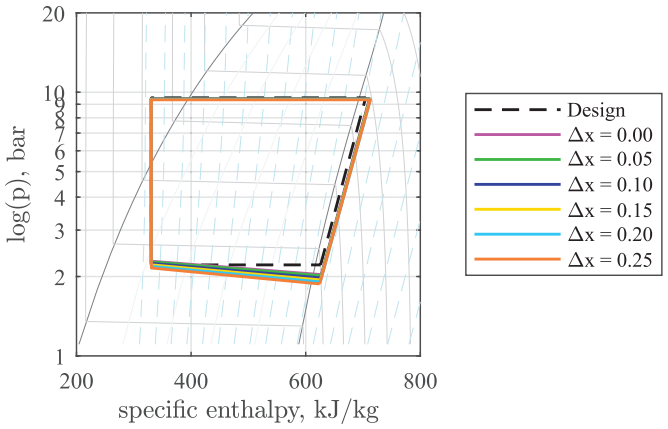

Fig. 9. Impact of maldistribution effects on the heat pump cycle for butane.

The effect of maldistribution on COP follows the same trend as the condenser heat flow rate for propane, propylene/butane and CO_2/DME, since the compressor power was not affected. The decrease of condenser heat flow rate was found to be dominating over the reduction of power consumption for butane, thereby entailing a COP reduction. The effect of end plates was however reduced compared to the evaporator, and the slope of the maldistribution rates (increasing Δx) is less steep.

By comparing the last columns of Tables 9 and 11, it may be observed that the PHE evaporator degradation was translated into a lower effect on the COP for all the working fluids, comparable to half of the evaporator degradation. The difference between the design and 1D model was reduced, as well as the effect of end plates, compared to the evaporator performance degradation. The relative ranking of the fluids with respect to each other was maintained, hence butane experienced the largest reduction of COP equal to 5.9%, followed by propylene/butane, CO_2/DME and propane.

The effect of maldistribution on the cycle thermodynamic performance is additionally presented in Fig. 9 by the log(p)-h diagram of the heat pump cycle at the design point compared to the different cases of maldistribution. Fig. 9 shows the case of butane, since it resulted as the most sensitive fluid to maldistribution. The trends for the other refrigerants were found to be similar. In agreement with the results shown in Fig. 7 (c), increasing Δx entails an increase of refrigerant pressure drop at the evaporator, as clearly shown by the evaporator outlet state point reported in the log(p)-h diagram. Fig. 9 shows that the cycle operation is significantly affected by the occurrence of maldistribution effects.

3.4. Economic analysis

The results of the economic analysis are presented solely for butane. The other working fluids showed similar trends yet with different magnitude of the impact. Moreover, the results of the economic analysis serve as a mere indication of the utilization of the simulation framework presented in this paper, since they are dependent on the assumptions made for the specific case study.

The economic performance indicator introduced by Eq. (3), namely the specific cost of heat, is shown in Fig. 10(a), while the two different revenue and cost streams associated with the chosen case study are reported in Fig. 10(b), for design case, the heat pump real operation and the different maldistribution rates. Since the heat pump was assumed to be operated for a fixed number of hours, the specific cost of heat was found to increase due to maldistribution effects. The heat load of the condenser (presented in Fig. 8 (a)) resulted to be decreasing with increasing Δx, and had

Table 11
COP degradation due to effect of end plates and liquid/vapour maldistribution.

Working fluid	COP_{design}, –	COP_{1D}, –	Real operation $\frac{COP_{1D} - COP_{design}}{COP_{design}}$, %	End plates effect $\frac{COP_{\Delta x=0} - COP_{1D}}{COP_{1D}}$, %	Liquid/vapour maldistribution $\frac{COP_{\Delta x=0.25} - COP_{\Delta x=0}}{COP_{\Delta x=0}}$, %	Overall effect $\frac{COP_{\Delta x=0.25} - COP_{1D}}{COP_{1D}}$, %
Butane	4.52	4.37	−3.4	−1.3	−4.7	−5.9
Propane	4.40	4.32	−1.8	−0.7	−1.8	−2.5
Propylene/Butane (0.5/0.5)	5.58	5.31	−4.8	−1.9	−1.8	−3.7
CO_2/DME (0.2/0.8)	5.63	5.59	−0.7	−2.5	−0.1	−2.6

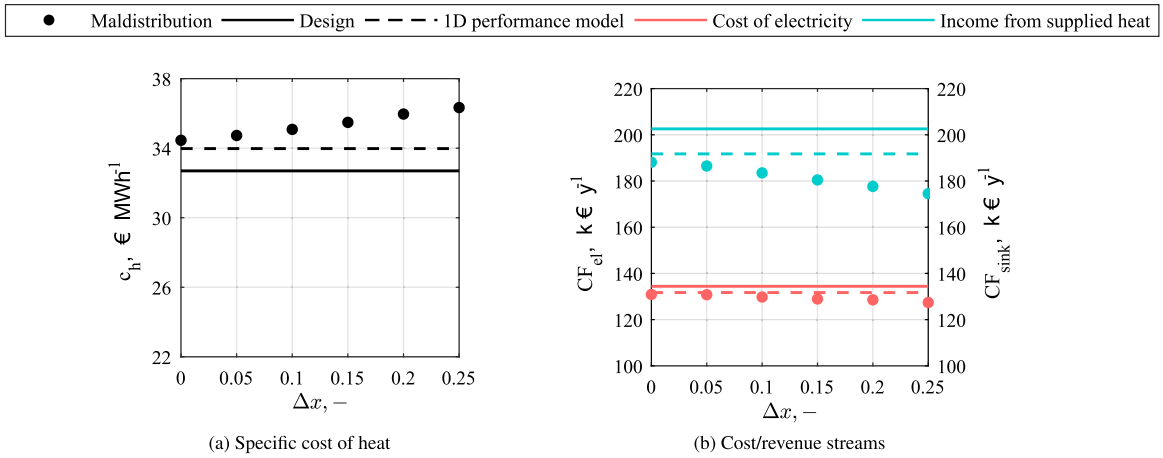

(a) Specific cost of heat (b) Cost/revenue streams

Fig. 10. (a) Specific cost of heat and (b) yearly cost and revenue streams as function of Δx for butane.

a dominating effect compared to the decrease in operating costs associated to the compressor. The heat source was considered to be free excess heat from a data centre, while the TCI was fixed in all the cases, hence constituting the heat sink and compressor costs to be the only influencing factors. Fig. 10(b) shows the yearly electricity cost of the compressor compared to the revenue stream (which is not considered for the computation of c_h). The revenue stream was determined by the heat of the condenser, which was supplied to the DH network. In agreement with the increasing trend of the specific cost of heat, the revenue stream was found to decrease with a steeper slope compared to the compressor running costs, thereby leading to an increase in the operation cost of the heat pump when maldistribution affects the operation of the evaporator.

4. Discussion

The results presented in this paper showed the application of a coupled PHE-cycle simulation framework, which can be used for system design and operation analysis when maldistribution occurs in PHE evaporators. The application of the procedure was demonstrated step-by-step for a case study and four different working fluids.

The results showed a general degradation of the evaporator and cycle performance both due to the effects of end plates and liquid/vapour maldistribution. The differences between working fluids were presented in light of several aspects contributing to such discrepancies, namely PHE design, obtained pressure drop and fluid properties.

The PHE design was carried out by fixing the plate geometry to typical dimensions available from suppliers, no numerical optimization was carried out for any working fluids and the designs were chosen to respect typical allowable limits for pressure drop. Since the pressure drop, which is strongly influenced by the geometry, was found to affect the refrigerant sensitivity to maldistribution effects, the results should not be taken as a final ranking of the different refrigerants. The results were instead presented as a way to use the simulation framework and to understand the different aspects to take into consideration during design and analysis of both evaporator and cycle. For instance, by looking at the results for PHE design for the two mixtures propylene/butane and CO_2/DME in Table 8, it can be observed that opposite evaporator designs were obtained: propylene/butane resulted in a configuration with a low number of channels, thereby higher pressure drop and low heat transfer area, whereas for CO_2/DME a higher plates number was employed, entailing higher heat transfer area and low pressure drop. It was therefore found that a lower evaporator investment could be required for propylene/butane. The maldistribution study showed however that propylene/butane, with this particular PHE design, experienced evaporator heat flow rate reduction of up 7%, leading to a 3.7% decrease of the system COP. The design for CO_2/DME was instead found to entail lower effects of maldistribution, leading to maximum 2.6% reduction of COP, almost entirely due to end plates. This means that, case by case, the trade-off between pressure drop and area investment must be decided also taking maldistribution effects into account, since they may impact the evaporator and cycle performance considerably, depending on the PHE geometry and pressure drop limit chosen during the design phase.

Moreover, the results of the study showed that the thermophysical properties of the refrigerant are a relevant aspect to consider. Brignoli et al. (2017) already stressed the importance of taking fluid characteristics into account to discriminate when combined optimization of cycle and HEX design leads to an effective increase of the cycle thermodynamic performance. They showed how a higher margin of COP improvement was obtained for those fluids for which increasing mass fluxes entailed a higher increase of heat transfer coefficient compared to pressure drop. They ad-

ditionally discussed how some fluid properties, such as vapour density and refrigerant temperature drop due to pressure drop, were influencing the trends. Maldistribution is another aspect to consider, since non-favourable thermo-physical properties (like the ones showed for butane in Table 10) implied higher performance degradation due to such effects. Choosing a PHE design leading to a lower impact of both end plates and liquid/vapour maldistribution is therefore particularly relevant for fluids with higher pressure drop sensitivity. For example optimizing the PHE design for butane in the chosen case study, would likely lead to higher benefits in terms of performance improvement compared to the other working fluids. This must also be considered when choosing empirical design criteria to size PHE, e.g. limiting velocities or pressure drop. Mancini et al. (2018c) showed how the usually employed design approaches do not necessarily lead to an optimal design for different working fluids, since different refrigerants are differently sensitive to pressure drop. This is in agreement with the findings of this work, which further stresses the importance of understanding maldistribution effects and of discriminating if it is relevant to consider them or to optimize the PHE design.

It is relevant to mention that the application of the simulation framework consisted of an economic analysis to study the effect of maldistribution on the operating costs of the heat pump. The results are strongly dependent on the assumption of this particular case study, especially regarding the values chosen for electricity cost and revenue from selling heat. Moreover, it was considered that the heat source comes at no cost from internal excess heat recovery from the data centre. These assumptions might completely change for different applications of heat pump integration, thereby stressing again that the economic analysis must be solely taken as an explanatory example of the procedure presented in the paper.

This study was focused on maldistribution effects in PHE evaporators only, thus neglecting potential maldistribution issues related to condenser design. Specifically, no liquid/vapour non-uniform distribution can occur at the condenser inlet, since the refrigerant is superheated vapour, hence only the effect of end plates may potentially be considered. Previous study by Zühlsdorf et al. (2018a) showed however that evaporator design affects the performance of heat pumps using mixed refrigerant to a larger extent compared to the condenser, and it was thus decided to limit the focus of this study on evaporator performance only.

Note that liquid/vapour maldistribution was evaluated by carrying out a sensitivity study on different slopes of vapour quality variation at the channel inlets. This was based on the assumption of linear vapour quality profiles, as experimentally shown for tubular manifolds for compact HEXs in Vist and Pettersen (2004). Moreover, a maximum variation of 0.25 was imposed as input to the model. Further experiments should therefore be carried out in order to validate the linear assumptions, as well as the slope of the distribution. Both evaporator and heat pump COP resulted to be largely affected, by limiting the maximum difference of the inlet vapour quality to 0.25, with maximum deviations due to liquid/vapour maldistribution obtained for butane of -8.5% and 4.7%, respectively. For a higher degree of maldistribution, it is thus expected to obtain even larger degradation of both PHE and heat pump performance.

Though not the focus of the present study, it is important to point out one aspect of condenser design and pressure drop prediction. The results of Table 8 showed that the frictional pressure drop evaluated using the Yan et al. (1999) correlation resulted in very low values of the frictional contribution. This led, for the case of propane, to have a dominant effect of gravity pressure recovery. However, it is again stressed that the conclusion on the dominating effect of gravity pressure recovery is strictly related to the chosen prediction method for frictional pressure drop, and using correlations recently published by Tao and Ferreira (2019) or Zhang et al. (2019) could lead to opposite results. However, Mancini et al. (2019) showed that the influence of condenser pressure drop is not relevant for the heat pump COP of the same case study and fluids considered in the present paper. The results on evaporator maldistribution effects presented in this paper are thus not sensitive to the chosen prediction method and to the resulting condenser design.

5. Conclusions

A coupled PHE-heat pump modelling framework was developed to evaluate the impact of end plates and liquid/vapour maldistribution at the inlet of PHE evaporators on heat transfer performance, heat pump COP and costs. A maldistribution parameter Δx was defined to describe the vapour quality difference between the outer-most evaporator channels. The procedure was applied to a case study, for which the pure fluids butane and propane and the two zeotropic mixtures propylene/butane and CO_2/DME were previously found as optimal working fluids.

A general reduction of the evaporator heat flow rate was obtained as a result of end plate effects. Propylene/butane was found as the working fluid that was most sensitive to end plates, with a 4.8% reduction of evaporator heat flow rate, followed by CO_2/DME and the two pure fluids. Butane was instead most sensitive to liquid/vapour maldistribution, with an impact equal to -8.5%, leading to an overall evaporator performance reduction of -10.5%. The high sensitivity was found to be related to the PHE design, and especially to the low working fluid vapour density, the higher temperature drop due to pressure drop and low evaporation pressure.

The impact of maldistribution effects was also translated into an estimation of COP degradation. The relative ranking of the working fluids was shown to be similar to the ones for the evaporator, i.e. with butane as the most sensitive fluid, with -5.9% due to end plates and vapour quality non-uniformity effects altogether and propane the least affected (-2.5%). The reduction of COP was lower compared to the evaporator performance degradation, around half of the value of all the working fluids.

The economic analysis showed the impact of COP reduction on the specific cost of heat, compressor running costs and revenue from the heat sink. It was shown that, despite a decrease in the electricity needed to run the compressor during off-design operation due to maldistribution, a lower yearly production of energy was achieved for a fixed number of operating hours. Therefore, an increase of the cost of heat was obtained, together with a steep drop in the revenue from selling the heat to the DH network. The economic analysis was highly dependent on the case study and related assumptions.

The results showed that both end plates and liquid/vapour maldistribution can have a considerable effect on evaporator and cycle performance, depending on the working fluid, PHE design, and case study. The presented simulation framework can be used as a comprehensive analysis tool to evaluate the impact on different PHE designs, with different rates of imposed maldistribution, on the thermodynamic and economic feasibility of heat pumps and to compare different refrigerants.

Acknowledgments

This research was funded by Innovations Fund Denmark - The Danish Council for Strategic Research in Sustainable Energy and Environment - under the project title “THERMCYC - Advanced thermodynamic cycles utilizing low temperature heat sources”. The first author acknowledges the support from the Modelling and Optimization Consortium (MOC) of the Center for Environmental Energy Engineering (CEEE) at University of Maryland.

References

ALFA LAVAL (2018). Alfa Laval, AlfaQ series http://gasketed-plate-and-frame-heat-exchangers/alfaq/gasketed-plate-and-frame-heat-exchangers/alfaq/.

Amalfi, R., Vakili-Farahani, F., Thome, J., 2016. Flow boiling and frictional pressure gradients in plate heat exchangers. Part 2: comparison of literature methods to database and new prediction methods. Int. J. Refrig. 61, 185–203. doi:10.1016/j.ijrefrig.2015.07.009.

Bassiouny, M., Martin, H., 1984a. Flow distribution and pressure drop in plate heat exchangers I U-type arrangement. Chem. Eng. Sci. 39 (4), 693–700. doi:10.1016/0009-2509(84)80176-1.

Bassiouny, M., Martin, H., 1984b. Flow distribution and pressure drop in plate heat exchangers II Z-type arrangement. Chem. Eng. Sci. 39 (4), 701–704.

Bell, I.H., Wronski, J., Quoilin, S., Lemort, V., 2014. Pure and pseudo-pure fluid thermophysical property evaluation and the open-source thermophysical property library coolprop. Ind. Eng. Chem. Res. 53 (6), 2498–2508. doi:10.1021/ie4033999.

Bell, K., Ghaly, M., 1973. An approximate generalized design method for multicomponent/partial condenser. AIChE Symp. Ser. 69, 72–79.

Bobbili, P.R., Sunden, B., Das, S.K., 2006. An experimental investigation of the port flow maldistribution in small and large plate package heat exchangers. Appl. Therm. Eng. 26 (16), 1919–1926. doi:10.1016/j.applthermaleng.2006.01.015.

Brignoli, R., Brown, J.S., Skye, H.M., Domanski, P.A., 2017. Refrigerant performance evaluation including effects of transport properties and optimized heat exchangers. Int. J. Refrig. 80, 52–65. doi:10.1016/j.ijrefrig.2017.05.014.

Chisholm, D., 1967. A theoretical basis for the Lockhart-Martinelli correlation for two-phase flow. Int. J. Heat Mass Transf. 10 (18), 1767–1778. doi:10.1016/0017-9310(67)90047-6. http://www.sciencedirect.com/science/article/pii/0017931067900476

Cooper, M., 1984. Heat flow rates in saturated nucleate pool boiling - a wide ranging examination using reduced properties. Adv. Heat Transf. 16, 59–156.

Eldeeb, R., Aute, V., Radermacher, R., 2016. An improved approach for modeling plate heat exchangers based on successive substitution in alternating flow directions. In: Proceedings of the International Refrigeration and Air Conditioning Conference, Purdue University, US. http://docs.lib.purdue.edu/iracc/1684

Godbole, P.V., Tang, C.C., Ghajar, A.J., 2011. Comparison of void fraction correlations for different flow patterns in upward vertical two-phase flow. Heat Transf. Eng. 32 (10), 843–860. doi:10.1080/01457632.2011.548285.

Gong, J., Gao, T., Yuan, X., Huang, D., 2008. Effects of air flow maldistribution on refrigeration system dynamics of air source heat pump chiller under frosting conditions. Energy Convers. Manag. 49 (6), 1645–1651. doi:10.1016/j.enconman.2007.11.004.

Granryd, E., Ekroth, I., Lundqvist, P., Melinder, Å., Palm, B., Rohlin, P., 2009. Refrigerating Engineering. Royal Institute of Technology, KTH, Department of Energy Technology, Division of Applied Thermodynamics and Refrigeration.

Jensen, J.K., Kærn, M.R., Ommen, T.S., Brix, W., Reinholdt, L., Elmegaard, B., 2015. Effect of liquid/vapour maldistribution on the performance of plate heat exchanger evaporators. In: Proceedings of the Twenty-Fourth IIR International Congress of Refrigeration.

Jin, S., Hrnjak, P., 2017a. A new method to simultaneously measure local heat transfer and visualize flow boiling in plate heat exchanger. Int. J. Heat Mass Transf. 113, 635–646. doi:10.1016/j.ijheatmasstransfer.2017.04.116.

Jin, S., Hrnjak, P., 2017b. Effect of end plates on heat transfer of plate heat exchanger. Int. J. Heat Mass Transf. 108, 740–748. doi:10.1016/j.ijheatmasstransfer.2016.11.106.

Kærn, M.R., Brix, W., Elmegaard, B., Larsen, L.F.S., 2011. Performance of residential air-conditioning systems with flow maldistribution in fin-and-tube evaporators. Int. J. Refrig. 34 (3), 696–706. doi:10.1016/j.ijrefrig.2010.12.010.

Lemmon, E., Bell, I., Huber, M., McLinden, M., 2018. NIST Standard Reference Database 23: Reference Fluid Thermodynamic and Transport Properties - REFPROP, Version 10.0.

Li, W., Hrnjak, P., 2016. Single Phase Pressure Drop and Flow Distribution in Brazed Plate Heat Exchangers. In: Proceedings of the International Refrigeration and Air Conditioning Conference. Purdue University, p. Paper1812. http://docs.lib.purdue.edu/iracc/1812

Li, W., Hrnjak, P., 2018. An experimentally validated model of single-phase flow distribution in brazed plate heat exchanger. In: Proceedings of the Seventeenth International Refrigeration and Air Conditioning Conference at Purdue.

Lockhart, R., Martinelli, R., 1949. Proposed correlation of data for isothermal two-phase, two-component flow in pipes. Chem. Eng. Prog. 45 (1), 39–48.

Madanan, U., Nayak, R., Chatterjee, D., Das, S.K., 2018. Experimental investigation on two-phase flow maldistribution in parallel minichannels with U-type configuration. Can. J. Chem. Eng. 96 (8), 1820–1828. doi:10.1002/cjce.23112.

Mader, G., Palm, B., Elmegaard, B., 2015. Maldistribution in air-water heat pump evaporators. Part 1: effects on evaporator, heat pump and system level. Int. J. Refrig. 50, 207–216. doi:10.1016/j.ijrefrig.2014.07.006.

Mancini, R., 2018. Numerical models for assessing the performance of heat pumps with maldistribution effects in plate heat exchanger evaporators doi:10.11583/DTU.7565279. https://data.dtu.dk/s/74a2e50d0cf215425d26

Mancini, R., Aute, V., Brix Markussen, W., Elmegaard, B., 2018a. Impact of liquid/vapor maldistribution on the performance of a plate heat exchanger evaporator for pure and mixed refrigerants. In: Proceedings of the Seventeenth International Refrigeration and Air Conditioning Conference at Purdue, West Lafayette, Indiana (US).

Mancini, R., Kjær Jensen, J., Brix Markussen, W., Elmegaard, B., 2018b. Comparison of heat transfer and pressure drop correlations for evaporation of zeotropic mixtures in plate heat exchangers. In: Proceedings of the Thirteenth IIR-Gustav Lorentzen Conference on Natural Refrigerants. International Institute of Refrigeration doi:10.18462/iir.gl.2018.1261.

Mancini, R., Zühlsdorf, B., Kjær Jensen, J., Brix Markussen, W., Elmegaard, B., 2018. Deriving guidelines for the design of plate evaporators in heat pumps using zeotropic mixtures. Energy 156. doi:10.1016/j.energy.2018.05.026.

Mancini, R., Zühlsdorf, B., Markussen, W.B., Elmegaard, B., 2019. Design recommendations for plate heat exchangers in heat pumps using pure and mixed refrigerants. In: Proceedings of the Twenty-Fifth IIR International Congress of Refrigeration, Montreal, Canada doi:10.18462/iir.icr.2019.853.

Martin, H., 1996. A theoretical approach to predict the performance of chevron-type plate heat exchangers. Chem. Eng. Process. 35 (4), 301–310. doi:10.1016/0255-2701(95)04129-X.

Mathworks, 2017a. fsolve - solve systems of nonlinear equations, Matlab 2017b. https://www.mathworks.com/help/optim/ug/fsolve.html

Mathworks, 2017b. Matlab R2017b. https://www.mathworks.com/help/matlab/

Moran, M., Shapiro, H., Boettner, D., Bailey, M., 2018. Fundamentals of Engineering Thermodynamics. Wiley. https://books.google.dk/books?id=QHJIDwAAQBAJ

Mueller, A.C., Chiou, J.P., 1988. Review of various types of flow maldistribution in heat exchangers. Heat Transf. Eng. 9, 36–50. doi:10.1080/01457638808939664.

Palm, B., Claesson, J., 2006. Plate heat exchangers: calculation methods for single and two-phase flow. Heat Transf. Eng. 27 (4), 88–98. doi:10.1080/01457630500523949.

Rao, B.P., Das, S.K., 2004. An experimental study on the influence of flow maldistribution on the pressure drop across a plate heat exchanger. J. Fluids Eng. Trans. ASME 126, 680–691. doi:10.1115/1.1779664.

Rao, B.P., Sunden, B., Das, S.K., 2005. An experimental and theoretical investigation of the effect of flow maldistribution on the thermal performance of plate heat exchangers. J. Heat Transf. Trans. ASME 127. doi:10.1115/1.1860568.

Sardesai, R.G., Shock, R.A., Butterworth, D., 1982. Heat and mass transfer in multicomponent condensation and boiling. Heat Transf. Eng. 3 (3-4), 104–114. doi:10.1080/01457638108939589.

Shah, R.K., Sekulic, D.P., 2002. Fundamentals of Heat Exchanger Design. Wiley doi:10.1002/9780470172605.

Silver, L., 1947. Gas cooling with aqueous condensation. Ind. Chem. Chem. Manuf. 23 (269), 380–386.

Smith, S.L., 1969. Void fractions in two-phase flow: a correlation based upon an equal velocity head model. Proc. Inst. Mech. Eng. 184 (1), 647–664. doi:10.1243/PIME_PROC_1969_184_051_02.

Srihari, N., Das, S.K., 2006. Transient response of multi-pass plate heat exchangers considering effect of flow maldistribution. Chem. Eng. Process. 47 (4), 695–707. doi:10.1016/j.cep.2006.12.011.

Srihari, N., Prabhakara Rao, B., Sunden, B., Das, S.K., 2005. Transient response of plate heat exchangers considering effect of flow maldistribution. Int. J. Heat Mass Transf. 48 (15), 3231–3243. doi:10.1016/j.ijheatmasstransfer.2005.02.032.

SWEP International AB, 2015. SWEP Products. https://www.swep.net/products/

Tao, X., Ferreira, C.A.I., 2019. Heat transfer and frictional pressure drop during condensation in plate heat exchangers : assessment of correlations and a new method. Int. J. Heat Mass Transf. 135, 996–1012. doi:10.1016/j.ijheatmasstransfer.2019.01.132.

Tereda, F.A., Srihari, N., Sunden, B., Das, S.K., 2007. Experimental investigation on port-to-channel flow maldistribution in plate heat exchangers. Heat Transf. Eng. 28 (5), 435–443. doi:10.1080/01457630601163769.

Thome, J.R., Shakir, S., 1987. A new correlation for nucleate pool boiling of aqueous mixtures. AIChE Symp. Ser. 83 (257), 46–51.

Vakili-Farahani, F., Amalfi, R.L., Thome, J.R., 2015. Two-phase heat transfer and pressure drop within plate heat exchangers. In: Thome, J.R., Kim, J. (Eds.), Encyclopedia of Two-Phase Heat Transfer and Flow II: Special Topics and Applications. Volume 2: Boiling Using Enhanced Surfaces, Plate Heat Exchangers and Two-Phase Devices. Chapter 4.. World Scientific Publishing, pp. 145–215. doi:10.1142/9789814623285_0011.

Vist, S., Pettersen, J., 2004. Two-phase flow distribution in compact heat exchanger manifolds. Exp. Therm. Fluid Sci. 28, 209–215. doi:10.1016/S0894-1777(03)00041-4.

Yan, Y.-Y., Lio, H.-C., Lin, T.-F., 1999. Condensation heat transfer and pressure drop of refrigerant R-134a in a plate heat exchanger. Int. J. Heat Mass Transf. 42 (6), 993–1006. doi:10.1016/S0017-9310(98)00217-8.

Zhang, J., Kærn, M.R., Ommen, T., Elmegaard, B., Haglind, F., 2019. Condensation heat transfer and pressure drop characteristics of R134a, R1234ze(E), R245fa and R1233zd(E) in a plate heat exchanger. Int. J. Heat Mass Transf. 128, 136–149. doi:10.1016/j.ijheatmasstransfer.2018.08.124.

Zühlsdorf, B., Jensen, J.K., Elmegaard, B., 2019. Heat pump working fluid selection economic and thermodynamic comparison of criteria and boundary conditions. Int. J. Refrig. 98, 500–513. doi:10.1016/j.ijrefrig.2018.11.034.

Zühlsdorf, B., Kjær Jensen, J., Cignitti, S., Madsen, C., Elmegaard, B., 2018a. Analysis of temperature glide matching of heat pumps with zeotropic working fluid mixtures for different temperature glides. Energy 153, 650–660. doi:10.1016/j.energy.2018.04.048.

Zühlsdorf, B., Meesenburg, W., Ommen, T., Thorsen, J., Brix Markussen, W., Elmegaard, B., 2018b. Improving the performance of booster heat pumps using zeotropic mixtures. Energy 154, 390–402. doi:10.1016/j.energy.2018.04.137.

Derivation of guidelines for the design of plate evaporators in heat pumps using zeotropic mixtures

Roberta Mancini[a], Benjamin Zühlsdorf[b] and Brian Elmegaard[c]

[a] Technical University of Denmark, Kgs. Lyngby, Denmark, robman@mek.dtu.dk
[b] Technical University of Denmark, Kgs. Lyngby, Denmark, bezuhls@mek.dtu.dk
[c] Technical University of Denmark, Kgs. Lyngby, Denmark, be@mek.dtu.dk

Abstract:

The present work derives design recommendations for plate heat exchangers used for evaporation of zeotropic mixtures in heat pumps. A parametric study is conducted on the geometry of the heat exchanger, and the analysis is carried out for four working fluids, based on a case study of heat pump integration in a spray drying facility. A numerical model of the evaporator is combined with cycle calculations, for estimating the impact of heat transfer area and pressure drop on the coefficient of performance and costs. Common trends are obtained as optimal configurations for the four considered fluids. It is recommended to minimize the hydraulic diameter by employing high corrugation height over low corrugation pitch. Moreover, an optimal range is found for the liquid Reynolds number at the evaporator inlet. The suggested values vary between 500 and 2000, depending on the fluid. Lastly, the trade-off between minimization of area and pressure drop is found by assessing the relative impact on costs of the heat exchanger area and pressure losses of both working fluid and heat source. The result shows that it is not always convenient to minimize the heat transfer area, since the mixture pressure drop negatively influences compressor investment and operating costs.

Keywords:

Plate heat exchangers, Waste heat recovery, Zeotropic mixtures, Heat pumps, Cost optimization.

1. Introduction

Implementation of energy efficiency measures in the industry sector is becoming imperative due to the increasing awareness of the environmental effects of fossil fuel consumption. The total energy consumption of the Danish industry sector accounted for 112 PJ in 2012. Drying processes alone constituted 19% of the consumption. Moreover, drying processes are a relevant source of waste heat, specifically around 7% of the total industrial waste heat [1]. Waste heat recovery is accordingly one suitable opportunity for increasing energy efficiency of drying processes. One possibility of recovering low grade thermal energy is the integration of heat pumps, which are able to lift the temperature level of the waste heat, in order to meet the energy needs of many industrial sectors [2].

Zeotropic mixtures constitute one possibility of optimizing the heat pump coefficient of performance (COP) by reducing the irreversibility in the heat exchangers. In fact, the exergy destruction in the evaporator and condenser due to finite temperature difference between the working fluid and the heat source or sink can be reduced by matching the mixture temperature glide with the heat source or heat sink temperature profiles [3].

However, the use of zeotropic mixtures implies a degradation of the heat transfer coefficient during both evaporation and condensation. During flow boiling in the heat exchanger channels, an additional mass diffusion resistance is created because of the more readily evaporation of the more volatile component. This phenomenon correspondingly entails an increase of the saturation temperature of the mixture, which becomes richer in the less volatile component. Moreover, a decrease of the nucleate boiling contribution is estimated, together with a degradation of the mixture transport properties with respect to pure components. Altogether, the aforementioned mechanisms lead to

worse heat transfer for zeotropic mixtures compared to pure fluids [4]. For this reason, when optimizing cycle performances by means of zeotropic working fluid mixtures, it is of high relevance to optimize the design of the heat transfer equipment, in order to avoid investing in higher heat transfer areas for the heat exchangers.

Plate Heat Exchangers (PHEs) offer a suitable solution for applications with zeotropic working fluid mixtures, since it is possible to achieve high heat transfer coefficients due to the flow turbulence generated by the characteristic plate corrugation patterns. Chevron-type plates are commonly employed to create such corrugations. Moreover, PHEs offer a modular and flexible solution, i.e. variation of thermal capacity can be simply obtained by changing the number of plates in the frame. Plate heat exchangers consist of thin parallel plates stacked together in order to form channels for fluid flow. Gasketed-type PHE consist of plates sealed by gaskets and held together by a frame. For higher operating temperature and pressure, the plates can be sealed together by brazing. The flow can be arranged in counter-current, thus making them a viable option to achieve the glide matching between zeotropic mixture and heat source or sink. At current state-of-the-art, the operability limits of gasketed-type PHEs is limited to 20.4 bar and 150°C as maximum pressure and temperature, respectively, hence offering a reasonable range for operation as evaporators in heat pumps [5].

Scientific literature provides a number of studies focusing on PHE design optimization for low temperature applications, most of them for organic Rankine cycles (ORCs). Gut and Pinto (2004) [6] developed an optimization program to determine the optimal configuration of PHEs for a given imposed maximum pressure drop and inlet fluid flow velocity; the optimization was based on the minimization of the heat transfer area. The work did not take an optimal choice of the pressure and velocity limitations for different applications into account, and did not consider the impact of the PHE on the thermodynamic cycle. Karellas et al. (2012) [7] investigated the influence of supercritical ORC parameters on PHE design. The study fixed the corrugation geometry and hydraulic diameter of the evaporator for the analysis, and assessed the difference of required heat transfer area for different fluids and cycle parameters, yet without considering pressure drops. Wang et al. (2013) [8] performed a multi-objective optimization procedure with the aim of minimizing heat transfer area and pressure losses of a PHE condenser in an ORC. The results showed the sensitivity of three design parameters of the PHE, namely plate length, width and corrugation height, on the heat exchanger area and pressure drop. Rohmah et al. (2014) [9] investigated the influence of plate spacing on condenser design for a ORC. It was shown that increasing the plate spacing led to an increase of the required area but a decrease of related pressure drop. Walraven et al. (2014) [10] developed a combined optimization procedure of a low temperature heat source ORC and heat exchangers, considering both PHE and shell and tube configurations. The optimization was aimed at maximizing the cycle exergy efficiency by changing both cycle and heat exchanger design parameters. The results showed that optimal PHE configurations performed better than shell and tube for most working fluids.

The main objective of the present work is to derive design recommendations for PHEs used as evaporator in heat pumps using zeotropic mixtures. The methodology is based on assessing the impact of the PHE design parameters on the cycle COP and Net Present Value (NPV). The analysis is based on four different working fluid mixtures, found as the best solutions for heat pump integration in a spray drying facility in [3]. The study focuses on the evaporator section of the PHE because the evaporator outlet condition is directly affecting the compressor work in the cycle. In order to carry out the analysis, a design model is developed to assess the required heat transfer area and resulting pressure losses for the working fluid and the heat source. The heat exchanger design model is coupled with heat pump calculations and the pressure drops are taken into account for the estimation of the COP and NPV of the cycle. The results are analysed in order to derive more general design guidelines for the evaporator section, which can be used in similar applications.

The framework of the analysis is given by a previously conducted study [3], assessing the integration of high temperature heat pumps in a spray drying facility, exploiting excess heat at 65°C for pre-heating of air up to 120°C. The advantage of using zeotropic mixtures was demonstrated by comparing the COP and NPV of a simple configuration of a vapor compression heat pump, in which

the working fluid was varied based on binary mixtures formed by combinations of six different hydrocarbons. It was shown that the best fluids corresponded to the ones better matching the heat sink and source temperature profiles, and a group of optimal mixtures was found. The sizing of the PHEs for economic calculations was based on a minimum pinch point temperature difference and maximum allowable velocities for liquid and gas phases, based on limiting values found in literature [11], and posing a constraint on the free flow area of the fluids in both evaporator and condenser. This criterion is based on empirical experience from manufacturers and the extension to other type of applications (e.g. phase change and/or zeotropic mixtures) is not trivial. Therefore, the derivation of specific design criteria for PHE design in such applications is the research question behind this work.

2. Methods

In order to derive design guidelines, a parametric study was conducted on the geometry of the PHE, used in the evaporator. For the assessment of the impact of the heat exchanger design on the cycle COP and NPV, a detailed numerical model of the heat exchanger was built and integrated with the previously presented heat pump model [3] in the Matlab [12] simulation environment. The working fluid properties were calculated by means of the database Refprop [13], using standard equation of states and mixing parameters.

Four different analyses were done to highlight common design trends of geometrical and fluid flow parameters, based on the four best working fluids found from the previous study [3]. Table 1 presents the evaporation pressure of the four cases, well below the maximum operability limit, showing that PHEs constitute a feasible design for all the cases. The working fluids are given by the four hydrocarbon mixtures reported in Table 1 with relative compositions. The heat pump was designed for waste heat recovery of air, with an available mass flow rate of 14.8 kg/s and inlet and outlet temperatures of 65°C and 40°C, resulting in a heat source capacity of 1544 kW. A minimum pinch temperature difference of 10°C was imposed over the heat exchanger. For all the cases, a minimum super-heating of 5°C before the compressor is included in the evaporator.

Table 1. Summary of the four cases considered in the analysis, with required evaporation pressure and results obtained from the study [3]

Case	Working fluid	p_{ev}, bar	$\dot{V}_{comp_{in}}$, m^3/h	COP, -	NPV, € 10^3
I	Propane – Iso-Pentane (0.5/0.5)	4.9	2220	3.08	921
II	Propane – n-Pentane (0.8/0.2)	8.4	1487	3.04	998
III	Propane – n-Pentane (0.4/0.6)	3.0	3288	3.02	419
IV	Butane – Hexane (0.9/0.1)	2.5	3668	3.07	509

2.1. Plate Heat Exchanger parametric analysis

The geometrical parameters of PHEs were given by the plate size, namely width W and length L_{th}, the number of channels N_{ch} and the corrugation characteristics, i.e. the corrugation height b, the corrugation pitch Λ, the chevron angle β and the plate thickness t. The plate thickness t was fixed to a constant value usually found in common PHE design, minimizing the conductive heat transfer resistance and providing acceptable mechanical strength. The port diameter size D_p was chosen between two values, depending on the plate size W. Fig. 1 shows the plate geometry and corrugations. The corrugation parameters determine the hydraulic diameter of the PHE channels, hence defining the fluid conditions during the flow inside the channels. The hydraulic diameter was estimated by (1), describing the relation between corrugation height b and enlargement factor Φ. The latter represents the ratio between the actual area of the corrugated plate and the projected flat plate area, and it is expressed by (2) as function of the corrugation pitch and height [14].

$$D_h = \frac{2b}{\Phi} \tag{1}$$

$$\Phi = \frac{1}{6}\left(1 + \sqrt{1 + \left(\frac{\pi b}{\Lambda}\right)^2} + \sqrt{1 + \frac{1}{2}\left(\frac{\pi b}{\Lambda}\right)^2}\right) \quad (2)$$

The design parameters were varied among the values reported in Table 2, investigating all possible combinations. The plate length, shown as L_{th} in Fig. 1, was calculated from the input geometry by means of the design model in order to match the heat transfer demand.

Table 2. Geometrical parameters of the PHE, with values considered in the parametric analysis

Parameter	Unit	Values
W	m	0.1 – 0.3 – 0.5 – 0.7 – 0.9
N_{ch}	-	10 – 20 – 40 – 70 – 100
β	°	20 – 45 – 60 – 80
b	mm	2 – 5 – 8
Λ	mm	2 – 5 – 8
t	mm	0.5
D_p	m	0.05 – 0.15

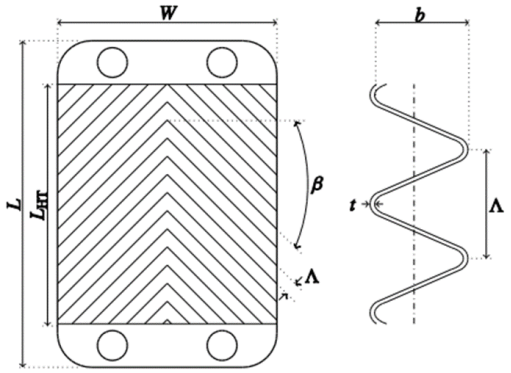

Fig. 1. Schematic view of a chevron-type PHE [15]

2.2. Mathematical model

In this section, the different parts of the numerical design model are presented and discussed, i.e. the heat transfer and fluid flow model describing the heat exchanger and the integration with the heat pump model, including economic calculations of the cycle.

2.2.1. Plate heat exchanger numerical model

The numerical model of the PHE was based on a one-dimensional discretization along the flow direction. The discretization took into consideration equidistant steps of enthalpy rate change for both the fluids. The heat transfer and fluid flow conditions were solved for each control volume (CV), hence heat transfer area and pressure drops were calculated for each element. The temperatures for heat transfer calculations were estimated at the CV centre points, interpolating the values between the nodes. Pressures and enthalpies were calculated at the nodes. The input to the PHE model were given by the cycle calculations, i.e. known inlet mass flow and thermodynamics for the two fluids, as well as outlet enthalpies. The model calculated the outlet temperature and pressure levels.

The heat transfer was solved by calculating the overall heat transfer coefficient in each CV [14], expressed by (3), with R^i_{wall} representing the specific conductive resistance of the plate wall, and h^i_{mix} and h^i_w representing the heat transfer coefficients of the mixture and water for the *i*-th CV.

$$U^i = \left(\frac{1}{h^i_{mix}} + R^i_{wall} + \frac{1}{h^i_w}\right)^{-1} \quad (3)$$

The heat transfer coefficients were calculated for each control volume, since they were dependent on the fluid properties, temperature and specific heat flux. The water side heat transfer coefficient was modelled by using the correlation of Martin (1996) [16], which is valid for PHEs with chevron-type corrugations and allows the estimation of the friction factor and Nusselt number for single-phase flow. The mixture heat transfer coefficient was estimated according to the CV location in the PHE; more specifically, if the fluid was in the evaporator section, a specific correlation developed for zeotropic mixtures was employed in order to consider the mixture effects on heat transfer. The correlation of Jung (1989) [17] was chosen for the analysis, based on a superposition model with two contributions from convective and nucleate boiling, and correction parameters taking into

consideration the deviation from ideal mixing. The super-heating section was modelled by considering the same correlation used for water, being the working fluid in the single-phase region.

The fluid flow was modelled by calculating the pressure level at each node of the CVs. The pressure drop along the channel derives from both friction and acceleration contributions. The pressure drop of the water flow and of the mixture flow in the super-heating section were calculated by considering the contributions of friction and acceleration, by using (4) [14], where the friction factor f derives from Martin (1996) [16]. The losses are expressed as function of the length of the CV, the fluid properties, mass velocity G and equivalent diameter D_e, equal to $2b$.

$$\Delta p_{\text{core}} = \Delta p_{\text{fr}} + \Delta p_{\text{acc}} = 4f\Delta L \frac{G^2}{2D_e}\left(\frac{1}{\rho}\right)_m + \left(\frac{1}{\rho_o} - \frac{1}{\rho_i}\right) G^2 \tag{4}$$

The frictional and acceleration pressure losses for the two-phase region of the zeotropic mixture were calculated by means of the Jung and Radermacher (1989) [18] correlation for the frictional contribution, while the Martinelli and Nelson (1984) [4] two-phase slip flow model was adopted to account for the acceleration term. In addition to the core pressure drop, another term was added to the heat source pressure drop: the port pressure drop of the PHE inlet was considered, since it has an impact on the overall pumping costs for the water side. On the other hand, it was decided to neglect the port pressure drop of the evaporator inlet for the mixture, since the throttling valve will implicitly balance the effect. The port pressure drop was calculated as reported in Shah (2002) [14].

The sizing procedure can be outlined as follow. First, the thermodynamics at each node of the heat exchanger was determined by assuming constant pressure over the length. The energy balance in each CV allowed the calculation of the UA value. The discretized area required for the heat transfer in each control volume was estimated by calculating the overall heat transfer coefficient *U*, as shown in (3). Once that the required length was determined from the area, the pressure drop of both fluids was determined and to the values of temperature and pressure at each node of the heat exchanger were found. The procedure of the PHE model is summarized in Fig. 2 (a). The convergence criterion was defined by a tolerance fixed to 10^{-4}. For the parametric analysis, a number of 20 control volumes and 21 nodes was used, chosen as a trade-off between computational cost and accuracy.

2.2.1.1. Analysis of flow parameters

When considering flow boiling of zeotropic mixtures, several parameters can be taken into account for a full description of the flow mechanism. Both vapour and liquid phases flow inside a channel, and the vapour and liquid mass flows and velocities strongly depend on the stage of the evaporation process. Moreover, the liquid and vapour phase compositions are not constant during evaporation of mixtures, because of the more volatile component evaporating first, hence a strong variation of the mixture properties was experienced during the process [4]. Despite the complexity of the physics, there is the need to choose a meaningful design parameter, which encapsulates information on the fluid, and on the conditions of the flow at some relevant positon along the PHE. Therefore, it was decided to analyse the influence of the Reynolds number of the liquid phase at the inlet of the evaporator. The parameter is defined by (5) [4], as function of the mass velocity G, vapor quality Q, channel hydraylic diameter D_h and viscosity of the liquid phase μ_L.

$$\text{Re}_L = \frac{G\,(1-Q)\,D_h}{\mu_L} \tag{5}$$

The mass velocity G was given by (6) [14], as function of the mass flow of the mixture and of the PHE geometrical parameters determining the free flow area , namely corrugation height b, plate width W and number of channels N_{ch}.

$$G = \frac{\dot{m}_{\text{mix}}}{bWN_{\text{ch}}} \tag{6}$$

The mass flux contains information on the fluid, as well as on the geometry of the PHE, i.e. hydraulic diameter, corrugation height, width and number of channels are considered for the calculation. Moreover Re_L was used for the estimation of the heat transfer coefficient in the correlations for flow boiling of zeotropic mixtures, hence its value was directly affecting the sizing of the PHE. Additionally, it was decided to analyse the behaviour of the Reynolds number at the location of evaporator inlet, because the inlet temperature and pressure are less affected by the pressure losses compared to the evaporator outlet. In fact, the inlet quality and viscosity were dependent only on the cycle configuration (state point at the evaporator inlet), and the design of the heat exchanger directly influenced the flow conditions at this position.

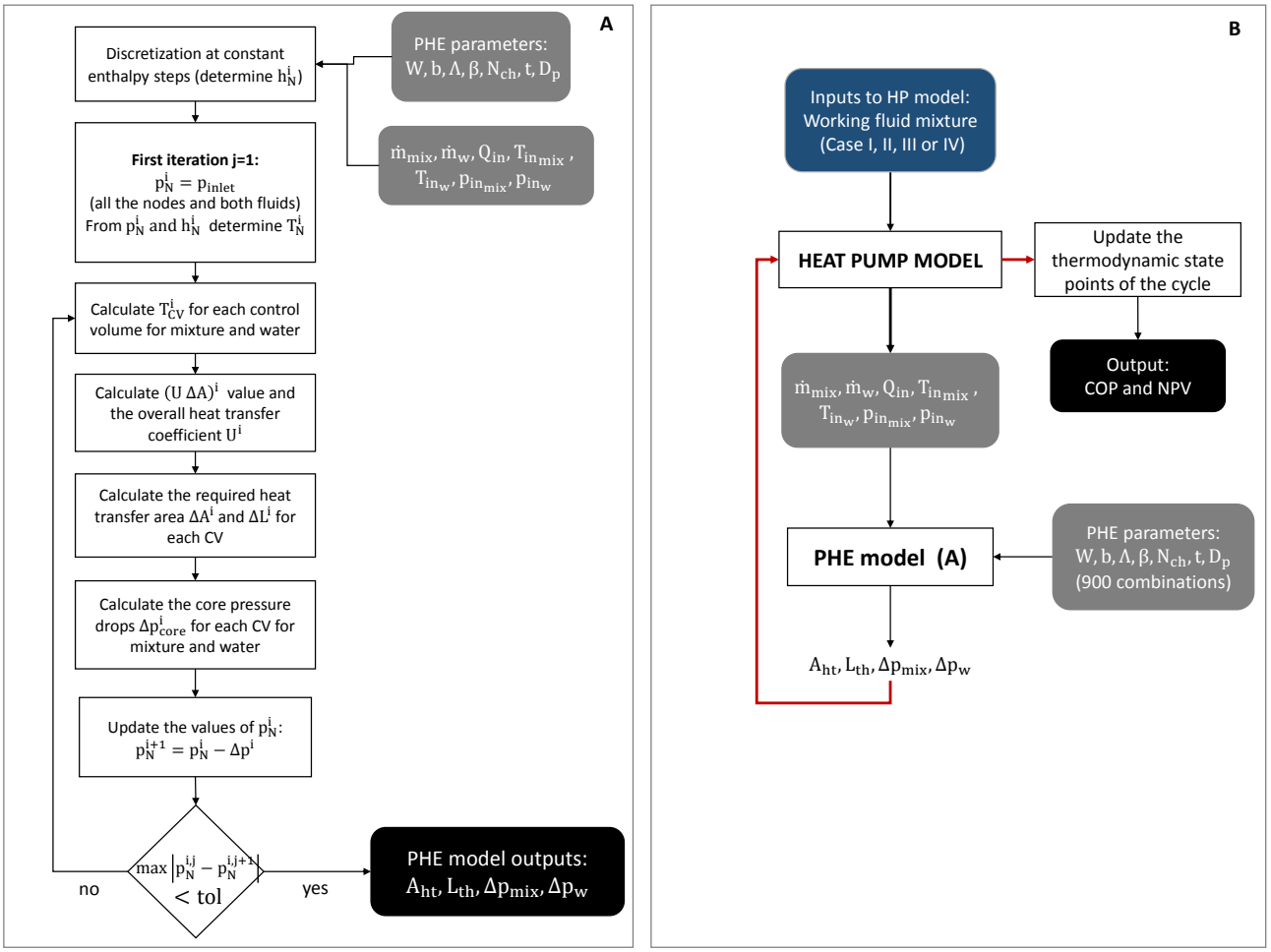

(a) (b)

Fig. 2. a) Procedure for PHE sizing and b) integration with the heat pump and overall methodology

2.2.2. Heat pump model and economic calculations

Fig. 2 (b) reports the procedure of the integration of the heat pump model with the PHE model. The procedure was carried for all the combinations of PHE design parameters and the four different working fluid mixtures. The heat pump was first solved for the calculation of the inlet and outlet states at the evaporator. Next, the PHE model solved the heat transfer and fluid flow equation, while determining the heat transfer area. This procedure was repeated for all the combinations of design parameters, each giving different required heat transfer areas and different outlet pressure and temperature (corrected by the pressure drop). The heat pump model received the output of the PHE model, and calculated the COP and the NPV again, by taking into account the updated temperature and pressure at the evaporator outlet. The COP was affected by the change in compressor power as function of the mixture pressure drop. On the other hand, different aspects of the PHE design

influenced the value of the NPV of the heat pump. The NPV was calculated by (7) [3], as function of the Total Capital Cost (TCI), Operation and Maintenance Cost (OMC), the Fuel Cost (FC_{hp}) due to the compressor, the required water pumping cost (FC_w), as well as the natural gas saving FC_{ng}.

$$NPV = -TCI - OMC - \frac{FC_{hp}}{CRF} - \frac{FC_w}{CRF} + \frac{FC_{ng}}{CRF} \tag{7}$$

OMC and F_{ng} are calculated as explained in [3], while the other contributions are adjusted according to the PHE model outputs. TCI accounts for the investment of condenser, compressor and evaporator. The latter was estimated using the sizing of the heat transfer area from the PHE model, while the condenser heat transfer area was fixed according to the design criterion applied in [3]. The TCI of each component was calculated from the Purchased Equipment Cost (PEC), scaled according to the component size with scaling factors reported by [19]. The TCI was increased by a factor 4.16 compared to the PEC, to account for the investment of the expansion of an existing facility, as reported in [19]. Since the compressor power was adjusted according to the PHE design, the investment cost varies accordingly. The running cost of the compressor, given by FC_{hp}, was adapted to the updated compressor power. The addition of the fuel cost term for the pressure losses of the heat source (water) side, is calculated by using (8), as function of the water mass flow rate $\dot{m}_w$, water density ρ_w, total water pressure drops $\Delta p_{w_{tot}}$,a pump efficiency η_{pump} equal to 95%, the electricity cost c_{el} assumed equal to 0.0783 €/kWh and annual operation hours τ_h equal to 7400 h/y.

$$FC_w = \frac{\dot{m}_w}{\rho_w}\frac{\Delta p_{w_{tot}}}{\eta_{pump}} c_{el}\tau_h \tag{8}$$

The interest and inflation rates were assumed equal to 7% and 2%, respectively, and then used for the estimation of the Capital Recovery Factor (CRF), with a plant economic lifetime of 20 years [19] [20]. The annual Operation and Maintenance Cost (OMC) were analogously to [3] calculated as a one-time fixed share of the initial investment cost of 20 % at the investment time, and the saving of natural gas consumption (F_{ng}) was calculated by considering a boiler efficiency of 90 % [19] [20] . The reader is referred to [3] for more details on how the heat pump model is built. Fig. 3 (a) shows the flow sheet of the heat pump model, with evaporator and condenser, and the processes occurring in the components. Fig. 3 (b) shows the log(p)-h diagram of the heat pump with and without pressure drops in the evaporator. It can be noticed how the outlet of the evaporator is affected by the pressure losses, thus changing the compressor power required. The pressure drop influences also the evaporator inlet location in the diagram, but to a lower extent compared to the outlet.

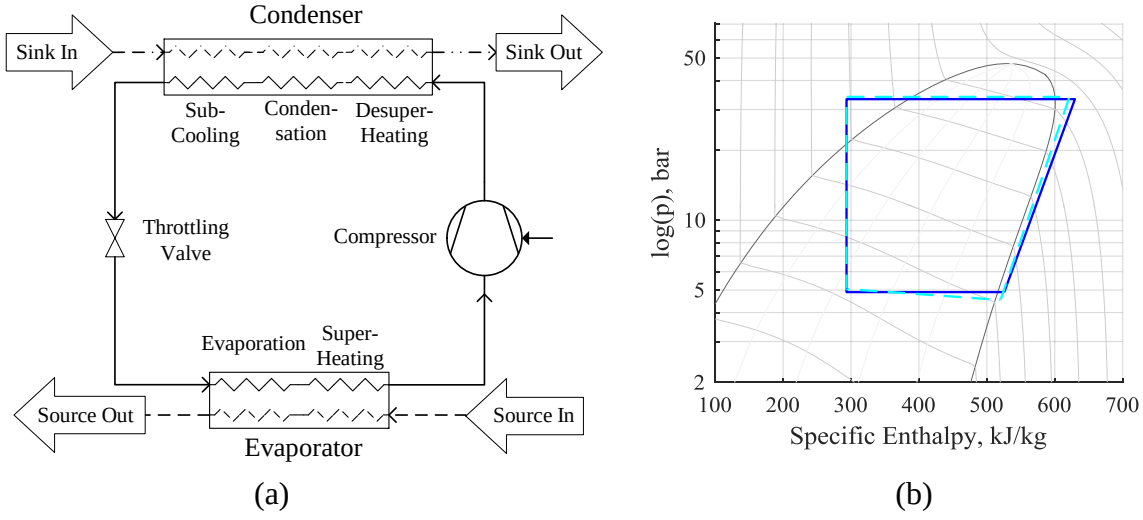

Fig. 3. (a) Flow sheet of the heat pump model and (b) log(p)-h diagram of the thermodynamic cycle without pressure drop (blue) and with 50 kPa pressure drop in the evaporator (light blue)

3. Results

3.1. Heat transfer area and pressure drop trade-off

Fig. 4 shows the NPV of the heat pump as function of the heat transfer area of the evaporator, for all the combinations of design parameters and for all the four zeotropic mixtures. Each point in the figure corresponds to one possible combination of the different design parameters. The colour scale represents the total pressure drop of the working fluid mixture. First, all the four cases considered reported similar trends on how the area and the pressure losses affect the performance of the system. By having high heat transfer area, the NPV decreased consistently because of the higher investment costs of the PHE. On the other hand, high pressure losses negatively affected the NPV even for those configurations with minimal PHE area.

This result highlights the importance of including the impact of pressure losses when assessing the profitability of the heat pump, since the impact on the NPV was relevant for all the cases. The optimal

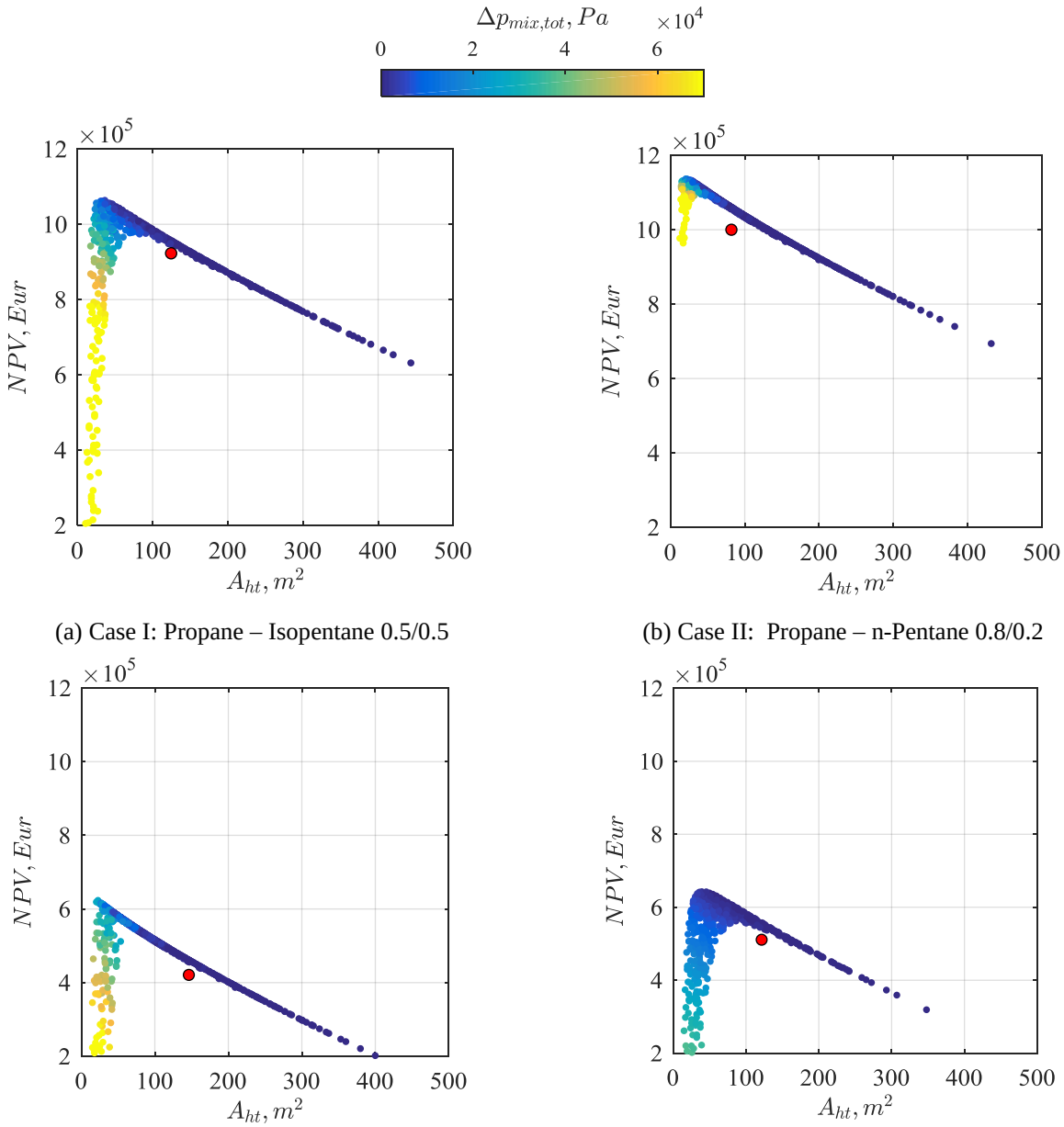

(a) Case I: Propane – Isopentane 0.5/0.5

(b) Case II: Propane – n-Pentane 0.8/0.2

(c) Case III: Propane – n-Pentane 0.4/0.6

(d) Case IV: n-Butane – n-Hexane 0.9/0.1

Fig. 4. NPV vs. PHE area, for Case I (a), Case II(b), Case III(c) and Case IV(d), with colour indicating the mixture pressure drop and red point showing the design criterion adopted in [3].

regions corresponded to combinations of design criteria giving small heat transfer area (hence low investment cost) together with reasonable pressure losses of the working fluid mixture. Values of pressure losses between 5 kPa and 30 kPa were optimal for all the four cases, as shown by the colour of the design points where NPV is maximal. Moreover, the red points in Fig. 4 indicate the design criterion adopted in the previous analysis of the case study [3]. As aforementioned, the design was based on posing a limitation on the inlet velocities of cold and hot fluids, not specifically derived for evaporation of zeotropic mixtures. It is shown that the economic optima did not coincide with the old design criterion, since a better NPV can be obtained by changing the design parameters in all the cases. The red point does not lie in the same design curve of the present analysis, since the reduction of required heat transfer area due to the pressure drop was not considered in the previous study [3].

The relative ranking of the four working fluid mixtures with respect to NPV was unchanged compared to the previous results [3], with Case I and Case II showing results with a more advantageous economy, i.e. NPV around the double for the optimal regions in both cases. Therefore, the PHE design does not affect the choice of the optimal mixture for this specific case study of heat pump integration. The following step of the results analysis consists in the identification of design and flow parameters describing the PHE in the optimal region. In order to do this, the relation between heat transfer area and NPV is presented as function of the main design parameters, so that the identified optimal region can be related to optimal values of the geometry and flow parameters of the heat exchanger.

3.2. Influence of the corrugation geometry

The corrugation height b, the corrugation pitch Λ and the chevron angle β are the geometrical parameters of the chevron-type PHE defining the type of corrugation used, influencing the flow condition inside the channels. The corrugation pitch and height define both the hydraulic diameter, used for heat transfer and pressure drop correlations, and a characteristic corrugation parameter X, defined as $b\pi/\Lambda$. The corrugation parameter X is directly related to the estimation of Φ, i.e. the ratio of the actual area over the projected flat area, introduced by (2). Fig. 5 represents the NPV and the heat transfer area A_{ht} for Case I. In Fig. 5(a) the colours indicate the hydraulic diameter of the channels, while in Fig. 5(b) the corrugation characteristic X is shown. It can be seen that it was optimal to employ corrugations leading to low hydraulic diameters, since a higher degree of turbulence was reached and heat transfer was enhanced. However, the best configurations were the ones for which the corrugation parameter X was very high. This means that it was preferred to achieve such small hydraulic diameter by manufacturing corrugation with high values of the corrugation height b and low values of the corrugation pitch Λ. From the analysis, it was shown that such configurations were the ones enhancing heat transfer without impacting negatively on the pressure losses. Therefore, it was concluded that all the optimal points in the figure were the ones corresponding to X above 10,

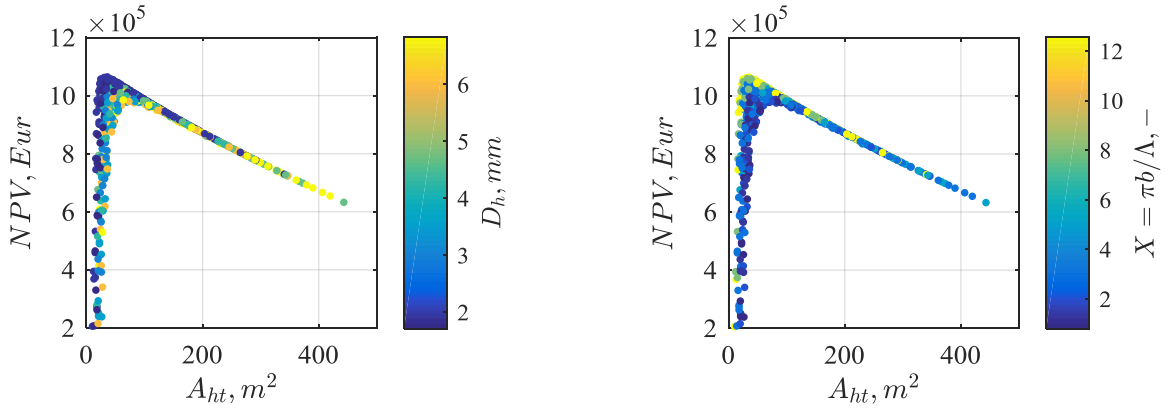

(a) (b)

Fig. 5. NPV as function of the heat transfer area, with colour indicating the magnitude of the hydraulic diameter (a) and the corrugation characteristic X (b). The results refer to Case I.

hence with b close to the value of 8 mm and Λ to the minimum value set as 2 mm. Analogous trends were observed for Cases II, III and IV, validating the conclusion, so they are not reported as figures.

Another parameter directly affecting the corrugation of the PHE, was the chevron angle β, with results shown in Fig. 6 (a) for Case I and Fig. 6 (b) for Case II. An analogous behaviour was observed for the two cases. There was not a clear trend as the one observed for the previous parameters, however it was shown that it was preferable to adopt angles in the higher range (above 60°), and that solutions around this median value seemed to be more optimal compared to the ones with very high angle (80°). Therefore, for this application, chevron angles within the range of 40° to 60° should lead to economically advantageous PHE design.

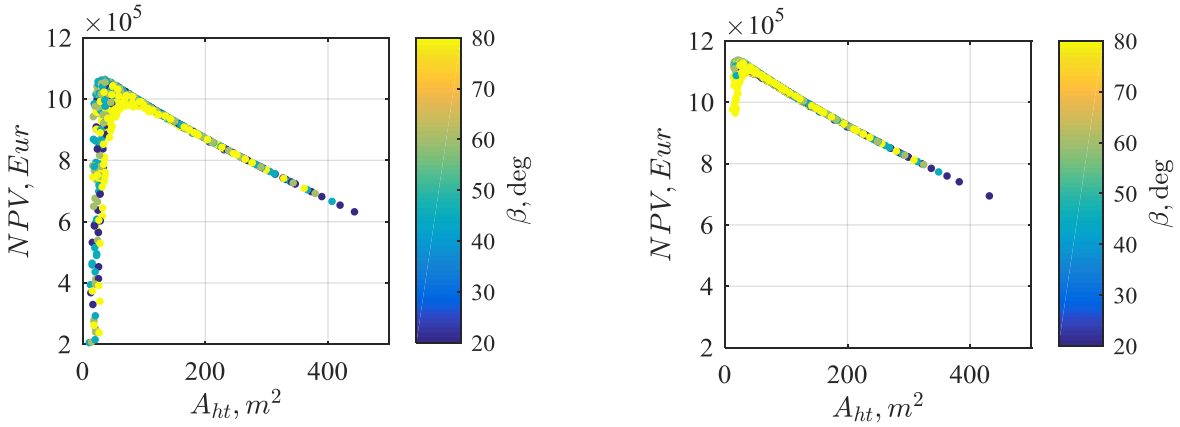

Fig. 6. NPV as function of the heat transfer area, with colour indicating the chevron angle for Case I (a) and Case II (b).

3.3. Influence of the plate size and numbers

Other geometrical parameters affecting the design of PHEs were the plate size and number of plates forming the flow channels. The results are reported in Fig. 7 (a), for Case I and Fig. 7 (b) for Case II.

The abscissa axis reports the values of the length-to-width ratio while the colour indicates the number of channels employed. It must be mentioned that configurations with length-to-width ratios below unity are not commonly found in the current market of PHEs, but usually ratio above 1 are adopted by manufacturers [21] [22]. However, it was decided not to limit the analysis to fixed values of the length-to-width ratio, in order to show the complete range of optimal solutions calculated by the PHE numerical model.

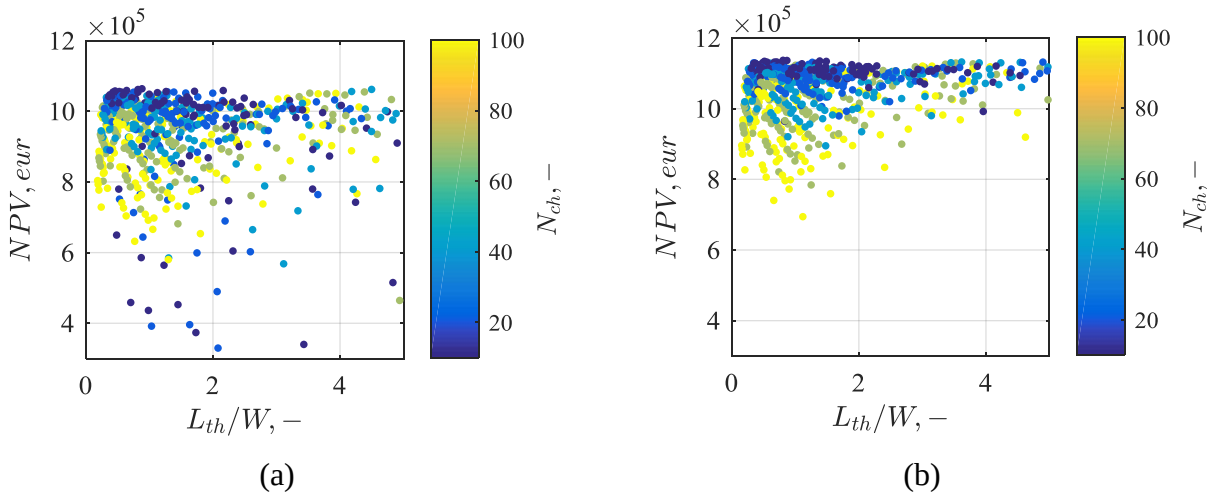

Fig. 7. NPV vs L/W , with colour indicating number of channels for Case I (a) and Case II (b)

From the results, it is shown that the highest values of NPV were reached by configurations with very different values of the ratio, and adjusting the number of channels used. Specifically, by employing plates with lower values of length-to-width ratio, a lower number of channels was required and preferred for optimal solutions, while the opposite trend is observed for higher values of ratio. Therefore, when designing a PHE, the plate size and number can be decided by considering other constraints, e.g. commercial availability or ease of manufacture, and the geometry of the corrugation might constitute the main parameters left as design variables. The plate size did not affect the results consistently, i.e. optimal configurations can be built by using different combinations of plate size and number of channels.

3.4. Flow parameters

Another analysis aimed at showing the relation between the flow conditions of the working fluid mixture inside the channels of the PHEs and the NPV of the cycle. The results are shown in Fig. 8, for the four cases considered, and it was observed that analogous trends were obtained with the optimal NPV lying in the same region of Reynolds numbers.

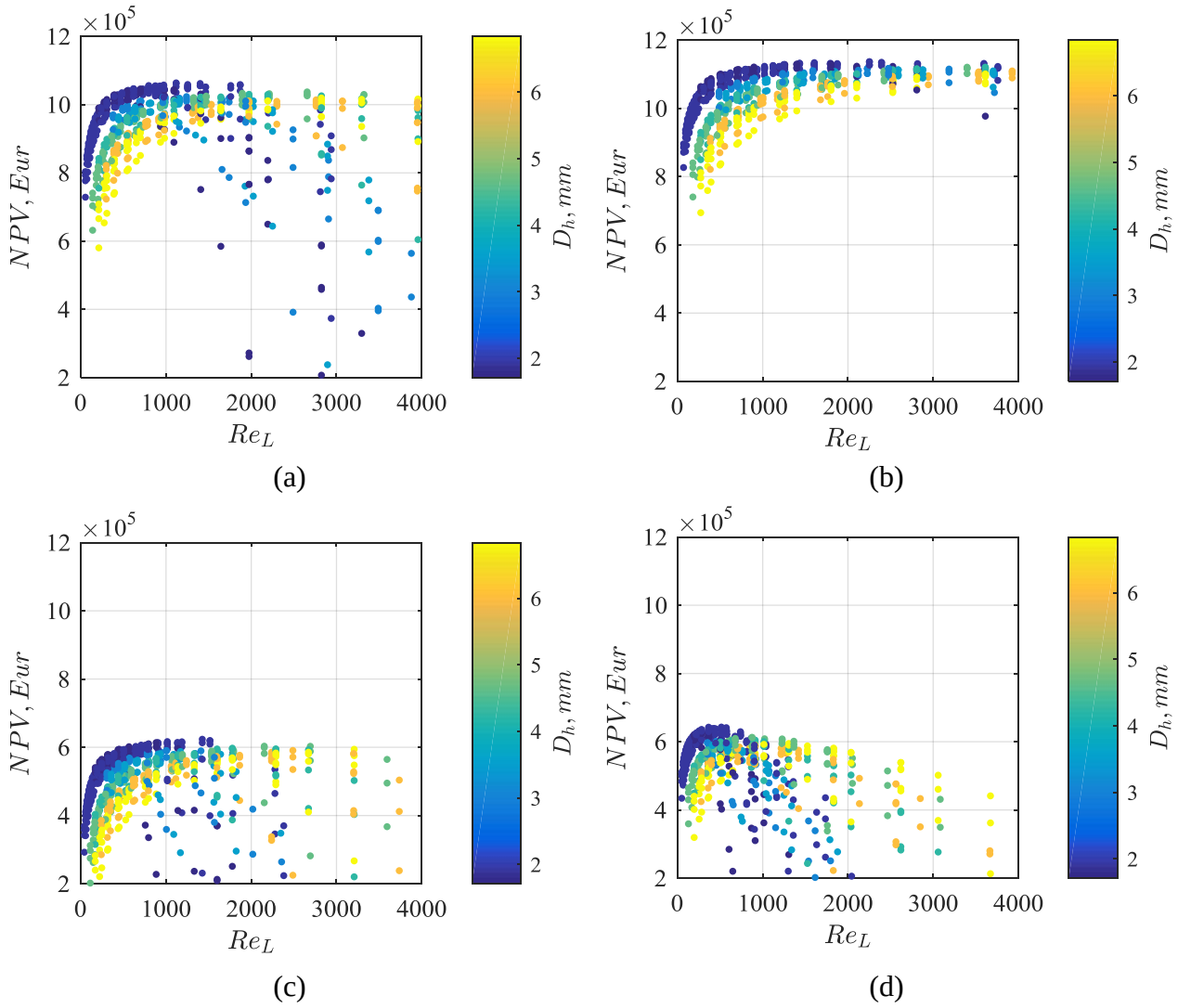

Fig. 8. Reynolds number of the liquid phase vs. NPV at the evaporator inlet for Case I (a), Case II (b), Case III (c) and Case IV (d), with colour indicating the value of hydraulic diameter.

The NPV is reported as function of Re_L. The point colour indicates the hydraulic diameter employed to achieve the flow condition. It can be seen that the highest curves for NPV are all obtained by choosing configurations with the minimum hydraulic diameters. Furthermore, it can be seen that the optimal range for Re_L lies within a range of 500-2,000, depending on the case considered. Case I and

III presented the peak of the NPV with a Reynolds number close to 1,000-1,500, while Case II showed a flatter trend of the NPV, with the highest points achieved around the value of 2,000. Case IV presented the maximum with lower Reynolds numbers between 500 and 1,000. The difference was related to the different properties of the working fluid mixtures. However, it was observed that the trends were analogous in all the cases, and the optimal range was within the specific region of 500-2,000, which could be therefore considered as a recommended range for the flow of the liquid phase at the evaporator inlet. Lastly, it is worth it to mention that a value of 1,000 for the Reynolds number for Case I corresponded to a liquid velocity of 5 m/s. The design criterion used in the previous analysis [3] was a limit velocity of 2 m/s. The results confirmed how the best NPV deviates from this value.

3.5. Cost analysis

As aforementioned in 2.2.2, the NPV was affected by the design parameters according to different contributions. The impact of the design on the various terms contributing to the NPV is shown for Case I. The PHE design was expressed by the heat transfer area A_{ht}, while the NPV value was divided into a term indicating the revenue (natural gas saving), and a term indicating the total cost, as shown in Fig. 9 (a) and (b). The former shows the variation of the cost for the total solution space, constituted by PHE with A_{ht} ranging from around 10 m^2 up to around 500 m^2; the latter shows a close-up of (a), where only solutions with area up to 50 m^2 are reported, so that the trends are better highlighted.

In the figure, the cost contribution is divided into the different terms, adjusted by the CRF as indicated by equation (5).

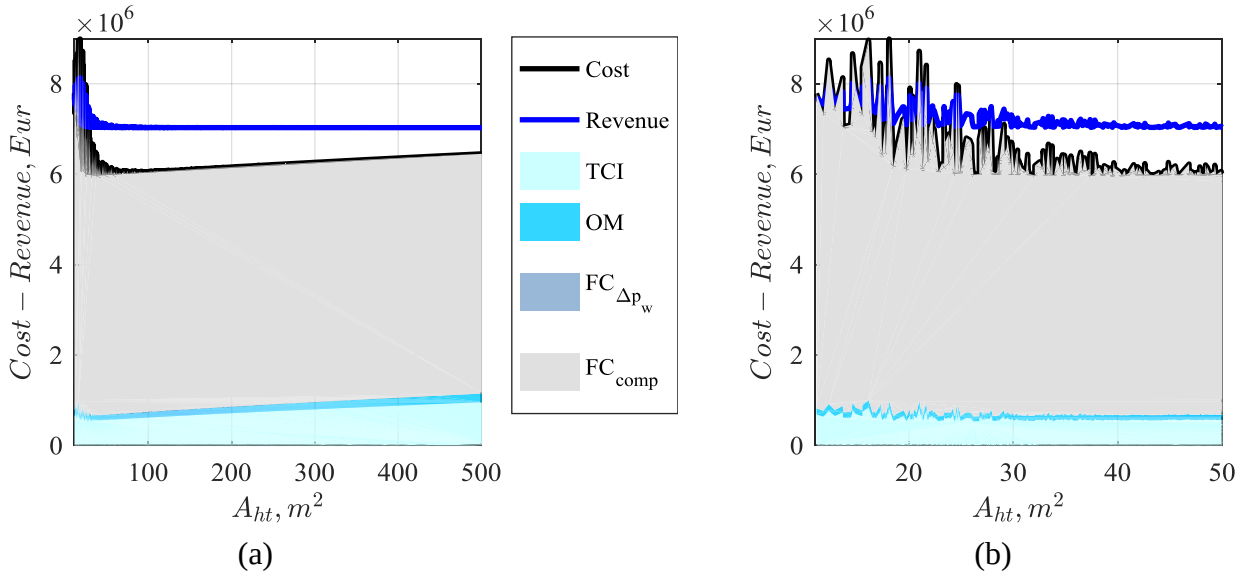

Fig. 9. Breakdown of the NPV terms as function of A_{ht}, with separation between annualised cost and revenue. The different coloured areas indicate the different contributions to the cost term. Results are reported for the whole solution space (a) and close-up with area up to 50 m^2 (b)

First of all, it was shown that the running costs for the water pressure drop are several orders of magnitudes lower than the other contributions, so that they are not visible in the cost breakdown. Moreover, it was observed that the most relevant contribution to the cost was given by the running cost of the compressor, indicated by the grey area. As expected, the running cost was not constant over the different PHE heat transfer areas. In fact, when the heat transfer area was minimized, the mixture experienced higher pressure losses, hence requiring a higher compressor work, and strongly impacting the economy of the heat pump. The cost line (in black) overcame the revenue line (in blue) for some configurations with small area, which is clearly visible in the close-up in Fig. 9 (b).

Lastly, it was shown that TCI and OMC constitute the other relevant sources of cost, and that the TCI tended to increase with increasing areas. However, the TCI oscillated in the lower range of PHE area, and despite the minimization of PHE investment costs, the compressor sizing influenced the results,

as shown in Fig. 10 (a), where the different investment costs are reported as function of the PHE heat transfer area. In fact, this region corresponded to the lowest contribution of the PHE to the TCI, yet the compressor sizing considering pressure drops could be consistently higher for those configurations with unfavourable pressure losses. Therefore, the figure shows the trade-off between compressor and evaporator contributions to the investment cost. The condenser curve was constant as the design was fixed based on the previous study design criterion [3].

Fig. 10 (b) summarizes the impact of the heat transfer area, i.e. the different design of the PHE, on the NPV, and colours indicating the liquid phase Reynolds number, chosen as flow design parameter. It was confirmed that the optimal region of Case I corresponded to values of Reynolds around 1,000 to 1,500.

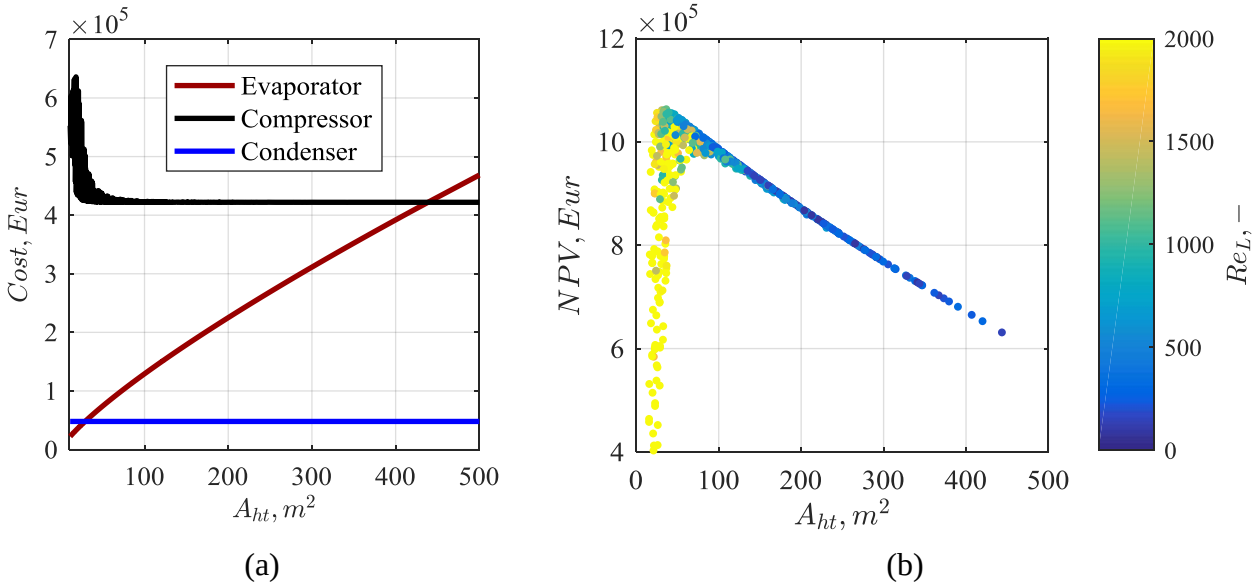

Fig. 10. (a) Investment costs of evaporator, compressor and condenser as function of the evaporator heat transfer area (b) NPV as function of the heat transfer area, with colours indicating the liquid Reynolds number at evaporator inlet

3.6. Design point

To conclude the results section, the trade-off between the PHE heat transfer area and the pressure losses is presented for the best solution of the four cases, corresponding to the heat exchanger configurations maximizing the NPV of the heat pump. The results are reported in Table 3, where heat transfer area, total capital investment cost, pressure drops of mixture and water and liquid Reynolds number at the evaporator inlet are indicated. It is shown that Case I and Case IV corresponded to the mixtures in which the optimal design required a lower pressure drop of the working fluids, thus a higher heat transfer area of the heat exchanger. Similarly to what was obtained in the preliminary analysis [3], Case I and II correspond to higher NPVs, due to the higher investment costs for Case III and Case IV, even for the best design solutions.

Table 3. Best solutions in terms of NPV for the four considered cases

	Unit	Case I	Case II	Case III	Case IV
COP	–	3.06	3.05	3.01	3.05
NPV	10^3 eur	1,060	1,135	617	641
A_{ht}	m^2	37.40	21.70	23.10	40.30
TCI	10^3 eur	548	461	852	885
Δp_{mix}	Pa	5,257	16,168	26,937	2,064
Δp_w	Pa	2,234	14,613	7,347	796
$Re_{L_{inlet}}$	–	1,128	2,260	1,434	523

It has to be mentioned that the parametric analysis considered 900 combinations of design parameters. Several optimal solutions, with very small differences of NPV, were found with different combinations of design parameters. Therefore, the comparison between the two most optimal solutions of Case I are presented in order to highlight the differences, and to show the obtained PHE design specifications; results are reported in Table 4. It is shown that the NPV of the second best solution differs of 0.025% compared to the best case, i.e. both points can be considered as optimal for the evaporator design.

The full specification set (plate size and plate corrugation) of the two solutions shows that in the first case, a design with wider plates and smaller number of channels is preferred, whilst in the second case higher length-to-width ratio is achieved, with a lower width and higher number of channels. This confirms the results shown in the previous section, which highlighted how optimal configurations could be achieved by different combinations of plate size and numbers. On the other hand, it is shown that similar corrugation characteristics are employed in both cases, lying in the optimal range before identified. Therefore, the results seem to be strongly influenced mostly by the plate corrugation.

Table 4. PHE specifications for Case I best solutions

	Unit	Case I – Best solution	Case I – Second best solution
COP	–	3.06	3.06
NPV	10^3 eur	1,060	1,059
General PHE design characteristics:			
A_{ht}	m^2	37.4	32.1
Δp_{mix}	Pa	5,256	8,139
Δp_w	Pa	2,234	46,132
$Re_{L_{inlet}}$	–	1,128	1,409
Plate size:			
W	m	0.5	0.1
N_{ch}	–	10	40
L_{th}	m	0.44	0.45
L_{th}/W	–	0.88	4.5
Plate corrugation:			
b	m	0.008	0.008
Λ	m	0.002	0.002
β	°	45	45
D_h	m	0.002	0.002
X	–	12.6	12.6

4. Discussion

The analysis presented in this work shows the influence of the design of a PHE evaporator on the NPV of a heat pump, using four different zeotropic mixtures as working fluid. The shown trends are similar for the four considered cases, yet the extension to more general applications with the use of zeotropic mixtures would require a more comprehensive study. In fact, it is very relevant to clarify the range of validity of the obtained results, tested considering only four possible working fluids used in a case study. The PHE optimal configurations, reported in Table 3, show the impact of using different working fluid mixtures on defining an optimal Reynolds number, thus the extension of the obtained recommendations to other type of mixtures requires validation.

Furthermore, the definition of an optimal Reynolds number might be dependent on cycle constraints, which make these design recommendations useful only when considering evaporators with similar conditions of the working fluid at the inlet. A similar consideration can be done on the water pressure

drop influence on the NPV, which is shown as negligible compared to the other contributions. Changing the temperature and pressure levels, and heat source medium, can influence the results.

Additionally, it was shown that the results were not dependent on the choice of the plate size, thus length-to-width ratio and number of channels could be adjusted according to the designer decision without affecting the possibility of reaching an economically optimal solution. However, the PHE numerical model does not take into account the mass flow distribution inside the channels, as well as the vapour and liquid distribution, which might lead to completely different results for some of the configurations. Therefore, an extension is required to describe the impact of the number of channels and distribution effect on the design.

A further point is given by the methodology followed in the work, which is based on a parametric study of the PHE, hence limiting the search space of the optimal solution. Implementing a full optimization procedure could be considered as a future extension.

Lastly, the results are dependent on the economic assumptions of interest rate, cost of electricity, as well as operational time of the plant. By changing these inputs, the impact on the NPV might be affected, hence requiring a further sensitivity study.

5. Conclusions

The parametric analysis conducted on the main parameters of the PHE shows that it is possible to derive design guidelines that can be potentially used in applications where PHEs are used as evaporators in heat pumps using zeotropic mixtures. The method applied is based on a combined evaluation of cycle performances and calculation of PHE required heat transfer area and pressure losses. The result shows that there are combinations of design parameters, which are optimal for the NPV of the heat pump, for all the considered cases. It is shown that the optimal design regions does not coincide with the design point adopted in a previous study, based on a practical limitations of the maximum inlet velocity, without accounting for the pressure losses of the PHE in the thermodynamics and economic calculations.

The results highlight design guidelines for the optimal PHE corrugation geometry, i.e. values of corrugation height around 8mm combined with low corrugation pitches around 2mm creates low hydraulic diameter, which are able to create a high degree of turbulence without increasing excessively the total pressure losses. From the results, it is obtained that the plate size, namely plate-to-width ration and number of channels, do not have a clear correlation with the NPV of the cycle, i.e. optimal solutions can be found by adopting different plate sizes, and adjusting number of channels and corrugation geometry accordingly. An optimal range is found for the liquid Reynolds number at the evaporator inlet, and it is recommended to keep the value within the range 500-2,000. The interval found is broad since the results are dependent on the working fluid considered.

Moreover, an in-depth cost analysis has shown the trade-off between heat transfer area and pressure losses, by considering all the contributions to the NPV calculations. It is obtained that it is not convenient to minimize the heat exchanger area without considering the mixture pressure drops, since the investment and running cost of the compressor are negatively impacted. On the other hand, the pressure losses of the heat source side, i.e. water, do not influence the results of the economic calculations.

Acknowledgments

This research project is financially funded by the Danish Council for Strategic Research in Sustainable Energy and Environment, under the project title: “THERMCYC – Advanced thermodynamic cycles utilising low temperature heat sources". The support is gratefully acknowledged.

Nomenclature

A	Area, m^2	NPV	Net Present Value, €
b	Corrugation height, mm	p	Pressure, Pa
c_{el}	Price of electricity, €/kWh	PEC	Purchased equipment cost, €
COP	Coefficient of Performance	Q	Vapour quality
CRF	Capital recovery factor	R	Thermal resistance, $(m^2K)/W$
D	Diameter, mm	Re	Reynolds number
f	Friction factor	t	Plate thickness, mm
FC	Fuel cost, €/yr	TCI	Total Capital Investment, €
G	Mass velocity, $kg/(m^2s)$	U	Overall heat transfer coefficient, $W/(m^2K)$
h	Heat transfer coefficient, $W/(m^2K)$	$\dot{V}$	Volumetric flow rate, m^3/h
L_{th}	Plate length, m	W	Plate width, m
$\dot{m}$	Mass flow, kg/s	X	Corrugation characteristic
N_{ch}	Number of channels		

Greek symbols

β	Chevron angle, °	ρ	Density, kg/m^3
Φ	Enlargement factor	μ	Viscosity, Pa s
Λ	Corrugation pitch, mm	τ	Time, h
η	Efficiency		

Abbreviations

CV	Control Volume	PHE	Plate Heat Exchanger
ORC	Organic Rankine Cycle		

Subscripts

acc	acceleration	*L*	liquid
core	core	*m*	median
e	equivalent	*mix*	mixture
fr	friction	*ng*	natural gas
h	hydraulic	*o*	outlet
hp	heat pump	*p*	port
ht	heat transfer	*w*	water
i	inlet		

References

[1] F. Bühler, T.-V. Nguyen, and B. Elmegaard, "Energy and exergy analyses of the Danish industry sector" *Applied Energy*, vol. 184, pp. 1447–1459, Feb. 2016.

[2] IEA Heat Pump Centre - Annex 35, "Application of Industrial Heat Pumps - Final report" Borås, Sweden, 2014.

[3] B. Zühlsdorf, F. Bühler, R. Mancini, S. Cignitti, and B. Elmegaard, "High Temperature Heat Pump Integration using Zeotropic Working Fluids for Spray Drying Facilities" in *Proceedings of the 12th IEA Heat pump conference, Rotterdam*, 2017.

[4] R. Radermacher and Y. Hwang, *Vapor Compression Heat Pumps with Refrigerant Mixtures*. CRC Press 2005, 2005.

[5] M. M. Abu-Khader, "Plate heat exchangers: Recent advances" *Renewable & Sustainable Energy Reviews*, vol. 16, no. 4, pp. 1883–1891, 2012.

[6] J. a. W. Gut and J. M. Pinto, "Optimal configuration design for plate heat exchangers" *International Journal of Heat and Mass Transfer*, vol. 47, no. 22, pp. 4833–4848, 2004.

[7] S. Karellas, A. Schuster, and A.-D. Leontaritis, "Influence of supercritical ORC parameters on plate heat exchanger design" *Applied Thermal Engineering*, vol. 33–34, pp. 70–76, 2012.

[8] J. Wang, M. Wang, M. Li, J. Xia, and Y. Dai, "Multi-objective optimization design of condenser in an organic Rankine cycle for low grade waste heat recovery using evolutionary algorithm" *International Commununications of Heat and Mass Transfer*, vol. 45, pp. 47–54, 2013.

[9] N. Rohmah, G. Pikra, A. J. Purwanto, and R. I. Pramana, "The Effect of Plate Spacing in Plate Heat Exchanger Design as a Condenser in Organic Rankine cycle for Low Temperature Heat Source" *Energy Procedia*, vol. 68, pp. 87–96, 2015.

[10] D. Walraven, B. Laenen, and W. D'Haeseleer, "Comparison of shell-and-tube with plate heat exchangers for the use in low-temperature organic Rankine cycles" *Energy Conversion and Management*, vol. 87, pp. 227–237, 2014.

[11] VDI-Gesellschaft, *VDI Heat Atlas*, vol. 1. 2015.

[12] Mathworks, "Matlab R2016b." [Online]. Available: https://www.mathworks.com/products/new_products/latest_features.html, accessed: 07th February 2017.

[13] National Institute of Standard and Technology, "Reference Fluid Thermodynamic and Transport Properties Database version 9.1" [Online]. Available: https://www.nist.gov/srd/refprop, accessed: 07th February 2017.

[14] R. K. Shah and D. P. Sekulic, *Fundamentals of Heat Exchanger Design*. 2002.

[15] J. K. Jensen, M. R. Kaernl, T. S. Ommen, W. Brix, L. Reinholdt, and B. Elmeegard, "Effect of liquid/vapour maldistribution on the performance of plate heat exchanger evaporators" in *Proceedings of the 24th IIR International Congress of Refrigeration*, 2015.

[16] H. Martin, "A theoretical approach to predict the performance of chevron-type plate heat exchangers" *Chemical Engineering and Processing: Process Intensification*, vol. 35, no. 4, pp. 301–310, 1996.

[17] D. S. Jung, M. McLinden, R. Radermacher, and D. Didion, "A study of flow boiling heat transfer with refrigerant mixtures", *International Journal of Heat and Mass Transfer*, vol. 32, no. 9, pp. 1751–1764, 1989.

[18] D. S. Jung and R. Radermacher, "Prediction of pressure drop during horizontal annular flow boiling of pure and mixed refrigerants," *International Journal of Heat and Mass Transfer*, vol. 32, no. 12, pp. 2435–2446, 1989.

[19] T. Ommen, J. K. Jensen, W. B. Markussen, L. Reinholdt, and B. Elmegaard, "Technical and economic working domains of industrial heat pumps: Part 1 - Single stage vapour compression heat pumps," *International Journal of Refrigeration*, vol. 55, pp. 168–182, 2015.

[20] A. Bejan, G. Tsatsaronis, and M. Moran, *Thermal design and optimization*. John Wiley and Sons, Inc., 1996.

[21] SWEP International AB, "SWEP." [Online]. Available: http://www.swep.net/, accessed: 07th February 2017.

[22] "Alfa Laval," 2015. [Online]. Available: http://www.alfalaval.com/, accessed: 07th February 2017.

DOI: 10.18462/iir.gl.2018.1261

COMPARISON OF HEAT TRANSFER AND PRESSURE DROP CORRELATIONS FOR EVAPORATION OF ZEOTROPIC MIXTURES IN PLATE HEAT EXCHANGERS

Roberta Mancini [(a)], Jonas Kjær Jensen [(a)], Wiebke Brix Markussen [(a)], Brian Elmegaard [(a)]

[(a)] Section of Thermal Energy, Department of Mechanical engineering, Technical University of Denmark, Nils Koppels Allé 403, Kgs. Lyngby, 2800, Denmark, robman@mek.dtu.dk

ABSTRACT

Zeotropic mixtures offer a possibility of optimizing heat pump cycle design by matching the working fluid temperature glide to the heat source and sink temperature profiles. Suitable heat transfer and pressure drop prediction methods are of paramount importance to evaluate the performance of plate heat exchangers (PHE) using such fluids. It is therefore relevant to evaluate the uncertainty in PHE performance estimation when zeotropic mixtures are used as working fluids. In this work, different correlations for the (Silver, 1947) and (Bell and Ghaly, 1973) method were compared to evaluate the evaporation heat transfer coefficient of mixtures of CO_2 and hydrocarbons at different mass compositions and subject to heat source temperature glides of 10 K, 15 K and 20 K. Moreover, the impact of using different pressure drop models and correlations was included in the sensitivity study on the evaporator performance. Maximum deviations of 6 % and 10 % were obtained on the total heat transfer rate, depending on the prediction method chosen for the heat transfer coefficient and pressure drop, respectively. Larger discrepancies were found in the estimation of the mean UA value and total frictional pressure drops. Working fluids subject to the largest glide of 20 K resulted to be more sensitive to the choice of the prediction method. No recommended set of correlation was found, but similarities and differences between the different mixtures were identified and discussed.

Keywords: Plate heat exchangers, Zeotropic mixtures, Evaporators, Prediction methods

1. INTRODUCTION

In the past two decades, increasing attention was posed on the utilization of natural refrigerants like hydrocarbons (HCs), proposed for their zero Ozone Depletion Potential and negligible Global Warming Potential. Hydrocarbons can be directly employed as pure fluids, but another possibility is to combine them in order to create refrigerant mixtures. For instance, the benefit of using mixtures of carbon dioxide (CO_2) and HCs leads to the advantage of reducing the typically high operating pressure of CO_2 systems and decreasing the flammability entailed by hydrocarbon utilization (Kim et al., 2008). Moreover, the so-called zeotropic mixtures offer the additional advantage of decreasing the irreversibility caused by temperature differences in the evaporator and the condenser by matching the heat source and sink temperature glides with the working fluid, due to its varying temperature during phase change. (Zühlsdorf et al., 2017a, 2017b) showed the possibility of increasing the heat pump coefficient of performance (COP) up to 27 % in two different case studies where different combinations of HCs and CO_2 were considered at different mass compositions.

The benefit obtained by using mixtures on the thermodynamic performance of the cycle entails however an increase in the necessary heat exchangers heat transfer area, due to mixture degradation of the heat transfer coefficient compared to pure fluids, observed in a number of experimental campaigns (Radermacher and Hwang, 2005). A number of reasons contribute to heat transfer degradation: (i) an earlier suppression of the nucleate boiling contribution. (ii) Formation of a mass diffusion resistance due to the more readily evaporation of the more volatile component. (iii) Reduction of effective super-heating and of the effective heat flow rate available for evaporation. (iv) Worse mixture transport properties (Collier and Thome, 1994).

This poses a major attention to the design and performance of heat transfer equipment when zeotropic mixtures are employed. Plate heat exchangers (PHEs) offer a suitable solution for the high heat transfer coefficient

achieved within their compact design and the possibility to arrange the flow in a counter-current mode, which is essential to achieve glide matching. Scientific literature collects different studies focused on experimental campaigns for deriving heat transfer coefficient and pressure drop correlations for two-phase flow in PHEs. (Vakili-Farahani et al., 2015) and (Eldeeb et al., 2015) carried out extensive literature reviews on the published experimental campaigns and prediction methods for evaporation and condensation in PHEs. In particular, (Vakili-Farahani et al., 2015) underlined the discrepancy of the different data and the difficulties of creating prediction models that are generally valid for PHEs, similarly to the ones existing for in-tube flow boiling. (Amalfi et al., 2016a) developed a correlation for heat transfer coefficient and friction factor during flow boiling in PHEs, based on the many experimental data sets available in literature. The developed prediction model showed better agreement with the experimental data than existing correlations. The databank was however limited to pure working fluids, with the exception of the near-azeotropic mixture R410a, the azeotropic mixture R507a and ammonia/water. The prediction method developed by (Amalfi et al., 2016a) is therefore not directly applicable to mixtures of natural refrigerants.

The difference between heat transfer in pure and multi-component working fluids was investigated in literature. (Silver, 1947) and (Bell and Ghaly, 1973) developed a method to account for the heat transfer degradation entailed by the mixture. The method uses weighted contributions of nucleate boiling, convective boiling and vapor phase heat transfer coefficients. In order to apply such method, different prediction methods can be chosen for the two-phase convective and nucleate boiling coefficients, as well as for the single-phase heat transfer coefficient. The objective of this paper was to estimate the impact of using different combinations of the heat transfer correlations developed for PHEs in the Silver and Bell-Ghaly method.

Moreover, the impact of employing different methods and correlations to calculate the frictional contribution to pressure drop was evaluated. The pressure drop literature review was based on the studies collected by (Amalfi et al., 2016b), and applied to the considered working fluids. Both sensitivity studies were carried out for a case study in which the heat exchanger (HEX) performance was estimated and the geometry of the PHE was fixed, thereby assessing the impact on the total heat flow rate at the evaporator.

2. METHODS

2.1 Case study and cycle boundary conditions

The comparison was based on a case study of a single-stage vapor compression heat pump, presented in (Zühlsdorf et al., 2017b), designed for delivering 2200 kW at the condenser, by heating up water from 40 °C to 80 °C. The inlet temperature of the heat source (water) was fixed to 40 °C, and different heat source temperature glides were assessed, namely 10 K, 15 K and 20 K, corresponding to Case I, II and III, respectively. Optimal zeotropic working fluid mixtures were found for the different temperature glides. These are reported in Table 1 with related mass composition, evaporation pressure, heat pump Coefficient of Performance (COP) and heat load at the evaporator.

Table 1: Evaporator boundary conditions for the different working fluids (Zühlsdorf et al., 2017b)

Case I, $\Delta T_{gl} = 10$ K				Case II, $\Delta T_{gl} = 15$ K				Case III, $\Delta T_{gl} = 20$ K			
Mixture	p_{ev} bar	COP -	$\dot{Q}_{ev}$ kW	Mixture	p_{ev} bar	COP -	$\dot{Q}_{ev}$ kW	Mixture	p_{ev} bar	COP -	$\dot{Q}_{ev}$ kW
CO_2/ DME (0.1/0.9)	7.5	5.62	1809	Propylene/ Butane (0.3/0.7)	4.0	5.40	1792	DME/ Pentane (0.3/0.7)	1.2	5.24	1780
DME/ Butane (0.5/0.5)	4.8	5.61	1807	Propane/ Butane (0.3/0.7)	3.9	5.38	1791	DME/Iso-Pentane (0.3/0.7)	1.7	5.19	1776
Ethane/ Propane (0.1/0.9)	12.3	5.60	1807	CO_2/DME (0.1/0.9)	7.0	5.32	1787	Propylene / Butane (0.5/0.5)	5.0	5.15	1773
Ethane/ Propylene (0.1/0.9)	14.5	5.57	1805	DME/Iso-Pentane (0.8/0.2)	4.5	5.31	1786				

The impact of the chosen prediction methods was assessed in a relevant practical situation, in which the geometry of the PHEs was entirely fixed and the suction volume of the refrigerant flow at the compressor inlet (corresponding to the evaporator outlet) and the super-heating were fixed by the control. The required number of channels was estimated for each working fluid with a preliminary evaporator sizing based on constant heat transfer coefficients in the different regions of evaporation and super-hating. The other HEX parameters were defined according to an existing evaporator model (V65) manufactured by SWEP (SWEP International AB, 2015). Its design parameters are reported in Table 2. The plate size was given by plate width W and port-to-port length L_p, while the corrugation characteristics were the chevron angle β, the corrugation height b and pitch Λ. The plate thickness t gives the trade-off between conductive resistance and mechanical strength. The PHE was assumed to be constructed in stainless steel, with a thermal conductivity equal to 16.2 $\mathrm{W(mK)^{-1}}$.

Table 2: Geometry of the PHE – SWEP Evaporator type V65 (SWEP International AB, 2015*)*

$\boldsymbol{W}$, m	$\boldsymbol{L_p}$, m	$\boldsymbol{\beta}$, °	$\boldsymbol{b}$, mm	$\boldsymbol{\Lambda}$, mm	$\boldsymbol{D_p}$, m	$\boldsymbol{t}$, mm
0.363	0.731	35	1.9	7	0.1	0.5

It was assumed to employ a thermostatic expansion valve, thus calculating the refrigerant super-heating in relation to inlet pressure. The refrigerant mass flow and saturation pressure were calculated in order to match the control values, and a numerical model was employed to estimate the PHE performance.

2.2 Plate heat exchanger numerical model

The numerical model of the PHE was based on an internal solver for the solution of heat transfer and fluid flow in the PHE, coupled with a Newton-Raphson solver iterating on the refrigerant operating conditions. Fluid thermo-physical properties were calculated using Refprop (Lemmon et al., 2013) and Coolprop (Bell et al., 2014), for mixtures and water, respectively. The tolerance of the Newton-Raphson solver was set to 10^{-3} on the relative residuals of the refrigerant suction volume and super-heating.

The internal solver was based on a successive substitution approach iterating on wall temperature and pressure drops. A one-dimensional (1D) discretization of the HEX was employed along the flow direction with equidistant heat transfer area steps. The solution strategy was built based on a combination of the SEWTLE solver presented in (Corberán et al., 2000) and an improved solution strategy based on alternate refrigerant and heat source iterations as suggested in (Eldeeb et al., 2016). A total number of 100 control volumes (CVs) was employed as a trade-off between accuracy and computational cost, with solver tolerance set to 10^{-5} for the norm of relative residuals of wall temperature and refrigerant and source pressure drops.

2.3 Prediction methods – heat transfer coefficient

The heat transfer coefficient in the two-phase region was estimated by using the (Silver, 1947) and (Bell and Ghaly, 1973) method, with the formulation expressed by Eq. (1).

$$h_{\mathrm{TP}} = \frac{1 + \dfrac{h_{\mathrm{NB_{mix}}}}{h_{\mathrm{C}}}}{\dfrac{1}{h_{\mathrm{C}}} + \dfrac{\bar{\mathrm{z}}}{h_{\mathrm{V}}}} \tag{1}$$

h_{TP} indicates the two-phase heat transfer coefficient and it is a function of the nucleate boiling (NB) contribution $h_{\mathrm{NB_{mix}}}$, the convective boiling (CB) heat transfer coefficient h_{C}, and the vapor phase heat transfer coefficient h_{V}.The nucleate boiling contribution $h_{\mathrm{NB_{mix}}}$ was calculated based on a dedicated experimental correlation, and corrected by a factor taking the degradation entailed by the mixtures into account. For this purpose the (Thome and Shakir, 1987) correlation was employed, as reported in Eq.(2). The mixture degradation is as a function of the difference between dew and bubble point temperatures $(\mathrm{T_{dew}} - \mathrm{T_{bubble}})$, the specific heat flux per unit area $\dot{\mathrm{Q}}''$, latent heat of evaporation h_{lat} and liquid density ρ_L. β_L represents the liquid mass transfer coefficient, equal to 0.0002 m/s.

$$\frac{h_{\mathrm{NB_{mix}}}}{h_{\mathrm{NB_{id}}}} = \left(1 + \frac{h_{\mathrm{NB_{id}}}}{\dot{\mathrm{Q}}''}(\mathrm{T_{dew}} - \mathrm{T_{bubble}})\left(1 - e^{-\frac{\dot{\mathrm{Q}}''}{\rho_L h_{\mathrm{lat}} \beta_L}}\right)\right)^{-1} \quad (2)$$

Last, the correction factor $\bar{z}$ of Eq.(1) was introduced by (Silver, 1947) and (Bell and Ghaly, 1973), as function of vapor quality x, vapor specific heat capacity c_{p_V} and the slope of evaporation curve $d\mathrm{T}/dh$, indicating the rate of sensible heat transfer over the total heat load.

$$\bar{z} = x \frac{d\mathrm{T}}{dh} c_{p_V} \quad (3)$$

The sensitivity analysis was based on the correlations reported in Table 3. (Hsieh and Lin, 2003) was developed as a superposition model, with distinct contributions for nucleate and convective boiling. (Longo et al., 2015) was developed by considering a transition point between nucleate and convective dominated regions, based on the Boiling number. Therefore, each term of both correlations was considered in the appropriate category, as reported in Table 3. The remaining two-phase correlations were categorized as convective or nucleate boiling methods, depending on the related authors observations on the heat transfer, which could be dominated by heat flux (nucleate boiling) or by vapor quality and mass flow (convective boiling). All possible combinations of the three terms were analyzed, leading to 75 different possibilities for each fluid.

Table 3: Summary of the considered experimental correlations for the different terms of Eq. (1)

h_C		$h_{\mathrm{NB_{id}}}$		h_V
Two-phase convective		Two-phase nucleate boiling		Single-phase
a	(Danilova et al., 1981)	A	(Cooper, 1984)	(Chisholm and Wanniarachchi, 1992)
b	(Hsieh and Lin, 2003)	B	(Hsieh and Lin, 2003)	(Wanniarachchi et al., 1995)
c	(Han et al., 2003)	C	(Palm and Claesson, 2006)	(Martin, 1996)
d	(Longo et al., 2015)	D	(Gorenflo and Kenning, 2010)	
e	(Amalfi et al., 2016a)	E	(Longo et al., 2015)	

The heat transfer coefficient of the heat source (water) was estimated using the single-phase correlations reported in the last column of Table 3. The single-phase heat transfer coefficient of the refrigerant in the super-heated region was estimated by the same correlation. A weighted interpolation was used in the transition between evaporation and super-heating from vapor quality of 0.9.

2.4 Prediction methods – frictional pressure drops

The pressure drops of the heat source and of the refrigerant were estimated as the sum of the contributions of acceleration, friction, gravity and manifolds. The acceleration and gravity contributions were estimated by assuming homogeneous flow (Vakili-Farahani et al., 2015), while manifold pressure drops were calculated using the correlation by (Shah and Focke, 1988). An upward refrigerant flow and downward water flow were considered, as typical in the considered PHE configuration (SWEP International AB, 2015).

The frictional pressure drop was estimated by using three different models found in literature. First, correlations calculating the two-phase Fanning friction factor were considered as indicated in the first column of Table 4. The second adopted model was the (Lockhart and Martinelli, 1949) method, consisting in the estimation of two-phase multipliers correlating the single-phase liquid and vapor pressure drops to the two-phase pressure drop. The (Palm and Claesson, 2006) coefficients were used, thereby assuming a Chisholm parameter of 4.67, found using experimental data for PHEs. Last, the kinetic energy model was used, assuming proportionality between the kinetic energy per unit volume and the frictional pressure losses, as proposed by (Longo and Gasparella, 2007). All the models were employed for the estimation of the frictional pressure drop

locally, thereby summing all the contributions of the CVs to obtain the total refrigerant and heat source frictional pressure drop in the PHE. In the super-heating region, the single-phase Fanning friction factor proposed by the single-phase correlations reported in the last columns of Table 3 was used.

Table 4: Prediction methods for the two-phase frictional refrigerant pressure drops

Two-phase Fanning friction factor		Lockhart-Martinelli multipliers
F 1	(Yan and Lin, 1999)	LM 1 (Palm and Claesson, 2006)
F 2	(Hsieh et al., 2002)	
F 3	(Hsieh and Lin, 2003)	Kinetic energy proportionality
F 4	(Han et al., 2003)	KE 1 (Longo and Gasparella, 2007)
F 5	(Amalfi et al., 2016a)	

3. RESULTS

Subsection 3.1 presents the results of the sensitivity analysis on the heat transfer coefficient, thereby illustrating the impact of the different correlations combinations on the mean UA value and on the UA development in the PHE. Subsection 3.2 presents the results of the sensitivity analysis of the different calculation methods for frictional pressure drops. Subsection 3.3 illustrates how the UA value and the frictional pressure drops impact the output of the performance model, i.e. the heat transfer rate at the evaporator.

3.1 Impact on the UA values

Fig. 1, Fig. 2 and Fig. 3 show the heat transfer correlation sensitivity analysis results for Case I, II and III, respectively. Fig. 1 (a), Fig. 2(a) and Fig. 3 (a) report the mean UA value for all the combinations: the abscissa indicates different combination of nucleate and convective boiling correlations, while the three different marker styles represent the three single-phase correlations. Different colors represent the different working fluids of the three cases. Fig. 1 (b), Fig. 2 (b) and Fig. 3 (b) represent the development of the UA value along the evaporator, as function of the cumulated heat flow rate. The results are shown for only two correlation combinations for each fluid, represented by a continuous and a dotted line. The former characterizes the combination estimating the highest mean heat transfer coefficient for the specific fluid, while the latter represents the correlations giving the lowest mean heat transfer coefficient.

Better heat transfer performance was obtained for smaller temperature glides, with mean UA values up to 400 kW/K for Case I against values not higher than 300 W/K for Case III. By looking at the UA distribution in the evaporator in Fig. 1 (b), Fig. 2 (b) and Fig. 3 (b), Case I yields a steeper heat transfer growth for increasing vapor quality compared to Case II and III for the best performing correlation combinations. This is due to the higher degradation of heat transfer for increasing temperature glide for both the case of nucleate and convective boiling, as it is expressed by Eq. (2) and (3), due to the larger sensible heat flow rate needed for increasing the mixture temperature during phase change. The fluid ranking in terms of heat transfer performance remains the same in all cases, regardless of the correlation applied. By looking at Case I in Fig. 1 (b), the UA value of DME/Butane (50/50) outperforms the other fluids for both the best and worst correlation combinations.

Similarities were found for the single-phase and nucleate boiling correlations. The single-phase correlation by (Chisholm and Wanniarachchi, 1992) led to higher heat transfer compared to (Martin, 1996) and (Wanniarachchi et al., 1995), which yielded the lowest UA. This holds for all the mixtures, as shown by the different markers in Fig. 1 (a), Fig. 2 (a) and Fig. 3 (a). (Hsieh and Lin, 2003) (B) underestimated the NB contribution compared to the other correlations, while (Palm and Claesson, 2006) (C) overestimated the nucleate boiling. The results, shown in Fig. 1 (b), Fig. 2 (b) and Fig. 3 (b), are the same for all the fluids.

By looking at convective boiling contributions, (Hsieh and Lin, 2003) (b) correlation led to the best heat transfer coefficient for all the working fluids of Case I, while (Longo et al., 2015) (d) yielded the best

DOI: 10.18462/iir.gl.2018.1261

performances for Case II and III. The lowest CB contribution to heat transfer was estimated by (Amalfi et al., 2016a) (e) and (Danilova et al., 1981) (a), depending on the working fluid.

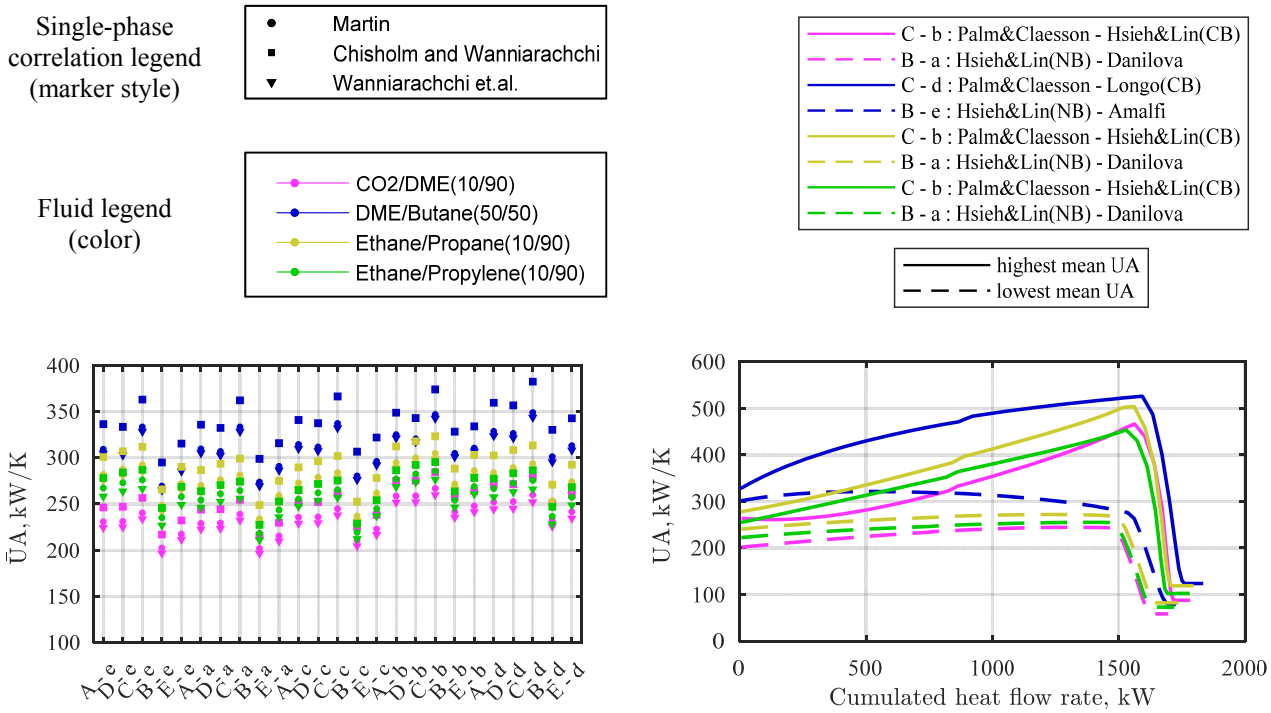

(a) Mean UA value

(b) UA value development in the evaporator

Fig. 1: Case I results (a) Impact of the different heat transfer correlations on the mean UA value; (b) UA as function of the cumulated heat flow rate in the evaporator.

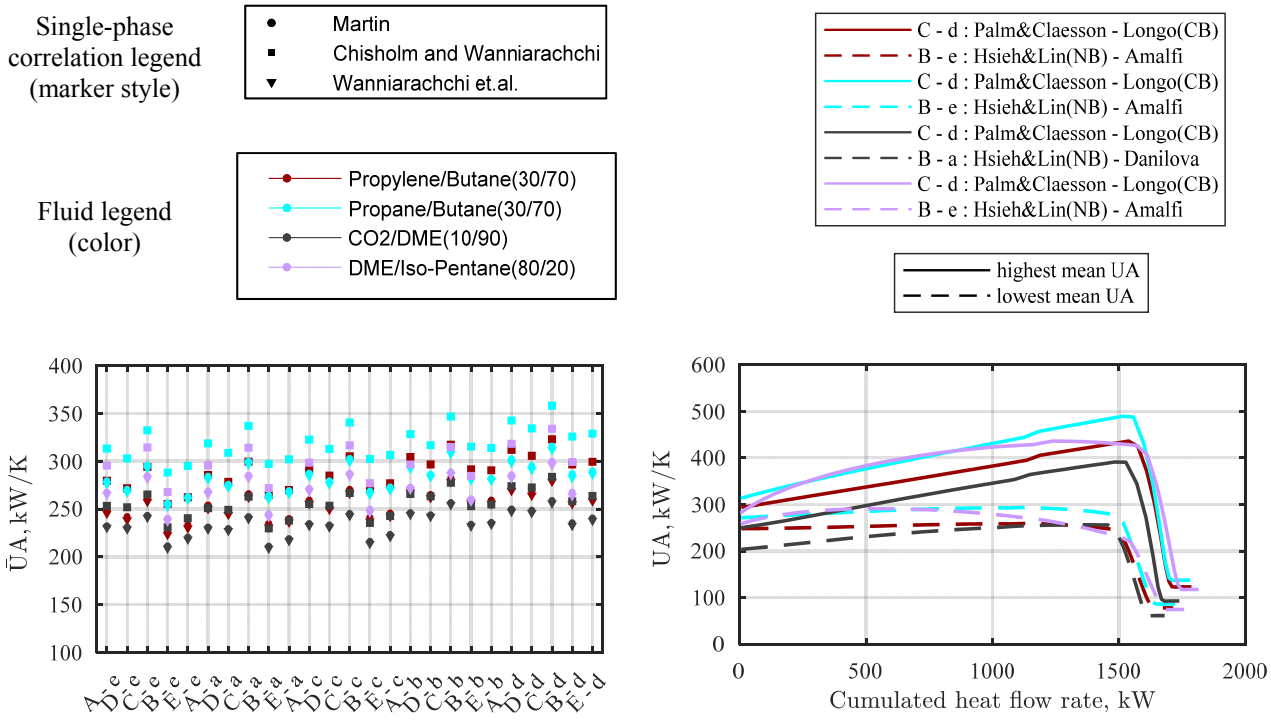

(a) Mean UA value

(b) UA value development in the evaporator

Fig. 2 Case II results (a) Impact of the different heat transfer correlations on the mean UA value; (b) UA as function of the cumulated heat flow rate in the evaporator.

DOI: 10.18462/iir.gl.2018.1261

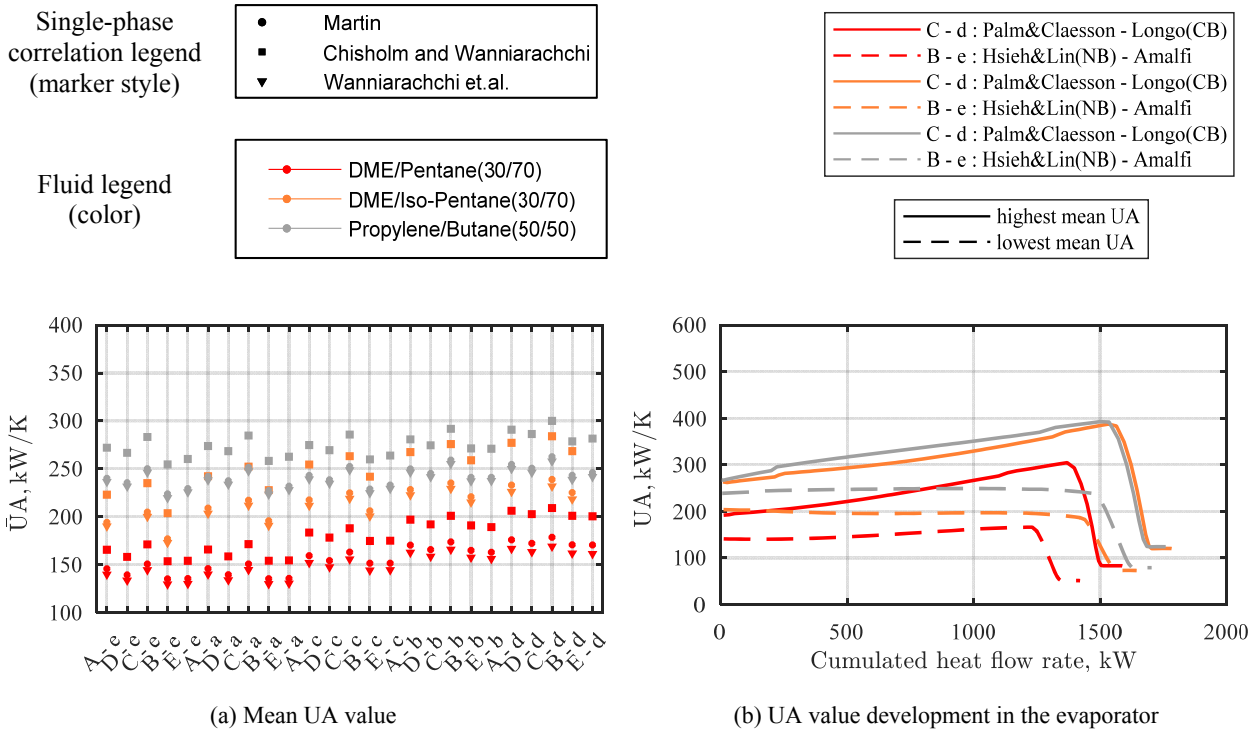

(a) Mean UA value

(b) UA value development in the evaporator

Fig. 3 Case III results (a) Impact of the different heat transfer correlations on the mean UA value; (b) UA as function of the cumulated heat flow rate in the evaporator.

3.2 Impact on the frictional pressure drops

Fig. 4 (a), (b) and (c) report the results of the pressure drop sensitivity analysis for Case I, II and III, respectively. The mixture temperature glide does not affect the results, opposite to the heat transfer coefficient behavior. The model by (Lockhart and Martinelli, 1949) with (Palm and Claesson, 2006) coefficients, the model by (Longo and Gasparella, 2007) and the friction factor correlations F 4 (Han et al., 2003) and F 5 (Amalfi et al., 2016a) led to similar pressure drop values. On the other hand, the Fanning friction factor correlations F 1, F 2 and F 3, namely (Yan and Lin, 1999), (Hsieh et al., 2002) and (Hsieh and Lin, 2003) over-estimated the pressure drop compared to the other correlations. DME/Iso-pentane(30/70) was the working fluid most sensitive to the choice of the correlation, with a large difference between (Lockhart and Martinelli, 1949) model and (Yan and Lin, 1999) correlation results. It must be noted that some results are not presented for DME/Pentane (30/70) in Case III, due to model convergence issues for very high pressure drops. It can be therefore be concluded that this fluid was very sensitive as well to the choice of the prediction method.

3.3 Impact on the performance model output

Fig. 5 reports the percentage deviation from the mean of all correlation combinations of the most deviating correlation combinations for heat transfer, which were identified in Fig. 1 (b), Fig. 2 (b) and Fig. 3 (b). The deviations are reported for the mean UA value, indicating the impact of the chosen correlations on the heat transfer coefficient calculation, and the consequent effect on the total heat flow rate at the evaporator, output of the performance model. Case I and Case II presented maximum differences in mean UA values around ±30 %, while Case III reported slightly higher deviations, with a maximum around ± 35%. A smaller effect was however found on the total heat flow rate. Despite larger discrepancies were obtained on the mean UA value, maximum deviations around ±2 % for Case I and II and ±6 % for Case III, can be observed in Fig. 5.

Fig. 6 reports the results of the frictional pressure drops. The maximum deviations were reported from the mean value obtained for each working fluids. As expected from the frictional pressure drop values presented in Fig. 4, a deviation of up 130 % was obtained for some of the fluids if correlations F 1, F2 and F 3 were employed. A much lower impact was however found on the total heat flow rate at the evaporator, similarly to the heat transfer correlation case. Case III was the most sensitive to the choice of the correlations, reporting maximum deviation on the total heat transfer rate around ±10 % for DME/Iso-Pentane(30/70).

DOI: 10.18462/iir.gl.2018.1261

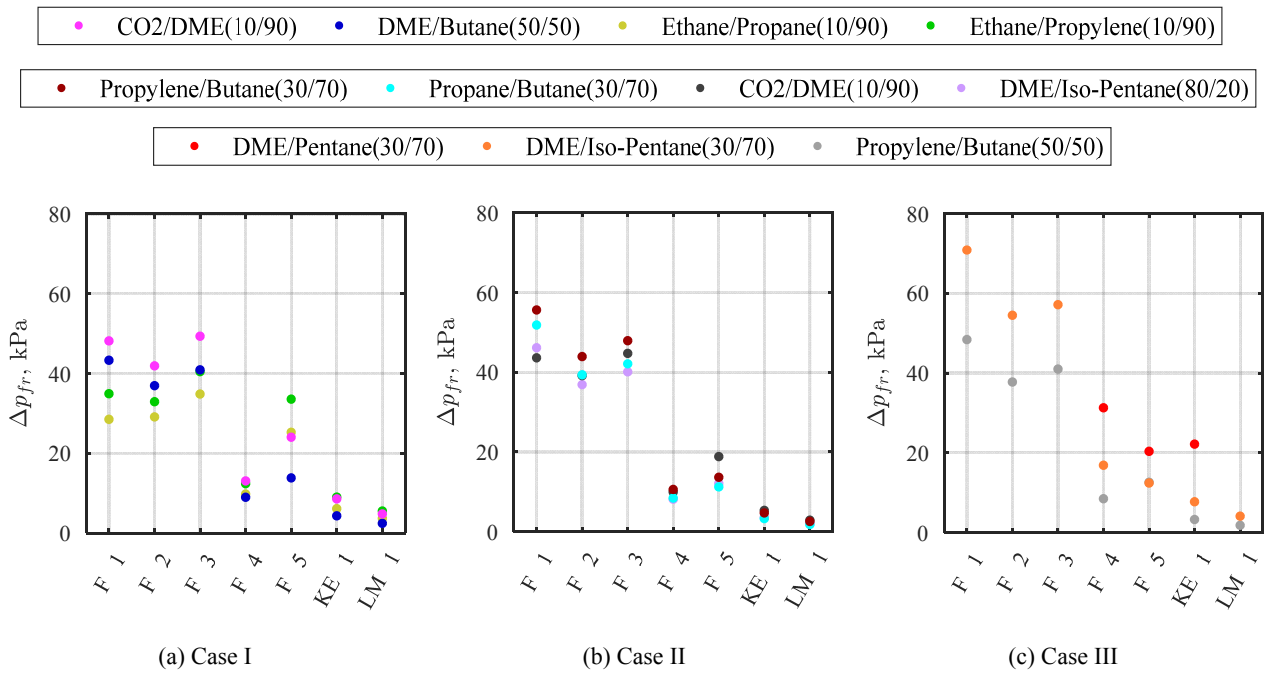

(a) Case I (b) Case II (c) Case III

Fig. 4 Frictional pressure drop estimated with the different correlations, for Case I (a), II (b) and III(c)

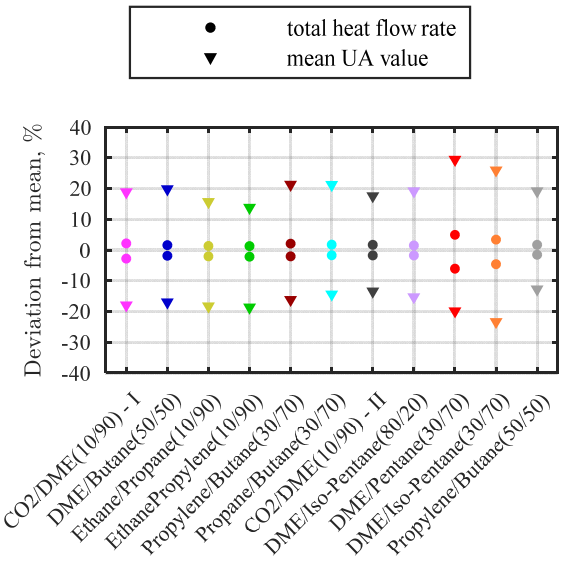

Fig. 5 Deviation from the mean of the UA value and of the total evaporator heat flow rate

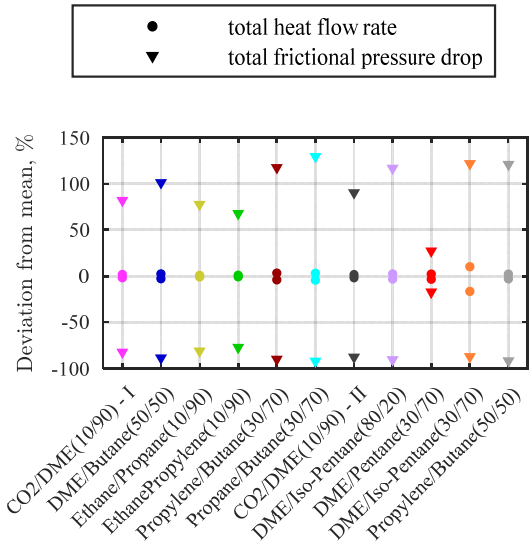

Fig. 6 Deviation from the mean of frictional pressure drops and of the total evaporator heat flow rate

4. DISCUSSION

The presented results suggest that the choice of the prediction method had a significant impact on the estimation of both the heat transfer coefficients and pressure drops. It is however not possible to conclude with a clear recommendation on a set of correlations. The working fluids presented similarities in terms of correlations overestimating or underestimating both UA and frictional pressure drop compared to the mean results and this must be taken into account when choosing a certain prediction method for other mixtures of natural refrigerants. It would however be necessary to compare the results with experimental data specifically obtained for zeotropic mixtures evaporation in PHEs, in order to identify a specific recommended set of correlations for both heat transfer and pressure drops.

Moreover, the results suggested that despite the large discrepancies on the absolute values of UA and pressure drops, a much smaller deviation was obtained on the output of the performance model, i.e. the heat transfer rate at the evaporator. It must be therefore taken into account that different degrees of uncertainties are related with the correlations choice depending on the scope of the analysis. For a user interested in analyzing the PHE performance impact on a thermodynamic cycle, the choice of the prediction method would not lead to large differences (max 6 % and 10% were found for heat transfer and pressure drop correlations, respectively). On the other hand, it would be very relevant to consider the much larger differences between correlations for a user focusing on detailed heat transfer and pressure drop mechanisms in the component.

A typical practical situation was assessed in the present study, i.e. evaluating the performance of the evaporator (with fixed geometry) as the operating conditions were adjusted according to control. The design problem represents an additional situation in which experimental correlations are used. In this case, the operating conditions are fixed and the PHE heat transfer area must be found to meet the design thermal load. A sensitivity analysis to assess the prediction methods impact on the design problem will be therefore part of future work. Last, it must be noted that the sensitivity analysis was limited to assess the impact of different correlations for the (Silver, 1947) and (Bell and Ghaly, 1973), and no correlation which was specifically derived for zeotropic mixtures was included in the analysis. This highlights one more time the importance of focusing further work on deriving experimental correlations for evaporation of different zeotropic mixtures in PHEs.

5. CONCLUSION

The impact of heat transfer and pressure drop correlations was estimated for evaporation of zeotropic mixtures in PHEs. The analysis was based on a performance problem, fixing the suction volume at the evaporator outlet and the mixture super-heating for a given case study. Different mixtures of HCs and CO_2 subject to three different temperature glides were evaluated. The main findings can be summarized as follow:

- Differences of up 30 % were obtained for the mean UA value for Case I and II, while Case III resulted in slightly larger deviation of up 35 %.
- Working fluids experiencing larger temperature glides presented a higher degradation of heat transfer, as well as a stronger dependence on the chosen prediction method.
- Differences of up 130 % were obtained for the frictional pressure drop estimation, with DME/Iso-pentane(30/70) being most sensitive to the correlation applied
- Smaller deviations were obtained on the performance model output, namely 6 % and 10 % for the heat transfer and pressure drop correlation choice, respectively.
- It was not trivial to identify a recommended combination of correlations, despite the similarities between the working fluids. Experiment validation is needed to clarify the results.

ACKNOWLEDGEMENTS

The research work was conducted within the frame of the THERMCYC project (Advanced thermodynamic cycles utilizing low temperature heat sources) funded by Innovation Fund Denmark: The Danish Council for Strategic Research in Sustainable Energy and Environment. The support is gratefully acknowledged.

REFERENCES

Amalfi, R., Vakili-Farahani, F., Thome, J., 2016a. Flow boiling and frictional pressure gradients in plate heat exchangers . Part 2: Comparison of literature methods to database and new prediction methods. International Journal of Refrigeration 61, 185–203. https://doi.org/10.1016/j.ijrefrig.2015.07.009

Amalfi, R., Vakili-Farahani, F., Thome, J., 2016b. Flow boiling and frictional pressure gradients in plate heat exchangers. Part 1: Review and experimental database. International Journal of Refrigeration 61, 166–184. https://doi.org/10.1016/j.ijrefrig.2015.07.010

Bell, I.H., Wronski, J., Quoilin, S., Lemort, V., 2014. Pure and pseudo-pure fluid thermophysical property evaluation and the open-source thermophysical property library coolprop. Industrial and Engineering Chemistry Research 53, 2498–2508. https://doi.org/10.1021/ie4033999

Bell, K., Ghaly, M., 1973. An approximate generalized design method for multicomponent/partial condenser. AIChE Symposium Series 69, 72–79.

Chisholm, D., Wanniarachchi, A.S., 1992. Maldistribution in single-pass mixed-channel plate heat exchangers. Compact Heat

Exchangers for Power and Process Industries (Heat Transfer Division, ASME) HTD-, 95–99.

Collier, J.G., Thome, J.R., 1994. Convective boiling and condensation, (3rd Ed.), Oxford University Press. https://doi.org/10.1016/0923-0467(95)80021-2

Cooper, M.G., 1984. Heat flow rates in saturated nucleate pool boiling - a wide ranging examination using reduced properties. Advances in Heat Transfer 16, 59–156.

Corberán, J.M., Fernández de Córdoba, P., Ortuno, S., Ferri, V., Montes, P., 2000. Modelling of compact evaporators and condensers. Computational Studies 3, 487–496.

Danilova, G.N., Azarskov, V.M., Zemskov, B.B., 1981. Teploobmen V plastinchatihispariteljan razichnole geometri (in Russian) - heat transfer in plates of different geometry. Kholodilnaya Tekhnika 4, 25–31.

Eldeeb, R., Aute, V., Radermacher, R., 2016. An Improved Approach for Modeling Plate Heat Exchangers Based on Successive Substitution in Alternating Flow Directions, in: Proceedings of the International Refrigeration and Air Conditioning Conference, Purdue University, US.

Eldeeb, R., Aute, V., Radermacher, R., 2015. A Survey of Correlations for Heat Transfer and Pressure Drop for Evaporation and Condensation in Plate Heat Exchangers. International Journal of Refrigeration 65, 12–26. https://doi.org/10.1016/j.ijrefrig.2015.11.013

Gorenflo, D., Kenning, D., 2010. Pool Boiling, in: Stephan, P. (Ed.), VDI Heat Atlas Second Edition Chapter H2. Springer Berlin Heidelberg, pp. 757–792.

Han, D.H., Lee, K.J., Kim, Y.H., 2003. Experiments on the characteristics of evaporation of R410A in brazed plate heat exchangers with different geometric configurations. Applied Thermal Engineering 23, 1209–1225. https://doi.org/10.1016/S1359-4311(03)00061-9

Hsieh, Y.Y., Chiang, L.J., Lin, T.F., 2002. Subcooled flow boiling heat transfer of R134a and the associated bubble characteristics in a vertical plate heat exchanger. International Journal of Heat and Mass Transfer 45, 1791–1806.

Hsieh, Y.Y., Lin, T.F., 2003. Evaporation Heat Transfer and Pressure Drop of Refrigerant R-410A Flow in a Vertical Plate. Journal of Heat Transfer-Transactions of the Asme 125, 852–857. https://doi.org/10.1115/1.1518498

Kim, J.H., Cho, J.M., Kim, M.S., 2008. Cooling performance of several CO2/propane mixtures and glide matching with secondary heat transfer fluid. International Journal of Refrigeration 31, 800–806. https://doi.org/10.1016/j.ijrefrig.2007.11.009

Lemmon, E.W., Huber, M.L., McLinden, M.O., 2013. NIST Standard Reference Database 23. Reference Fluid Thermodynamic and Transport Properties (REFPROP), Version 9.1.

Lockhart, R.W., Martinelli, R.C., 1949. Proposed correlation of data for isothermal two-phase, two-component flow in pipes. Chemical engineering progress 45, 39–48.

Longo, G.A., Mancin, S., Righetti, G., Zilio, C., 2015. A new model for refrigerant boiling inside Brazed Plate Heat Exchangers (BPHEs). International Journal of Heat and Mass Transfer 91, 144–149. https://doi.org/10.1016/j.ijheatmasstransfer.2015.07.078

Longo, G., Gasparella, A., 2007. Refrigerant R134a vaporisation heat transfer and pressure drop inside a small brazed plate heat exchanger. International Journal of Refrigeration 30, 821–830. https://doi.org/10.1016/j.ijrefrig.2006.11.011

Martin, H., 1996. A theoretical approach to predict the performance of chevron-type plate heat exchangers. Chemical Engineering and Processing: Process Intensification 35, 301–310. https://doi.org/10.1016/0255-2701(95)04129-X

Palm, B., Claesson, J., 2006. Plate Heat Exchangers: Calculation Methods for Single and Two-Phase Flow. Heat Transfer Engineering 27, 88–98. https://doi.org/10.1080/01457630500523949

Radermacher, R., Hwang, Y., 2005. Heat Transfer of Refrigerant Mixturers, in: Vapor Compression Heat Pumps with Refrigerant Mixtures. CRC Press 2005, pp. 237–278. https://doi.org/doi:10.1201/9781420037579.ch8

Shah, R.K., Focke, W.W., 1988. Plate heat exchangers and their design theory, in: Shah, R.K., Subbarao, E.C., Mashelkar, R.A. (Eds.), Heat Transfer Equipment Design. Hemisphere Publishing, Washington DC, pp. 227–254.

Silver, L., 1947. Gas cooling with aqueous condensation. Industrial Chemist and Chemical Manufacturer 23, 380–386.

SWEP International AB, 2015. SWEP products - V65 [WWW Document]. URL https://www.swep.net/products/v65/ (accessed 12.12.17).

Thome, J.R., Shakir, S., 1987. A new correlation for nucleate pool boiling of aqueous mixtures. AIChE Symposium Series 83, 46–51.

Vakili-Farahani, F., Amalfi, R.L., Thome, J.R., 2015. Two-Phase Heat Transfer and Pressure Drop within Plate Heat Exchangers, in: Thome, J.R., Kim, J. (Eds.), Encyclopedia of Two-Phase Heat Transfer and Flow II : Special Topics and Applications. Volume 2: Boiling Using Enhanced Surfaces, Plate Heat Exchangers and Two-Phase Devices. Chapter 4. World Scientific Publishing, pp. 145–215.

Wanniarachchi, A.S., Ratnam, U., Tilton, B.E., Dutta-Roy, K., 1995. Approximate correlation for chevron-type plate heat exchangers, in: 30th National Heat Transfer Conference.

Yan, Y., Lin, T.F., 1999. Evaporation heat transfer and pressure drop of refrigerant R134a in Plate Heat Exchanger. Journal of Heat Transfer-Transactions of the Asme 121, 118–127.

Zühlsdorf, B., Bühler, F., Mancini, R., Cignitti, S., Elmegaard, B., 2017a. High Temperature Heat Pump Integration using Zeotropic Working Fluids for Spray Drying Facilities, in: Proceedings of the 12th IEA Heat Pump Conference. Rotterdam.

Zühlsdorf, B., Kjær Jensen, J., Cignitti, S., Madsen, C., Elmegaard, B., 2017b. Improving efficiency of heat pumps by use of zeotropic mixtures for different temperature glides, in: Proceedings of ECOS 2017 - 30th International Conference on Efficiency, Cost, Optimization, Simulation and Environmental Impact of Energy Systems. San Diego.

Impact of Liquid/Vapor Maldistribution on the Performance of a Plate Heat Exchanger Evaporator for Pure and Mixed Refrigerants

Roberta MANCINI[1]*, Vikrant AUTE[2], Wiebke BRIX MARKUSSEN[1], Brian ELMEGAARD[1]

[1]Section of Thermal Energy, Department of Mechanical Engineering,
Technical University of Denmark, 2800 Kongens Lyngby, Denmark
Tel: +45 4525 4161, Fax: +45 4525 1961,
Emails: robman@mek.dtu.dk*, wb@mek.dtu.dk, be@mek.dtu.dk

[2]Center for Environmental Energy Engineering,
Department of Mechanical Engineering, University of Maryland,
College Park, MD 20742, USA
Email: vikrant@umd.edu

* Corresponding Author

ABSTRACT

This paper presents an estimation of the degradation in heat transfer performance in plate heat exchanger (PHE) evaporators due to flow maldistribution. A booster heat pump system integrated in a district heating network is used as a case study. Butane and two zeotropic mixtures, namely Propylene/Butane (0.5/0.5) and R1234yf/R1233zdE (0.5/0.5) were evaluated as working fluids. A two-dimensional (2D) numerical model was developed for the evaluation of the total heat flow rate degradation due to the imposed uneven liquid/vapor distribution at the inlet of the PHE channels. Butane showed the largest sensitivity to both the effect of end plates and maldistribution, with an overall reduction of the heat flow rate equal to - 11.2 %. Both the zeotropic mixtures were only insignificantly affected by the uneven quality distribution at the inlet, and suffered a slight reduction of the overall heat flow rate of - 0.9 % and - 0.8 % respectively, due to effect of end plates. Last, the sensitivity to the boundary conditions of the case study was assessed for the mixture Propylene/Butane (0.5/0.5), evaluating the dependence of the obtained results from superheat and number of channels, since both parameters impact the degradation of heat transfer performance.

1. INTRODUCTION

Plate heat exchangers (PHEs) have been increasingly employed in a range of different applications, such as food, chemical and process industries, as well as in the energy sector. They are widely used as evaporators and/or condensers for refrigerating cycles and heat pumps, thus constituting a key component for cycle design and optimization. PHEs are comprised of thin parallel plates stacked together to form parallel channels for fluid flow, which can be arranged in co- or counter-current configurations. The typical chevron corrugation of the plates allows achieving high heat transfer coefficients within a compact design, constituting the key-advantage compared to other heat exchanger (HEX) configurations (Shah and Sekulic, 2002). The occurrence of flow maldistribution can however degrade the performance of multiple channels HEXs. Mueller and Chiou (1988) conducted an extensive review on the main causes of maldistribution, which can be induced by fluid flow characteristics (two-phase flow), fouling, corrosion and nozzle design. It is therefore of paramount importance to estimate the impact of maldistribution on the performance of PHEs.

Bassiouny and Martin (1984a, 1984b) studied the uneven distribution of liquid-to-liquid PHEs for both U-type and Z-type flow arrangements by an analytical model, proposing to compensate the effect by tuning the area ratio between inlet and outlet fluid ports. Rao and Das (2004) studied the maldistribution effect on fluid pressure drop for a PHE for single-phase applications experimentally. Rao et al. (2005) further studied the effect on PHE thermal performances and they found that the deterioration of heat transfer and increase of pressure losses were affected by port size, number of channels, and mass flow rate. Srihari et al. (2005) and Srihari & Das (2006) developed analytical models based on the work of Bassiouny and Martin (1984a, 1984b), in order to study the transient response of PHEs in single pass and multi-pass configurations, showing how flow maldistribution affected the performance of the component in both

steady state and transient operations. Further works by Bobbili et al. (2006) and Tereda et al.(2007) demonstrated the occurrence of flow maldistribution in U-type configuration PHEs experimentally, with more severe maldistribution occurring for higher mass flow rates, smaller port diameters and higher number of channels. Their experimental results showed a good agreement with the analytical treatment first developed by Bassiouny and Martin (1984a, 1984b). Li and Hrnjak (2016) assessed the impact of flow maldistribution of upward nitrogen flow experimentally, using the results to validate a Computational Fluid Dynamics (CFD) model of the PHE header, while Jin and Hrnjak (2017a) evaluated the overestimation of the PHE heat transfer coefficient when the end plate effect is not considered.

Literature reports a limited number of studies focusing on two-phase flow maldistribution in PHEs. Vist and Pettersen (2004) investigated two-phase flow distribution in HEX manifold experimentally, dividing the mass flow into ten channels, in both upward and downward flow configurations. The occurrence of uneven quality distribution was detected for different mass flow rates, resulting in large differences between the thermal load of the various channels. They observed that the vapor phase distributed more easily in the first channels for upward flow, while higher quality was detected in the last channels for downward flow arrangement. Jensen et al. (2015) assessed the impact of such maldistribution by a numerical model, imposing different rates of linear quality variation at the PHE channels inlet. The study was conducted for an evaporator using R134a as working fluid, resulting in a 25 % reduction of the overall heat transfer coefficient when a severe rate of maldistribution was imposed. Jin and Hrnjak (2017b) investigated the distribution of R245fa in a plate channel experimentally, showing large non-uniformities of the flow, heat transfer affected by local heat flux, and occurrence of dry-out zones.

The present work aims at investigating the impact of uneven quality distribution at the inlet channels of PHEs using further numerical modeling. An evaporator of a booster heat pump system for ultra-low temperature district heating (DH) systems is used in the analysis. Zühlsdorf et al. (2018) optimized the coefficient of performance (COP) of the heat pump for different pure fluids and zeotropic mixtures. Due to the non-isothermal nature of mixture phase-change, it is possible to reduce the heat transfer irreversibility in the heat exchangers, by matching the refrigerant temperature profile with the heat source and sink temperature glides. The use of zeotropic mixtures entails however a degradation of the heat transfer coefficient compared to pure fluids (Radermacher and Hwang, 2005), as well as requiring larger heat transfer area for the HEX. The objective of this work is to assess the impact of uneven liquid/vapor distribution imposed at the PHE inlet during evaporation for both pure fluids and zeotropic mixtures.

2. METHODS: CASE STUDY AND MODELLING

2.1 Case study

The assessment of flow maldistribution was carried out for a PHE evaporator for a booster heat pump, for preparation of domestic hot water in ultra-low temperature district heating systems, presented in (Zühlsdorf et al., 2018). A single-stage vapor compression heat pump was suggested for increasing the temperature of one part of the DH forward water stream from 40 °C up to 60 °C, with a total thermal load of 13.9 kW at the condenser. The evaporator heat source (secondary fluid), was taken from the forward DH stream, entering the HEX at 40 °C and then discharged to the return DH line at 25 °C. Different pure and mixed refrigerants were analyzed and ranked with respect to the system COP. The screening was based on a number of natural refrigerants and hydrofluoroolefins (HFOs). Butane, a mixture of Propylene/Butane at 0.5/0.5 mass composition and a mixture of R1234yf/R1233zdE at 0.5/0.5 mass composition were found to be among the best performing fluids, and hence were chosen for the present study. The boundary conditions of the PHE evaporator are reported in Table 1.

Table 1: Evaporator design conditions and COP for the considered working fluids (Zühlsdorf et al., 2018)

Working fluid	$\dot{Q}_{\mathrm{eva}}$, kW	p_{eva}, bar	T_{bubble}, ° C	T_{dew}, ° C	$\dot{m}_{\mathrm{ref}}$, kg/s	$\dot{m}_{\mathrm{w}}$, kg/s	ΔT_{sh}, K	$\dot{V}_{\mathrm{out}}$, m^3/h	COP, -
Butane	11.6	2.25	22.5	22.5	0.0360	0.1857	5	23.1	6.15
Propylene/Butane (0.5/0.5)	12.3	6.29	19.8	37.0	0.0373	0.1967	0	9.9	8.85
R1234yf/R1233zdE (0.5/0.5)	12.3	3.67	18.9	37.3	0.0796	0.1967	0	15.0	8.87

2.2 Plate heat exchanger geometry

The thermodynamic variables at the design point shown in Table 1 were used in order to conduct preliminary sizing of the PHEs for the different working fluids. Each fluid requires a different heat transfer area and thus leads to a

different design. The plate geometry was obtained from a commercial manufacturer and was fixed for all heat exchangers. The total number of channels was determined to meet the design thermal load for all the fluids. The design specifications are reported in Table 2 with the chosen PHE plate size, defined by plate width W and length L. The PHE was assumed to be constructed in stainless steel, with a thermal conductivity equal to 16.2 $\mathrm{W(mK)^{-1}}$. Moreover, the PHEs were designed to operate with counter-current flow arrangement, which is essential to achieve the temperature glide match between the mixtures and the secondary fluid.

Table 2: Evaporator SWEP V80 (SWEP International AB, 2015) plate dimensions and count

W, m	L, m	$N_{\mathrm{ch_{tot}}}$,-		
		Butane	Propylene/Butane (0.5/0.5)	R1234yf/R1233zdE (0.5/0.5)
0.117	0.524	23	49	57

As shown in Table 2, the sizing led to a very different number of required channels for the pure fluid case compared to the two zeotropic mixtures. A higher heat transfer area is required for the lower mean temperature difference during evaporation due to mixture glide and to account for the heat transfer degradation compared to pure fluids.

2.3 Imposed vapor quality maldistribution

The uneven vapor quality maldistribution was imposed and used as input to the PHE numerical model. Vist and Pettersen (2004) showed that the vapor phase distribution changed monotonically with increasing distance from the inlet manifold, depending on the flow direction (upward or downward). A linear variation of the vapor quality at the inlet of the channels was therefore assumed, similar to (Jensen et al., 2015). The variation was imposed by a vapor quality difference parameter Δx, indicating the absolute difference between the vapor quality in the first and last refrigerant channel. The vapor quality at the inlet of the j^{th} channel is hence estimated by Eq. (1):

$$x_{\mathrm{IN_j}} = x_{\mathrm{IN_1}} + \frac{j-1}{N_{\mathrm{ch_{ref}}} - 1} \Delta x \tag{1}$$

$x_{\mathrm{IN_j}}$ was expressed as function of the total number of refrigerant channels $N_{\mathrm{ch_{ref}}}$ and of the inlet vapor quality at the first channel $x_{\mathrm{IN_1}}$. The study was carried out for different quality difference values ranging from 0.00 up to 0.25 with steps of 0.05. When Δx is equal to zero, a uniform quality distribution is assumed and the mass flow of both refrigerant and secondary fluid is solely affected by the end plates.

2.4 Heat pump boundary conditions

With the occurrence of flow maldistribution, the PHE operation shifts from design conditions. In practical applications, the operating conditions of the refrigerant are adjusted in order to respect the control values. According to the case study boundary conditions (Zühlsdorf et al., 2018), the suction volume flow rate at the evaporator outlet and the refrigerant superheat were fixed to the design values, reported in Table 1. The refrigerant saturation pressure and mass flow rate were estimated accordingly for each case. Note that a different superheat was imposed for Butane and Propylene/Butane (0.5/0.5). Due to the temperature glide during evaporation, zeotropic mixtures offer the possibility of determining the outlet quality by measuring pressure and temperature as independent variables also in the two-phase region. This implies that superheat may not be necessary for control.

2.5 PHE modeling

The heat transfer and fluid flow were solved by an internal solution procedure based on a two-dimensional (2D) discretization of the PHE. An external solver called the internal 2D PHE model for the solution of the mass flow distribution and operating conditions. They are presented in subsections 2.5.1 and 2.5.2, respectively.

2.5.1 Heat transfer and fluid flow

The internal solver iterated on wall temperatures and refrigerant and secondary fluid pressure drops based on a successive substitution approach. The discretization was applied in 2D: lengthwise along the flow direction and with respect to the different PHE channels. The lengthwise discretization divided the PHE in 50 elements of equal heat transfer area. Each element was further divided into a number of control volumes (CVs) equal to the total number of

channels for the refrigerant and secondary fluid, i.e. $N_{\mathrm{ch_{tot}}} = N_{\mathrm{ch_{ref}}} + N_{\mathrm{ch_{hs}}}$. Each CV was therefore representing either the refrigerant or the heat source flow. The PHE was solved with the following assumptions:

1. steady state;
2. adiabatic end plates
3. no longitudinal conduction through the walls;
4. homogeneous two-phase flow.

Based on a linear distribution of wall temperature guess and uniform pressure drops for both fluids, the momentum and energy balance equations were solved iteratively for each CV. Figure 1 shows the structure of the 2D discretization, together with wall temperature and pressure drops used as iteration variables. The tolerance of the solver was given by a 2-norm of the relative residuals of wall temperature and refrigerant and secondary side pressure drops of 10^{-5}. Fluid thermo-physical properties were evaluated using Coolprop (Bell et al., 2014) for pure fluids and water, and REFPROP (Lemmon et al., 2013) for mixtures.

Empirical correlations were used for the evaluation of local heat transfer coefficients and pressure drops. The two-phase refrigerant heat transfer coefficient was estimated by Amalfi et al. (2016) in case of pure fluids. Collier and Thome (1994) recommended the use of the Silver (1947) and Bell and Ghaly (1973) method for the estimation of the two-phase mixture heat transfer coefficient, in order to take the degradation of heat transfer into account. The method estimates the mixture flow boiling heat transfer coefficient as function of the nucleate boiling, convective boiling and vapor only heat transfer coefficients, evaluated by Cooper (1984), Amalfi et al. (2016) and Martin (1996) correlations, respectively. The Thome and Shakir (1987) correction factor was applied to account for the mixture degradation to the nucleate boiling contribution. The single-phase heat transfer coefficient in the superheated region was estimated by using Martin (1996) correlation for both pure and mixed refrigerants, and it was also applied to estimate the heat source heat transfer coefficient. A smooth transition was ensured at the transition between two-phase and superheated region, by calculating the refrigerant heat transfer coefficient as a weighted interpolation of the two-phase and single-phase contributions. The smoothing was applied to the CVs with local vapor quality included in the interval [0.9, 1). Pressure drops were computed for both fluids by applying the steady-state momentum equation, considering the contributions of friction, acceleration and gravity. The two-phase frictional pressure drops were assessed by applying the Lockhart and Martinelli (1949) method, with coefficients proposed by Palm and Claesson (2006). The single-phase pressure drop of the superheated refrigerant and of the heat source were estimated by Martin (1996). The acceleration and gravity pressure drops in the two-phase region were calculated by using the void fraction model by Smith (1969) for the estimation of the momentum density and cross section average density.

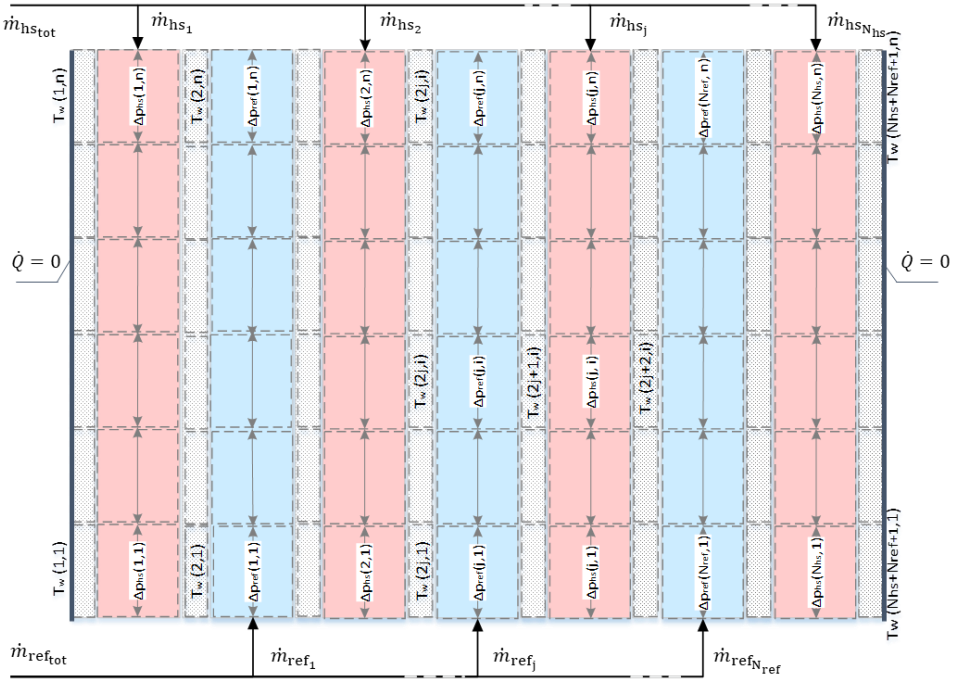

Figure 1: Structure of the discretized 2D PHE model with iteration variables

2.5.2 Solution procedure for flow distribution and operating conditions

The internal solver for heat transfer and fluid flow was coupled with a solver to determine the mass flow distribution of both refrigerant and heat source at the inlet of each channel. The solver determined the refrigerant operating conditions according to the boundary conditions imposed by the cycle, as explained in subsection 2.4. The external solver was based on *fsolve* (Mathworks, 2017), coupled with the user-supplied internal solver for heat transfer and fluid flow. A system of $N_{\mathrm{ch_{ref}}} + N_{\mathrm{ch_{hs}}} + 3$ equations was therefore solved for the same number of unknowns. The unknowns were the total mass flow rate of the refrigerant, the mass flow rate distribution of both heat source and refrigerant, the refrigerant inlet saturation pressure and the inlet vapor quality of the first channel. The equations are reported in Table 3. The average values of refrigerant temperature and density at outlet conditions were estimated by considering the mixing enthalpy of the refrigerant mass flow from all the channels at the refrigerant outlet pressure.

Table 3: Governing equations of the flow distribution solver

Flow distribution solver governing equations		
Mass conservation of manifold		
$\sum_{\mathrm{j}=1}^{N_{\mathrm{ch_{ref}}}} \dot{m}_{\mathrm{ref_j}} = \dot{m}_{\mathrm{ref_{tot}}}$	$\sum_{\mathrm{j}=1}^{N_{\mathrm{ch_{hs}}}} \dot{m}_{\mathrm{hs_j}} = \dot{m}_{\mathrm{hs_{tot}}}$	$\sum_{\mathrm{j}=1}^{N_{\mathrm{ch_{ref}}}} \dot{m}_{\mathrm{ref_j}} x_{\mathrm{ref_{in_j}}} = \dot{m}_{\mathrm{ref_{tot}}} x_{\mathrm{ref_{in}}}$
Pressure drop equalization		
$\sum_{\mathrm{i}=1}^{n} \Delta p_{\mathrm{ref_{i,j}}} = \sum_{\mathrm{i}=1}^{n} \Delta p_{\mathrm{ref_{i,j+1}}}$	$\sum_{\mathrm{i}=1}^{n} \Delta p_{\mathrm{hs_{i,j}}} = \sum_{\mathrm{i}=1}^{n} \Delta p_{\mathrm{hs_{i,j+1}}}$	
$\mathrm{j} = 1, \dots, N_{\mathrm{ch_{ref}}} - 1$	$\mathrm{j} = 1, \dots, N_{\mathrm{ch_{hs}}} - 1$	
Superheat		**Compressor suction volume flow**
$\bar{T}_{\mathrm{ref_{out}}} - T_{\mathrm{dew}} = \Delta T_{\mathrm{SH}}$		$\dot{m}_{\mathrm{ref_{tot}}} \cdot \bar{\rho}_{\mathrm{ref_{out}}} = \dot{V}_{\mathrm{out}}$

2.5.3 Comparison with one-dimensional (1D) model

In order to separate the effect of uneven vapor quality distribution at the PHE inlet channels from the effect of end plates, the results of the flow distribution solver were compared with a 1D model of the component, discretized along the flow direction. The heat transfer and fluid flow equations were solved iteratively by considering 50 PHE elements, without further discretizing across the PHE channels. The solution procedure was implemented analogously to the 2D model, and the same boundary conditions for superheat and suction volume flow rate were imposed.

2.5.4 Model validation

The 2D heat transfer and fluid flow numerical model coupled with the flow distribution and operating conditions solver was validated against 316 experimental data points for evaporation of R134a, R1234yf and R1234ze (Zhang et al., 2017). The model reported a normalized root mean square error on the total heat flow rate equal to 2.9 % and on the refrigerant pressure drop equal to 23.8 %.

3. RESULTS

3.1 Mass flow distribution and temperature profiles

Figure 2 shows the refrigerant mass flow distribution for the three working fluids at different maldistribution rates, under the design considered in Table 2. The case Δx = 0 corresponds to the uniform distribution of vapor quality at the inlet channels, wherein the non-uniform mass flow distribution is solely due to the effect of the end plates. The ordinate reports the percentage deviation of the mass flow rate in each channel with respect to the average mass flow rate per channel. The average value is estimated by dividing the total mass flow rate, reported in Table 4 for the different maldistribution cases, by the total number of refrigerant channels. Figure 2 (a) shows that the pure fluid Butane was the most affected by maldistribution, compared to both Propylene/Butane (0.5/0.5) (b) and

R1234yf/R1233zdE (0.5/0.5) (c). The latter was the working fluid being least affected by uneven quality distribution, with maximum differences equal to - 3.3 % for the case of Δx = 0.25, followed by Propylene/Butane (0.5/0.5) with a maximum deviation of - 6.1 %. Butane showed consistently higher deviations, reaching up to + 46.7 %. Furthermore, Figure 2 reports opposite mass flow trends for the pure fluid compared to the two zeotropic mixtures. In the case of Butane, a higher mass flow rate was obtained in the channels where the inlet vapor quality was lower. This is due to the higher pressure drop entailed by the vapor phase, thereby causing a mass flow reduction in those channels where the complete evaporation and superheat were reached earlier. On the other hand, both Figure (b) and (c) show that the mass flow of the two zeotropic mixtures is only slightly affected by maldistribution. Moreover, Table 4 shows that the total refrigerant mass flow rate of the two mixed refrigerants is only slightly affected by the maldistribution parameter Δx, while the total mass flow of Butane decreases with increasing Δx, thereby implying an expected reduction of the total evaporator heat flow rate.

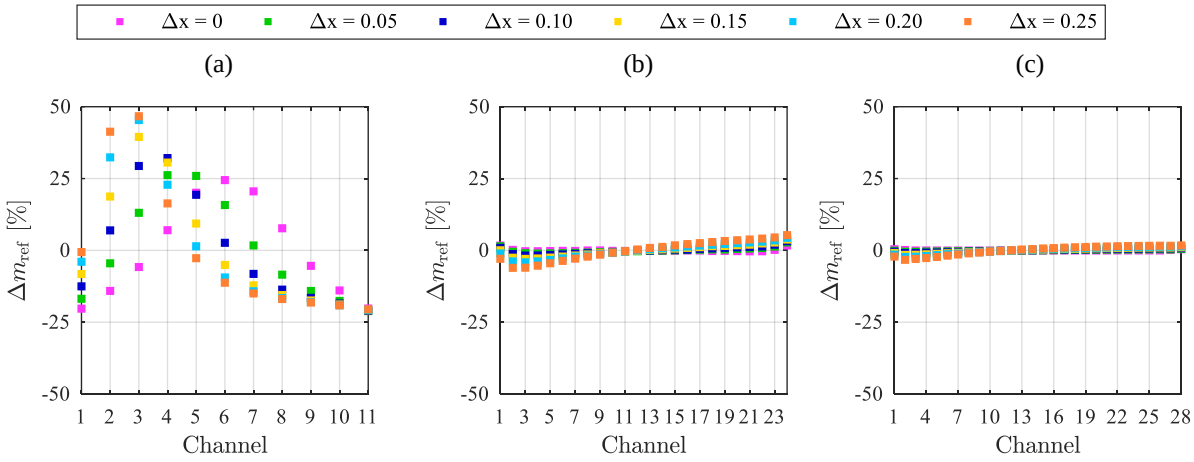

Figure 2: Deviation from average value of refrigerant mass flow rate in each channel at different rates of maldistribution, for (a) Butane, (b) Propylene/Butane (0.5/0.5) and (c) R1234yf/R1233zdE (0.5/0.5)

Table 4: Total refrigerant mass flow rate at different maldistribution rates for the three considered working fluids

Working fluid	$\dot{m}_{\mathrm{ref_{tot}}}$, kg/s					
	$\Delta x = 0$	$\Delta x = 0.05$	$\Delta x = 0.10$	$\Delta x = 0.15$	$\Delta x = 0.20$	$\Delta x = 0.25$
Butane	0.0347	0.0346	0.0344	0.0340	0.0337	0.0334
Propylene/Butane (0.5/0.5)	0.0355	0.0354	0.0354	0.0355	0.0354	0.0354
R1234yf/R1233zdE (0.5/0.5)	0.0745	0.0750	0.0751	0.0750	0.0751	0.0750

The higher sensitivity to maldistribution of the pure fluid can also be observed in the temperature distribution of the refrigerant, heat source and wall temperature in the different channels, which is shown in Figure 3 for the case of severe maldistribution (Δx = 0.25). The refrigerant flows upward in the even channels, while the water flows downward in the odd ones. Figure 3 (a) shows the results for Butane. The channels with a low refrigerant mass flow rate experienced a large region of superheat, where the temperature level of the refrigerant outlet reached the inlet heat source temperature. The effect on the overall outlet superheat was however compensated by the channels with lower outlet temperature. For instance, incomplete evaporation occurs in channels 4 and 6 of Figure 3 (a), presenting outlet refrigerant temperature equal to the saturation level.

Figure 3 (b) shows the same temperature distribution for the case of Propylene/Butane (0.5/0.5) at Δx = 0.25. The temperature profiles for R1234yf/R1233zdE (0.5/0.5) were similar to those of Propylene/Butane (0.5/0.5), and hence are not reported here. Compared to the pure fluid, a refrigerant temperature rise can be observed during the evaporation process, due to the characteristic temperature glide of zeotropic mixtures. The effect of end plates can be noticed in the outmost refrigerant channels (channels 2 and 48 of Figure 3 (b)) presenting a slightly higher outlet temperature compared to the inner ones. The effect of maldistribution, namely the slightly uneven mass flow distribution presented in Figure 2 (b), can however not be detected.

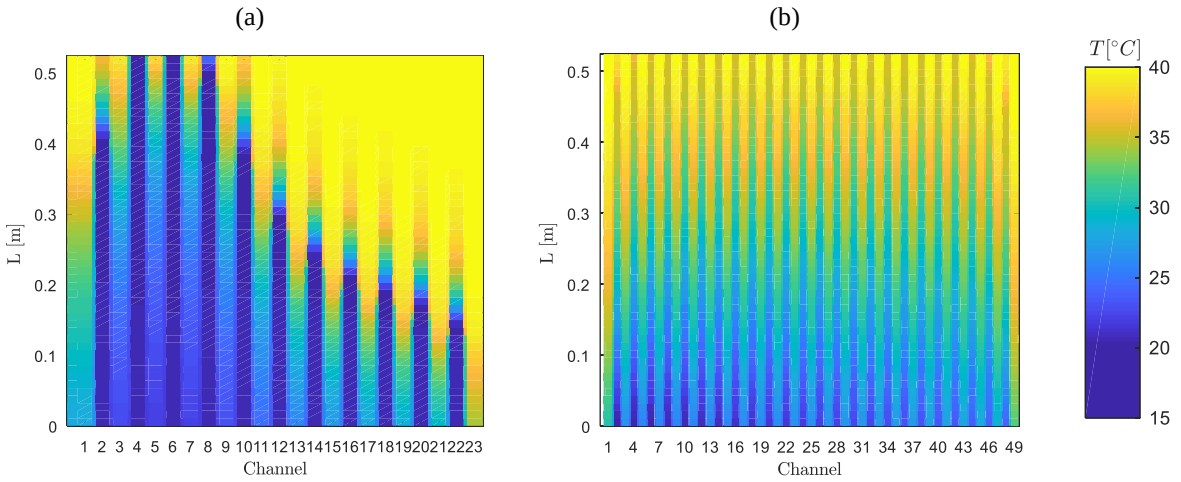

Figure 3: Temperature distribution in the different channel and across the plate length, for (a) Butane and (b) Propylene/Butane (0.5/0.5), for the case of severe maldistribution rate Δx = 0.25

3.2 Degradation of heat transfer performance

Figure 4 reports the total heat flow rate for the three working fluids as function of the maldistribution parameter Δx. The results are compared with the value obtained by considering a 1D discretization of the PHE along the flow direction, thereby neglecting the effect of end plates. Note that the same boundary conditions on superheat and suction volume were applied to the 1D case. The heat transfer performance for Butane (shown in Figure 4 (a)) was considerably affected by both the effect of end plates and liquid/vapor maldistribution. A reduction of -5.2 % on the total heat flow rate was obtained between the 1D model and the 2D model with Δx = 0, accounting for the effect of end plates. A further reduction of -6.3 % was obtained between the uniform distribution case and the severe maldistribution imposed by setting Δx = 0.25.

On the other hand, both zeotropic mixtures Propylene/Butane (0.5/0.5) and R1234yf/R1233zdE (0.5/0.5) (shown in Figure 4 (b) and (c)) report a negligible effect of the liquid/vapor maldistribution on the total heat flow rate, performing with a constant heat flow rate as function of the maldistribution rate Δx. The trend is consistent with the slight impact on the total refrigerant mass flow presented in Table 4. A small effect of the end plates was estimated, equal to a reduction of the heat flow rate of -0.9 % and -0.8 %, for Propylene/Butane (0.5/0.5) and R1234yf/R1233zdE (0.5/0.5), respectively. It must be noted that the lower impact of end plates in the case of the zeotropic mixtures was also affected by a larger number of plates employed by both the designs, namely 49 and 57 against the 23 channels used for Butane.

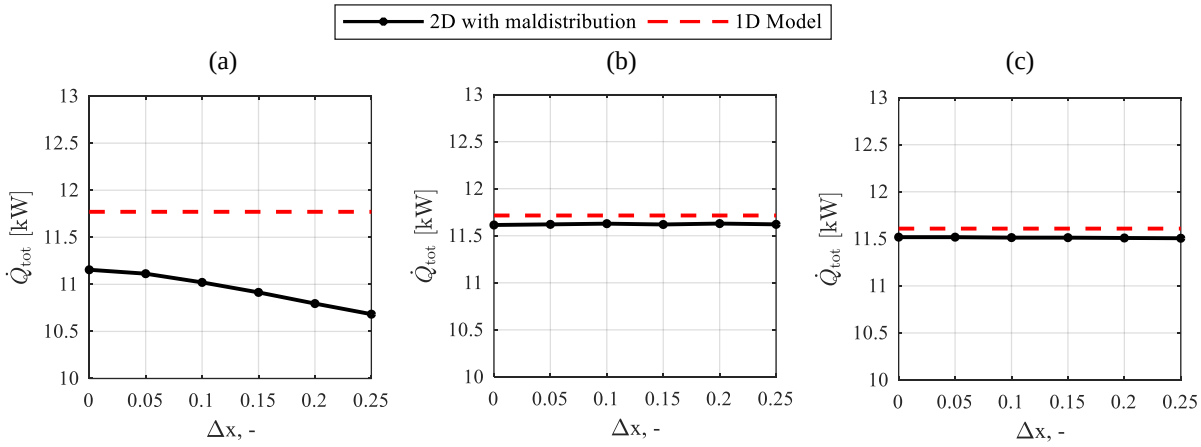

Figure 4: Total heat flow rate as function of the maldistribution rate for (a) Butane, (b) Propylene/Butane (0.5/0.5) and (c) R1234yf/R1233zdE (0.5/0.5)

4. DISCUSSION

5.1 Impact of number of channels and superheat

The results suggest that the zeotropic mixtures may show operating advantages compared to Butane for the heat pump system, due to a considerably reduced impact of flow maldistribution on the PHE performance. Despite the higher initial investment for the larger heat transfer area required by the use of mixtures, both Propylene/Butane (0.5/0.5) and R1234yf/R1233zdE (0.5/0.5) were only slightly affected by the occurrence of maldistribution, while Butane suffered from a performance reduction equal to -11.2 % due to flow maldistribution and end plate effects altogether.

These considerations are however dependent on the boundary conditions used in the study. Among these, the different superheat and the number of channels could largely affect the outcome of the analysis. The larger number of channels employed for both the mixtures reduced the effect of end plates from -5.2 % for Butane down to less than -1 % for both the mixtures. Moreover, a larger imposed superheat is likely to increase the vapor phase pressure drop, thereby leading to a further reduction of the mass flow in the channels reaching a higher degree of superheat. In order to compare performance under same boundary conditions for the pure and mixed refrigerants, a comparison was carried out between Butane and Propylene/Butane (0.5/0.5) for the same number of channels, e.g. 23, and the same controlled value for superheat e.g. 5 K. The plate geometry was kept constant as presented in Table 2.

Figure 5 (a) shows the obtained refrigerant mass flow distribution of Propylene/Butane (0.5/0.5). Compared to the results of Butane (Figure 2 (a)), the same trend was obtained. As expected, the larger superheat implied a reduction of the refrigerant mass flow rate for the channels with higher inlet vapor quality, reaching the superheated region earlier. It is however shown that the magnitude of this effect is much lower in the case of the mixture compared to the pure fluid, with maximum percentage deviations of the mass flow rate of – 5.8 % from the average, in the case of Δx = 0.25, against the +46.7 % of Butane, as reported in the first two columns of Table 5.

The mass distribution effect was translated into heat transfer performance degradation, as shown in Figure 5 (b) for the case of Propylene/Butane (0.5/0.5). The trend is similar to the one of Butane (shown in Figure 4 (a)), with a first decrease in the total heat flow rate due to the effect of end plates, and a further decrease in performance when a larger non-uniform vapor quality distribution was imposed at the inlet. The percentage deviations are reported in the last four columns of Table 5 using the 1D-model results as reference case. Propylene/Butane (0.5/0.5) experienced a degradation of heat transfer due to end plates equal to around 1/3 of the same effect for the pure fluid. The degradation due to non-uniform quality distribution was smaller, causing an additional -0.4% loss in total heat flow rate. Butane, on the other hand was largely influenced by both end plates and the maldistribution, leading to an equal degradation of heat transfer, around -6 % for each.

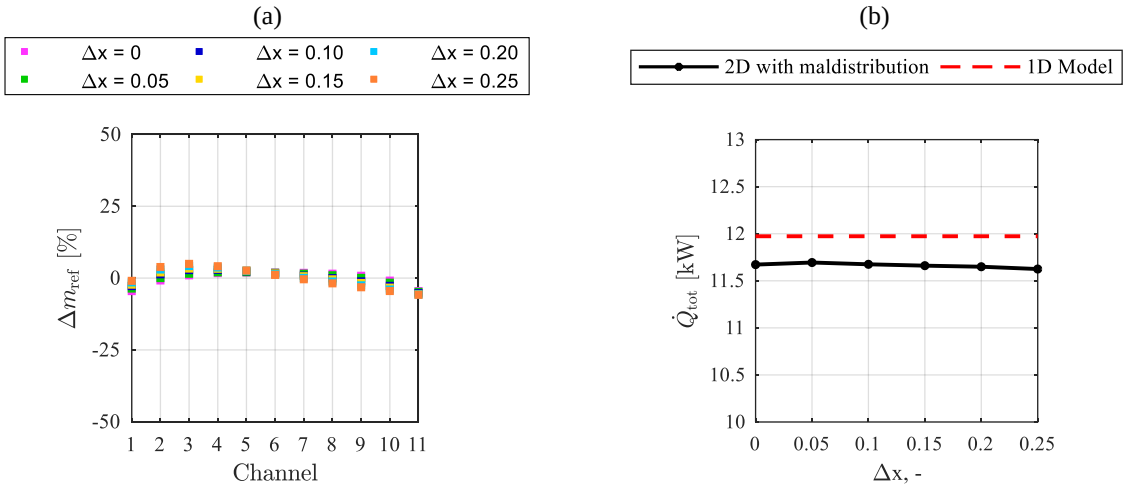

Figure 5: (a) Deviation from average refrigerant mass flow rate in each channel and (b) total heat flow rate as function of the maldistribution rate for Propylene/Butane (0.5/0.5) with 23 total channels and 5 K superheat

Table 5: Mass flow maximum deviations and maximum estimated degradation of total heat flow rate due to end plates and to liquid/vapor maldistributions for Butane and Propylene/Butane (0.5/0.5)

Working fluid	$\dot{m}_{\mathrm{ref_{tot}}}$, (Δx = 0.25), kg/s	max($\Delta\dot{m}_{\mathrm{ch}}$) (Δx = 0.25), %	$\dot{Q}_{\mathrm{tot}}$ (1D – ref.), kW	$\dot{Q}_{\mathrm{tot}}$ (Δx = 0), kW	$\Delta\dot{Q}_{\mathrm{tot}}$, %	$\dot{Q}_{\mathrm{tot}}$ (Δx = 0.25), kW	$\Delta\dot{Q}_{\mathrm{tot}}$, %
Butane	0.0334	+ 46.7	11.8	11.2	- 6.3	10.4	- 11.2
Propylene/Butane (0.5/0.5)	0.0349	- 5.8	12.0	11.7	- 2.5	11.6	- 2.9

5.2 Limitations and future work

The flow distribution was solved by imposing equal pressure drops of both fluids across the channels, thereby entailing a strong dependence of the results on the chosen empirical correlation for the frictional contribution to pressure drop. The study was however carried out by applying the same model to pure fluid and mixtures, and hence led to a reasonable comparison between the fluids, regardless of the uncertainties in the calculation. Investigating the effect of using alternative correlations would be a further step to validate the present results. Moreover, the study was carried out for a specific application of a booster heat pump for a DH network, thus further validation would be obtained by evaluating additional refrigerants and different operating conditions for various applications. Last, the economic benefit of PHE performance entailed by mixture utilization, avoiding a likely degradation of the heat pump COP, could be compared with the increasing investment due to larger required heat transfer area.

5. CONCLUSIONS

The impact of uneven liquid/vapor distribution at the inlet of a PHE evaporator was evaluated for the case study of a booster heat pump for a DH network. Three different refrigerants were compared, namely Butane, Propylene/Butane (0.5/0.5) and R1234yf/R1233zdE (0.5/0.5). The degradation of PHE performance was evaluated for different cases of maldistribution, imposed by assuming a linear variation of the inlet vapor quality across the PHE channels. Butane was the most affected by maldistribution, with a consistent reduction of the mass flow rates in the channels with higher inlet quality, reaching the superheated region earlier. A degradation of the heat flow rate equal to - 6.3 % was estimated as the sole effect of end plates, while an overall reduction of - 11.2% was estimated in case of severe maldistribution. Both zeotropic mixtures were only slightly affected by end plates, with heat transfer rate decrease of - 0.9% and - 0.8 %, while the uneven vapor/quality distribution resulted in a negligible effect on the total heat flow rate.

NOMENCLATURE

COP	coefficient of performance	(-)	$\dot{Q}$	heat flow rate	(kW)
L	plate length	(m)	T	temperature	(K or °C)
$\dot{m}$	mass flow rate	(kg/s)	$\dot{V}$	volume flow rate	(m^3/hr)
N_{ch}	number of channels	(-)	W	plate width	(m)
p	pressure	(bar)	x	vapor quality	(-)
Greek letters					
Δ	difference	(-)	ρ	density	(kg/m^3)
Subscripts					
ch	channel		out	outlet	
eva	evaporator		ref	refrigerant	
hs	heat source		sh	superheating	
in	inlet		tot	total	

REFERENCES

Amalfi,R.,Vakili-Farahani, F., Thome, J., 2016. Flow boiling and frictional pressure gradients in plate heat exchangers part 2 Comparison of literature methods to database and new prediction methods. Int. J. Refrig. 61, 185–203.

Bassiouny, M.K., Martin, H., 1984a. Flow distribution and pressure drop in plate heat exchangers—I U-type arrangement. Chem. Eng. Sci. 39, 693–700. https://doi.org/10.1016/0009-2509(84)80176-1

Bassiouny, M.K., Martin, H., 1984b. Flow distribution and pressure drop in plate heat exchangers—II Z-type arrangement. Chem. Eng. Sci. 39, 701–704.

Bell, I.H., Wronski, J., Quoilin, S., Lemort, V., 2014. Pure and pseudo-pure fluid thermophysical property evaluation and the open-source thermophysical property library coolprop. Ind. Eng. Chem. Res. 53, 2498–2508.

Bell, K., Ghaly, M., 1973. An approximate generalized design method for multicomponent/partial condenser. AIChE Symp. Ser. 69, 72–79.

Bobbili, P.R., Sunden, B., Das, S.K., 2006. An experimental investigation of the port flow maldistribution in small and large plate package heat exchangers. Appl. Therm. Eng. 26, 1919–1926.

Collier, J.G., Thome, J.R., 1994. Convective boiling and condensation, (3rd Ed.), Oxford University Press.

Cooper, M.G., 1984. Heat flow rates in saturated nucleate pool boiling - a wide ranging examination using reduced properties. Adv. Heat Transf. 16, 59–156.

Jensen, J.K., Kaern, M.R., Ommen, T.S., Brix, W., Reinholdt, L., Elmeegard, B., 2015. Effect of liquid/vapour maldistribution on the performance of plate heat exchanger evaporators, in: Proceedings of the 24th IIR International Congress of Refrigeration.

Jin, S., Hrnjak, P., 2017a. Effect of end plates on heat transfer of plate heat exchanger. Int. J. Heat Mass Transf. 108, 740–748. https://doi.org/10.1016/j.ijheatmasstransfer.2016.11.106

Jin, S., Hrnjak, P., 2017b. A new method to simultaneously measure local heat transfer and visualize flow boiling in plate heat exchanger. Int. J. Heat Mass Transf. 113, 635–646.

Lemmon, E.W., Huber, M.L., McLinden, M.O., 2013. NIST Standard Reference Database 23. Ref. Fluid Thermodyn. Transp. Prop. (REFPROP), Version 9.1.

Li, W., Hrnjak, P., 2016. Single Phase Pressure Drop and Flow Distribution in Brazed Plate Heat Exchangers, in: International Refrigeration and Air Conditioning Conference. Purdue university, p. Paper 1812.

Lockhart, R.W., Martinelli, R.C., 1949. Proposed correlation of data for isothermal two-phase, two-component flow in pipes. Chem. Eng. Prog. 45, 39–48.

Martin, H., 1996. A theoretical approach to predict the performance of chevron-type plate heat exchangers. Chem. Eng. Process. Process Intensif. 35, 301–310. https://doi.org/10.1016/0255-2701(95)04129-X

Mathworks, 2017. fsolve, Matlab 2017b URL https://www.mathworks.com (accessed 3.5.18).

Mueller, A.C., Chiou, J.P., 1988. Review of various Types of Flow Maldistribution in Heat Exchangers. Heat Transf. Eng. 9, 36–50. https://doi.org/10.1080/01457638808939664

Palm, B., Claesson, J., 2006. Plate Heat Exchangers: Calculation Methods for Single and Two-Phase Flow. Heat Transf. Eng. 27, 88–98. https://doi.org/10.1080/01457630500523949

Radermacher, R., Hwang, Y., 2005. Heat Transfer of Refrigerant Mixturers, in: Vapor Compression Heat Pumps with Refrigerant Mixtures. CRC Press 2005, pp. 237–278. https://doi.org/doi:10.1201/9781420037579.ch8

Rao, B.P., Das, S.K., 2004. An Experimental Study on the Influence of Flow Maldistribution on the Pressure Drop Across a Plate Heat Exchanger. J. Fluids Eng. - Trans. ASME 126, 680–691. https://doi.org/10.1115/1.1779664

Rao, B.P., Sunden, B., Das, S.K., 2005. An Experimental and Theoretical Investigation of the Effect of Flow Maldistribution on the Thermal Performance of Plate Heat Exchangers. J. Heat Transf. Asme 127.

Shah, R.K., Sekulic, D.P., 2002. Fundamentals of Heat Exchanger Design, … to Thermo-Fluids Systems Design.

Silver, L., 1947. Gas cooling with aqueous condensation. Ind. Chem. Chem. Manuf. 23, 380–386.

Smith, S.L., 1969. Void fractions in two-phase flow: a correlation based upon an equal velocity head model. Proc. Inst. Mech. Eng. 184, 647–664. https://doi.org/10.1243/PIME_PROC_1969_184_051_02

SWEP International AB, 2015. SWEP Products URL https://www.swep.net/products/ (accessed 2.23.18).

Tereda, F.A., Srihari, N., Sunden, B., Das, S.K., 2007. Experimental investigation on port-to-channel flow maldistribution in plate heat exchangers. Heat Transf. Eng. 28, 435–443.

Thome, J.R., Shakir, S., 1987. A new correlation for nucleate pool boiling of aqueous mixtures. AIChE Symp. Ser. 83, 46–51.

Vist, S., Pettersen, J., 2004. Two-phase flow distribution in compact heat exchanger manifolds. Exp. Therm. Fluid Sci. 28, 209–215. https://doi.org/10.1016/S0894-1777(03)00041-4

Zhang, J., Desideri, A., Kærn, M.R., Ommen, T.S., Wronski, J., Haglind, F., 2017. Flow boiling heat transfer and pressure drop characteristics of R134a, R1234yf and R1234ze in a plate heat exchanger for organic Rankine cycle units. Int. J. Heat Mass Transf. 108, 1787–1801. https://doi.org/10.1016/j.ijheatmasstransfer.2017.01.026

Zühlsdorf, B., Meesenburg, W., Ommen, T., Kjaer Jensen, J., Brix Markussen, W., Elmegaard, B., 2018. Improving the performance of booster heat pumps using zeotropic mixtures. Energy.

ACKNOWLEDGEMENT

This research was funded by Innovations Fund Denmark under the project title “THERMCYC - Advanced thermodynamic cycles utilizing low temperature heat sources”. The first author would like to acknowledge the support of the MOC consortium of the Center for Environmental Energy Engineering (CEEE) at University of Maryland.

Manuscript ID: 853
DOI: 10.18462/iir.icr.2019.853

Design recommendations for plate heat exchangers in heat pumps using pure and mixed refrigerants

Roberta MANCINI [(a)], Benjamin ZÜHLSDORF [(a)], Wiebke BRIX MARKUSSEN[(a)], Brian ELMEGAARD[(a)]

[(a)] Section of Thermal Energy, Department of Mechanical Engineering, Technical University of Denmark (DTU), 2800 Kgs. Lyngby, Denmark, Tel: +45 45254161
Emails: robman@mek.dtu.dk*, bezuhls@mek.dtu.dk, wb@mek.dtu.dk, be@mek.dtu.dk

ABSTRACT

This paper aims at deriving design recommendations for plate heat exchanger (PHE) evaporators and condensers in heat pump (HP) systems using different refrigerants. A coupled HP - PHE simulation framework was used to carry out cycle and component design for a case study, with different combinations of PHE geometrical parameters, and propane, butane and propylene/butane (0.5/0.5) as refrigerants. An operating model subsequently evaluated the heat pump thermodynamic and economic performance with the different designed PHEs: the trade-off between heat transfer area and refrigerant pressure drops was therefore taken into account for both components. Only evaporator pressure drops affected the Coefficient of Performance (COP), and different refrigerants presented dissimilar slopes of degradation. Condenser design did not influence the COP, and the economic optimum corresponded to the lowest size. The evaporator design at minimum cost was instead found as a trade-off between heat transfer area and pressure drops for all the working fluids. Despite the different rates of COP drop, the three refrigerants resulted in the same optimal pressure drop at the evaporator, equal to around 5 kPa.

Keywords: Pressure drops, Zeotropic mixtures, Evaporators, Condensers, Economic analysis

1. INTRODUCTION

Optimal design of evaporators and condensers in heat pumps plays a key-role for overall system thermodynamic and economic optimization. Plate heat exchangers (PHEs) offer a compact design that is feasible for both pure fluids and zeotropic mixtures. Contrary to the most common configurations of micro-channel heat exchangers (HEXs), PHE allows counter-current flow arrangement, which is essential for temperature glide matching between mixed refrigerants and heat source/sink. Nonetheless, HEX design often relies on criteria based on heuristics, such as maximum allowable inlet velocities or maximum pressure drop, possibly leading to suboptimal solutions, depending on the working fluid (Mancini et al., 2018). Previous studies (Muralikrishna and Shenoy, 2000; Wang and Sundén, 2003) attempted at establishing trade-off criteria between pressure drops and investment in heat transfer area, yet mostly focusing on single-phase application or without considering the impact on the thermodynamic cycle performance. On the other hand, HEX design optimization (with or without system integration) was addressed by several works in literature, also focusing on PHEs (Walraven et al., 2014; Xu et al., 2015). However, a simultaneous component/system optimization may entail a high computational cost, especially during the preliminary system design phase and working fluid selection. For example, screening of multiple combinations of pure fluids at different compositions to evaluate the performance of mixed refrigerants (Zühlsdorf et al., 2019), may require too many evaluations of system performance.

In this context, the present work aims at: (i) comparing the relative impact of condenser and evaporator design on the heat pump thermodynamic and economic performance, by looking at both area investment and pressure drops. (ii) Estimating the differences between three working fluids (pure and mixed refrigerants), for a case study. (iii) Discussing similarities and differences considering fluids thermo-physical properties. (iv) Attempting at the definition of general design recommendations for PHE evaporator and condenser in HP systems to be used during the preliminary system design phase.

2. METHODS

This section describes the chosen case study, the overall procedure and the numerical modelling.

2.1. Case Study

A case study previously published in (Zühlsdorf et al., 2019) was chosen for the analysis. A heat pump (HP) was integrated in a data centre facility for waste heat recovery purposes, with the aim of supplying heat to the district heating (DH) network. Propane, butane and a mixture of propylene/butane at (0.5/0.5) mass composition were found among the best performing working fluids. The heat pump was sized by fixing the heat transfer rate at the evaporator, i.e. 500 kW to use as waste heat. Moreover, the heat source was considered to be water entering the evaporator at 50 °C and leaving at 25 °C, while the heat sink was considered to be water entering the condenser at 50 °C to be heated up to 75 °C, i.e. the temperature level required by the DH network.

Table 1. Heat pump design and operating parameters for the three considered refrigerants

Working fluid	$\dot{Q}_{\mathrm{cond}}$, kW	$\dot{Q}_{\mathrm{eva}}$, kW	p_{cond}, bar	p_{eva}, bar	COP, -	$\dot{V}_{\mathrm{out,eva}}$, m^3/h
Propane	638	500	28.1	8.8	4.4	370
Butane	630	500	9.5	2.2	4.5	1100
Propylene/Butane	600	500	16.4	5.6	5.6	460

2.2. Coupled heat pump-plate heat exchanger simulation framework

The simulation framework structure is shown in Figure 1. The models were built in MATLAB (Mathworks, 2017), and fluid properties were estimated by REFPROP 10 (Lemmon et al., 2018). The reader is referred to (Mancini et al., 2018) for a detailed description of the PHE design models, and to (Mancini et al., 2019) for a comprehensive description of the heat pump design and operating models, with detailed PHE characterization.

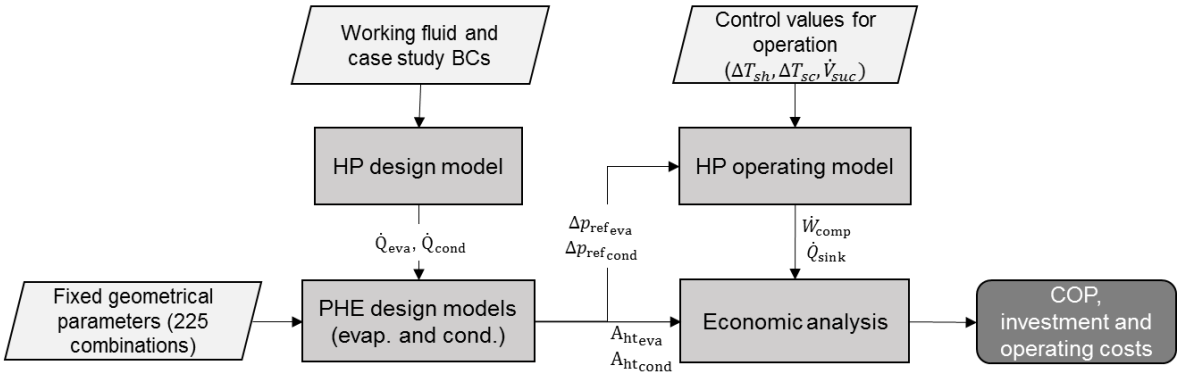

Figure 1: Workflow of the overall method

First, the working fluid and the case study boundary conditions (BCs) were defined and used in the HP design model. The PHE evaporator and condenser designs were subsequently carried out, for different combinations of geometrical parameters. The aim of the parametric analysis was to obtain PHE designs with different heat transfer areas and pressure drops. The resulting configurations were finally used in a HP operating model, which additionally received as input the control values chosen for the operation, namely a fixed superheat, subcooling and suction volume flow rate at the compressor inlet. The resulting HP operating conditions, affecting the compressor power requirement and the heat supply of the condenser, were used in an economic analysis to estimate the COP and operating costs.

2.2.1. Parametric Analysis on PHE geometry

A parametric study was conducted on the geometry of both evaporator and condenser. It was decided to fix the corrugation geometry of the PHEs and to carry out a sensitivity study on the plate size and count. The plate width W and number of channels N_{ch} were varied for both the components, while the plate length was estimated as an output of the design model. The values used in the parametric analysis are reported in Table 2.

Table 2: Plate width and number of channels values used in the parametric study

Parameter	Working fluid	Values	Unit
W_{eva}	All fluids	0.250 – 0.400 – 0.600	m
$N_{\mathrm{ch,eva}}$	Propane	50 – 100 – 150 – 200 – 250	-
	Butane	70 – 120 – 170 – 220 – 270	
	Propylene/butane	80 – 130 – 180 – 230 – 280	
W_{cond}	All fluids	0.200 – 0.400 – 0.600	m
$N_{\mathrm{ch,cond}}$	Propane	50 – 100 – 150 – 200 – 250	-
	Butane	70 – 120 – 170 – 220 – 270	
	Propylene/butane	50 – 100 – 150 – 200 – 250	

2.2.2. Evaluation of thermodynamic and economic performances

The thermodynamic and economic performance of the heat pump for different PHE geometries of both evaporator and condenser were assessed by means of performance indicators. The COP, estimated by Eq. (1), indicated the thermodynamic performance.

$$\mathrm{COP} = \frac{\dot{Q}_{\mathrm{sink}}}{\dot{W}_{\mathrm{comp}}} \qquad \text{Eq.(1)}$$

The specific cost of heat, calculated by means of Eq. (2) and expressed in €/MWh, was instead chosen to quantify the economic performance (Zühlsdorf et al., 2019). In Eq. (2), CF represents the fuel cost to run the compressor, TCI the total capital investment and CRF the capital recovery factor, estimated as function of an effective interest rate. OH represents the HP yearly operating hours.

$$\mathrm{c_h} = \frac{\mathrm{CF_{el}} + \mathrm{TCI} \cdot \mathrm{CRF}}{\dot{Q}_{\mathrm{sink}} \cdot \mathrm{OH}} \qquad \text{Eq.(2)}$$

The use of the specific cost of heat allows estimating the price at which the heat must be sold to the DH network in order to compensate for the investment and running cost of the HP. In this specific case study, the heat source was assumed as free waste heat from the data centre facility.

3. RESULTS

Section 3.1 deals with the impact of PHE designs on the heat pump COP, while Section 3.2 introduces the results of the economic analysis. Section 3.3 presents optimal designs obtained for the different refrigerants. Design recommendations are finally summarized in Section 3.4.

3.1. Impact of Evaporator and Condenser Design on Thermodynamic Performance

Figure 2 shows how the refrigerant pressure drops of the evaporator affected the heat pump COP. Each point corresponds to one combination of the design variables reported in Table 2, e.g. different evaporator and condenser geometries. The different marker styles and colours represent the working fluid. The COP value was reported by scaling it with respect to the design value. The thermodynamic performance degradation due to pressure drops for the different PHE evaporator designs was fitted linearly for each working fluid, and Figure 2 also reports the value of the slopes. For example, choosing a design with 30 kPa pressure drops entails around 4 % COP drop for butane, 3 % for propylene/butane, while it stays lower than 2 % for propane.

It must be noted that only few design points are visible in the figure compared to the 225 different combinations evaluated in the sensitivity study. This is due to the condenser design, which does not affect the COP, hence the points with the same evaporator geometry and different condenser designs overlap. Figure 3 (a) further illustrates this result, reporting the COP for the three working fluids vs. the total refrigerant pressure drops at the condenser. There is no dependency between the COP and the condenser design, and the colour scale – indicating different normalized evaporator pressure drops – shows that maximum COP was obtained for minimum evaporator pressure drops in all the cases. Note that Figure 3 (a) shows that the relative ranking of the working fluids in terms of COP was slightly affected by the PHE designs. Propylene/butane remained the refrigerant with the highest COP regardless of the evaporator and condenser configuration, while butane and propane were found to overlap depending on the evaporator design (pressure drops).

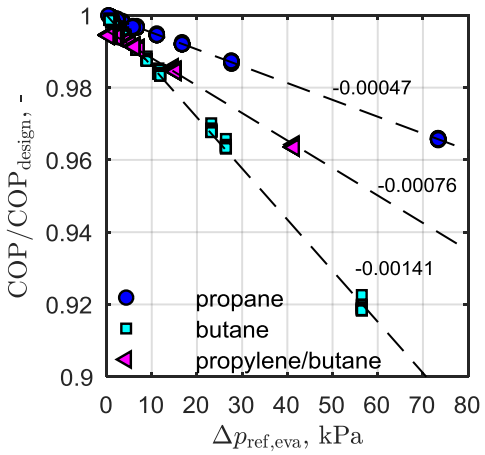

Figure 2: Normalized COP as a function of total refrigerant pressure drop in the evaporator

Table 3: Bubble and dew temperatures and thermo-physical properties at design pressure

Working fluid	p_{eva}, bar	ρ_V, kg/m^3	dT_{bubble}/dp K/kPa
Propane	8.8	19.1	0.044
Butane	2.2	5.7	0.140
Propylene/Butane	5.6	13.6	0.054

The stronger dependence of the COP to the evaporator pressure drops was related to a number of reasons. First, a higher value of pressure drops entailed a decrease in the heat output of the condenser. This was due to the impact of evaporator operation on the operating parameters of the cycle, i.e. refrigerant mass flow rate and pressures. The mass flow rate was in fact diminished at fixed superheat and subcooling, and the HP operated at a lower pressure ratio, i.e. a lower compressor power was required. However, the decrease in total heat flow rate of the condenser affected the COP negatively to a larger extent, as shown in Figure 3 (b): the condenser total heat flow rate – normalized by the design value – is plotted as a function of the evaporator pressure drops, with different colours representing different magnitudes of normalized condenser pressure drops. Similarly to the COP degradation reported in Figure 2, butane reports the steepest degradation, followed by propylene/butane and propane. The slopes of degradation were found to be similar to the COP drop plotted in Figure 2. Condenser pressure drops, represented by the different colour scale, were found not to affect the total heat flow rate at the condenser, and different condenser designs overlap in Figure 3 (b) similarly to Figure 2.

The higher drop of heat pump COP for butane compared to the other two fluids is due to another main reason: evaporator pressure drops also imply a saturation temperature drop, which increases the exergy destruction due to finite temperature differences in the evaporator component, thus contributing to the COP degradation. Depending on some relevant fluid thermo-physical properties, refrigerants can be more or less subject to this effect.

(Brignoli et al., 2017) identified the ones characterizing refrigerants sensitivity to pressure drops, namely vapour density and saturation temperature drop due to pressure drop. These are reported in Table 3 for the three working fluids at design conditions. Lower vapour density implies higher pressure drops for the same mass flux and PHE geometry. Therefore, a design that is feasible for propane and propylene/butane, possibly enhancing the heat transfer coefficient, might entail too large pressure drops for butane, with vapour density much lower than the other two refrigerants. This was one of the reasons why the bounds for plate width and number of channels variation in the sensitivity study (see Table 2) were chosen differently for the working fluids, i.e. to ensure feasible PHE designs with similar values of pressure drops.

The refrigerant vapour density is thus a property that must be carefully taken into account when choosing the working fluid and subsequently selecting the HEX design. Higher saturation temperature drop due to pressure drop, estimated by the Clapeyron relation (Moran, 2017), entails a larger drop of the saturation temperature due to pressure drop, thereby increasing the exergy losses due to the temperature difference between the refrigerant and the heat source side in the evaporator. Table 3 shows how the ranking between the working fluids in terms of vapour density and dT_{bubble}/dp respects the slopes of the COP degradation reported in Figure 2. Therefore, despite both propane and propylene/butane reported similar slopes for the degradation of condenser heat flow rate, the mixture was found to be more sensitive to saturation temperature drop due to pressure drop, resulting in a steeper COP drop.

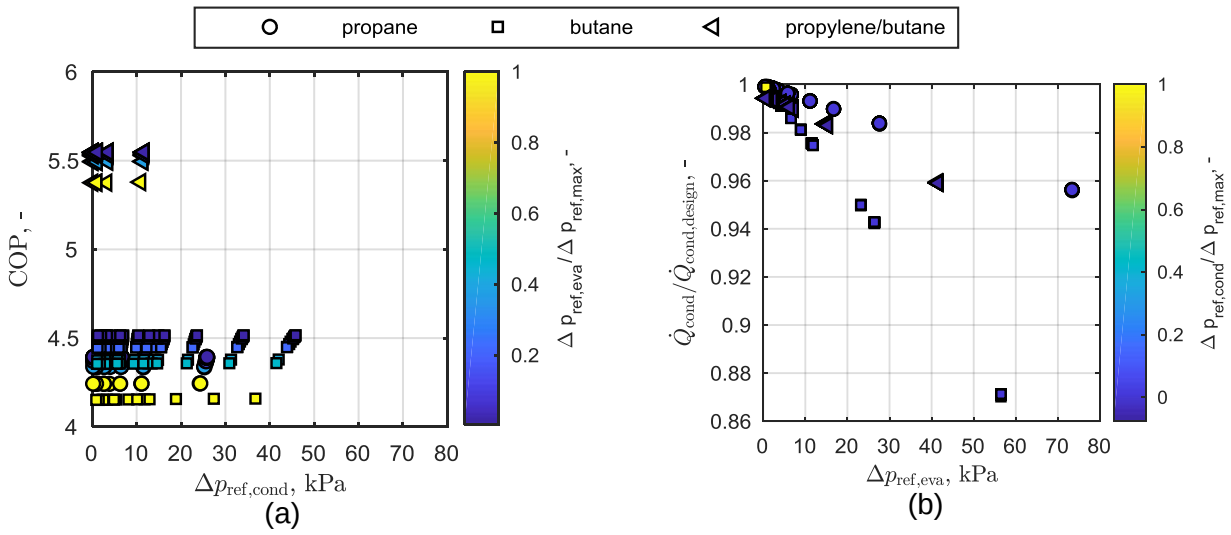

Figure 3: (a) COP as a function of total refrigerant pressure drop in the condenser; (b) Normalized condenser heat flow rate as function of total refrigerant pressure drop in the evaporator

3.2. Impact of Evaporator and Condenser Design on Economic Performance

The economic performance was evaluated by looking at the specific cost of heat, which is influenced by both condenser and evaporator design. The TCI is dependent on both HEX sizes (related to the heat transfer area), while the operating costs are strongly related to the heat pump COP. The economic performance indicator is reported in Figure 4 (a) for the three refrigerants as function of the pressure drop at the evaporator. The three working fluids present similar trends, with a trade-off and a minimum for a certain value of refrigerant pressure drops. Figure 4 (a) reports a close-up for the case of propane, where the colours represent different values of condenser heat transfer area. The results show that evaporator and condenser have different types of impact on the specific cost of heat. For a fixed condenser design – thus a fixed value of heat transfer area shown by the colours of Figure 4 (b) – the economic performance was a trade-off between heat transfer area and pressure drops of the evaporator. The minimum cost was determined by a certain value of evaporator pressure drops, which was similar for all the different condenser designs.

On the other hand, the condenser design influences the economic performance in a different manner: it was always desirable to employ condenser designs with minimum heat transfer area (shown by the darker blue colour in Figure 4 (b)). In fact, since the COP was not found to be affected by condenser pressure drops, the operating costs were not influenced by its design. The TCI was instead related to the heat transfer area, thereby suggesting a minimization of the condenser size. A relevant finding shown by Figure 4 is thus given by the fact that the evaporator and condenser geometry optimization, despite aimed at minimizing the cost of the overall system, could be considered as decoupled problems. The designer can choose to optimize the evaporator geometry and to find the design leading to the minimum cost, regardless of the condenser design (and the opposite holds). One additional relevant aspect highlighted by Figure 4 (a) is that all the refrigerants presented a minimum of specific cost of heat for similar values of refrigerant pressure drops. These values lie in the interval 5 – 10 kPa, which is relatively low, compared to usual manufacturer guidelines setting the limitation to around 50 kPa (SWEP International AB, 2015).

The results might therefore suggest that in this particular case study – regardless of the refrigerant chosen – an optimal value of pressure drops could be defined preliminarily to the refrigerant selection and HEX sizing. In this way, it is possible to define a guideline – based on optimal pressure drops – to design the PHE evaporators and condensers prior to the working fluid screening. This would enable the screening to avoid suboptimal solutions or the computational cost of optimizing the HEX design for all the working fluids, some of which the screening will in any case subsequently disregard. This result might seem contradictory if one thinks about the different slopes of COP degradation for the different fluids, previously shown in Figure 2. However, Figure 4 (a) reports an effective steeper increase of the specific cost of heat for butane rather than propane and propylene/butane. This increase started however after reaching the minimum specific cost of heat (after around 30 kPa), thus the different slopes of the working fluids for the COP degradation were not relevant to define the optimum. Moreover, since the optimal values of refrigerant pressure drops was found to be as

low as 5 kPa to 10 kPa, the COP degradation (shown in Figure 2) admissible for this case was found to be lower than 2 %.

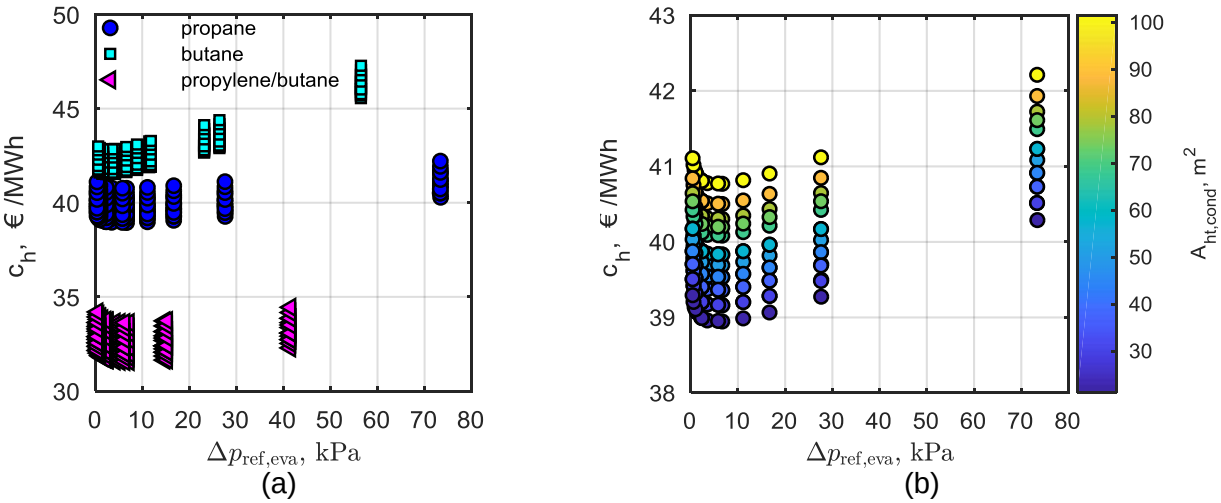

Figure 4: Specific cost of heat as function as a function of total refrigerant pressure drops in the evaporator for: (a) all fluids, (b) propane (close-up)

3.3. Economic Optimum: PHE Designs

Table 4 shows the geometrical specification of the PHE evaporator and condenser designs corresponding to the economic optimum shown in Figure 4. Moreover, heat transfer area, total refrigerant pressure drops and heat pump COP and specific cost of heat are reported. The designs minimizing the specific cost of heat are in agreements with the results presented above. The PHE evaporator design was limited to pressure drops from 4.2 kPa for butane and 7.2 kPa for propylene/butane. The optimal values are thus close for all the working fluids. Similar plate size was found for propane (P) and propylene/butane (P/B), while a plate with a lower aspect ratio (length-to-width ratio) was obtained for butane (B). Due to the lower vapour density, butane is in fact subject to higher pressure drops for the same velocity and channel geometry. The condenser design was instead found to be similar for propane and butane, e.g. high pressure drops over 100 kPa were allowed. With similar channel geometry, the condenser design for propylene/butane led instead to low pressure drops, e.g. 11.5 kPa. This was likely due to the lower dependency of the total heat flow rate at the condenser on the pressure drops, as previously explained in Section 3.1. Note that the condenser design corresponding to the economic optimum is an extreme design case of very high aspect ratio, due to the large bounds for variation of width and channels imposed in the sensitivity study. Such designs might be unrealistic compared to commercial plate size. The economic optimum would in any case correspond to the same evaporator design and more realistic plate size for the condenser could be easily obtained by choosing solutions with higher condenser heat transfer area (e.g. going up in the parallel curves reported in Figure 4).

Table 4: PHE designs corresponding to the economic optimum

	Evaporator design					Condenser design						
	W	L	N_{ch}	A_{ht}	Δp_{ref}	W	L	N_{ch}	A_{ht}	Δp_{ref}	COP	c_h
	m	m	-	m^2	kPa	m	m	-	m^2	kPa	-	€/MWh
P	0.250	0.460	150	20.5	6.7	0.200	1.768	50	21.1	113.3	4.4	38.9
B	0.400	0.447	170	36.0	4.2	0.200	1.472	80	28.1	140.2	4.5	41.5
P/B	0.250	0.655	180	35.1	7.1	0.200	1.774	100	42.3	11.5	5.5	31.6

3.4. Design Recommendations

The results presented so far led to the following findings, summarized as design recommendations for evaporator and condenser design in heat pump systems:

- Design criteria such as maximum allowable pressure drops and fixed velocities possibly lead to suboptimal solutions depending on the case study and the working fluid.
- Evaporator and condenser designs can be carried out as decoupled geometry optimization problems, e.g. the design of each component does not affect the other.
- Evaporator design influences the heat pump COP to a large extent, while the condenser design is not found to be relevant for the thermodynamic performance.
- Both components influence the economic performance: the minimum cost is found by defining optimal trade-offs between heat transfer area and pressure drop in the evaporator, while it is always desirable to minimize condenser heat transfer area.
- The economic optimum could be defined by a maximum allowable COP degradation, which theoretically corresponds to different allowable pressure drops for each refrigerant.
- The same optimal evaporator pressure drop was found for different refrigerants for this case study. This is not necessarily a general conclusion, given the very low allowable COP degradation and the dependence of the results from the economic boundary conditions.

4. DISCUSSION

The results presented in this paper were based on numerical modelling of PHE and HP, in both design and performance mode. The PHE models were based on a 1D discretization along the fluid-flow direction, thus neglecting the occurrence of channel-to-channel maldistribution effects. (Mancini et al., 2019) showed that refrigerant pressure drops have a major impact on the heat transfer degradation due to maldistribution effects, causing an additional COP degradation. This implies that the optimal value of refrigerant pressure drops found in this study could be even lower for those refrigerants (like butane) that are particularly sensitive to maldistribution effects. The results of economic analysis are strongly dependent on the boundary conditions assumed for the case study. The heat from the source was considered to come at no cost, and the COP degradation solely implied an increase of the compressor running cost. A COP decrease could also imply a reduction of the heat source utilization, which might partially counteract the cost increase in those cases where the heat source is not free (e.g. district heating applications). Last, the importance of tailoring design criteria depending on the working fluid and application is stressed: designers must be aware that limiting inlet velocities or imposing allowable pressure drops can lead to suboptimal solutions, since the slope of COP degradation has a strong dependence on refrigerant properties. For example, for the economic analysis of propane shown in Figure 4(b), choosing an evaporator design with pressure drops around 50 kPa would entail an increase of almost 1 €/MWh in the specific cost of heat.

5. CONCLUSIONS

This paper presented an approach to derive recommendations for PHE design in HP using pure and mixed refrigerants. A sensitivity study was carried out by simultaneously varying plate size and count for both evaporator and condenser, and PHE geometrical configurations with different trade-offs between heat transfer area and pressure drops were obtained. This study constitutes an attempt to derive design guidelines during a preliminary cycle design phase, where a full component optimization is computationally expensive, and adopting heuristics criteria might lead to suboptimal solutions. The results showed that only evaporator pressure drops affected the COP, and the different refrigerants were subject to different degradation slopes. Butane, with lowest vapour density and higher saturation temperature drop due to pressure drop, resulted in the steepest drop, with 30 kPa generating a 4 % COP drop. Condenser design solely influenced the economic performance, thus a minimization of the size was always preferable. The trade-off between evaporator size and pressure drops was found to be independent from the condenser design, and the analysed case study resulted in optimal COP degradation of maximum 2 % for all the working fluids, thereby defining optimal pressure drop values in a narrow range, around 5 kPa.

ACKNOWLEDGEMENTS

This research was funded by Innovations Fund Denmark with project title "THERMCYC".

NOMENCLATURE

A_{ht}	heat transfer area (m^2)	Abbreviations	
c_h	specific cost of heat (€×MWh^{-1})	BC	boundary conditions
$\mathrm{CF_{el}}$	annual cost of electricity (€)	HEX	heat exchanger
COP	coefficient of performance (-)	HP	heat pump
CRF	capital recovery factor (-)	PHE	plate heat exchanger
L	plate length (m)	Greek symbols	
N_{ch}	number of channels (-)	ρ	density (kg×m^{-3})
OH	operating hours (h)	Δ	Difference (-)
p	pressure (bar)	Subscripts	
$\dot{Q}$	heat flow rate (W)	comp	compressor
T	temperature (K)	cond	condenser
TCI	total capital investment (€)	eva	evaporator
W	plate width (m)	V	vapour

REFERENCES

Brignoli, R., Brown, J, Skye, H, Domanski, P.A., 2017.Refrigerant performance evaluation including effects of transport properties and optimized heat exchangers. Int. J. Refrig. 80, 52–65.

Lemmon, E.W., Bell, I.H., Huber, M., McLinden, M.O., 2018. NIST Standard Reference Database 23: Reference Fluid Thermodynamic and Transport Properties - REFPROP, version 10.0.

Mancini, R, Zühlsdorf, B, Jensen, J., Brix Markussen, W., Elmegaard, B., 2018. Deriving guidelines for the design of plate evaporators in heat pumps using zeotropic mixtures. Energy 156.

Mancini, R., Zühlsdorf, B, Aute, V, Markussen, W., Elmegaard, B., 2019. Performance of heat pumps using pure and mixed refrigerants with maldistribution effects in plate heat exchanger evaporators. Submitt. to Int. J. Refrig.

Mathworks, 2017. Matlab R2017b URL https://www.mathworks.com/products/new_products/latest_features.html (accessed 11.7.17).

Moran, M.J., 2017. Engineering thermodynamics: Fundamentals, in: CRC Handbook of Thermal Engineering, Second Edition. pp. 3–14. https://doi.org/10.4324/9781315119717

Muralikrishna, K., Shenoy, U.V., 2000. Heat Exchanger Design Targets for Minimum Area and Cost. Chem. Eng. Res. Des. 78, 161–167. https://doi.org/10.1205/026387600527185

SWEP International AB, 2015. SWEP Products URL https://www.swep.net/ (accessed 2.23.18).

Walraven, D, Laenen, B, D'Haeseleer, W, 2014. Comparison of shell-and-tube with plate heat exchangers for the use in low-temperature organic Rankine cycles. Energy Convers. Manag. 87, 227–237.

Wang, L., Sundén, B., 2003. Optimal design of plate heat exchangers with and without pressure drop specifications. Appl. Therm. Eng. 23, 295–311.

Xu, J., Luo, X., Chen, Y., Mo, S., 2015. Multi-criteria Design Optimization and Screening of Heat Exchangers for a Subcritical ORC. Energy Procedia 75, 1639–1645.

Zühlsdorf, B., Jensen, J.K., Elmegaard, B., 2019. Heat pump working fluid selection – Economic and thermodynamic comparison of criteria and boundary conditions. Int. J. Refrig. 98, 500–513.

If we knew what it was we were doing,
it would not be called research, would it?

— Albert Einstein

This thesis presents detailed numerical models to design and evaluate the performance of plate heat exchangers (PHEs) integrated in heat pump systems using pure fluids and zeotropic mixtures as working fluids. The models are verified and validated with experimental data. They are subsequently applied to address open research questions in the field of PHE technology. First, a comparison of different prediction methods to compute the heat transfer coefficient of zeotropic mixtures in PHEs is presented, with the aim of identifying the most suitable correlations to apply. Second, design guidelines for PHE evaporators and condensers in heat pumps are derived, and a methodology to derive simplified guidelines for optimal evaporator design is illustrated. Last, a study on flow maldistribution in PHE evaporators is carried out, with the aim of quantifying the performance degradation due to liquid/vapour maldistribution and effect of end plates. The impact of maldistribution is evaluated in terms of heat transfer performance degradation of the component, as well as thermodynamic performance decrease of the cycle.

DTU Mechanical Engineering
Section of Thermal Energy
Technical University of Denmark

Nils Koppels Allé, Bygn. 403
DK-2800 Kgs. Lyngby
Denmark

Tlf.: +45 4525 4131
Fax: +45 4525 1961
www.mek.dtu.dk

May 2019

ISBN: 978-87-7475-578-4

DCAMM
Danish Center for Applied Mathematics and Mechanics

Nils Koppels Allé, Bld. 404
DK-2800 Kgs. Lyngby
Denmark
Phone (+45) 4525 4250
Fax (+45) 4525 1961

www.dcamm.dk

DCAMM Special Report No. S268

ISSN: 0903-1685